PROCEEDINGS
SECOND WORKSHOP
GEOTHERMAL RESERVOIR ENGINEERING
December 1-3, 1976

Paul Kruger and Henry J. Ramey, Jr., Editors
Stanford Geothermal Program
Workshop Report SGP-TR-20*

*Conducted under Grant No. NSF-AER-72-03490 supported by the RANN program of the National Science Foundation and Contract No. E043-326-PA-50 from the Geothermal Energy Division, Energy Research and Development Administration.

TABLE OF CONTENTS

Field Development

Well Stimulation

Modeling

INTRODUCTION

The Arab oil embargo of 1973 focused national attention on energy problems. A national focus on development of energy sources alternative to consumption of hydrocarbons led to the initiation of research studies of reservoir engineering of geothermal systems, funded by the National Science Foundation. At that time it appeared that only two significant reservoir engineering studies of geothermal reservoirs had been completed.

Many meetings concerning development of geothermal resources were held from 1973 through the date of the first Stanford Geothermal Reservoir Engineering workshop December 15-17, 1975. These meetings were similar in that many reports dealt with the objectives of planned research projects rather than with results. The first reservoir engineering workshop held under the Stanford Geothermal Program was singular in that for the first time most participants were reporting on progress in active research programs rather than on work planned. This was true for both laboratory experimental studies and for field experiments in producing geothermal systems. The Proceedings of the December 1975 workshop (SGP-TR-12) is a remarkable document in that results of both field operations and laboratory studies were freely presented and exchanged by all participants. With this in mind the second reservoir engineering workshop was planned for December 1976. The objectives were again two-fold.

First, the workshop was designed as a forum to bring together researchers active in various physical and mathematical branches of the developing field of geothermal reservoir engineering, to give participants a current and updated view of progress being made in the field. The second purpose was to prepare this Proceedings of Summaries documenting the state of the art as of December 1976. The workshop proceedings will be distributed to all interested members of the geothermal community involved in the development and utilization of the geothermal resources in the world.

Many notable occurrences took place between the first workshop in December 1975 and this present workshop in December 1976. For one thing, the newly formed Energy Research and Development Administration (ERDA) has assumed the lead role in geothermal reservoir engineering research. The second workshop under the Stanford Geothermal Program was supported by a grant from ERDA. In addition, two significant meetings on geothermal energy were held in Rotarua, New Zealand and Taupo, New Zealand. These meetings concerned geothermal reservoir engineering, and the reinjection of cooled geothermal fluids back into a geothermal system. It was clear to attendees of both the New Zealand and the December workshop meetings that a great deal of new information had been developed between August and December 1976. Another exciting report made at the meeting was a successful completion of a new geothermal well on the big island of Hawaii which

produces a geothermal fluid that is mainly steam at a temperature in excess of 600 degrees F.

Although the total developed electrical power generating capacity due to all geothermal field developments in 1976 is on the order of 1200 megawatts, it was reported that rapid development in geothermal field expansion is taking place in many parts of the world. Approximately 400 megawatts of geothermal power were being developed in the Philippine Islands, and planning for expansion in production in Cerro Prieto, Mexico was also announced. The Geysers in the United States continued the planned expansion toward the level of more than 1000 megawatts.

The Second Workshop on Geothermal Reservoir Engineering convened at Stanford December 1976 with 93 attendees from 4 nations, and resulted in the presentation of 44 technical papers, summaries of which are included in these Proceedings. The major areas included in the program consisted of reservoir physics, well testing, field development, well stimulation, and mathematical modeling of geothermal reservoirs.

The planning for this year's workshop and the preparation of the proceedings was carried out mainly by my associate Paul Kruger and his secretary for the program, Marion Wachtel. A great deal of the work involved in conducting the workshop was also carried out by students in the Stanford Geothermal Program under Dr. Paul Atkinson, Program Manager. We would like to express our deep gratitude to the Energy Research and Development Administration whose financial support of this workshop made the program and these proceedings possible.

Henry J. Ramey, Jr.
Stanford University
December 3, 1976

GEOTHERMAL RESERVOIR ENGINEERING RESEARCH

H. J. Ramey, Jr. and Frank G. Miller
Department of Petroleum Engineering
Stanford University
Stanford, CA 94305

Before discussing reservoir engineering research, it is useful to consider the place of reservoir engineering within the broad field of study of petroleum engineering. Petroleum engineering includes the major specialties of drilling, production, and reservoir engineering. Other specialties important to development and production include petroleum geology, geophysics, geochemistry, fluid transmission, marine operations, refining, natural gas production and processing, computer science and reservoir simulation, and economics. Although petroleum engineering is frequently involved in planning the drilling of an exploration target, the main activity actually begins upon completion of an exploratory well.

Unfortunately, the objectives of the three major petroleum engineering specialties of drilling, production, and reservoir engineering are often antagonistic. The drilling engineer has a responsibility to complete the well as rapidly as possible with due regard for safe procedures and low drilling costs. The production engineer has the responsibility of maintaining high producing rates from wells and is frequently involved in the well completion phase of the drilling. He must analyze well logs and drill stem tests and make decisions concerning the running of pipe and completion of the well. He must determine whether the well is damaged and when and how to stimulate the well. In addition, he will be involved in the completion design of the well and will decide which portion of the interval to complete. The reservoir engineer is interested in the total reservoir-producing well system. He seeks such information as the permeability, porosity, and fluid content within the entire reservoir volume and the condition of the well. The reservoir engineer will be involved in planning the development of the entire reservoir, and will decide the number of wells required for a given reservoir, which well pattern should be used and what recovery process should be used. He usually establishes the potential producing life and oil recovery of the system. Generally, all three branches of engineers employ economics in making engineering decisions.

Obtaining necessary engineering data frequently involves extended periods of testing during the drilling of a well. In this respect, the drilling objectives of fast, low-cost completion are diametrically opposed to production and reservoir engineering objectives to obtain reliable data. On the other hand, the production engineer also is reluctant to expose the formation to drilling fluid for extended periods of time. This may result in formation damage and a poor producing well. Often, the technology employed by drilling, production, and reservoir engineers is compartmentalized or segregated. The specialty of formation evaluation is often considered

to be involved with the drilling and completion of a well only, although important information useful in reservoir engineering may be obtained during this phase. This specialty should cross all three engineering specialties.

Fortunately, there are three good reference books available describing the functions of drilling, production, and reservoir engineering. Good examples include the text Drilling and Well Completions, by Carl Gatlin, Principles of Oil Well Production, by P.E.W. Nind and Applied Reservoir Engineering, by B. Craft and M. Hawkins. The text by Nind is a McGraw-Hill publication. The other two are Prentice-Hall publications.

In the light of important cross-purposes in the three major petroleum engineering specialties, it is imperative that engineering data not be taken for frivolous reasons. Engineering data should be gathered with firm objectives in mind. Data-taking procedures should be carefully planned so that the desired information will be obtained, and proper interpretive techniques established. Thus it is basic to review the principles involved in sound reservoir engineering research.

Reservoir Engineering Research

Reservoir engineering generally follows a specific pattern. First, field performance is observed and data obtained. From the observed performance, it is possible to generate a hypothesis as to the nature of the system. The hypothesis is then tested either by operating physical models in the laboratory or by computer investigation of mathematical formulations describing the hypothesis. From these results the physical laws involved in the operation of the reservoir can be formulated. It is also necessary to collect physical and thermodynamic data for the reservoir rock and fluids. These steps frequently involve running well tests. Pressure transient information and fluid samples may be obtained. The fluid samples can be used for pressure-volume-temperature studies in the laboratory, or used to select correlated properties from the literature. Using this information, one can write and solve pertinent equations describing the reservoir system. The mathematical model solutions are usually compared with field behavior to establish the validity of the simulation. Given a reasonable correlation between the mathematical model and the field performance, it is then possible to study the effect of various development and production plans for the system. Final decisions as to development plan are usually based on comparative economics of various operating schemes.

One danger in the preceding method lies in searching for field performance data to match a preconceived notion about important reservoir mechanisms. It is difficult to differentiate between a sound hypothesis and an incomplete mathematical model which includes only selected fact. One good example which occurs often in geothermal reservoir production is the idea that precipitation from geothermal fluids will plug the producing sand face of a well and result in declining production rates. The fact that all

geothermal wells do appear to decline in productivity over short periods of time is sometimes thought to prove that precipitation is responsible for rate decline. However, many other factors may cause declining production rates in wells. One is declining formation pressure causing a decreasing driving force to move fluids into the wellbore. Often this is the factor responsible for declining geothermal well production rates rather than precipitation from geothermal fluids.

It is therefore important to keep an open mind. A proper reservoir engineering study searches for the hypothesis derived from all known facts. It is not valid to select only facts that substantiate a preconceived concept. The researcher should observe facts, then produce a hypothesis to explain field behavior and from this test the hypothesis with physical and mathematical models.

Geothermal reservoir engineering research is currently similar to oil and gas reservoir engineering research performed during the first quarter of this century. At that time workers were trying to decide the true nature of gas and oil reservoirs. Almost every scientific discipline made a contribution. There were many debates as to the essential behavior of oil, water and gas within the pore space of rock. Incorrect theories were offered and defended vigorously. Debate often gave way to rancor and personal animosity. Scientific reputations crumbled. There exist many scientific textbooks written during 1900-1925 which are now only historical curiosities. The final result, however, was a sound technology presently heading into a second generation of accomplishment and discovery.

Gas and oil reservoir engineering flourished immediately after World War II. The return of servicemen from war-time duties provided a new pool of engineering talent needed for the rapidly growing oil industry. The modern geothermal industry also dates essentially from the end of World War II. However, application of reservoir engineering to geothermal systems essentially began in the early 1960's. Geothermal reservoir engineering has come a long way in the last ten years. We have reached a stage of development that is comparable to the early 1950's in gas and oil reservoir engineering research. This can be seen in the report on the first geothermal reservoir engineering workshop held at Stanford in December of 1975. Perhaps the greatest reason for rapid advance has been development of field studies recently. The concept of jointly funded field studies supported by federal funding and combining the talents of private industry, university staffs, and the U.S. Geological Survey, has permitted rapid strides in the field of reservoir engineering research.

Geothermal reservoir engineering research is destined to blossom and bear significant fruit for the nation's energy appetite. We confidently forecast that the December 1977 workshop will reveal that geothermal reservoir engineering research has finally reached the decade of the 1970's.

GEOTHERMAL RESERVOIR ENGINEERING IN INDUSTRY

Stephen C. Lipman
Union Oil Company of California
Santa Rosa, California 95406

The status of geothermal reservoir engineering in industry is highly encouraging. The "state of the art" has grown steadily over the years and has been accelerating rapidly in the last few years. Geothermal engineers in industry have had an advantage over their counterparts in research and government in that they have had actual reservoirs and producing wells on which to apply their engineering skills. This involvement with field testing and development has created an ideal environment for advancing the technology of geothermal reservoir engineering.

I tend to view geothermal reservoir engineering in a much broader context than the five general topics being discussed in this workshop. For reservoir engineers in private industry, a geothermal project begins when a potential geothermal prospect is being evaluated for leasing. The reservoir engineer must be involved with his exploitation and land acquisition groups so that the terms of the eventual lease are achievable within the framework of the existing stage of technology, regulatory control and appropriate economics.

Once the lease is consummated, the reservoir engineer must be involved in the exploration and initial drilling program. The exploration data acquired and evaluated by the exploration geologist is of vital importance to the reservoir engineer in his evaluation of the reservoir. He must work closely with the design and execution of the initial drilling program so that the maximum reservoir information can be obtained from the drill cuttings, coring, logging, bottomhole fluids, temperatures and pressures. The casing design and well completion program will be of important concern to the reservoir engineer, since they will play a large role in limiting or contributing to the productivity of the well.

Nowadays in the United States, very little new industrial development can occur without a thorough analysis of the environmental impacts of the operation. The reservoir engineer in industry must play a role in contributing necessary information in these analyses. He can provide details on the anticipated well testing and field evaluation programs and on the estimated extent of development and on the quantity and characteristics of the fluids which will be produced. The quantity of information required before these projects are well defined may seem unmanageable, but the reservoir engineer is the most qualified to supply much of this information.

There is another aspect of regulatory control in which the reservoir engineer should play an active role. The regulations which generally fall into the category of environmental protection have been in a general state of flux by local, state and federal agencies. Geothermal development is very new to these agencies, and there is an urgent need to educate them on the exact nature of the operations. Without this education, industry has and will continue to experience long delays in receiving governmental approval for future development.

While I am on the subject of delays, we should examine an important responsibility the reservoir engineer has in shortening the long lead time from initial discovery to commercial production. In an oil or gas reservoir, field production facilities can be installed shortly after the first few wells are drilled and tested. The reservoir evaluation proceeds concurrent with the development of the field. We are not provided with this luxury in geothermal development. Small geothermal power plants are not economically attractive, and it takes extenuating circumstances to justify their installation. We tend to view a 55 MW plant as the smallest economic size unit under normal circumstances. This means that a reservoir will have to contain close to 300 billion pounds of steam to support this plant for a 30-year life. Of course the required minimum reserve will vary depending upon the power cycle used and the nature of the fluids in the reservoir. If the reservoir fluid is hot water, the required fluid reserves may be four to five times as large. The challenge to the reservoir engineer in industry is to determine how large his reserves are within the shortest possible time and with the minimum amount of wells and testing.

It is toward achieving this goal that the reservoir engineer must constantly strive. I feel that the industry is moving rapidly in this direction. Well testing and evaluation techniques have been vastly improved in the last few years. In this respect, the bottomhole pressure measurement techniques are meeting our needs, but there is an obvious absence of equally sensitive temperature tools. We must find a way to measure temperature changes in the reservoir with greater accuracy.

There are considerable chemical data becoming available on existing geothermal reservoirs. I feel there is an urgent need to analyze these data with respect to what they are telling us on reservoir performance. I refer not only to ion concentration changes, but also to isotope chemistry. The performance of a geothermal field will be controlled by, among other factors, the hydrology of the area. Monitoring the changes of isotopes, such as H, O, C and S, will provide insight into how the hydrology of the area is responding to geothermal operations. The results of these chemical investigations need to be integrated with flow behavior and the physical properties of the reservoir fluids. We feel that the reservoir evaluation and prediction techniques will eventually have to account not only for the mass and energy changes during exploitation, but also for the chemical changes.

There has been considerable interest in the last few years on the consequences of cold fluid injection into geothermal reservoirs. Industry has been aware of this potential problem for a number of years, so it is gratifying that more research is being undertaken to determine the physical characteristics of its effect. Such research will aid in designing successful reinjection programs, but industry will have the responsibility of developing field trials and making the system work beneficially for additional heat recovery and not to detrimentally inhibit our producing wells. An unknown in calculating the heat recovered from the rock during water injection is the fracture intensity. In all the mathematical derivations, we use the assumption of instantaneous heat transfer from the rock to the fluid to achieve thermal equilibrium. This assumption has

to be verified in the laboratory using larger rock than in past experiments and also in the field by conducting pilot tests. The technology development for fluid injection into geothermal reservoirs should proceed much like the development of water-flooding in oil reservoirs. Theoretical and laboratory analyses went hand in hand with field testing.

I should point out that Union Oil has been involved in water injection at The Geysers since 1969, in New Mexico since 1973, and for over one year in Imperial Valley. These injection programs were initiated to dispose of the produced liquids in an environmentally acceptable manner. I anticipate that reinjection of produced liquids will become the only acceptable method of water disposal for geothermal operations in the United States. Therefore, it is mandatory that we develop techniques that minimize the detrimental effects. Our experience to date indicates that if the injection program is designed carefully, water injection can be carried out successfully.

Though we are confident in cold fluid injection, there is still a considerable amount of field data and experience needed. We intend to concentrate on reservoir analyses on the heat transfer characteristics in these operations in the coming year. We have experimented with the use of tracers in our injection water in the past, and we plan to expand this work in the future. It is our hope that the use of tracers will provide us with information on the orientation and intensity of the fractures and how effectively we are mining the heat from the rock.

In summary, I feel that geothermal reservoir engineering in industry is extremely important in advancing the development of these needed resources. The engineering going on in the field is highly complementary to the current research activity. There is considerable work ahead for both industry and research, but through information exchanges such as this workshop, we can shorten the time-lag in our knowledge about geothermal reservoirs.

GEOTHERMAL RESERVOIR ENGINEERING IN THE EPRI GEOTHERMAL PROGRAM

V. W. Roberts
Electric Power Research Institute
Palo Alto, Ca. 94303

Early optimism about the rate at which geothermal energy might be developed in the United States appears to have diminished over the past two years, and the formula for accelerating the development of geothermal energy has proven elusive both for industry and the federal government. Certainly, the geothermal resource base has not changed, and several of the liquid-dominated fields have been better defined by continuing drilling programs. The technical problems have not changed significantly and progress has been made in the art of handling geothermal brines, notably the work with the hypersaline brines of the Salton Sea deposit. More applied research is underway and beginning to yield results. Why, then, has optimism diminished?

One of the main reasons is that power is not yet being generated in the United States from geothermal energy outside of The Geysers. Furthermore, there still are no firm plans to construct power plants at hot water-dominated resource sites. The nearest thing to a planned commercial size generating facility of this type is the Heber 50 MWe demonstration plant project initiated by EPRI and conceived for completion in 1980 with broad support from EPRI, the San Diego Gas and Electric Company (the lead utility), a number of other participating utilities, Chevron Oil, and ERDA. Many of the details of cooperation must be resolved in the next few months if the project is to remain on schedule. Including the possibility of another 10 MWe at the Geothermal Loop Experimental Facility at Niland and 10 MWe at East Mesa in California, the hydrothermal growth rate is far from impressive. If this slow trend is to be reversed and the commercialization of hydrothermal resources is to accelerate, more geothermal power plants must begin to appear in utility construction plans. In order for this to happen, the industry needs more precise estimates of the commercial potential of hydrothermal reservoirs both from the standpoint of energy production and energy conversion.

Although there are few firm plans, several utilities have tentative plans to use hydrothermal resources providing: (1) they have access to commercial quality resources; (2) the cost of geothermal power is competitive with other available energy sources; (3) that regulatory approval for such plants is forthcoming; and (4) environmental acceptance of geothermal power is achieved.

Although several of the known resource sites appear to have the potential for satisfying all of these conditions, the truth is that we have not yet satisfied all of these conditions at any of the sites. This, then, is one of the main reasons that utilities are cautious in regard to making firm commitments to plans that include geothermal power plant construction. A further cause for reluctance is that the potential of geothermal energy to displace other energy sources on a large scale has not been demonstrated. We do not yet know how much geothermal power we can depend on for electrical power generation.

The present status of geothermal development is somewhat disappointing, but may not be quite as grim as it seems. It appears to be a case of a young industry wanting to grow somewhat faster than could reasonably be expected. Both the potential and the challenge are still there and efforts should continue to establish the credentials of hydrothermal energy in the market place.

Importance of Reservoir Engineering

Aside from technology adaptation, verification of commercial viability and environmental acceptance, one of the most crucial efforts in the commercialization of hydrothermal resources will be reservoir assessment. It seems reasonable to speculate that as reservoir production and geothermal fluid characteristics are defined with better accuracy and greater confidence, geothermal power plants will begin to appear with increasing frequency in the future plan of utilities.

A decision on the part of a utility to construct a geothermal power plant naturally involves a host of considerations, but most relate one way or another to the results of reservoir assessments. Overall reservoir capacity, rate of sustained production, fluid heat content, fluid purity and the amount and species of non-condensible gases, are important considerations, particularly as they relate to power needs, selection of appropriate conversion processes and environmental controls. Reservoir assessment is one of the most important links in the development of geothermal energy, and reservoir engineering is an exceedingly important part of reservoir assessment.

Rationale for Including Reservoir Assessment Projects in the EPRI Program

For all practical purposes geothermal energy is a sole source commodity. It cannot be transported except over short distances; therefore, power plants must be sited near the source. Once a commitment is made to a particular reservoir, the commitment is irreversible in that fuel substitution is not a likely possibility.

Geothermal power plants must be designed to operate with low enthalpy fluids, making it unlikely that higher grade fuels could be sacrificed to continue operation of geothermal plants, if the reservoir fails to produce as expected. In such an event, the utility could experience capital losses associated with the plant as well as loss of generating capacity required to meet public need. The inherent nature of this type of arrangement suggests that the utility seek assurances that the reservoir will sustain production of fluids with consistent purity and energy content for the life of the power plant prior to commitment of funds to construct a plant.

Assurances of reservoir production may conceivably be obtained in two ways. The first would be for the resource company to assume all of the risk by guaranteeing the flow of energy, and indemnification against capital loss and loss of generating capacity. This could be achieved only by guaranteeing alternate fuels that could be used at other plants to make up any lost capacity, should the reservoir fail. However, such a complete guarantee is not likely. A more probable approach would be for the utility to share some of the risk, in which case it would want to participate in reservoir assessment either directly or through qualified consultants. In either case, the utility would have a need to be conversant with the technical disciplines of reservoir assessment, as they reflect reservoir reliability and longevity, fluid purity, long-term temperature stability, production capacity and the capacity of the reservoir formation to accept injected supersaturated brines. For the foregoing reasons and EPRI's emphasis on acceleration of geothermal development, EPRI has an interest in advancing the art of reservoir assessment and reservoir engineering.

Scope of EPRI's Current Effort

Several of the projects in the current EPRI geothermal program are loosely related to reservoir assessment. Only one is directly related. The brine chemistry project is intended to improve the capability to analyze the performance of brine systems as a function of the chemical and thermal properties of geothermal brines and the thermodynamics, hydrodynamics and chemical kinetics of the brine processing system. Although the project is oriented toward power plant analysis, the analytical techniques are expected to be useful in assessing the economic value of different geothermal brines for electric power generation. Two heat exchanger tests at Heber, one completed last year and a second almost complete, were conducted to develop data on heat exchanger performance as an aid in developing design criteria for commercial size heat exchangers. Here again the results should be useful in making first order approximations of the economic worth of brines, particularly brines similar to those found at Heber. In our

feasibility study for the 50 MWe low salinity hydrothermal demonstration plant project, a significant portion of the effort was devoted to reservoir analysis. The mobile laboratory project is intended to increase and improve the information base on geothermal brine properties and their economic potential through standardized field testing.

Reservoir Assessment Guideline Manual

This project is more directly related to reservoir assessment. Its purpose is to develop a guideline manual on reservoir assessment primarily for use by utilities; however, the intent is to include sufficient information to make it useful to practicing reservoir engineers as well. The objective of the effort is not necessarily to advance the state-of-the-art, but to consolidate the existing body of information into a central source. The need for the manual stems from the fact that many techniques presently used to assess geothermal reservoir potential are not well documented in the open literature and have not been standardized by the industry.

For the purpose of this effort, reservoir assessment is viewed as that spectrum of activities and technical displines that, when combined into a logical sequence, are expected to lead to optimum choices regarding: (1) where to search for geothermal energy; (2) where to locate exploratory wells; and (3) assessment of the commercial potential of reservoirs. The relative role of reservoir assessment in the electric power development cycle is illustrated in Figure 1.

Since some assessment techniques are new and others are expected to emerge from current research, standardization of techniques is probably premature: however, the absence of standardization makes it difficult to compare results obtained by one group with those obtained by another, and a common reference may be useful in this context. Some standardization would be beneficial to the power generating industry in that it could serve to remove some of the ambiguities that arise from different sets of assumptions, different computational procedures, and sometimes different standards of measurement, test and data interpretation. It could increase the level of confidence placed on projections of reservoir power potential and lower the perceived risk of investment in geothermal power plants.

The approach is to include the following sections or chapters in the manual:

Geothermal Reservoir Assessment Philosophy and Rationale
Prospecting
Exploration
Reservoir Development
Production Facilities

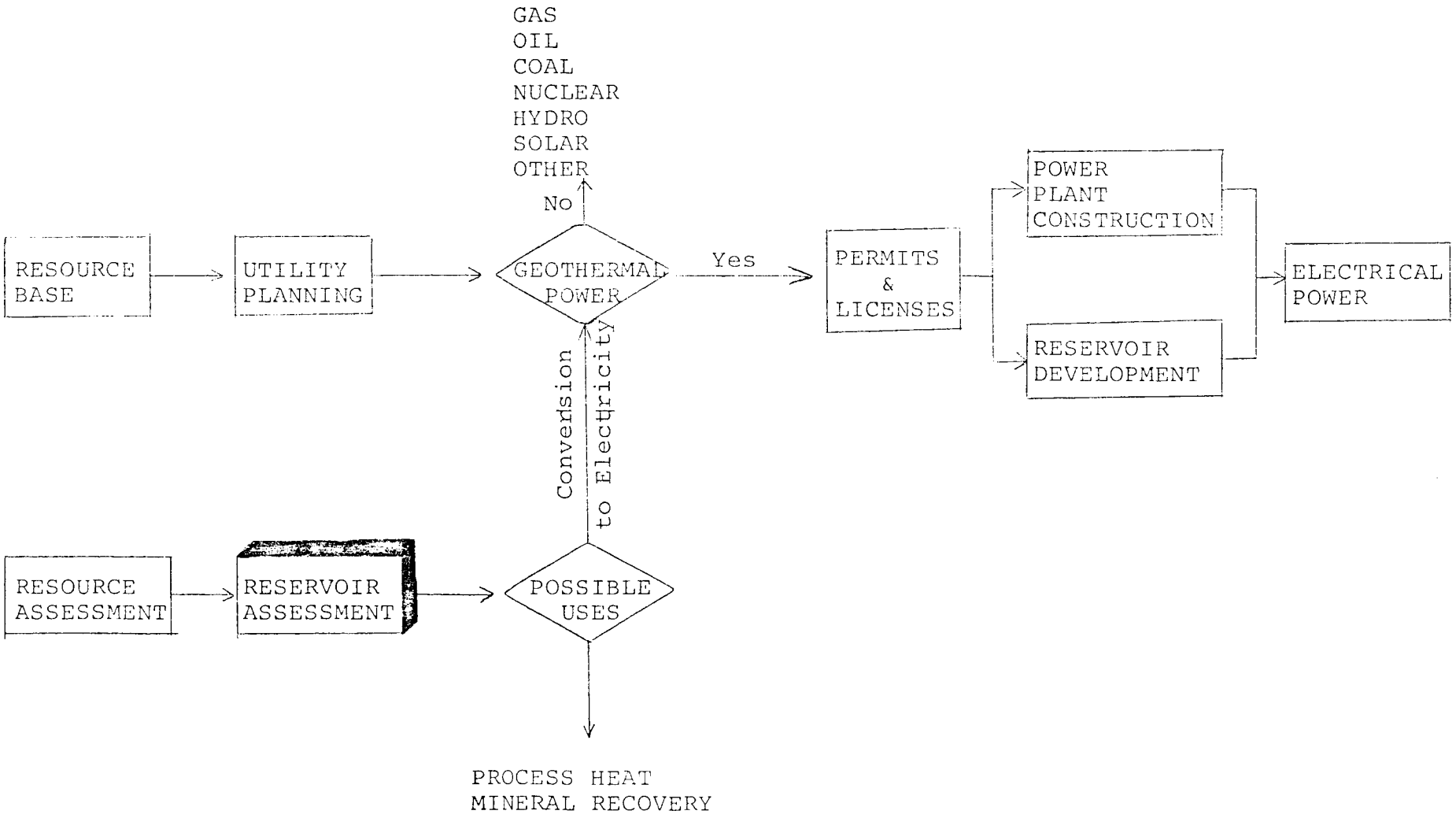

FIGURE 1. GEOTHERMAL ELECTRIC POWER DEVELOPMENT CYCLE

Production Test
Reservoir Management
Case Studies

The major emphasis will be on:

Geophysical Data Analysis
Geochemical Data Analysis
Well Log and Core Analysis
Well Test Data Analysis
Reservoir Performance Prediction
Well Bore Engineering

The text will contain concise descriptions of scientific principles and calculation procedures. Each calculation step will be illustrated by practical examples. The number of calculations required of the user will be minimized by making use of parametric charts covering the range of expected values. The charts will be developed using dimensionless variables so that a relatively small number of charts can be used for a large range or reservoir conditions. Direct readings from tables, charts, and nomograms, supplemented by a few calculations on a small calculator, should be sufficient for rough assessments. The manual will include conversion tables, tables of relevant mathematical functions, and a selected bibliography.

Gross Heat and Fluid Reserves: Common geophysical exploration techniques will be described. Examples of simplified, approximate techniques of deriving useful reservoir information from geophysical data will be included. Some examples include areal extent of the reservoir, subsurface geological structure, depth to the geological basement, presence of faults, fault activity and, in some cases, the reservoir temperature and salinity of the water. Inferences about locations of active faults can indicate the seismic risks. The techniques of estimating reservoir temperature from chemical analysis of water will be discussed. A brief account will be given of the principles of assessment of corrosion, scaling, and environmental pollution potential from chemical analysis of the water.

Recoverable Energy: Acquisition of qualitative and quantitative information on reservoir thickness, rock type, pay zones, porosity, permeability, water quality and temperature, will be discussed. Common well logs will also be discussed.

Flow Rates, Well Stimulation Pumping: Techniques of deriving important reservoir information from well tests will be reviewed. The information that can be derived from such tests include reservoir pressure, well productivity, reservoir boundaries, continuity and interconnection of various producing layers, expected flow rates, the need for well stimulation and pumping requirements.

Temperature Performance: Simplified techniques for predicting pressure, temperature, and flow behavior of a reservoir for at least 30 years will be discussed. Temperature decline will dictate increased production with corresponding escalation of operational costs. Temperature performance of a reservoir is almost as important as the heat reserve. Techniques for estimating temperature, pressure, density, and quality (proportions of steam and water) of the fluid as it flows up the well bore will also be presented in the manual.

The first issue of the Reservoir Assessment Manual is planned for completion by the end of this year.

Conclusion

Modest progress has been made in the definition of hydrothermal resources and development of the geothermal information base. The reluctance to build hydrothermal power plants thus far is a function of many factors but one important factor is the need for more complete and more accurate reservoir assessments for hydrothermal fields. EPRI's geothermal program has a small effort in reservoir assessment at this time, but a strong interest in advancing the art, and hopes to be in a position to expand the effort in the future.

STEAM ZONE TEMPERATURE GRADIENTS AT THE GEYSERS

J. R. Hite and E. L. Fehlberg
Shell Oil Co.
P. O. Box 831
Houston, Texas 77001

Temperature logs, which have been run routinely in The Geysers geothermal wells, have been used to indicate the depth corresponding to the top of the steam zone (1). This steam chest is marked by temperatures which exceed 400°F and by a sharp change in temperature gradient. Above the steam chest heat transfer is largely by conduction, so that the gradient depends on heat flux and thermal conductivity. Within the steam chest, which is highly fractured, heat is transferred via the vertical fractures by convective reflux as well. This being a much more effective mechanism, the temperatures are more nearly isothermal (2). The existence of this abrupt gradient change has been confirmed directly in U.S. Geothermal C-4 and C-5, where the temperature was logged from the surface into the upper unproductive portion of the steam chest.

This report describes a model of the heat transfer within the steam chest. By comparing the model with temperature gradient data from a well, one can estimate the average vertical permeability within the reflux system.

Vertical Heat Transfer Mechanisms

The model is based principally on the description of the reservoir by Truesdell and White (2). They argue that the steam chest is a highly fractured rock system. Flow conductivity is due largely (or solely) to the fractures. The effective vertical permeability of the matrix rock is unknown as yet, but is probably quite small. Fluid storage is known to be relatively large, although its distribution with depth remains a matter of some controversy. It could be either in rock matrix porosity or in a bottom water zone at some unknown depth (15,000 ft?) or both. To yield the anticipated reserves at The Geysers, the fluid storage must be equivalent to a porosity of 6% over a depth of 5000 ft. on 40-acre spacing. The top of the steam chest is presumed to be an unfractured rock seal. (The seal is probably at least partially broken in the Old Geysers Area.)

To model the temperature gradient within the steam chest the equations of continuity were solved for a combination of steam reflux within the fractures and thermal conduction through the rock matrix. Steady state conditions were assumed and horizontal gradients were neglected. Rock and fracture properties were constant with depth. Flow in the fractures (vapor phase up, liquid phase down) was modeled using Darcy's Law, assuming straight line relative permeabilities for each phase ($k_{rp} = S_p$). This would be correct for laminar flow in fracture geometries equivalent to narrow slits. At the top of the steam chest it was assumed that the net mass flux was zero and that the heat flux was equal to $-k^T \left.\frac{dT}{dz}\right|_o$ where k^T is the thermal conductivity and $\left.\frac{dT}{dz}\right|_o$ is the temperature gradient

just above the steam chest. The resulting equations the predict temperature and pressure versus depth as a function of 1) steam properties, 2) the assumed pressure at the top of the steam chest, P_o, 3) the ratio of thermal conductivity k^T, to the average vertical permeability in the reflux system, k_v, and 4) the product of this ratio and the gradient $\left.\frac{dT}{dz}\right|_o$.

U.S. Geothermal C-4 and C-5 Temperature Gradients

The temperature vs. depth curves shown in Fig. 1 were derived from Horner-type buildup analyses as suggested by Dowdle and Cobb [3]. Two separate log runs were made in each well, one at the 13-3/8" casing point and one at the 9-5/8" casing point. Each run consisted of several traverses over depth and a build-up at TD. The surveys did not include the productive part of the steam zone.

The data show a sharp gradient change approximately corresponding to the top of the steam reflux zone. Below that depth the gradient is greatly reduced, although still significantly greater than that which would result from a static steam phase.

Results

The calculated temperature gradients are compared to the well data in Fig. 2 for several assumed values of k_v. The assumed values for the other parameters are:

C-4	C-5
$\left.\frac{dT}{dz}\right\|_o$ = 12.2° F/100 ft (222°C/km)	$\left.\frac{dT}{dz}\right\|_o$ = 11.3°F/100 ft (206°C/km)
k^T = 29.0 Btu/day-ft-°F (.005 cal/sec-cm-°C)	k^T = Same as C-4
P_o = 425 psia (29.32 bars)	P_o = 316 psia (21.77 bars)
T_o = 450.6°F (232.6°C)	T_o = 422.0°F (216.7°C)

The pressure, P_o, is the saturation pressure corresponding to the measured temperature, T_o, at the top of the steam chest. The best match of computed and actual gradients corresponds to k_v = 0.5 md for C-4 and k_v = 0.2 md for C-5. The accuracy of this result is affected by the accuracy of the temperature measurements as well as by the many assumptions in the model. A study of the sensitivity of k_v to the other parameters shows that it is roughly proportional to the assumed values of k^T and $\left.\frac{dT}{dz}\right|_o$.

These results were obtained using data from the unproductive part of the steam chest. As a result the calculated permeability values are much less than would be expected from a productive interval.

The model can also be used to extrapolate pressure and temperature to greater depths whenever the temperature gradient at those depths can be reliably predicted.

Conclusions

The model suggests that the average vertical permeability at The Geysers is less than 1 md in the upper unproductive portion of the steam chest.

Temperature data taken from this portion of the steam chest indicate that the reservoir is considerably less isothermal than previously assumed. The dynamic effects of the reflux system should be included in any study of transient well behavior or in any estimate of deliverable reserves.

References

(1). Fehlberg, E. L. (1975), "Shell's activity in The Geysers Area," presented at the Stanford Geothermal Workshop, Stanford University, December 15-17.

(2). Truesdell, A. M., and White, D. E. (1973), "Production of superheated steam from vapor-dominated geothermal reservoirs," Geothermics, Vol. 2, p. 154.

(3). Dowdle, W. L., and Cobb, W. M. (1974), "Estimation of static formation temperature from well logs," SPE Preprint SPE 5036.

FIGURE 1
ESTIMATED STATIC TEMPERATURE GRADIENTS

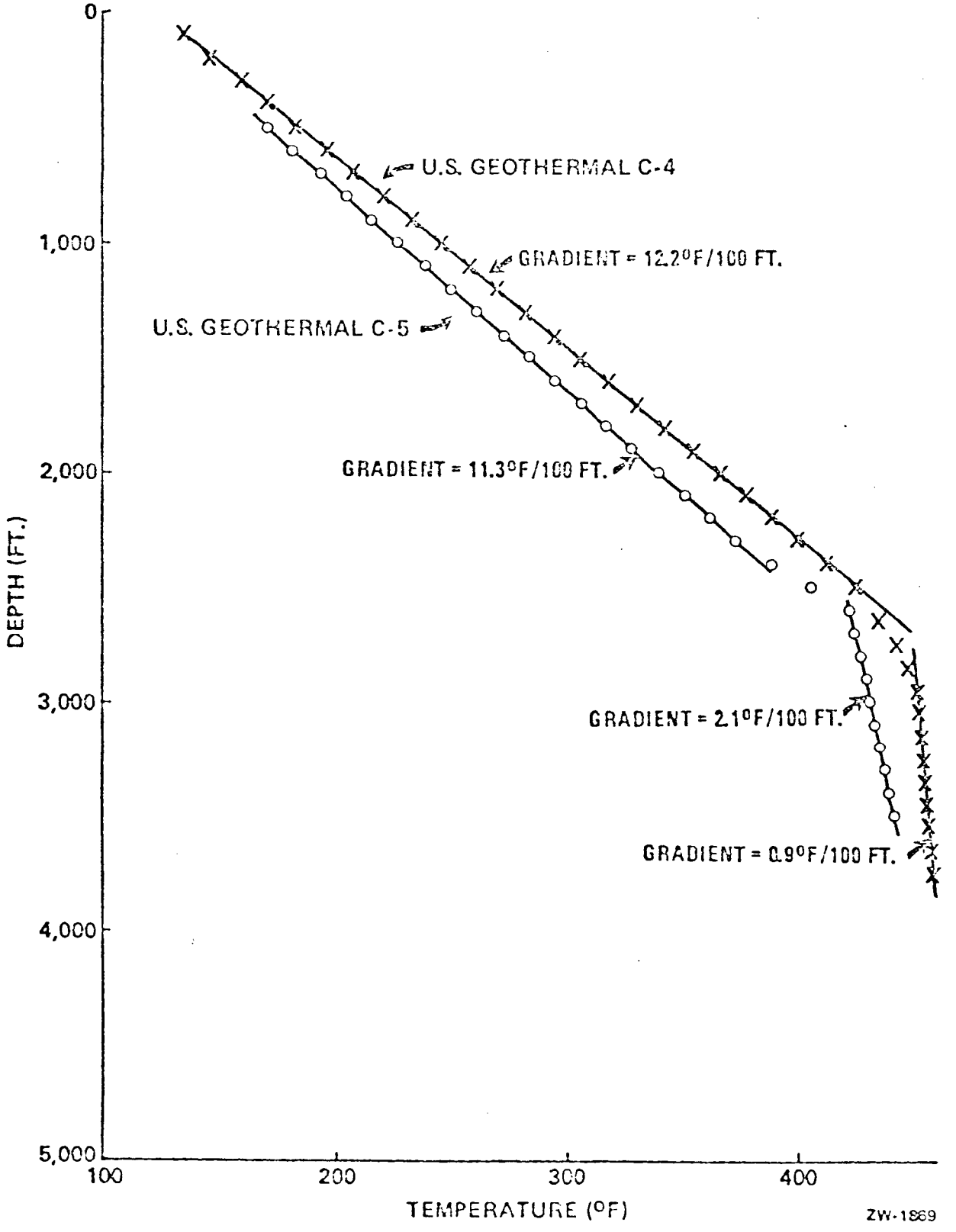

FIGURE 2
TEMPERATURE GRADIENTS
IN STEAM REFLUX ZONE

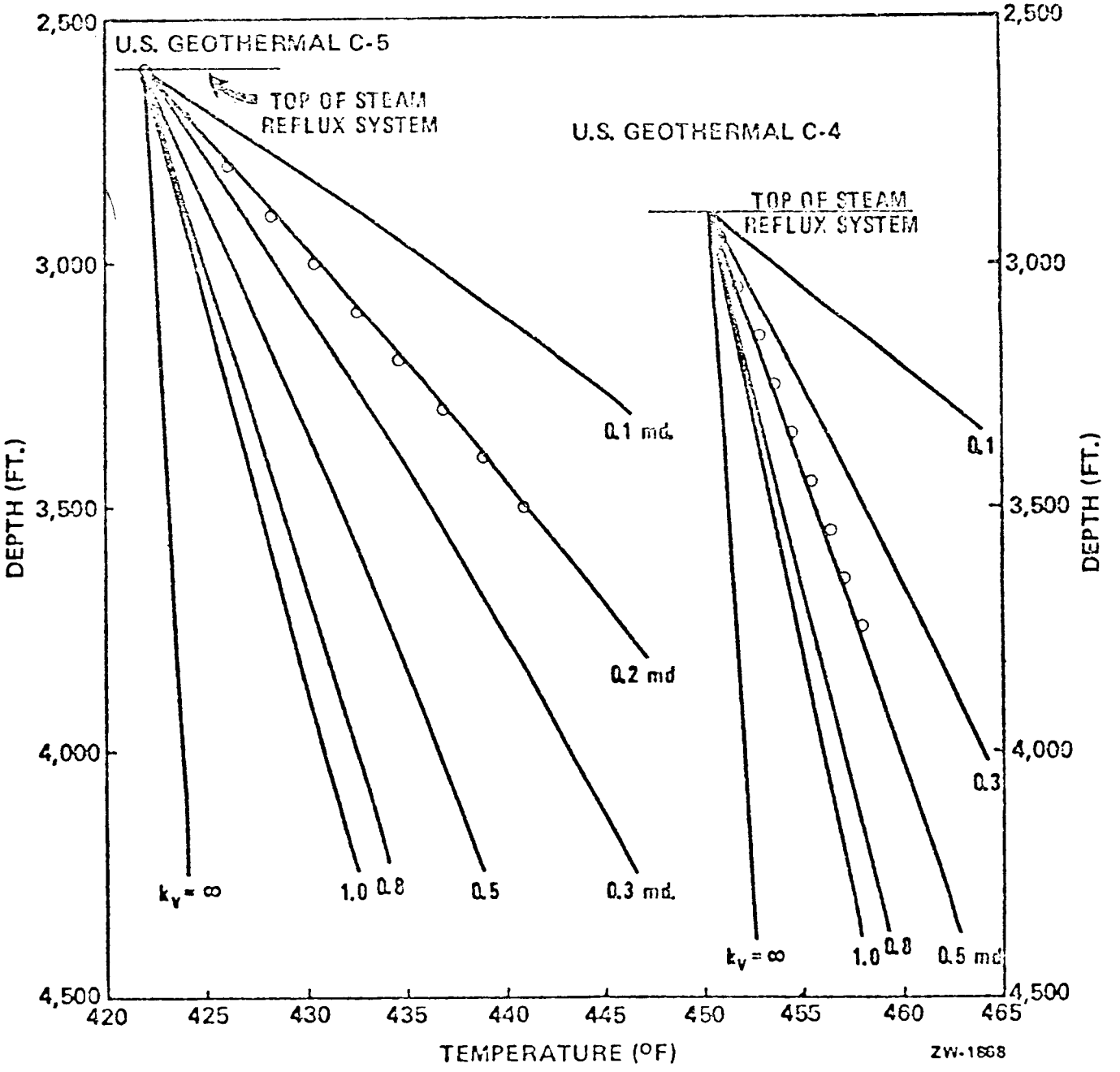

WATER INFLUX IN A STEAM PRODUCING WELL

R. Celati*, V. Cillerai**, R. Marconcini** and G. Neri**

Castelnuovo area, in Larderello geothermal field, was exploited intensively over a period of more than 35 years, with productive wells that are generally 300-500 m deep. As a consequence of this exploitation the formation pressure in the upper part of the reservoir decreased below 4 ata. A few deeper wells, to∿800 m depth, have shown shut-in pressures in the 6 - 10 ata range during these last few years.

In 1974 a deep well, Sperimentale 2, was drilled in this area in order to test steam production possibilities from deep horizons of the reservoir where sufficiently high pressures were still expected to be found. Having reached a depth of 1266 m (Fig. 1) the hole was cased from the surface to 829 m in order to isolate the shallower formations. A circulation loss occurred at 834 m, which represented the only fracture identified during drilling in the open-hole section of the well. No other eventual fractures were noted at greater depths as drilling continued without a fluid return.

The stratigraphic reconstruction of the well is given in Fig. 1.

The stratigraphic and tectonic study of Larderello region shows that the tectonic contacts crossed by this well are connected to regional-type overthrust planes (1).

These overthrusts generally correspond to the most fractured zones of the reservoir.

The well blew out on January 3, 1975. After a short period of steam and liquid water production a first measurement gave:

flow-rate - 26 t/h, no liquid water;
wellhead temperature - 175°C;
wellhead pressure - 7.9 ata.

---

*Istituto Internazionale Ricerche Geotermiche, CNR, Pisa, Italy.

**Gruppo Minerario Larderello, ENEL, Larderello, Italy.

In the period from May to October 1975, superheating of the steam increased and wellhead temperature reached 204°C at a delivery pressure of 5 ata. In October the temperature decreased to saturation point and wet steam production began.

A well-testing program was set up to study the phenomenon of two-phase production and to assess well performance. A separation plant was installed and separate measurements taken of the steam and liquid water produced at different back-pressures. The corresponding wellhead and bottom-hole back-pressure curves are shown in Fig. 2.

The pressures plotted in the bottom-hole curve were measured at 1000 m depth because, as will be made clear later, below this depth the hole was, on several occasions, filled with liquid water.

A nearly constant flow-rate of liquid water ($\sim$2 m^3/h) was produced, along with the steam at wellhead pressures below about 9 ata, whereas dry steam only was produced at wellhead pressure above 10 ata.

At a wellhead pressure of about 10 ata the flow regime corresponding to the upper part of the well-head curve became unstable and a slight increase in wellhead pressure was sufficient to cause a sudden drop in flow-rate.

While liquid water was produced with the steam in the upper part, dry steam only reached the wellhead in the lower part. In the latter case large pressure differences were observed between wellhead and bottom-hole. Pressure and temperature logs were also run along the borehole during the back-pressure test.

Fig. 3 shows these logs in flow conditions of point 3, Fig. 2.

The fluid inside the hole is shown to be saturated above 834 m, where the first fracture was found. The pressure drop in this section of the hole is greater than that occurring in the flow of steam only and can probably be attributed to the presence of a two-phase mixture.

The pressure and temperature measured between 834 and 1150 m indicate the existence of superheated steam. The pressure in the final section of the hole is clearly indicative of a liquid phase which, within the limits of error in measurement, seems to be in boiling conditions. Liquid temperature, therefore, is controlled by the pressure and the lowest value is found at the liquid-steam interface (1150 m).

Borehole conditions at point 5 in Figure 2 are represented in Fig. 7. The well was shut-in for an eight-day period. Steam filled the borehole down to a depth of 1130 m below which it was filled with liquid water.

There is no water at the bottom of the hole in the conditions shown in Fig. 8. The measurements were taken during a pressure build-up 24 hours after shut-in.

The liquid observed on some occasions in the final section of the hole is probably due to a complete lack of permeability below 1130 m. The presence of the water depends on several factors, including pressure, temperature and radial temperature gradient at the well sides, the time elapsed with the well in particular flow or shut-in conditions, past history etc.

The low permeability between 1130 and 1000 m probably caused the water-level to rise when the water "rained" on bottom-hole.

In conclusion the following interpretation seems valid in light of the above facts.

1. Two-phase production derives from the mixing of fluids entering the borehole at different depths. Fractures below 834 m produce superheated steam, whereas liquid water or a water-steam mixture enters the borehole near the top of the open-hole section of the well.

   It is possible that the water eventually mixed with the steam came from the fracture at 834 m depth. In this case the water carried after a few months of superheated steam production could be tied to the drop in pressure and change in flow patterns in the zone around the borehole consequent to production.

   Another possibility is that water enters the well from the bottom of the casing due to a failure in casing cementing after a work period in high temperatures.

   It is well-known that the shallower permeable geological formations (mainly the sandstone outcropping over a wide area very near the field) carry the meteoric waters into the field (2). We can thus assume that the water came from the sandstone and reached the borehole by seeping down along the casing.

2. There are probably several fractures at different depths in the open-hole section of the well. The fluid in these fractures has probably different pressures and no separate

From the temperature and pressure distribution it can be deduced that the water enters the hole near the fracture at 834 m depth and, in these flow conditions, all the water is carried upwards along with the steam.

Between 834 and 1000 m there would seem to be some fractures that produce superheated steam; between 1000 m and the steam-liquid interface, on the other hand, the temperature is probably controlled by the weak steam flow produced by the boiling liquid.

Figure 4 gives the temperature and pressure distribution inside the hole at point 2 of Figure 2.

The temperature log is incomplete as no measurements were taken in the section of the borehole characterized by the two-phase mixture.

In this case superheated steam exists from 834 m down to bottom-hole and the trend taken by the still unstabilized temperature distribution is still affected by the distribution resulting previously from the boiling of the liquid. The temperature and pressure distribution in the hole in flow conditions of point 4, Fig. 2, is given in Fig. 5.

The pressure loss in the cased section of the borehole increased even though the flowrate decreased. The steam at wellhead is slightly superheated, whereas it is saturated in the uncased section above the water-level. The water-level rose to about 1030 m.

The pressure distribution in the borehole is given in greater detail in Fig. 6, which represents a pressure log run one day after that shown in Fig. 5. The low pressure gradient from about 400 m to the surface indicates a steam flow separated from the liquid. The steam velocity is so reduced as to be incapable of carrying the liquid to wellhead.

The 830-1030 m section is now also affected by the two-phase flow: the water entering the borehole in the zone between the bottom of the casing and the first fracture is partly held up by the rising steam and partly falls to bottom-hole, so causing the water-level to rise. The high pressure gradient between 834 and 900 m may indicate that most of the steam produced originates in this section.

The temperature distribution in Fig. 3, on the other hand, would appear to be evidence of a very low steam supply from the formation below 1000 m.

The temperature distribution near bottom-hole in Fig. 5 is probably still affected by a previous flow regime with the water-level at 1130 m.

pressure measurements for them are available. From some build-up tests run on the well, a final shut-in pressure of about 20 ata may be inferred.

This pressure is certainly affected, to an unknown degree, by fluid flow inside the borehole from one fracture to another. However, there is obviously a considerable vertical component of pressure gradient in the zone, due to the long and intensive exploitation by relatively shallow wells.

3) Several problems still remain unsolved as regards the contribution to production from the different depth intervals in the open-hole section. A flow-meter log, which is now in project, will provide some useful information in this regard.

References

(1) M. Puxeddu, P. Squarci, A. Rau, M. Tongiorgi, P. D. Burgassi, "Stratigraphic and Tectonic Study of Larderello-Travale Basement Rocks and its Geothermal Implications," International Congress on Thermal Waters, Geothermal Energy and Volcanism of the Mediterranean Area, Athens, 1976.

(2) R. Celati, P. Noto, C. Panichi, P. Squarci, L. Taffi, "Interactions Between the Steam Reservoir and Surrounding Aquifers in Larderello Geothermal Field," Geothermics, V. 2, Nos. 3-4, 1973.

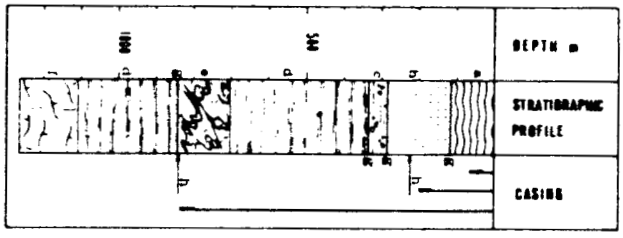

Fig. 1 - Stratigraphic profile of Sperimentale 2 well (1).

a - flysch: shales, marls, marly limestones (U. Jurassic-Eocene)

b - sandstone "macigno" (Oligocene)

c - brecciated magnesian limestones and anhydrites (U. Trias)

d - Triassic quartzites and phyllites

e - Paleozoic quartzites and phyllites

f - marbles and magnesian limestones (of unknown age)

g - tectonic contacts

h - circulation losses

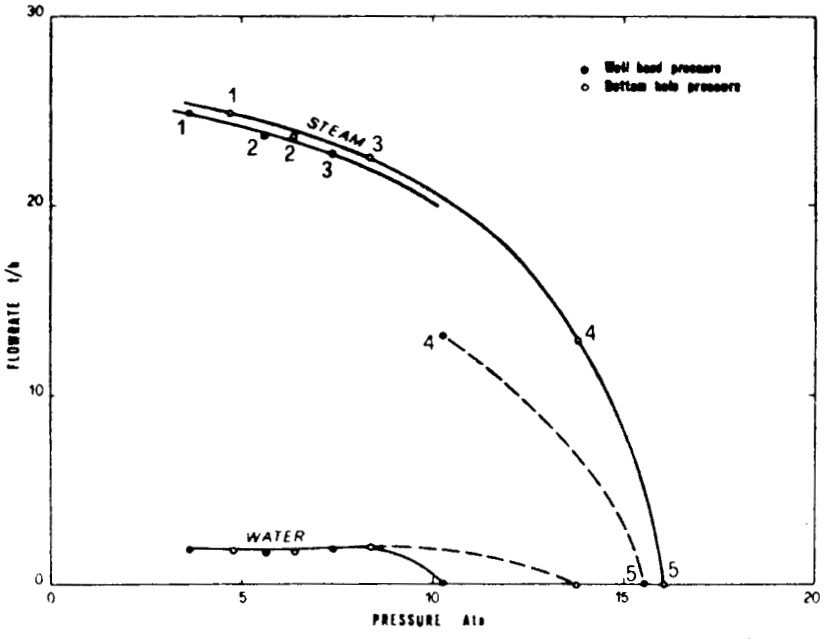

Fig. 2 - Back-pressure curves of Sperimentale 2 well.

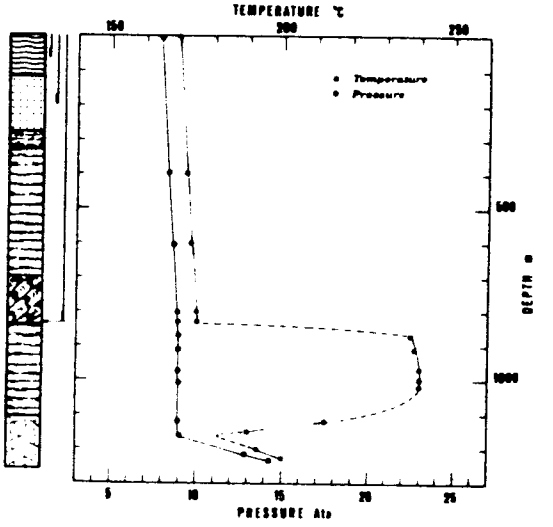

Fig. 3 - Pressure and temperature logs in flowing conditions of point 3 in Fig. 2.

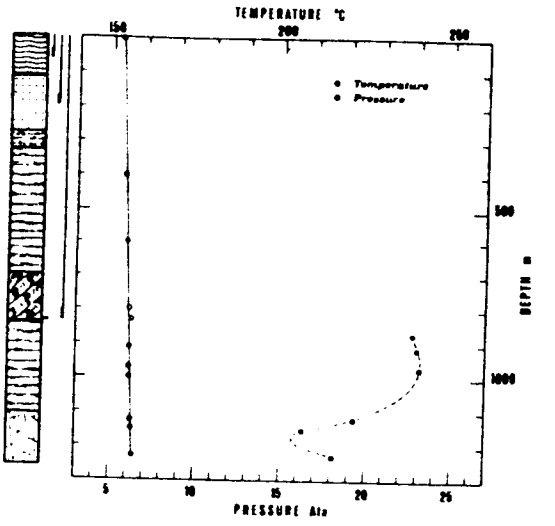

Fig. 4 - Pressure and temperature logs in flowing conditions of point 2 in Fig. 2.

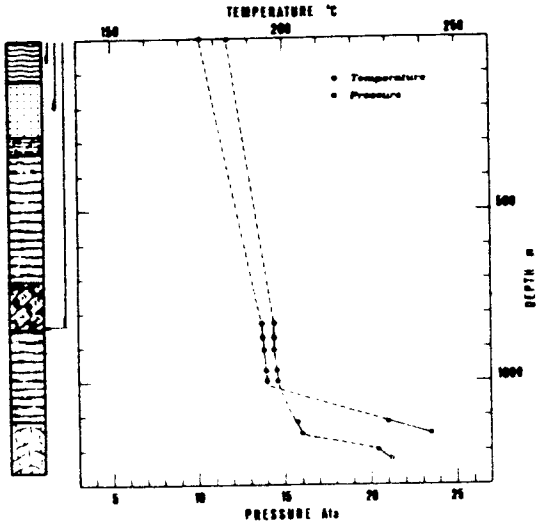

Fig. 5 - Pressure and temperature logs in flowing conditions of point 4 in Fig. 2.

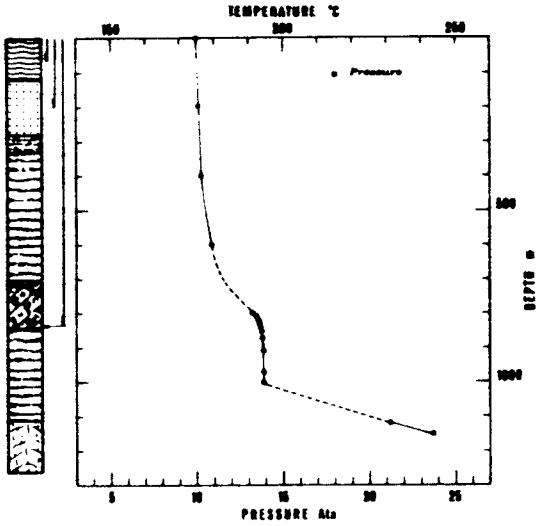

Fig. 6 - Pressure log in flowing conditions of point 4 in Fig. 2.

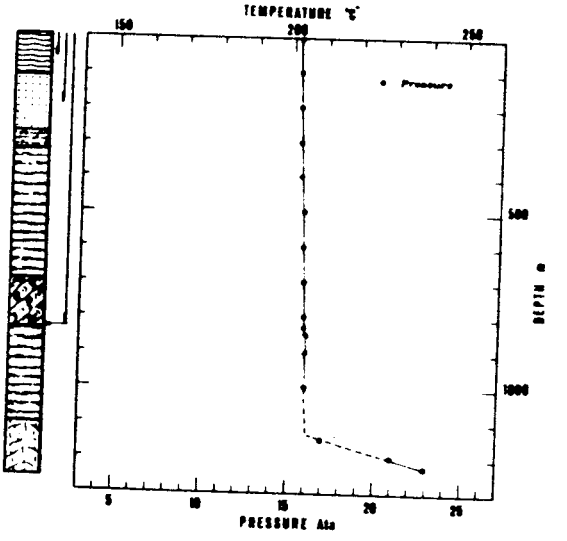

Fig. 7 - Pressure log in conditions of point 5 in Fig. 2.

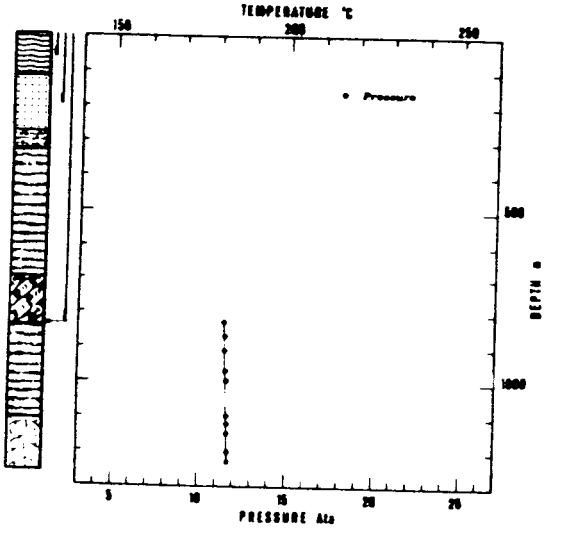

Fig. 8 - Pressure log 24 hours after well shut-in.

INVESTIGATION OF A FLUID BOUNDARY

George A. Frye
Aminoil USA, Inc.
P.O. Box 11279
Santa Rosa, CA 95406

Aminoil is a subsidiary of R. J. Reynolds Industries, Inc., and successor to Burmah Oil and Gas Company. Our drilling activities in the southeast part of The Geysers area have proved geothermal steam reserves to power 300 megawatts of electric generating capacity. In the past year Aminoil has conducted exploratory drilling activities outside of the proven productive area in order to establish additional reserves. One of these areas is discussed in the paper.

The area of investigation is characterized by the intersection of at least three regional lineaments. These lineaments are discernible from satellite imagery of the NASA LANDSAT (formerly ERTS) program. The lineaments are confirmed by medium to low altitude color stereo pair photographs. On the surface these lineaments sometimes lack enough discernible ground displacement to be characterized as faults. These lineaments do coincide with cliffs, truncated ridges, major creeks and stream offsets. Figure 1 indicates the location of these lineaments by long, dashed lines.

Shown also on Figure 1 by smooth, continuous lines are isopleths of heat flow gradients. They were obtained from Aminoil's extensive shallow (300 to 1000 feet) hole drilling in the area. The intersection of the lineaments also coincides with closely spaced isopleths. Heat flow gradients, while a good indication of geothermal resources at depth, do not always assure commercially productive wells.

Locations A through E indicate holes drilled to at least 7200 feet on Figure 1. Locations B and C are commercially productive steam wells. Even though Locations A and E are located in areas of higher heat flow than C, only minor steam entries were encountered at depths from 6000 to 8000 feet. A minor steam entry was also encountered in Location D.

The rocks of the steam-producing zones of Aminoil's proven areas are predominately silicified metagraywackes and lesser varying proportions of greenstone, chert, serpentine and argillite and may be more accurately described as a melange unit of the Franciscan formation. Locations B and C fit this description. Comparison of the productive sections with those encountered in Locations A, D, and E show the sections of the two areas to be quite different. The last three holes all drilled thick sections of arguillite with minor metagraywacke.

These three holes never drilled out of this sequence. The entire sequences in these three holes are also characterized by their general lack of silica. Silica is common in the majority of Aminoil's producing wells. A few of these deeper wells may have penetrated an argillite section below

productive metagraywacke and show minor or no production from those zones. Argillites did occur in the steam zone of one well but were associated with up to 60% silica.

Of particular interest is Location E. A water entry encountered at approximately 5100 feet was analyzed and is shown on Fig. 2. A sample was collected while air drilling and this analysis shows the water to be considerably more saline with less hardness than the water entries reported at the 1975 Stanford Geothermal Reservoir Engineering Workshop. Additional drilling encountered a minor steam entry below 7500 feet. The hole is now suspended and surface wellhead pressure is approximately 50 psia. The steam to noncondensible gas molar ratio is about 50 or more than a tenfold decrease of Location B. Methane and nitrogen account for most of the increase of noncondensible gases. An analysis of the steam condensate is shown on Fig. 2. The sulfide content, over twice Aminoil's field average, is consistent with the overall increased amount of noncondensible gases.

Fifteen days after the drilling rig was released at Location E, a static temperature and pressure survey was conducted. Saturated steam was recorded to a 7070 foot fluid level. Below this fluid level the liquid continually increased in enthalpy with increasing depth. A maximum temperature of 464^{o}F was recorded at total depth.

The phenomena discussed above led to the tentative conclusion that there is a fluid boundary with Locations B and C on the productive side and A, D, and E, all nonproductive. Aminoil believes the change in rock types to be significant. The change may be attributed to the lineaments although structural correlations in the Franciscan formation are difficult to substantiate. Even though there were minor steam entries in the nonproductive holes, the heat gradient surveys indicates a rapidly decreasing heat flux from the productive area. Changes in gas to steam molar ratio and the increased hydrogen sulfide at Location E may be attributable to the small volume of the steam entry with relation to the open hole surface area. However, the increased percentage of methane supports a fluid boundary conclusion. Further examination of the water in the hole at Location E is planned using a bottom hole sampler. These analyses will be designed to test for thermodynamic phase equilibrium of the fluid with known equilibria phenomena of the productive area.

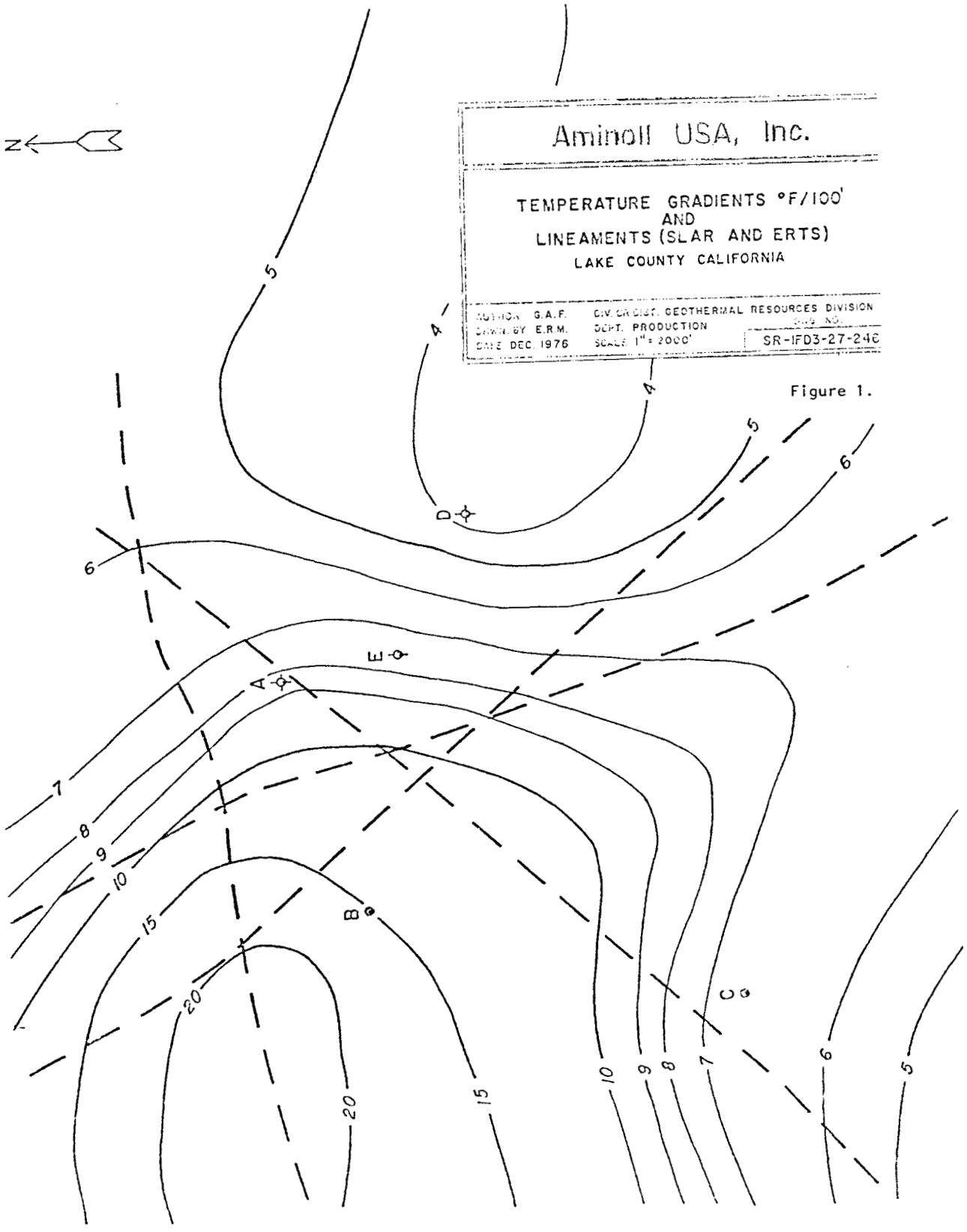
N
Aminoil USA, Inc.
TEMPERATURE GRADIENTS °F/100'
AND
LINEAMENTS (SLAR AND ERTS)
LAKE COUNTY CALIFORNIA
AUTHOR G.A.F.
DRAWN BY E.R.M.
DATE DEC. 1976
DIV. OR DIST. GEOTHERMAL RESOURCES DIVISION
DEPT. PRODUCTION
SCALE 1" = 2000'
SR-IFD3-27-246
A
B
C
D
E
4
5
6
7
8
9
10
15
20

Figure 1.

CHEMICAL ANALYSES, LOCATION E

	Water Entry	Condensate
pH	9.0	6.1
Specific Conductance μmhos/cm @ 25° C	2250	400
Calcium, mg/l	< 1.0	< .4
Magnesium, mg/l	< 1.0	< .2
Sodium, mg/l	530	0.6
Potassium, mg/l	55	0.05
Sulfate, mg/l	65	< 0.5
Chloride, mg/l	480	1.5
Boron, mg/l	66	.06
Fluoride, mg/l	5.2	< .01
Aluminum, mg/l	< 0.1	-
Mercury, μg/l	< 0.002	.0
Silica, mg/l	205	1.3
Sulfide, mg/l	-	210
Ammonia	1.5	35
Bicarbonate	-	240

Figure 2. Chemical Analyses, Location E

EFFECTS OF HYDROTHERMAL CHEMISTRY ON RESERVOIR EVOLUTION

Charles G. Sammis, Todd M. C. Li, and William F. Downs
Department of Geosciences
Pennsylvania State University
University Park, PA 16802

Although the corrosion and scaling problems associated with handling geothermal fluids are well known, the effects of hydrothermal reactions are often overlooked in geothermal reservoir modeling. Water-rock chemistry can be expected to affect the evolution of a reservoir in at least three ways: (a) the heats of reaction may contribute directly to the energy production, (b) the viscosity and thermodynamic properties of water are affected by the dissolved solids--this is especially important in two-phase regimes, and (c) the porosity and permeability change with time due to dissolving and precipitation as well as due to the volume change associated with alteration.

Chemical Energy

Table 1 summarizes the important hydrothermal reactions in a granitic source rock together with the heats of reaction and associated volume changes. Note that the available chemical energy is comparable to the thermal energy while the associated volume changes are an order of magnitude larger than those due to thermal contraction.

Table 1

IMPORTANT REACTIONS IN GRANITIC ROCK
(CHEMICAL REACTIONS TAKEN FROM HELGESON, 1969)

PROCESS	Heat released per mole of initial min. ΔH(kcal/mole)	Heat released per 100g of initial min. ΔH(kcal/100g)	Solid volume change per 100g of initial min. ΔV_s(cm^3/100g)
HYDROTHERMAL ALTERATION			
$2NaAlSi_3O_8(s)+2H^+ + H_2O \longrightarrow Al_2Si_2O_5(OH)_4(s)+4SiO_2(s)+2Na^+$ (Low Albite → Kaolinite + α-quartz)	11.21	4.27	-1.882
$3KAlSi_3O(s)+2H^+ \longrightarrow KAl_3Si_3O_{10}(OH)_2(s)+6SiO_2(s)+2K^+$ (Microcline → muscovite + α-quartz)	2.95	1.063	-5.907
DISSOLVING AND PRECIPITATION			
$SiO_2(s) + 2H_2O \longrightarrow H_4SiO_4(aq)$ (α-quartz)	-6.22	-10.352	-37.760
COOLING			
GRANITIC ROCK (300°C) → GRANITIC ROCK (65°C) (ρ_R = 2.65 g/cm^3, C_R = 0.25 cal/g°C, β_R = 2.5 x 10^{-5}/°C)	-	5.875	-0.2217

Although significant chemical energy exists, it cannot always be extracted. One of the first questions we addressed (Morris, 1975; Morris and Sammis, 1975) was the delineation of reservoir conditions under which one could expect to extract significant chemical heat. For the case of dissolving-precipitation reactions, a comparison of thermal energy with chemical energy leads to a simple relation between solubility and heat of reaction for a given ratio of chemical to thermal energy extracted. Because the rate of dissolving is controlled by the solubility at the outlet temperature, the resulting relation is independent of all crack and flow parameters. In the case of quartz, the solubility at 300°C is too low for chemical heat to make a contribution - thermal energy is extracted far faster than chemical energy under all flow conditions.

In the case of alteration reactions, however, the reaction rate is not limited by solubility and, depending on the alteration rate, significant chemical energy may be extracted. Morris (1975) has delineated the combinations of flow parameters, crack parameters, heats of reaction and alteration rates for which chemical energy associated with the alteration may be extracted. One of the objectives of our experimental program is to determine alteration rates in typical reservoir rocks, and thus assess the importance of such reactions to the total thermal regime.

Numerical Model for Single-phase Flow Including Porosity and Permeability Changes

The changes in porosity and permeability associated with both dissolving and alteration reactions are easily incorporated into the standard finite difference schemes commonly used in numerical reservoir modeling. The molality of each important solute may be treated as a dependent variable to be found together with the temperature and velocity fields. In addition to the standard three equations for the conservation of mass, momentum, and energy, an equation may be written for the conservation of each solute species. Such an equation directly incorporates permeability changes associated with dissolving and precipitation. It requires, as an additional constitutive relation, the experimentally determined rate equation. Permeability changes associated with alteration reactions may be written explicitly in terms of the temperature, flow velocity, crack parameters, water chemistry, and appropriate alteration rate equation. This larger system of equations may be combined and solved using exactly the same numerical scheme employed by Harlow and Pracht (1972). Using their notation (variables are defined in Table 2), the energy balance equation is

$$\frac{\partial}{\partial t}\{[b_R\rho_R(1-\theta) + b_w\rho_w\theta]T\} + \vec{\nabla}\cdot\rho_w b_w\theta\vec{u}T = \vec{\nabla}\cdot[K_R(1-\theta)\vec{\nabla}T] + \rho_w b_w T_s S \qquad (1)$$

and the mass and momentum balance equations may be written in the form

$$\frac{\partial\theta}{\partial t} - \vec{\nabla}\cdot\left\{\frac{k\rho_0}{\mu}[\vec{\nabla}\phi + \vec{g}\beta_w(T-\langle T\rangle)]\right\} = S \qquad (2)$$

$$\vec{u}\theta = \frac{-k\rho_0}{\mu}[\vec{\nabla}\phi + \vec{g}\beta_w(T-\langle T\rangle)] \qquad (3)$$

The equation of state of water

$$\rho_w = \rho_0[1-\beta_w(T-T_0)] \qquad (4)$$

and a porosity-permeability relation

$$k = \left(\frac{4d_c^2}{5}\right)\left[\frac{\theta^3}{(1-\theta)^2}\right] \tag{5}$$

are also required. It also is important to include the temperature dependence of the viscosity of water

$$\mu = \frac{0.279}{T(°C)-3.8} \quad \left(\frac{gm}{cm\ sec}\right) \tag{6}$$

If we only consider the dissolution and precipitation of SiO_2

$$SiO_2\ (S) + 2H_2O \rightleftharpoons H_4SiO_4 \tag{7}$$

we can write two more balance equations: the conservation of SiO_2 during the reaction,

$$\frac{\partial}{\partial t}[W_R\rho_R(1-\theta)] + \frac{\partial}{\partial t}\left[\frac{m_{H_4SiO_4}\bar{M}_{SiO_2}}{10^3}\rho_w\theta\right]_R = 0 \tag{8}$$

and the mass balance for SiO_2 in solution

$$\frac{\partial}{\partial t}\left[\frac{m_{H_4SiO_4}\bar{M}_{SiO_2}}{10^3}\rho_w\theta\right] = \frac{\partial}{\partial t}\left[\frac{m_{H_4SiO_4}\bar{M}_{SiO_2}}{10^3}\rho_w\theta\right]_R - \vec{\nabla}\cdot\left[\frac{m_{H_4SiO_4}\bar{M}_{SiO_2}}{10^3}\rho_w\theta\vec{u}\right] + \rho_w M_s S \tag{9}$$

The subscript R indicates that we only consider the part of the subscripted expression which is due to the reaction. The time rate of change of molality $[\partial m/\partial t]_R$ is given in terms of experimentally determined rate constants, k_+ (for the forward dissolution reaction) and k_- (for the reverse precipitation reaction) by the rate equation

$$\left(\frac{\partial a_{H_4SiO_4}}{\partial t}\right)_{P,T,M} = \frac{A}{\rho_w V}\{k_+ a_{SiO_2} a_{H_2O}^2 - k_- a_{H_4SiO_4}\} \tag{10}$$

If we assume a pure quartz-water system $a_{SiO_2}=a_{H_2O}=1$. The activity of H_4SiO_4 may be written in terms of the molality

$$a_{H_4SiO_4} = \frac{\gamma_{H_4SiO_4} m_{H_4SiO_4}}{\gamma^0_{H_4SiO_4} m^0_{H_4SiO_4}} \tag{11}$$

The reference state is chosen such that $\gamma^0=m^0=1$. If we also assume $\gamma_{H_4SiO_4}=1$ (true only for pure water) equation (10) may be written

$$\left[\left(\frac{\partial m_{H_4SiO_4}}{\partial t}\right)_{P,T,M}\right]_R = \frac{1}{\rho_w}\left(\frac{A}{V}\right)\left[k_+ - k_- m_{H_4SiO_4}\right] \tag{12}$$

In general we can write A/V=(Fracture Parameter)/θ where the fracture parameter can be readily found for simple assumed fracture geometries.

Following Harlow and Pracht (1972), these equations may be solved in the following sequential order: (a) the energy balance equation (1) (in finite difference form) is solved for T at the new time step using the values of θ, u, and T at the previous time step; (b) equations (8), (9), and (12) are used to find θ and m at the new time step; (c) equation (2) is solved for new values of ϕ; and (d) equation (3) is solved for new values of u. The procedure is then repeated for the next time step. We are currently working on such a solution procedure for simple reservoir configurations.

Kinetics of the Dissolution and Precipitation of SiO_2

In order to implement the above scheme, the rate constants k_+ and k_- must be known. These have been determined experimentally by measuring m as a function of time in the apparatus shown in Figure 1 (Barnes and Rimstidt, 1975)

$$k_+ = 2.03\ e^{-28.3/RT}\ \text{moles/cm}^2\text{sec}$$

$$k_- = 3.30\ e^{-22.5/RT}\ \text{moles/cm}^2\text{sec}$$

where the activation energies are in kcal/mole. The rate-constants are only weakly dependent on pressure and salinity of the solution. In the case of saline brines, the major effect on the kinetics of quartz dissolution is to lower a_{H_2O} in (10) (Lindsay and Liu, 1968) and slightly lower $\gamma_{H_4SiO_4}$ in (11).

References

Barnes, H.L., and J. D. Rimstidt, Control of Silica Scaling, in Geothermal Reservoir Engineering, ed. P. Kruger and H.J. Ramey, Jr., SGP-TR-12, Stanford University, 1975.

Harlow, F.H., and W.E. Pracht, A Theoretical Study of Geothermal Energy Extraction, J. Geophysical Research, 77, 7038-7048, 1972.

Helgeson, H.C., Thermodynamics of Hydrothermal Systems at Elevated Temperatures and Pressures, American Journal of Science, 267, 729-804, 1969.

Lindsay, W.T., Jr., and C.T. Liu, Vapor Pressure Lowering of Aqueous Solutions at Elevated Temperatures, U.S. Office of Saline Research and Development, Progress Report No. 347, 235 p., 1968.

Morris, J.R., A Preliminary Study of the Importance of Hydrothermal Reactions on the Temperature History of a Hot, Dry Rock Geothermal Reservoir, M.S. Thesis, Pennsylvania State University, 1975.

Morris, J.R., and C.G. Sammis, The Recovery of Chemical Energy from a Dry-Rock Geothermal Reservoir (abstr.), Trans. Am. Geophys. Union, 56, 1073, 1975.

Table 2 Summary of Notation

θ	porosity, open volume for water flow (per unit volume)
ρ_w	density of water, a function of temperature
ρ_R	density of rock
$\vec{u}$	water velocity
S	source or sink of water from surface pipes (volume per unit volume per unit time)
p	water pressure
g	acceleration of gravity
μ	coefficient of water viscosity
k	permeability
b_R, b_w	specific heats of rock and water, respectively
T	temperature
<T>	average water temperature at a given depth
T_0	reference temperature for thermal expansion
T_s	source or sink temperature
K_R	thermal conductivity of rock
ϕ	$(p-p_0)/\rho_0$ where p_0/ρ_0 is a function of depth only
d_c	measure of average crack spacing
β_w	volumetric expansion coefficient of water
m	molality
$\overline{M}$	molecular weight
W_R	grams quartz per gram of rock
a	activity
(A/V)	surface area per unit water volume, a function of fracture geometry
k_+	rate constant for the forward dissolving reaction
k_-	rate constant for the reverse precipitation reaction
γ	activity coefficient
M	mass

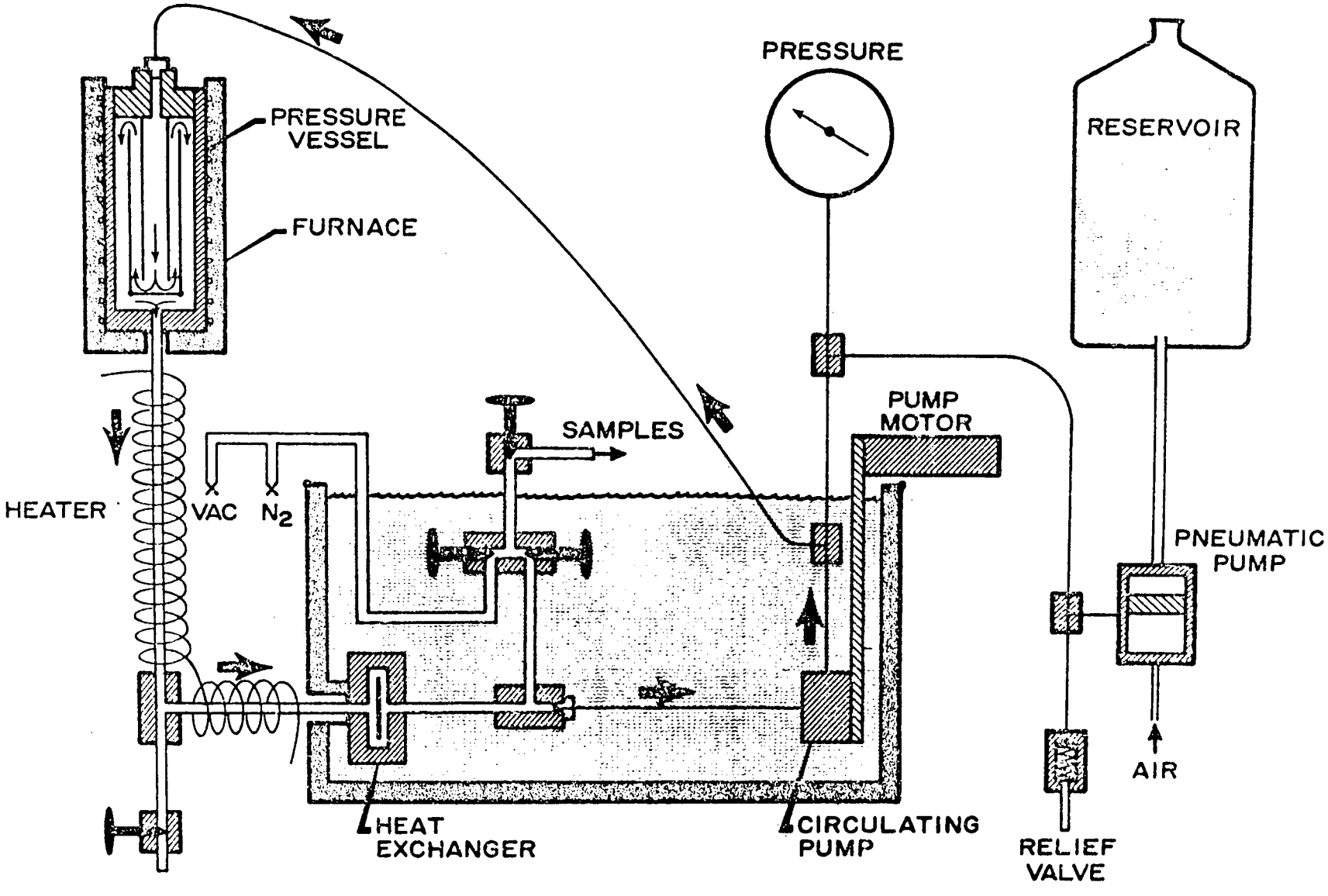
PRESSURE
RESERVOIR
PRESSURE VESSEL
FURNACE
SAMPLES
PUMP MOTOR
HEATER
VAC
N_2
PNEUMATIC PUMP
AIR
HEAT EXCHANGER
CIRCULATING PUMP
RELIEF VALVE

Figure 1

THE EFFECTS OF A STEP CHANGE IN WATER FLOW ON AN INITIALLY LINEAR PROFILE OF TEMPERATURE

Manuel Nathenson
U.S. Geological Survey
Menlo Park, CA.

In recent analyses of the hot-water system at Wairakei, New Zealand (Mercer, Pinder, and Donaldson, 1975) and the vapor-dominated system at Larderello, Italy (Petracco and Squarci, 1975), it has been suggested that large quantities of cold water are entering the reservoir by flowing down from the surface and then horizontally into the reservoir because of decreased reservoir pressures. It is also suggested that decreased reservoir pressures should increase these downward flows above their pre-exploitation levels. In order to estimate the effects of vertical flows on the temperature distribution, two idealized problems are analyzed in this paper. In both problems, the initial condition is a linear temperature increase with depth, and the flow starts at time equal to zero. In the first problem, the flow is through a semi-confining layer with the temperature fixed at the top and bottom of the layer. In the second problem, the flow is into a half-space with the surface temperature fixed.

The governing equation is conservation of energy in a porous medium (e.g., Bredehoeft and Papadopulos, 1965) which can be written in the form

$$\phi^* \frac{\partial T}{\partial t} + q\frac{\partial T}{\partial y} = \kappa \frac{\partial^2 T}{\partial y^2} \qquad (1)$$

where $\phi^* = (\phi\rho_w c_w + (1-\phi)\rho_r c_r)/\rho_w c_w$ combines the volumetric specific heats (ρc) of water and rock with the porosity ϕ, $\kappa = k_m/\rho_w c_w$ is an effective thermal diffusivity involving the thermal conductivity of the rock plus water and the volumetric specific heat of the water, and q is the seepage velocity. For the first problem of flow through a semi-confining bed of thickness ℓ the constant temperature at the top and bottom of the bed and the initial condition of constant gradient may be written as

$$T(0,t) = T_o \qquad (2a)$$
$$T(\ell,t) = T_1^o \qquad (2b)$$
$$T(y,o) = T_o + (T_1 - T_o)\, y/\ell. \qquad (2c)$$

The boundary and initial conditions for the half-space are written as

$$T(0,t) = T_o \qquad (3a)$$
$$\lim_{y\to\infty} \frac{\partial T}{\partial y} \text{ exists} \qquad (3b)$$
$$T(y,o) = T_o + Gy \qquad (3c)$$

where (3b) insures that there is no perturbation to the gradient at infinity and G is the temperature gradient at time equal zero.

The solution to equations (1) and (2) is obtained by changing to dimensionless variables that reduce the problem to homogeneous boundary and initial conditions. The form of the differential equation is then modified by the transformation $\tilde{T} = T^* \exp(q''y'')$ to an inhomogeneous equation but with no linear gradient term. The reduced problem is solved by classical techniques (see e.g., Berg and McGregor, 1964) to give

$$y = y''\ell \qquad t = \phi^*\ell^2 t''/\kappa \qquad q = 2\kappa q''/\ell \tag{4a}$$

$$\frac{T-T_o}{T_1-T_o} = y''-4q'' \; e^{q''y''} \sum_{n=1}^{\infty} \frac{n\pi}{\lambda_n^2}(1-e^{-q''}\cos n\pi)(1-e^{-\lambda_n t''})\sin n\pi y'' \tag{4b}$$

$$\lambda_n = q''^2 + (n\pi)^2. \tag{4c}$$

The location of a fluid particle that started at the origin (y=o) at t=o may be written in terms of dimensionless variables as

$$y''_c = 2\phi^* \, q''t''/\phi. \tag{5}$$

The solution to equations (1) and (3) is obtained by a similar transformation to a homogeneous problem. The form of the differential equation is modified by the transformation $T' = T^* \exp(x'-t')$ as suggested by Brenner (1962) and the equations are solved by obtaining an ordinary differential equation by Laplace transforms, solving it, and using the inversion given in Carslaw and Jaeger (1959, p. 496). The solution may be written as

$$y = 2\kappa y'/q \qquad t = 4\phi^*\kappa t'/q^2 \tag{6a}$$

$$\frac{T-T_o}{\frac{2\kappa}{q}G} = (t' - \tfrac{y'}{2})\,\operatorname{erfc}\left[\frac{y'/2-t'}{t'^{1/2}}\right] + (t' + \tfrac{y'}{2})\,e^{2y'}\operatorname{erfc}\left[\frac{y'/2+t'}{t'^{1/2}}\right] - 2t' + y' \tag{6b}$$

$$y'_c = \frac{2\phi^*}{\phi}t'. \tag{7}$$

Some sample solutions are presented in Fig. 1 for the semi-confining layer. The values for infinite time are obtained from Bredehoeft and Papadopulos (1965) formula $(T-T_o)/(T_1-T_o) = (\exp(2q'' y/\ell)-1)/(\exp(2q'')-1)$ as it is easier to evaluate. The solution is presented in terms of dimensionless variables for a flow rate q'' = 1 (top) and 2.5 (bottom) with the location of a fluid particle that started at the origin at t=o marked with a horizontal line. Choosing a layer thickness of 100 m, diffusivity of 23 m^2/yr, ϕ = 0.2, and ϕ^* = 0.68, the dimensionless flow rates correspond to seepage velocities of 0.46 and 1.2 m/yr and the inset table shows the

correspondence between physical and dimensionless time. The figures show that times greater than 60 years are required to reach the steady state solution. For a layer that is 10 m thick, this time is reduced to 0.6 year (while the velocities are 1/10 the values in Fig. 1).

Fig. 2 shows the results for a half-space. Because of the non-dimensionalization (equations 6a), different values of y' and t' are required to obtain the same values of physical length when changing the flow rate. The top of Fig. 2 is for the same flow rate as the bottom of Fig. 1. The solution in Fig. 2 is useful in enabling the influence of the upper boundary condition to be studied without having the bottom boundary condition of the solution in Fig. 1 propagate upwards. The major region of curvature in the profiles is well behind the location of the fluid particle that started at y=o at t=o, and fairly modest velocities show easily measured temperature changes in only a few years. In the model for Wairakei of Mercer, Pinder, and Donaldson (1975), the area of downflow needed to supply the natural recharge appears from the temperature contours to be about 10 km^2 although it could be larger. The velocity needed to supply the natural recharge of 440 kg/sec is 1.5 m/yr, about the same as that in Fig. 2 (top). The velocity of 4.6 m/yr in Fig. 2 (bottom) is roughly that which would be required if the current production were to be obtained without recourse to removing stored water but as steady state flow (Bolton, 1970) with recharge over the same 10 km^2. These assumptions, if true, indicate that large temperature differences should be easily found in such an area of recharge.

For Larderello, the maximum value of recharge as suggested by a hydrologic study is 9×10^6 m^3/yr (Petracco and Squarci, 1975). If this were to be distributed over an area equivalent to the entire productive area (200 km^2 from Gabbro to Carboli), the seepage velocity would be 0.05 m/yr and the effects would be small for a 100 m thick confining bed. If the recharge area were restricted to 20 km^2, the flow corresponds to Fig. 1 (top) and the effect should be easily measurable. The magnitudes of the effects for the two cases considered suggest that monitoring temperatures in undisturbed wells on the margins of producing geothermal areas should give a measure of the change in the fairly local recharge. If the amount of total recharge is known, subtracting the localized recharge should give an estimate of the recharge derived from deep circulation that originates at large distances from the reservoir.

References

Berg, P. W., and McGregor, J. L., 1964, Elementary partial differential equations-preliminary edition: San Francisco, Calif., Holden-Day, 383 p.

Bredehoeft, J. D., and Papadopulos, I. S., 1965, Rates of vertical ground water movement estimated from the Earth's thermal profile: Water Resources Research, v. 1, p. 325-328.

Brenner, Howard, 1962, The diffusion model of longitudinal mixing in beds of finite length: Chemical Engineering Science, v. 17, p. 229-243.

Bolton, R. S., 1970, The behavior of the Wairakei geothermal field during exploitation: Geothermics Special Issue 2, v. 2, pt. 2, p. 1426-1439.

Carslaw, H. S., and Jaeger, J. C., 1959, Conduction of heat in solids: Oxford University Press, 510 p.

Mercer, J. W., Pinder, G. F., and Donaldson, I. G., 1975, A Galerkin-finite element analysis of the hydrothermal system at Wairakei, New Zealand: Jour. of Geophysical Research, v. 80, p. 2608-2621.

Petracco, Cesare and Squarci, Paolo, 1975, Hydrological balance of Larderello geothermal region: United Nations Symposium on the Development and Use of Geothermal Resources, abs. no. II-38.

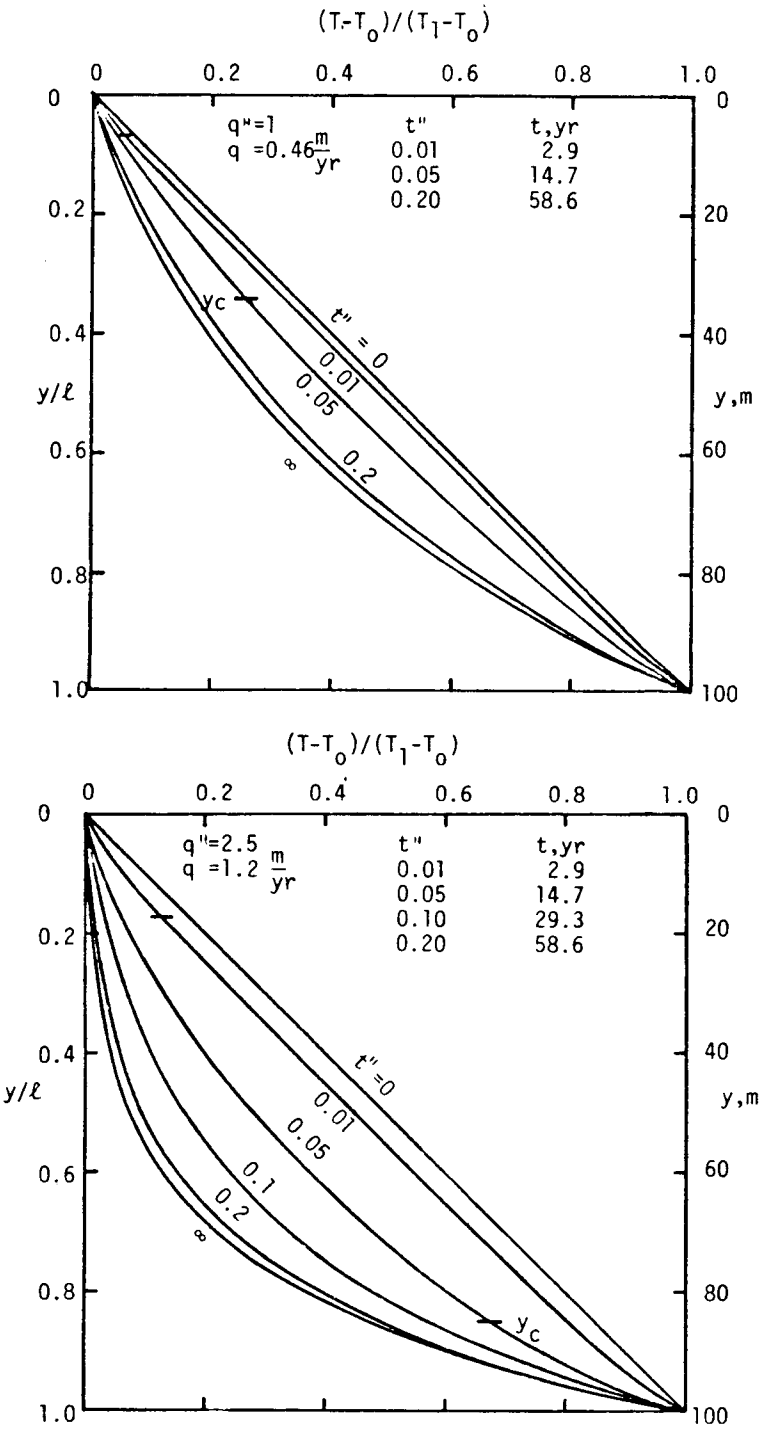

Figure 1.--Temperature versus depth in semi-confining layer for several times at dimensionless flow rates of 1 (top) and 2.5 (bottom).

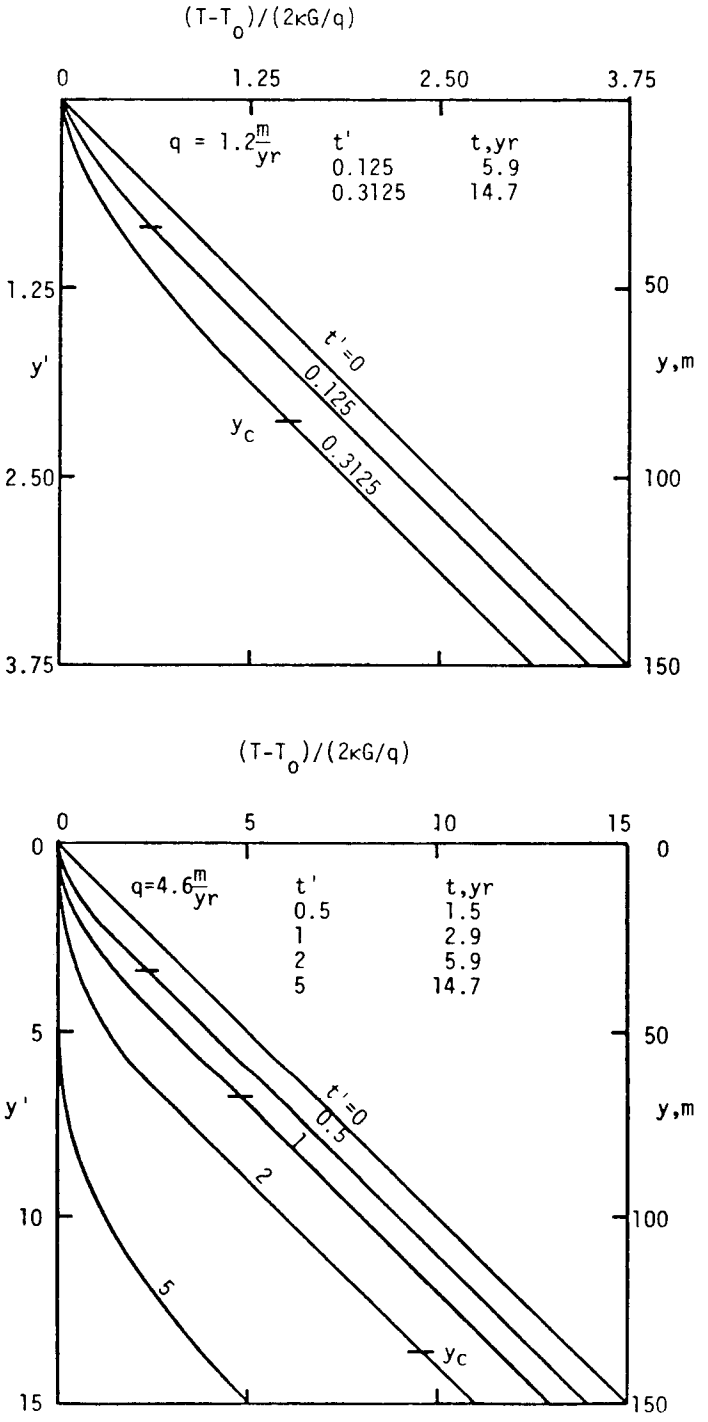

Figure 2.--Temperature versus depth for half-space for several times.

HEAT TRANSFER IN NONISOTHERMAL LIQUID INJECTION EXPERIMENTS IN POROUS MEDIA

Paul G. Atkinson
Department of Petroleum Engineering
Stanford University
Stanford, California 94305

This paper presents a study of heat transfer phenomena in bench-scale experiments of heat and mass flow in porous media (Atkinson, 1976). The intent of this work was to determine which heat transfer mechanisms are important in the bench-scale experiments being carried out in the Stanford Geothermal Program. The initial analysis considered the relatively simple case of nonisothermal single-phase liquid flow. However, the results can be applied to bench-scale experiments involving boiling water or brine flow (such experiments have been described by Chen, 1976).

Mathematical Modeling

A series of simplified mathematical models of heat and mass transport in fine-grained porous media were developed. The basis for the models was a physical system which consisted of cylindrical consolidated sandstone cores mounted in a Hassler-type coreholder. The coreholder system was placed inside a uniform temperature airbath. Hot or cold liquid water was injected into the core, and temperature distributions within it were measured as functions of time. These experimental results were reported by Arihara (1974).

The Arihara data were analyzed with new, simple models. Such models can be used to gain insight into the physical system because they display the interaction of the various assumed heat transfer mechanisms. Furthermore, since they contain fewer unknown or uncertain parameters, the comparison of the models with experimental results is easier than with more complicated models.

Four mathematical models have been developed. All of the models account for convective energy transfer, heat losses from the core, and thermal energy storage. However, each one includes different assumptions about heat conduction along the axis of the system, and about the nature of heat losses from the core. Easch of the models was studied and compared with both of the other models and with the experimental data of Arihara. The development of analytical solutions for the models simplified comparisons. None of the mathematical models could match observed experimental behavior accurately for the entire time of the experiments. However, each model did exhibit behavior which was important during some stage of the experiments, and as a group these models were able to isolate the important heat transfer mechanisms in the Arihara experiments. These theoretical results are discussed in the next section.

Results

It was determined that longtime, steady-state temperature behavior in the core was dominated by convection energy transfer in conjunction with steady heat losses from the sides of the core. This should cause the steady-state temperature profiles to be semi-log straight lines, as can be seen to be the case in Fig. 1. The slopes of the semi-log straight lines have negative values of $hP/(2.303\ wC_w)$ on $\log_{10}$ graph paper, where h is the overall heat loss coefficient from the core, P is the perimeter of the core, w is the mass flowrate through the core, and C_w is the specific heat of the flowing liquid. The one experiment which did not graph as a straight line in this figure had not reached steady-state.

During the early stages of hot or cold liquid injection, an effective axial thermal conduction mechanism was found to affect the temperature profiles strongly. This effect was not reduced at higher mass injection rates, because of the increased effect of mixing and dispersion mechanisms with increasing injection rate.

Early- and medium-time stages of hot or cold liquid injection were found to be affected strongly by transient heat losses through the core-holder system. These transients were caused primarily by the thermal capacity of the viton sleeve which surrounded the core. It was also found that the transients were controlled by a flowrate-dependent film coefficient between the core and coreholder sleeve.

The functional dependence between the core-coreholder film coefficient and the mass injection rate was estimated by comparing calculated temperatures with those reported by Arihara. The results of these comparisons are presented in Fig. 2. This figure also presents the results of Crichlow (1972), derived from experiments on an unconsolidated sandpack, and those of Colburn (1931), whose smallest particles were 1/8 in. granules. Figure 2 suggests an interesting trend in the data, particularly since Arihara's experiments were carried out on consolidated porous media with effective particle sizes of as much as ten times smaller than those of Crichlow. Experimental investigation of this functional dependence is continuing.

A Critique of Previous Modeling of Arihara's Liquid Injection Experiments

The single- and two-phase nonisothermal fluid flow experiments of Arihara have been used by various authors (Garg, et al., 1975; Faust and Mercer, 1976; Thomas and Pierson, 1976) as a basis for checking sophisticated computer model results.

None of these computer models incorporated the phenomenon of transient heat losses through the coreholder.

For example, Garg, et al., presented calculations for the CWI-S-4 experiment of Arihara, and compared computed and measured temperatures. Their model could handle only steady heat losses through the coreholder system. Their comparison appeared plausible for the limited range of time presented. However, analysis of the steady-state profile for this experiment

(See Fig. 1) indicates an overall heat loss coefficient from the core of 1.98 Btu/(hr ft^2 ^oF) while Garg, et al., used an effective value of 4.2 Btu/hr ft^2 ^oF). This higher heat loss coefficient caused the appearance of higher calculated heat losses from the core during the early stages of the experiment. This calculated behavior is consistent with the observed early-time behavior of the experiments. At longer times, however, the experiments showed a lower heat loss rate. If Garg, et al., had presented calculated temperatures for times greater than 45 minutes, these values would have been close to the values presented for 45 minutes. Thus, their model would have reached steady-state for the given physical parameters. Fig. 3 shows that the temperatures in the core actually continued to change for 105 minutes.

It can thus be seen that care must be taken if one wishes to avoid a situation where a mathematical model is calibrated against experimental results using incorrect values for some physical parameters. It is important that all of the relevant physics be discovered and incorporated into the mathematical model before doing such a calibration.

Summary

This paper has discussed an analysis of the heat transfer phenomena in the bench-scale experiments being carried out in the Stanford Geothermal Program. The basis of this analysis was a series of simplified mathematical models of heat and mass transport in fine-grained porous media. The analysis determined that the thermal capacity of the coreholder system caused heat losses from the core which were not steady at early and medium times. This phenomenon had not been recognized previously. This was in spite of the fact that various authors previously had attempted to match the experimental behavior under discussion with their sophisticated computer models. These computer models did not account for the transient nature of the heat losses from the core.

References

Arihara, N.: "A study of nonisothermal single and two-phase flow through consolidated sandstones," Stanford Geothermal Program, Report SGP-TR-2, November 1974.

Atkinson, P. G.: "Mathematical modelling of single-phase nonisothermal fluid flow through porous media," Ph.D. Dissertation, Stanford University, May 1976; to be issued as Stanford Geothermal Program Report SGP-TR-14.

Chen, H. K.: "Measurement of water content in porous media under geothermal fluid flow conditions," Ph.D. Dissertation, Stanford University, November 1976; to be issued as Stanford Geothermal Program Report SGP-TR-15.

Colburn, A. P.: "Heat transfer and pressure drop in empty, baffled, and packed tubes," Ind. Eng. Chem., 23 (1931), p. 910.

Crichlow, H. B.: "Heat transfer in hot fluid injection in porous media," Ph.D. Dissertation, Stanford University, May 1972.

Faust, C. R., and Mercer, J. W.: "An analysis of finite-difference and finite-element techniques for geothermal reservoir simulation," Proceedings for the Fourth SPE Symposium on Numerical Simulation of Reservoir Performance, held in Los Angeles, Calif., Feb. 19-20, 1976.

Garg, S. K., Pritchett, J. W., and Brownell, D. H., Jr.: "Transport of mass and energy in porous media," Second United Nations Symposium on the Development and Use of Geothermal Resources, San Francisco, Calif., May 20-29, 1975.

Thomas, L. K., and Pierson, R.: "Three dimensional geothermal reservoir simulation," presented at the 51st Annual Fall Technical Conference and Exhibition of the Society of Petroleum Engineers of AIME, held in New Orleans, Oct. 3-6, 1976.

FIGURE 1. GRAPH OF log ($T_{external}$ - T) VS DISTANCE ALONG THE CORE FOR THE COLD WATER INJECTION EXPERIMENTS OF ARIHARA

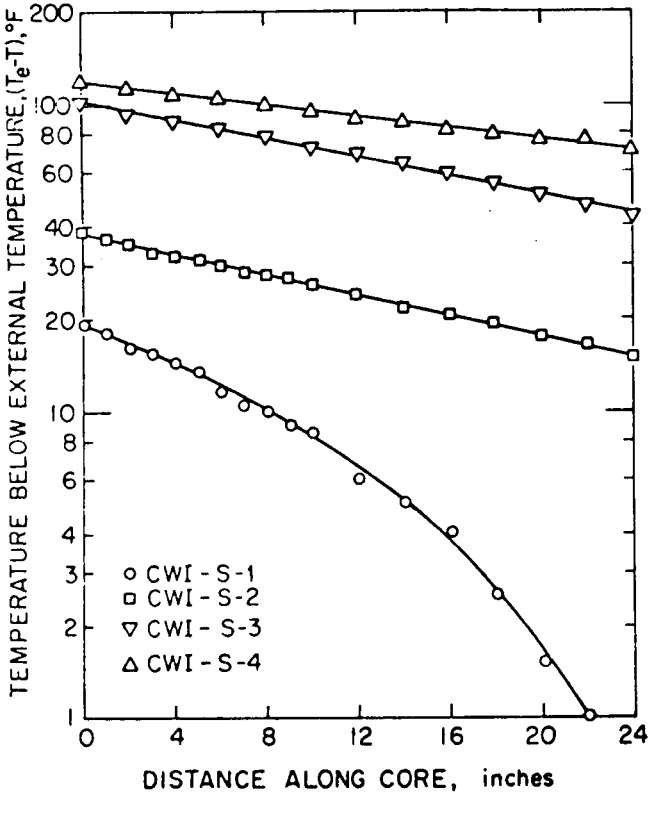

FIGURE 2. GRAPH OF THE CORE-COREHOLDER FILM COEFFICIENT, h_f, VS. MASS VELOCITY, w"

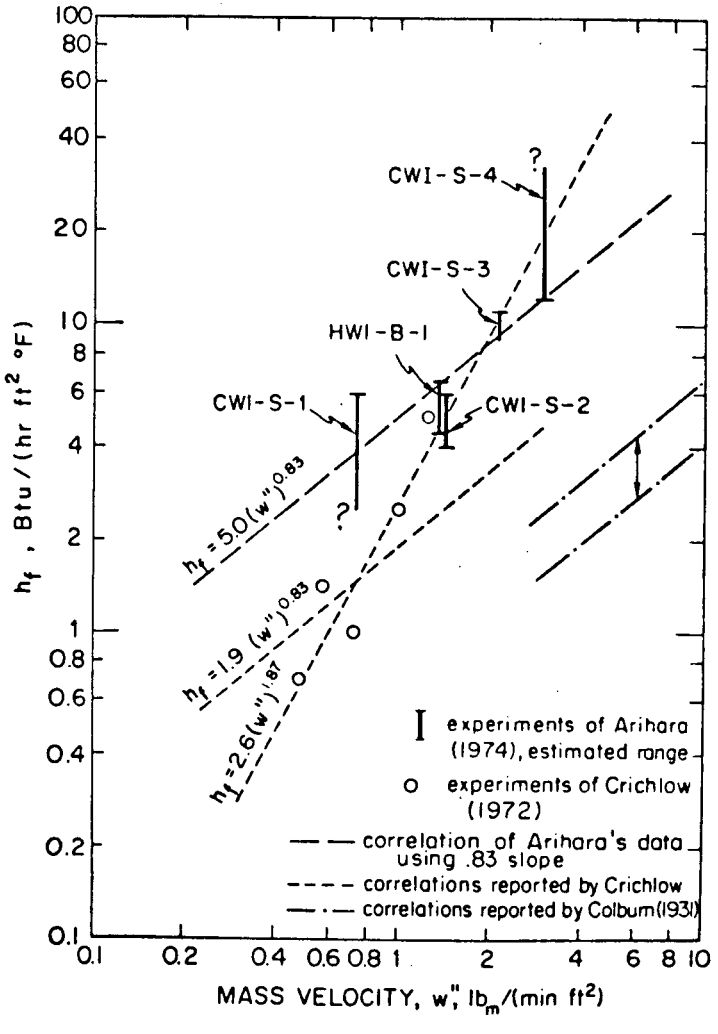

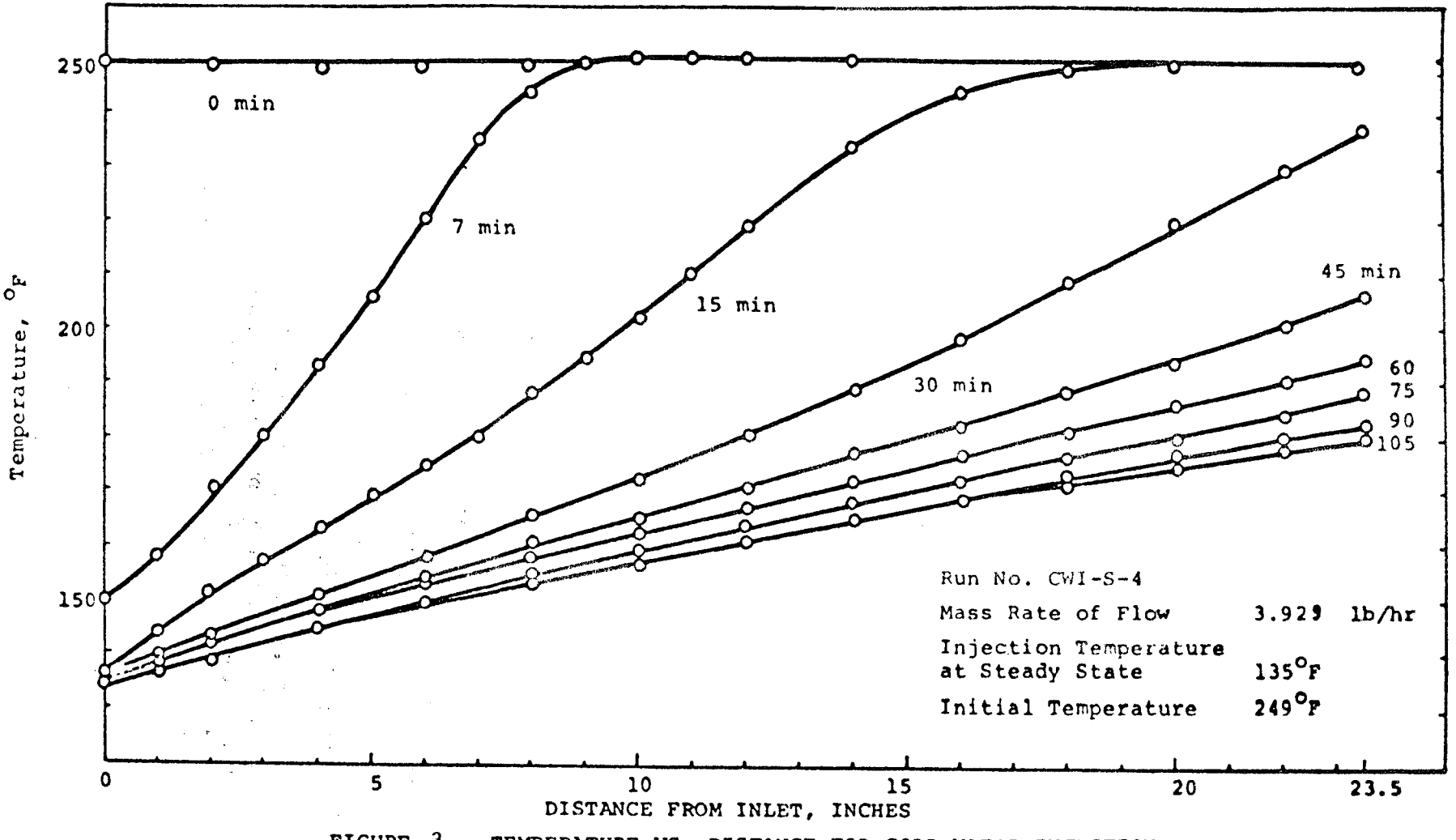

FIGURE 3. TEMPERATURE VS. DISTANCE FOR COLD WATER INJECTION SYNTHETIC SANDSTONE; RATE = 3.929 lb/hr, TEMP. = 135°F

FORCED GEOHEAT EXTRACTION FROM SHEET-LIKE FLUID CONDUCTORS

G. Bodvarsson and J. M. Hanson
School of Oceanography
Oregon State University
Corvallis, OR. 97331

Geoheat is now being extracted for electrical power generation from a number of resources in thermally active regions. The most notable examples are The Geysers, California; Larderello, Italy, and Wairakei, New Zealand. Common to all these cases is that the energy is being extracted from natural hydrothermal resources on the basis of free flowing boreholes. This type of operation may be termed as free geoheat production.

Large scale space heating by geoheat has been carried out in Iceland for more than three decades. The Reykjavik District Heating System, which now supplies energy for domestic heating for more than 100,000 people, is a low-temperature operation where large scale resource stimulation by borehole pumping is being applied.

The free and stimulated production methods as described above are based on the presence of natural fluid conducting openings in the resource formations and on a natural recharge of the withdrawn fluid. One can also envision forced geoheat extraction systems (FGES) with an artificial recharge of the heat extracting fluid which flows to some extent through artificial openings created by hydraulic fracturing or other pressurizing operations. For the operation of such systems to be successful, the openings have to provide adequate contact areas or contact volumes between the fluid and the rock such that a sufficient amount of heat can be extracted from the hot formations.

In the following, we will discuss a number of economical and physical aspects of FGES with emphasis on heat extraction from sheet-like natural fluid conductors in volcanic formations such as sufficiently open (conducting) fault zones, dikes and formation contacts. We envision applications of our results in some regions in the western U. S., the Pacific Northwest, in particular.

Limitations on Geoheat Transport

Thermal waters and natural steam are bulky heat carriers which cannot be transported economically over long distances. In the case of power generation the limits are of the order of a few kilometers only. For direct uses such as space heating, the maximum distances

may in extreme cases amount to a few tens of kilometers. At the present state-of-art where only natural convective type sources are being harnessed, geoheat utilization, non-electrical uses, in particular, are therefore severely limited by the low transportability. The major convective sources are not favorably located with regard to the heat market. There is consequently a great interest in the possibility of extracting geoheat at suitable temperatures over much wider areas than has been possible so far.

FGES in Regions of Moderately High to Normal Heat Flow

The FGES which we envision involve the circulation of a heat extracting fluid through hot formations at depth between sets of injection and production boreholes. The principal factors that have to be considered in the design of such systems are the following:

(1) thermal properties of the formations
(2) fluid conductivity at the depth of interest
(3) drilling and equipment costs
(4) pumping power required to provide the necessary penetration and contact area
(5) fluid losses, scaling.

Minimum Contact Area

The size of the fluid-rock contact area required to produce a sufficient amount of hot fluid to amortize a given system investment depends critically on factors (1) to (5) above. The minimum economic area can be estimated on the basis of an idealized model. We assume that the circulating fluid is water absorbing heat from the rock in uniform and unidirectional flow through an infinitesimally thin fracture in a large volume of homogeneous rock which is isothermal at the initiation of the process. Using theoretical results by Bodvarsson (1974), the contact area as a function of plant investment and value of the energy produced can easily be calculated. The results for a single borehole-pair producing heat for building heating are shown in Fig. 1 and the corresponding results for electrical power generation are shown in Fig. 2. In both figures the useful life of the system is assumed to be 20 years, the interest on capital 8% and the operational and maintenance costs are 10% of capital per annum. Other factors are given in the figures. In the electrical case, the required power per borehole pair amounts to a few MW.

Suitable Fluid Conductors

There are two main possibilities of realizing FGES of the above type, viz., by using (a) natural subsurface fluid conductors or (b) artificial conductors obtained by hydraulic fracturing. The second

FIGURE 1.

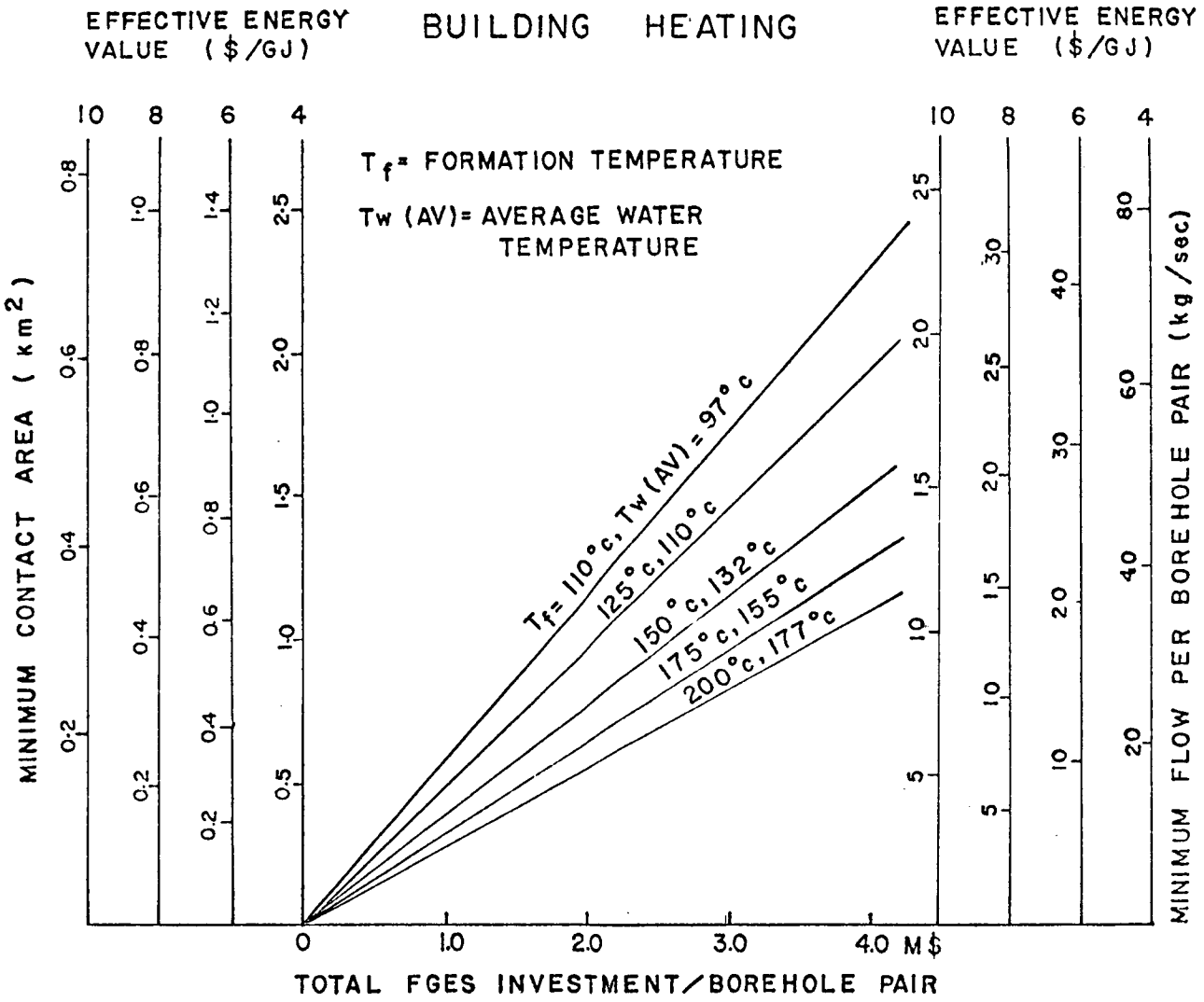
BUILDING HEATING
EFFECTIVE ENERGY VALUE ($/GJ)
EFFECTIVE ENERGY VALUE ($/GJ)
10 8 6 4
10 8 6 4
T_f = FORMATION TEMPERATURE
Tw (AV) = AVERAGE WATER TEMPERATURE
T_f = 110°c, Tw (AV) = 97°c
125°c, 110°c
150°c, 132°c
175°c, 155°c
200°c, 177°c
MINIMUM CONTACT AREA (km^2)
0.8 0.6 0.4 0.2
1.0 0.8 0.6 0.4 0.2
1.4 1.2 1.0 0.8 0.6 0.4 0.2
2.5 2.0 1.5 1.0 0.5
25 20 15 10 5
30 25 20 15 10 5
40 30 20 10
80 60 40 20
MINIMUM FLOW PER BOREHOLE PAIR (kg/sec)
0 1.0 2.0 3.0 4.0 M$
TOTAL FGES INVESTMENT/BOREHOLE PAIR

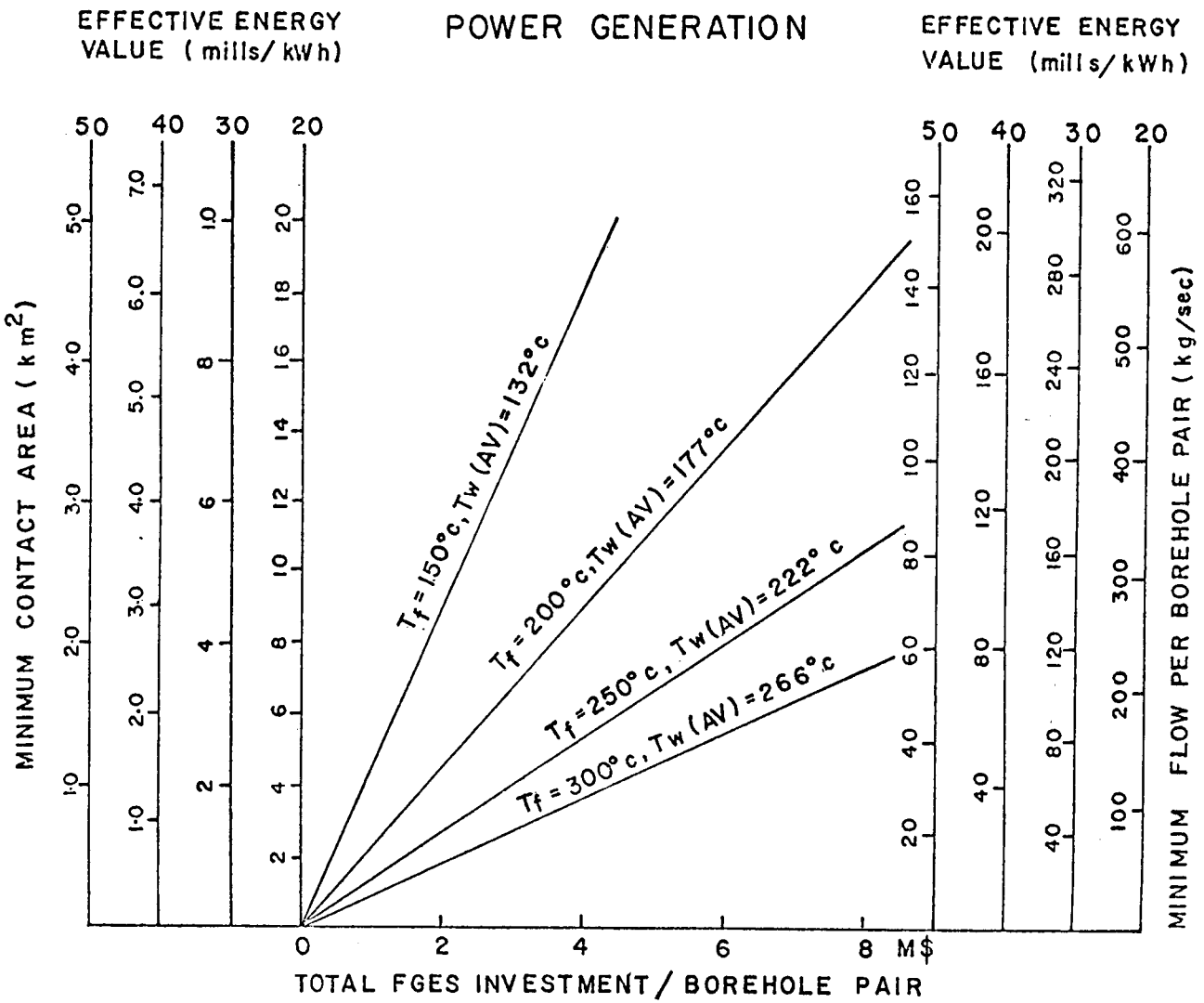
POWER GENERATION
EFFECTIVE ENERGY VALUE (mills/ kWh)
EFFECTIVE ENERGY VALUE (mills/ kWh)
MINIMUM CONTACT AREA (k m²)
MINIMUM FLOW PER BOREHOLE PAIR (kg/sec)
Tf = 150°c, Tw (AV) = 132°c
Tf = 200°c, Tw (AV) = 177°c
Tf = 250°c, Tw (AV) = 222°c
Tf = 300°c, Tw (AV) = 266°c
TOTAL FGES INVESTMENT / BOREHOLE PAIR
0 2 4 6 8 M$

Figure 2

possibility is now under thorough investigation including field testing by the Los Alamos Scientific Laboratory Dry-Hot-Rock Group in Los Alamos, N.M. (ERDA, 1976). In this note we will concentrate on the natural conductors. The results for the minimum contact area given in Fig. 1 and 2 will obviously apply to both cases (a) and (b).

The natural fluid conductors which have the potential of providing sufficient fluid-rock contact and some relevant data are listed in Table 1 below.

Due to great horizontal extent, major open fault zones and basaltic dikes have very large wall surfaces which in a sufficiently hot environment could be used for heat extraction provided an adequate and sufficiently uniform longitudinal fluid conductivity is available. It is to be emphasized that the fluid conductivity can be enhanced by an increased injection pressure.

Table 1

Potential Fluid Conductors

Type	Field observations on large scale fluid conductivity	Role in geoheat extraction
(1) Fault zones	Many major geothermal systems are controlled by faults, e.g. in the Basin and Range Province.	Borehole production obtained by intersecting fault zones.
(2) Basaltic dikes in flood-basalt areas	Many geothermal systems in Iceland are controlled by dikes.	Boreholes in Central North Iceland produce by intersecting dikes.
(3) Other intrusions	Few data available, but columnar structure possibly indicative of conductivity.	Some production in Iceland appears to be obtained from thin basaltic sills.
(4) Formation contacts	Lava-bed contacts are major aquifers in the flood-basalt plateau of Iceland.	Major production in Southwestern Iceland obtained from lava-bed contacts.
(5) Sedimentary horizons	Many major sedimentary basins contain large volumes of thermal water.	Large scale forced geoheat production from sedimentary basins in France (DGRST, 1976).

Factors Affecting the Efficiency of FGES

The estimates given in Fig. 1 and 2 are based on an idealized model. Deviations from the assumed conditions will in one way or another affect the results and will have to be considered carefully.

First, rock temperatures are generally not uniform. The water may therefore flow along rock surfaces where the temperature varies in the direction of flow. Second, the load on FGES will vary considerably, in particular in cases where the heat is to be used for building heating. A varying production rate will usually be required in such cases. A somewhat more elaborate computer modeling indicates that these two effects will not be of major importance and can quite easily be taken into account.

Of greater concern is the rather complex interaction of three phenomena affecting the flow of thermal water in subsurface natural conductors, viz., (i) natural flow channeling, (ii) thermoelastic effects and (iii) buoyancy of convective effects. The quantitative theory of these effects in the natural environment is both uncertain and basically difficult. By nature, these flow phenomena are non-linear effects.

Table 2 has been designed to furnish a very brief qualitative overview of the adverse influence of the above three flow effects on the design factors listed in section (3) above.

Experimental Preliminary Design of a Sheet-Controlled FGES

The fluid conductors under (1) to (4) in Table 1 appear suited for the type of FGES under consideration. The basically horizontal conductors such as the formation contacts and intrusive sills have, however, very frequently the disadvantages of not being directly observable. Lack of field data can in such cases greatly reduce the possibilities for arriving at a rational design of the heat extraction system. This type of difficulty is of much less concern in the case of the quasi-vertical conductors, such as (1) and (2) in Table 1, where surface outcrops can be inspected. Quite frequently the position of such conductors can be mapped with considerable precision.

We have therefore chosen to base our first attempt at the design of a FGES on the assumption of a sufficiently open quasi-vertical conductor such as a basaltic dike or a fault zone. We make the *ad hoc* assumption that such a conductor is available. Depending on the position of the injection-production boreholes, the main flow in systems of this type can be vertically up (Fig. 3), vertically down (Fig. 4) or quasi-horizontal. Considering the various phenomena indicated in Table 2 there appear grounds for assuming that the up-flow systems will exhibit the highest degree of flow stability and thereby achieve the most favorable conditions for heat extraction.

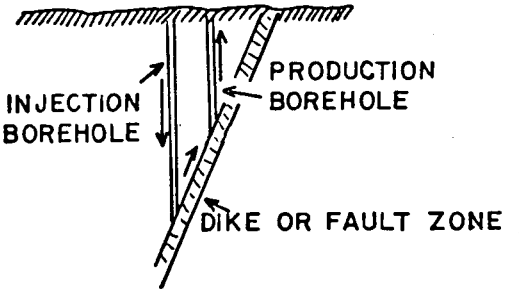

Figure 3. Upflow system.

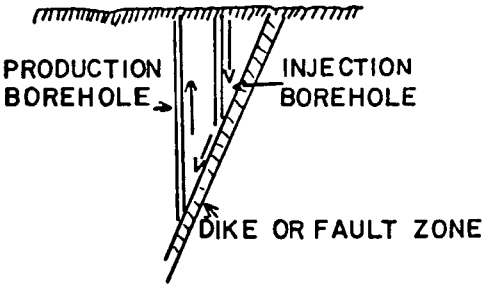

Figure 4. Downflow system

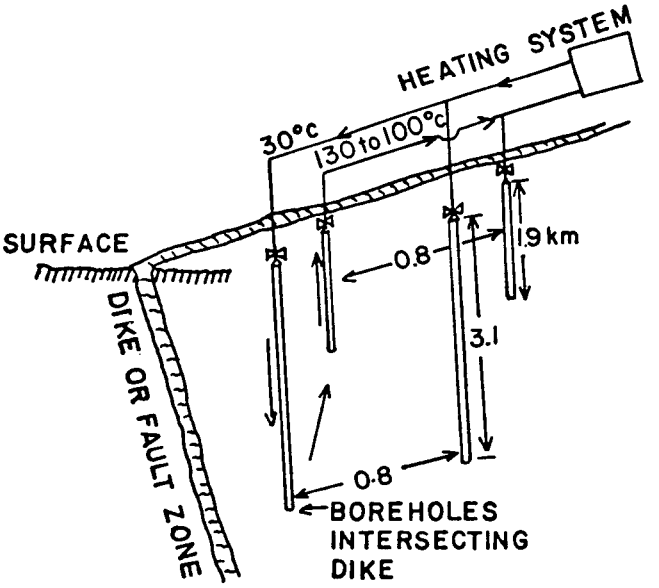

Figure 5. An experimental design of a multihole FGES system for building heating. The minimum flow per borehole pair is 25 kg/sec.

Table 2

Adverse flow phenomena

Type of phenomena	Potential effects: Inefficient heat extraction	Potential effects: Pumping power	Potential effects: Water losses
(1) Non-uniform conductivity, flow channeling	Potentially major factor	High pumping pressure may be required to overcome non-uniformity.	Can be a major factor in channeling injected cold water out of the heating zone.
(2) Thermoelastic effects	Enhances channeling of water colder than the rock.	Narrowing of fractures carrying water hotter than the rock requires increasing pumping pressure.	May increase water losses by enhanced channeling.
(3) Buoyancy and convection	Enhanced channeling in down-flow systems		Downward convective penetration of cold water may enhance losses.

A preliminary experimental design of a multihole upflow FGES is shown in Figure 5. The system is to produce water in the temperature range 130-100°C for building heating purposes. The system is envisioned to operate in an environment where the geothermal gradient is 50°C. The effective contact area per borehole pair is to amount to 0.5 km^2, the flow per hole is 25 kg/sec and the effective thermal power relative to an effluent temperature of 40°C is 3.1 MW.

Physical Parameters

The following rock and fluid parameters were used in the computations underlying Figures 1 and 2; rock thermal conductivity k_r = 2.1 W/(m.deg), density ρ = 2700 kg/m^3, specific heat of rock C_r = 1000 J/(kg.deg), and specific heat of water C_w = 4186 J/(kg.deg). The injection temperature was 30°C.

Epilogue

Having come to the conclusion that the estimated subsurface dimensions of the FGES under consideration are not unreasonable, our principal task will be to demonstrate that nature complies with our basic assumptions.

References

Bodvarsson, G., 1974, Geothermal resource energetics, Geothermics, 3(3), p. 83-92.

Delegation Generale á la Recherche Scientifique et Technique (DGRST), Report, 1976, Paris.

ERDA, 1976, Geothermal Project Summaries, Report 76-53, Washington, D.C.

RADON IN GEOTHERMAL RESERVOIR ENGINEERING

Paul Kruger and Gary Warren
Civil Engineering Department
Stanford University
Stanford, CA 94305

Radon is a potentially-useful internal tracer for the study of geothermal reservoirs (Stoker and Kruger, 1975; Kruger, Stoker, and Umaña, 1975). The naturally-occurring gaseous radioactive element radon exists essentially as the longest-lived isotope, 3.83-day ^{222}Rn, produced by alpha decay of 1620-year ^{226}Ra, which in turn is produced in the natural uranium series originating with 4.5×10^9-year ^{238}U. Thus radon, which decays with its characteristic half-life of 3.83 days when separated from its parent radium, will be produced "forever" from the radium found rather uniformly distributed in crustal rocks at a mean concentration of about 1 pg/g/. However, radium as a chemical homolog of the alkaline earth elements calcium, strontium, and barium, can undergo hydrothermal processes in geothermal systems and may be redistributed in a geothermal reservoir.

Stoker and Kruger (1975) noted that radon concentration in geofluids produced from active geothermal resources depends on several independent factors, among them the distribution of radium in the formation (a function of the hydro- and thermo-chemical history of the formation), the emanating power of the produced radon (a function of the physical state of the formation), and the transport time of the radon from emanation site to sampling site (a function of the hydrodynamic properties of the reservoir). Because of its relatively short half-life of 3.83-days, in contrast to the stable chemical components CO_2, H_2S, $\delta(^{18}O)$, etc., radon offers a uniquely sensitive tracer for transport time measurements in geothermal reservoirs.

Two general types of information related to transit time are amenable to radon measurement experiments. Under steady flow conditions, changes in the radon source will result in changes in the radon concentration in produced geofluids. And under steady emanation conditions, changes in the flow regime will also result in changes in the radon concentration.

Short-term changes in radon emanation can be induced by seismic activity affecting the reservoir. Such an effect seems to have occurred during experiments run for other purposes (Kruger, Stoker, and Umaña, 1975). The possibility of relating changes in radon concentration during periods of steady geofluid production with seismic events is being explored as a potential means of studying earthquakes. Short-term changes in radon emanation can also be induced by artificial fracture stimulation of low productivity hydrothermal reservoirs or of hot dry rock formations. The initial radon research program (Kruger and Ramey, 1973) was undertaken to study the possibility of determining the effectiveness of fracture stimulation methods.

Long-term changes of radon concentration in high-productivity reservoirs should be associated with long-term changes in reservoir characteristics, such as fracture density, permeability changes, lowering of boiling fronts, or redistribution of alkaline earth elements. One example of such change was

noted when two wells at The Geysers sampled for radon by Stoker and Kruger (1975) were resampled two years later. The data are given in Table 1.

TABLE 1

Long-Period Sampling of Steam Wells

Well No.	Date	Flow (klb/hr)	Wellhead Pressure (psig)	Wellhead Temperature (°F)	Radon Concentration (nCi/lc)
I D	Apr '74	22.1	130	351	26.7 ± 1.0
	May '76	25.0	131	342	40.8 ± 2.8
II A	Apr '74	59.0	88	368	26.3 ± 1.0
	May '76	51.5	84	350	32.9 ± 2.2

The radon concentration (in nanocuries per liter condensate) shows a significant change over the two-year period of steady production and extensive seismic history. Although these fragmentary data are insufficient to indicate any of the long-term changes in reservoir characteristics noted above, they do indicate a reasonable justification for long-term measurement of radon emanations in several wells over the reservoir.

Current interest has focused on the relationship between radon concentration and the flow regime in producing geothermal reservoirs. Steady-state production should result in a steady-state concentration of radon gas on the basis of a constant emanation rate of radon from the reservoir rock, a constant permeability field in the reservoir, and thus a constant transport time from the emanation or boiling site to the wellhead.

Several indications of a dependence of radon concentration on flow rate in producing geothermal reservoirs have been observed. The basis for flow models in vapor-dominated and liquid-dominated reservoirs was given by Stoker and Kruger (1975). For a one-dimensional linear vertical model of a steam reservoir, in which the radon is boiled out with the steam from a deep liquid zone, and little radon emanates into the dry steam zone below the well, the concentration should be directly related to the flow rate, for which the transit time is a function of the permeability-distance product, Kh. A model of such flow is given in Muscat (1946) as the "open-bottom" well, a three-dimensional reservoir of great thickness. Figure 1 shows the first test of radon concentration dependence on flow rate at The Geysers well (Kruger, Stoker, and Umaña, 1975). The transient, following a flow rate shut-in from ∿100 Mt/hr to ∿50 Mt/hr, shows a period of about 21 days in change of concentration from an average of 16.5 ± 2 to a test termination value of ∿8 ± 1 n Ci/lc.

Several attempts have been made to reproduce this observed linear change in concentration with flow rate. Samples taken weekly at another well at The Geysers this summer in preparation for a double draw down test showed a qualitative dependence during a period of shut-in unknown to us. Figure 2 shows the data during this period. Completed analysis of 19 samples

obtained during the period 1 to 2 months prior to the shut-in showed a mean concentration of 18.4 $\pm$ 0.4 nCi/lc at a steady flow rate of 130 klb/hr. The random samples taken after the then unknown shut-in period showed a curious pattern. The first sample taken 15 days after the initial shut-in showed a significant decrease; the second sample, showing a major decrease, was taken 18 and 11 days respectively after the second and final flow rate changes. The third sample was taken 15 days after the return to full flow and the fourth sample was taken one day later. The similarity in patterns between flow rate and radon concentration with an apparent 15-16 day phase lag is qualitatively striking.

Current experiments include a full 24 day, double flow rate shut-in at The Geysers with samples taken daily at this and a nearby monitoring well without change in flow rate. A two-week half-flow shut-in test is scheduled for a well in the Larderello steam fields for November, 1976. The results of these experiments is expected to assist in the formation of a quantitative model of radon flow in steam reservoirs.

Other experiments are underway to obtain steady flow rate radon concentrations in liquid-dominated reservoirs in anticipation of flow rate change experiments when sufficient periods of production are available and reduction in flow does not interfere with production operations. Tests are underway at Well 6-1 of the East Mesa facility operated by the Bureau of Reclamation, at Cerro Prieto through the courtesy of the Comision Federal de Electricidad and at Heber in conjunction with a long-term heat exchange test supported by the Electric Power Research Institute. A model for radon concentration change with flow rate change was suggested by Stoker and Kruger (1975) as the horizontal flow confined aquifer, in which the concentration would be dependent on the logarithm of 1/Q rather than directly proportional to Q itself. Verification of this model requires substantial sampling under steady operating conditions to obtain a sufficiently small standard deviation in the mean concentration of radon which should vary logarithmically with flow. The results of these tests will be given in subsequent reports.

References

Kruger, P. and H. J. Ramey, Stimulation of Geothermal Aquifers, Progress Report No. 1 to National Science Foundation, SGP-TR-5, March, 1973.

Stoker, A. K. and P. Kruger, Radon in Geothermal Reservoirs, Proc., Second UN Symposium on the Development and Use of Geothermal Resources, San Francisco, May, 1975.

Kruger, P., A. K. Stoker, and A. Umaña, Radon in Geothermal Reservoir Engineering, Proc., Application of Nuclear Techniques to Geothermal Studies (International Atomic Energy Agency, Vienna, 1975) in press.

Muscat, M., The Flow of Homogeneous Fluids through Porous Media (Edwards, Ann Arbor, 1946).

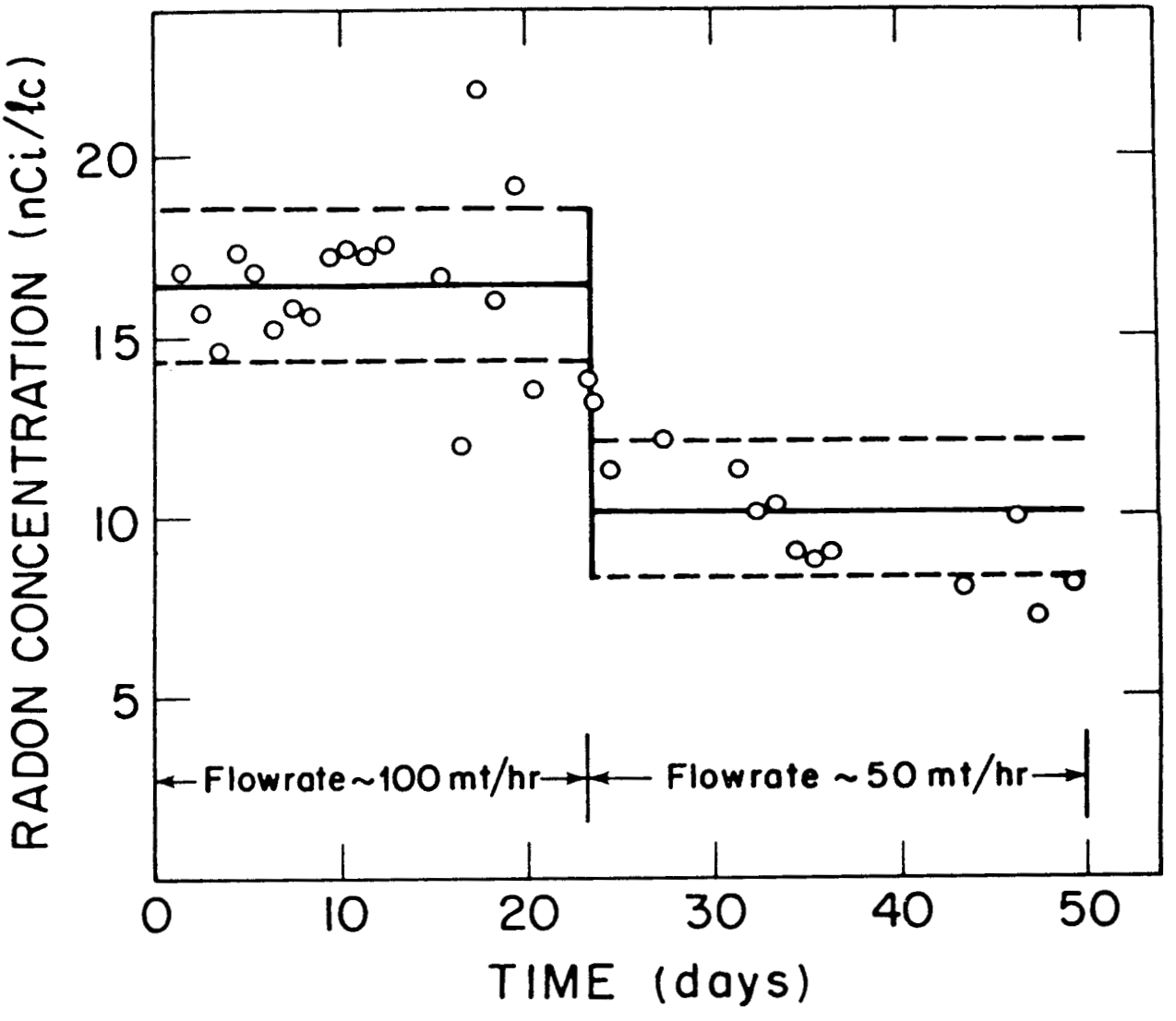

Figure 1. Radon concentration during a flow rate change. Solid lines are mean values over the flow rate period; broken lines represent one standard deviation.

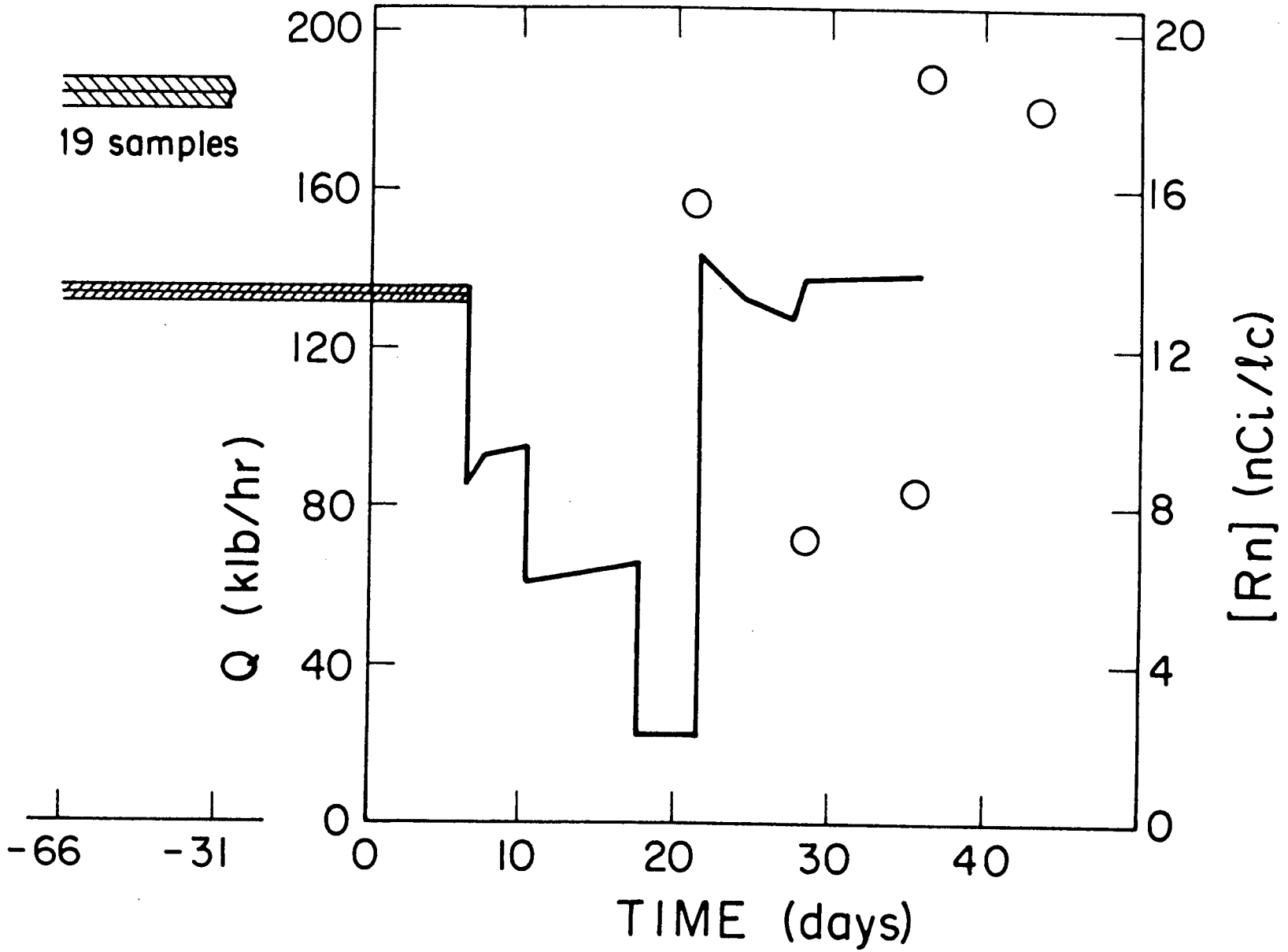

Figure 2. Radon concentrations during a period of changes in steam flow rate

BOREHOLE GEOPHYSICS IN GEOTHERMAL WELLS--PROBLEMS AND PROGRESS

W. Scott Keys
U. S. Geological Survey
Denver, Colorado 80225

Surface geophysical techniques are readily adaptable to exploration for and evaluation of geothermal reservoirs because existing equipment and interpretive models can be used. In contrast, the application of borehole geophysics for these same purposes requires the development of equipment to operate dependably in the very hostile environment of some geothermal wells. After equipment has been developed and tested, its response must be calibrated with respect to required parameters such as lithology and porosity. This is difficult in geologic environments where there is practically no experience in well-log interpretation. The desired final products are reliable data to guide exploration for geothermal systems, and to aid in reservoir evaluation, modeling, and development, in the ways in which well logs are routinely used in the petroleum industry. Researchers in geothermal exploration are still some years from achieving the level of application already attained in petroleum exploration and development. This deficiency is receiving some attention from the U.S. Energy Research and Development Agency (ERDA) and the U.S. Geological Survey. The two agencies cosponsored a workshop on Geophysical Measurements in Geothermal Wells in September 1975 (Baker, Baker, and Hughen, 1975). Sandia Laboratories had previously summarized the state-of-the-art in a report on "Well-Logging Technology and Geothermal Applications" (Baker, Campbell, and Hughen, 1975). For several years the U.S. Geological Survey has had a research program to develop logging instrumentation and log-interpretation techniques for geothermal applications. This summary describes some of the results of that research effort.

Equipment Problems

The research project on borehole geophysics in the U.S. Geological Survey has several high-temperature logging systems under development and test. The following probes rated at 250°C and 10,000 PSI ($6.896 \times 10^7 N/m^2$) are being used for experimental geothermal well logging: temperature, fluid conductivity, caliper, natural gamma, spectral gamma, non-compensated gamma-gamma, non-compensated neutron, 16 inch and 64 inch normal resistivity, spontaneous potential, single-point resistance, and acoustic televiewer. Upgrading for high-temperature operation is planned for several other logging probes which now operate to approximately 150°C (Celsius); these include acoustic velocity, focused resistivity, induction, compensated gamma-gamma and flowmeter probes, and a water sampler. Many of these probes are of stainless steel; development of probes that are more resistant to long exposure to the highly corrosive fluids found in some geothermal wells has not yet been started.

The logging probes listed above are operated on two research trucks that utilize high-temperature (250°C) armored cable; 6,000 feet (ft) (1829 meters (m) of four-conductor and 16,000 ft (4877 m) of seven-conductor

cable. Both trucks are capable of recording data from wells simultaneously in analog and digital forms. Digital data can be recorded on computer-compatible 7- or 9-track magnetic tape, or punched or printed on paper tape. Data are usually recorded at 0.5 ft (0.15 m) intervals, and output from as many as seven sensors can be recorded simultaneously along with depth information to the nearest 0.01 ft (0.003 m). We also have magnetic-tape systems for recording gamma spectra and the full acoustic wave form digitally. All these digital data are then entered without modification into the Survey's computer in Denver for quantitative analysis.

Two general approaches are used to develop geophysical logging probes capable of operating at high temperatures. The simplest method is to isolate all the electronic components and sensors from the borehole environment by means of a stainless steel dewar flask inside a high-pressure housing. Heat-sink material that changes state below the maximum operating temperature of the components is incorporated in the flask. These tools are usually designed for 10 hours of operation at 250°C. The major drawback to this approach, which we use for several high temperature probes, is the build-up of heat from power dissipation in the electronics. Internal heat, which cannot escape from the flask, may cause drift in output signal.

A second approach is to replace all electronics, mechanical components, and materials for operation at 250°C. For most logging probes this is not possible because many of the necessary high-temperature components and materials do not exist. The Energy Research and Development Agency is funding a number of development efforts in private industry to correct this deficiency. In the meantime development of a dependable high-temperature acoustic televiewer, so important to the geothermal industry, has been an expensive and time-consuming project. Our approach for the televiewer has been a combination of the two techniques described above. All electronics are installed in a dewar flask with heat sink-material and the motor-magnetometer-transducer section is designed for operation in high temperature fluids. The status and application of this one-of-a-kind probe will be described later.

Testing of probes developed for geothermal logging has also been a problem. Components and sections can be tested in laboratory ovens, but until recently there has been no high-temperature, high-pressure, wet chamber available for testing assembled probes. Even this kind of a test does not fully simulate logging environments. There is no substitute for actually logging a hot well. We are attempting to combine in-hole testing with development of calibration data and log-interpretation techniques for the probes listed above. Some of our high-temperature probes are dependable and stable and others are not, which is similar to the experience users have had with commercially available high-temperature logging services.

In-Hole Gamma Spectrometry

The natural gamma log provides no information on the relative concentrations of uranium, thorium, and potassium which contribute to the total gamma radiation emitted by all rocks. In-hole gamma spectrometry does provide data on the relative concentrations of these naturally

occurring radioisotopes and has several potential applications to studies of geothermal reservoirs. This log provides more diagnostic information on lithology than can be obtained from the gross radiation recorded as a natural gamma log, and the concentrations of the radio-elements are related to sources of radiogenic heat in rocks.

Several geothermal investigators in Los Alamos report that the gamma spectral log is one of the most useful logs run in the crystalline basement rocks penetrated by their deep wells (West and Laughlin, 1976). The spectral logs provided unique data for the identification of such rock types as hornblende-biotite schists and leucocratic monzogranite, and for correlation between holes. The presence of high concentrations of radium-equivalent uranium in fracture zones is evidence of the mobility of uranium and aids in the location of fracture zones that formerly had a relatively high intrinsic permeability. The spectral log may therefore provide information related to the source of radon gas reported to be abundant in some geothermal waters and which might constitute an environmental problem in the development of geothermal energy.

Continuous spectral logs are available from one commercial service company and we developed and are now testing a high-temperature spectral logging probe. We have developed the capability of transmitting the spectral data through 16,000 ft (4877 m) of logging cable and of digitizing the spectra in the logging trucks. Project personnel also wrote computer programs for energy shifting and stripping of complex gamma spectra (Eggers, 1976). By means of these techniques, quantitative analyses for radioisotopes can be made with equipment that is properly calibrated for the borehole environment. Calibration is now done by utilizing laboratory analyses of core.

Acoustic Televiewer

The acoustic televiewer provides the most reliable and accurate data on the location and orientation of fractures and other types of secondary porosity. The probe employs an acoustic transducer which is rotated at three revolutions per second. Each rotation of the transducer is displayed as a sweep on an oscilloscope at the surface, and the sweeps are triggered on magnetic north by a magnetometer in the probe. The intensity of the scope trace is a function of the amplitude of the acoustic signal reflected from the wall of the borehole. A camera is used to record the successive sweeps, which are combined to produce a picture of the borehole wall as if it had been split along the north side and opened out into the plane of the picture. The strike and dip of fractures and other planar features can be calculated from the televiewer log and a caliper log (Zemanek, 1969). The acoustic televiewer log can resolve features as small as 1.5 mm, and it can be used in holes filled with drilling mud, water, or oil. Our televiewer systems also have available oriented acoustic caliper outputs that produce four very high resolution traces at North, East, South and West. These data, combined with the televiewer log, provide a three-dimensional model of fractures and other openings.

While televiewer probes were developed 8 years ago and have been used by several service companies, the only high-temperature televiewer probe built to date is being developed under contract for, and tested by, the U.S. Geological Survey. It has been used experimentally to log geothermal wells at Marysville, Mont.; Raft River, Idaho; Long Valley, Calif. and Los Alamos, New Mexico. Although it has operated at temperatures as high as 200°C for many hours it is still not dependable, and all component and material problems have not yet been solved. Despite these problems we are encouraged by progress to date and look for further improvement of the system.

The potential significance of a probe that reveals individual openings in the borehole wall is illustrated by a statement by geologists for a major company involved in the development of one important geothermal reservoir, that the orientation of fractures would be the most important data that could be obtained from geophysical logs. This statement is based on the hypothesis that fractures of one orientation are more likely to produce steam than those of another, and that information on the distribution and orientation of fractures as a function of depth would allow wells to be drilled directionally at the best angle to intersect the producing fractures.

Natural fractures are very abundant in most of the geothermal wells we have logged; some of these wells attain depths as great as 10,000 ft (3048 m). Fracture sets have been observed with favored orientations that may be consistent over several thousand feet of hole. Log A in Fig. 1 is a section of televiewer log made with the high temperature probe in a well in Long Valley, Calif. Several fracture sets with different orientations are clearly shown. Considerable difference in the character of fractures has been noted in such logs, and the data being collected will make possible a study of the relationship of water contribution to the orientation and character of the fractures. We have also used the televiewer to log a well before and after hydraulic fracturing as an essential part of state-of-stress studies in California and in Colorado. Fractures induced artificially as part of the Los Alamos Scientific Laboratory's hot-dry-rock program were observed during logging in a deep well in New Mexico. Log B in Fig. 1 was made in this well and shows a section of a hydraulically induced fracture system, which is apparently both vertical and branching. If hydraulic fracturing becomes an important procedure for the stimulation of geothermal wells the televiewer will be needed to provide information on the fractures produced. Study of subsidence caused by the withdrawal of geothermal fluids is another potential application of the televiewer; this may prove to be one of the best ways of estimating the amount of compaction in sediments penetrated by wells. It has high resolution and can therefore be used to measure the shortening of each length of casing caused by compaction. This can be done by locating very accurately collars, perforations, or other irregularities in casing.

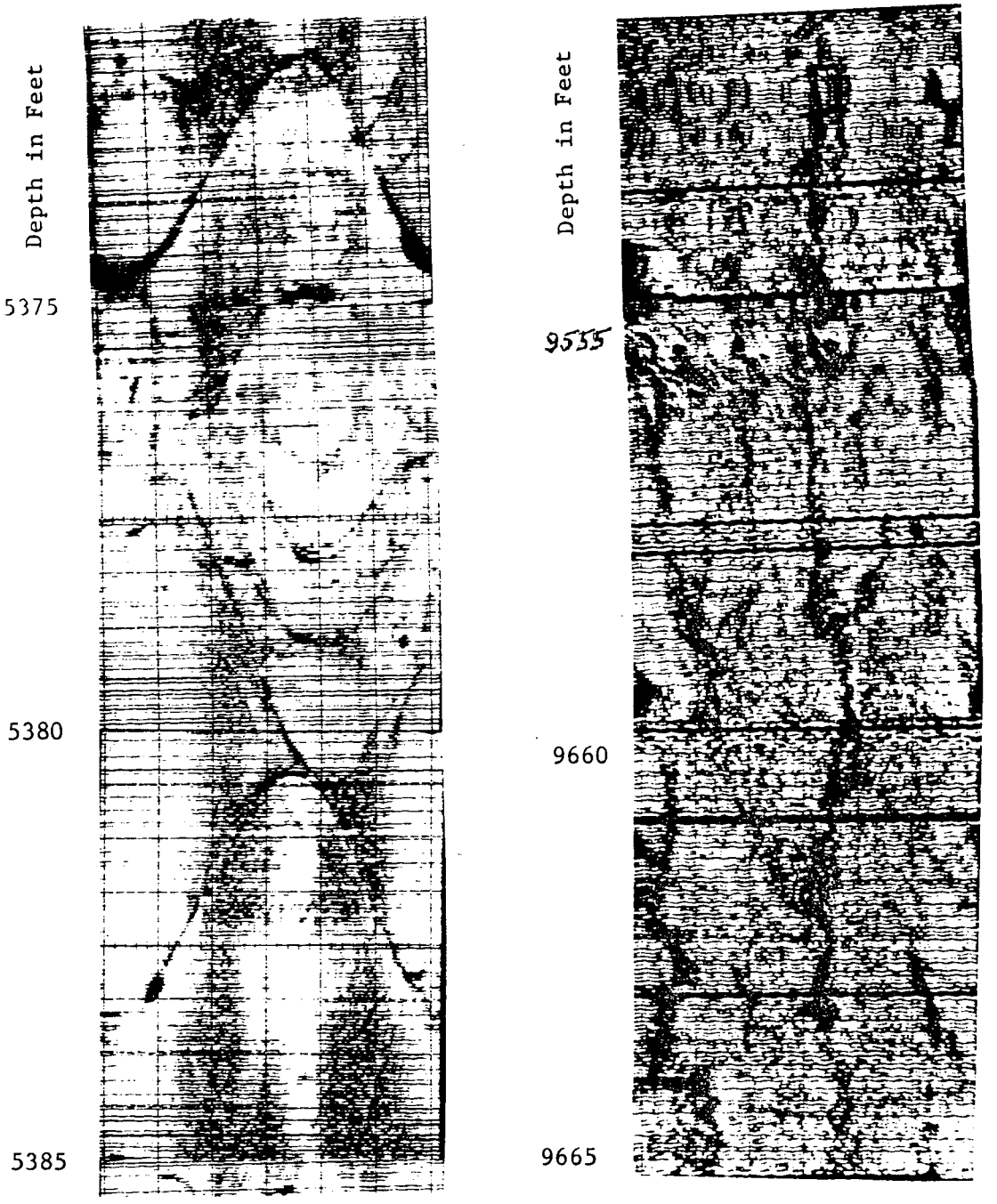

Log A--Long Valley, California

Log B--Los Alamos, New Mexico

Figure 1.--Acoustic televiewer logs made in geothermal wells

Computer Interpretation of Logs

Four types of logs respond to changes in porosity in a lithology-dependent manner: the neutron, acoustic velocity, gamma-gamma, and resistivity logs. Resistivity logs, however, also depend on the conductivity of the interstitial fluid. A typical petroleum-oriented technique is to crossplot two of the three lithology-dependent porosity logs. If the rock type is limestone, sandstone or dolomite, or a mixture of any two of these, the cross-plots may indicate lithology and provide estimates of porosity values corrected for lithologic or matrix effects. We are attempting to use this technique to interpret geophysical logs of the wells in the Raft River Basin, Idaho.

Fig. 2 is a computer-generated plot of density from a commercial gamma-gamma log and of porosity from a commercial neutron log, assuming a sandstone matrix. The plot is for the depth interval 5400 to 5900 ft (1646 to 1798 m) in the Idaho National Engineering Laboratory's well RRGE-2. It is apparent from the plot that two distinct lithologies or porosities are present. Nearly all the points clustered around 13% apparent porosity and a bulk density of 3.0 g/cc correspond to the depth interval from 5690 to 5760 ft (1734 to 1756 m). The cut-off at 3.0 g/cc is due to setting of the scale for the gamma-gamma log at value suitable for a typical oil-field environment. A more effective scale would have accommodated the higher densities encountered in the igneous and metamorphic rocks. This demonstrates the importance of having a log analyst at the site who is familiar with the geothermal environment. Data from cuttings and core indicate that the interval from 5690 and 5760 ft (1734 to 1756 m) is biotite schist. Biotite has a bulk density of 2.8 to 3.4 g/cc.

The cluster of points at a bulk density of approximately 2.6 g/cc and an apparent porosity of 2 percent represents quartz monzonite, which is found above and below the biotite schist. If the sandstone, limestone, and dolomite lines were added to the plot in Fig. 2 the quartz monzonite would fall between 0 and 5 percent on the line representing sandstone porosity. This relationship is quite reasonable because the minerals in quartz monzonite have grain densities that average near 2.65 g/cc, a value commonly assumed for sandstone. The crossplot points for biotite schist do not fall near any of the lithologic types on available cross-plots. This illustrates the need for development of calibration data and interpretive techniques for the rock types found in geothermal areas but not found in petroleum-producing areas.

Project personnel have developed computer techniques to compute lithology-corrected porosity, matrix density, matrix velocity, acoustic porosity, secondary porosity, apparent water resistivity, mineralogy, thermal conductivity, and heat flow in a limestone-dolomite section in Texas (Merkel, MacCary and Chicko, 1976). Figure 3 shows some of these curves generated by the computer. Lithology was solved as a function of the three porosity logs (neutron, gamma-gamma, and acoustic velocity) by means of a linear programming algorithm.

Figure 2.--Computer-generated crossplot of neutron and gamma-gamma logs for Raft River well GE2, depth interval 5,400-5,900 feet (1646 to 1798 m)

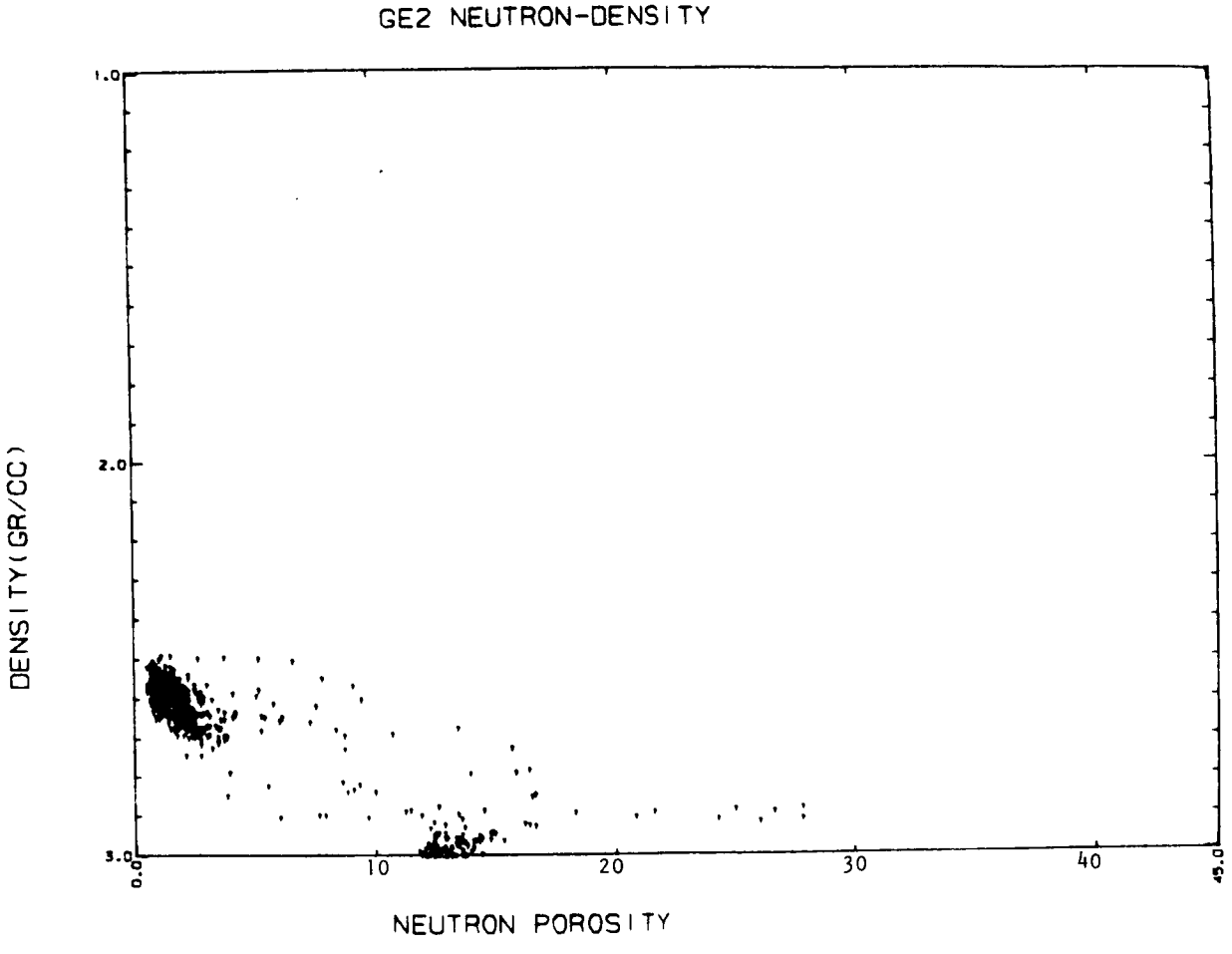

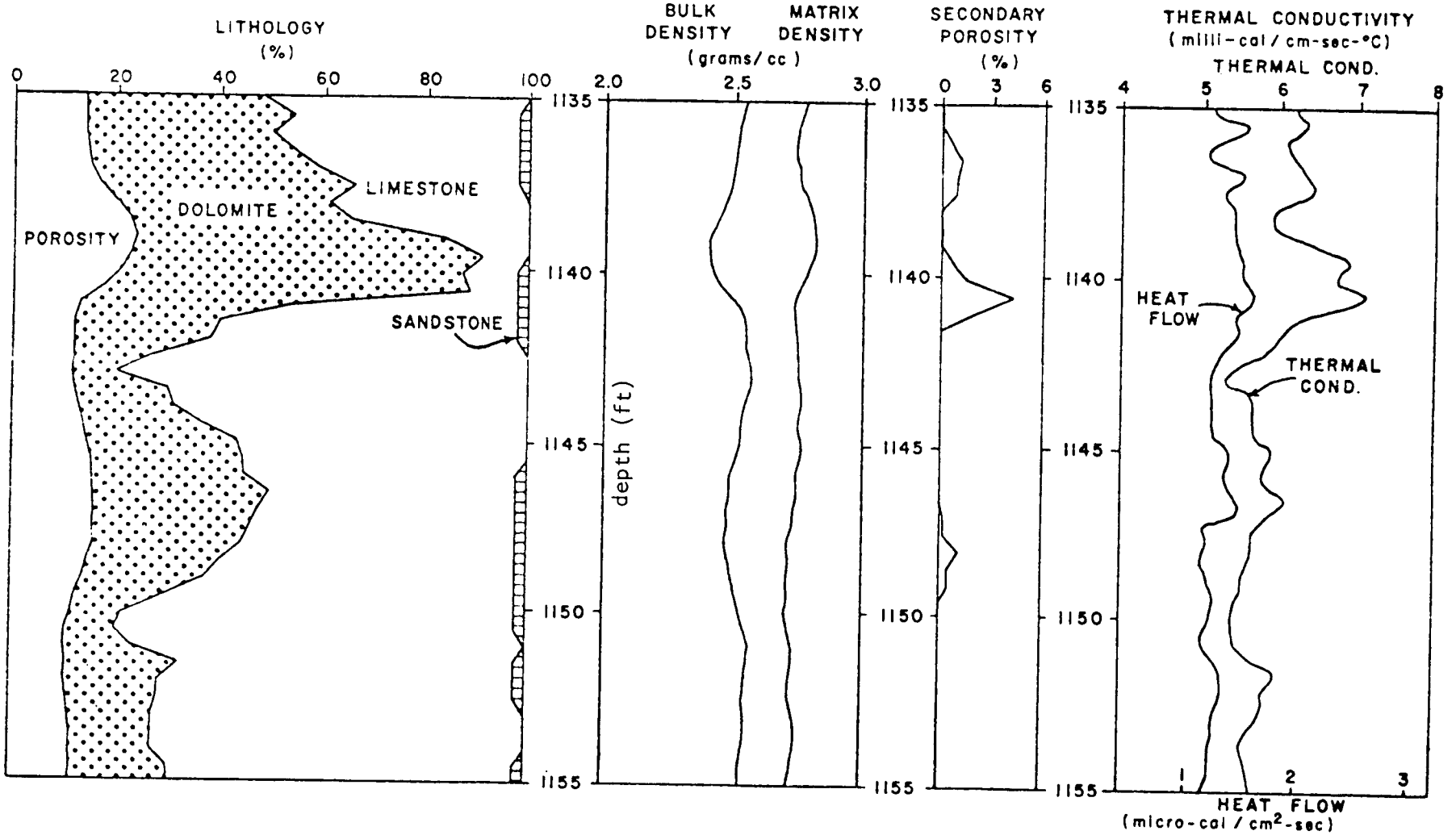

Figure 3.--Computer-generated curves for the Randolph number 1 test hole near San Antonio, Texas

A thermal conductivity log was generated in the computer using the results of the mineralogy program and a geometric mean equation that has been found to represent most effectively the relationships between mineralogy and thermal conductivity (Sass and others, 1971); Merkel, 1975). A temperature-gradient log was generated using the temperature log and a delta-Z of 10 ft. The product of thermal conductivity and thermal gradient produced a heat-flow log.

Conclusions

The application of borehole geophysics to the development of geothermal energy is still in its infancy but equipment problems are being solved and progress is being made toward quantitative interpretation of the logs in environments where previous experience does not exist. These efforts will be furthered by the availability of core, core analyses, and test information from various geothermal environments and by increasing time available for logging those wells where other data are available.

References

Baker, L. E., Baker, R. P., and Hughen, R. L., 1975, Report of the geophysics measurements in geothermal wells workshop, Issued by Sandia Corporation, Albuquerque, New Mexico, for U. S. Energy Research and Development Administration: SAND75-0608, 69 p.

Baker, L. E., Campbell, A. B., and Hughen, R. L., 1975, Well-logging technology and geothermal applications--a survey and assessment with recommendations, Issued by Sandia Corporation, Albuquerque, New Mexico, for U.S. Energy Research and Development Administration: SAND75-0275, 75 p.

Eggers, D. E., 1976, The application of borehole geophysics to the selection and monitoring of nuclear waste disposal sites in 17th U.S. Symposium on rock mechanics, proceedings, Snowbird, Utah, complied by Brown, W. S., Green, S. J., and Hustrulid, W. A.: Utah Univ. Engineering Experiment Station, p. 4B3-1-4B3-7.

Merkel, R. H., 1975, The generation of thermal-conductivity and heat-flow logs from conventional borehole logs (abs.): Geophysics, v. 40, no. 1, p. 176.

Saas, J. H., Lachenbruch, A. H., and Munroe, R. J., 1971, Thermal conductivity of rocks from measurements on fragments and its application to heat flow determination: Jour. Geophys. Research, v. 76, no. 14, p. 3391-3401.

West, F. G. and Laughlin, A. W., 1976, Research notes: Spectral gamma logging in crystalline basement rocks in Geology: Geol. Soc. America, v. 4, no. 10, p. 617-618.

Zemanek, J. 1969, The borehole televiewer--A new logging concept for fracture location and other types of borehole inspection: Jour. Petroleum Technology, v. 21, June 1969, p. 762-774.

ANALYSIS OF WELL TESTS WITH VARIABLE DISCHARGE

Chin Fu Tsang, D. G. McEdwards, T. N. Narasimhan
and P. A. Witherspoon
Lawrence Berkeley Laboratory
University of California
Berkeley, California 94720

The conventional methods of well tests analysis usually assume a constant rate of discharge of the producing well. The procedure involves matching a log-log plot of test data (drawdown versus time) to analytic or semi-analytic solutions that are based on a model of the production well as a line source of constant strength in an infinite reservoir. However, variable discharge well test conditions may arise under a variety of conditions, such as existing well-field production schedules, step-drawdown tests, and influence of the pumping water level on the production rate. It is very desirable to have the capability to reliably interpret data from the tests. In fact, the present study was prompted by a set of recent geothermal well test data in which due to various mechanical problems, the flow rate during the first 70 hours of production varied widely and could not effectively be treated as a mean constant rate. The present paper reports the development of a general technique of analyzing well tests with variable flow rates.

Method of Analysis

The variable flow is approximated by a series of sequential straight line segments of arbitrary length and slope (Figure 1). The pressure response of each linearly varying production pulse at any time is derived analytically in terms of the well-known exponential integral. The change in pressure head at time t and distance r from the producing well that is caused by a production pulse n, occurring between τ_n and τ_{n+1} is given by

$$\Delta h_n(t,r) = \frac{1}{4\pi kH} \int_{\tau_n}^{\tau_{n+1}} Q_n(\tau) \frac{e^{-\frac{r^2}{4\alpha(t-\tau)}}}{t-\tau} d\tau$$

If we define

$$x_1 = \frac{1}{4\pi kH}$$

$$x_2 = \frac{r^2}{4\alpha} = \frac{\mu\phi CHr^2}{4kH}$$

and the linear flow rate is given by

$$Q_n(\tau) = A_n + B_n(\tau - \tau_n)$$

then

$$\Delta h_n(t,r) = x_1 \int_{\tau_n}^{\tau_{n+1}} \left[A_n + B_n(\tau - \tau_n)\right] \frac{e^{-\frac{x_2}{t-\tau}}}{t-\tau} d\tau$$

The result of the integration is given by

$$\Delta h_n(t,r) = x_1 \left\{ \left[A_n + B_n(\tau_n + x_2)\right] \left[W(u_n) - W(u_{n+1})\right] - \left[B_n \tau_n e^{-u_n} - \tau_{n+1} e^{-u_{n+1}}\right] \right\}$$

where

$$u_n = \frac{x_2}{t-\tau_n}$$

$$u_{n+1} = \frac{x_2}{t-\tau_{n+1}}$$

and $W(u)$ is the well function, which is related to the exponential integral $Ei(x)$ by

$$W(u) = -Ei(-u)$$

The total pressure drop as a function of time is obtained by a superposition of the reservoir responses attributable to each production pulse:

$$\Delta h(t,r) = \sum \Delta h_n(t,r)$$

To account for the influence of one linear boundary, a third parameter is defined as

$$x_3 = \frac{\mu\phi C H r_i^2}{4kH}$$

where r_i is the image well distance, and the pressure drop is then given by

$$\Delta h(t,r) = \sum \Delta h_n(t,r) \pm \Delta h_n\ t, r_i$$

where the position or negative sign indicated an impermeable or fully leaky boundary respectively.

These equations are used to calculate pressure drawdown values that correspond to a specific flow rate variation and a given set of reservoir parameters. Thus with a set of initial guess values of reservoir parameters a multiparameter least-square-fit computer routine is employed to compare well-test data with predicted values in a search for the best set of reservoir parameters. Input data for the program are A_n and τ_n, coordinate points on the production history record, Δh and t, coordinate points on the well-test pressure drawdown record, and a few program control parameters.

Corresponding to optimal values of x_1, x_2, and x_3 obtained, the program assigns values respectively to transmissivity, kH; storativity, ϕCH; and the image well distance r_i. Both interference and production tests can be analyzed. In the latter case, work is in progress to account for the influence of wellbore storage and skin effects, also in a parametric fashion.

Applications

The method has been applied to data from seven well tests to evaluate its utility (see Table 1). Three of the analyses involve theoretically generated well-test data and four analyses involve field data.

The field data were from two well tests conducted at the East Mesa Geothermal field in southern California and from two well tests conducted at the Raft River in southern Idaho. The three theoretical cases involve well test data calculated assuming: (1) constant discharge; (2) variable discharge in steps, and (3) exponentially decaying discharge. Three of the four field tests were constant discharge interference tests, two of which indicated the presence of a boundary. The last remaining field test involved a discharge rate with a very wide fluctuation.

In all of these cases, a solution was possible and an unambiguous set of reservoir parameters was determined. In the three tests using generated data, known parameters are reasonably reproduced. The first three field interference tests analyses yielded reasonable parameters. Figures 2, 3 and 4 show respectively the theoretical case of exponentially decaying discharge rate, the East Mesa 31-1 constant discharge interference field tests analysis involving the detection of a barrier boundary, and the analysis of the Raft River #3 production test, in which the flow rate varied markedly. In the figures, the circles represent observed drawdown data and the squares represent the best-fit drawdown values. The close agreement with analytical and conventional results in cases where they are available indicates the validity of the method. Furthermore, the results of the RRGE 3 production test analysis indicate that the methods can successfully analyze variable flow field data.

Conclusions

This method will make it possible to do well test analyses when a constant discharge flow rate is difficult to maintain, and permit detection of boundaries even in situations where there is a markedly varying flow rate. Work is currently in progress to extend the analysis to the study short-term data.

Nomenclature

Δh	Pressure head drop
n	Designation of production segment
t	Time
r	Distance from well
k	permeability
H	Thickness of aquifer
τ	Time
Q	Flow rate
α	$k/(\phi\mu C)$
ϕ	Porosity
C	Total compressibility
r_i	Image well distance

TEST CASES	DISCHARGE		BARRIERS		TYPE TEST	
	Constant	Variable	None	Impermeable	Interference	Production
Synthetic Data						
Constant Discharge	●		●		●	
Stepped Discharge		●	●			●
Exponential Decay Discharge		●	●			●
Field Data						
Raft River No. 2	●			●	●	
East Mesa Well 31-1	●			●	●	
East Mesa Well 6-2	●		●		●	
Raft River No. 3		●	●			●

TABLE 1. WELL TESTS ANALYZED.

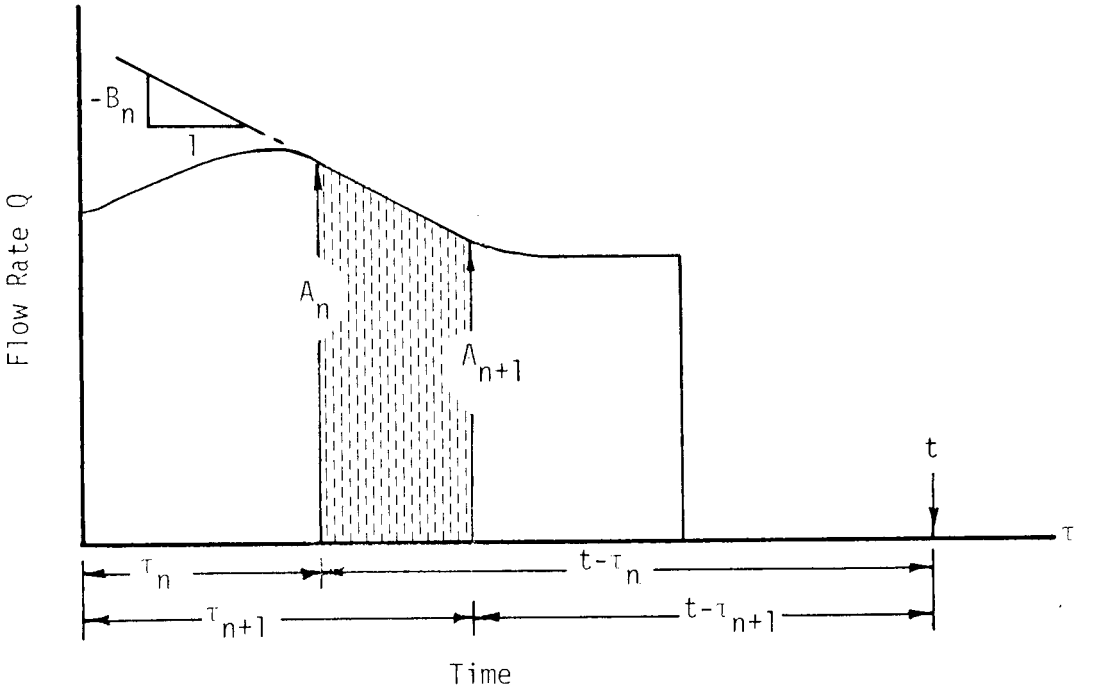

Figure 1. Time-Dependent Flow Rate

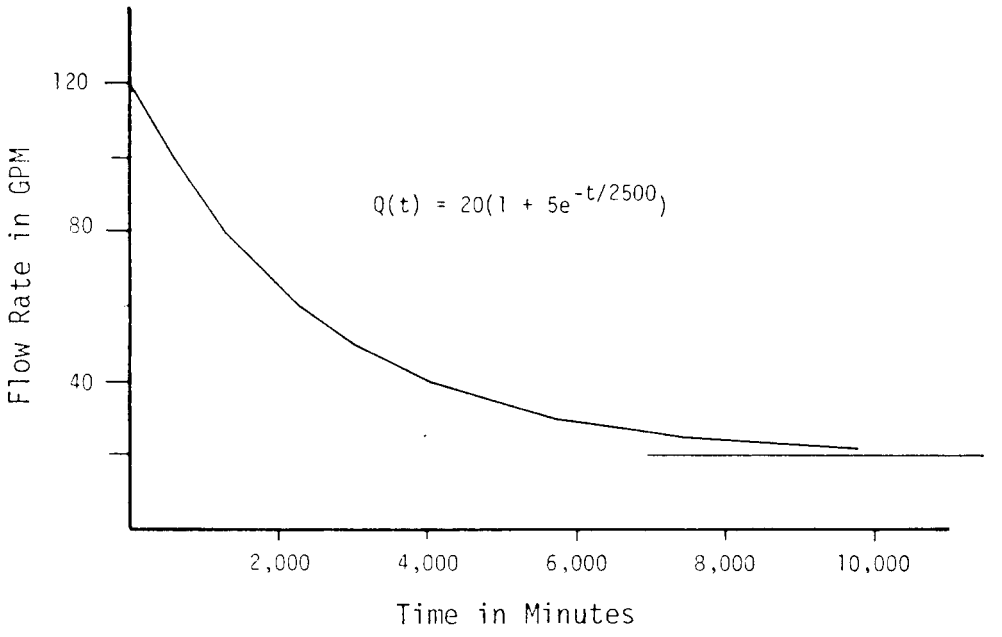

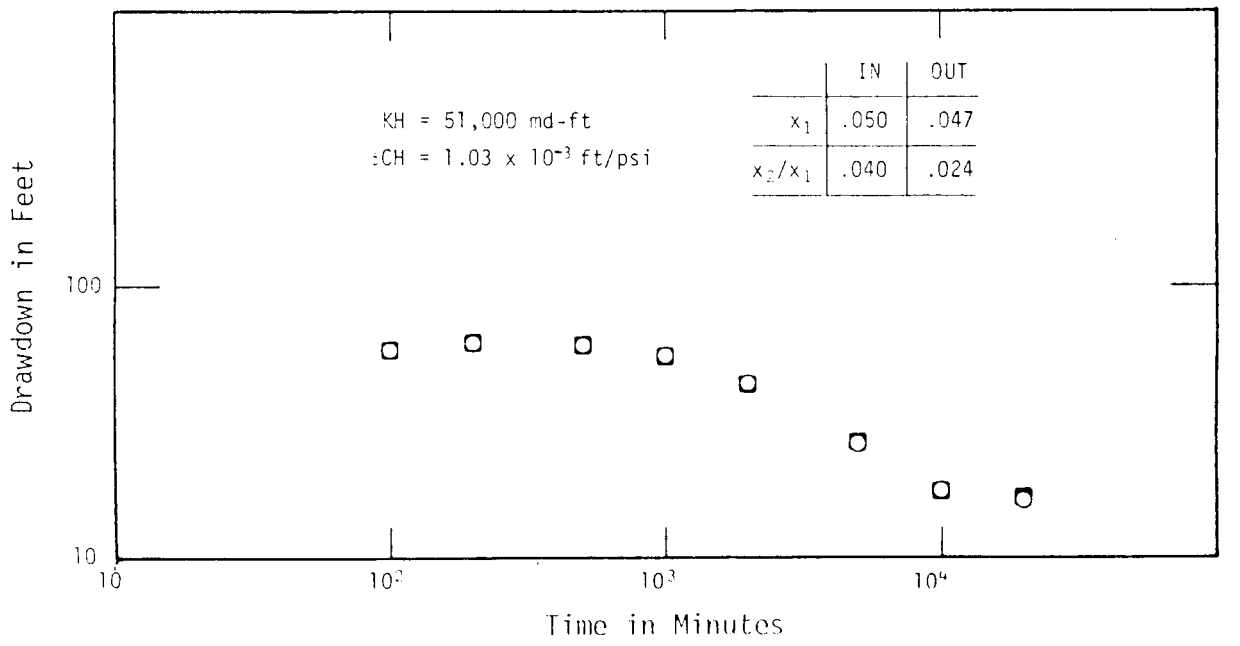

Figure 2. Exponential Decay of Discharge

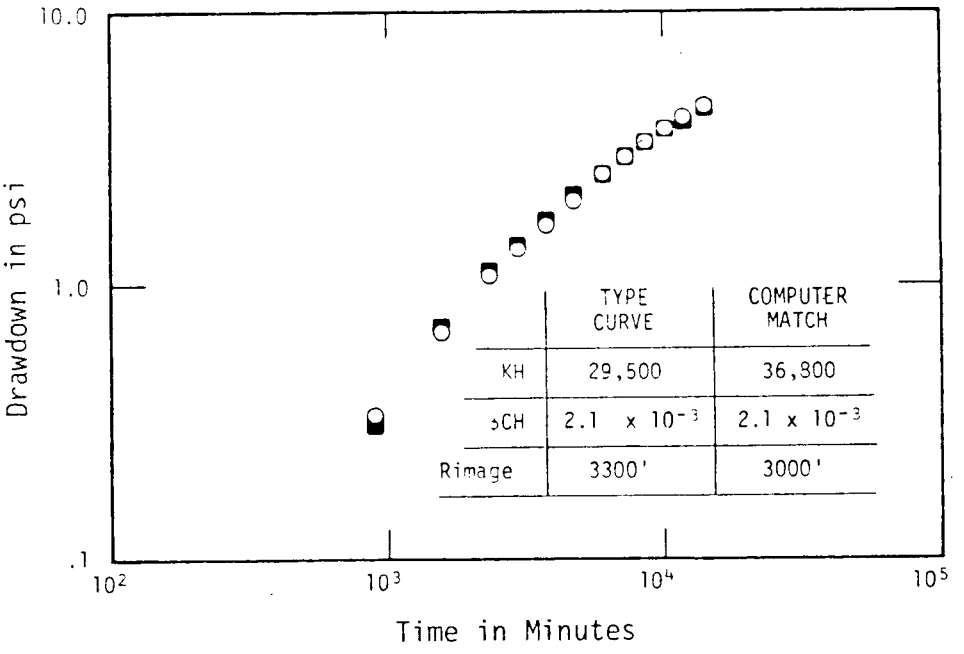

Figure 3. East Mesa 31-1 Interference Test

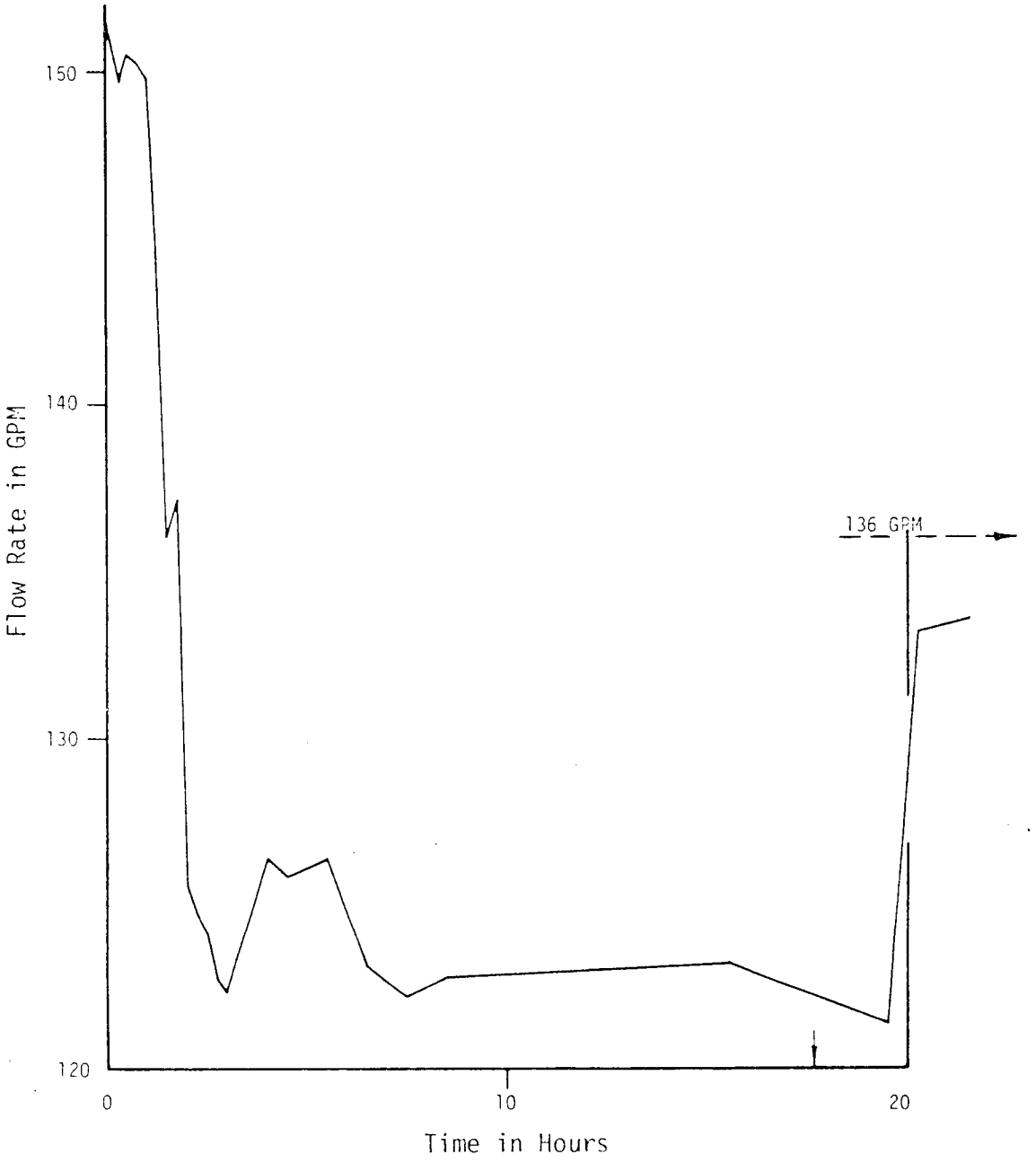

Figure 4a. RRGE 3 Production History

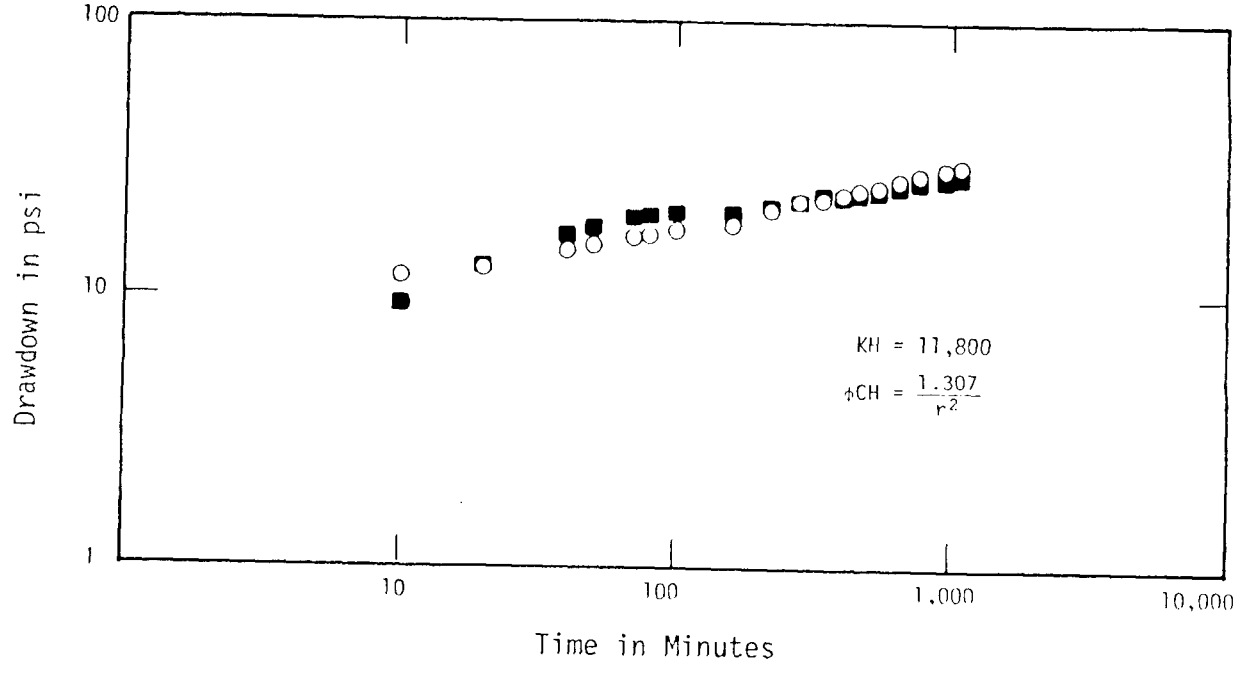

Figure 4b. RRGE 3 Production Test

RESERVOIR TESTING USING SIMULTANEOUS MEASUREMENTS IN MORE THAN ONE WELL

C. F. Tsang and R. C. Schroeder
Lawrence Berkeley Laboratory
University of California
Berkeley, California 94720

The results of a preliminary study of transient well test analysis using simultaneous pressure measurements in two wells is reported. Using the simultaneous measurements from production-injection or production-production doublets results in a straight line plot of the ratio

$$\frac{\Delta P_1 - \Delta P_2}{q_1 - q_2}$$

versus a function of time. The straight lines are the results of cancellation of terms when the contribution from the two wells are combined, as will be shown below. The use of simultaneous well test analysis can be used in conjunction with single well analysis methods to provide redundant estimates for the effective formation parameters, and for non-linear effects.

In this report we will assume an infinite reservoir with the well represented by a line-source approximation (Theis Curve). The solution is given by*

$$\Delta P = \frac{q}{4\pi T} \; Ei\left(-\frac{Sr^2}{4Tt}\right) \tag{1}$$

The transmissivity is determined by

$$T = \frac{kh}{\mu} \tag{2}$$

and the storativity is determined by

$$S = \phi c h \tag{3}$$

The principle of linear superposition of pressure is used to write the drawdown for two wells as the sum of two Theis (line source)

*See the Appendix for symbol definition

function (Eq. 1). When two wells labeled 1 and 2 are separated by a distance D and have identical formation properties and both wells begin flowing at time $t = 0$ we have for the drawdown at well 1

$$\Delta P_1 = \frac{q_1}{4\pi T} \; Ei\left(-\frac{S}{4T}\frac{r_w^2}{t}\right) + \frac{q_2}{4\pi T} \; Ei\left(-\frac{S}{4T}\frac{D^2}{t}\right) \tag{4}$$

with a similar equation for well 2. The behavior of ΔP_1 is shown in Figure 1. When $q_1 \neq -q_2$ the behavior of ΔP_1 is linear with t. But when $q_1 = -q_2$ the drawdown ΔP_1, tends to a constant value as t increases. This functional dependence is explainable when the exponential integral is expanded as the sum of a log function plus an infinite series. Thus, for large values of t

$$\Delta P_1 \longrightarrow \frac{q}{4\pi T} \ln\left(\frac{r_w^2}{D^2}\right) \tag{5}$$

With values of quantities used given by Table 1, this limit is found to be 1.275 MPa. From Equation (5) it is clear that the limiting value of ΔP_1 gives only T but not S, and from Figure 1 we see that the asymptotic value is not reached for about 1 week.

A more useful function which gives both S and T and can give these values in 1 or 2 days of well testing is defined by

$$\frac{\Delta P_1 - \Delta P_2}{q_1 - q_2} = \frac{1}{4\pi T}\left[Ei\left(-\frac{S}{4T}\frac{r_w^2}{t}\right) - \left(Ei - \frac{S}{4T}\frac{D^2}{t}\right)\right] \tag{6a}$$

$$\approx \frac{1}{4\pi T}\left[2\ln\left(\frac{r_w}{D}\right) - \frac{S}{4T}\left(r_w^2 - D^2\right)\frac{1}{t} + \frac{1}{2}\left(\frac{S}{4T}\right)^2\left(r_w^4 - D^4\right)\frac{1}{t^2}\right] \tag{6b}$$

Note the interesting point that the righthand side of the equation is independent of q_1 and q_2.

In Figures 2a and 2b the exact functional dependence (Eq. 6a) is shown where the straight line defines both S and T. In Figure 2 we see that in the absence of barriers or inhomogeneities the straight line segment is well defined within half to two days of testing, using values of S and T given in Table 1.

When this same problem is considered with the exception that well 2 begins flowing at $t = t_1 > 0$ while for well 1 the flow begins at $t = 0$, we have the approximate expression for large times given by

$$\frac{\Delta P_1 - \Delta P_2}{q_1 - q_2} \approx \frac{1}{4\pi T}\left[\ln\left(\frac{r_w^2}{D^2}\right) - \frac{S}{4T}\left(\frac{r_w^2 - D^2}{q_1 - q_2}\right)\left(\frac{q_1}{t_1 + \Delta t} - \frac{q_2}{\Delta t}\right)\right.$$
$$\left. + \frac{1}{2}\left(\frac{S}{4T}\right)^2\left(\frac{r_w^2 - D^2}{q_1 - q_2}\right)\left(\frac{q_1}{(t_1 + \Delta t)^2} - \frac{q_2}{\Delta t^2}\right)\right] \qquad (7)$$

Figures 3a and 3b display the time dependence of the drawdown difference function (using the correct expression in terms of exponential integrals) when plotted against a function of the time, i.e.

$$\left(\frac{q_1}{t_1 + \Delta t} - \frac{q_2}{\Delta t}\right)\frac{1}{(q_1 - q_2)}$$

Again the straight line is well defined for $\Delta t > 10$ hours ($t_1 = 3$ days).

When we consider buildup tests using simultaneous well measurements, we have for the drawdown function,

$$\frac{\Delta P_1 - \Delta P_2}{q_1 - q_2} = \frac{1}{4\pi T}\left[Ei\left(-\frac{S}{4T}\frac{r_w^2}{t_1 + \Delta t}\right) - Ei\left(-\frac{S}{4T}\frac{r_w^2}{\Delta t}\right)\right.$$
$$\left. - Ei\left(-\frac{S}{4T}\frac{D^2}{t_1 + \Delta t}\right) + Ei\left(-\frac{S}{4T}\frac{r_w^2}{\Delta t}\right)\right] \qquad (8)$$
$$\approx \frac{S}{16\pi T^2}\left(r_w^2 - D^2\right)\left(\frac{t_1}{t_1 + \Delta t}\frac{1}{\Delta t}\right)$$

where t_1 is the flowing time before shut-in. We see from the approximate function expansion in (8) that the function passes through the origin with slope

$$\frac{S}{16\pi T^2}\left(r_w^2 - D^2\right) \qquad (9)$$

when plotted as a function of

$$\frac{t_1}{t_1 + \Delta t}\frac{1}{\Delta t}$$

In Figures 4a and 4b we see that the straight line is well established after about 10 hours.

The usual individual well buildup curves are also obtained in the case of simultaneous measurements, that is

$$\Delta P_1 \approx \left(\frac{q_1 + q_2}{4\pi T}\right) \ell n\left(\frac{\Delta t}{t_1 + \Delta t}\right) + \frac{1}{4\pi T}\left(\frac{S}{4T}\right)\left(\frac{t}{t_1 + \Delta t}\right)\left(\frac{1}{\Delta t}\right)\left(q_1 r_w^2 + q_2 D^2\right) \quad (10)$$

The dependence of ΔP_1 is shown in Figure 5 and is approximately linear in $\ell n \frac{\Delta t}{t_1 + \Delta t}$ for times longer than about 3 days. However, since we could obtain $\frac{S}{T^2}$ from Figure 4, the linear term in Equation (10) may be subtracted from the measured value of ΔP_1, and we extend the straight line log plot to times as short as a few hours indicated by the dashed line in Figure 5, for the case of $q_1 = 0.02 \frac{m^3}{s}$ and $q_1 = -0.6\ q_1$. The value of T can then be obtained from the dashed line by determining its slope (or from a similar plot for ΔP_2) and S may be obtained from Figure 4 by evaulating the ratio of $\frac{S}{T^2}$ (see Equation 9).

Situations will be much simpler if we set $q_1 = -q_2$, i.e., for an injection-production doublet. In this case, the first term in Equation (10) drops out and a straight line plot against $\frac{t}{t + \Delta t}\ \frac{1}{\Delta t}$ is obtained after only a few hours.

In simultaneous well test analysis skin and wellbore storage effects can be handled in a simple manner. Consider first only skin effect, then

$$\Delta P_1 = \frac{q_1}{4\pi T}\left[Ei\left(-\frac{S}{4T}\frac{r_w^2}{t}\right) + 2s_1\right] + \frac{q_2}{4\pi T}, Ei\left(-\frac{S}{4T}\ \frac{D^2}{t}\right) \quad (11)$$

with a similar equation for ΔP_2. When we form the function

$$\frac{\Delta P_1 - \Delta P_2}{q_1 - q_2}$$

we have

$$\frac{\Delta P_1 - \Delta P_2}{q_1 - q_2} = \frac{1}{4\pi T}\left[Ei\left(-\frac{S}{4T}\frac{r_w^2}{t}\right) - Ei\left(-\frac{S}{4T}\frac{D^2}{t}\right)\right] + \frac{1}{2\pi T}\left(q_1 s_1 - q_2 s_2\right) \quad (12)$$

Thus, the function

$$\frac{\Delta P_1 - \Delta P_2}{q_1 - q_2}$$

when plotted against $\frac{1}{t}$ is a straight line (see Equation 6) with intercept

$$\frac{1}{4\pi T} \ell n\left(\frac{r_w^2}{D^2} + 2 \cdot \frac{q_1 s_1 - q_2 s_2}{q_1 - q_2}\right)$$

When we also analyze ΔP_1 and ΔP_2 separately and combine the results with the analysis of

$$\frac{\Delta P_1 - \Delta P_2}{q_1 - q_2}$$

we obtain not only the formation parameters T and S, but the skin effects s_1 and s_2 also.

In the case of wellbore storage the drawdown can be written

$$\Delta P_1 = \Delta P_1(C=0) - \frac{q_1 C_1}{4\pi T} \int_0^t \frac{\partial \Delta P_1}{\partial t'} \left(\frac{e^{-\frac{S}{4T}\frac{r_w^2}{t-t'}}}{t-t'}\right) dt' \qquad (13)$$

where we have used the instantaneous line source formulation and the relationship between sand-face flow rate and time given by

$$q_{SF} = q\left(1 - C\,\frac{\partial \Delta P}{\partial t}\right) \qquad (14)$$

C is the wellbore storage coefficient. A similar expression can be written for ΔP_2, and it can be shown that for small t

$$\frac{\partial \Delta P_1}{\partial t} \approx \frac{1}{4\pi T}\, q_1 \left(\frac{e^{-\frac{S}{4T}\frac{r_w^2}{t}}}{t}\right) \qquad (15)$$

Substitution of (15) into (13) gives

$$\Delta P_1 \approx \Delta P_1\ (C=0) - \left(\frac{q_1^2 C_1}{4\pi^2 T S r_w^2}\right) A(u)$$

where the function of $A(u)$ is defined by

$$A(u) \equiv \int_0^u \left(\frac{e^{-\frac{1}{u'}}}{u'}\right)\left(\frac{e^{-\frac{1}{u-u'}}}{u-u'}\right) du' = \left(\frac{2}{u}\right)\left(e^{-\frac{2}{u}}\right) K_0\left(\frac{2}{u}\right)$$

However, if we note that C is the wellbore storage constant, i.e., the fluid storage capacity in the wellbore (cc/atm), it follows that for identical formation parameters S and T, and for wells of equal radius and height the wellbore storage terms approximately cancel when the function $\frac{\Delta P_1 - \Delta P_2}{q_1 - q_2}$ is formed.

The central theme of this report has been the advantage of using two simultaneous well measurements whenever possible. The reasons for this are that

1. Redundant, independent estimates for formation properties can be obtained,
2. Wellbore storage effects will cancel in certain cases, and skin effects may be determined,
3. Orientation and distance of linear boundaries relative to the two wells can be obtained in one set of measurements. (This has also been worked out, though not presented in this summary.)
4. In many cases straight line approximations are valid within one or two days of testing.

APPENDIX

Symbols:

p	Pressure
q	Volumetric flow rate
$\Delta P = P - Po$	Drawdown
r	Radial distance
t	Time
k	Permeability
h	Formation thickness
μ	Fluid viscosity
ϕ	Porosity
c	Compressibility (total)
D	Distance between the two wells
$\ell n(\gamma)$	Euler's constant = 0.57722. . .
C	Wellbore storage constant
s	Skin effects

Subscripts:

o	Initial value
w	Wellbore value

Functions:

$\ell n(x)$	Natural log of x
$-Ei(-x)$	Exponential Integral of x defined by

$$-Ei(-x) = \int_0^x \frac{e^{-u}}{u}\, du$$

where u is a dummy variable.

$K_0(x)$	The modified Bessel function of the second kind of order zero.

TABLE I

Parameters Used in Calculations in this Paper

$r_w = 0.1$ m

$D = 300$ m

$T = 5 \times 10^{-8}$ $(m^3/s)\frac{1}{Pa}$

$\frac{S}{T} = \frac{1}{3}$ s/m^2

$q_1 = 0.02$ m^3/s

$q_2 = q_1, -0.8\ q_1, -0.6\ q_1$

$t_1 = 3$ days

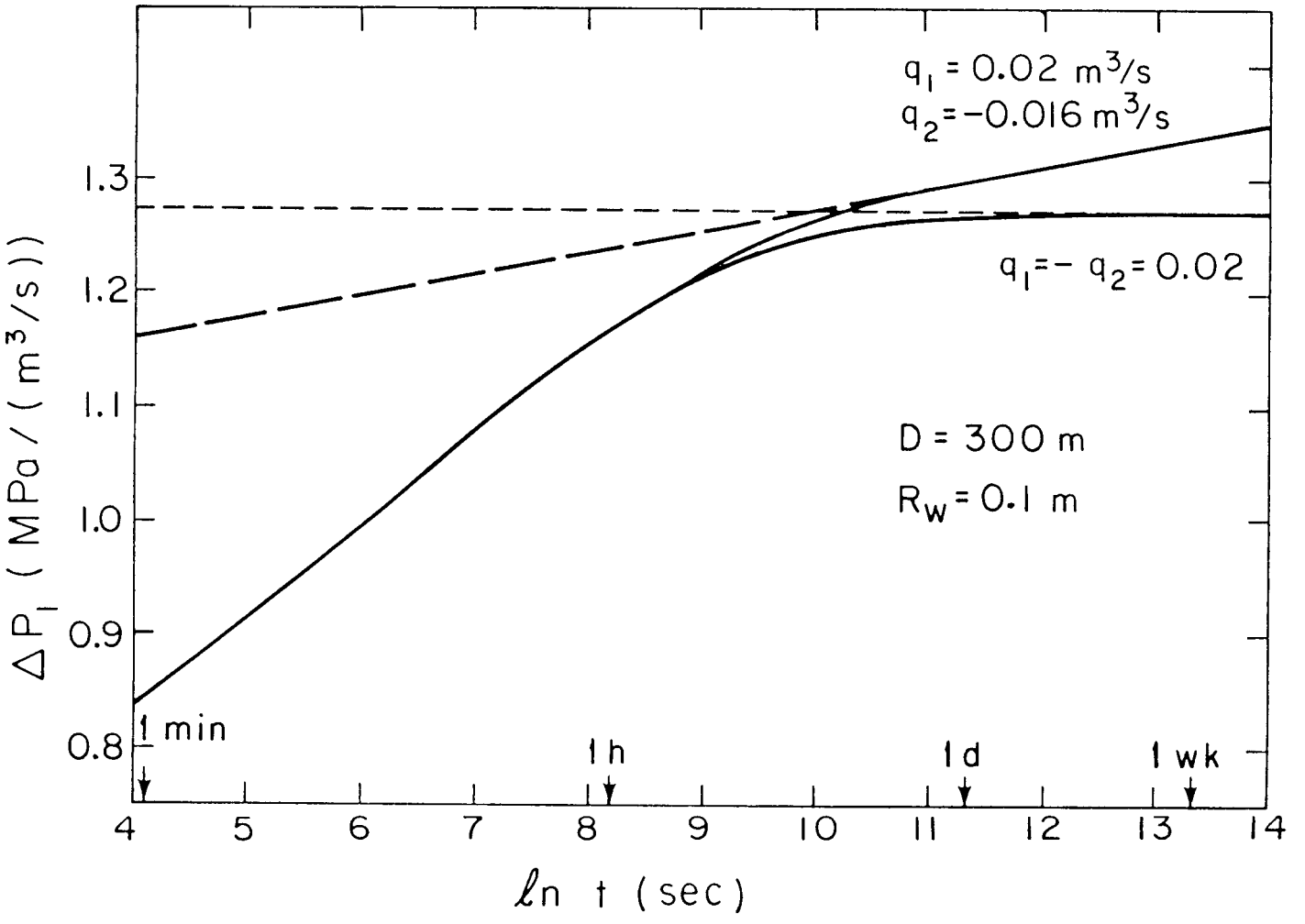
$q_1 = 0.02\ m^3/s$
$q_2 = -0.016\ m^3/s$
$q_1 = -\ q_2 = 0.02$
D = 300 m
R_w = 0.1 m
ΔP_1 (MPa / (m^3/s))
1.3
1.2
1.1
1.0
0.9
0.8
1 min
1 h
1 d
1 wk
4
5
6
7
8
9
10
11
12
13
14
ℓn t (sec)
XBL7612-11199

Figure 1.

Figure 2a.

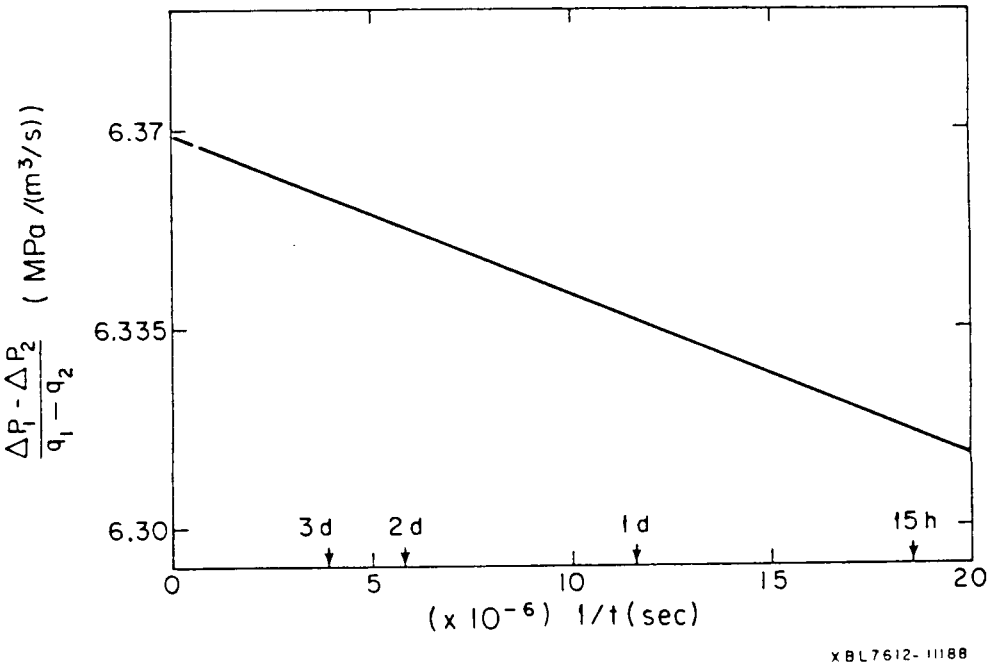

Figure 2b.

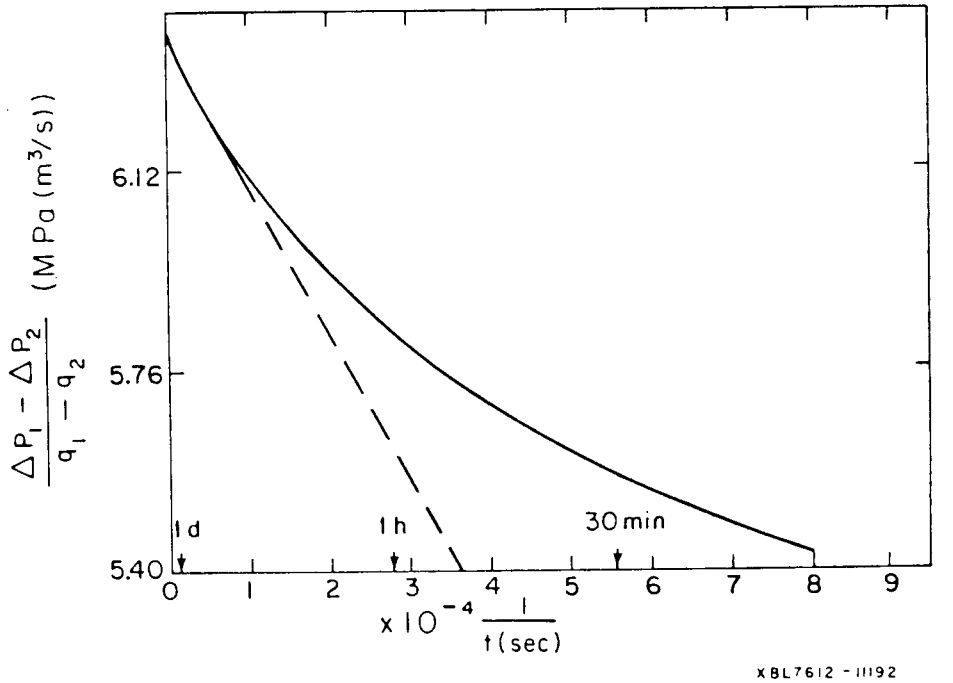

Figure 3a

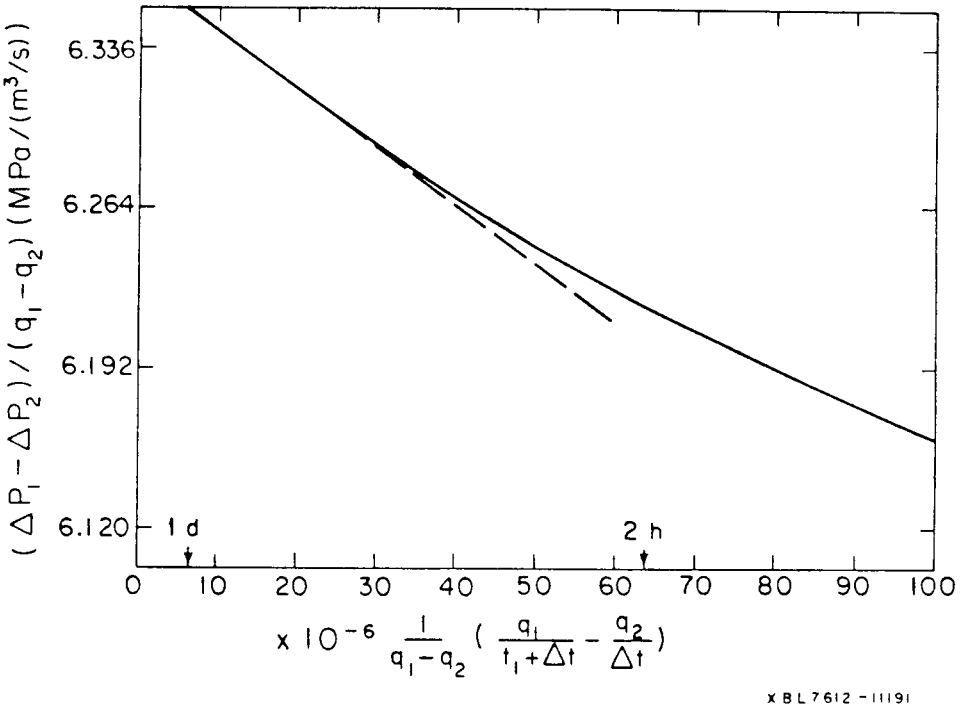

Figure 3b

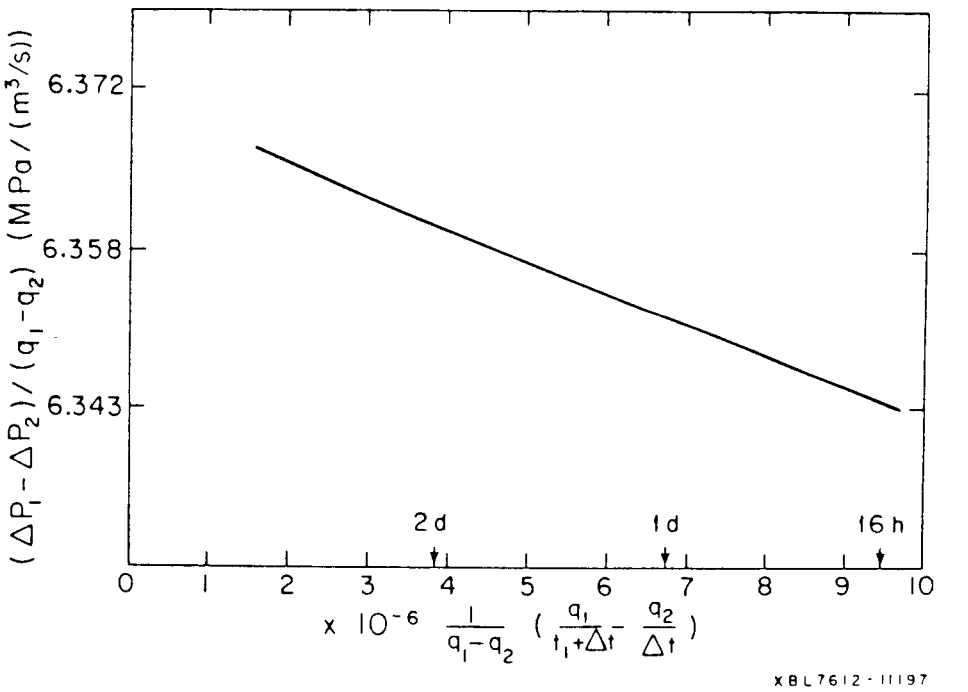

Figure 4a.

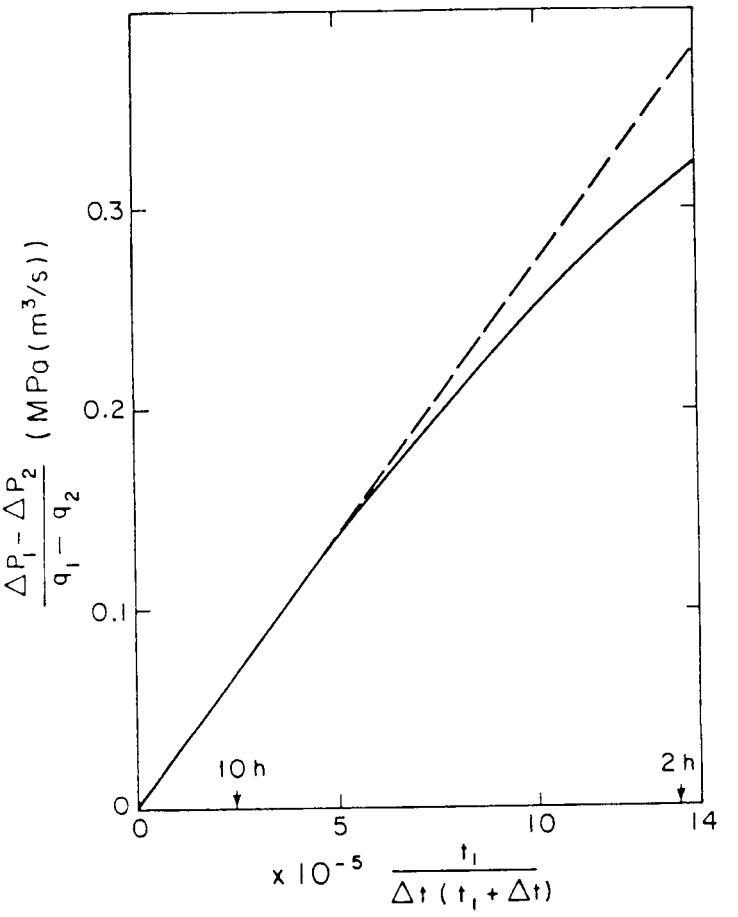

XBL7612-11193

Figure 4b.

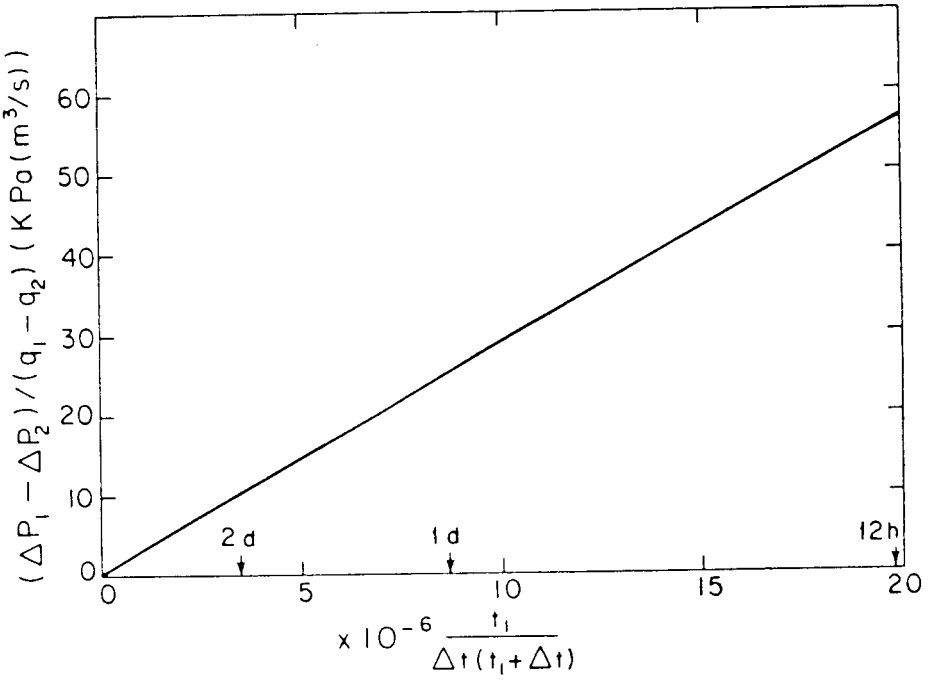

XBL7612-11194

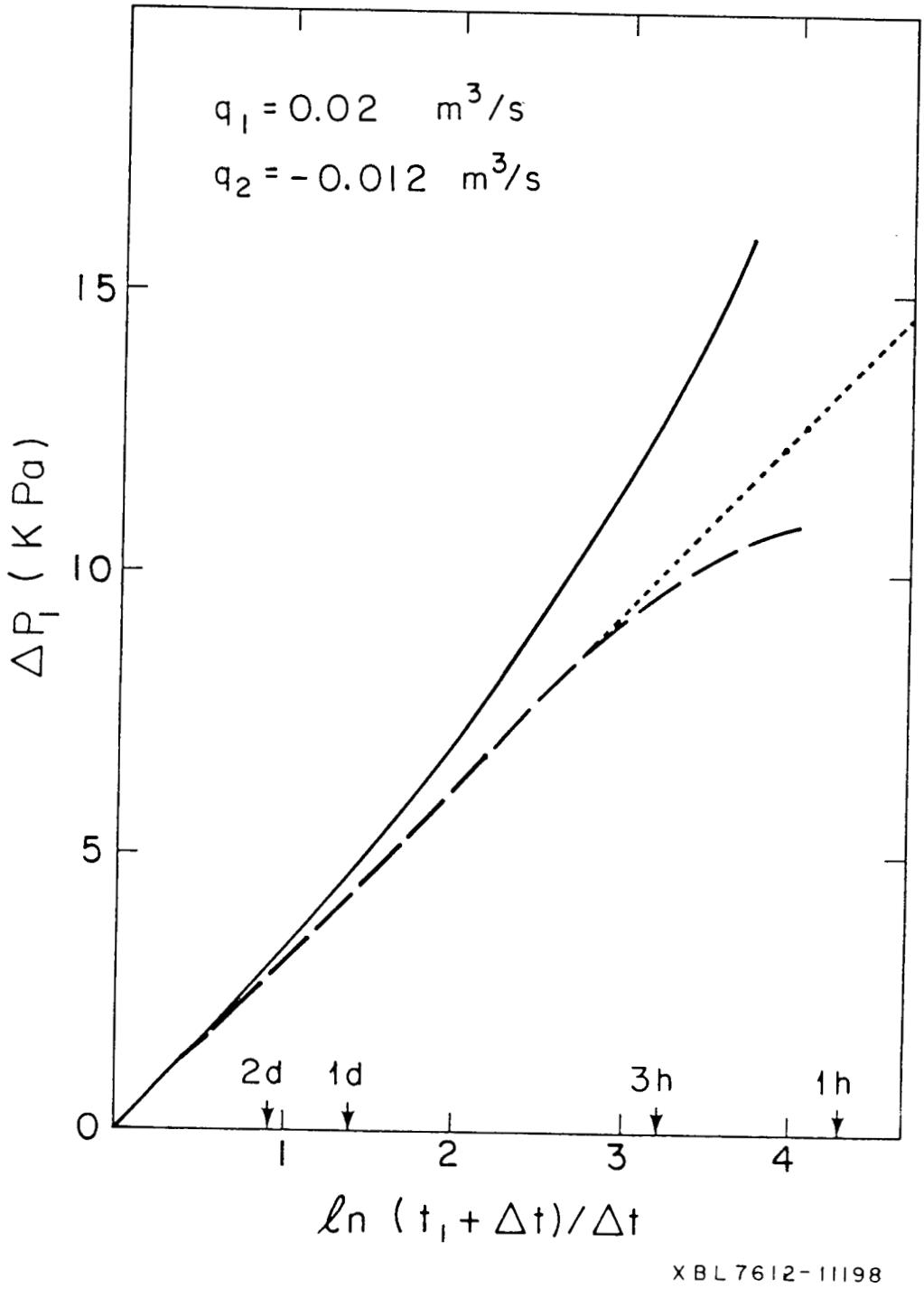
$q_1 = 0.02 \quad m^3/s$
$q_2 = -0.012 \quad m^3/s$
15
10
5
0
ΔP_1 (K Pa)
2d
1d
3h
1h
1
2
3
4
$\ell n\ (t_1 + \Delta t)/\Delta t$
XBL 7612-11198

Figure 5.

FUTURE WELL TESTING AND INJECTION AT THE EAST MESA FIELD

K. E. Mathias
U. S. Bureau of Reclamation
P. O. Box 416
Holtville, CA 92250

The Bureau of Reclamation has established an ongoing program for the analysis and evaluation of the East Mesa Geothermal Field. This presentation will discuss the recent history of the field including testing methods and results. Future testing plans will also be discussed.

The East Mesa Field

Located from various geophysical studies including heat flow, gravity, seismic noise, and resistivity, the field lies on the east flank of the Salton trough. Mesa 6-1 was drilled to a depth of 2443 meters in 1972 at a common anomaly to the above geophysical parameters. The well was initially completed by a hanging slotted liner and later the uphole casing was perforated opposite permeable sand horizons. Produced fluid is of a sodium chloride type having a total dissolved solids (TDS) content of 26,300 mg/1 (unflashed wellhead sample).

Mesa 6-6 was drilled as a step-out well one-fourth mile west of Mesa 6-1. Completed to 1916 meters, produced fluid is of the sodium chloride type having a TDS content of 5000 mg/1 (unflashed wellhead sample).

In 1974 three additional wells were drilled, based on additional heat flow and seismic monitoring work. These wells are designated Mesa 5-1, Mesa 8-1, and Mesa 31-1. They flow a sodium chloride type water with a TDS content of about 2500 mg/1.

Table 1 describes the casing and completion program of each well. Well locations are shown in Figure 1.

Well Testing

Flow Testing. The portable flash tank and weir box has been most useful in obtaining flow information at East Mesa wells. A pipeline is connected directly to the flash tank from the well where fluid is flashed to atmospheric conditions. Steam from the well bore and flashoff evolve from the flash tank. Liquid passes into a weir

box where level over a V-notch weir is measured. Clock-driven pressure, temperature, and level gauges monitor surface conditions, and calculations are made to determine total well flow. This technique was described by Mathias in 1975. Flow tests have been performed at all wells and represent conditions which exist at the wellhead during flows at various rates for a total flow period of several days. Low flow conditions are generally not at pressure, temperature or flow equilibrium due to the extended time required to heat surrounding uphole rock formations.

Pressure Testing. Downhole pressures have been measured using standard oil field type mechanical clock-driven recording instruments. In addition, a very sensitive downhole quartz pressure gauge was used to conduct interference tests in the East Mesa Field. This test was reported by Witherspoon, Narasimhan, and McEdwards in 1976. The results of mechanical gauge work and electronic precision gauge work were combined with flow data and used to evaluate and model the East Mesa Reservoir (TRW-Intercomp, 1976). The results of this work are presented elsewhere in these proceedings (Spivak and Rice, 1976).

Temperatures. Surface and downhole temperature have been measured both at shut-in and under flowing conditions. Standard oil-field type mechanical clock-driven recording instruments have been used for downhole measurements. A summary of bottomhole temperatures at shut-in equilibrium conditions is shown on Table 2.

Injection Operations

Mesa 5-1 has been used as an experimental injection well. It was located in an area of low heat flow and approximately two kilometers from the nearest microearthquake epicenter (Combs, 1974). The lower 305 meters were slotted opposite sand horizons having an average Saraband permeability of 69 millidarcies. During initial tests, water having a TDS of 50,000 mg/l and a dissolved oxygen content of 6.9 mg/l was injected. After 48 hours of pumping at a rate of 1000 m^3/day, water level reached the surface and pressure pumping began. At the end of ten days, surface pressure had risen to about 5.5 bars gauge. Average injection pumping was then 400 m^3/day. Intermittent pumping was then begun, as required pressure was above pumping equipment capacity on hand. Surface pressure varied between 0 and 14 bars while pumping intermittently at a wide range of rates. A summary of injection activities from February 28 through April 2, 1975 is tabulated on Table 3.

An average of 0.0923 grams per liter suspended solids was measured in the injection fluid. A sample of the fluid filtrate was analyzed by X-ray diffraction techniques. The primary constituents were found to be quartz, clay-sized particles, and other material that would be wind blown into a pond in a desert area. From the above concentration value, a total weight of 1030 kilograms of solid material is calculated to have been pumped down the well.

Piping at the test site was revised so that fluid blowdown from geothermal operations would be transported directly into the injection system with minimal contact to air and no contact with the brine holding pond. As high corrosion was noted in the lower portion of the downhole wireline equipment, it was suspected that corrosion damage to the casing may have resulted. A Schlumberger casing thickness log was run in December of 1975 and no damage was detected.

A high pressure pump of capacity to pump up to 138 bars gauge pressure at 1088 m^3/day was added to the wellhead. Fluid was injected using this pumping arrangement from January 14, 1976 to January 28, 1976. A summary of wellhead pressures is shown on Figure 2. It was noted that at a pressure of near 85 bars gauge, wellhead pressure decreased. Sufficient pumping capacity was not available to increase the volume of fluid injected to maintain the 85 bars gauge wellhead pressure.

In May, 1976, the injection well was acid treated with 38 m^3 of 15% HCl, 38 m^3 of mud acid, and 19 m^3 of 5% HCl. Short term pumping concluded that the treatment had resulted in improved acceptance characteristics of the well.

Future Testing

General. A testing program involving all operators at the East Mesa Field is scheduled for early 1977. The testing program will search two main areas. First, a flow profile test for each well connected into a disposal system (Mesa 8-1, 6-1, and 6-2) will be run to ascertain the latest characteristics of the wells at low flow rates. As these wells will be used to supply the ERDA test pad at the test site, it is important to know each well characteristic at the range of flows to be utilized. The second parts of tests involves interference tests. The details of this test program are outlined below. This testing program and others in the future will involve other equipment and programs at the site. These include injection, seismic monitoring, chemical, and other geophysical monitoring. These will also be discussed in detail.

Interference Testing. The interference test will be of a duration of at least 30 days. Precision quartz pressure gauges will be placed in select wells operated by Republic, Magma Power Co., and the Bureau. The Bureau's production well Mesa 6-2 will be operated at a low flow rate (about 800 m^3/day). Magma Power Company will provide a continuously recording surface readout downhole capillary type pressure gauge to be placed in this well. Fluid will be injected at well Mesa 5-1. The effects of pressure drawdowns and buildups in the field will be analyzed and used to refine the already existing model developed by TRW and Intercomp.

Precision pressure gauges, operating personnel and analysis of results will be supplied by Lawrence Berkeley Laboratory.

Injection Equipment. Fluid conveyed to Mesa 5-1 wellsite will be moved downhole by a high speed centrifugal pump. Bypass equipment has been installed at the pump to maintain a steady and optimum flow of about 1088 m^3/day at 60 bars pressure through the pump while allowing less fluid to be injected. The Mesa 5-1 wellhead is fully instrumented to indicate wellhead pressure, temperature, flowrate, and totalized flow. This apparatus is shown on Figures 3 and 4.

Seismic Monitoring. The Bureau six-station seismic monitoring array is situated within an area of about 6 km radius of the test site office. Each station is comprised of three component seismometers of which signals are telemetered by FM radio link to the Bureau office. The data is recorded on magnetic tape at that location. Correlation between seismic activity and reservoir parameters have been observed in the past. In one case, (Witherspoon, Narasimhan, McEdwards, 1976), 14 local seismic events in a time period of less than one hour corresponded directly to a rise in pressure in well Mesa 8-1 but not in Mesa 6-1. These events were located two to four miles east and northeast of Mesa 8-1. It is possible that a reservoir boundary prevented a pressure signal from being transmitted to Mesa 6-1. Differing frequency content and anomalous travel time delays from events occurring outside the field have led us to believe that there exists an anomalous region in the East Mesa Field (Combs, 1975). A set of calibration blasts was arranged to learn more about this phenomena; the results of this work are not yet completed.

Seismicity in the Imperial Valley has been seen to affect the chemical content of wells during production. The most remarkable change has been the association of area seismic activity with increases in wellhead CO_2 at Mesa 6-2 during production. Additional seismic recording equipment is being installed to help further define this observation.

REFERENCES

1. Combs, J., 1974; Microearthquake Investigation of the Mesa Geothermal Anomaly, Imperial Valley, California, Report prepared for Bureau of Reclamation, Lower Colorado Regional Office under Contract Number 14-06-300-2390.

2. Combs, J., 1975; Microearthquake Studies Before and During Fluid Withdrawal and Reinjection Test; Mesa Geothermal Field, Imperial County, California, Report prepared for Bureau of Reclamation, Lower Colorado Regional Office under Contract Number 14-06-300-2563.

3. Mathias, K. E., 1975; The East Mesa Geothermal Field - A Preliminary Evaluation of Five Geothermal Wells, Second UN Symposium on the Development and Use of Geothermal Resources, San Francisco, Proceedings, Lawrence Berkeley Lab., University of California.

4. Spivak, A.; Rice, L. F., 1976; A Reservoir Engineering Study of the East Mesa KGRA, Second Workshop on Geothermal Reservoir Engineering, Stanford University, Proceedings.

5. Staff, 1976, TRW Defense and Space Systems Group, Intercomp, Inc.; Study of the Geothermal Reservoir Underlying the East Mesa Area, Imperial Valley, California, Report prepared for Bureau of Reclamation, Lower Colorado Regional Office under Contract Number 14-06-300-2604.

6. Witherspoon, P. A.; Narasimhan, T. N.; and McEdwards, D. G., 1976; Results of Interference Tests from Two Geothermal Reservoirs: Lawrence Berkeley Laboratory, Soc. Petroleum Engineers of AIME 51st Fall Meeting, New Orleans.

Table 1

Casing and Completion Records,
Geothermal Resource Investigations,
Imperial Valley, California

Mesa well number	Casing outside diameter (in.)	Depth interval (m)	Slotted interval (m)	Perforated interval (m)	Average Saraband sand permeability (md)
6-1	20	0-116			
	13 3/8	0-763			
	9 5/8	0-2223		2075-2179/1868-2075	230
	7	2213-2443	2238-2433		1.5
6-2	20	0-19			
	11 3/4	0-301			
	7 5/8	0-1816	1663-1816	1392-1662	70
5-1	20	0-18			
	13 3/8	0-312			
	7 5/8	0-1830	1525-1830		69
8-1	20	0-18			
	13 3/8	0-304			
	7 5/8	0-1829	1508-1829		39
31-1	20	0-18			
	13 3/8	0-309			
	7 5/8	0-1882	1652-1882		62

Table 2

Bottom-hole shut-in temperatures,
Geothermal Resource Investigations,
Imperial Valley, California

Mesa Well Number	Depth Measured (m)	Bottom-hole temperature (^{o}C)
6-1	2442	204
6-2	1816	188
5-1	1830	157
8-1	1830	179
31-1	1882	154

Table 3

Injection Schedule, Mesa 5-1,
February 28-April 2-1975

Date 1975	Time	Operation	Average flow rate (m^3/day)	Cumulative quantity flowed (m^3)
Feb. 28	1015	Begin Injection	1 090	0
Mar. 11	1730	Stop Injection	398	6 968
Mar. 11	1020	Begin Injection	398	-
Mar. 12	1745	Stop Injection	125	7 222
Mar. 12	1840	Begin Injection with Booster pump	1 281	-
	1330	Stop Injection	600	7 416
	1450	Begin Injection	441	-
	2100	Stop Injection	578	7 490
Mar. 13	0915	Begin injection	1 128	-
		Average flow during injection	273	
Mar. 25	1525	Stop Injection	343	11 184
Apr. 2	0955	Begin injecting shallow well water	300	-
Apr. 2	1300	Stop Injection	300	11 441

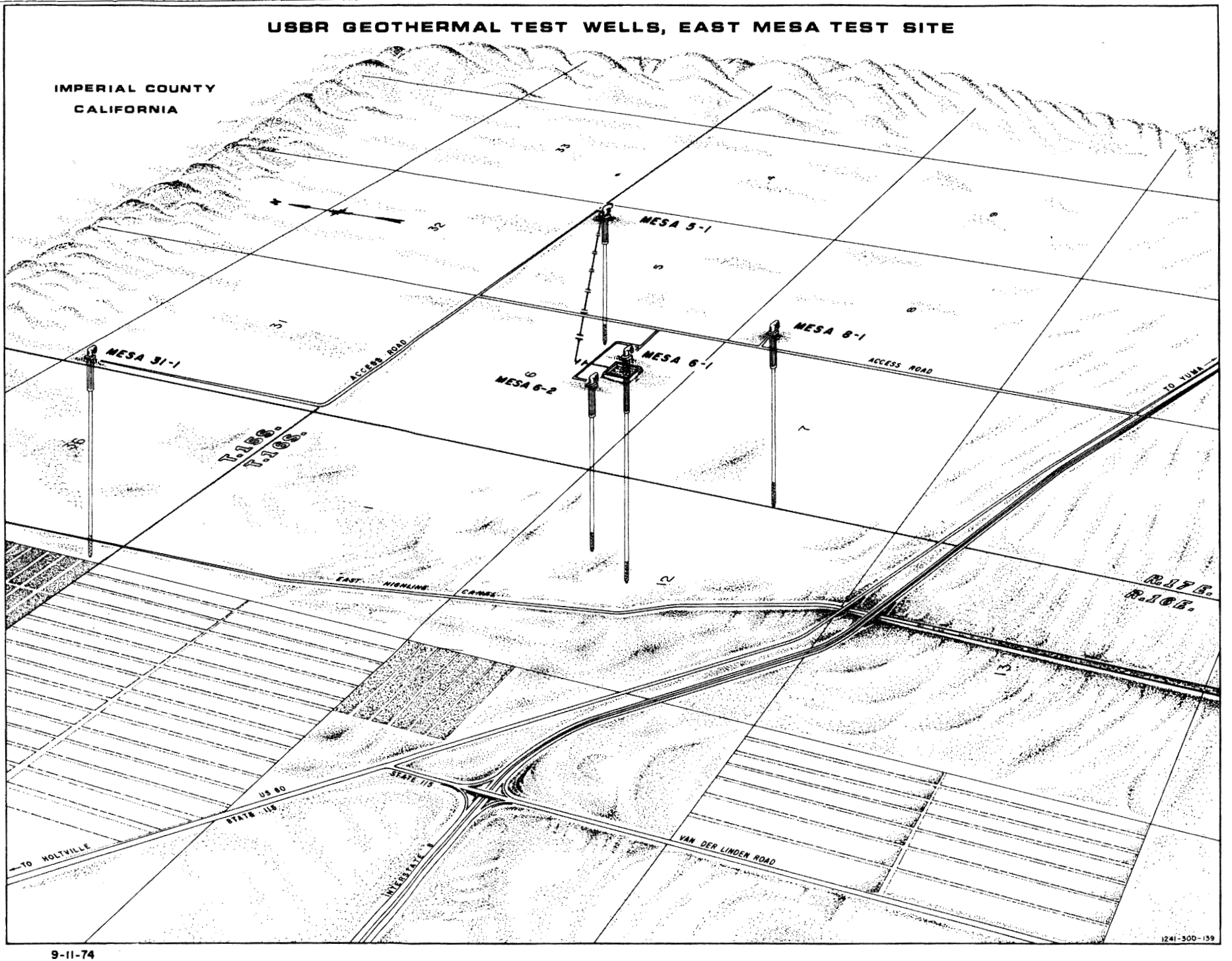

Figure 1. Locations of U.S. Bureau of Reclamation Geothermal Test Wells, East Mesa Test Site.

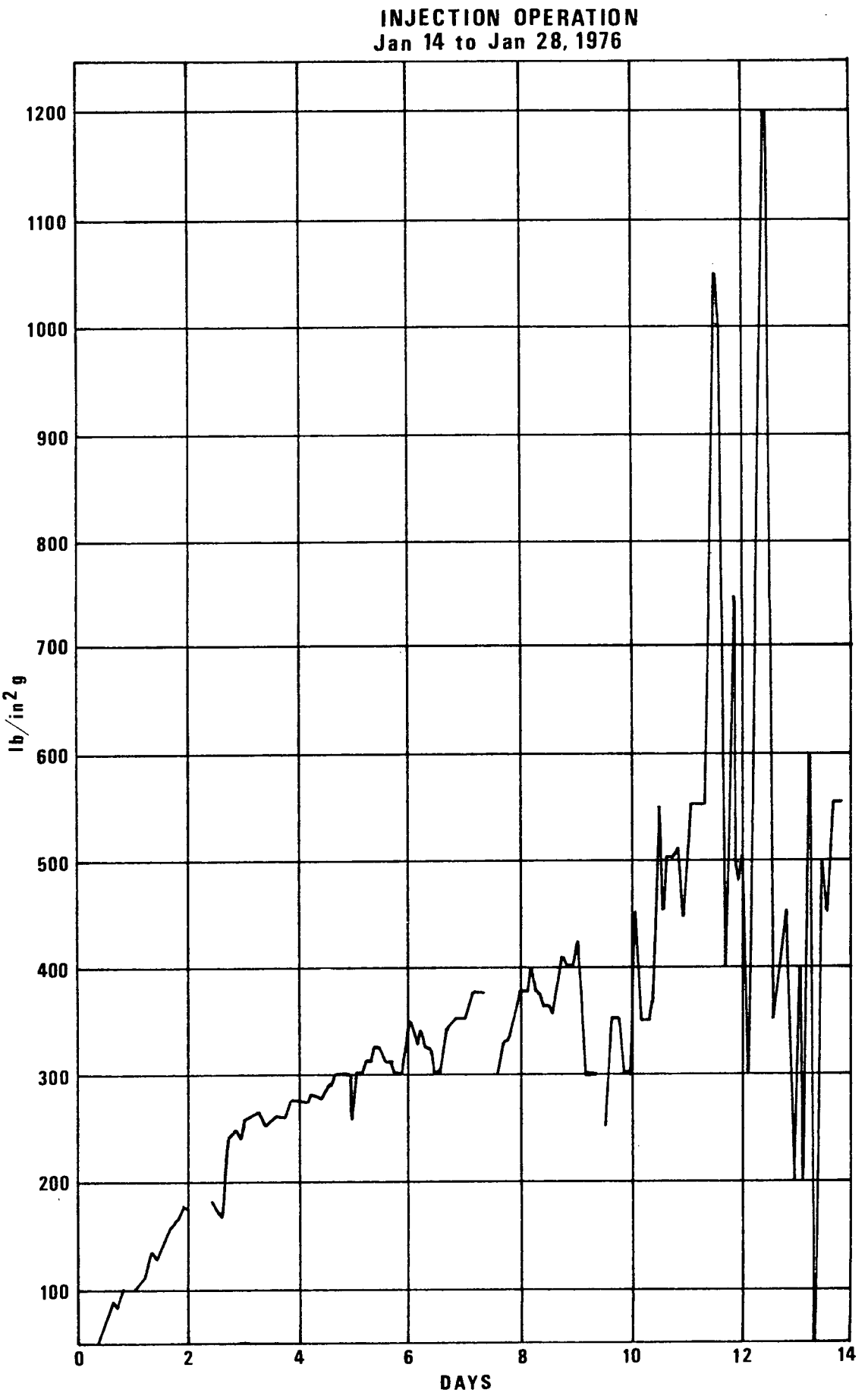

Figure 2. Summary of Well-head Pressures, Mesa 5-1 Injection, January 14 to January 28, 1976.

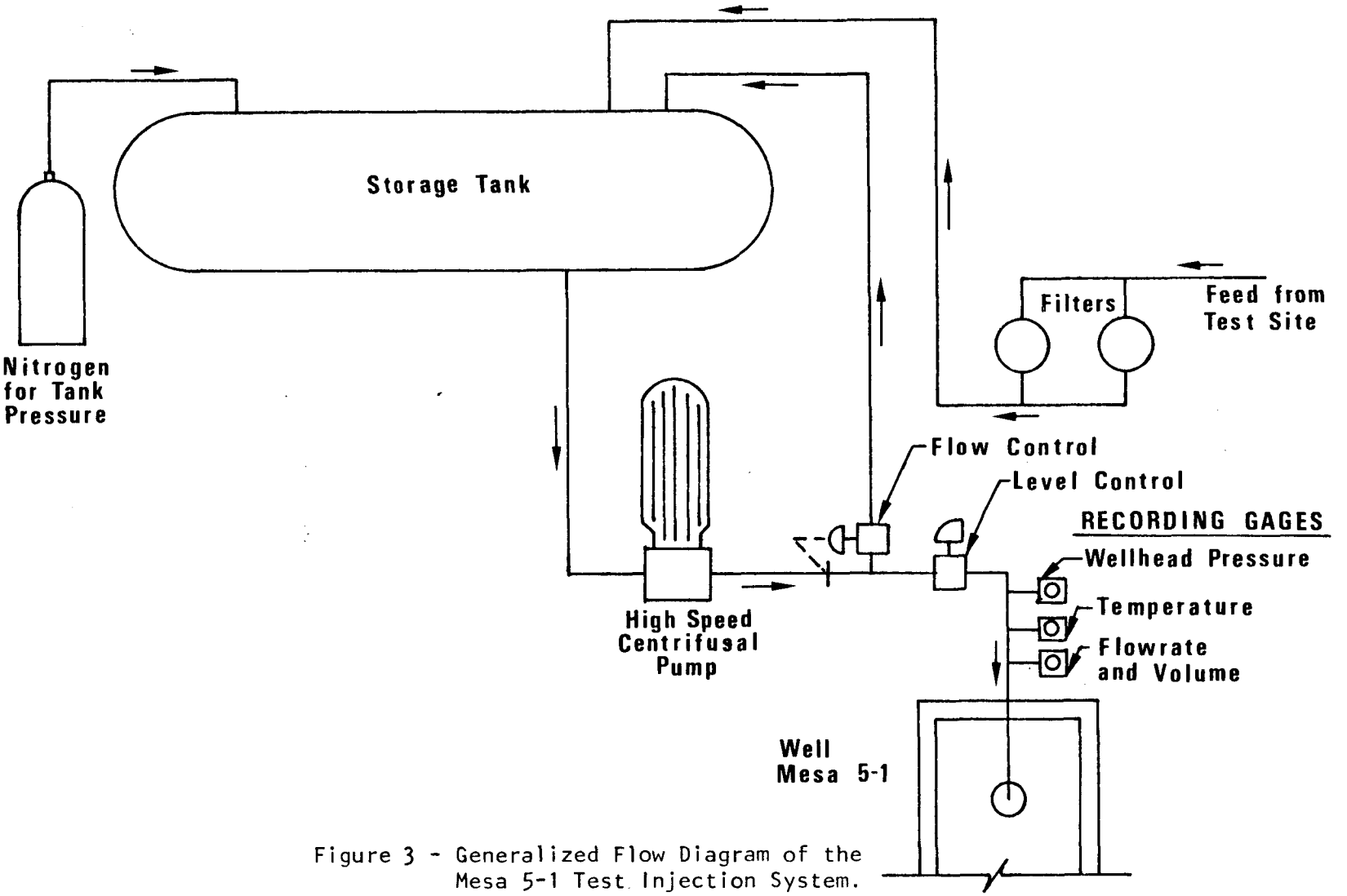

Figure 3 - Generalized Flow Diagram of the Mesa 5-1 Test Injection System.

Test Injection System

Fig. 4. Mesa 5-1 Test Injection System during Fabrication. Well Mesa 5-1 is out of view to the right.

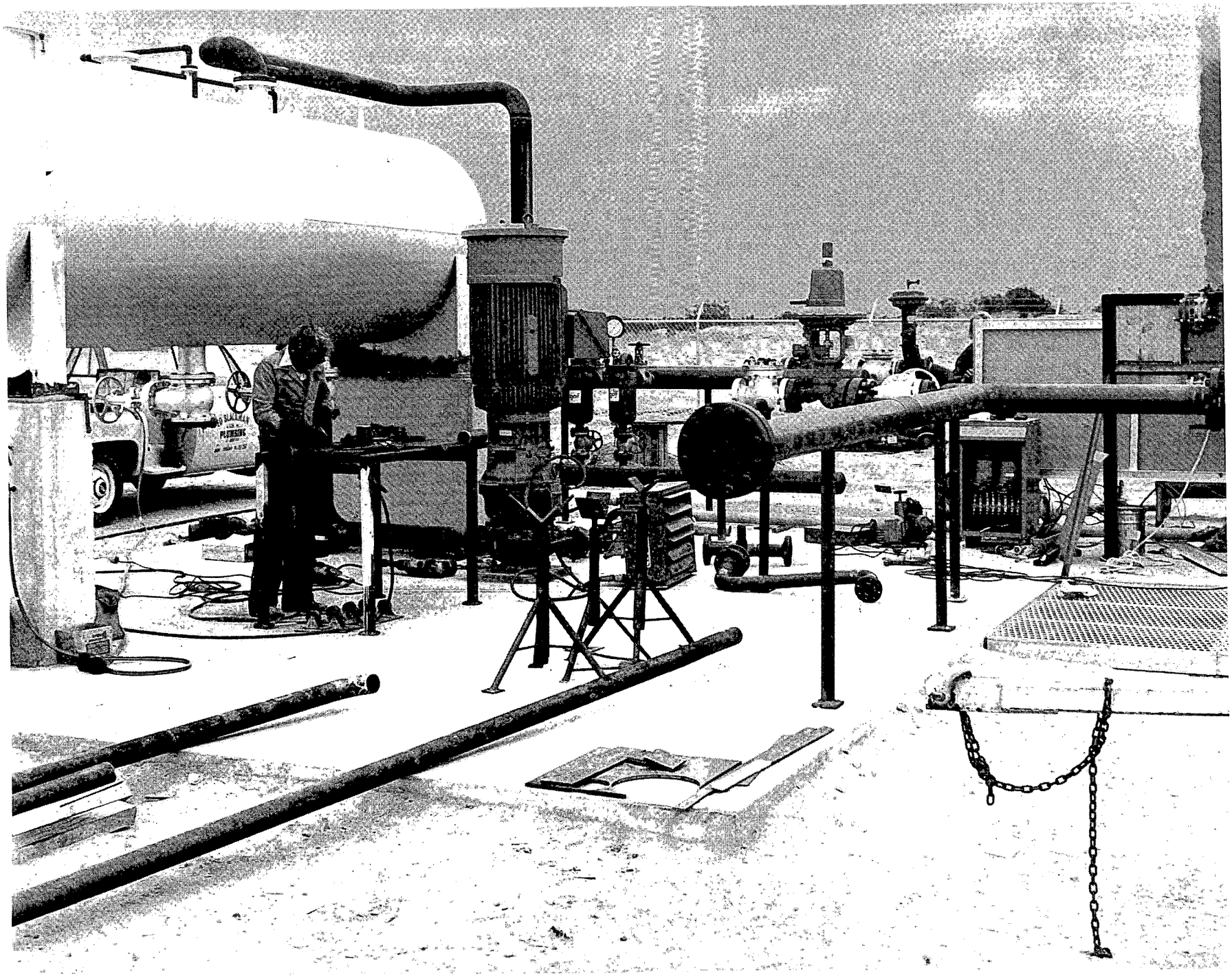

INSTRUMENTATION AND TEST RESULTS FOR HAWAII GEOTHERMAL PROJECT'S HGP-A WELL

Deane Kihara, Bill Chen, Patrick Takahashi
College of Engineering
University of Hawaii
Honolulu, Hawaii 96822

With the completion of the drilling of HGP-A and indications of extremely high bottom hole temperatures, the next major phase in the Hawaii Geothermal Project is a test and analysis program designed to determine the properties of the well, the fluid, and the reservoir. The program described below was formulated as a first step to obtain this information.

The objectives of the well test and analysis program are:

1. Determine well and reservoir characteristics.
2. Obtain data useful for drilling future wells.
3. Determine problem areas and possible solutions relative to well production.
4. Determine possible environmental problems.
5. Remedy possible skin damage in well.

Drilling of HGP-A was completed on April 27, 1976. The slotted liner at the bottom of the well was installed during the period May 27 to June 1. Water injection tests were completed on June 6 using the mud pumps that were still present at the drill site. HGP-A has been flashed four times for varying periods, once on July 2, a second time on July 19, a third time on July 21 to check instrumentation, and then a longer period of four hours on July 22 to obtain preliminary values for wellhead pressure and temperature, and total mass flow rate. Beginning April 29, temperature and pressure profiles in the wellbore have been obtained at various times, and beginning August 19, water at different depths in wellbore has been sampled in order to obtain chemical analyses of the water.

The four-hour well flashing on July 22 was accomplished using the wellhead instrumentation shown in Figure 1. The sonic flow, lip pressure method of James[1] was used to obtain total mass flow with lip pressure being measured at the end of a vertical 6"

[1] James, Russell, "Measurement of Steam-Water Mixtures Discharging at the Speed of Sound to the Atmosphere." New Zealand Engineering, pp. 437-41, October 1966.

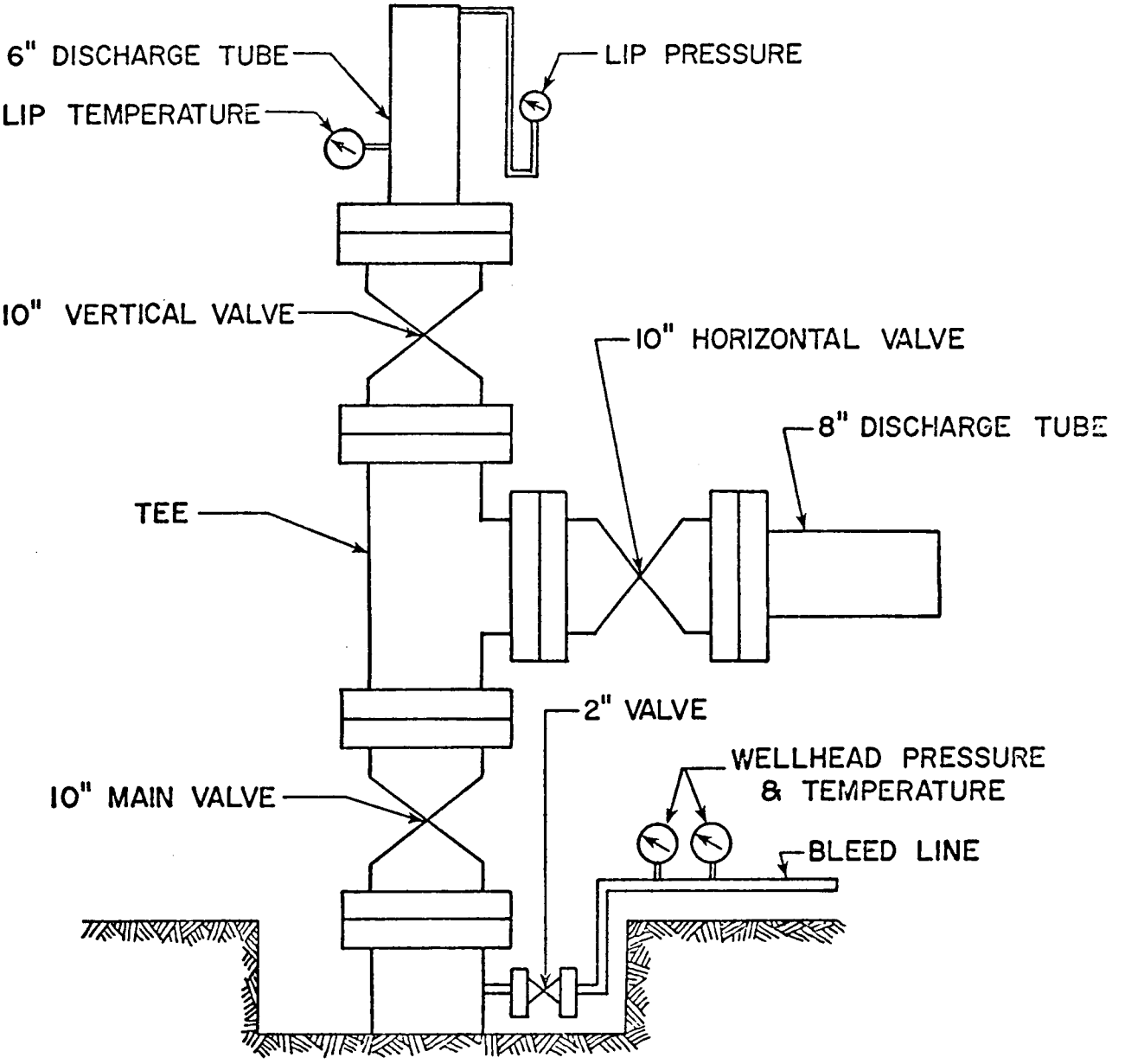

SCHEMATIC OF HGP-A WELLHEAD INSTRUMENTATION

Figure 1

discharge tube. In addition, an 8" discharge tube mounted horizontally was also flowed for a brief time. Wellhead pressure and temperature were obtained from a bleed line controlled by a 2" valve.

Results of the four-hour flashing are shown in Figure 2 which gives wellhead and lip pressure. The lip pressure at the end of four hours was 23 psig, which corresponds to a mass flow of about 220,000 lbs. per hour, assuming a specific enthalpy of 600 BTU per lb. Using this figure for specific enthalpy and assuming a conversion efficiency of 15% leads to a usable electric power equivalent to a little over 5 megawatts.

Figure 3 are plots of temperature versus depth and pressure versus depth for HGP-A for the indicated times after the flashing on July 22, 1976. The temperature profile obtained one week after the flashing was fairly close to equilibrium, except that the portion of the well that is cased continues to decrease slowly in temperature. The temperature profiles also appear to indicate that the major production region is probably between 3,500 and 4,500 feet and that a lesser producing zone of probably lower temperature may exist around 6,000 feet.

The following tests and analyses are planned for the next period:

1. Temperature and pressure profiles
2. Sustained long-term discharge
3. Variable flow-rate discharge
4. Pressure drawdown and buildup
5. Steam quality
6. Cold fluid influx
7. Interference tests using observation waterwells
8. Scaling and corrosion effects of effluent
9. Chemical analyses of downhole water samples

Figure 4 is a sketch of the equipment and instrumentation for the discharge test. As shown, the method involves basically the James technique for measuring total mass flow with twin cyclone separators for silencing and separation of steam and water. A 90^{o} V-notch weir is used to measure the liquid flowrate, permitting steam quality and specific enthalpy to be calculated. In addition, a calorimeter will be used to provide an independent measurement of the specific enthalpy. A 2" twin cyclone sampler will be used to obtain gas and vapor samples for chemical analyses and a recovery tube will be mounted on the wellhead to permit temperature and profiles to be obtained during the flow test.

In order to heat up the casing slowly and prevent damage, the well will be flowed through the 2-inch bleed line with the flow

FIGURE 2.

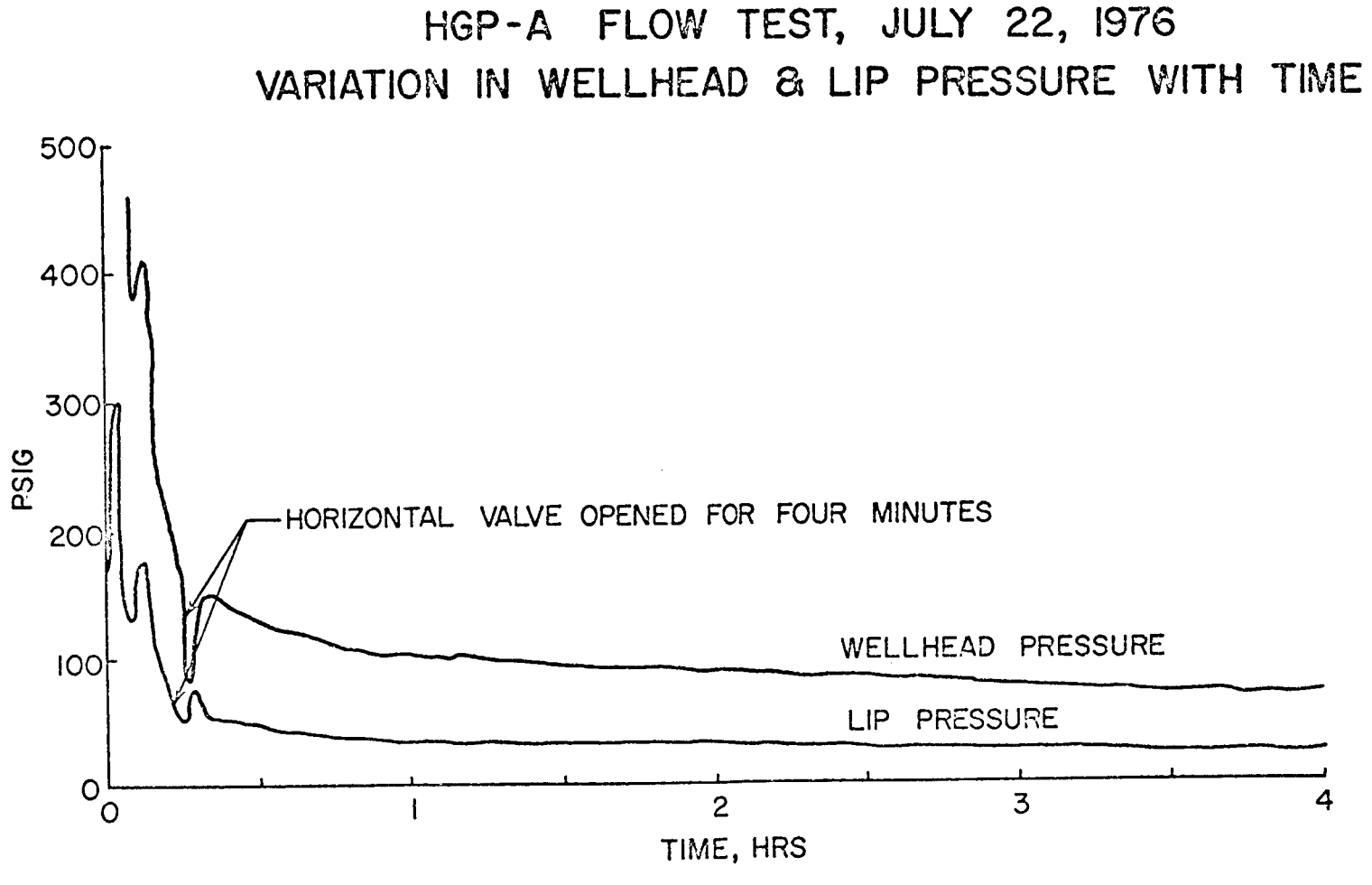
HGP-A FLOW TEST, JULY 22, 1976
VARIATION IN WELLHEAD & LIP PRESSURE WITH TIME
500
400
300
200
100
0
PSIG
HORIZONTAL VALVE OPENED FOR FOUR MINUTES
WELLHEAD PRESSURE
LIP PRESSURE
0
1
2
3
4
TIME, HRS

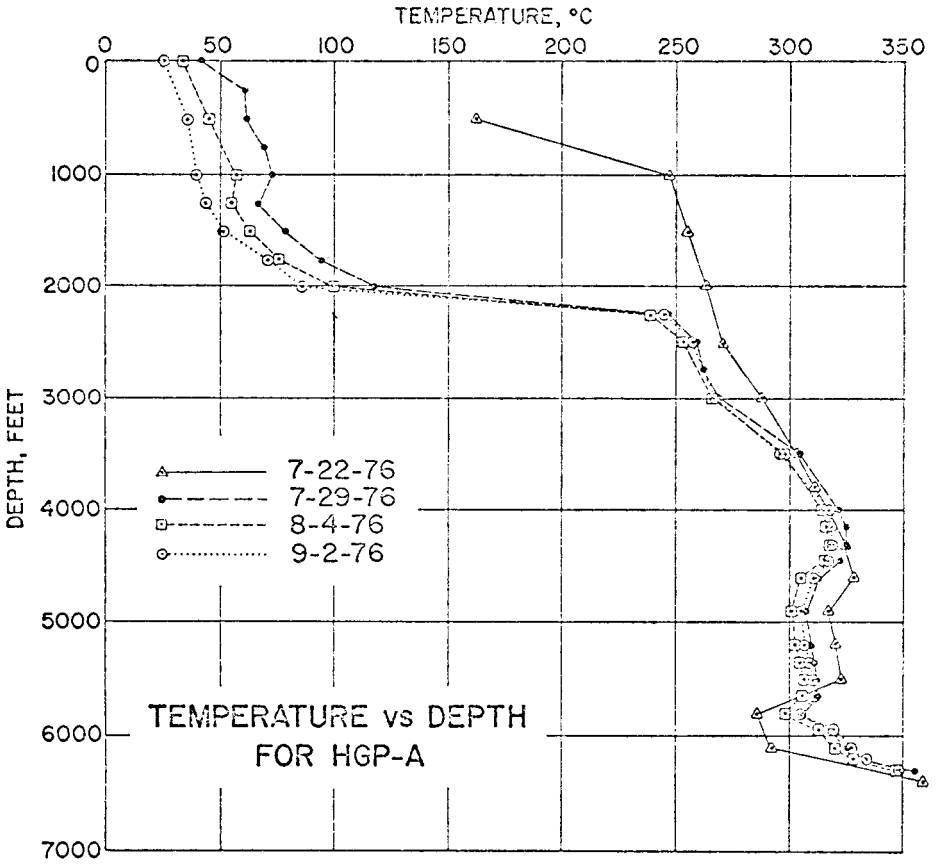
TEMPERATURE, °C
0
50
100
150
200
250
300
350
DEPTH, FEET
0
1000
2000
3000
4000
5000
6000
7000
7-22-76
7-29-76
8-4-76
9-2-76
TEMPERATURE vs DEPTH
FOR HGP-A

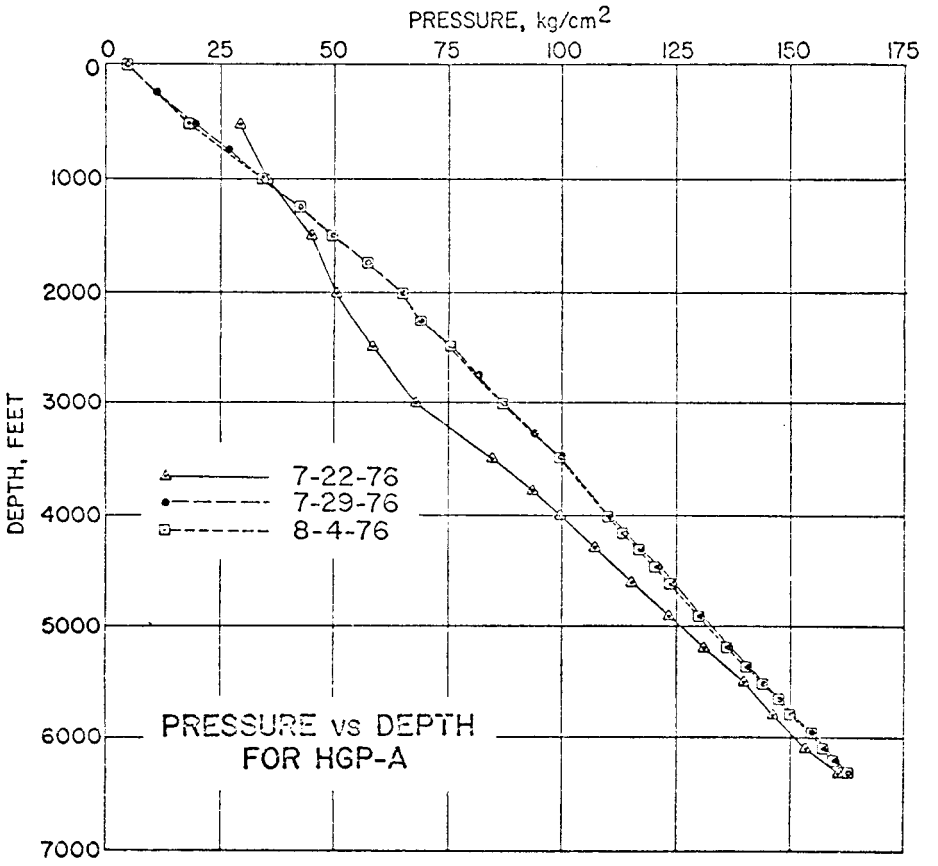
PRESSURE, kg/cm2
0
25
50
75
100
125
150
175
DEPTH, FEET
0
1000
2000
3000
4000
5000
6000
7000
7-22-76
7-29-76
8-4-76
PRESSURE vs DEPTH
FOR HGP-A

Figure 3

FIGURE 4.

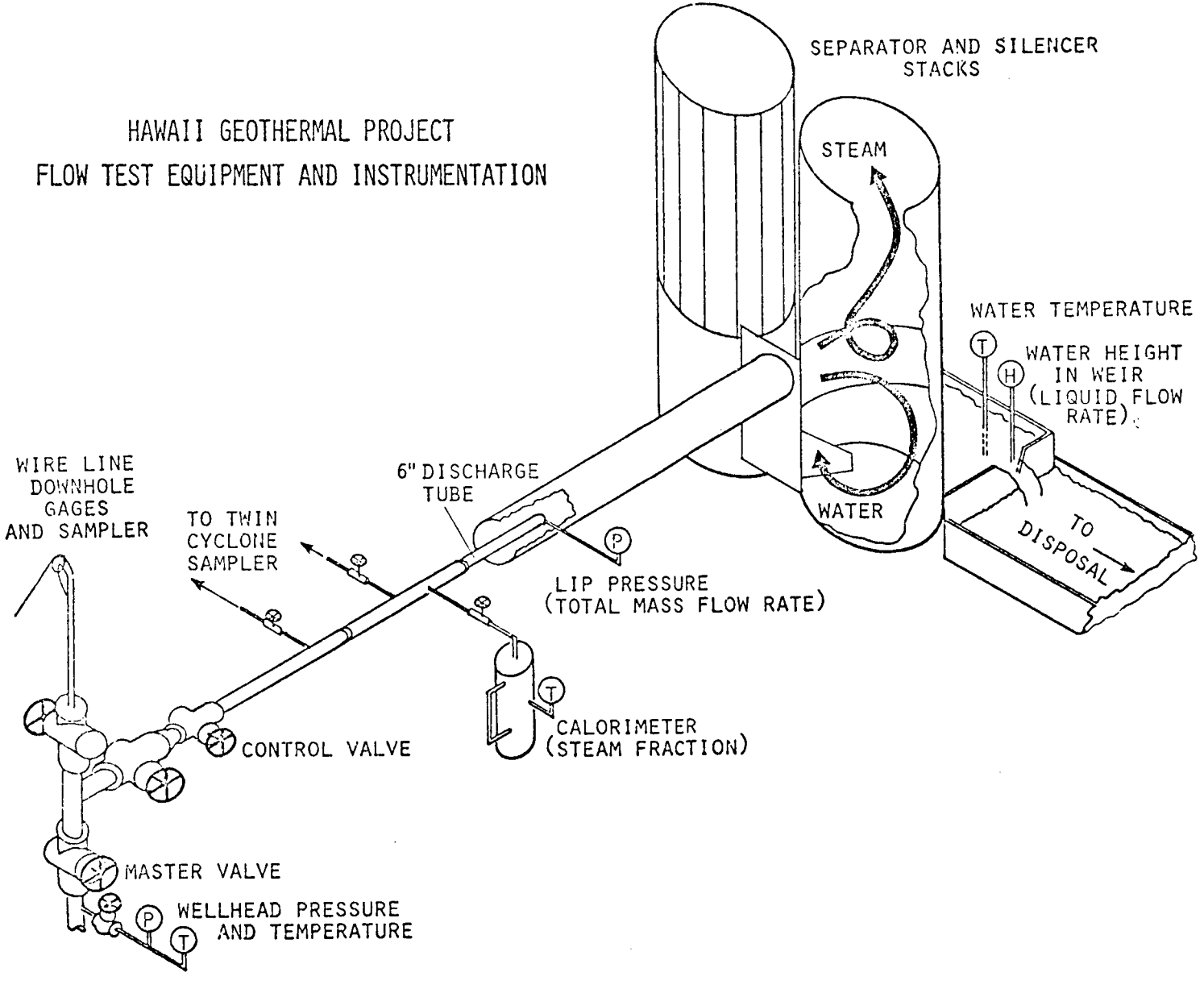
HAWAII GEOTHERMAL PROJECT
FLOW TEST EQUIPMENT AND INSTRUMENTATION
SEPARATOR AND SILENCER STACKS
STEAM
WATER TEMPERATURE
WATER HEIGHT IN WEIR (LIQUID FLOW RATE)
WATER
TO DISPOSAL
WIRE LINE DOWNHOLE GAGES AND SAMPLER
TO TWIN CYCLONE SAMPLER
6" DISCHARGE TUBE
LIP PRESSURE (TOTAL MASS FLOW RATE)
CALORIMETER (STEAM FRACTION)
CONTROL VALVE
MASTER VALVE
WELLHEAD PRESSURE AND TEMPERATURE

increased gradually until flashing flow is achieved. Once the temperatures of the system are at operating levels, tests to determine the production capacity of HGP-A will be undertaken. During this phase, the well will be allowed to flow at various fractions of wide open flow. Measurements taken during this series of tests will allow determination of production flow rate and steam fraction as functions of wellhead conditions. This information, along with chemical analyses of samples of steam, liquid, and noncondensable gases, will aid in the future selection of an energy conversion system--whether it be a permanent unit or a small portable unit to be used in conjunction with further testing of HGP-A.

A longer term, sustained discharge test will follow for the purpose of estimating reservoir characteristics. For this phase, the well will be flowed at a constant rate for periods of two weeks or longer and transient pressure measurements taken at the bottom of the well. The pressure drawdown and buildup (after the well is shut in) data will allow a rough estimate of the permeability and extent of the reservoir to be made. Also to be measured are the characteristics of the effluent (temperature, specific enthalpy, chemical composition, etc.) in order to detect any changes in the producing zones or alleviation of possible skin damage.

In conjunction with these sustained long-term discharges, the water levels of several water wells in the immediate vicinity will be monitored. Any measurable changes will be incorporated in the evaluation of the reservoir.

Concurrent with the well production testing and reservoir evaluation phases, tests will be conducted to evaluate the scaling and corrosion effects of the effluent. Specimens of various materials will be located on the separator wall and in the liquid behind the weir.

Throughout the course of the well testing program, downhole water samples and temperature and pressure profiles will be taken during those intervals when the well is shut in or is being bled through the 2-inch bleed line.

EAST MESA--GEOLOGY, RESERVOIR PROPERTIES AND AN APPROACH TO RESERVE DETERMINATION

J. H. Barkman, D. A. Campbell, J. L. Smith and R. W. Rex
Republic Geothermal, Inc.
11823 E. Slauson Avenue, Suite One
Santa Fe Springs, CA 90670

The East Mesa KGRA is located in an area of anomalously high heat flow on the east flank of the Salton Trough, at the southeast corner of the Imperial Valley of California (see Fig. 1). This geothermal field has been the object of numerous academic and industrial studies, several of which are being reported on at this workshop.

Ten producing wells have been drilled within the East Mesa KGRA, including three by Republic Geothermal in the northern portion, five by the U.S. Bureau of Reclamation in the central area, and two by Magma Power Co. to the south (see Fig. 2). The early drilling by the Bureau at locations near the apparent center of the shallow thermal anomaly unfortunately resulted in wells of low productivity. This information became well known and led to the feeling by some that East Mesa would be disappointing. The more recent drilling by Republic and Magma has shown that high productivity wells can be brought in with flow rates that are commercial for electric power generation.

Due to the already extensive investigations, a great deal is known about the East Mesa reservoir and its properties. Republic now believes this large body of knowledge provides the confidence needed to proceed with commercial development at the northern end of the field, starting with a minimum 48-megawatt project. Development drilling is expected to begin early next year with funds provided by the Bank of America under the ERDA loan guaranty program.

The intent of this presentation is primarily to illustrate an approach to reserve determination applicable to Republic's lease area.

RESERVE DETERMINATION

The reserve determination approach used is analogous to a volumetric calculation for determination of conventional oil and gas reserves. It is comprised of essentially three steps. First, the total initial heat content (enthalpy) of the reservoir was calculated between a bottom of 9000 feet and a top defined by the 300°F surface. Second, an estimate was made of the portion of this initial heat content that can be expected to be recovered during the economic producing life of the area by using reservoir simulation studies of a single five-spot reinjection pattern. Lastly, a conversion efficiency was developed that relates the heat content of the produced water to the electrical energy output.

Note that this approach is very conservative in two major respects. First, no credit is taken for recharge of the reservoir due to thermal convection through the fracture system. There is good geological and geochemical evidence that this will probably occur, with the net effect being higher temperatures and longer reservoir life. Second, the reservoir model assumes that a five-spot pattern will be employed to reinject the cooled residual water. In reality, it is planned to prolong reservoir life and to improve sweep efficiency by using a peripheral flood or an inverted nine-spot pattern. Therefore, the five-spot prediction will probably prove to be pessimistic.

We believe a more sophisticated approach will only be warranted after additional drilling has yielded a refined picture of reservoir property distribution, and after long-term production testing has yielded information on aquifer influx. The following discussion deals with the application of this approach to Republic's reserves in Sections 29 and 30.

Total Initial Heat Content

The first step in calculating the total initial heat content of the reservoir for Sections 29 and 30 was to construct a set of isothermal surface maps which show the depth to each of four selected reservoir temperatures (see Figure 6 for an example of the 350°F map). The maps were based on the static temperatures measured in the wells, with additional input provided by the data from the existing network of shallow temperature observation holes.

Using the maps, the bulk volume of each 1000-foot depth interval and its average temperature were determined from isothermal surfaces by numerical integraion. The total initial heat content of each interval can then be calculated by:

$$\text{Total Heat Content} = \text{Bulk Volume} \cdot (T-T_o) \cdot \rho c \qquad (1)$$

Where T is the reservoir temperature, T_o is the reference temperature (taken as 32°F), and ρc is the effective volumetric heat capacity of the total rock and fluid system. The last term (ρc) may be calculated as follows:

$$\rho c = \rho_r c_r (1-\phi \cdot NS) + \rho_w c_w \phi \cdot NS \qquad (2)$$

Where ρ_r and ρ_w are densities of the rock and fluid, respectively, c_r and c_w are the specific heat capacities of the rock and fluid, respectively; ϕ is the porosity of the productive portion of the rock; and NS (net sand) is the fraction of the interval which is productive.

Basis input and summary results of the calculation for each Section are shown in Table VII. Porosity and net sand values derived from RGI 16-29 and 38-30 were taken to be representative of Sections 29 and 30, respectively. Total initial heat content for the two sections is shown to be 2.14×10^{15} BTU. The amount of this initial heat that can be recovered from the produced hot water and converted to electrical energy is the subject of the following two subsections.

Reservoir Simulation

Simulation studies were carried out using the geothermal simulator developed by INTERCOMP. These studies will be described in detail in INTERCOMP's presentation to this workshop and are merely summarized here for completeness.

The objectives of the numerical model studies were to predict the temperature, pressure, and rate behavior of the producing wells as a function of time. The type of field development considered included: (1) straight depletion without reinjection; (2) peripheral reinjection; and (3) five-spot reinjection. Various rates and pattern sizes were investigated as well as the effect of an infinite aquifer.

In summary, it was found that: (1) An aquifer alone (having the same properties as the reservoir) is insufficient to maintain pressure; (2) For some combinations of withdrawal rate, spacing and permeability, peripheral injection combined with the contributions from the aquifer will maintain adequate pressure; (3) Whenever the peripheral flood fails to maintain adequate pressure for the desired withdrawal rate, pressure can always be maintained by going to a pattern flood such as a five-spot. This last result was true for both the 50 and 10 md permeability models. The average permeability on the RGI Sections 29 and 30 is expected to be approximately 50 md based on the previously discussed data from RGI 38-30 and 16-29.

Although many combinations of pattern size, production rate, porosity and interval thickness were investigated for a five-spot pattern, it was found that the results could be expressed by a single dimensionless curve relating temperature and time. This resultant curve is shown in Figure 7. The producing temperature (T) is made dimensionless by expressing it as a function of the initial producing temperature (T_i) and the reinjected water temperature (T_f) as in the equation:

$$T_D = \frac{T - T_f}{T_i - T_f} \qquad (3)$$

The time (t) is made dimensionless by multiplying it by the flow rate (Q) and dividing by the total pore volume (ϕAh). This is equivalent to the number of pore volumes produced:

$$t_D = \frac{Qt}{\phi Ah} \qquad (4)$$

This curve appears valid over the range of parameters of interest, but in extreme cases a separate simulator run with the actual parameter values may be required. One of the interesting features of the curve without aquifer influx (i.e., no convection) is that the final temperature, namely that of the reinjected hot water (200°F) is approached very slowly because of the heat influx from the cap and base rock. Secondly, thermal breakthrough occurs at about one pore volume, whereas fluid breakthrough in a five-spot occurs at about 0.7 $\pm$ PV. This difference is due to heating of the injected fluid by the formation and mixing with the formation water.

A dimensional "base case" is illustrated in Figure 8 for a 40,000 B/D producer on 40-acre spacing, which initially produces at 355°F. The reinjected water temperature is assumed to be 200°F. The economic life of this well is approximately 30 years or 265°F. For the reserve calculation, this "base case" is used to determine the fraction of original heat content of the rock and fluid system which would be produced in the hot water over the economic life of the well. The total amount of heat (enthalpy) contained in the produced fluids is equivalent to over 90 percent of the original heat-in-place in the reservoir, but about half of this heat is returned to the reservoir by means of the reinjected water. Therefore, the net heat produced is about 45 percent of the original heat-in-place. During the 30-year period, approximately three pore volumes of water were produced and reinjected. Thus, it is concluded for East Mesa conditions that the gross producible heat is approximately equal to 90 percent of the original heat-in-place of 1.92×10^{15} BTU for Sections 29 and 30 combined.

Conversion to Electricity

It is desirable to express geothermal reserves in electrical terms (i.e., megawatt-years), rather than in volume or mass of hot water. Reference must therefore be made to a specific power plant design. A number of such studies have been made in the industry, the results of which are in general agreement and widely known. For example, Figure 9 shows a typical power output for the one-stage and two-stage flashed steam process as a function of temperature.

For the proposed 48-megawatt East Mesa power plant, a two-stage flash process is planned. The reasons for selecting this process are: (1) it relies on proven, existing technology; (2) it utilizes standard and well-understood design features; (3) it can be designed and built in time to meet the incremental power needs of the Imperial Irrigation District by 1980; (4) it is well suited to the low salinity and low noncondensables found in Republic wells; and (5) it will probably generate the lowest-cost electricity under the specific East Mesa temperature and water chemistry conditions.

Assuming a produced water temperature of 335°F and two-stage flash, the calculated conversion efficiency, based on Figure 9, is approximately 5.5 percent, which is in general agreement with values quoted in the literature. A conversion efficiency of five percent was used in the reserve calculation and was assumed to apply throughout the range of temperatures expected.

The resulting calculated electrical energy reserve for Sections 29 and 30 is shown in Table VII. These calculations are based on a gross producible heat equal to 90 percent of the original heat-in-place (as determined from the five-spot simulation results) and a conversion efficiency of five percent. The total reserve amounts to 3215 megawatt-years, which is 107 megawatt installed capacity for a 30-year life. These reserves are clearly adequate to support the proposed 48-megawatt project, even after discounting for the numerous uncertainties involved.

References

Biehler, S., Kovach, R. L., and Allen, C. R., 1964, Geophysical framework of northern end of Gulf of California structural province: in Marine Geology of Gulf of California, T. Van Andel and G. Shor (eds.), Am. Assoc. Petroleum Geologists Mem. 3, p. 126-143.

Hileman, J. A., Allen, C. R., and Nordquist, J. M., 1973, Seismicity of the Southern California region, 1 January 1932 to 31 December 1972; Seis. Lab., Cal. Inst. Tech., P. 492.

Rex, R. W., 1966, Heat Flow in the Imperial Valley of California (abstr.): Am. Geophys. Union Trans., 47, p. 181.

Rex, R. W., 1971, Geothermal Resources in the Imperial Valley in California Water, David Seckler, (ed.), Univ. Calif. Press, Berkeley, p. 190-205.

Cooperative geological-geophysical-geochemical investigations of geothermal resources in the Imperial Valley area of California: Final Report (FY 1971), Contr. No. 14-06-300-2194, U.S. Bureau of Reclamation.

U.S. Bureau of Reclamation, 1974, Geothermal resource investigations, East Mesa test site, Imperial Valley, California: status report, p. 64.

Biehler, S., 1971, Gravity studies in the Imperial Valley: in Cooperative geological-geophysical-geochemical investigations of geothermal resources in the Imperial Valley area of California. Univ. of Calif., Riverside, Education Research Service, p. 29-14.

Meidav, T., and Furgerson, R., 1972, Resistivity studies of the Imperial Valley geothermal area, California: Geothermics, v. 1, p. 47-62.

Combs, J., and Hadley, D. M., 1973, Micro-earthquake investigation of the Mesa geothermal anomaly, Imperial Valley, California: EOS, v. 54, p. 1213-1214.

Hoagland, J. R., 1976, Petrology and hydrothermal alteration in borehole Mesa 6-2, East Mesa geothermal area, Imperial County, California, Thesis, Dept. of Geol. Sci., Univ. of California, Riverside.

Witherspoon, P. A., Narasimhan, T. N., and McEdwards, D. G., 1976, Results of Interference Tests from Two Geothermal Reservoirs: Lawrence Berkeley Laboratory, Soc. Petroleum Engrs. of AIME 51st Fall Meeting, New Orleans.

TABLE I

EAST MESA WELL FLUID COMPARISON (mg/l)

Water	RGI 38-30	RGI 16-29	RGI 18-28*	RGI (450') Water Well	Bu-Rec 6-1	Bu-Rec 6-2	Bu-Rec 8-1	Bu-Rec 31-1	Bu-Rec 5-1
Total Dissolved Solids	1907	1978	2950	1600	26300.	5000.	1600.	2900.	1575.
Sodium	630	623	980	410	8100.	1700.	610.	730.	593.
Potassium	39	39	40	12	1050.	150.	70.	85.	29.
Calcium	4.3	3.2	0.1	68	1360.	16.4	8.5	8.9	16.2
Magnesium	0.1	0.1	0.1	19	17.2	0.24	0.05	0.05	2.1
Iron	1.5	1.9	2.3	0.1	8.8	0.1	0.1	0.1	N/A
Silicon	518	489	167	10	320.	269.	389.	274.	201.
Boron	2.6	3.2	4.5	0.9	9.7	7.8**	1.6	2.5	N/A
Arsenic	0.13	0.1	N/A	N/A	0.26	0.22	0.053	0.025	N/A
Chloride	565	514	600	760	15850.	2142.	500.	510.	454.
Fluoride	3.2	4.0	2.5	0.5	0.9	1.2	1.6	1.42	N/A
Bromide	0.70	N/A	N/A	N/A	N/A	1.66**	N/A	N/A	N/A
Sulfate	142	169	64	9.0	42.	156.	173.	183.	N/A
Carbonate	128	188	0	4.0	0.0	0.0	0.0	0.0	N/A
Bicarbonate	312	342	1340	76	202.	560.	417.	845.	331.
pH (pH Units)	8.9	9.0	8.3	8.3	5.4	6.1	6.2	6.2	9.1
Chem. Thermometer**									
Alkali	460°F	424°F	417°F	202°F	449°F	429°F	432°F	440°F	332°F
Silica	442°F	436°F	329°F	80°F	383°F	365°F	410°F	369°F	334°F

*Analysis of 18-28 sample made shortly after completion & may be contaminated with drilling fluids.

**RGI measured or calculated

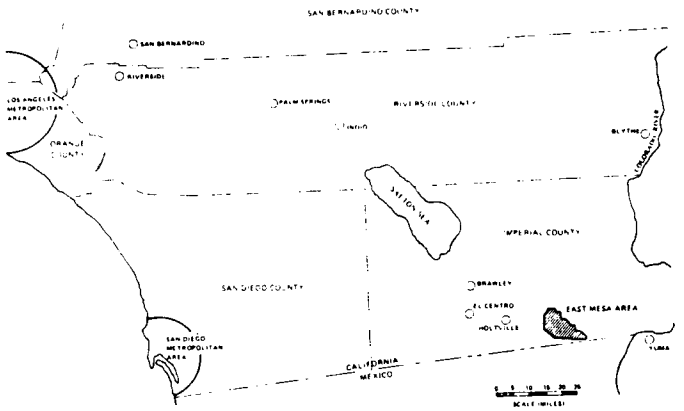

Figure 1. Location Map, East Mesa K.G.R.A.

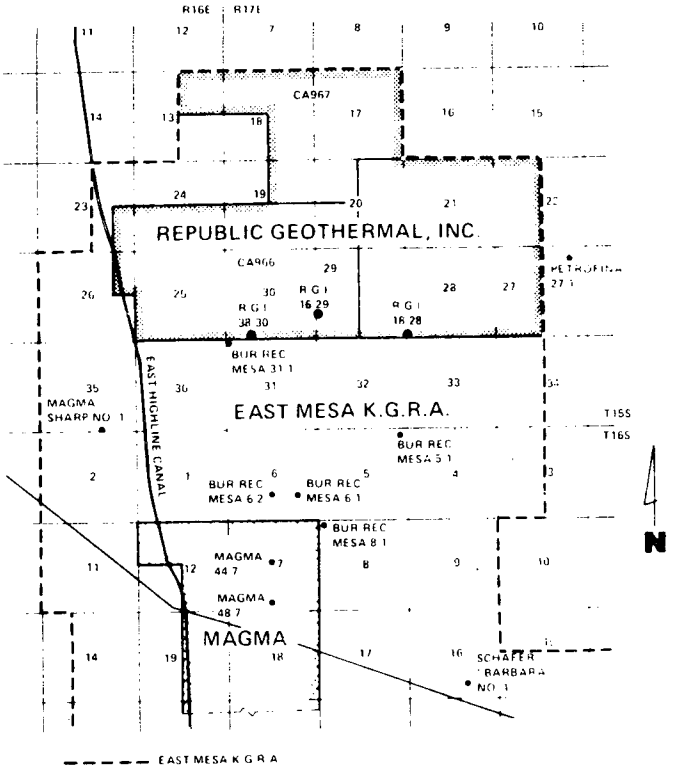

Figure 2. Plat of East Mesa

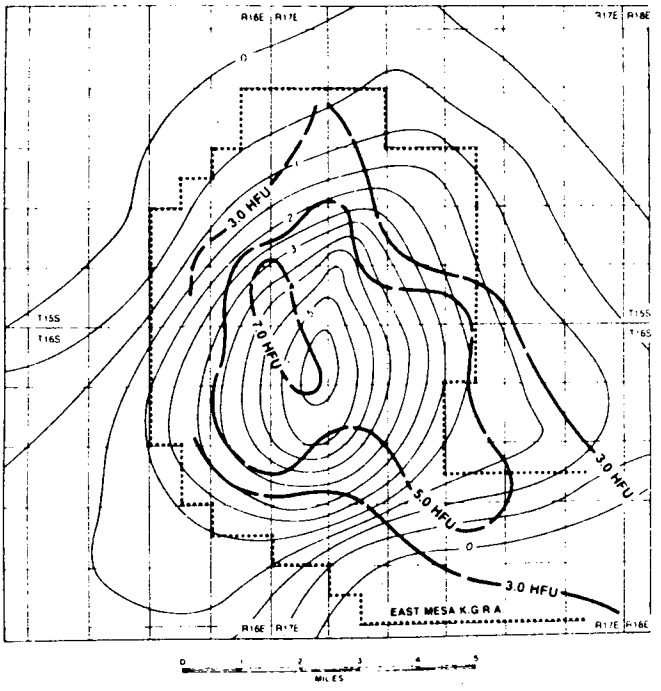

Figure 3. Residual Gravity Anomaly Map of the East Mesa Geothermal Field (Biehler, 1971) with superimposed Surface Heat Flow Anomaly Contours (U.S.B.R. 1974).

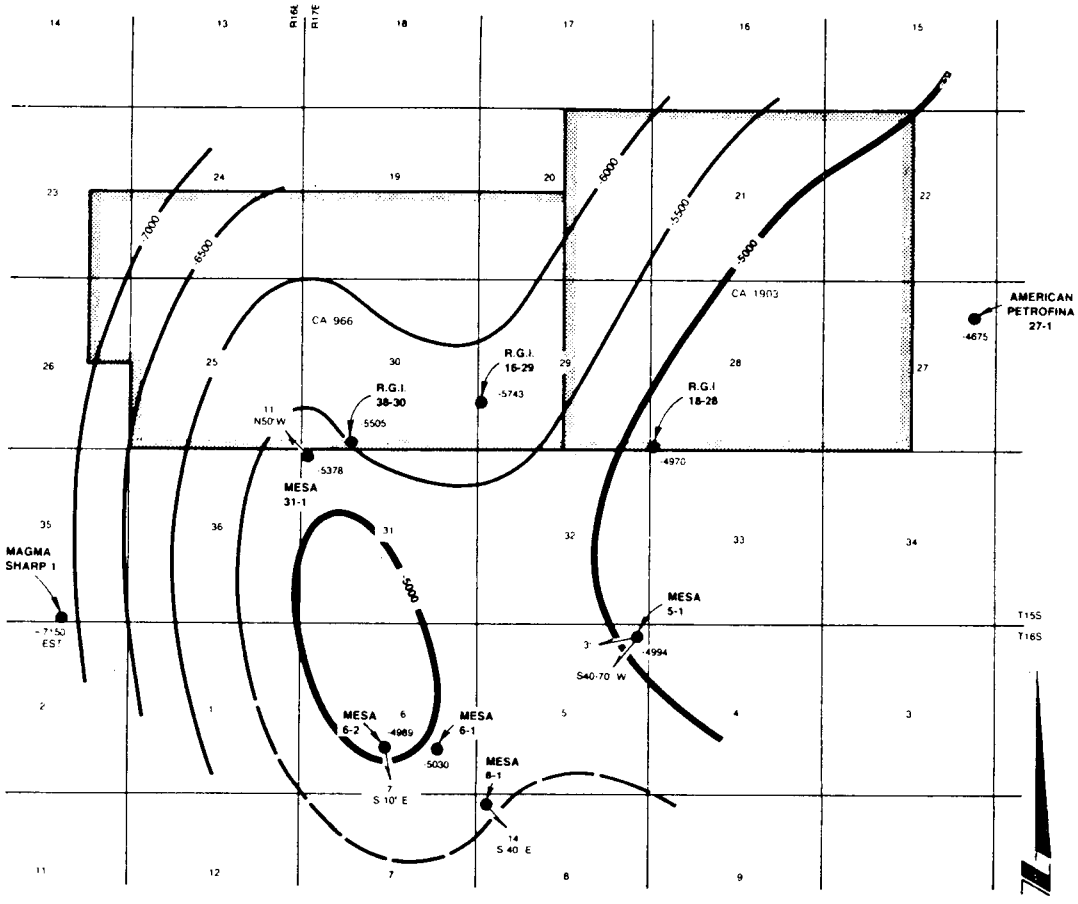

Figure 4. East Mesa Structure Contour Map.

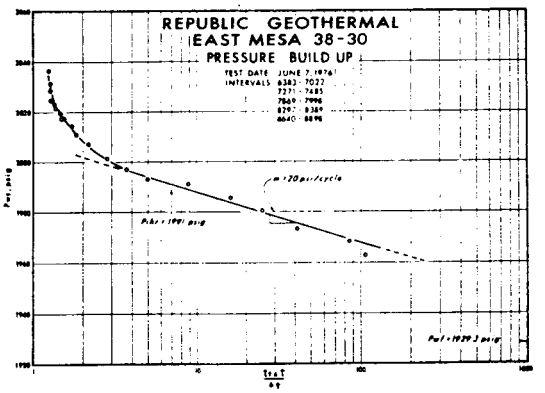

Figure 5

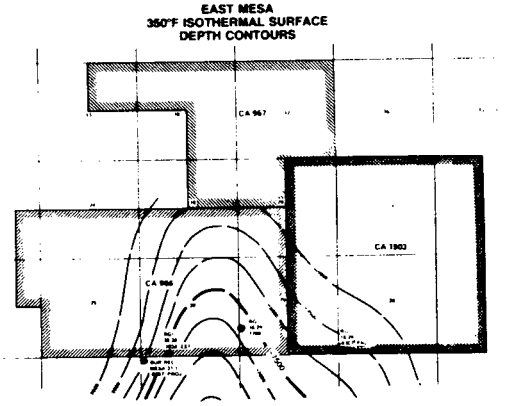

Figure 6

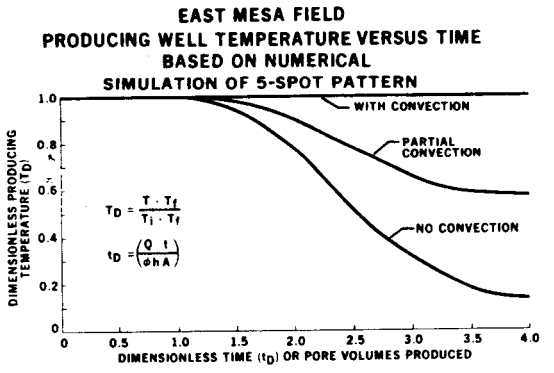

Figure 7

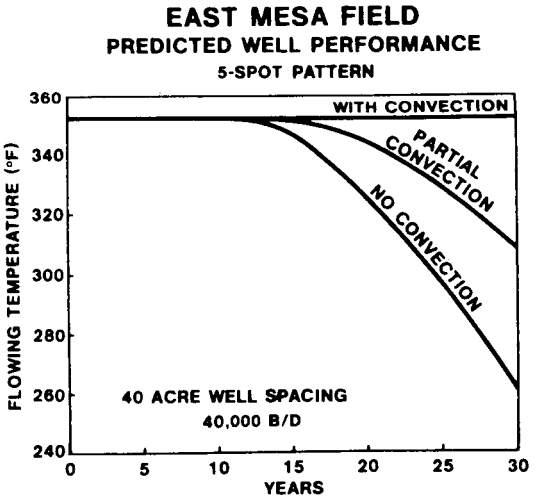

Figure 8

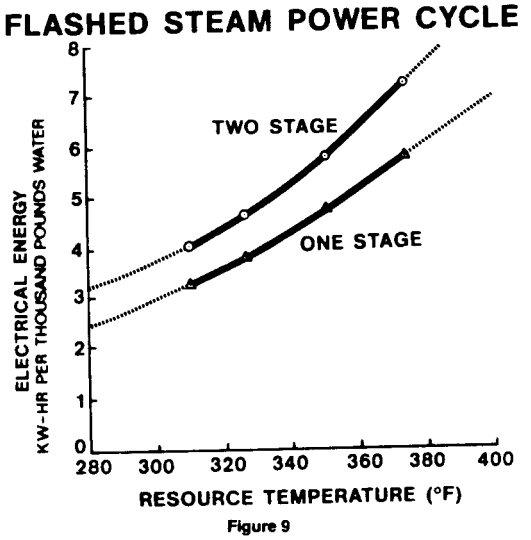

Figure 9

TABLE II

CHEMICAL ANALYSIS OF FLASHED STEAM — REPUBLIC 16-29

Total Noncondensables	—	0.64 wt. % of steam
Constitutents		
Carbon dioxide	—	91.4 vol. % of noncondensables
Nitrogen	—	4.3
Methane	—	3.9
Alkanes	—	0.4
Hydrogen sulfide	—	None detected

TABLE III

EAST MESA WELL DATA

Well	T.D.	Temp. at T.D.	Flowing downhole Temp. (Above Producing Interval)	Flow Rate lb mass/hr	Flow Rate 10^6BTU/hr	MW	Net Sand	Completion Date
Republic Geothermal								
38-30	9009'	374°F (est)	338°F	670,000*	5000	3.5	736'	10-75
16-29	7998'	365°F	332°F	419,000**	3060	2.1	827'	12-75
18-28	8001'	326°F	310°F (est)	36,000	230	0.1	794'	1-76
Bureau of Reclamation								
31-1	6231'	323°F	300°F (est)	300,000	1800	0.9	593'	6-74
8-1	6205'	354°F	320°F (est)	228,000	1580	1.0	916'	6-74
6-1	8030'	399°F	330°F	211,000	1530	1.0	942'	8-72
6-2	6005'	370°F	304°F	152,000	990	0.6	904'	8-73
5-1	6016'	315°F	305°F	117,000	770	0.5	790'	5-74

NOTES
All data are actual measured values unless indicated to be estimated.
* Fill at 6910' (348°F)
** Liquid rate only — vapor phase (10 ± %) not measured)

TABLE V

PRESSURE BUILDUP DATA AND RESULTS

	RGI WELLS		
TEST DATA	**18-28**	**16-29**	**38-30**
Flow duration, hrs	21.5	5.53	5.47
Shut-in time, hrs	9.3	22.40	24.39
Cumulative production, STB	1,264*	4,525	5,907
Last rate before shut-in, STB/D	2,517	19,668	25,462
Producing time, hrs	17.05	5.902	6.097
RESERVOIR AND FLUID PROPERTY DATA			
Water viscosity, μ_w	0.210	0.185	0.185
Water FVF, RB/STB	1.078	1.085	1.088
Porosity, fraction	0.220	0.223	0.249
Total compressibility, psi^{-1}	7.570×10^{-6}	7.904×10^{-6}	8.202×10^{-6}
Wellbore radius, ft	0.375	0.443	0.510
Estimated net thickness, ft	794	827	736
Open intervals	6105-6210 6440-8000	6413-6984 7231-7996	6383-7022 7271-7485 7869-7998 8297-8384 8640-8898
RESULTS			
Average permeability, md	7.95	41.96	56.61
Flow capacity, md-ft	6,309	34,698	41,666
Formation damage (skin)	−0.91	−2.28	−2.81
Distance to nearest boundary, ft	451	893	692

*Estimated

TABLE IV

REPUBLIC GEOTHERMAL WELLS ZONE SUMMARIES

Well	Interval	Net Sand (ft)	Average Porosity $\bar{\phi}$	Geometric Average Permeability (md) $\bar{k}_{(h)}$	$\bar{k}_{(v)}$	Perm.-Thickness (Darcy-ft)
38-30	4001-5000	640	0.29	174	115	111
	5001-6000	735	0.27	109	74	80
	6001-7000	782	0.29	170	112	133
	7001-8000	399	0.19	9	7	4
	8001-8900	293	0.10	1	< 1	~ 1
16-29	5001-6000	746	0.23	26	19	20
	6001-7000	768	0.24	44	32	34
	7001-7900	431	0.21	12	9	5
18-28	5100-6000	733	0.29	126	85	93
	6001-7000	608	0.22	16	12	10
	7001-7900	325	0.23	35	25	11

TABLE VI

COMPARISON OF PERMEABILITY AND FLOW CAPACITY OF EAST MESA WELLS

Well	Max. observed flow rate, BD	Avg. Permeability from buildup (md)	Permeability-Thickness (Darcy-ft) buildup	logs
Republic Geothermal				
38-30	50,300	57	41.7	44.
16-29	31,400	42	34.7	30.
18-28	2,600	8	6.3	14.*
Bureau of Reclamation				
31-1	21,200	30	22.2	N/A
5-1	8,300	6	5.7	N/A
6-1	14,800	0.5	0.3	N/A
6-2	10,700	N/A	N/A	N/A
8-1	16,100	13	13.5	N/A

Lawrence Berkeley Laboratory Interference Results:
38-30 and 31-1 pair: kh = 29.8 Darcy-ft
6-1 and 6-2 pair: kh = 11.2 Darcy-ft

*RGI 18-28 has 14 Darcy-ft in the slotted interval plus another 99.7 Darcy-ft behind blank pipe (below 5100 ft).

TABLE VII

EAST MESA FIELD — SECTIONS 29 & 30 (Republic)

PRELIMINARY RESERVE ESTIMATE

Section	Average Reservoir Temperature (°F)	Average Sand Porosity (fraction)	Net Sand (fraction)	Bulk Volume ($ft^3 \times 10^{10}$)	Total Initial Heat Content (Btu x 10^{14})	Reserve (MW-Years)
29	334	0.17	0.60	8.363	8.732	1315
30	335	0.23	0.58	11.701	12.625	1900
	335	0.20	0.59	20.064	21.357	3215

$\rho_r = 165 \frac{lbs}{ft^3}$, $\rho_w = 56.7 \frac{lbs}{ft^3}$, $c_r = .19 \frac{Btu}{lb°F}$, $c_w = 1.12 \frac{Btu}{lb°F}$

A SEMI-ANALYTICAL APPROACH TO GEOTHERMAL RESERVOIR PERFORMANCE PREDICTION

S. K. Sanyal, M. Sengul and H. T. Meidav
Geonomics, Inc.
3165-7 Adeline Street
Berkeley, CA 94703

This paper presents a simplified analytic treatment of the problem of fluid flow and heat transfer in a hot water reservoir. A multi-layered reservoir is considered, with a circular array of producing wells surrounded by a concentric, circular array of injection wells. Complete injection of produced water, and hence an eventual steady state, is assumed for the flow system. A temperature gradient is assumed in the radial direction. The rock properties are allowed to vary from layer to layer, but are considered uniform within a particular layer. The heat transfer problem is handled by a modification of the solution to the problem of heat extraction from fractured dry rocks proposed by Gringarten, et al. (1975). The reservoir is represented as a vertical stack of horizontal layers, with permeable and impermeable layers alternating. The pressure distributions in various layers are calculated by spatial superposition of the continuous line source solution for the given geometry, with average fluid and rock properties within the system. This approach can yield results such as the breakthrough time of injected water in each layer, pressure distribution in space and time and the temperature of the produced water over time. In a study of the Heber geothermal reservoir in the Imperial Valley of California such results have shown reasonably close agreement with the results from computer simulation.

Many hot water geothermal reservoirs display a closed temperature anomaly, i.e., the temperature of the reservoir is highest near the center and gradually declines towards the periphery. For such reservoirs a logical development plan is to produce hot water from the central part of the reservoir through an array or cluster of production wells. The heat is extracted from the produced water for power generation, and the cooled water is injected into the cooler marginal areas of the reservoir through an array of injection wells. This paper presents a semi-analytic method for analyzing the heat and fluid flow characteristics of such a system.

HEAT FLOW ANALYSIS

The objective of this analysis is to be able to forecast the outlet temperature which, together with the fluid production rate at the production wells, determines the heat flow rate.

Physical and Mathematical Model. As shown in Figure 1a, the reservoir consists of thin sand and shale layers with differing thickness, permeability and porosity for each sand layer, and with shale layers all having the same thickness and assumed to be located between these sand layers. Cold water is injected through the injection wells located on a circle with radius R_2 and hot water is produced at the production wells located on a circle with radius R_1 as shown in Figure 1b. Initially the reservoir temperature increases linearly from the injection wells to the production wells.

The mathematical model is based upon Figure 2 where the relevant information concerning the heat flow for a sand layer is represented. Z_E is the distance from the bottom of the shale layer to the no heat flow boundary within it. If the average water flow rate for all the sand layers is the same and the thickness of the sand layers and the shale layers is constant then Z_E will be half of the shale thickness.

The following assumptions are made in simplifying the physical model:

1. The sand layers and the shale layers are homogeneous and isotropic.

2. The density, heat capacity, and thermal conductivity of water, of the solid matrix of the sand layer, and of the shale layer are constant. Further, the density, specific heat, and thermal conductivity of the shale and of the solid matrix of the sand layer are the same.

3. The water temperature T_w is only a function of radial coordinate, r, and time, t, and does not vary with the vertical coordinate, z.

4. Heat conduction in the radial direction in both sand and shale layers is negligible.

5. Initially, both the sand and shale layers are at the same temperature at any given r. Taking the temperature gradient in the r direction into account, the initial temperature distribution at any given r is given by the initial rock temperature T_{ro} at the point of production minus the product of the temperature gradient, a, and the distance from the production well.

Heat flow for a single layer, shown in Figure 2, is governed by two differential equations

$$\frac{h}{2}\rho_1 C_1 \frac{\partial T_w(r,t)}{\partial t} + \frac{h}{2}\rho_w C_w V_w \frac{\partial T_w(r,t)}{\partial r} = k_R \frac{\partial T_R(r,z,t)}{\partial z}\Big|_{z=h/2} \qquad (1)$$

where $\rho_1 C_1 = (1-\phi)\rho_R C_R + \phi\rho_w C_w$

and
$$\frac{\partial^2 T_R(r,z,t)}{\partial z^2} = \frac{1}{D_R} \frac{\partial T_R(r,z,t)}{\partial t} \tag{2}$$

$T_w(r,t)$ and $T_R(r,z,t)$ are water and rock temperatures respectively.

The temperatures must also satisfy the following initial and boundary conditions:

$$T_R(r,z,t) = T_w(r,t) = T_{R0} - a(R_2-r), \quad t<r/v \tag{3}$$

$$T_R(R_2,z,t) = T_w(R_2,t) = T_{R0} \qquad t<0 \tag{4}$$

$$T_R(R_2,z,t) = T_w(R_2,t) - T_{wo} \qquad t\geq 0 \tag{5}$$

$$T_w(r,t) = T_R(r,Z_E,t) \qquad \text{for all } r \text{ and } t \tag{6}$$

$$\partial T_R(r,z,t)/\partial z\Big|_{z=Z_E} = 0 \tag{7}$$

For a single layer, taking Z_E at infinity, Lauwerier (1955) gave a solution for the above problem in Cartesian coordinates. In order to use Lauwerier's solution the shale layers separating the sand layers should be thicker than they are assumed to be in this study. Carslaw and Jaeger (1959) gave the solution to the same problem as Lauwerier except that they considered a single fracture instead of a porous sand layer. Recently, Gringarten et al. (1975) gave the solution for the mathematical problem above in Cartesian coordinates, but they solved the problem for an infinite series of parallel, equidistant fractures of uniform thickness rather than for sand layers. Gringarten gave the solution, dimensionless temperature $T_{wD}(r,t_D)$, in the form of a graph as a function of two dimensionless numbers, given in our notation as follows:

$$Z_{ED} = (\rho_w C_w/k_R)(\bar{q}/r)Z_E \tag{8}$$

$$t'_D = [(\rho_w C_w)^2/k_R\rho_R C_R](\bar{q}/r)^2 t' \tag{9}$$

where $t' = t-(R_2-R_1)/\bar{v}_w$. The second term $(R_2-R_1)/\bar{v}_w$ is the breakthrough time, i.e., the time taken by the injected water to arrive at the production well. The dimensionless temperature, T_wD, is given by:

$$T_{wD} = [T_{RO}-T_w(r,t)]/(T_{RO}-T_{wo}) \quad (10)$$

For given values of Z_{ED} and t'_D, T_{wD} is read from the graph.

Defining an average flow rate, $\bar{q}$, per sand layer per unit length, one can use the solution given by Gringarten et al. in the analysis of the problem at hand. This application is summarized in the following section.

Application of Gringarten's Solution. In order to use the solution given in graphical form to find the produced water temperature, one needs to determine the dimensionless numbers given by Eqs. 8 and 9. Assuming the thermal properties of the water and shale are known, still to be found are the values of the breakthrough time, $(R_2-R_1)/v_w$, and the ratio between the average flow rate, $\bar{q}$, and the distance $r = R_2-R_1$.

Given the total injection rate Q, the average flow rate, $\bar{q}$, is given by the expression:

$$\bar{q} = Q/\pi(R_1+R_2) \quad (11)$$

Based on the relative magnitude of the $(kh)_i$ product of each layer, the average flow rate for each layer is found as:

$$\bar{q}_i = \bar{q}(kh)_i / \sum_{i=1}^{m} (kh)_i, \quad i=1,2,\ldots,m \quad (12)$$

where $(kh)_i$ is the product of permeability and thickness of the i^{th} layer, and m is the number of sand layers.

Dividing the rate, $\bar{q}_i$, for a sand layer by the product of its thickness and porosity $(h\phi)_i$, the average velocity in the layer is obtained:

$$\bar{v}_{wi} = \bar{q}_i/(h\phi)_i, \quad i=1,2,\ldots,m \quad (13)$$

Using these values of $\bar{q}_i$, and $\bar{v}_{wi}$ together with $r = R_2-R_1$ in Eqs. 8 and 9, the values of Z_{ED} and the breakthrough time, $(R_2-R_1)/\bar{v}_{wi}$, are found.

To obtain the water outlet temperatures for each layer at different times, now the task is to determine the dimensionless time, t'_D, which is taken as zero for $t<(R_2-R_1)/\bar{v}_{wi}$. However, in the application of Gringarten's solution to the problem under investigation one faces two problems:

(1) as pointed out earlier, Gringarten's solution assumes that all the flow rates are the same and therefore that Z_{EDi}'s are the same, whereas here they are different for each layer, and
(2) Gringarten assumes that there is no temperature gradient along the fracture, whereas there is a temperature gradient along the sand layer in the present problem.

Pertaining to the first of these problems, if the values of Z_{EDi}'s for the layers expected to have significant outlet temperature drops all fall in a narrow range, then the errors introduced by the variance of Z_{ED} from layer to layer can be considered acceptable for engineering purposes. As for the second problem, to relax the assumption of no temperature gradient in the radial direction and to include the effect of this temperature gradient in the solution, all of the layers can be divided into several concentric sections. Initially all the sections are assumed to be at a uniform temperature which is given by their median temperature, and the temperature gradient in each of these sections is neglected. Also the area weighted average flow rate, $\overline{q}$, is calculated for each section of every sand layer and thus the same is done for $\overline{v}_{wi}$.

In finding the outlet temperature history of a layer at $t = t_1 < t_2 < \ldots < t_m$, one first calculates the outlet temperature at the production end of the first section, which will have the shortest breakthrough time. Using Gringarten's solution, the outlet temperature of this section is obtained at time t_2 with time interval $\Delta t_1 = t_1, t_2$. If during this first time period Δt_1, not only the first section but the next section (or sections) breaks through, then first the outlet temperature of this second section is found. The average of this outlet temperature is used as the injection temperature for the first section to find its outlet temperature by superposition.

The above procedure is repeated for all the layers and their outlet temperature histories are found. Taking the density and the specific heat of water constant, the average bottom hole water outlet temperature history is found by the following expression:

$$T(t)_{av} = \sum_{i=1}^{m} (\overline{q}_i / \overline{q}) T_{wi}(R_1, t) \qquad (14)$$

FLUID FLOW ANALYSIS

The objective in this section is to be able to predict the pressure behavior of production and injection wells again for the system shown in Figure 1. In order to get a better understanding of the fluid flow characteristics of the system, both early and late pressure histories will be investigated.

The following assumptions are made in order to simplify the physics of the problem:

(1) the reservoir is infinitely large, compared to the well bore radius
(2) homogeneous and isotropic medium
(3) formation has a uniform thickness
(4) porosity, permeability, and viscosity are constant (independent of pressure and temperature)

Further, for simplicity, the radii of the production and injection wells are taken to be the same, and the production and injection wells are assumed to have constant production and injection rates and show no skin effect.

The solution giving the pressure history of a production well producing at a constant rate located in a reservoir for which the above assumptions hold is the continuous line source solution given as follows:

$$\frac{kh}{141.3q_p\mu B_w}[P_i - P(r,t)] = P_D(r_D,t_D) = \frac{1}{2}\,Ei\left(-\frac{r_D^2}{4t_D}\right) \tag{15}$$

where $r_D = r/r_w$, $t_D = 0.000264\ kt/\phi\mu c_t r_w^2$, and

$$-Ei(-x) = \int_o^\infty \frac{e^{-u}}{u}du \quad \text{(exponential integral)}$$

For an injection well the production rate, q_p, in Eq. 15 will be replaced by the injection rate with negative sign $(-q_{in})$.

In an infinite reservoir where there are N production and M injection wells, the pressure history of any given production or injection well can be found through the solution given above with spatial superposition if the injection and production rates are constant with time or are a step function of time.

Taking q_p as the production rate for all the production wells and q_{in} as the injection rate for all the injection wells, the pressure history of a production well will be given by:

$$P_p(r,t) = P_i - \left[\frac{141.3\mu B_w q_p}{kh}\right]\sum_{i=1}^{N} -\frac{1}{2}E_i\left(-\frac{r_{Di}^2}{4t_D}\right)$$
$$+ \left[\frac{141.3\mu B_w q_{in}}{kh}\right]\sum_{j=1}^{M} -\frac{1}{2}E_i\left(-\frac{r_{Dj}^2}{4t_D}\right) \tag{16}$$

A similar expression will be obtained for the injection pressure history, $P_{in}(r,t)$, for an injection well.

To find $p_p(r,t)$ for a given value of dimensionless time t_D one needs to find the dimensionless radial distance r_{Di} to all of the production wells and r_{Dj} for all of the injection wells, and then to find all of the values of the exponential integral for all of the arguments $(r^2_{Di}/4t_D)$, $i = 1,\ldots, N$, and $(r^2_{Dj}/4t_D)$, $j = 1,\ldots,M$.

For the system under investigation the values of r_{Di} and r_{Dj} can be evaluated through the following expressions (see Figure 3):

$$r_{Di} = 1, \quad i = 1 \tag{17}$$

$$r_{Di} = \frac{R_1}{r_w}\sqrt{2\left[1-\cos\frac{2\pi(i-1)}{N}\right]}, \quad i = 2,\ldots,N \tag{18}$$

$$r_{Dj} = \frac{1}{r_w}\sqrt{R_1^2 + R_2^2 - 2R_1R_2\cos\frac{2\pi(j-1)}{M}}, \quad j = 1,2,\ldots M \tag{19}$$

A computer program is developed and production and injection pressure histories are computed for various values of the variables affecting the fluid flow characteristics of the system.

NOMENCLATURE

B_w	=	formation volume factor for water
c_t	=	total system effective isothermal compressibility
C_R	=	specific heat of shale or the solid matrix of the sand layers
k	=	formation permeability
k_R	=	thermal conductivity of shale or the solid matrix of the sand layer.
P_D	=	dimensionless pressure
P_i	=	initial pressure
r_w	=	radius of the production or injection wells
T_{RO}	=	rock temperature at the point of injection
T_{wo}	=	water injection temperature
v_w	=	water velocity
ρ_R	=	density of shale or the solid matrix of the sand layers
ρ_w	=	density of water
μ	=	viscosity of water
ϕ	=	porosity
θ	=	angle

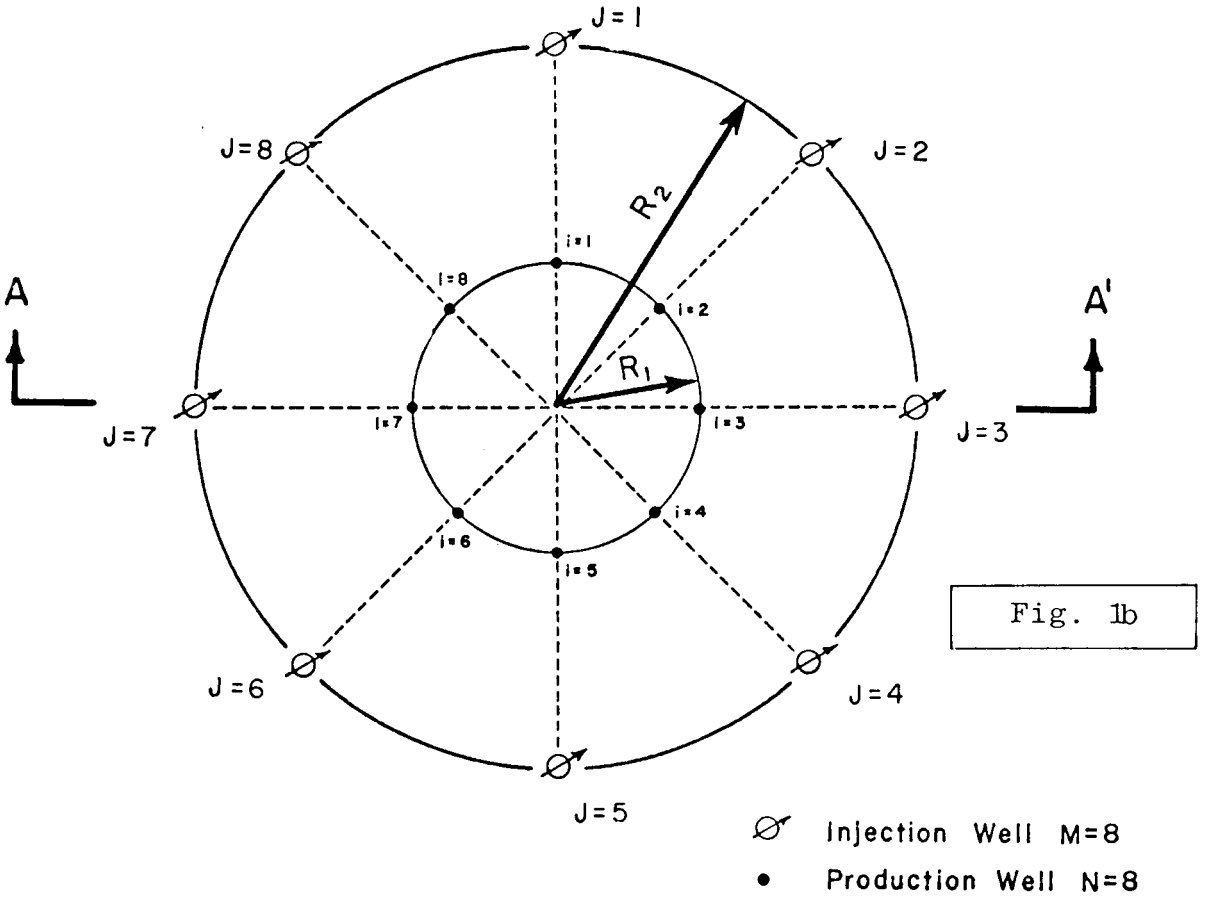

Fig. 1b

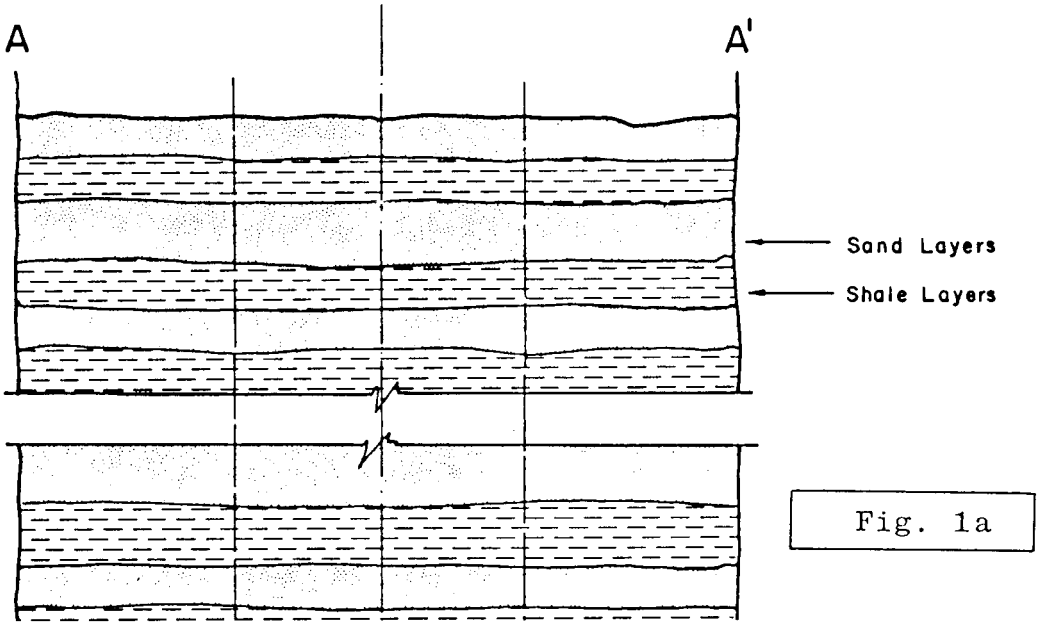

Fig. 1a

Figure 1. Physical system

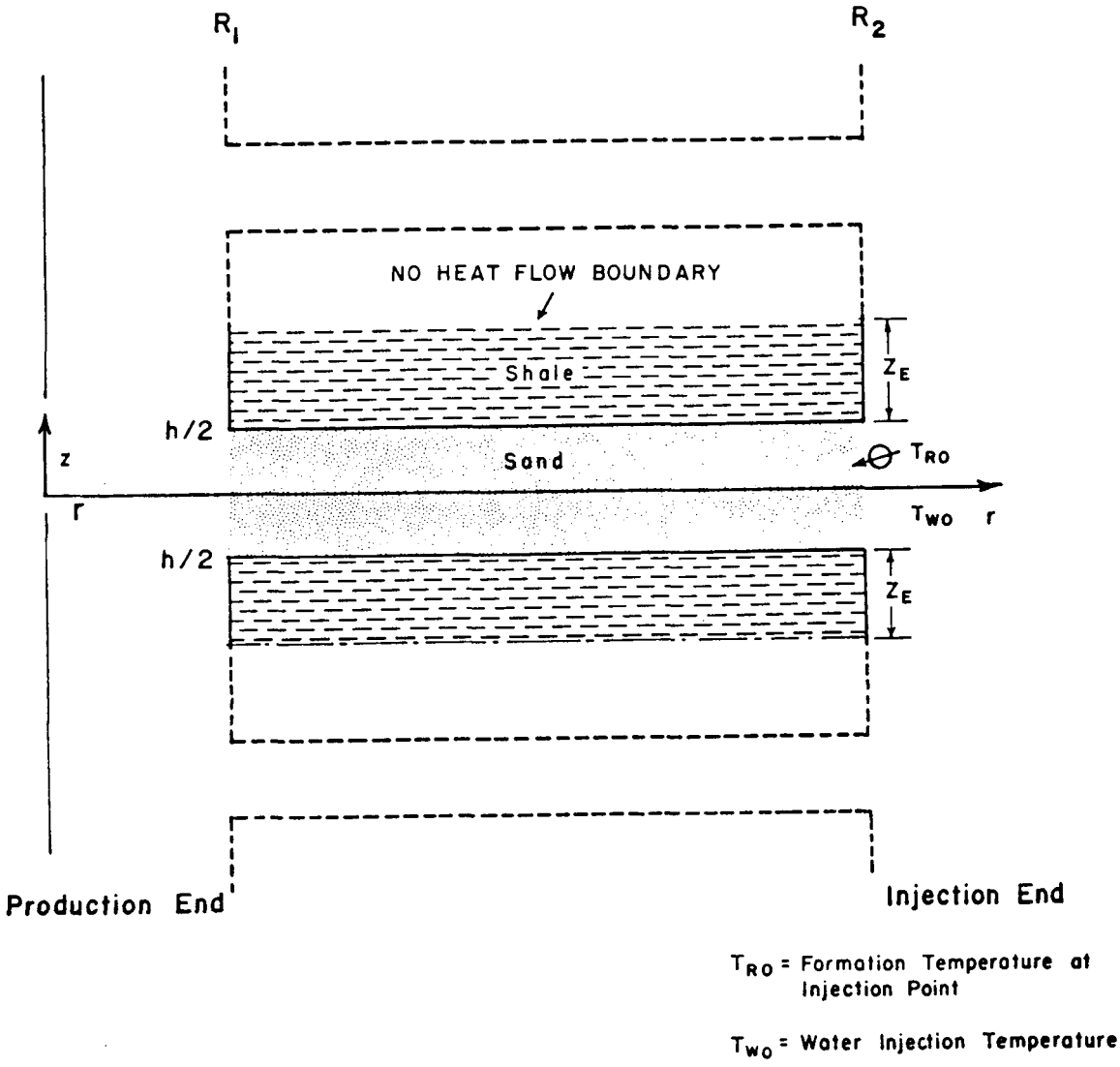

Figure 2. Mathematical model

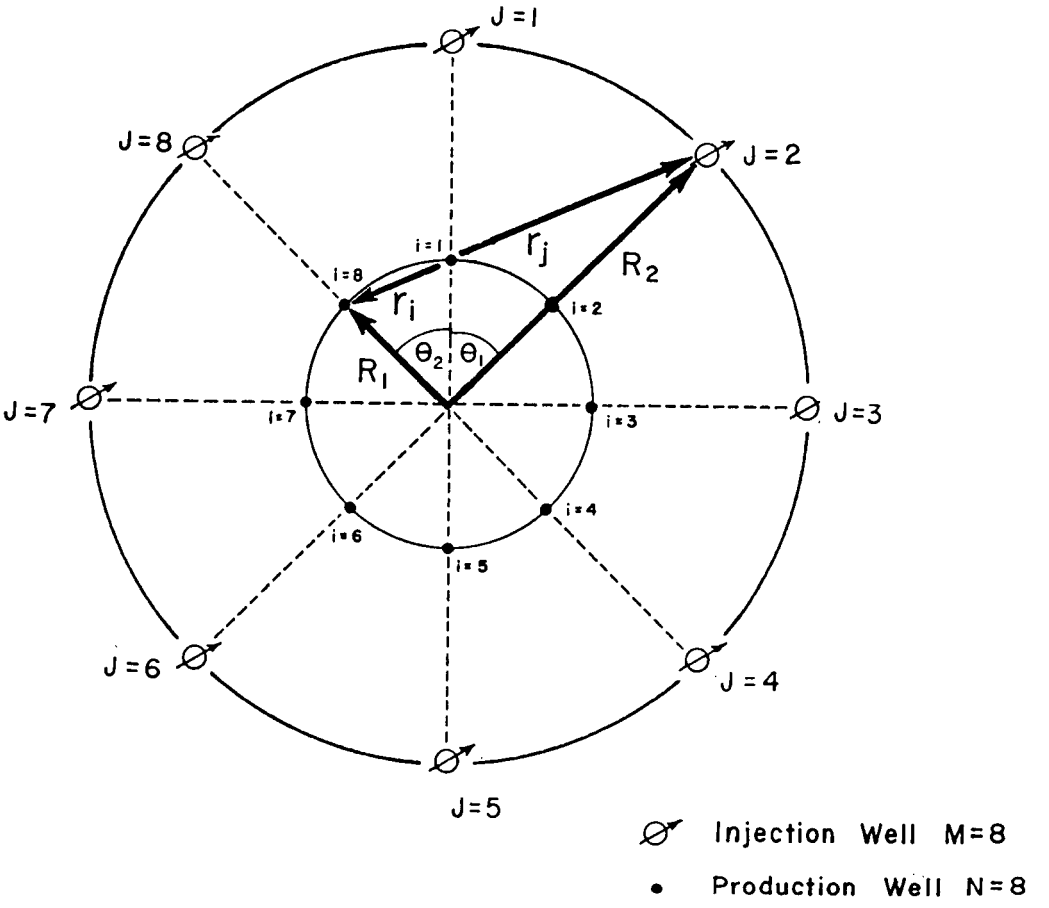

Figure 3. Explanation of symbols

ESTIMATION OF STATIC RESERVOIR TEMPERATURE DURING DRILLING OPERATIONS

P. H. Messer
Union Oil Company
P. O. Box 6854
Santa Rosa, CA 95406

A reliable static formation temperature is valuable in determining casing depths, establishing geothermal gradients, analyzing logs and estimating fluid potential for geothermal reservoirs. The conventional drilling mud fluid systems associated with geothermal well drilling distort the static formation temperature near the wellbore because the circulating mud temperature is normally much less than the static formation temperature. As a result, a wellbore temperature recorded during drilling operations does not reflect the static formation condition.

The use of a Horner-type temperature buildup plot, similar to the conventional pressure buildup method, has been suggested [1] for estimating static formation temperature. The method has proven satisfactory in a number of oil and gas field cases. Recently, Dowdle and Cobb [2] investigated the conditions under which the Horner temperature plot can be used to yield representative static formation temperatures. They concluded that the method is reliable if both the wellbore temperature gradient changes very slowly and the mud circulation time is short. However, in geothermal operations, temperature gradients are usually more extreme and longer circulation times are required to cool the wellbore sufficiently for logging. Therefore, the method has proved to be less reliable.

As an alternate solution, dimensionless Horner temperature type curves have been developed for determining reliable static formation temperatures under normal geothermal drilling conditions in the Imperial Valley, California.

Basic Temperature Equation

The temperature distribution near the wellbore at any time is described in the following differential equation [3]:

$$\frac{\partial T}{\partial r^2} + \frac{1}{r}\frac{\partial T}{\partial r} = \frac{C_p \rho}{K}\frac{\partial T}{\partial t} \qquad (1)$$

Subject to the assumptions of conductive heat flow in the horizontal, cylindrically symmetrical, homogeneous medium surrounding the wellbore, the solution to the above equation is dependent on a set of boundary conditions. Unlike the "diffusivity" equation used in describing pressure behavior, the inner boundary condition is not constant because the wellbore temperature gradient is changing during circulation.

Edwardson et al. [4] numerically solved the above equation at various distances from the wellbore for a $K/C_p\rho r^2$ parameter value of 0.4. This number is derived from the following estimates from limestone, sandstone and shale hydrocarbon reservoir properties: K = 1.303

Btu/hr-ft-°F; C_p = 0.21 Btu/lb-°F; and ρ = 144 lbs/cu ft. The wellbore diameter was assumed to be 7.875 inches. The numerical solution in the form of a dimensionless Horner temperature type curve is shown in Fig. 1 for r_D = 1. Dowdle and Cobb[2] demonstrated that the nonlinearity of these Horner temperature curves is due to the slow change in wellbore temperature gradient during the mud circulation period.

Although the dimensionless curves in Fig. 1 are based on the $K/C_p\rho r_w^2$ value of 0.4, their adaption to reservoirs with different thermal properties has been demonstrated [2] [4]. The values of circulation time (t_k) in Figure 1 can simply be replaced with values corresponding to another set of conditions. For a case of $K/C_p\rho r_w^2$ equal to 0.8, the curve for t_k = 2.4 hours in Fig. 1 would be redesignated t'_k = 1.2 hours. Empirical data determined during drilling operations can be plotted on Fig. 1 and a representative $K/C_p\rho r_w^2$ value for the system can be determined.

Figure 2 shows actual data points collected during Imperial Valley drilling operations plotted on the theoretical Horner buildup curves for $K/C_p\rho r_w^2$ equal to 0.4. Clearly, a circulation time in excess of 14 hours would be required to define the $K/C_p\rho r_w^2$ value or to use the curves shown in Fig. 1.

Circulation times on this order are excessive and costly. For these theoretical type curves to be useful in Imperial Valley geothermal reservoirs, t_k values down to 0.05± would need to be generated.

Development of Empirical Type Curves

Rather than expanding the numerical solutions presented by Edwardson et al., sufficient temperature data has been collected from the drilling operations in more than one geothermal area of the Imperial Valley to construct an empirical set of Horner temperature buildup curves. Various scheduled operations during drilling provided opportunities to measure directly wellbore temperatures at various depths and times after mud circulation was stopped. For instance, multiple maximum recording thermometers were run during logging operations and also during hole deviation surveys. In addition, Amerada-type temperature recorders were run at various depths and circulation histories.

Wellbore temperature change with time after circulation stopped was recorded in several wells at various formation depths for a wide range of circulation times. Following completion, a history of temperature gradient surveys defined the static formation temperature at any particular depth. Having measured the static formation temperature and recording the wellbore temperature changes with time after various circulation periods, the curves in Fig. 3 were constructed.

Accuracy of the Static Formation Temperature Estimation

The empirical set of curves in Fig. 3 was developed from data obtained over a formation depth interval in excess of 4500 feet in one area of the Imperial Valley. The uniform spacing of the curves suggests that there was no

appreciable change in the reservoir thermal properties with depth or temperature variation. The curves in Fig. 3 have been quite accurate in estimating static formation temperature as demonstrated in the following examples.

Field Examples of Estimating Static Formation Temperature

Example 1

The following data was obtained at a specific depth after 14 hours of circulating (t_k).

T_m = Datum circulating mud temperature, 164°F.

Δt = Time since circulation stopped, 10.75 hours.

T_{ws} = Datum shut-in temperature at time Δt, 282°F.

Solve for Horner dimensionless time:

$$\frac{t_k + \Delta t}{\Delta t} = \frac{14 + 10.75}{10.75} = 2.30$$

From graph:

$$\frac{T_i - T_{ws}}{T_i - T_m} = .446$$

$$\frac{T_i - 282}{T_i - 164} = .446$$

$$T_i = 377^{\circ}F$$

The static temperature recorded at this datum several months after completion was 377°F.

Example 2

The following data was obtained at a different datum in another well after 2.22 hours of circulation (t_k):

$$T_m = 180^{\circ}F$$

$$t = 6.62 \text{ hours}$$

$$T_{ws} = 225^{\circ}F$$

$$\frac{t_k + \Delta t}{\Delta t} = 1.335$$

From graph: $\frac{T_i - 255}{T_i - 180} = .50$

$T_i = 330^{\circ}F$

The static temperature recorded at this datum more than 7 months after completion was $334^{\circ}F$.

References

(1) Timko, D. J., and Fertl, W. H.: "How downhole temperatures, pressures affect drilling," World Oil (October, 1972).

(2) Dowdle, W. L., and Cobb, W. M.: "Static formation temperature from well logs--an empirical method," J. Pet. Tech. (November, 1975) pgs. 1326-1330.

(3) Carslaw, H. S., and Jaeger, J. C.: "Conduction of heat in solids," The Clarendon Press, Oxford University (1947).

(4) Edwardson, M. J., Girner, H. M., Parkison, H. R., Williamson, C. D., and Matthews, C. S.: "Calculation of formation temperature disturbances caused by mud circulation," J. Pet. Tech. (April, 1962) pgs. 416-426, Trans., AIME, 225.

(5) Ingersoll, L. R., Zobel, O. J., and Ingersoll, A. C.: "Heat conduction," U. Wisconsin Press, Madison, Wisconsin, (1954).

Nomenclature

C_p = Specific heat capacity, Btu/lb-°F.

K = Thermal conductivity, Btu/hr-ft-°F.

r = Radial distance, feet.

r_w = Wellbore radius, feet.

r_D = r/r_w, dimensionless radius.

t_k = Circulation time, hours.

Δt = Shut-in time since circulation, hours.

T_i = Static formation temperature, °F.

T_m = Datum circulating mud temperature, °F.

T_{ws} = Datum shut-in temperature at time Δt, °F.

ρ = Density, lbs/cu ft.

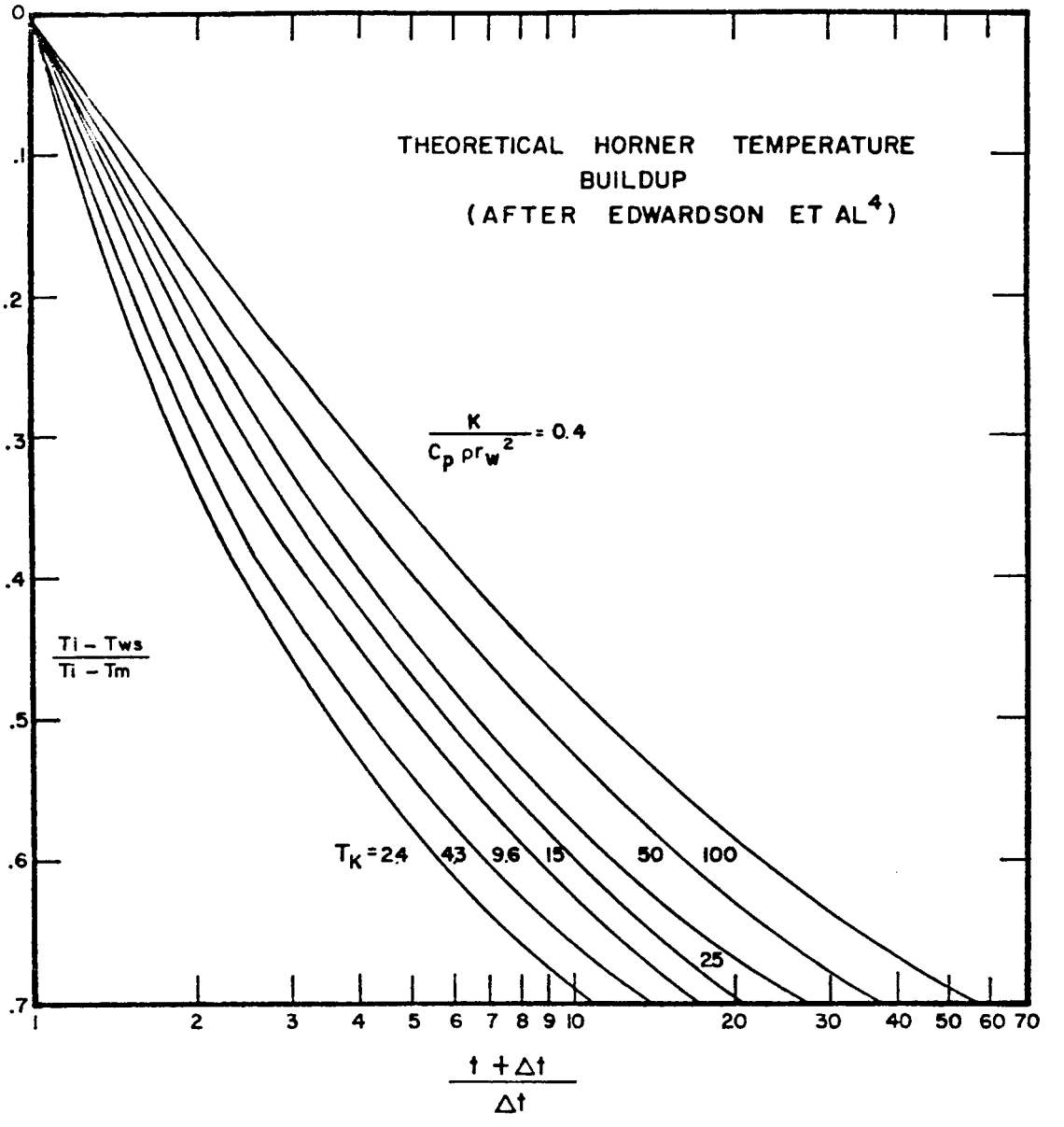
THEORETICAL HORNER TEMPERATURE BUILDUP
(AFTER EDWARDSON ET AL[4])
$\frac{K}{C_p \rho r_w^2} = 0.4$
$\frac{Ti - Tws}{Ti - Tm}$
T_K = 2.4 4.3 9.6 15 25 50 100
0 .1 .2 .3 .4 .5 .6 .7
1 2 3 4 5 6 7 8 9 10 20 30 40 50 60 70
$\frac{t + \Delta t}{\Delta t}$

FIGURE 1.

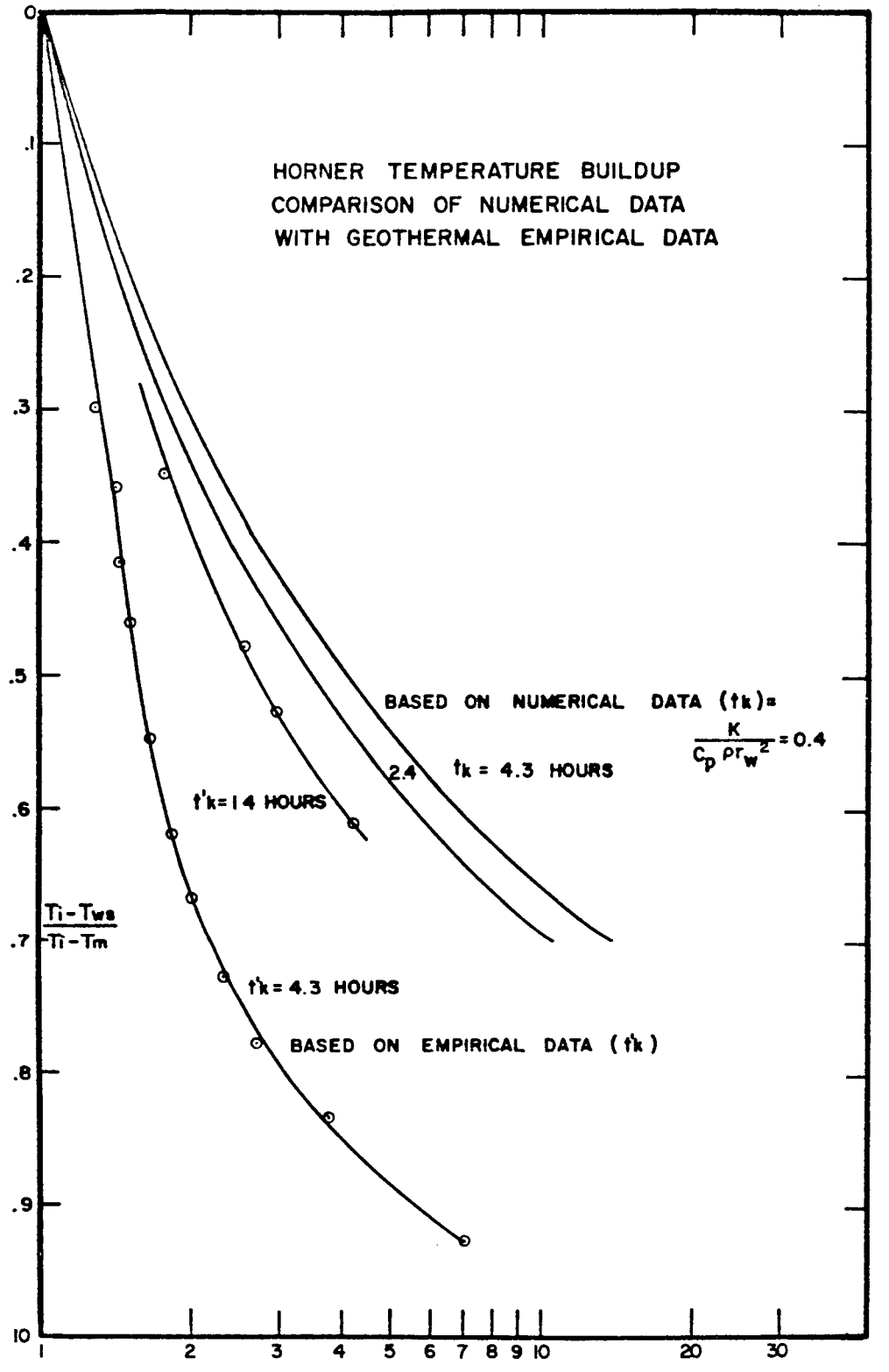
HORNER TEMPERATURE BUILDUP
COMPARISON OF NUMERICAL DATA
WITH GEOTHERMAL EMPIRICAL DATA
BASED ON NUMERICAL DATA (tk)=
K / Cp ρrw² = 0.4
2.4
tk = 4.3 HOURS
t'k=14 HOURS
t'k = 4.3 HOURS
BASED ON EMPIRICAL DATA (t'k)
(Ti-Tws)/(Ti-Tm)
0
.1
.2
.3
.4
.5
.6
.7
.8
.9
10
1
2
3
4
5
6
7
8
9
10
20
30

FIGURE 2.

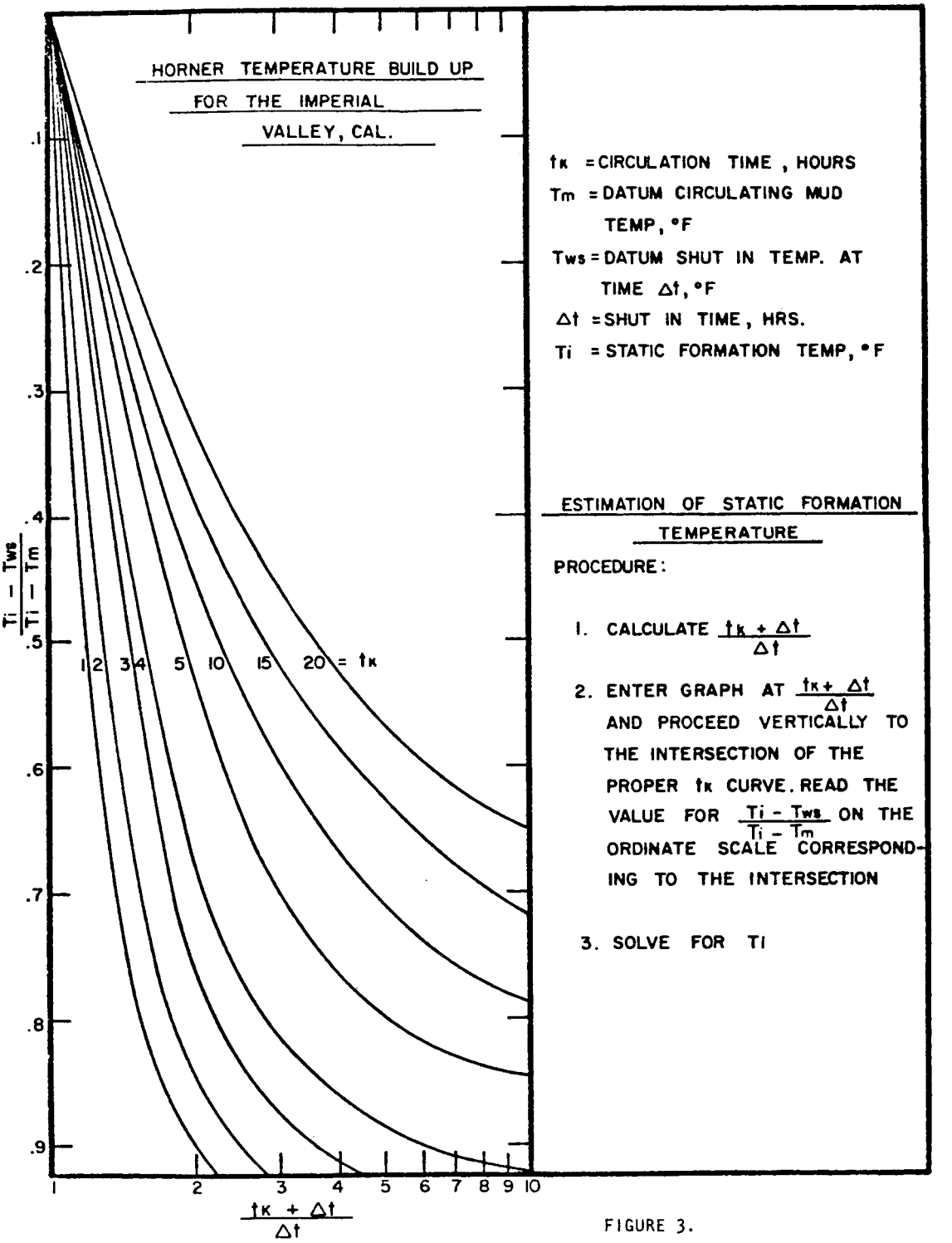
HORNER TEMPERATURE BUILD UP
FOR THE IMPERIAL
VALLEY, CAL.
t_K = CIRCULATION TIME, HOURS
T_m = DATUM CIRCULATING MUD TEMP, °F
T_{ws} = DATUM SHUT IN TEMP. AT TIME Δt, °F
Δt = SHUT IN TIME, HRS.
T_i = STATIC FORMATION TEMP, °F
ESTIMATION OF STATIC FORMATION TEMPERATURE
PROCEDURE:
1. CALCULATE $\frac{t_K + \Delta t}{\Delta t}$
2. ENTER GRAPH AT $\frac{t_K + \Delta t}{\Delta t}$ AND PROCEED VERTICALLY TO THE INTERSECTION OF THE PROPER t_K CURVE. READ THE VALUE FOR $\frac{T_i - T_{ws}}{T_i - T_m}$ ON THE ORDINATE SCALE CORRESPONDING TO THE INTERSECTION
3. SOLVE FOR T_I
$\frac{T_i - T_{ws}}{T_i - T_m}$
.1
.2
.3
.4
.5
.6
.7
.8
.9
1 2 3 4 5 10 15 20 = t_K
1 2 3 4 5 6 7 8 9 10
$\frac{t_K + \Delta t}{\Delta t}$

FIGURE 3.

FIELD CASE STUDIES OF PRESSURE BUILDUP BEHAVIOR IN GEYSERS STEAM WELLS

Calvin J. Strobel
Union Oil Company
1250 Coddington Center
P.O.Box 6854
Santa Rosa, CA. 95406

The purpose of this paper is to illustrate and discuss practical application of pressure buildup test theory in The Geysers steam reservoir. This field, located in Sonoma County in Northern California, has installed generating capacity of 522 MW. Total withdrawal rate is approximately 8.5 million pounds per hour from 93 wells.

The reservoir is naturally fractured greywacke, a very competent rock with low interstitial porosity and permeability. It is underpressured, initial pressure being approximately 520 psia at sea level datum. Static pressure gradient is that of saturated steam to total depths reached to date.

Application

Practical application of pressure buildup analysis at The Geysers has been used to make qualitative interpretations about such things as fracture geometry and boundary conditions.

Quantitative estimates of reservoir permeability are made on a routine basis. Quantitative estimation of porosity using pressure buildup analysis requires a very accurate knowledge of reservoir geometry, so this application must be approached with caution, since the reservoir is still being delineated by exploratory drilling.

The pressure buildup can conveniently be divided up into three general periods for purposes of discussion: (1) short-time, (2) radial flow, and (3) late-time. During short-time, pressure buildup is dominated by either wellbore storage and skin effect, linear flow along a fracture plane, or a combination of these. After these short-time effects die out, pressure becomes a linear function of the logarithm of time. This semi-log straight period will be called radial flow for purposes of discussion in this paper. At late-time, pressure departs from semi-log straight in various ways depending upon boundary conditions.

Any or all of the above three periods typical of pressure buildup behavior at wells in The Geysers reservoir may be masked by such unpredictable things as condensation in the wellbore.

Short-Time Behavior

The short-time behavior designated by straight lines on Figs. 1 and 2 commonly lasts for no more than a few minutes. This data, recorded by hand using a test gauge and a stop watch, is valuable in characterizing

fracture geometry and in doing type curve matching to identify the proper semi-log straight line. The wellhead data is converted to datum (usually midpoint of steam entries) using the Cullender-Smith Method of calculating bottomhole pressure [1].

Short-time buildup behavior at The Geysers generally falls into one of the two types: (1) half-slope as in Fig. 1, and (2) unit slope, as in Fig. 2. Ramey [2] identified the significance of these two types, showing that unit slope behavior is characteristic of a well with storage and skin, and that half-slope behavior is characteristic of flow along a linear fracture plane. Unit slope behavior is most common at The Geysers; however, fractured wells commonly exhibit storage effects with early behavior showing anything from 1/2 to unit slope. Certain methods of analysis discussed in Reference 3 are used to avoid labeling a particular buildup a storage case when it is actually a fracture case with storage.

For pressure buildup analysis in wells exhibiting fracture flow, Wattenbarger's "double delta p" rule, discussed in Reference 3, has been used successfully to find the start of the proper semi-log straight line. As noticed by Wattenbarger [4], dimensionless pressure at the start of the semi-log straight line is approximately twice the dimensionless pressure at the top of the one-half slope line. This rule also helps to differentiate between fracture cases with wellbore storage, and cases that are only storage and skin effect because in the latter case, application of the "double delta p" rule will lead to a pressure difference for greater than possible for the start of a semi-log straight line. Applying the "double delta p" rule to Fig. 2 shows that this buildup might be a fracture case, even though it has a unit slope. Comparison of this buildup to type curves for a vertically fractured well having wellbore storage effects verified that this was a fracture case.

Log-log graphs such as Figs. 1 and 2 require an accurate knowledge of flowing pressure prior to shut-in. Flowing pressure measured at the wellhead is generally not directly usable for constructing a log-log graph. This is because wellhead flowing pressure reflects friction pressure losses, and small inaccuracies in estimating friction pressure drop lead to very substantial changes in the log-log graph. The most useful procedure for identifying the proper value to use for graphing has been to record short-time data at 5-second intervals for the first minute of the buildup, then visually inspect the data to determine incremental rise in pressure per 5-second interval. Best estimate of this can usually be made using data beyond 10 seconds. Pressure at time zero is then corrected to make it consistent with the observed incremental pressure rise beyond 10 seconds.

Radial Flow Behavior

Pressure buildup beyond the short-time period is a linear function of the logarithm of time. Fig. 3, showing this behavior for a steam well at The Geysers, describes a semi-log straight line for five log cycles. Quantitative estimates of permeability-thickness, kh, made from graphs such as this, give remarkably consistent values from test to test on a given well.

The most prevalent problem with testing the dry steam wells at The Geysers has been condensation, which causes erratic pressure behavior. In serious cases, wellhead pressure may even drop as the wellbore loads with water condensation. The data scatter on Fig. 3 is probably due to condensation and revaporization effects. Fig. 4 is a more dramatic case, showing that a part of the semi-log straight line has been masked by these two-phase wellbore effects. In very serious cases, a long vaporizing period may be mistaken for a semi-log straight line. This mistake can be avoided by comparing the buildup to the appropriate log-log type curve.

The two-phase effects illustrated in Fig. 4 have been most common in wells shut-in on small vents, i.e., 1/2" or less. This problem is eliminated by doing two-rate buildup tests. The two-rate tests require that the well be choked back to a second rate high enough to avoid condensation. The pressure buildup analysis method, developed from Chapter 6 of Reference 5, for use at The Geysers, accounts for this second rate, resulting in the analytic method shown on Fig. 5. The two-rate method gives results that compare well with conventional buildup tests. For example, kh obtained from Fig. 5 was within 13% of the kh value obtained on the same well using conventional buildup test procedures.

Late-Time Behavior

When drainage boundaries or other reservoir heterogeneities begin to affect pressure buildup at a well, the data will no longer be a semi-log straight function of time. Boundary conditions at The Geysers are not well understood, so that our analysis of boundary effects on pressure buildup must be confined to qualitative comparisons with type curves. For example, the theoretical behavior for the case of a vertically fractured well in a closed square (Fig. 6) was published by Gringarten, et al [6]. Theoretical behavior for the system shown on Fig. 6, with uniform flux along the fracture, is illustrated on Fig. 7. The field data shown on Fig. 7, from a non-commercial well at The Geysers, matches a type curve from the first data point, recorded at 10 seconds shut-in time, up until a shut-in time of 147 hours. Fig. 7 shows the importance of recording accurate short-time data. Field cases of this type are extremely rare.

The most common type of late-time behavior observed at The Geysers conforms to the theoretical behavior for the drainage system illustrated in Fig. 8. This system, and the corresponding type curves shown on Fig. 9, are from work published by Ramey, et al [7]. Field data graphed on Fig. 9 follow the general shape and timing of events characteristic of the type curves; deviation of the field data from the type curves during late-time is probably due to the condensation effects discussed earlier. The type curves shift upward and to the right correspondingly as producing time prior to shut-in is increased. This behavior, peculiar to systems with strong pressure support, is exhibited by most wells in The Geysers reservoir.

Type curve matches, such as Fig. 9, can be used to make reliable, quantitative estimates of reservoir pore volume and porosity, provided the system is at initial conditions and location and nature of drainage

boundaries can be reasonably identified. Practical application of this has been demonstrated in a naturally fractured gas field [8]. Obviously, geologic and engineering investigations must be a joint cooperative effort.

Concluding Remarks

Pressure buildup behavior recorded at wells in The Geysers dry steam field has been valuable in gaining insight into reservoir mechanics. Modern well test analysis methods have been applied successfully to describe field data and extract practical information. Buildup testing, however, is not an end in itself, but must be harmonized with other engineering and geological methods. Analysis of pressure buildup behavior along with geologic information, is a logical first stage of analysis leading to more sophisticated methods such as reservoir simulation using digital computers.

Nomenclature

L	=	Fracture length, wellbore to tip
P	=	Pressure
T	=	Flowing Time
ΔT	=	Shut-in Time
W	=	Flow Rate, lbs/hr
X_E	=	Linear Distance, boundary to boundary
X_F	=	Linear Distance, fracture tip to tip

Subscripts

D	=	Dimensionless
TF	=	Wellhead flowing
TS	=	Wellhead shut-in
WF	=	Bottomhole flowing
WS	=	Bottomhole shut-in

References

(1) Theory and Practice of the Testing of Gas Wells, Oil and Gas Conservation Board, Calgary, Alberta, Second Edition (1965), pg. 161.

(2) Ramey, H.J., Jr.: "Short-time Well Test Data Interpretation in the Presence of Skin Effect and Wellbore Storage," J. Pet. Tech. (Jan., 1970) pg. 97.

(3) Ramey, H.J., Jr.: "Practical Use of Modern Well Test Analysis," SPE 5878, 46th Annual California Regional Meeting, SPE of AIME, Long Beach (April 8-9, 1976).

(4) Wattenbarger, R.A., and Ramey, H.J., Jr.: "Well Test Interpretation of Vertically Fractured Gas Wells," J. Pet. Tech. (May, 1969) pgs. 625-632.

(5) Matthews, C.S., and Russell, D.G.: Pressure Buildup and Flow Tests in Wells, Soc. Pet. Eng. Monograph Series, Volume 1, SPE, Dallas (1967).

(6) Gringarten, C.A., Ramey, H.J., Jr., and Raghavan, R.: "Unsteady-State Pressure Distributions Created by a Well with a Single Infinite--Conductivity Vertical Fracture," Soc. Pet. Eng. J. (August, 1974) pgs. 347-360; AIME Trans., Volume 257.

(7) Ramey, H.J., Jr., Kumar, A., and Gulati, M.S.: Gas Well Test Analysis Under Water-Drive Conditions, American Gas Association Monograph, 1973.

(8) Strobel, C.J., Gulati, M.S., and Ramey, H.J., Jr.: "Reservoir Limit Tests in a Naturally Fractured Reservoir--A Field Case Study Using Type Curves," J. Pet. Tech. (September, 1976) pg. 1097.

FIGURE 1

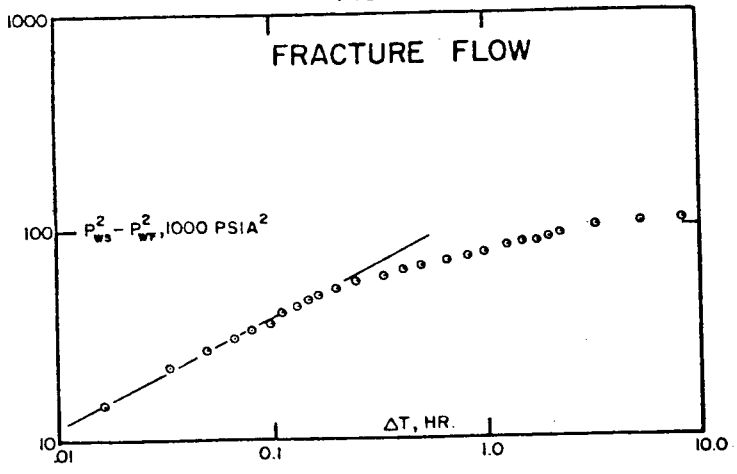

FIGURE 2

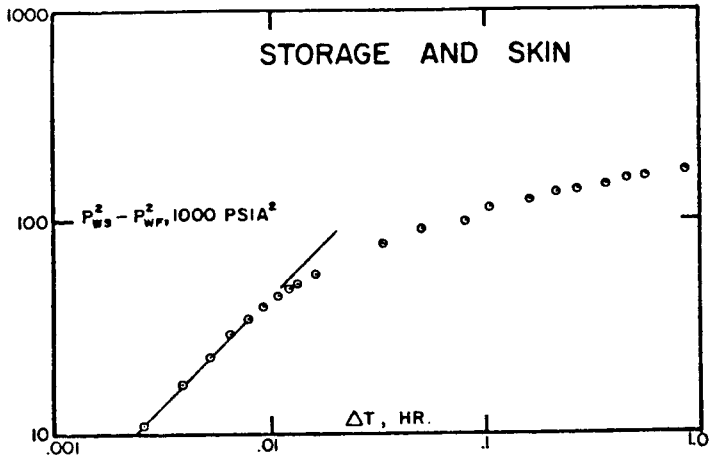

FIGURE 3

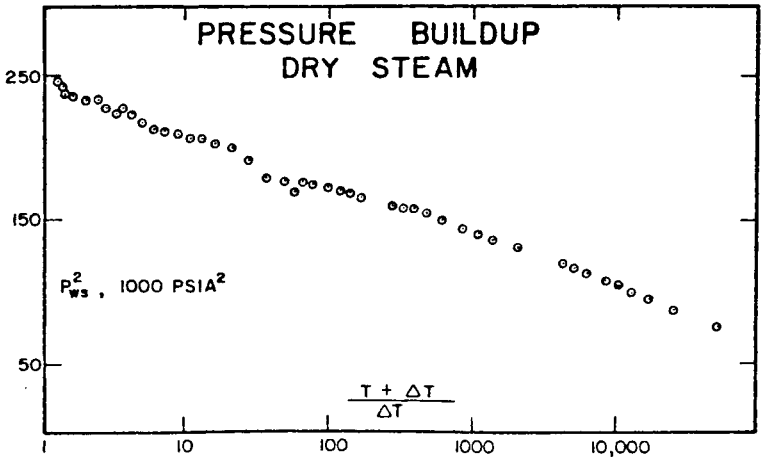

FIGURE 4

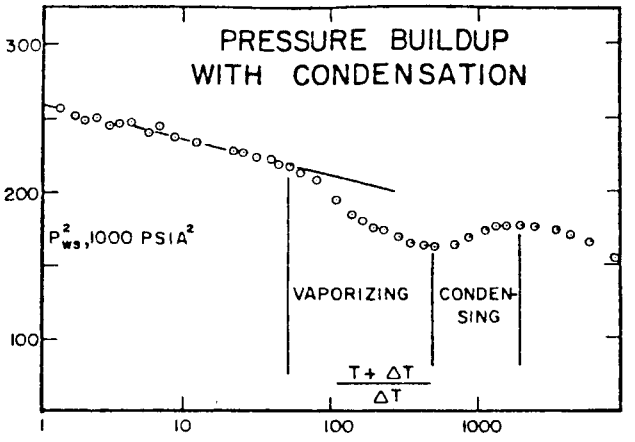

FIGURE 5

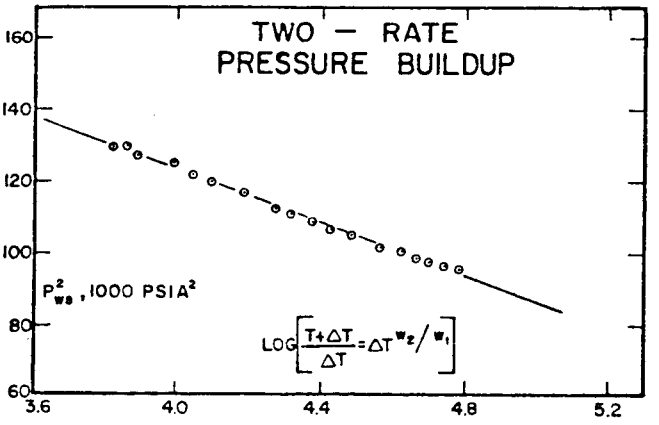

FIGURE 6

DRAINAGE AREA

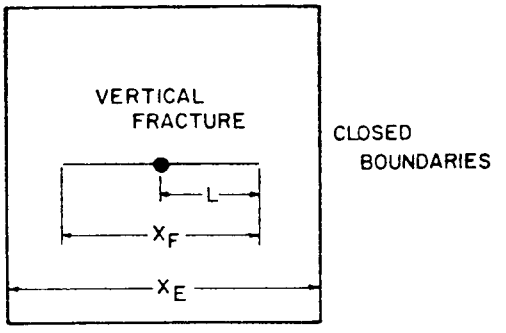

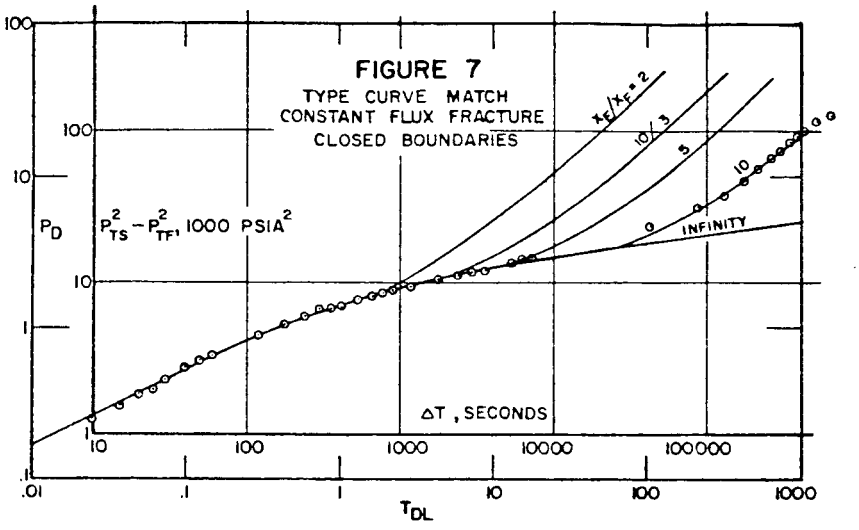

FIGURE 8
DRAINAGE AREA
CONSTANT PRESSURE BOUNDARIES

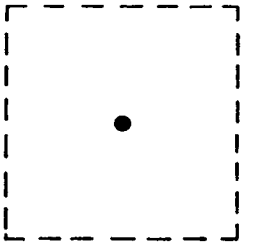

FIGURE 9

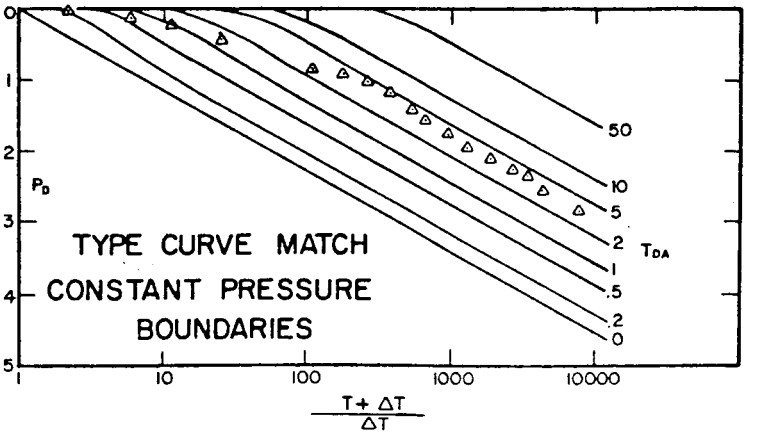

A RESERVOIR ENGINEERING STUDY IN GABBRO ZONE (NORTHERN PART OF LARDERELLO FIELD)

R. Celati*, G. Manetti**, R. Marconcini***, G. Neri***

Gabbro zone, located north of the old geothermal field of Larderello, was explored after 1960 by several wells, as shown in Fig. 1.

The geology of the area can be summarized by grouping the different terrains into three main complexes as follows.

1. An upper complex, consisting of Neogenic deposits, and allochthonous flysch facies formations with ophiolites (Jurassic-Eocene). Because of its predominantly argillaceous nature, this complex is practically impermeable.

2. A discontinuous layer represented by brecciated carbonate rocks associated with evaporitic deposits (Trias), characterized by high secondary permeability.

3. A lower complex, consisting mainly of Triassic and Paleozoic metamorphic clastic formations (quartzites and phyllites). In this case too the permeability is tied to the existence of fractures.

Gabbro zone represents a structural high, separated from the culmination of the main Larderello-Castelnuovo structure.

On the E-NE side, this structure borders on an important direct fault which, on a regional scale, represents the western boundary of a large tectonic depression trending NW-SE (Era Graben).

On the north side of the Gabbro structure, the layer of Triassic breccias is lacking. This is probably one cause of the decrease in permeability observed in the northern marginal zone.

*C.N.R., Istituto Internazionale per le Ricerche Geotermiche, Pisa, Italy.

**ENEL, Centro Ricerca Geotermica, Pisa, Italy.

***ENEL, Gruppo Minerario Larderello, Larderello, Italy.

Only a few wells were productive. The extension of research showed that the high productivity zone (G1, G3, G6, G9) is surrounded by dry or low productivity wells (Fig. 1). Therefore it can be said that the wells inside the circle in Fig. 1 are producing from a reservoir closed in on every side except that of the old Larderello area. In particular, 90% of production is concentrated in an area smaller than 1 km^2, including wells G1, G3, G6 and G9.

Other producing wells in this area are SD2, G7, SD4, G4, G8, 155. The non-commercial wells as, for example, SD4, G4, G8, have been shut-in since they were first drilled.

The producing wells deliver superheated steam at a well-head pressure between 5 and 8 ata (kg/cm^2a) and at a temperature of 230 C. This work sets out to analyze shut-in pressure and flow-rate declines. The first wells drilled north of Larderello area where N.155 and SV9 which, after their shut-in, reached the pressures of 25.8 and 25 ata, respectively, at well-head.

The small difference between the shut-in pressures of the two wells is not surprising considering their topographic position, which is along a line parallel to the area containing the producing wells of Larderello and Castelnuovo fields.

We can assume that the isobars of the drainage volume of Larderello-Castelnuovo wells lie parallel to the line joining wells SV9 and 155 and so the pressure gradient has its greatest value perpendicular to this line. These considerations are confirmed (Fig. 2) by the value (31 ata) of the shut-in pressure of Gabbro 1 well, drilled in 1962, which is about 5 ata more than the shut-in pressure of well 155 and also by shut-in pressures of wells G3 and SD2, drilled in 1963.

In that period the shut-in pressure in the old Larderello area was 8 ata and the flow-rate in Larderello field was 1500 t/h at a delivery pressure of about 5 ata.

It appears from these considerations that Gabbro zone is drained by the wells in old Larderello field.

The development of production in Gabbro zone is shown in Fig. 3 and the pressure decline in the closed wells is shown in Figs. 4 and 5.

The well-head pressure measurements for wells G4 and G8 are not completely reliable because their behavior is probably affected by the existence of liquid water inside the wells (Fig. 4).

However, an interference of G9 production on the pressure trend is apparent.

The pressure histories of SD2, G7 and G9 are available for a limited period of time.

Figure 5 shows that SD2 pressure history is affected by exploitation of G6 and G9.

We first of all tried applying the analysis methods used for gas reservoirs. As the available data are insufficient for defining a reliable average reservoir pressure history, shut-in pressures of the individual wells were plotted versus cumulative production of the entire zone (Figs 6 and 7). Considering the pressure values, well conditions and location, we can assume that the average pressure of the zone is higher than G8 pressure and lower than SD4 one. (As a matter of fact, well G6 has recently been shut-in for two days and its pressure reached 14.4 ata). Furthermore, in the final section all the curves appear to be parallel to one another. The extrapolations of these curves to 1 ata give an evaluation of steam reserves between 100 and 115 x 10^9 kg.

To obtain an alternative estimate of initial fluid in place, we analyzed the flow-rate decline curves.

Assuming the following rate and pressure decline equations:

$$Q = C(\overline{P}^2 - P^2)^n \qquad (1)$$

$$\overline{P} = P_i - KQ_{ex} \qquad (2)$$

$$K = P_i/Q_{tot} \qquad (3)$$

Q	= flow-rate	kg/h
$\overline{P}$	= reservoir average pressure	ata
P	= flowing pressure	ata
P_i	= initial reservoir pressure	ata
Q_{ex}	= steam produced	kg
Q_{tot}	= initial steam in place	kg

we obtain,

$$(Q/Q_1)^{1/n} = \frac{1-A^2}{1-B^2} - \frac{2R-R^2}{1-B^2} \qquad (4)$$

$$A = P/P_i$$

$$B = P_1/P_i \qquad R = Q_{ex}/Q_{tot}$$

Q_1, P_1 are Q and P at t = 0

To obtain this equation, C and n are supposed to remain constant throughout the production period. The values of n were taken from the back-pressure tests performed a short time after the wells blew out.

To establish whether equation (4) describes the temporal evolution of flow-rate in the wells examined, we plotted the actual values of $(Q/Q_1)^{1/n}$ versus time.

The diagram $(Q/Q_1)^{1/n}$ appearing in the figure is due to the fact that delivery pressures were considerably lowered during short periods.

The best value for Q_{tot} was chosen.

A 10% Q_{tot} variation is easily detected by this method.

Diagram $\ln(Q/Q_1)^{1/n}$ versus Pnt shows that production in wells G6 and G9 clearly interferes with the previously producing wells.

The interference effects change the drainage volumes of a well so that C is no longer constant and the equations no longer valid. Better results will probably be gained by varying C and n according to suitable criteria.

In order to obtain an evaluation of Q_{tot} and an indication of the effect of a variation in n, the analysis was repeated using n values covering all the possible range.

The sum of Q_{tot} for all the wells in the area is $70 \cdot 10^9$ kg, assuming $n = 0.5$, whereas, using the maximum value $n = 1$ for all the wells, ΣQ_{tot} becomes $130 \cdot 10^9$ kg.

Thus an evaluation of the initial steam-in-place gives:

pressure decline analysis : $100 \div 115 \times 10^9$ kg

flow-rate decline analysis: $70 \div 130 \times 10^9$ kg

These values are in sufficient agreement, considering the limits of the methods employed. However, assuming that the reservoir was initially filled with steam (specific volume of 0.07 m^3/kg) and considering a porosity of 5%, the bulk volume should be 100 km^3. Since the area concerned covers 7 km^2, the reservoir depth should be 14 km.

From the last consideration, the hypothesis of a closed gas reservoir, as assumed for the analysis, does not seem to work in our case, especially in view of the fact that an unknown amount of fluid is flowing from this area towards the old Larderello zone.

Some sort of water recharge, a feeding from deep subvertical fractures, or the initial presence of liquid and steam simultaneously in the reservoir, must be admitted.

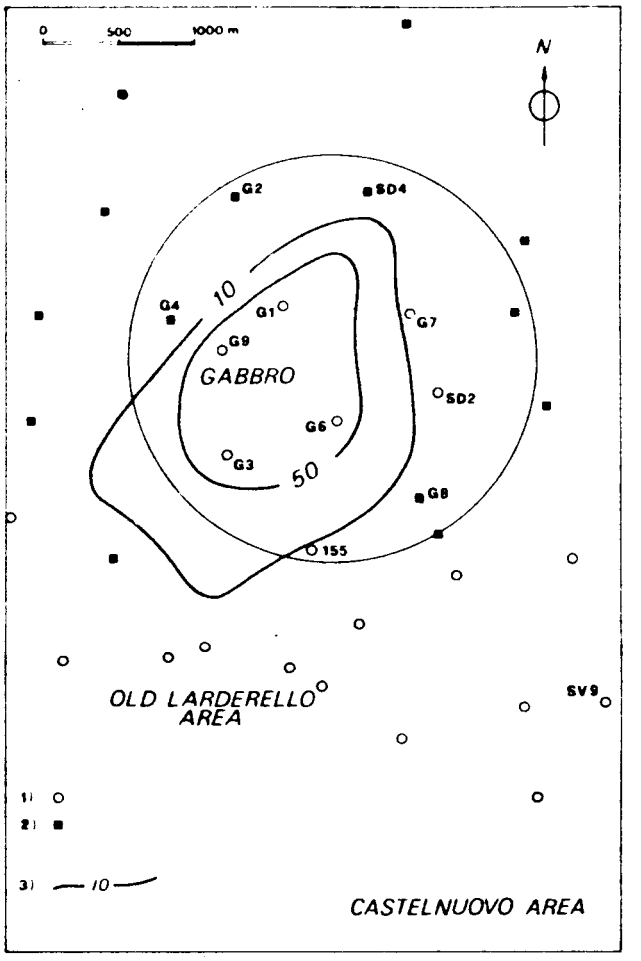

Fig. 1 - Location of the wells in Larderello field. Gabbro zone lies within the circle.

1: producing wells.
2: dry or non-commercial wells.
3: Kh contours (Darcy m).

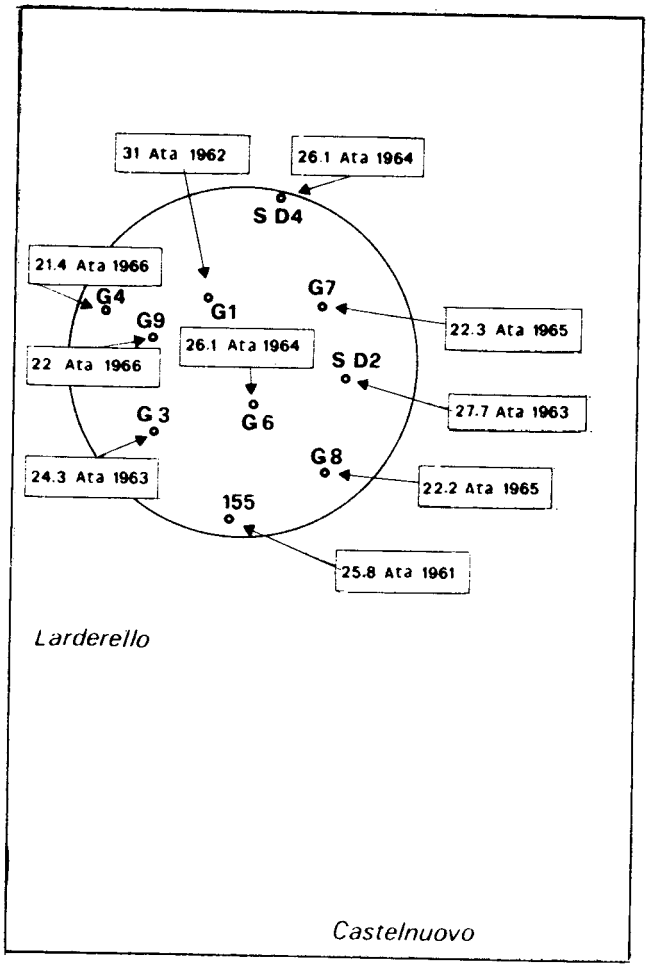

Fig. 2 - Initial shut-in pressures of the wells drilled in Gabbro zone.

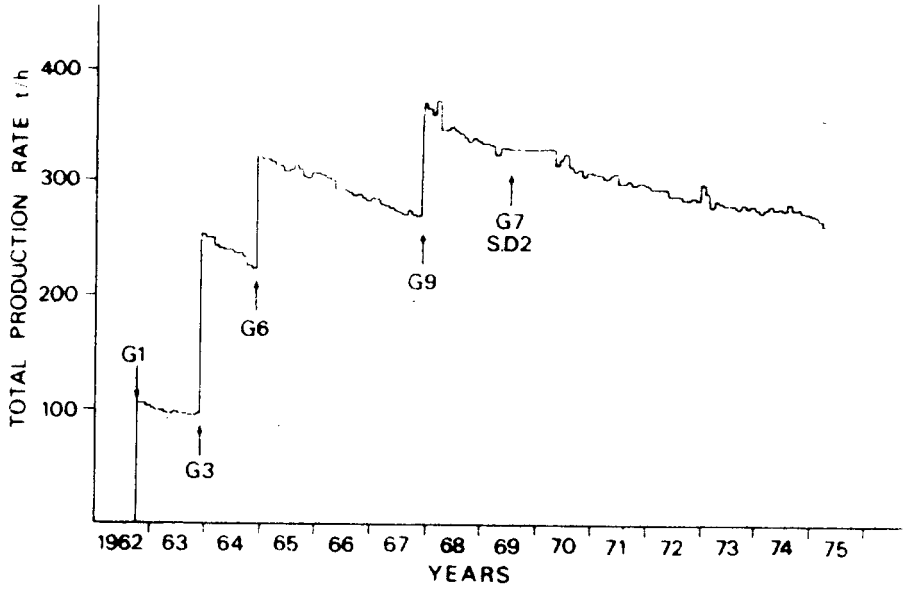

Fig. 3 - Total flow-rate of the wells in Gabbro zone during 1962-1975 period. Well No. 155 is not included.

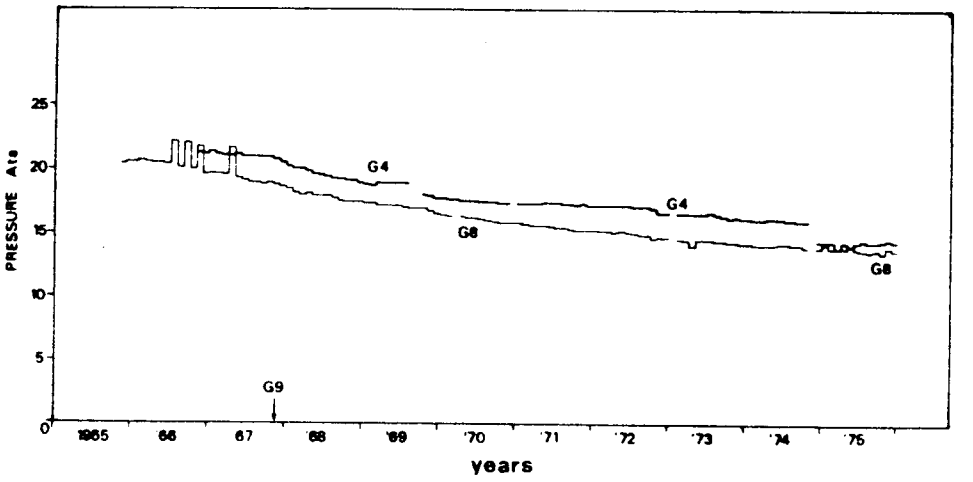

Fig. 4 - G4-G8 well-head shut-in pressures versus time.

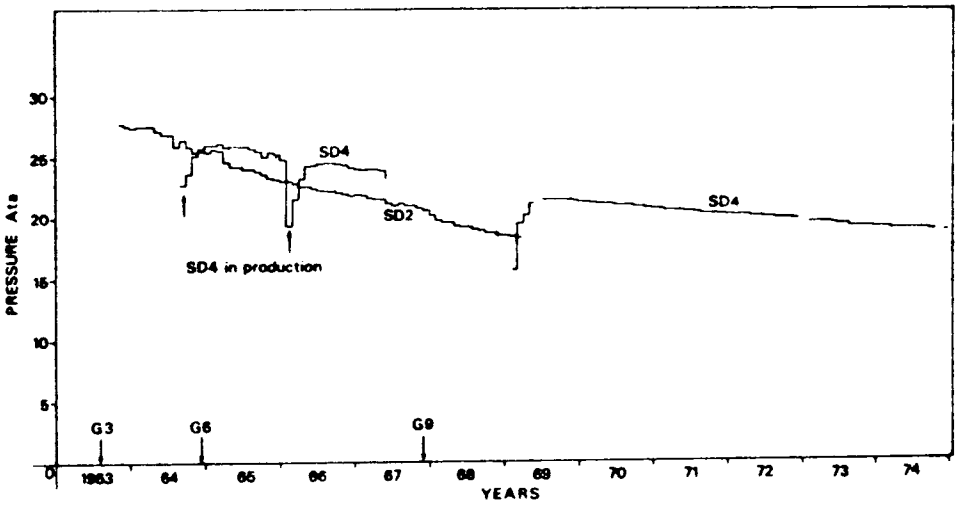

Fig. 5 - SD4 - SD2 well-head shut-in pressures versus time.

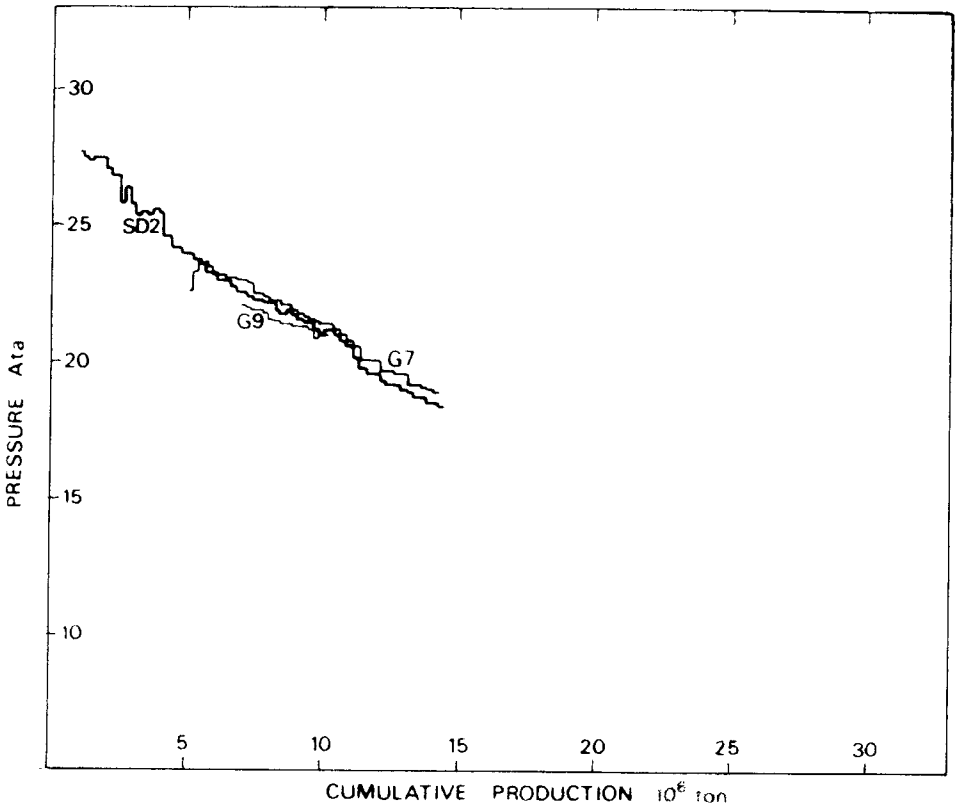

Fig. 6 - G9 - G7-SD2 well-head shut-in pressures versus cumulative production.

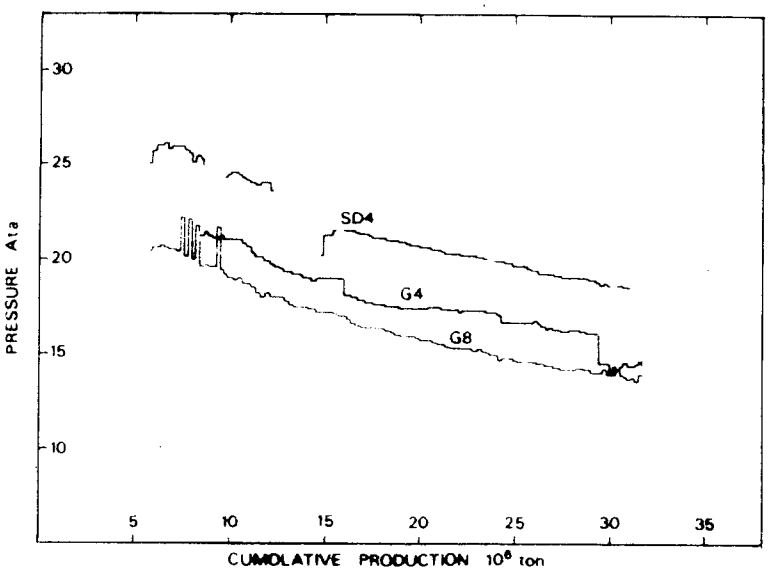

Fig. 7 - G4 - G8-SD4 well-head shut-in pressures versus cumulative production.

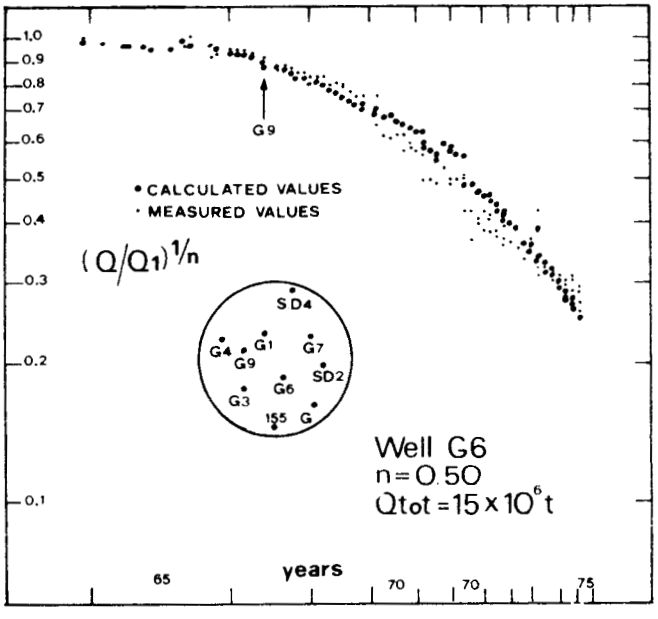

Fig. 8 - $(Q/Q_1)^{1/n}$ ratio versus time on logarithmic paper.

A RESERVOIR ENGINEERING STUDY OF THE EAST MESA KGRA

A. Spivak and L. F. Rice
INTERCOMP Resource Development and Engineering, Inc.
1201 Dairy Ashford, Suite 200
Houston, Texas 77079

The East Mesa area is located on the east side of the Imperial Valley approximately seven miles southeast of Holtville and 110 miles east of the San Diego metropolitan area. This area presently contains ten deep geothermal wells, five of which have been drilled by the Bureau of Reclamation, three by Republic Geothermal and two by Magma Power Company. Four older, abandoned deep holes are also in the general area.

Summary

The East Mesa Reservoir has been analyzed from a reservoir engineering point of view using a three-dimensional Geothermal Reservoir Simulation Model (1). The model treats transient two-phase (steam-water) flow in permeable rock and solves the energy and mass equations using finite-difference methods.

The basic objectives of the study were to determine the following:

1. Expected reservoir life when fluids at temperatures greater than 300°F are produced at flow rates of

   10,000 lb/min (600,000 lb/hr)
   100,000 lb/min (6,000,000 lb/hr)
   1,000,000 lb/min (60,000,000 lb/hr)

2. Optimum production and injection well spacing design for the above flow rates.

Results of the study showed that under certain assumptions concerning the level of permeability and the extent of the reservoir, all of the above rate objectives could be met for a period in excess of 30 years.

Basic Data

1. Petrophysics and Geology

Basic petrophysical characterization of the reservoir (porosity and permeability distribution) were obtained from the following sources:

(a) flow test data from the five Bureau of Reclamation wells and the three Republic wells,

(b) interwell interference data obtained by Lawrence Berkeley Laboratory using an ultra-sensitive pressure gauge, and

(c) analysis of all the log and core data in the Bureau of Reclamation and Republic wells.

2. Subsurface Temperature Distribution

A three-dimensional subsurface temperature distribution was determined by TRW using measured temperature profiles in deep wells and heat flow determinations in numerous shallow holes throughout the area.

Two-Dimensional Areal Calculations

A network of 40 acre (1320' x 1320') grid blocks was set up to enclose the 300°F isotherm at a depth of 6000 ft. The grid network comprised 14 grid blocks in the x (east-west) direction and 20 grid blocks in the y (north-south) direction. A northwest-southeast fault was accounted for by zeroing interblock transmissibilities along a series of grid block interfaces approximating the fault. (See Figure 1.)

A total thickness of 1000' representing the interval from 5000' to 6000' was simulated. This is approximately the interval in which all of the Bureau wells are completed with the exception of the 6-1 well which is completed below 6000'. The average temperature in this interval is 355°F.

Heat lost to or gained from the rock volume above and below the interval being simulated is computed from the one-dimensional heat conduction equation:

$$K_{ob} \frac{\partial^2 T}{\partial Z^2} = (\rho C_p)_{ob} \frac{\partial T}{\partial t}$$

where

K_{ob} = rock thermal conductivity (BTU/°F-ft-day)

ρ = rock density (lb/cu.ft.)

C_p = rock specific heat (BTU/lb-°F)

This equation is solved numerically in conjunction with the mass and energy balance equations.

In practice, the over and underburden almost always supplies heat to the reservoir in that injected fluid is almost always cooler than the in-place reservoir fluid. Accordingly, the reservoir either remains constant in temperature or declines, and as a result, the heat flux is from the over and underburden into the reservoir. It should be noted that the over and underburden heat supply is completely independent of heat supplied to the reservoir by convection.

The two-dimensional simulation runs were made under either of two assumptions: The reservoir is closed and limited to the 11,200 acres of the grid model or the reservoir is effectively infinite so that the 11,200 acre grid model is only a part of a much larger hydrologic system. The portion of this system outside the grid will be referred to as the "aquifer," although, strictly speaking, the total system is an aquifer and the grid is simply a region of anomalous temperature.

The pressure support supplied by the aquifer to the grid has been calculated using the method of Carter and Tracy (2) which is, in turn, an approximation of the rigorous superposition calculation described by Van Everdingen and Hurst (3) for an infinite circular system.

Production wells produce fluid at an assigned rate or whatever the well is capable of producing against a flowing bottomhole pressure of 1000 psi, whichever is less. In most cases, the assigned rate was 500,000 lb/hr. For a water specific gravity of 1.02, 500,000 lb/hr. is equivalent to 981 gpm or 33,634 barrels per day. The production capability of a well is calculated as follows:

$$Q = \frac{.001127\ 2\pi kh}{\mu_w \left(\ell n \frac{r_e}{r_w} - 1/2\right)} \left(p_{i,j,k} - p_{wf}\right)$$

where

Q = flow rate (B/D)

k = grid block permeability (md)

h = formation thickness (ft)

$p_{i,j,k}$ = grid block pressure (psi)

p_{wf} = flowing bottomhole pressure (psi)

r_w = wellbore radius (ft)

$r_e = \sqrt{\frac{\Delta x \cdot \Delta y}{\pi}}$

Δx = x-direction grid block dimension (ft)

Δy = y-direction grid block dimension (ft)

Low Rate

For the low rate case (600,000 lb/hr), one producing well and one injection well were employed. The wells were in the central portion of the reservoir, a distance of 1-1/4 miles apart. All of the produced fluid was reinjected at a temperature of 200°F. The average reservoir permeability was 50 md. After 30 years, the production well had sustained its initial rate and initial temperature of 355°F. The temperature front created by the bank of 200°F water had only progressed approximately 1/4 the distance between the two wells. Results for this case were similar, for an average permeability of 10 md.

Intermediate Rate

For the intermediate rate case (6,000,000 lb/hr) 12 production wells were employed. These wells were placed within the central portion of the grid model. For an average permeability of 50 md and assuming that the system is infinite, the total rate can be sustained for at least 30 years. If the reservoir is closed and limited to the 11,200 acres within the grid model, then the production rate drops very rapidly and within 6 years the average reservoir pressure falls to the limiting bottomhole pressure of 1000 psi.

With twelve injection wells located around the periphery of the 300°F contour and the twelve production wells in the interior as before, the intermediate rate can be maintained for 30 years. The cooling caused by the reinjection is limited to the regions immediately around the injection wells so that the producing wells remain essentially at the initial temperature of 355°F.

High Rate

For the high rate case (60,000,000 lb/hr) both peripheral and pattern injection were looked at. In the peripheral injection case, 60 producing wells were located in the central portion of the reservoir and 60 injection wells were located around the periphery of the 300°F contour. As before, the minimum flowing bottomhole pressure was 1000 psi and the injected water temperature was 200°F. For both the 10 md and 50 md case, the production rates dropped rapidly at first and then stabilized at rates below the desired 60,000,000 lb/hr. These stabilized rates were 48,000,000 lb/hr and 33,000,000 lb/hr for the 50 md and 10 md cases, respectively. The stabilized rates could be higher if a lower limiting bottomhole pressure could be tolerated.

Since there was some question as to whether the high rate case was feasible with peripheral injection, a series of pattern

injection cases was run. For all pattern cases, a 5-spot pattern was assumed.

Simulation runs were made for 5-spot patterns with wells drilled on 20, 40 and 80 acre spacing. All runs were made using a 2-D areal 10 x 10 grid for 1/4 of a 5-spot. Production and injection rates were approximately 500,000 lb/hr per well. In each case, the temperature of the produced water was determined as a function of time. For 80 acre spacing, there was no decline in the temperature of the produced water, even after 30 years. For 40 acre spacing the produced water temperature dropped to 250°F after 27 years and for 20 acre spacing, the produced water dropped to 250°F after about 15 years. (See Figure 2.)

A summary of the Two Dimensional Areal Calculations is presented in Table 1.

Two-Dimensional Cross-Sectional Calculations

The two-dimensional areal simulations assume uniform permeability in the vertical direction. In order to look at the effects of vertical heterogeneity, a two-dimensional x-z cross-sectional grid was utilized. The grid has four layers in the vertical direction and 19 columns in the x-direction. Fluid was injected at one end (x=1) and produced from the other end (x=19). Thickness in the y-direction decreases from the center toward the injection and production ends to represent approximately the shape of the area that would be swept in a 5-spot pattern. The distance between the production and injection wells is 933 ft. corresponding to a 40 acre 5-spot (wells drilled on 20 acre spacing). (See Figure 3.)

The assumed reservoir thickness is 1000 feet with the thickness of each layer being 250 feet. The horizontal permeabilities for the four layers from top to bottom are 111 md, 54 md, 20 md and 15 md, respectively. Vertical permeabilities were assigned as one-half of the horizontal permeabilities. This permeability distribution was based on data from the East Mesa 6-1 well.

Production and injection rates were set at 125,000 lb/hr for the simulated one-quarter 5-spot (500,000 lb/hr for the full 5-spot). For this case, the producing well temperature dropped to 250°F after about 12 years. The producing well temperature was calculated using the temperatures in the four layers weighted by their respective kh's. At the end of 12 years, the top layer has almost been completely swept by the relatively cold 200°F injection water, whereas temperatures in the bottom two layers remain greater than 300°F. Figure 4 shows the temperature distribution after four years.

In order to investigate the effects of a convective heat source from below, this case was repeated with the total injection of 125,000 lb/hr distributed as follows:

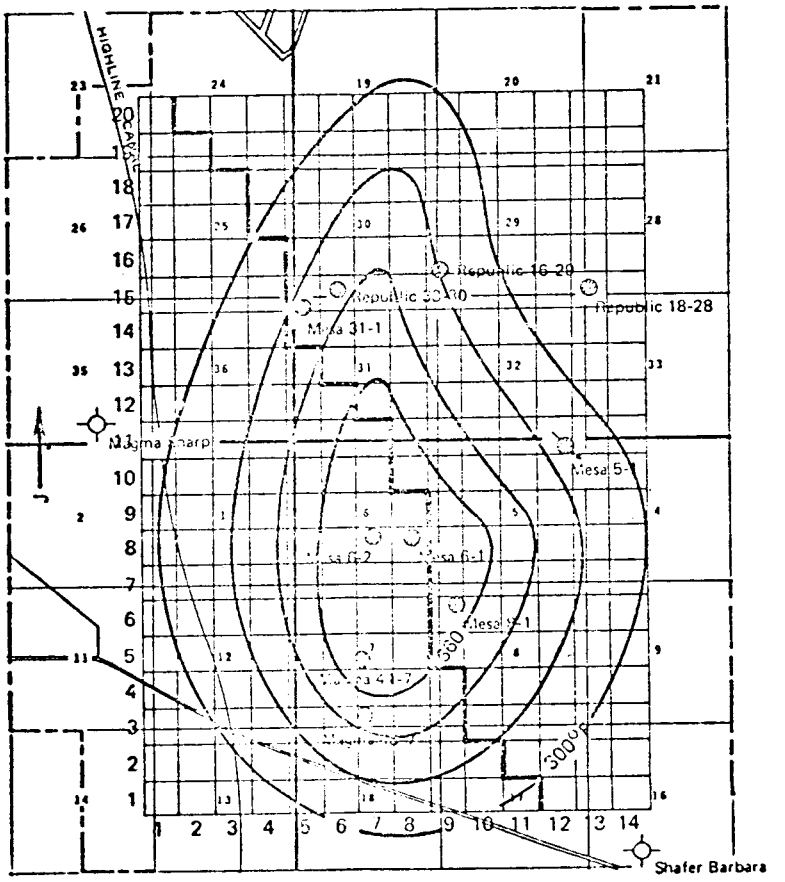

Figure 1. Grid for Two-Dimensional Areal Calculations

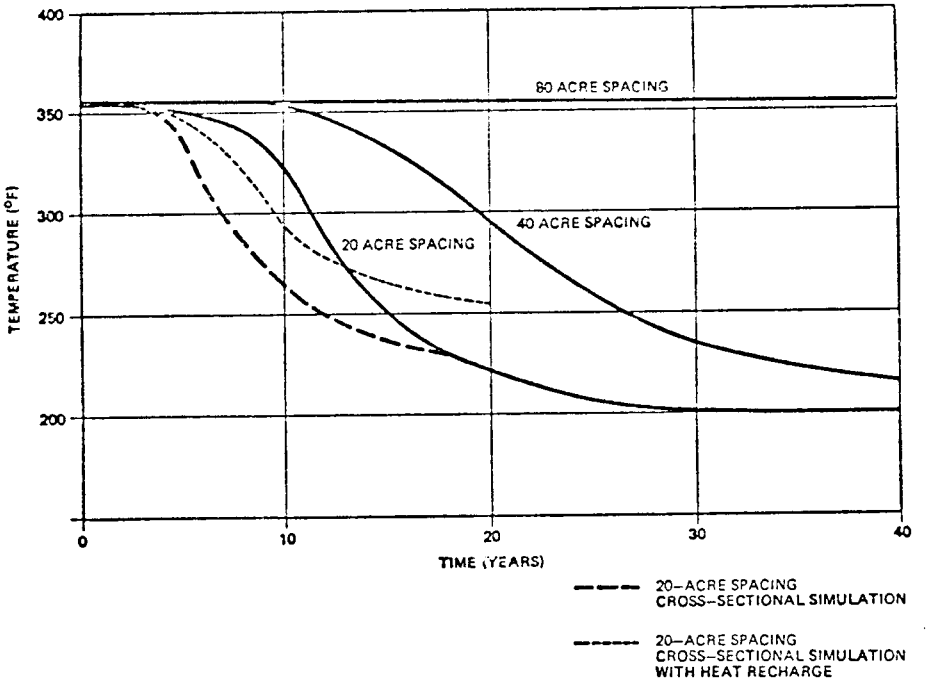

Figure 2. Produced Fluid Temperature as a Function of Time

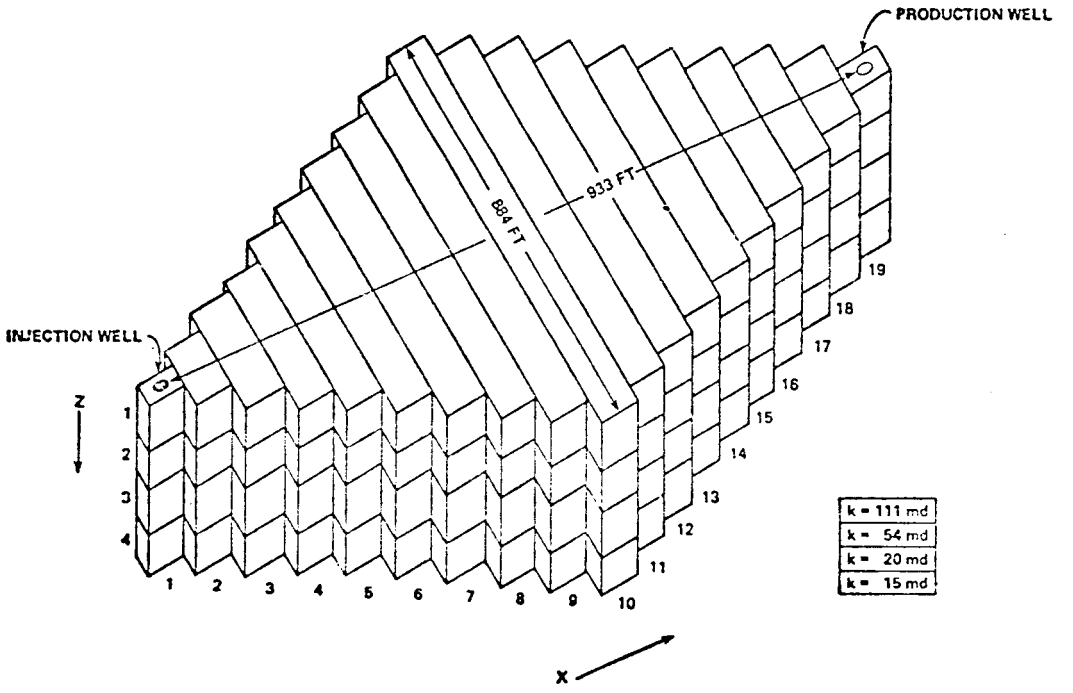

Figure 3. Five-Spot Cross-Sectional Simulation Grid

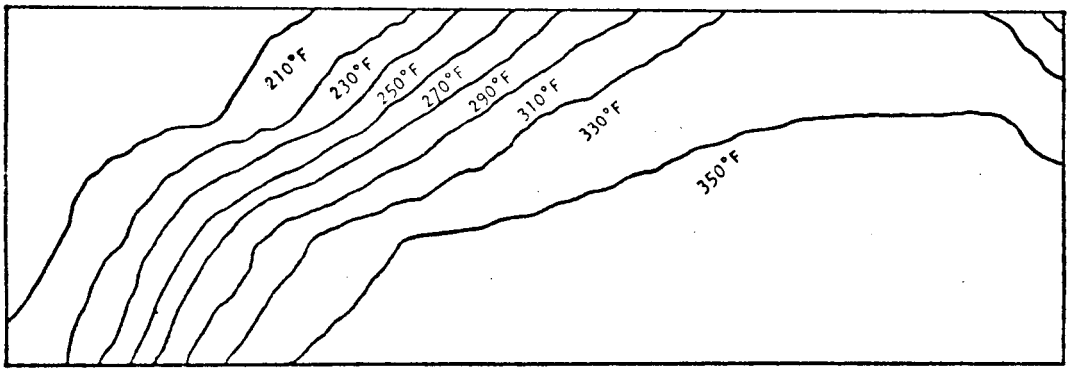

Figure 4. Temperature Distribution Contour Map at 1460 Days: Cross-Sectional Simulation

Table 1. Two Dimension Areal Simulation Summary

Case No.	Permeability (Millidarcies)	Fluid Injection	Aquifer Support	Reservoir Longevity	Notes
Low Flow Rate (10,000 lb/min)					
1	50	No	Yes	Exceeds 30 years	
2	50	No	No	Less than 15 years	Flow not sustained
3	50	Yes	No	Exceeds 30 years	
4	10	No	Yes	Less than 30 years	Flow not sustained
5	10	Yes	Yes	Exceeds 30 years	
6	10	No	No	Less than 30 years	Flow not sustained
7	10	Yes	No	Exceeds 30 years	
Intermediate Flow Rate (100,000 lb/min)					
8	50	No	Yes	Exceeds 30 years	
9	50	No	No	Approx. 6 years	Flow not sustained
10	10	No	Yes	Less than 30 years	Flow not sustained
11	10	No	No	Less than 30 years	Flow not sustained
12	10	Peripheral	Yes	Exceeds 30 years	Flow decreases by 10%
High Flow Rate (1,000,000 lb/min)					
13	10	Peripheral	Yes	Approx. 6 years	Flow not sustained
14	50	Peripheral	Yes	Exceeds 30 years	Flow decreases by 20%
15	50	Pattern 20-acre spacing	—	Approx. 2 years	Pressure not maintained Injected fluid volume not equal to produced fluid volume
16	50	Pattern 20-acre spacing	—	Approx. 12 years	Longevity limited to 300°F
17	50	Pattern 40-acre spacing	—	Approx. 20 years	Longevity limited to 300°F
18	50	Pattern 80-acre spacing	—	Exceeds 30 years	

(a) 100,000 lb/hr @ 200°F into the injection well, and

(b) 25,000 lb/hr @ 500°F at the bottom, half-way between the injection well and the production well.

Performance in this case was considerably improved over the preceding case.

References

1. "Study of the Geothermal Reservoir Underlying the East Mesa Area, Imperial Valley, California," TRW/INTERCOMP Final Report No. 28859-6001-RU-00, prepared for the United States Department of the Interior, December, 1976.

2. Carter, R. D. and Tracy, G. W.: "An Improved Method for Calculating Water Influx," Trans. AIME (1960) 219 p. 415.

3. Van Everdingen, A. F. and Hurst, William: "The Application of the LaPlace Transform to Flow Problems in Reservoirs," Trans. AIME (1949) 181 p. 305.

STUDIES ON THE 3-WELL RESERVOIR SYSTEM IN RAFT RIVER

J. F. Kunze, R. C. Stoker, D. Goldman and L. G. Miller
EG&G
Idaho National Engineering Laboratory
Box 1625
Idaho Falls, ID. 83401

The geothermal reservoir at Raft River, Idaho, was penetrated with a third deep well in the spring of 1976. The information deduced from this well and the subsequent testing of all three wells is presented in this report. This supplements the paper presented at the 1975 Reservoir Engineering Conference (1), which discussed in detail the experiences with the first two wells (5000 ft and 6500 ft deep, respectively, 4000 ft apart). Figure 1 shows the location of these wells, and the pipeline between them.

The Third Well

The third well, about 7000 ft southeast of the other two, was drilled with water and rather thoroughly tested on the way down until it appeared the resource of the desired temperature had just been entered. Casing was then installed (before the well became too difficult to handle) and drilling proceeded into the resource again with water. However, the well was initially a poor (<100 gal/min) producer from depth.

It has been planned to dig several channels at depths below the casing, each at a 10° to 15° angle away. Calculations had indicated that up to 50% increase in flow might be expected if the second channel could be 300 to 400 ft separated from the first in the main producing zone. It was decided, nevertheless, to try the technique on this poor producer. Shortly after beginning the second channel (from 4500 ft depth), the well began to produce significant artesian pressures. Yet a third channel was drilled, and after completion the well developed artesian flows of 800 gpm (51 liters/sec) initially. Flow was 350 gpm when steam flashing choked the flow in the well bore.

(1) Raft River Geothermal Reservoir Engineering and Well Stimulation, J. F. Junze, L. G. Miller, and R. C. Stoker, page 117 of SGP-TR-12, December 15-17, 1975 Conference.

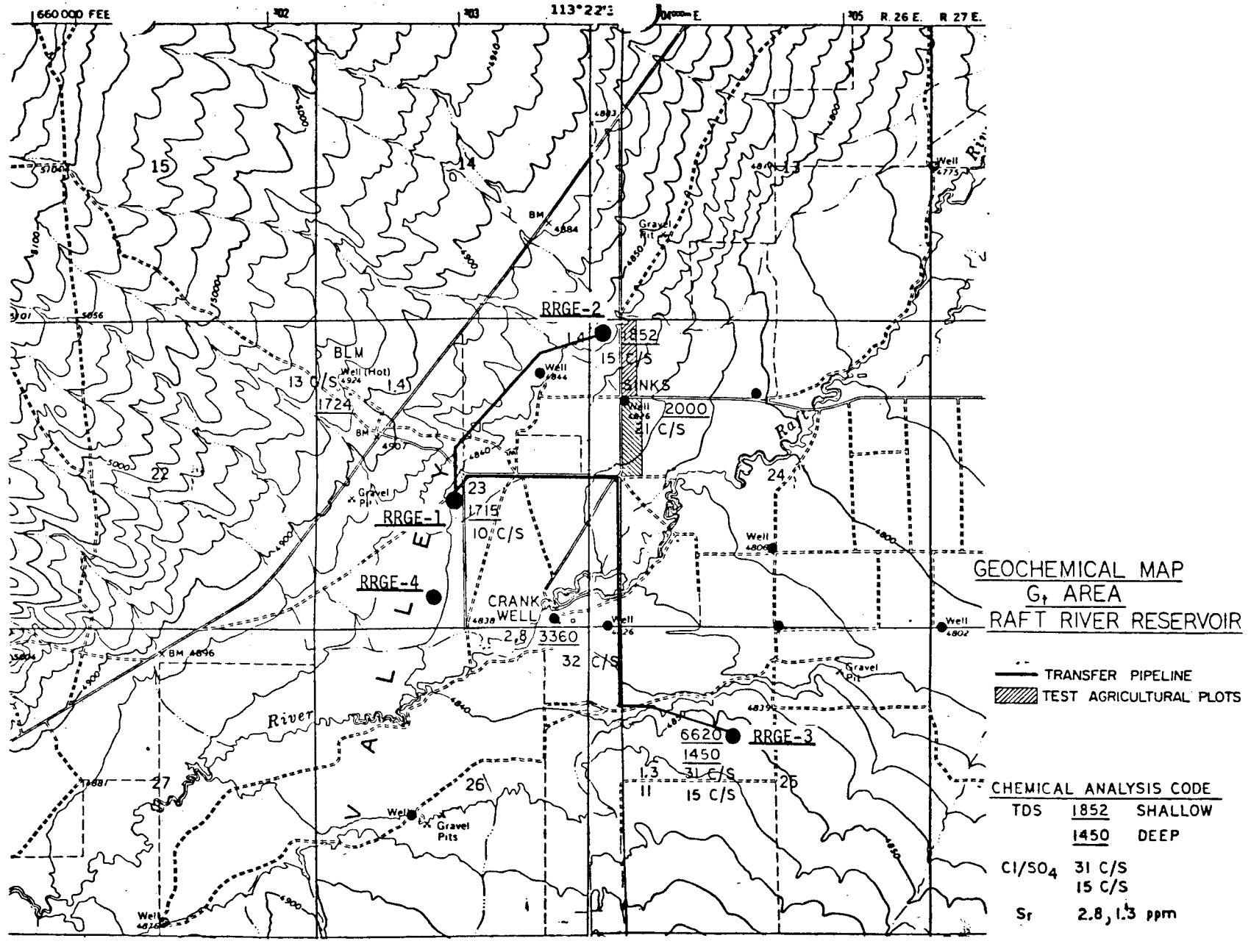
660000 FEET
113°22'30"E
R. 26 E.
R. 27 E.
RRGE-2
1852
15 C/S
SINKS
2000
21 C/S
RRGE-1
1715
10 C/S
RRGE-4
CRANK WELL
2.8 3360
32 C/S
RRGE-3
6620
1450
1.3
31 C/S
11
15 C/S
BLM
13 C/S
1724
Well (Hot)
Gravel Pit
Gravel Pits
BM 4896
River
Raft River
GEOCHEMICAL MAP
G_t AREA
RAFT RIVER RESERVOIR
TRANSFER PIPELINE
TEST AGRICULTURAL PLOTS
CHEMICAL ANALYSIS CODE
TDS 1852 SHALLOW
1450 DEEP
Cl/SO4 31 C/S
15 C/S
Sr 2.8, 1.3 ppm

FIGURE 1

FIGURE 2.

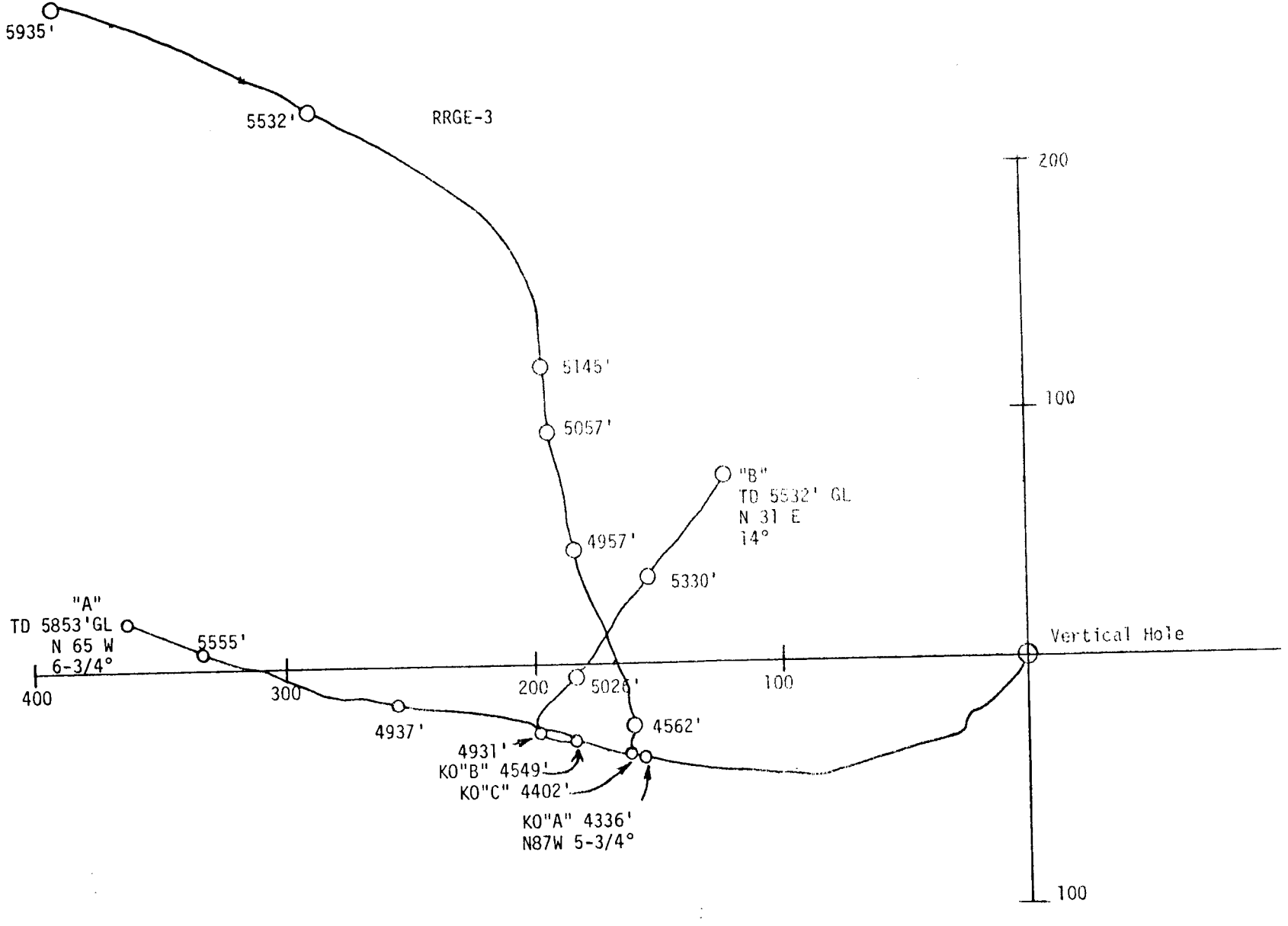
5935'
5532'
RRGE-3
5145'
5057'
"B"
TD 5532' GL
N 31 E
14°
4957'
5330'
"A"
TD 5853'GL
N 65 W
6-3/4°
5555'
400
300
200
5026'
100
Vertical Hole
4937'
4931'
4562'
KO"B" 4549'
KO"C" 4402'
KO"A" 4336'
N87W 5-3/4°
200
100
100

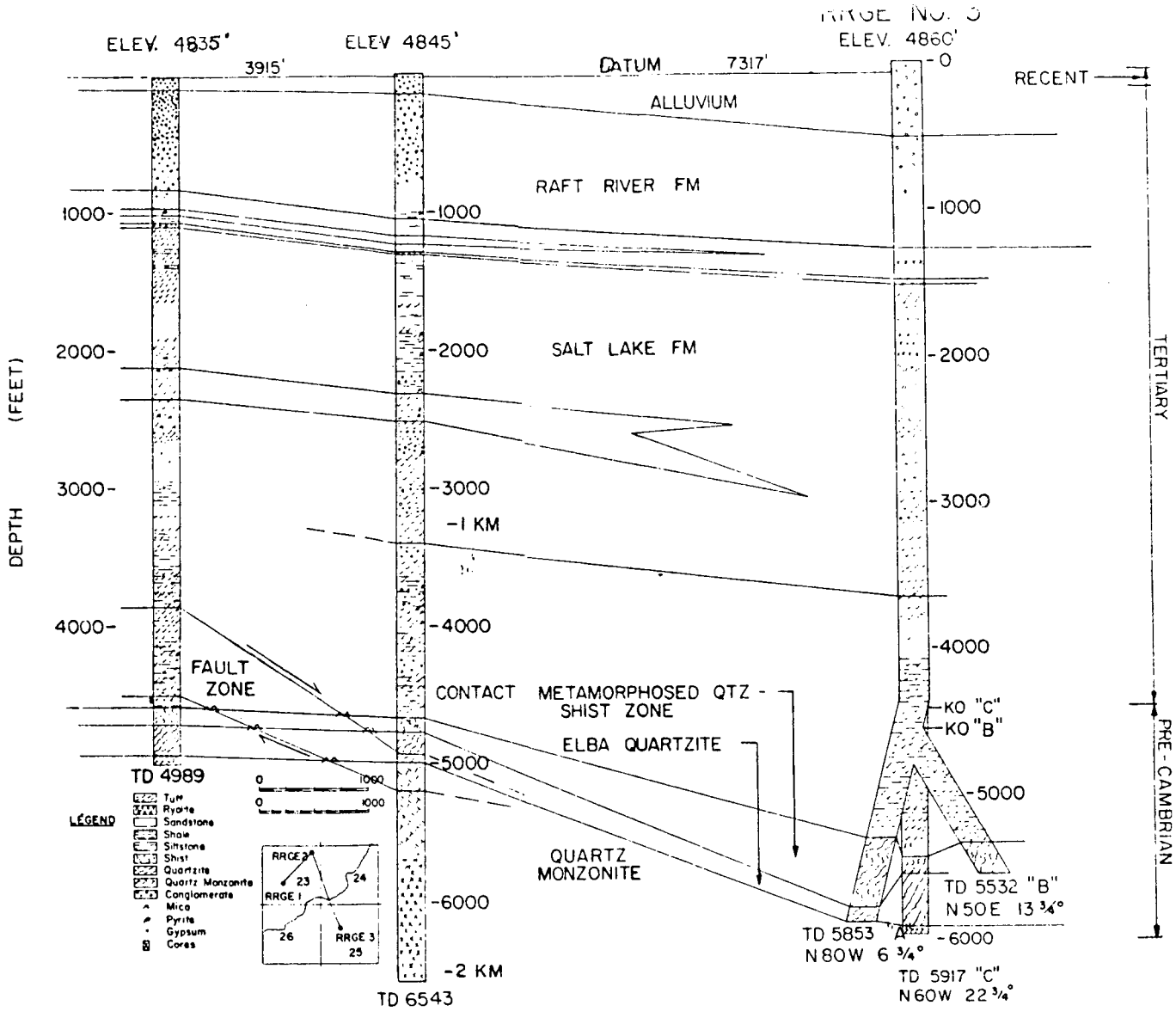
RRGE NO. 3
ELEV. 4835'
ELEV 4845'
ELEV. 4860'
3915'
DATUM 7317'
0
RECENT
ALLUVIUM
RAFT RIVER FM
1000-
-1000
1000
2000-
-2000
SALT LAKE FM
2000
3000-
-3000
-1 KM
3000
DEPTH (FEET)
4000-
-4000
4000
FAULT ZONE
CONTACT METAMORPHOSED QTZ - SHIST ZONE
KO "C"
KO "B"
ELBA QUARTZITE
-5000
TD 4989
TERTIARY
PRE-CAMBRIAN
LEGEND
Tuff
Rhyolite
Sandstone
Shale
Siltstone
Schist
Quartzite
Quartz Monzonite
Conglomerate
Mica
Pyrite
Gypsum
Cores
RRGE 2
RRGE 1
RRGE 3
23
24
26
25
QUARTZ MONZONITE
-6000
-2 KM
TD 6543
TD 5532 "B"
N50E 13 3/4°
TD 5853 "A"
N80W 6 3/4°
TD 5917 "C"
N60W 22 3/4°

FIGURE 3

Figure 2 shows a cross section of this well, in comparison with the other wells. Figure 3 shows the paths of the three channels of the third well, shown on a horizontal projection.

Logging, Coring, and Reservoir Analysis

A full complement of the standard logs was taken on each well. Though neutron and sonic logs give some clue (after the fact) of where the production zones might be, there is still no reliable correlation to use such logs to indicate producing regions prior to running production casing. (In the case of fracture permeability, the well must be left open hole or slotted casing installed.) Perhaps the main difficulty is that to date it is not positively known where the producing zones are. Flow meters from a number of organizations have failed to work in the down hole environment. Re-injection of cold water into formation has, where done, given clues from resulting temperature logs where the formation is taking water. These might correspond to the producing zones.

A number of simulated in situ permeability measurements were taken on the cores withdrawn. The results varied by several orders of magnitude, even from samples a foot apart. This further supports the contention that the production is from fractures and not from homogeneous permeability.

Well down hole pressure response has been measured, both in the producing wells and in the other two wells, for several combinations of the producing well. From the data the product of permeability and reservoir thickness has been calculated, where definitive results were obtained.

Wells #1 and #2 communicate quite readily with each other, with an observable pressure drop within six hours of flowing the other well. Drawdown of 3.6 psi was observed over a month of flowing the other well at 400 gpm.

On the other hand, well #3 appears to be communicating very poorly with the other two. Over a two-month period of flowing well #1 continuously (180 to 350 gpm) and well #2 intermittently (180 gpm for 4 weeks), the well #3 observed only a total drop of 1.3 psi. It also exhibits notably different chemistry than the first two. RRGE #1 and #2 have 2000 gpm dissolved solids, while RRGE #3 has nearly twice this amount.

Summary

The Raft River producing formation itself is tight (low permeability) except for fractures, which are the key to getting

adequate production from its wells. To the extent this area is typical of western valleys, the experience in discovering and extracting the resource is instructive. Since one never knows in advance where the resource is, drilling it with water is essential. Though drill stem testing should overcome the effects of a mud column, the test involved dangers of hole collapse and may be testing a region of no fractures (as occurred in RRGE #2 on a test of a 100 ft column just above the region that first started producing). The advantage of a light density column of drilling fluid, whether water or aerated water, should not be underestimated in allowing the geothermal fluid to enter the hole during drilling.

The variable nature of the distribution of the fractures makes it appropriate to consider multiple channeling below the production casing. Each such directionally drilled channel adds only 10 to 15% to the total well cost, and can mean the difference between a successful producer and a failure. Such channels can also provide an increment to total flow in a homogeneous formation exceeding the incremental cost increase.

To date, logging methods during drilling are inadequate to tell where the resource is. The expense is usually prohibitive for maintaining a drill rig over the well while it is tested adequately prior to a decision on casing the well or drilling further. For this reason, a light drilling fluid that will not even temporarily block the fractures is important. Multiple channeling in the case of Raft River was undertaken in a relatively consolidated region, and the use of only water did not involve problems of hole stability.

The producing zones in the wells have been inferred indirectly from temperature profiles taken after the re-injection of cool water. Further attempts at use of flow meters will be made. Currently, the following conclusions about the individual wells producing zones can be drawn:

1. Various producing zones from 3700 to 4600 ft. No production below 4600 to T.D. at 5000 ft, this latter 400 ft being quartzite and quartz monzonite.

2. Principal producing zones at 4400, 4900, 5200, 5800, and 5900 ft. Essentially no production below. The principal production appears to be at 4400 and 4900 ft, before reaching quartz monzonite.

3. Production from 4500, 4900, 5300 and 5400 ft depths; most of these are fractured zones in the Pre-cambrian.

Re-injection experience with the wells shows almost a direct comparison with the production flow and pressure data, i.e., 400 psi pressure to re-inject 1200 gpm to 1500 gpm typically. None of the three wells was designed specifically for re-injection. Current preference is that such a well should consider regions of good permeability not only in the main producing reservoir but somewhat above it in the mixing zones where already lower temperature water exists. Reduced pumping costs for re-injection are a major emphasis for future efforts.

None of the wells has had the opportunity to be fully developed for long periods of flow, and likewise to be monitored to confirm the deduced Theis Equation parameters reported above from short flow periods. The reason is simple that environmental considerations have necessitated disposing of the water in places other than the surface waterways. For a while the No. 2 well was used to inject over 8 million gallons of cooled geothermal water that had been stored in the reserve pit for a long period of time. Presently this well is being flowed in attempts to restore it to its former production characteristics. Tables I and II list the characteristics known about the wells at this time.

TABLE I

NOMINAL WELL FLOW CHARACTERISTICS
(Values in gallons/min of water)
Artesian

Well	Initial, Cold	Steady State Hot and Flashing	Pumped
No. 1	600	350 +	870 with 450 ft drawdown
No. 2	800 (200)*	400 ± (350)*	---
No. 3	800 +	350	---

* Recently, since its use to dispose of 8 million gallons of cold water.

TABLE II

WELLHEAD PRESSURE CHARACTERISTICS

Well	Condition	Pressure
RRGE-1	Cold	~50 psig
	Quiescent	146 psig
	Hot	175 psig
RRGE-2	Cold	~60 psig
	Quiescent	129 psig
	Hot	165 psig
RRGE-3	Cold	~40 psig
	Quiescent	100 psig
	Hot	140 psig

SCALING TESTS ON A SALTON SEA GEOTHERMAL BRINE

W. F. Downs, H. L. Barnes and J. D. Rimstidt
Department of Geosciences
The Pennsylvania State University
University Park, PA. 16802

As part of the Penn State scaling project sponsored by the U. S. Bureau of Mines, we designed a field test to determine scaling rates from homogeneous geothermal fluids. This technique has been used on the concentrated brines of the Salton Sea K.G.R.A. The principle adopted for the test was to cool the brine abruptly to a controlled temperature and then to maintain flow until sufficient scale was deposited to determine scale composition and amount deposited along the flow path.

Figure 1 is a schematic diagram of our experimental apparatus. A selected proportion of the geothermal brine is mixed with irrigation or other water at ambient temperatures to produce a mixed fluid at the required temperature. The remainder of the geothermal brine flows through a small heat exchanger where it is cooled to the chosen temperature and maintained as a single phase. The small-volume heat exchanger (Figure 2) was constructed from a two-foot length of six inch-diameter pipe. Both end plates are identical and contain ports for entry and exit of both the geothermal brine and the cooling fluid. The brine is quenched within a 25-foot, helical coil of 1/4 inch-diameter copper tubing. The coil has a four-inch outside diameter which gives each turn a total length of approximately one foot. Flow rates were determined by measuring the time to collect measured volume of effluent in a barrel.

The brine from Magmamax I (courtesy of San Diego Gas and Electric Company) was introduced into the heat exchanger at 225°C and 25 bars. A constant flow rate of 1 ± 0.1 gallons per minute was maintained for the four hour duration of each run. Experiments were repeated at intervals of 25°C for quench temperatures between 225°C and 75°C. Temperatures were monitored every 15 minutes and flow rates every half hour. Due to scaling within the tube and fluctuations in the flow rate of the well, minor periodic adjustments had to be made to maintain the constancy of temperature and flow rate. During the course of individual experiments, the chloride content of the incoming brine was monitored to determine whether upstream flashing was significantly altering the composition of the incoming brine. Any runs which included flashed brines were discarded. Upon completion of the experiment, the coils were removed, weighed and stored.

When the entire suite of coils were returned to our laboratory, they were dried in a nitrogen stream, any exterior scale from the cooling fluid was removed and the coils were reweighed. Figure 3 is a plot of the total weight of the cleaned coil as a function of quench temperature. The maximum amount of scale was formed at quench temperatures between 125 and 150°C. At higher temperatures, the brine was only slightly supersaturated and at lower temperatures, the rates of precipitation were slow enough that only a relatively small amount of scale was precipitated during flow through the tube.

The coils were cut into individual loops and the distribution of scale along the coils was determined by weighing. Several scale samples from different coils were mounted and analyzed by x-ray diffraction, scanning electron microscopy--including x-ray emission spectroscopy, and standard polished section microscopic techniques. Scales formed from the Salton Sea Brines are a complex mixture of carbonate, sulfide and silicate minerals. The majority of the scale is composed of Pbs and copper-iron sulfide phases dispersed in a carbonate matrix--largely aragonite. The crystal habit of the aragonite and the abundance of copper-iron sulfides is a function of both the rapidity of the quench and the quench temperature.

The resulting easily acquired data show the dependence on temperature decrement and distance, of the amount and composition of scale that is likely to form during geothermal development of a well. These data apply to a fluid of fixed initial composition being cooled, either before or after, but not during flashing. The kinetics of flashing, where volatite components are partially removed, may be significantly different both in rates and in composition of resulting scale. Further experiments have been designed to determine the effects of flashing on the kinetics of scale formation.

FIGURE 1. TOP VIEW OF A SCALING TEST APPARATUS.

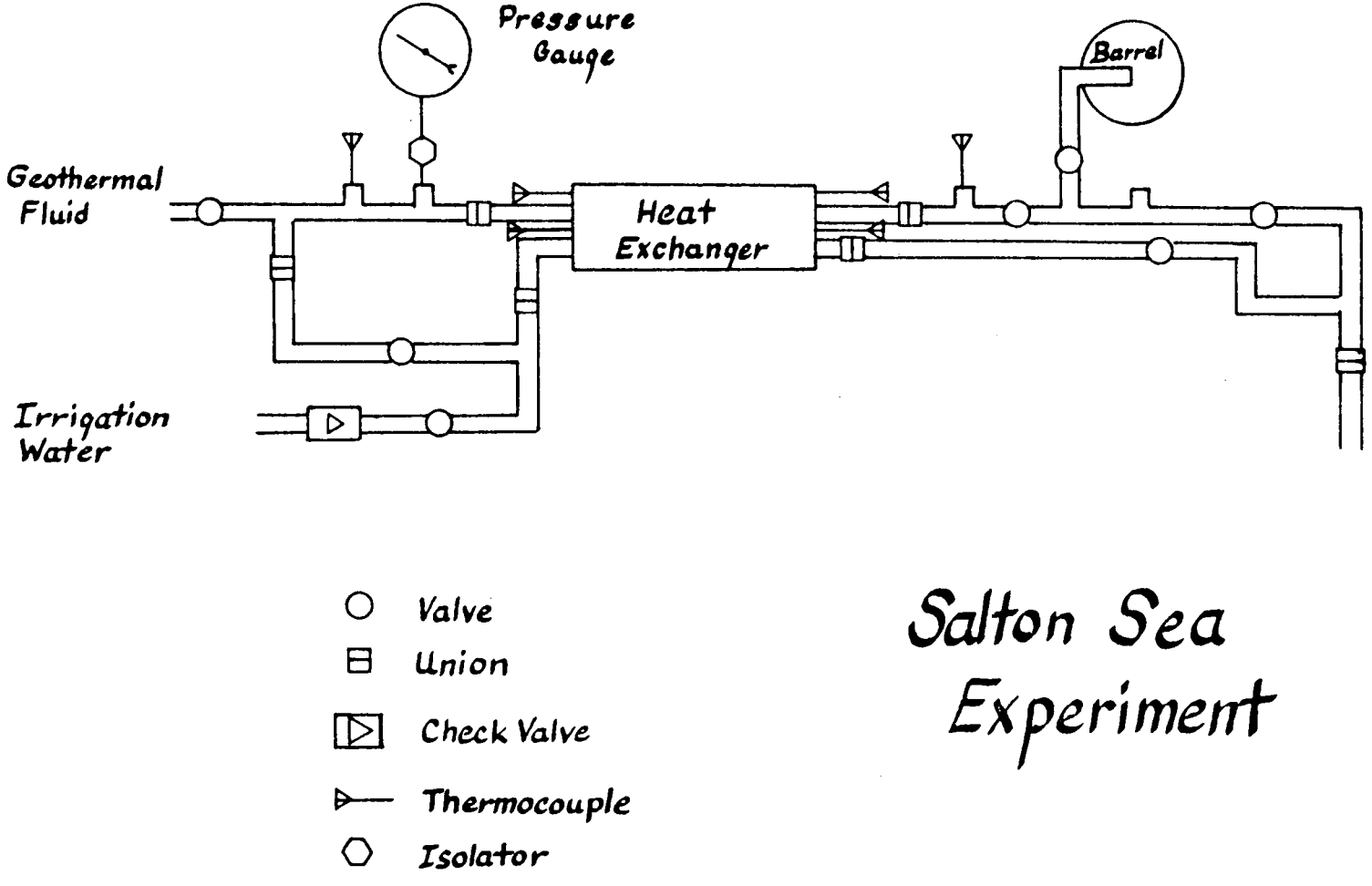

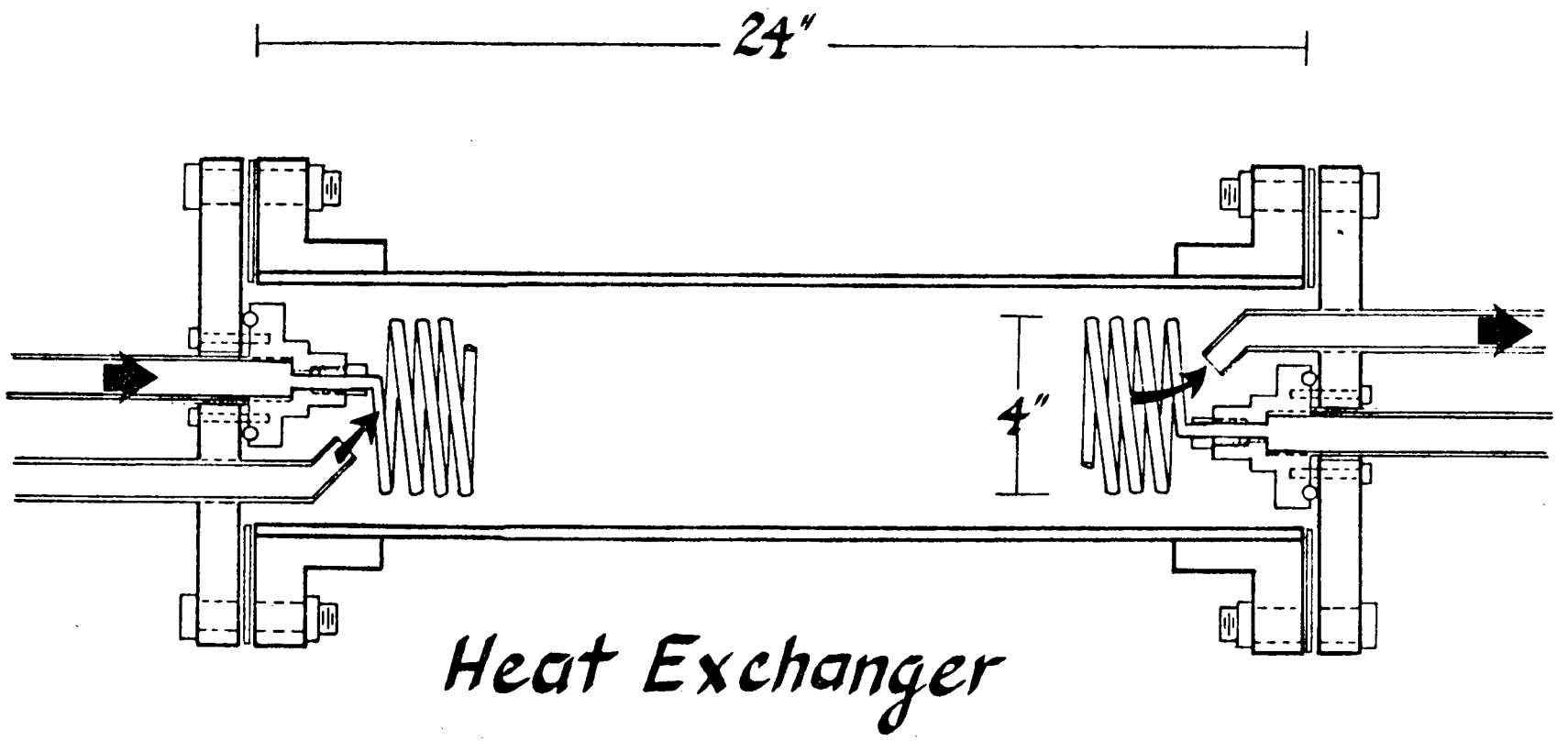

FIGURE 2.

FIGURE 3. Weight change of coils as a function of quench temperature. The 175°C experiment was duplicated and both values are plotted.

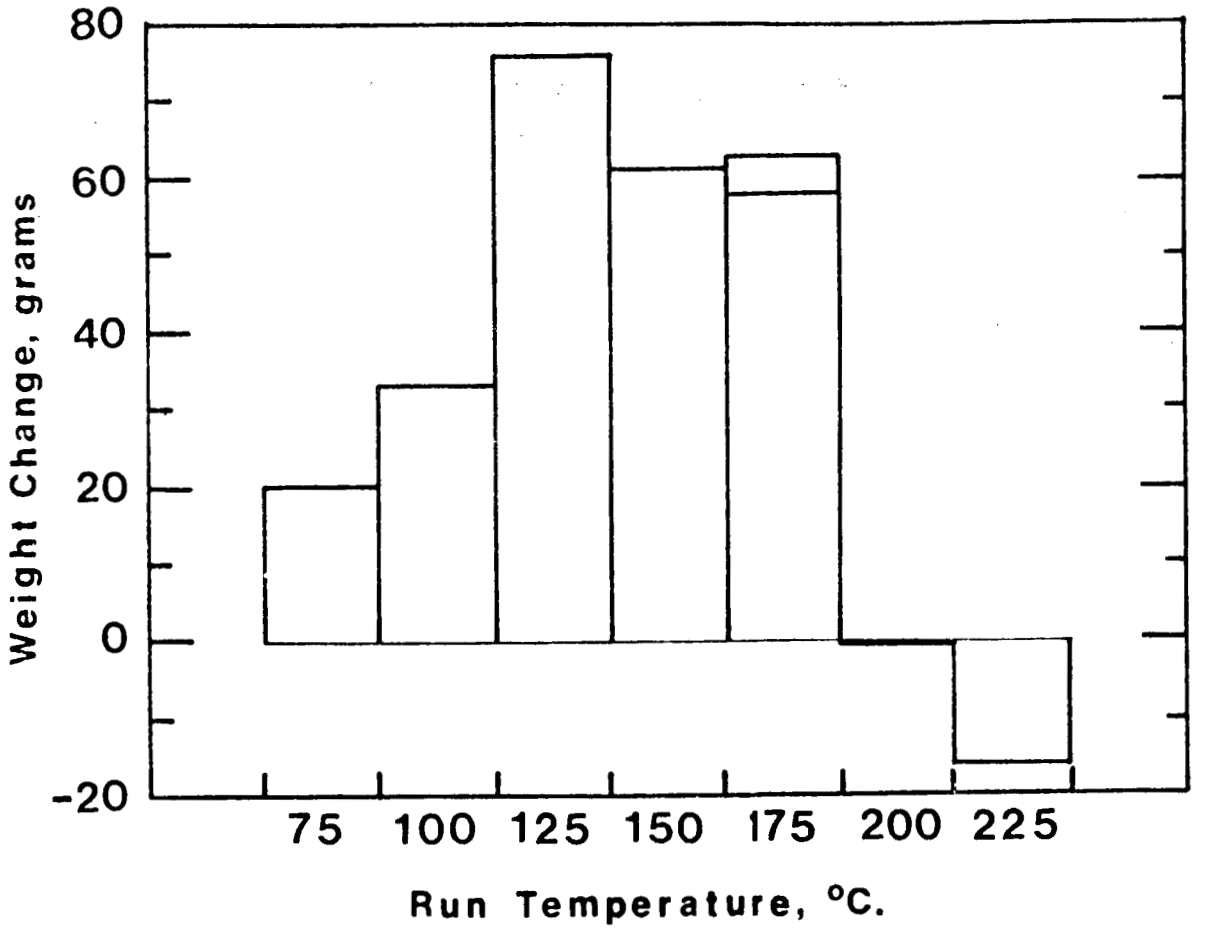

OPTIMAL MANAGEMENT OF A GEOTHERMAL RESERVOIR

Kamal Golabi and Charles R. Scherer
University of California
Los Angeles, CA. 90024

In a presentation to the First Stanford Geothermal Workshop last year, we outlined the basic philosophy, assumptions and general approach to finding an optimal rate of energy extraction from a hot water geothermal field. In this paper, we present the explicit relationships governing the physical processes and economic factors of our model, as well as the modifications to the model that have been necessary to accommodate the more specific articulation of these relationships. The conceptual modifications of the earlier model are subtle, but of great importance in making our work more useful for geothermal resource management.

This study is concerned with the optimal management, and in particular the optimal timing of energy extraction from a geothermal reservoir. For the conclusions of this optimization problem to be meaningful, the analysis must be carried out in the context of a particular hydro-thermal model. Furthermore, some assumption regarding the future value of geothermal energy must be made. Accordingly, we adopt the hydro-thermal model developed by Gringarten and Sauty (1), and assume that the value of geothermal energy is known as a function of time and the quantity of the extracted energy. We note however that our optimization model can be modified to accommodate other hydro-thermal models such as that of Kasameyer and Schroeder, which combines fractured and porous media flow (2). In view of the increase in the attractiveness of geothermal energy for space heating (3,6), we also assume that the extracted energy is used for generation of steam to be used for this purpose. However, we are well aware that the hot brine, depending on the parameters of a particular field, may be more economically utilized for some other purpose (e.g., electric power generation, direct utilization of hot water for domestic and industrial use, mineral extraction and desalination). In this paper, we restrict our attention to the case where the decision has already been made to use the geothermal energy for space heating.

The quantity of the extracted energy is a function of both the rate at which hot brine is extracted and the degree to which it is cooled before reinjection in the reservoir. Hence, we seek an extraction rate, a reinjection temperature and an economic life that maximize the net discounted value of the extracted energy.

The Hydro-Thermal Model

The hydro-thermal model adopted for this study was developed by Gringarten and Sauty (1). It assumes a pumped production well for a single phase saturated confined hot water aquifer with a recharge well as shown in Fig. 1 (actually each well can represent a cluster of wells). Although the aquifer is confined vertically, it is assumed to extend horizontally to infinity.

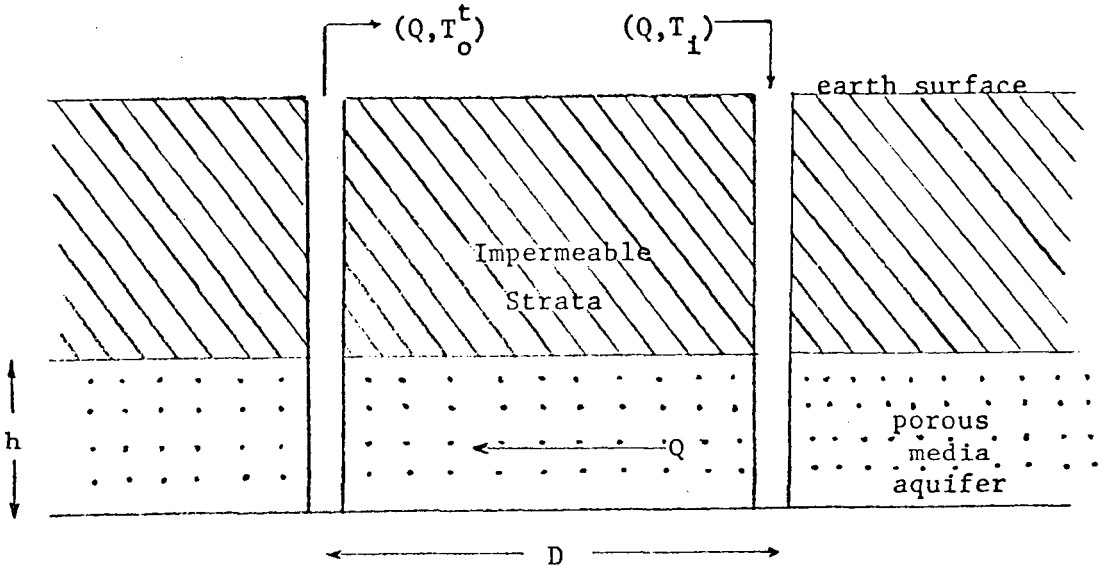

Figure 1

Fluid is withdrawn at the rate Q and recharged at the same rate. The temperature of extracted fluid at time t is T_o^t. Recharged fluid enters the ground at temperature T_i^t at time t.

The recirculated fluid is heated by the aquifer matrix from T_i^t to T_o^t (and this tends to cool the matrix). For the first τ years ($0^o \leq t \leq \tau$), $T_o^t = T_o^o$ where T_o^o is the initial equilibrium temperature of the unexploited anomaly and τ denotes the time until reduced fluid temperature "breaks through" to the production well. The breakthrough time is function of Q and is described by:

$$\tau(Q) = \frac{t_u}{6} \quad ,$$

where t_u is a dimensionless expression for time,

$$t_u = \frac{2\pi h D^2 \rho_a c_a}{Q \rho_f c_f}$$

h is the thickness of the aquifer, D the well separation, Q the pumping rate and $\rho_a c_a$ and $\rho_f c_f$ the heat capacities of the aquifer matrix and the fluid, respectively. Thus $\tau(Q)$ is inversely proportional to Q.

The temperature after breakthrough is given by a function $\bar{g}(T_i^t, t/t_u)$ which gives the ratio of the temperature drop through the heat exchanger experienced by the brine at the time t, to the analogous drop at time zero:

$$\frac{T_o^t - T_i^t}{T_o^o - T_i^t} = \bar{g}\,(T_i^t,\ t/t_u)$$

It can be easily shown that the variation in T_i^t is small. Hence, we have used the results of the hydro-thermal model to approximate $\bar{g}$ by a function g which assumes T_i does not vary with time. However, althouth T_i may be assumed constant with time, its value does affect heat removed per unit of time (for a given Q), and hence discounted net revenues. That is, for a given steam temperature, lower values of T_i yield greater heat flows per time but require more expensive heat exchangers and also cause the aquifer to cool more rapidly.

The expression for g has been developed (5) and is given by

$$g\,(t/t_u) = \begin{cases} 1 & \text{if } 0 \le t \le \tau \\ 0.338e^{-0.0138t/t_u} + 0.337e^{-0.656t/t_u} + 1.368e^{-8.006t/t_u} & \text{if } t \ge \tau. \end{cases}$$

Therefore, after the τ^{th} year, T_o^t drops exponentially toward T_i at a rate $g(t/t_u)$ as shown in Figure 2.

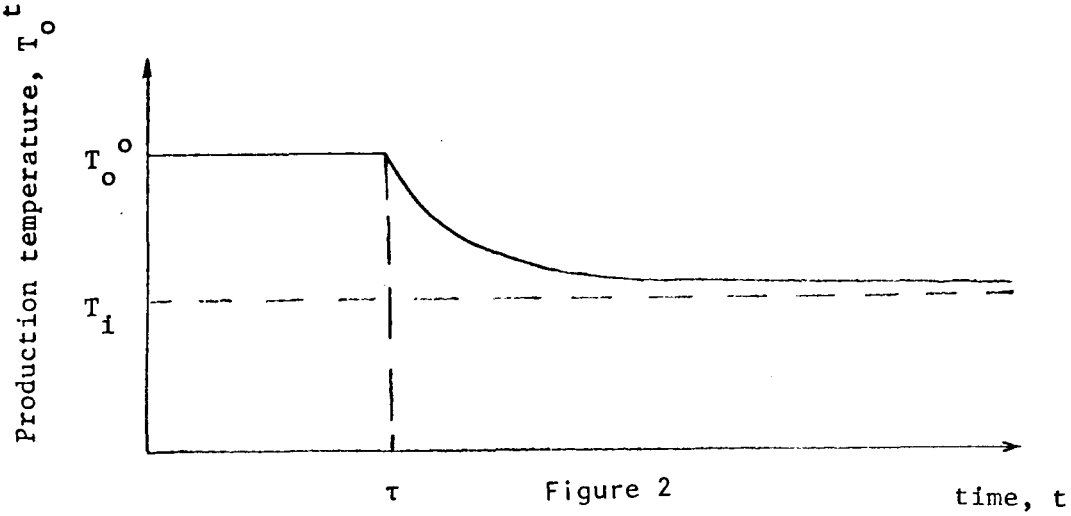

Figure 2

The Economic Model

We have now described the fundamental relationship between temperature and time for a given Q. Since extractable energy is proportional to $T_o^t - T_i$, it is possible to take T_o^t as the quality of the resource. As $T_o^t \to T_i$ the cost of heat extraction (per BTU) increases and there is a time when it is no longer economical to extract more heat. Since a certain amount of heat is lost in transfer and transmission, we need the difference between the production and injection temperatures to remain greater than a prespecified number δ. Thus we will need L^*, the optimal lifetime of the project, to be no greater than L_δ, where L_δ is such that $T_o^{L_\delta} - T_i = \delta$ and is a decreasing function of δ.

There are at least two ways to consider the value of the energy. The first is to assume that the value of the energy increases with time at the rate of e^{rt} where r is the (continuous) rate of increase of real (as opposed to inflated) energy price with time, i.e. $P_t = P_o e^{rt}$ where P_t is the value of the energy at time t and P_o is determined by the cost of alternative sources of energy. The second approach is to assume that demand for the energy is price sensitive, using the area under the demand curve as an index of willingness to pay, and hence benefit or value to society. If demand y, is price dependent, then we can write:

$$y=f(p).$$

This can be mathematically inverted, yielding:

$$p=f^{-1}(y).$$

Then willingness to pay for y_o BTU/hr, $w(y_o)$ is:

$$w(y_o) = \int_0^{y_o} p\,dy = \int_0^{y_o} f^{-1}(y)\,dy.$$

We will assume $w_t(y_o)$ increases with time so that

$$w_t(y_o) = w_o(y_o)e^{rt}$$

For the first criterion, the basic optimization problem (θ_1) is then

$$\theta_1: \quad \underset{Q,T_i,L}{\text{Maximize}}\ \Pi = \int_0^{\tau(Q)} P_o e^{rt} Q c_f \rho_f\ (T_o - T_i)\ e^{-it} dt$$

$$+ \int_{\tau(Q)}^{L} P_o e^{rt} Q c_f \rho_f (T_o - T_i) g(t/t_u) e^{-it} dt$$

$$- \int_0^{L} C(Q, T_i) e^{-it} dt$$

subject to

$$T_o^L - T_i \geq \delta$$

$$Q \geq 0 \ ,$$

where Q is the extraction rate, τ the breakthrough time, $c_f \rho_f$ the heat capacity of the brine, i the discount rate, L the economic life of the project and $C(Q,T_i)$ the function describing the annual capital and operting costs.

For the second criterion the problem (θ_2) is

$$\theta_2: \quad \underset{Q,\ T_i,\ L}{\text{Maximize}}\ \Pi = \int_0^{\tau(Q)} w_o (Q c_f \rho_f\ (T_o - T_i)) e^{rt - it} dt$$

$$+ \int_{\tau(Q)}^{L} w_o (Q c_f \rho_f (T_o - T_i) g(t/t_u)) e^{rt - it} dt$$

$$- \int_0^{L} C(Q, T_i) e^{-it} dt$$

subject to $T_o^L - T_i \geq \delta$

$Q \geq 0.$

A study of the various components of the production and surface equipment has established the relationship between the capacity of each component and the decision variables. By combining these relationships with empirical cost data, we have obtained the function C enabling us to obtain optimal solutions to problems Θ_1 and Θ_2. The components of C are costs for wells and casing, pipes and pipe cleaning, heat exchangers, well assemblies, pumps and pump operating costs. The pump cost is dependent both on the flow rate and the drawdown generated in the production well, which is in turn dependent on the flow rate. An important part of the cost function is the relationship between heat exchanger area A and effectiveness of exchange:

$$\varepsilon = 1-e^{-kA/Q}$$

where k is a constant. We have combined this with the definition of effectiveness.

$$\varepsilon = \frac{T_o^t - T_i}{T_o^t - T_s} \quad ,$$

to incorporate heat exchanger area and T_i into the cost function. A linear demand curve has been assumed to solve Θ_2.

A final note on the optimization model is that the maximum possible flow, $\bar{Q}$, from each production well is determined not only by pump technology, but by the requirement that the flow into the production well be laminar in order to be consistent with the assumption of the Gringarten-Sauty model. Hence, we assume the total flow Q, is achieved by using a number of wells drilled reasonably apart from each other to minimize pressure interference. Each of these wells has an upper bound of $\bar{Q}$ on capacity.

Proposed Work

The next step in our study is a sensitivity analysis indicating the relative importance of the physical, cost and economic parameters of our model in determining the optimal policy.

A logical extension of our work is the development of a dynamic decision process in which the extraction rate Q will be allowed to vary with time. An extraction strategy is then defined in terms of a vector of pumping rates:

$$Q = (Q_1, Q_2, \ldots\ldots\ldots, Q_L)$$

where Q_t is the pumping rate in the t^{th} year. We will seek an optimal strategy that maximizes the total discounted net revenues. Initial consideration of this extension has shown that the dynamic programming approach, suggested in last year's presentation, is not consistent with the Gringarten & Sauty model. This is because the derivative of T^t with respect to t ($t>\tau$) is dependent on the history of Q (i.e. ${}^{o}Q_{t-1}, Q_{t-2}, \ldots\ldots Q_1$) in the Gringarten and Sauty model. This dependence is effectively precluded by the dynamic programming approach. The solution to the multiple extraction rate problem is therefore not yet at hand. However, since multiple extraction policies may have advantages for the optimal management of geothermal resources, we intend to consider this problem further. Another extension would be to investigate various geometries and spacing of production and recharge wells. The geometry and well separation not only affect the breakthrough time, but also the hydraulic drawdown and hence pumping costs and production well capacities. Heat losses in surface piping will also be considered in this extension.

Our optimization model can be extended to cases where the hot brine is intended for uses other than space heating, in particular, electric power generation.

References

1. Gringarten, A.C. and J.P. Sauty, "A Theoretical Study of Heat Extraction for Aquifers with Uniform Regional Flow," Bureau de Recherches Geologiques et Minières, Orléan, France.

2. Kasameyer, P.W. and R.C. Schroeder, "Thermal Depletion of a Geothermal Reservoir with Both Fracture and Pore Permeability," Lawrence Livermore Laboratory, Preprint UCRL-77323, August 1976.

3. Maugis, P., "Exploitation d'une Nappe d'Eau Chaude Souterraine pour le Chauffage Urbain dans la Region Parisienne," Annales des Mines, p. 135, May 1971 (in French).

4. Scherer, C.R., "On the Optimal Rate of Geothermal Energy Extraction," Proceedings of the First Workshop on Geothermal Reservoir Engineering, Stanford University, December 1975.

5. Tsang, C.F. and P. Witherspoon, "The Physical Basis for Screening Geothermal Production Wells from the Effects of Reinjection," Lawrence Berkeley Laboratory, Rep. LBL 5914, 1976.

6. Zöega, J. and G. Kristinsson, "The Reykjavik District Heating System."

PRELIMINARY ASSESSMENT OF A HOT DRY ROCK GEOTHERMAL ENERGY RESERVOIR FORMED BY HYDRAULIC FRACTURING

Hugh D. Murphy, Robert G. Lawton, Jefferson W. Tester,
Robert M. Potter, Donald W. Brown, and R. Lee Aamodt
Los Alamos Scientific Laboratory
P. O. Box 1663
Los Alamos, N.M. 87545

If a mass of relatively impermeable hot rock can be hydraulically fractured and if a heat extraction fluid can be circulated through the fracture and recovered, appreciable amounts of energy can be extracted from the rock. The Los Alamos Hot Dry Rock Geothermal Energy Project is designed to investigate and demonstrate this concept. A series of field experiments have been carried out at a site called Fenton Hill, located on the west flank of the Valles Caldera in the Jemez mountains of northern New Mexico.

In December, 1974, the first deep borehole, GT-2 was completed to a depth of 2.929 km (9609) ft) in granite, where the temperature was 197°C (386°F). A hydraulic fracture was then created near the bottom of this borehole, and a second borehole, EE-1, was drilled to complete the circulation loop, but it failed to intersect the fracture by about 8 m (26 ft). Communication between the wellbores was established by initiating a fracture from EE-1. This paper discusses some aspects of what has been learned about this dual fracture system by subsequent experiments.

Permeation Studies and Minimum Earth Stress

By assuming constant, one-dimensional, permeable flow into a homogeneous porous media with constant properties, and by also assuming that the hydraulic conductivity of the fracture is very large compared to that of the rock, it can be shown that if water is injected into a fracture at a constant rate, q, the change in fracture pressure, P, is[1]:

$$P = \frac{2\mu q}{kA}\sqrt{\frac{\kappa t}{\pi}} \quad \ldots\ldots\ldots\ldots\ldots\ldots \quad (1)$$

Because the hydraulic diffusivity, κ, is

$$\kappa = k/\mu\,\bar{\beta} \quad \ldots\ldots\ldots\ldots\ldots\ldots \quad (2)$$

the product of the fracture area times the square root of permeability, $A\sqrt{k}$, is given by rewriting Eq 1.

$$A\sqrt{k} = 2\sqrt{\frac{\mu}{\pi\bar{\beta}}}\,\frac{q\sqrt{t}}{P} \quad \ldots\ldots\ldots\ldots\ldots\ldots \quad (3)$$

Typical data for the EE-1 fracture are presented in Fig. 1. The experiment was conducted by pumping into the EE-1 wellbore at a constant rate of 2.1 ℓ/s (34 gal/min), corrected to downhole conditions. A good linear fit to the data is obtained on P versus $\sqrt{t}$ coordinates. Deviation of the later time data from the linear fit is thought to be due to pressure dependent permeability, or a "leak" from the EE-1 fracture to the GT-2 fracture via a flow connection, as will be discussed.

Since the porosity of the granite is less than 1%, the mean compressibility, $\bar{\beta}$, is essentially that of the rock which, based upon the results of sonic velocity logs, is estimated to be 2.7×10^{-6} bar^{-1} (1.9×10^{-7} psi^{-1}; 1 bar = 10^5 N/m^2 = 14.5 psi). Using available properties of water at 200°C, [2] and the above values of $\bar{\beta}$ and q, it can be shown that the $A\sqrt{k}$ value for the EE-1 fracture at the time this experiment was conducted was 2.2×10^{-5}m^3 (7.8×10^{-4}cu ft). Since this result was obtained with an initial pore pressure of zero (taking hydrostatic pressure as the baseline), the $A\sqrt{k}$ derived is more properly designated as $(A\sqrt{k})_o$, where the subscript represents the change in the initial pore pressure.

It is found that values of $(A\sqrt{k})_o$ are most useful when they are interpreted as a parameter which characterizes a fracture. Changes in $(A\sqrt{k})_o$ indicate irreversible changes in a fracture, examples being fracture extension due to pressurization or changes in k due to potential geochemical effects such as the formation and precipitation of rock-water interaction products or the dissolution of rock mineral components, particularly silica (SiO_2).

A historical summary of the $(A\sqrt{k})_o$ for both fractures is presented in Fig. 2. At the top of this figure are identified the various flow experiments, while near the bottom, the maximum EE-1 wellhead pressure achieved during each experiment is indicated. Since the creation of the EE-1 fracture in October, 1975, its $(A\sqrt{k})_o$ has increased during several of these flow experiments. Furthermore, these increases have been observed only when the EE-1 pressure has exceeded 90 to 94 bars (1300 to 1360 psi). Thus, it is believed that these increases in $(A\sqrt{k})_o$ are due to increases in A (fracture extensions) and that the fracture extension pressure, P_e, is approximately 92 bars (1330 psi) above hydrostatic. Since its creation, $(A\sqrt{k})_o$ of the GT-2 fracture has not changed significantly. The maximum sustained pressure ever reached at the GT-2 wellhead was 91 bars (1320 psi), i.e., below P_e. The permeability of the rock surrounding the GT-2 fracture has apparently not changed, in spite of the potential geochemical effects cited above.

If it is assumed that the fracture extension pressure for large fractures is approximately equal to the minimum earth stress less hydrostatic pressure, the value of the minimum earth stress, S_3, in the EE-1 and GT-2 fractures is approximately 375 bars (5440 psi) or 50% of the overburden pressure, S_1.

Pore Pressure Dependent Permeability

The effects of pore pressure upon $A\sqrt{k}$ are indicated in Fig. 3. The results were obtained from an experiment in which the sequence of operations was to first inject water into the EE-1 fracture at a constant rate until

a pressure of 28 bars (400 psi) above hydrostatic was reached, and then adjust the flow rate such that this pressure was maintained constant for two hours. In such a manner a new pore pressure was established in the rock adjacent to the fracture face. Following the two-hour "soak" the procedure was repeated at the additional pressure levels shown on the figure. The start of each new change in pressure level was taken as a new zero time and the results, when plotted versus $\sqrt{t}$, yielded straight lines as shown. Using a modified principle of superposition, the $A\sqrt{k}$ for each increment of pressure can be calculated and the results are indicated on the figure. As can be seen, increasing the pore pressure from 0 to 69 bars (1000 psi) above hydrostatic resulted in a factor of 3.8 increase in $A\sqrt{k}$. Since A did not change (pressure levels were below the fracture extension pressure) the permeability apparently increased by a factor of 15.

Additional results, obtained from another flow experiment, indicate that the permeability increases even more sharply (up to a factor of 80!) as the pore pressure increases to 83 bars (1200 psi) above hydrostatic. These results are qualitatively similar to those of Brace, et al. [3] for westerly granite and to those of Potter, et al. [4] for GT-2 core specimens. If one interprets the "effective" stress holding microcracks closed as simply the difference between the earth stress and the pore pressure, then Brace, et al. [3] have shown that reducing the effective stress by increasing the pore pressure tends to open the microcracks, leading to large changes in the effective permeability of the rock.

Fig. 4 presents a summary of all the data we have measured pertaining to pore-pressure-dependent permeability. Included are data from the EE-1 fracture, the present GT-2 fracture (roughly centered at 2.81 km) and an early, now-inactive fracture in GT-2. Empirically we have found that the square root of the ratio of the permeability at zero wellhead pressure to the permeability at elevated pressured, $\sqrt{k_o/k}$, is reasonably linear with pressure as shown. A value of zero for the ratio $\sqrt{k_o/k}$ at the intercept with the abscissa mathematically implies infinite permeability at the face of the fracture plane. A reasonable interpretation would be that when the pressure approaches the maximum horizontal component of earth stress, S_2, (the intermediate earth stress, aligned horizontally and parallel to the fracture plane) the effective stress in the S_2 direction approaches zero with concomitant opening of microfractures. The least squares line using the entire data set has the equation:

$$\frac{k_o}{k} = 1.00 - 0.0098\ P(\text{Bars}) \quad \ldots\ldots\ldots\ldots \quad (4)$$

and the extrapolated pressure, at $\sqrt{k_o/k} = 0$, of 102 bars (1480 psi) above hydrostatic is believed to be an estimate of S_2. Thus the absolute value of S_2 is about 390 bars (5660 psi), or only 15 bars above S_3.

References

1 Gringarten, A. C., Ramey, H. J., Jr., and Raghavan, R. "Unsteady-state pressure distribution created by a well with a single infinite-conductivity vertical fracture," Soc. Petr. Engr. Jour. (Aug 1974), 347.

2 ASME Steam Tables (1967)

3 Brace, W. F., Walsh, J. B., and Frangos, W. T. "Permeability of granite under high pressure," J. Geophys. Res. (1968) 73, 2225-2236.

4 Potter, J. M., Balagna, J. R., and Charles, R. W.: "Permeability of granitic rock at elevated pressures and temperatures," Los Alamos Scientific Laboratory report (to be published).

Nomenclature

A = Area (both sides) of fracture
k = permeability of rock
P = pressure change in the fracture
P_e = fracture extension pressure
q = volumetric flow rate entering the fracture
S_1, S_2, S_3 = maximum, intermediate and minimum compressive earth stress
t = time
$\bar{\beta}$ = mean compressibility ($=\phi\beta_f + (1 - \phi)\beta_r$)
β_r = compressibility of rock
β_f = compressibility of water
κ = hydraulic diffusivity ($= k/\mu\bar{\beta}$)
μ = viscosity of water
ϕ = porosity

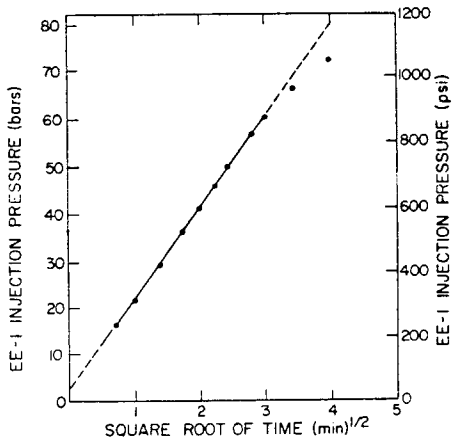

Fig. 1 - Transient increase in well-head pressure due to water injection.

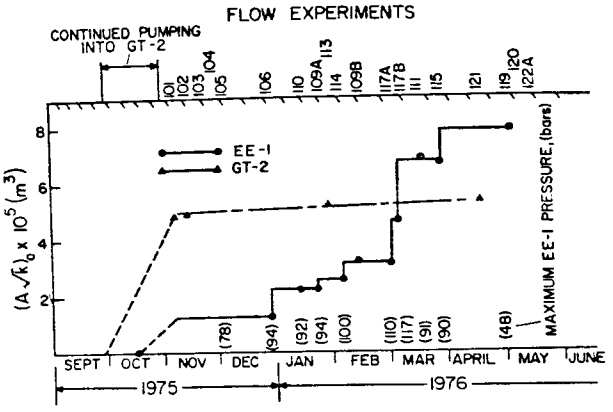

Fig. 2 - Variation of $(A\sqrt{k})_o$ product.

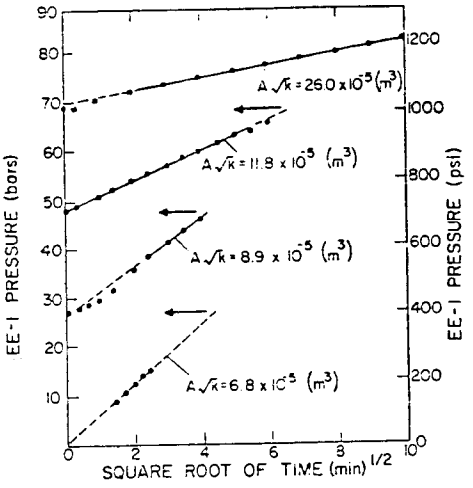

Fig. 3 - Transient pressure increases at elevated pore pressures.

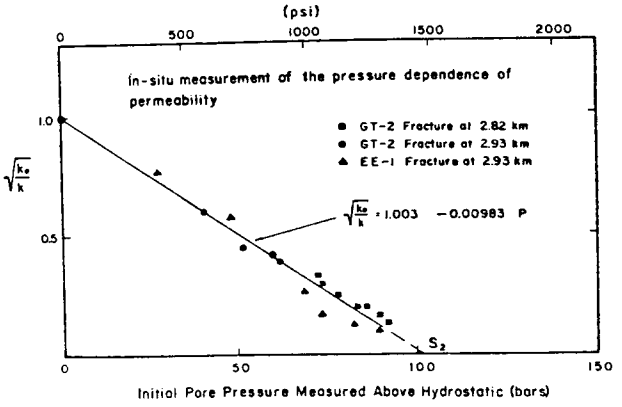

Fig. 4 - Summary of all pore pressure dependent permeability data and extrapolation to intermediate principal stress.

FLUID FLOW THROUGH A LARGE VERTICAL CRACK IN THE EARTH'S CRUST

J. Weertman
Departments of Materials Science & Engineering and Geological Sciences
Northwestern University, Evanston, Ill. 60201
S. P. Chang
Engineering Sciences Department, Northwestern University

In this investigation, we are primarily concerned with modeling fluid flow through vertical cracks that were created for the purpose of extracting heat from hot, dry rock masses. The basic equation for the two-dimensional problem of fluid flow through a crack is presented and an approximate solution is found. The basic equation is a nonlinear, Cauchy-singular integro-differential equation. Moderately simple formulae for the crack opening displacement and the effective pressure difference between the crack tips are derived. The results are valid for arbitrary vertical cracks, provided that the fluid injection and removal points are not placed too close to the crack tips. (A more complete treatment of this problem is given by us in a paper to appear in the Journal of Geophysical Research.)

The Basic Equation

Consider a vertical, liquid-filled, two-dimensional crack the center of which, at $y = 0$, is assumed to be at a depth below the earth's surface that is large compared with the half height L of the crack. Let $D(y)$ represent the crack opening displacement at the vertical distance y from the crack center. $D(y)$ is determined by the following nonlinear, Cauchy-singular integro-differential equation:

$$\frac{\mu}{2\pi(1-\nu)} \int_{-L}^{L} \frac{B(y')dy'}{y-y'} + \frac{\mu}{\pi(\lambda+2\mu)} \int_{-L}^{L} \frac{\tau(y')dy'}{y-y'} =$$

$$-T(y) + P_0 - P_0' - (\rho-\rho')gy - \int_0^y P'_g(y)dy \qquad (1)$$

where $B(y) = -dD(y)/dy$, P_0 is the overburden pressure within the rock mass at $y = 0$, P_0' is the hydrostatic pressure within the liquid at $y = 0$, $T(y)$ is any tensile or compressive tectonic stress component within the rock mass whose axis is perpendicular to the crack plane,

ρ is the density of rock and ρ' is the density of the liquid, g is the gravitational acceleration, P'_g is the component of the pressure gradient within the liquid that drives fluid flow, ν is Poisson's ratio, μ is the shear modulus and λ is the other Lamé constant, and $\tau(y)$, which is equal to $-P'_g(y)D(y)/2$, is the shear stress exerted parallel to the crack faces that is produced when fluid flows through the crack.

When the fluid flow is laminar and when the crack faces are nearly parallel to each other, the pressure gradient P'_g is equal to or very nearly equal to (Batchelor, 1967)

$$P'_g(y) = -12V\eta/D^3(y) \tag{2}$$

where η is the viscosity of the fluid and V is the volume of fluid that moves past the point y in unit time per unit length of crack. In the cases of interest to us, the fluid flow will always be laminar or not strongly turbulent.

It is unlikely that fluid used to extract geothermal energy from a vertical crack in a hot, dry rock mass would be injected exactly at the lower crack tip and removed exactly at the upper crack tip (or vice versa). A more realistic situation is one in which water is injected at $y = -L'$ and is removed at $y = L'$ where $L' < L$. In this situation, $P'_g = 0$ in the region $L' \leq |y| \leq L$. Thus, Eq. (1) can be written as (on inserting Eq. (2) into Eq. (1) and also using the relationship $2\tau(y) = D(y)P'_g(y)$).

$$\frac{\mu}{2\pi(1-\nu)} \int_{-L}^{L} \frac{B(y')dy'}{y-y'} = -\frac{6V\eta\mu}{\pi(\lambda+2\mu)} \int_{-L'}^{L'} \frac{dy'}{D^2(y')(y-y')}$$

$$-T(y) + P_0 - P'_0 - (\rho-\rho')gy + 12V\eta \int_0^y \frac{H(L'-|y|)dy}{D^3(y)} \tag{3}$$

where H is the Heaviside step function.

Solution by Linearization

An approximate solution of Eq. (3) may be obtained by setting up a perturbation scheme and solving, with increasing labor, the resulting equations. However, a reasonably good approximate solution

can be found by using the following simple physical arguments. The crack opening displacement is not a rapidly varying quantity near the center of the crack. Furthermore, the integral terms on the right-hand side of Eq. (3) can be shown, a posteriori, to be relatively small in magnitude compared with the other terms for any reasonable values of V. Therefore, if the value of L' differs appreciably from the value of L, which we now assume it does, the crack opening displacement D(y) in the two integrals in question may be considered to have a constant value in a first approximation. It will be obvious later that there will be no need to carry the solution to a higher approximation in which D(y) is not considered to be a constant in the two integrals. We also assume that the tectonic stress T(y) is equal to a constant and is independent of the variable y.

Under these assumptions the crack opening displacement D(y) is found to be

$$
\begin{aligned}
D(y) = {} & \{(1-\nu)/\mu\}\{2(T-P_0+P_0') + (\rho-\rho')gy\}(L^2-y^2)^{\frac{1}{2}} \\
& + \left[\frac{12V\eta(1-\nu)}{\pi\mu D_c^3}\right]\left[-(\pi\mu D_c/[\lambda+2\mu])\{(L'-y)H(L'-y) + [1-H(L'+y)](L'+y)\}\right. \\
& + \{\pi-2\sin^{-1}(y/L)\}\{L'D_c\mu/[\lambda+2\mu]\} - 2y(L^2-y^2)^{\frac{1}{2}}\sin^{-1}(L'/L) \qquad (4) \\
& - 2L'y\log|\{L^2-y^2)^{\frac{1}{2}}+(L^2-L'^2)^{\frac{1}{2}}\}/\{(L^2-y^2)^{\frac{1}{2}}-(L^2-L'^2)^{\frac{1}{2}}\}| \\
& \left. + (y^2+L'^2)\log|\{y(L^2-L'^2)^{\frac{1}{2}}+L'(L^2-y^2)^{\frac{1}{2}}\}/\{y(L^2-L'^2)^{\frac{1}{2}}-L'(L^2-y^2)^{\frac{1}{2}}\}|\right]
\end{aligned}
$$

where for $|y|>L$ the displacement $D(y) = 0$. The term D_c is equal to

$$
\begin{aligned}
D_c = (2L')^{-1}\int_{-L'}^{L'} D(y)dy = {} & \{(1-\nu)(T-P_0+P_0')/\mu\}\{L^2-L'^2)^{\frac{1}{2}} \\
& + (L^2/L')\sin^{-1}(L'/L)\} \qquad (5)
\end{aligned}
$$

and is not a function of V and η.

The crack opening displacement $D(y)$ produces stress singularities at the crack tips. The tensile stress T' acting across the crack plane just ahead of the crack tip is equal to

$$T' = K/\sqrt{2\pi r} \tag{6}$$

where $r(<<L)$ is the distance measured from a crack tip and K is the stress intensity factor which is defined as the limit

$$K_{\pm} = \pm \left[\{\mu/(1-\nu)\}\{(\pi/4L)(L^2-y^2)\}^{\frac{1}{2}}B(y)\right]_{y \to \pm L} \tag{7}$$

where the $+$ sign is used in the limit of $y - L$ (K at upper crack tip) and the $-$ sign when $y \to -L$ (K at lower tip). On substituting Eq. (5) into Eq. (8) the following values of the stress intensity factor are found:

$$K_{\pm} = (T-P_0+P_0')(\pi L)^{\frac{1}{2}} \pm (\pi L)^{\frac{1}{2}}\{[\rho-\rho')gL/2]$$

$$- (12V\eta/\pi D_c^{\,3})[(L'/L)(L^2-L'^2)^{\frac{1}{2}} \tag{8}$$

$$+ L \sin^{-1}(L'/L) - \{\mu L' D_c/L(\lambda+2\mu)\}]\}.$$

For the situation in which $V = 0$, the longest possible crack half height that can exist without K_- taking on negative values for a given value of $(T-P_0+P_0')$ is equal to

$$L = 2(T-P_0+P_0')/g(\rho-\rho'). \tag{9}$$

A crack of this length has a displacement at $y = 0$ equal to

$$D(0) = (\rho-\rho')g(1-\nu)L^2/\mu. \tag{10}$$

The stress intensity factor is equal to

$$K_+ = (\rho-\rho')gL(\pi L)^{\frac{1}{2}} \tag{11}$$

when $K_- = 0$. If K_+ is equal to or larger than the critic value K_c for crack propagation, the crack will propagate to the upper surface by breaking rock open at the upper tip while simultaneously closing itself up at the lower tip (Weertman 1971a, 1971b, 1973; Secor and Pollard 1975).

Now consider the case in which V is not zero. Because $D_c << L$, if can be shown (Weertman and Chang) that the terms that contain the factor $\eta/(\lambda+2\mu)$ in Eqs. (4) and (8) can be dropped from these equations without introducing any appreciable error. It can further be shown that except for cracks with half heights smaller than 50 m the terms in Eqs. (5) and (8) that contain the expression $(12V\eta/\pi D_c^3)L$ are small in magnitude compared with the terms that contain the expression $(\rho-\rho')gL$ or $(T-P_0+P_0')$. Thus the crack profile and the stress intensity factor of a large crack with water flowing is essentially the same as that of a water-filled crack in which the fluid is stationary.

A Remark on Two Corrections

There are two corrections that can be made to our results. One of these is for the influence of the earth's surface. Another correction takes into account the force in the vertical direction produced at the crack walls by the fluid pressure because the crack walls are not vertical when the crack is filled with fluid. It can be shown (Weertman and Chang) that both of these corrections are negligibly small.

Conclusion

We conclude from this analysis that the crack profile and stress intensity factors of any large vertical fluid-filled crack for heat extraction purposes will not be changed appreciably when fluid is forced to flow through the crack at physically practical velocities.

References

Batchelor, G. K., An Introduction to Fluid Dynamics, Cambridge University Press, 1967.

Secor, D. T. and Pollard, D. D., On the Stability of Open Hydraulic Fractures on the Earth's Crust, Geophys. Res. Lett., 2, 510-513 (1975).

Weertman, J., Theory of Water-Filled Crevasses in Glaciers Applied to Vertical Magma Transport Beneath Ocean Ridges, J. Geophys. Res., 76, 1171-1183 (1971a).

Weertman, J., Velocity at Which Liquid Filled Cracks Move on the Earth's Crust or in Glaciers, J. Geophys. Res., 76, 8544-8553 (1971b).

Weertman, J., Ocean Ridges, Magma Filled Cracks and Mantle Plumes, Geofisica International, 13, 317-336 (1973).

Weertman, J. and Chang, S. P., Fluid Flow Through a Large Vertical Crack in the Earth's Crust, J. Geophys. Res. (in press).

LABORATORY EXPERIMENTS ON HYDROFRACTURE AND THE PERMEABILITY OF HOT GRANITE

J. Byerlee, D. Lockner, R. Summers
U.S. Geological Survey
Menlo Park, CA 94025

It has been proposed that an artificial geothermal reservoir could be created by injecting water under high pressure through a hole drilled into a hot dry batholith. By drilling a second hole to intersect the plane created by hydraulic fracture, a fluid circulation system could be created by pumping cold water into one hole and extracting hot water or steam through the other hole. We have carried out a number of laboratory experiments to investigate various aspects of this project.

It is usually assumed that during hydraulic fracture a single tension fracture is formed with its plane parallel to the direction of maximum principal stress. In laboratory experiments we have found that at high injection rates this is correct, but if the rock is under shear stress and the fluid is injected slowly enough, shear fractures are formed with their planes oriented about 30° to the direction of maximum principal stress. This occurs not only in sandstone, but also in very low permeability rocks such as oil shale and Westerly Granite. The efficiency of an artificial geothermal reservoir depends in part on the surface area of the hot rock with which the circulating fluid comes in contact. Our laboratory results suggest that it may be possible, in regions of high tectonic stress, to increase the fracture surface area simply by varying the fluid injection rate and thus to create not only a tension fracture but shear fractures as well.

A major problem in creating a fluid circulation system is knowing exactly where to drill the second hole to intersect the fractures. We found that the spacial distribution of the fracture planes can be determined accurately by determining the location of the acoustic emission events that occur during fracture. This technique should be applicable in large-scale field projects as well. It should also be possible to calculate the three-dimensional distribution of the fracture planes from the change in magnetic field at the earth's surface caused by the injection of material of high magnetic susceptibility into the fracture.

Once the circulating system is formed, how does the permeability of the system change with time? We have measured the permeability of granite under confining pressure and differential stress at temperatures to 400°C. In all cases the initial permeability at elevated temperature was found to be higher than the permeability at room temperature. This was probably caused by thermal cracking that could be detected by monitoring the acoustic emission from the rock during the experiments. The high initial permeability, however, did not persist and in nearly all cases decreased significantly during the first half day of water flow through the rock. Dissolution of the minerals was concentrated near the inlet where the pressure was highest,

and precipitation occurred throughout the sample owing to oversaturation as the pressure dropped. This precipitation almost certainly caused the reduction of permeability. In many cases, particularly at the highest temperatures, measurable flow of water through the sample ceased after a few days, even in samples that contained a pre-existing fracture plane. If the same phenomenon occurs in a large-scale field project, then our results suggest that the system would tend to clog unless preventive steps were taken.

REFERENCES

1. D. Lockner and J. Byerlee, Hydrofracture in Weber Sandstone at high confining pressure and differential stress, submitted to J. Geoph. Res., 1976.

2. P. Solberg, D. Lockner, and J. Byerlee, Shear and tension hydraulic fractures in low-permeability rock, submitted to Pure and Applied Geoph., 1976.

3. J. Byerlee and M. Johnston, A magnetic method for determining the geometry of hydraulic fractures, Pure and Applied Geoph, v. 114, p. 425-433, 1976.

4. R. Summers, K. Winkler, and J. Byerlee, Permeability changes during the flow of water through Westerly Granite at temperatures of 100°C to 400°C, submitted to J. Geoph. Res., 1976.

HEAT EXTRACTION FROM A HYDRAULICALLY FRACTURED PENNY-SHAPED CRACK IN HOT DRY ROCK

H. Abé,† T. Mura and L. M. Keer
Northwestern University
Evanston, Illinois 60201, U.S.A.

Heat extraction from a penny-shaped crack having both inlet and outlet holes is investigated analytically by considering the hydraulic and thermal growth of the crack when fluid is injected at a constant flow rate. The rock mass is assumed to be infinitely extended, homogeneous, and isotropic. The equations for fluid flow are derived and solved to determine the flow pattern in the crack. Temperature distributions in both rock and fluid are also determined. The crack width change due to thermal contraction and the corresponding flow rate increase are discussed. Some numerical calculations of outlet temperature, thermal power extraction, and crack opening displacement due to thermal contraction of rocks are presented for cracks after they attain stationary states for given inlet flow rate and outlet suction pressure.

The present paper is a further development of the previous works of Bodvarsson (1969), Gringarten et al. (1975), Lowell (1976), Harlow and Pracht (1972), McFarland (1975), among others, and considers the two dimensional rather than the one-dimensional crack. Furthermore, the crack radius and width are quantities to be determined rather than given a priori.

FLUID FLOW IN A PENNY-SHAPED CRACK

Consider a large penny-shaped crack having a radius R and width w (in the z-direction) as shown in Fig. 1. Fluid is injected from the inlet at the center of the crack and removed in part at the outlet, x = a, where x is the distance measured in the vertical direction from the center. The radii of the inlet and outlet holes are denoted by R_0 and R_a, respectively.

The total mass flow rate at the inlet wellbore can be written in the form:

$$q_0 = q_a + q_E + q_L + q_T \tag{1}$$

where q_a is the effective flow rate equal to the outlet flow rate, q_E is the total mass change in the crack, q_L corresponds to the total fluid loss in the crack per unit time, and q_T is the increase of the crack volume due to the thermal contraction of the rock and can be neglected.

If the crack is subjected to a constant inlet flow rate and the crack radius is sufficiently large, the fluid viscosity can be neglected from the equation of linear momentum as shown in a previous paper (Abé, Mura and Keer, 1976):

---

†Permanent address, Tohoku University, Sendai, Japan.

$$\frac{\partial p}{\partial r} = -\rho_f\, g \cos\theta, \quad \frac{\partial p}{\partial \theta} = \rho_f\, g r \sin\theta \tag{2}$$

where p is the fluid pressure in the crack, g is the acceleration due to gravity, and ρ_f is the fluid density. Equation (2) is integrated as

$$p(r,\theta,t) = p_0(t) - \rho_f\, g r \cos\theta \tag{3}$$

where p_0 is the fluid pressure at $r = 0$ and t is time. The density ρ_f has been assumed to be constant.

The fracture mechanics is introduced here by considering a crack opening stress $(\sigma_z)_{z=0} = -p + (S_0 - K_a \rho_\gamma g x)$ where S_0 is the tectonic stress at $r = 0$, K_a is the coefficient of active rock pressure, and ρ_γ is the density of the rock.

The stress intensity factor at the crack tip and the opening displacement are easily obtained from the results derived by Keer (1964):

$$K = \lim_{r \to R} (r - R)^{1/2}\, \sigma_z = \frac{\sqrt{2R}}{\pi}\left[p_0 - S_0 + \frac{2}{3} g R (K_a \rho_\gamma - \rho_f)\cos\theta\right] \tag{4}$$

and

$$w(r,\theta) = \frac{3}{\rho_f D}\left[p_0 - S_0 + \frac{2}{3}(K_a \rho_\gamma - \rho_f) g r \cos\theta\right]\sqrt{R^2 - r^2} \tag{5}$$

where

$$D = \frac{3\pi E}{8(1-\nu^2)\rho_f} \tag{6}$$

with E and ν being Young's modulus and Poisson's ratio respectively.

The flow rate q_E, defined in (1), is

$$q_E = \frac{d}{dt}\int_0^R \int_{-\pi}^{\pi} \rho_f w r \, d\theta dr = \frac{d}{dt}\left\{\frac{2\pi}{D} R^3 (p_0 - S_0)\right\}. \tag{7}$$

Now the average stress intensity factor is introduced by the definition

$$\bar{K} = \frac{1}{2\pi}\int_{-\pi}^{\pi} K \, d\theta = \frac{\sqrt{2R}}{\pi}(p_0 - S_0). \tag{8}$$

It is assumed that when the crack is expanding

$$\bar{K} = \text{constant } K_c. \tag{9}$$

The flow loss is defined by

$$q_L = 2\rho_f \int_0^{2\pi}\int_0^R u_L \, r \, dr d\theta, \tag{10}$$

where u_L is the fluid loss rate per unit area of the crack surface and is assumed here to be a linear function of p;

$$2\rho_f u_L = C_{L0} + C_{L1}(p_0 - \rho_f g r \cos\theta) \tag{11}$$

where C_{L0} and C_{L1} are constant. Then, (10) becomes

$$q_L = \pi R^2 (C_{L0} + C_{L1} p_0). \tag{12}$$

Finally, the flow rate q_a in (1) is evaluated from the Bernoulli equation applied to the flow in the neighborhood of the throat of the outlet. Then

$$p_0 - g\rho_f a = -p_a^* + g\rho_f (h_0 - a) + \frac{1}{2\rho_f}\left(\frac{C_v q_a}{\pi R_a^2}\right)^2 \tag{13}$$

where p_a^* is the suction pressure by the outlet pump and the constant C_v (> 1) is an outlet head loss.

Equations (1), (7), (12) and (13) provide a functional form of R with respect to t for given values of q_0, p_a^* and other physical constants and geometrical values of h_0, a, R_a; p_0 is expressed in terms of K_c and R through the relations (8) and (9). The crack radius R increases with time from the initial value R_s which is the value of R before the outlet is introduced. R reaches a stationary value after some time when

$$q_E > 0 \quad \text{and} \quad p_a^*/S_0 < 1/\Delta - 1 \tag{14}$$

where $\Delta = S_0/\rho_f g h_0$. We call this case Case (I). On the other hand, the crack can remain at the initial size R_s when

$$q_E \leq 0 \quad \text{and} \quad \bar{K} < K_c. \tag{15}$$

We call this case Case (II). Here, $R = R_s$ and p_0 is obtained as a function of t from (1), (7), (12) and (13) for given values of q_0, p_a^* and other physical and geometrical constants. In the next section we shall calculate the quantity of heat extracted from the outlet in each case (I) and (II). Several numerical examples for $R = R(t)$ and $p_0 = p_0(t)$ were shown in a previous paper (Abé, Keer, Mura 1976).

HEAT EXTRACTION FROM OUTLET

In this section a stationary penny-shaped crack (after R and p_0 have attained their stationary values) is treated as a starting point for the analytical study of two-dimensional heat transmission problems.

We have to determine first the velocity field of the fluid inside the crack. Assumptions of incompressibility and irrotationality of fluid lead to

$$\frac{1}{r}\frac{\partial}{\partial r}(r\, q_r) + \frac{1}{r}\frac{\partial q_\theta}{\partial \theta} + 2\rho_f u_L = 0 \tag{16}$$

$$\frac{\partial}{\partial r}(r\, q_\theta) - \frac{\partial q_r}{\partial \theta} = 0 \tag{17}$$

where

$$q_r = \rho_f w \bar{u}_r, \quad q_\theta = \rho_f w \bar{u}_\theta \tag{18}$$

and $\bar{u}_r$ and $\bar{u}_\theta$ are the components of velocity averaged through the width w. The boundary condition is $q_r = 0$ at $r = R$. The inlet and outlet are treated as a point source and sink, respectively, since R_0 and R_a are sufficiently small

when compared with R. The solution is obtained as

$$q_r = \frac{q_a}{2\pi}\Big[\sum_{n=1}^{\infty} \frac{a^n}{R^{2n}} r^{n-1} \cos n\theta - \frac{a}{r} \frac{r\cos\theta - a}{(r\cos\theta - a)^2 + r^2\sin^2\theta}\Big]$$

$$+ \frac{1}{2}(R^2 - r^2)\Big[\frac{1}{r}(C_{L0} + C_{L1}p_0) - \frac{3}{4}\rho_f g C_{L1}\cos\theta\Big]$$

$$q_\theta = -\frac{q_a}{2\pi}\Big[\sum_{n=1}^{\infty} \frac{a^n}{R^{2n}} r^{n-1}\sin n\theta + \frac{a\sin\theta}{(r\cos\theta - a)^2 + r^2\sin^2\theta}\Big] \qquad (19)$$

$$+ \frac{1}{8}\rho_f g C_{L1}(3R^2 - r^2)\sin\theta.$$

It should be noticed that (19) is valid even for a non-stationary crack.

Next, the energy equation for the fluid is derived. For heat transfer problems at small fluid velocity, the mechanical energy terms are small in the energy equation. The effect of heat conduction in fluid (water) may also be small compared with those of heat convection and transfer terms. Furthermore, the time derivative term of the fluid temperature T can be neglected because of smallness (Bodvarsson, 1969, Lowell, 1976). It is assumed that the rock temperature T_r is approximately equal to T on the crack surface and T is constant through the crack width (Bodvarsson, 1969, Gringarten et al., 1975, Lowell, 1976). In this way the energy equation for the fluid, after averaging through the crack width, can be written in the form:

$$q_r \frac{\partial T}{\partial r} + q_\theta \frac{\partial T}{r\partial\theta} = \frac{2\lambda}{C_f} \frac{\partial T_r}{\partial z}\Big|_{z=0} \qquad (20)$$

where C_f and λ are the specific heat of the fluid and the heat conductivity of the rock respectively. The position of the boundary $z = w/2$ has been replaced by $z = 0$, since w is very small compared with the radius R and the distance a.

When the energy system operates effectively, the thermal penetration depth in the rock is very small compared with R and a so that the heat flux is almost perpendicular to the fracture surface. Thus the rock temperature T_r may simply be governed by the following equation:

$$\frac{\partial^2 T_r}{\partial z^2} = \frac{C_\gamma \rho_\gamma}{\lambda} \frac{\partial T_r}{\partial t} \qquad (21)$$

where C_γ is the specific heat of the rock. It is noted that this simplification does not mean that T_r is independent of r and θ. Harlow and Pracht (1972) have used the same equation as (21).

The temperatures $T(r,\theta,t)$ and $T_r(r,\theta,z,t)$ which are the solutions of (20) and (21) must satisfy the following conditions:

$$T_r(r,\theta,z,t_s) = T_\infty \qquad (22a)$$

$$T(0,\theta,t) = T_0 \qquad (22b)$$

$$T(r,\theta,t) = T_r(r,\theta,0,t) \tag{22c}$$

where T_∞ is the initial temperature (or the far-field tectonic temperature), T_0 is the temperature of the inlet fluid, and t_s is the time at which the outlet is provided.

The solution of (20) and (21) is written as

$$T_r = T_0 + (T_\infty - T_0)\operatorname{erf}\left[\frac{1}{\sqrt{t-t_s}}\left\{\sum_{n=0}^{\infty} f_n(r)\cos n\theta + \tfrac{1}{2}\left(\frac{C_\gamma \rho_\gamma}{\lambda}\right)^{1/2} z\right\}\right] \tag{23}$$

with

$$f_n(0) = 0, \tag{24}$$

where f_n are solutions of

$$a_0 \frac{df_0}{dr} + \tfrac{1}{2}\sum_{n=1} a_n \frac{df_n}{dr} - \frac{1}{2r}\sum_{n=1} nb_n \frac{df_n}{dr} = kr\left(1 + \frac{r^2}{a^2}\right)$$

$$a_0 \frac{df_1}{dr} + a_1 \frac{df_0}{dr} + \tfrac{1}{2}\sum_{n=1}\left(a_{n+1}\frac{df_n}{dr} + a_n \frac{df_{n+1}}{dr}\right) - \frac{1}{2r}\sum_{n=1}\left\{nb_{n+1}f_n + (n+1)b_n f_{n+1}\right\}$$

$$= -2k\,\frac{r}{a} \tag{25}$$

$$a_0 \frac{df_p}{dr} + a_p \frac{df_0}{dr} + \tfrac{1}{2}\sum_{n=1}\left(a_{n+p}\frac{df_n}{dr} + a_n \frac{df_{n+p}}{dr}\right) - \frac{1}{2r}\sum_{n=1}\left\{nb_{n+p}f_n + (n+p)b_n f_{n+p}\right\}$$

$$+ \tfrac{1}{2}\sum_{n=1}^{p-1} a_n \frac{df_{p-n}}{dr} + \frac{1}{2r}\sum_{n=1}^{p-1}(p-n)b_n f_{p-n} = 0 \qquad (p \geq 2)$$

where

$$k = \frac{2\pi}{C_f q_0}(C_\gamma \rho_\gamma \lambda)^{1/2},$$

$$a_0 = \left(1 - \frac{r^2}{R^2}\right)\left[1 + \frac{\pi R^2}{q_a}\left\{\left(1 + \frac{r^2}{a^2}\right)\left(C_{L0} + C_{L1}p_0\right) + \tfrac{3}{4}\rho_f g\, C_{L1}\frac{r^2}{a}\right\}\right]$$

$$a_1 = r\left(1 - \frac{r^2}{R^2}\right)\left[\frac{a}{R^2}\left(1 - \frac{R^2}{a^2}\right) - \frac{\pi R^2}{a q_a}\left\{2\left(C_{L0} + C_{L1}p_0\right) + \tfrac{3}{4}\rho_f g\, C_{L1} a\left(1 + \frac{r^2}{a^2}\right)\right\}\right]$$

$$a_2 = r^2\left(1 - \frac{r^2}{R^2}\right)\left[\frac{a^2}{R^4}\left(1 - \frac{R^2}{a^2}\right) + \frac{3\pi R^2}{4 a q_a}\rho_f g\, C_{L1}\right]$$

$$a_m = \frac{r^m a^m}{R^{2m}}\left(1 - \frac{r^2}{R^2}\right)\left(1 - \frac{R^2}{a^2}\right) \qquad (m \geq 3); \tag{26}$$

$$b_0 = 0$$

$$b_1 = -\frac{2r}{a} - \frac{ra}{R^2}\left(1 - \frac{r^2}{R^2}\right)\left(1 - \frac{R^2}{a^2}\right) + \frac{3\pi R^2}{4q_a}\rho_f g C_{L1} r\left(1 - \frac{r^2}{3R^2}\right)\left(1 + \frac{r^2}{a^2}\right)$$

$$b_2 = -\frac{r^2a^2}{R^4}\left(1 - \frac{r^2}{R^2}\right)\left(1 - \frac{R^2}{a^2}\right) - \frac{3\pi R^2}{4aq_a}\rho_f g C_{L1} r^2\left(1 - \frac{r^2}{3R^2}\right)$$

$$b_m = -\frac{r^m a^m}{R^{2m}}\left(1 - \frac{r^2}{R^2}\right)\left(1 - \frac{R^2}{a^2}\right) \qquad (m \geq 3).$$

The heat extraction rate or thermal power output at the outlet is

$$Q_f = q_a C_f (T_a - T_0) \tag{27}$$

where T_a is the fluid temperature at the outlet, or by (23) and (22c)

$$Q_f = q_a C_f (T_\infty - T_0)\operatorname{erf}\left[\frac{1}{\sqrt{t - t_s}} \sum_{n=0}^{\infty} f_n(a)\right]. \tag{28}$$

ILLUSTRATIVE EXAMPLES

The data employed here and in the following are given below:

R_a/R_0	= 0.5	C_f	= 1.0 cal/gr °C
C_v	= 1.25	C_γ	= 0.25 cal/gr °C
ρ_f	= 1.0 gr/cm^3	λ	= 6.2×10^{-3} cal/cm sec °C
ρ_γ	= 2.65 gr/cm^3	T_∞	= 250°C
K_a	= 0.49	T_0	= 65°C
ν	= 0.25	α_T	= 8.0×10^{-6}/°C
$S_0/\rho_f g h_0$	= 1.3	$\pi K_c/\sqrt{2R_0}\cdot S_0$	= 1.118.

Furthermore, B_1 is taken as zero since the effect of the pressure on the fluid loss should not be large as discussed by Hall and Dollarhide (1964).

The outlet fluid temperature T_a and the thermal power output Q_f in Case (I) are graphed as functions of time in Figs. 2a and 2b. The corresponding relations in Case (II) are graphed in Figs. 3a and 3b. The effect of the position of the outlet hole is also shown in Figs. 2a and 2b. The outlet flow rate q_a considered here is not necessarily large (Table 1).

REFERENCES

Abé, H., T. Mura and L. M. Keer, 1976. Growth rate of a penny-shaped crack in hydraulic fracturing of rocks, J. Geophysical Res., 81, pp. 5335-5340.

Abé, H., L. M. Keer and T. Mura, 1976. Growth rate of a penny-shaped crack in hydraulic fracturing of rocks, 2, J. Geophysical Res., 81, pp. 6292-6298.

Bodvarsson, G., 1969. On the temperature of water flowing through fractures, J. Geophysical Res., 74(8), pp. 1987-1992.

Delisle, G., 1975. Determination of permeability of granite rocks in GT-2 from hydraulic fracturing data, Rep. LA-6169-MS, Los Alamos Scientific Lab., Los Alamos, N.M., pp. 1-5.

Gringarten, A. C., P. A. Witherspoon and Y. Ohnishi, 1975. Theory of heat extraction from fractured hot dry rock, J. Geophysical Res., 80(8), pp.1120-1124.

Hall, C. D., Jr. and F. E. Dollarhide, 1964. Effects of fracturing fluid velocity on fluid-loss performance, Trans. AIME, 231, pp. 555-560.

Hall, C. D., Jr. and F. E. Dollarhide, 1968 (July). Performance of fracturing fluid loss agents under dynamic conditions, J. Pet. Tech., pp. 763-769.

Harlow, F. H. and W. E. Pracht, 1972. A theoretical study of geothermal energy extraction, J. Geophysical Res., 77(35), pp. 7038-7048.

Keer, L. M., 1964. A class of non-symmetrical punch and crack problems, Q. J. Mech. and Appl. Math., 17(4), pp. 423-436.

Lowell, R. P., 1976. Comments on 'Theory of heat extraction from fractured hot dry rock' by A. C. Gringarten et al., J. Geophysical Res., 81(2), pp. 359-360.

McFarland, R. D., 1975. Geothermal reservoir models — crack plane model, Rep. LA-5947-MS, Los Alamos Scientific Lab., Los Alamos, N.M., pp. 1-18.

Table 1. Stationary Cracks

Case		h_0 m	q_0 gr/sec	p_a^*/S_0	q_a gr/sec	$\Delta p_0/S_0$	R/R_0
I	1	3000	1.451×10^5	-0.23916	5.305×10^4	0.24009	11500
	2	2000	1.409	-0.24264	5.151	0.24396	5750
II	A	3000	1.289	-0.23852	4.647	0.23923	10000
	B		1.232	-0.23882	4.649	0.23954	
	C		1.162	-0.23916	4.653	0.23988	
	D	2000	1.183	-0.24172	3.819	0.24245	5000
	E		1.127	-0.24215	3.823	0.24288	
	F		1.059	-0.24264	3.827	0.24337	

$\Delta p_0/S_0 \equiv p_0/S_0 - 1/\Delta$

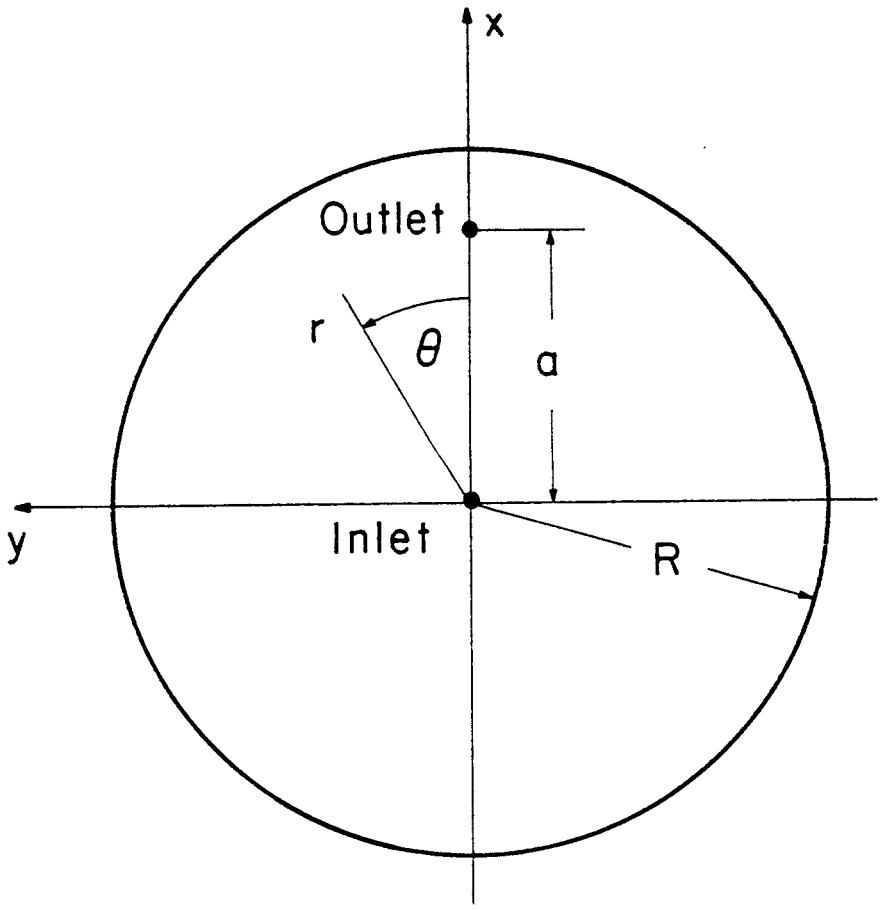

Fig. 1

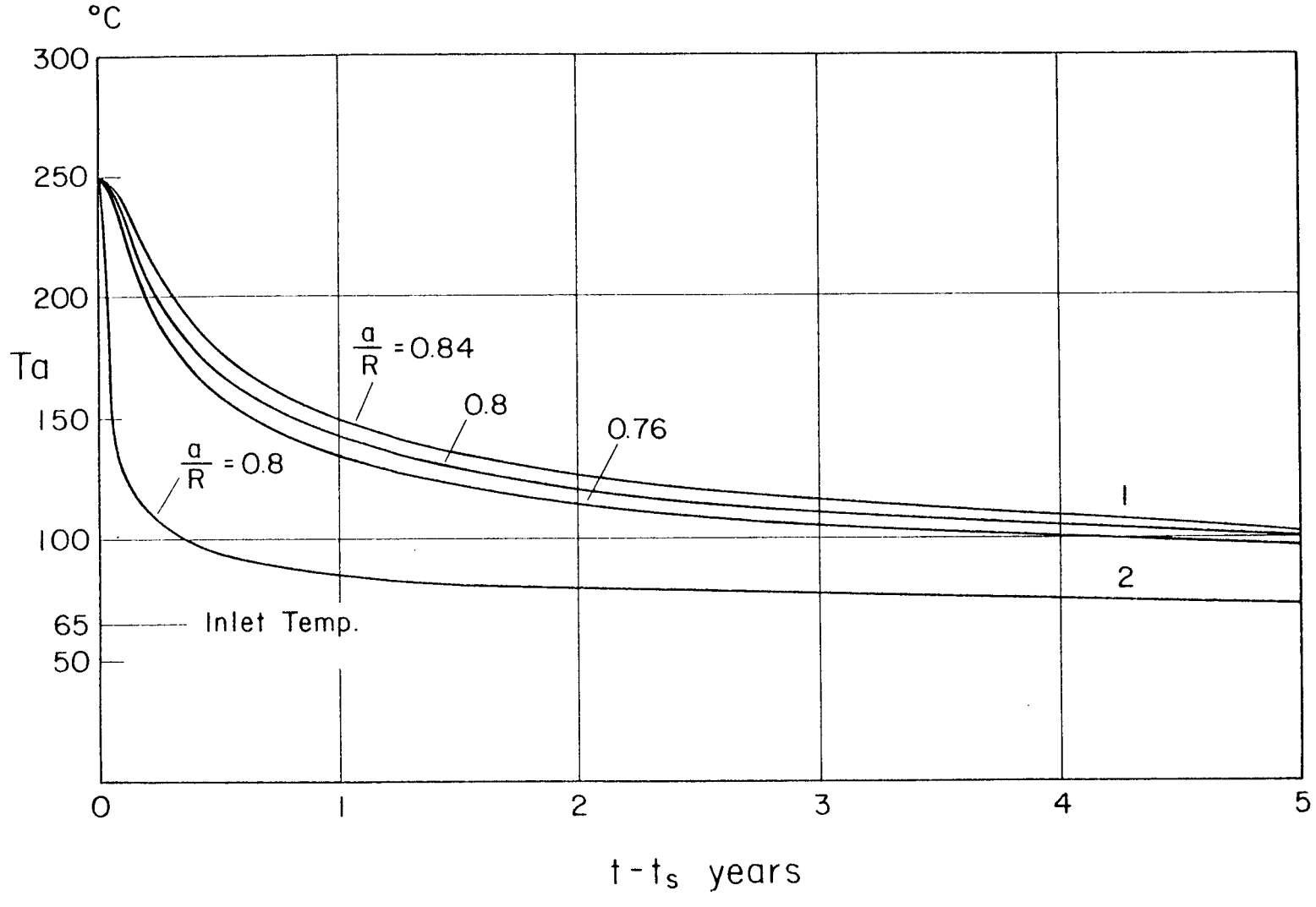
°C
300
250
200
150
100
65
50
Ta
a/R = 0.84
0.8
0.76
a/R = 0.8
1
2
Inlet Temp.
0
1
2
3
4
5
t - ts years

Fig. 2a

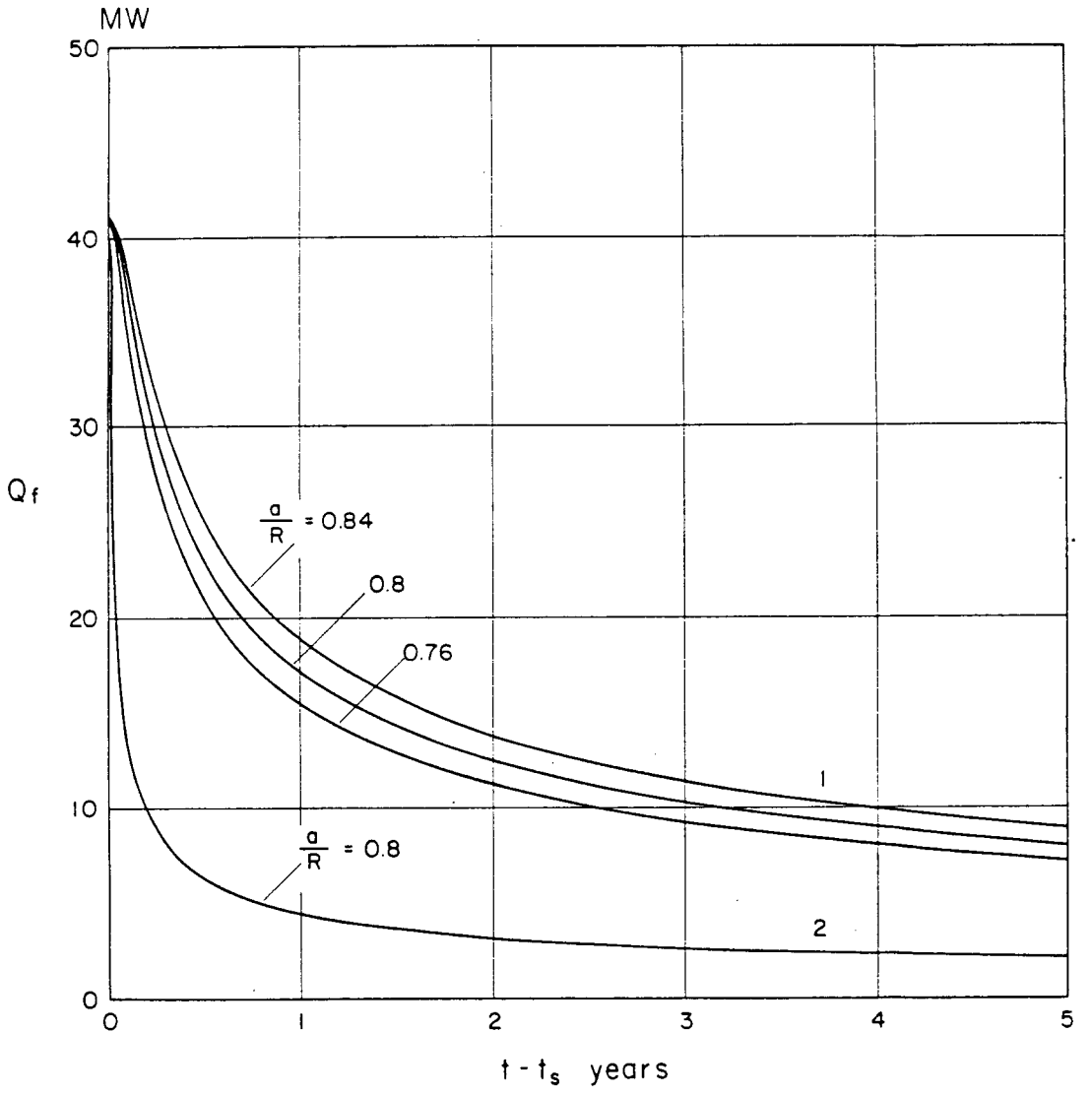
MW
50
40
30
20
10
0
Q_f
$\frac{a}{R}$ = 0.84
0.8
0.76
1
$\frac{a}{R}$ = 0.8
2
0
1
2
3
4
5
$t - t_s$ years

Fig. 2b

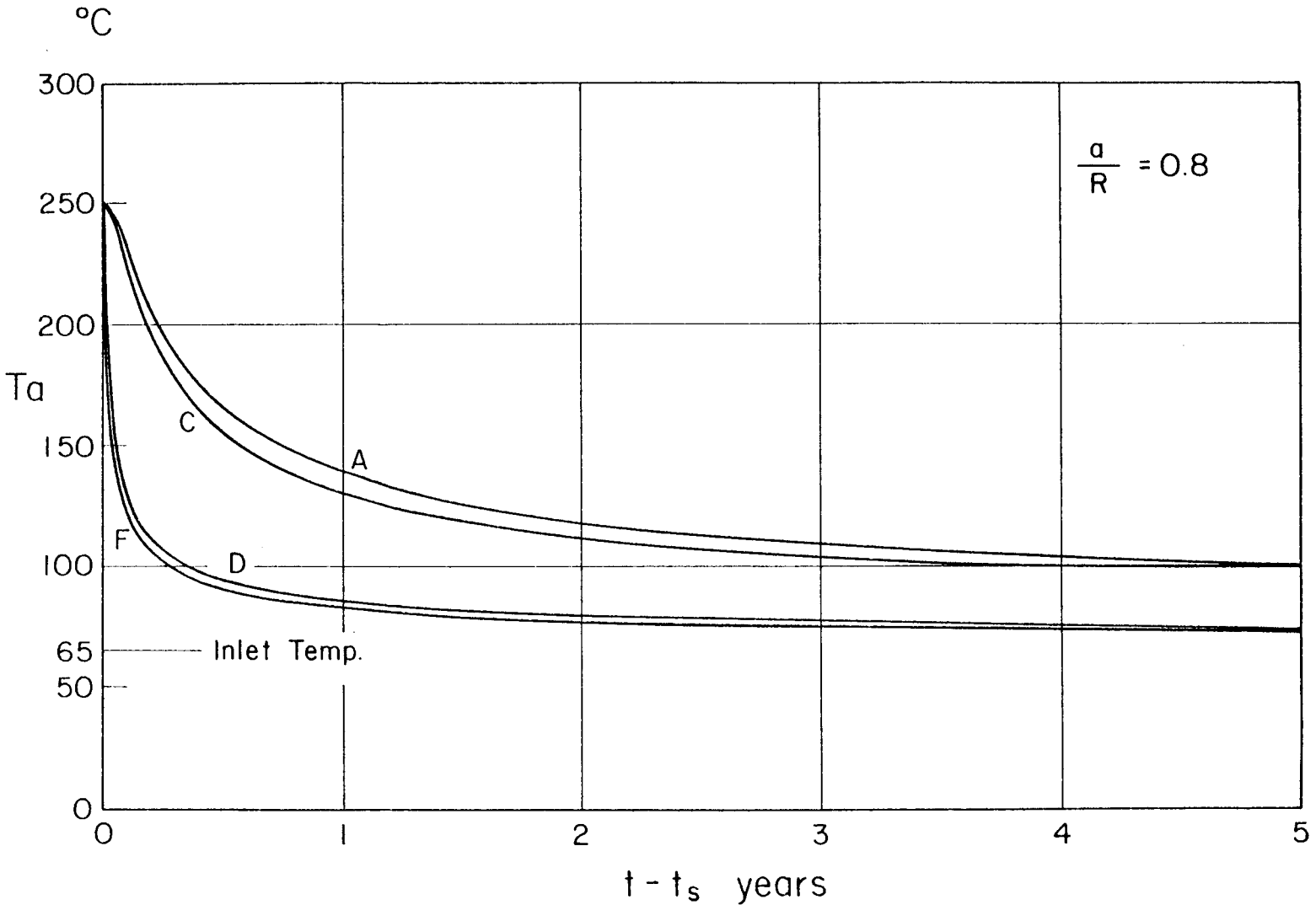
°C
300
250
200
Ta
150
100
65
50
0
0
1
2
3
4
5
t - ts years
a/R = 0.8
A
C
D
F
Inlet Temp.

Fig. 3a

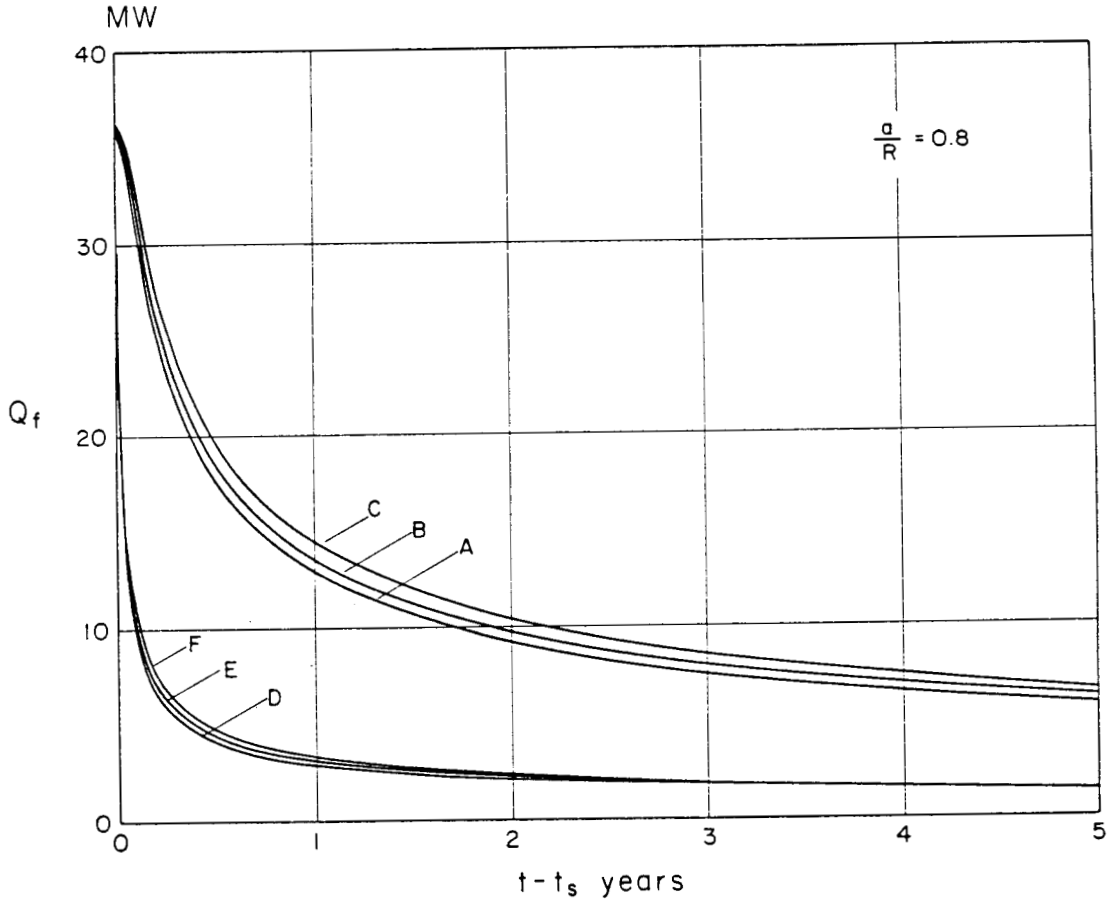

Fig. 3b

PHYSICAL MODEL STUDIES OF EXPLOSION-FRACTURED GEOTHERMAL RESERVOIRS

Anstein Hunsbedt,* Roberto Iregui, and Paul Kruger
Civil Engineering Department
and A. Louis London
Mechanical Engineering Department
Stanford University
Stanford, CA 94305

Large scale utilization of geothermal energy will require means for enhanced energy extraction from geothermal reservoirs since the higher quality hydrothermal resources adequate for commercial electricity generation represent only a small fraction of the estimated resource base. Technologies are being developed for artificial fracturing of hydrothermal and dry hot rock geothermal resources to obtain adequate permeability for water circulation and to expose new rock surface area. Non-isothermal processes such as in-place boiling or artificial circulation of cooler fluids can be used to extract the energy from the fractured formation. To evaluate non-isothermal heat transfer processes, physical model studies were conducted in the Stanford Geothermal Program fractured-rock reservoir model capable of operating at a maximum pressure of 800 psig at 500°F. The 17-ft^3 physical model has been described previously [Hunsbedt, Kruger, and London (1975), Hunsbedt (1975), and Hunsbedt, Kruger and London (1976)]. A summary of the characteristics of the relatively large fracture-permeability rock systems tested in the model are summarized in Table 1. The porosity and permeability characteristics of these systems resembled those of fracture-stimulated created by high-energy explosives.

TABLE 1

Summary of Rock System Characteristics

	Rock System		
	1	2	3
Rock type	Gabbro	Granite	Granite**
Mean rock equivalent diameter, inches	0.99	2.65	1.62
Drainage porosity, percent	44	35	43

A description of the in-place boiling experiments (flashing by pressure reduction) conducted with the first two rock systems were given by Hunsbedt (1976) and by Hunsbedt, Kruger and London (1976). The results showed that

*Now at General Electric Company, Sunnyvale, CA 94086

**Obtained from the underground "Piledriver" rock chimney.

the fraction of rock energy extracted by in-place boiling* was in excess of 75 percent of maximum for a broad range of production conditions. Heat transfer from the rock resulted in an increase in the total energy extraction from the hydrothermal (liquid and rock) system ranging from 1.25 to 2.57 times the energy obtained by flashing the fluid alone. Gravity segregation resulted in the production of slightly superheated steam from the producing zone located at the top of the reservoir model. Fluid production and rock heat transfer analyses were developed which closely predict the behavior of the physical model as long as the axial liquid temperature gradients are small. Application of the rock heat transfer analysis to large-scale systems with a 30-year production time showed that a maximum rock size of about 200 feet would give energy extraction fractions of the same order as those obtained experimentally.

Non-isothermal production of the reservoir model was also achieved by recharging cool fluids at the bottom, a process often referred to as the sweep process. Experiments of this type were conducted with the second rock system. The results of one such experiment are given in Fig. 1 which show the axial temperature profiles measured at various times during production. The zone of production at the top is seen to remain at nearly constant temperature until cool fluid recharged at the bottom breaks through to the producing zone after about 4 hours. At that time there is a rapid drop in the temperature of the liquid being produced. It is also noted that significant thermal energy still remains in the top rock zone when liquid production was terminated. This also tends to be true in large-scale systems because the power generating equipment requires fluids at temperatures above a minimum level to operate efficiently. In analogy to the experimental results, there will be a tendency to achieve incomplete energy extraction from the rock near the producing zone of a large-scale system as well. The estimated mean rock temperatures also given in Fig. 1 are seen to be only slightly higher than the liquid temperature indicating effective heat transfer from the rock. The liquid temperature distribution and the mean rock to liquid temperature difference at the end of production both determine the magnitude of the rock energy extraction fraction defined in terms of the initial and recharge fluid temperatures. The rock energy extraction fraction for this experiment was estimated to be 0.85. The rock heat transfer analysis developed for the model system was used to estimate the mean rock size of a large-scale system. The results show that a maximum rock size of about 150 feet would give rock energy extraction fractions of the same order as those achieved in the model. This assumes a 30-year production time, mean rock to liquid temperature difference of 15°F, and similar permeability characteristics of the model and large-scale systems.

Fluid production experiments were conducted with the producing zone located at the bottom of the model to investigate the possible development of axial temperature gradients in the steam zone observed to occur in the in-place boiling experiments. The fluid production reservoir pressure behavior for one such experiment is shown in Fig. 2. The results show that all liquid was produced at nearly constant pressure (between points D and D') followed

*The rock energy extraction factor is defined as the thermal energy extracted from the rock to the thermal energy stored in the rock between initial and final liquid temperatures.

by a sharp pressure decline when vapor production is initiated (at point D'). It is noted that the corresponding reservoir pressure characteristic for in-place boiling with vapor production from the top, also shown in Fig. 2, declines more uniformly. Note also that only 60 percent of the fluids were produced (as high enthalpy superheated steam) in the in-place boiling experiment while about 99 percent of the fluids were produced (as low enthalpy liquid) in the steam drive experiment. The rock temperature decreased only slightly during the production process indicating that this is an ineffective rock energy extraction process. Examination of the temperature behavior in the model reservoir showed that the axial temperature profiles were nearly uniform and that the liquid was slightly subcooled, indicating the presence of a non-condensable gas (argon used for pressurization during heatup) in addition to water vapor in the zone above the liquid. Further evaluation of this steam/gas drive production process appears warranted to determine the major parameters and the extent to which it may be important in large-scale systems.

Experiments are currently in progress with the third rock system. The rock was obtained from the rubble chimney formed by collapse of the overburden formation into the cavity created by the 61 kt "Piledriver" nuclear explosion. The Piledriver nuclear explosive was detonated on June 2, 1966 at a depth of 1,500 feet in a formation of granodiorite. The explosion produced a cavity radius of 131.5 feet and a collapsed rubble chimney 890 feet high and 160 feet in width measured in the reentry tunnel 103 feet above the explosive. The rubble chimney is estimated to contain about 67 million ft^3 of fractured rock with a zone of fractures created by the immense shock wave out to a distance of more than 1,000 feet. The rubble rock is expected to be microfractured, and thus may have thermal properties measurably different from naturally fractured granites.

The current rock system in the physical model consists of Piledriver rock obtained from the reentry tunnel at a distance of about 100 feet from the chimney axis. The size distribution after conveyance in 30-gallon drums to Stanford from the Nevada Test Site was still approximately log normal. Six of the rocks of various sizes have thermocouples installed to obtain center rock temperature measurements.

In-place boiling and cool fluid recharge energy extraction experiments similar to those performed previously with the first two rock systems will be performed with the current rock system under similar test conditions to provide comparative rock thermal transient data. Furthermore, the steam production rates will be as high as practical to obtain large rock/steam temperature differences and consequently lower measurement uncertainties. An analysis of the conduction error in the rock center temperature measurements will be performed and corrections will be applied to both previous experimental data and the Piledriver rock system data. An improved analysis for predicting the rock/steam temperature differences for non-constant cooling rate will be developed using the shape factor correlation proposed by Kuo (1976). Kuo has shown from sensitive heat transfer experiments that the heat transfer behavior of irregularly-shaped rocks can be correlated to equivalent spherical rocks of equal mass, to a sphericity shape parameter and to the rock surface area to volume ratio.

A qualitative assessment of microfractures on the heat transfer and energy extraction processes will be made by comparing the measured rock temperature transient with those obtained for the second rock loading. The rock/steam temperature difference measurements will be compared to analytic predictions for individual instrumented rocks before applying it to the model rock system as a whole. The ultimate goal of this analysis is to develop a generalized thermal model for a collection of rocks that can be applied to large-scale fracture-stimulated geothermal systems with known or assumed rock-size and shape-factor distributions.

Future experimental efforts are anticipated with two other rock systems. Experiments with a fourth rock system will explore the effect of finite permeability and low porosity on the energy recovery process from fractured geothermal systems. Experiments with a fifth rock system will explore the potential improvement in the heat transfer by thermal cracking processes. Measurements of radon emanation from the Piledriver granites into surrounding air and water are underway in the Stanford Geothermal Program. Radon emanation characteristics appear promising as an indicator of changes in rock surface area. Thus, it is anticipated that changes in the radon emanation rate as well as in the heat transfer rate from the rock system will be important indicators that thermal cracking and exposure of new heat transfer surface area have occurred.

References

Hunsbedt, A., P. Kruger, and A. L. London, "A laboratory model of stimulated geothermal reservoirs," SGP-TR-7, Report to National Science Foundation, Grant No. GI-34925, February, 1975.

Hunsbedt, A., "Laboratory studies of stimulated geothermal reservoirs," SGP-TR-11, Report to National Science Foundation, Grant No. NSF-03490, December, 1975.

Hunsbedt, A., P. Kruger, and A. L. London, "Recovery of energy from fractured geothermal reservoirs," 46th Annual California Regional Meeting of the Society of Petroleum Engineers of AIME, Long Beach, CA, April 8-9, 1976.

Kuo, Ming-Ching T., "Shape factor correlations for transient heat conduction from irregular shaped rock fragments to surrounding fluid," SGP-TR-16, Report to National Science Foundation, Grant No. NSF-03490, June, 1976.

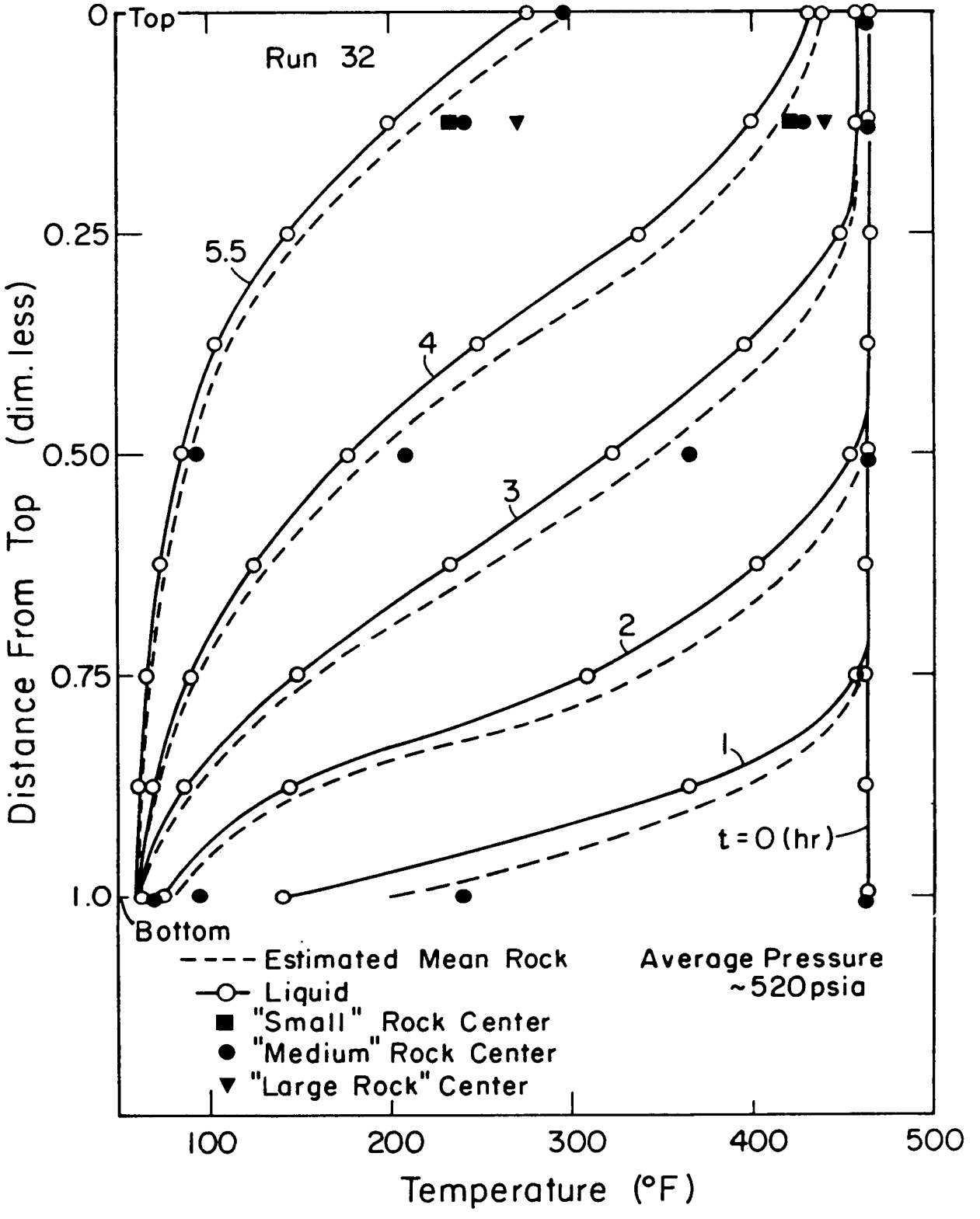

Figure 1 Liquid and rock temperature distributions as functions of time with cool liquid recharge

Figure 2. Pressure as a function of mass production.

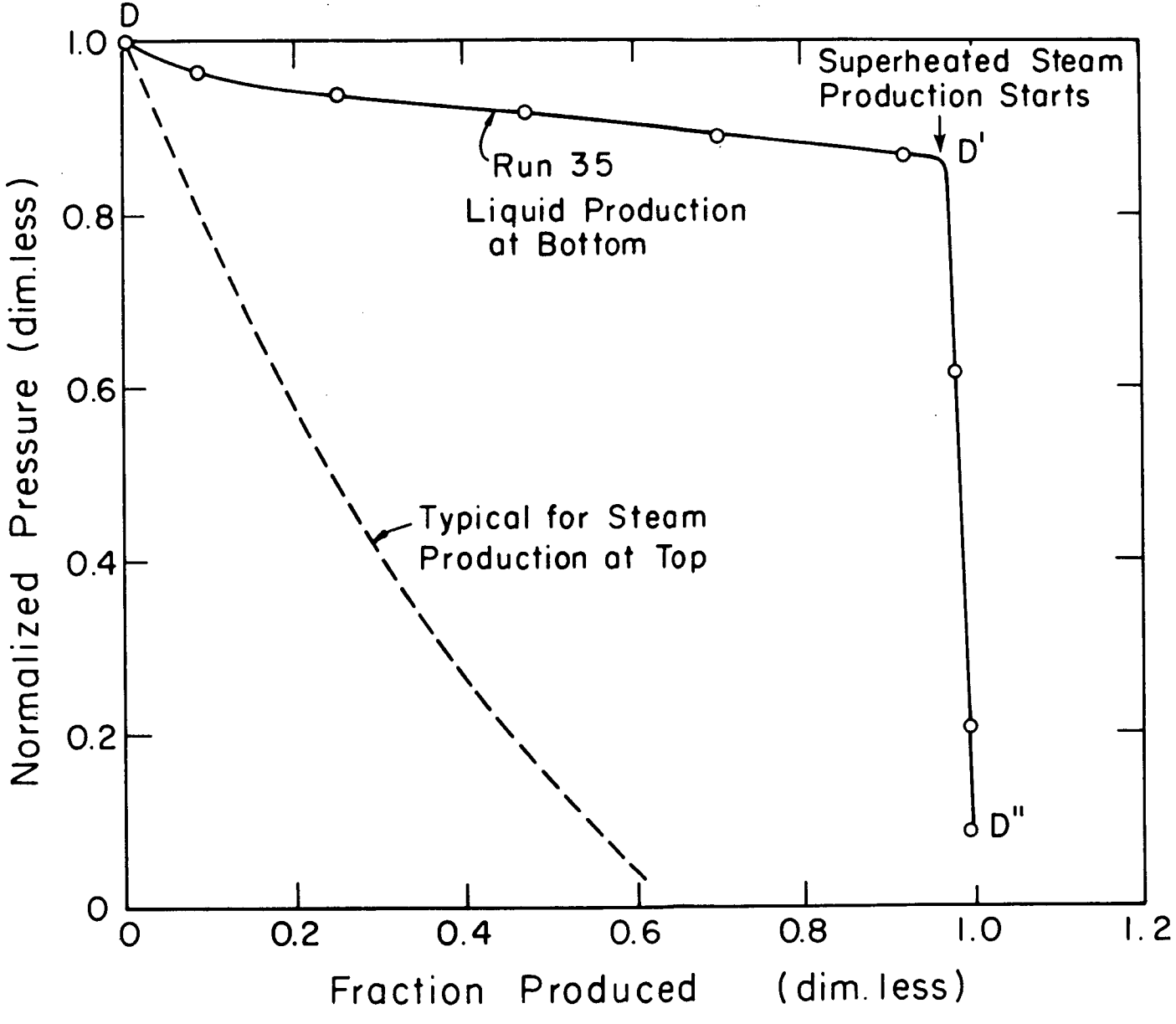

EXPLOSIVE STIMULATION OF GEOTHERMAL WELLS

M. E. Maes
Energy Sciences Associates
Seattle, WA 98101

The widespread, economic utilization of geothermal energy is at least partly dependent on efficient methods for stimulation of geothermal wells and formations. Well stimulation has become routine in the petroleum industry and yet, in spite of decades of downhole experience, most of the successful petroleum techniques cannot be used in a geothermal application. The principal problem is temperature, which imposes chemical, physical and mechanical limitations on equipment and stimulation fluids. The restrictions become particularly serious when formation temperatures exceed the 350° to 400°F range which of course are the better geothermal zones. Ironically, one stimulation technique which has lost favor in oil and gas fields offers promise geothermally. Explosive fracturing, particularly bore shooting, can be used to fracture formations adjacent to the well bore.

The first requirement for explosive geothermal stimulation is an explosive which will tolerate the temperature environment. An important distinction must be made between conventional explosives which can be adapted one or another for experimental purposes, and a true geothermal explosive which is capable of being routinely under a wide variety of commercial field conditions. In the first case, special methods can be employed to protect the explosive from the heat, such as insulative packaging, the design of explosive containers to allow for expansion and melting, forced cooling of the charges, and continuous water flooding of the well to drop local temperatures. These methods will allow a variety of common explosives to be tried for research purposes but are prohibitively expensive and fundamentally unsafe for commercial application. There are some advanced military explosives in existence now which will tolerate temperatures up to 500-600°F, but are specially synthesized and cost from $125 to over $500 per pound. They are therefore impractical economically except for very small charges. Fortunately, compositions have recently been discovered at a substantial cost advantage. These new materials have demonstrated thermal stability to 600°F and should be available for a few dollars a pound in quantity.

The object of any stimulation technique is to increase the ability of the surrounding formation to accept or release fluids more readily. Explosives achieve this by punching into or cracking the formation around the well bore. Explosive stimulation can be divided into three principal techniques: perforation, bore shooting, and massive formation fracturing. Perforation involves the use of shaped charges, which focus explosive shock waves to produce an intense, ultra-high velocity jet of molten metal which punches through the steel casing, cement and into the formation beyond. Perforating shaped charges are used extensively in the oil and gas industry to open well bores to production zones, but since the penetration is limited to a few feet and hole sizes are typically under one inch, they are of little value in opening up tight formations.

Bore shooting with cans of desensitized nitroglycerine was quite common in oil and gas wells until about 20 years ago, when it was gradually replaced by hydraulic fracturing. It involves the detonation of one or more charges of substantial size in the well bore in order to shatter the surrounding formation. Canisters of explosive are lowered to the zone selected for fracturing (after the casing has first been removed) and detonated. Single charges can be employed or multiple charges can be used to effect reinforced shock waves. The extent of the fractures still depends on many factors including the type of rock, existence of nearby discontinuities, depth, and the design and size of the charge. Typically, a six-inch diameter canister, with an explosive loading of about ten lbs. per linear foot, would be expected to create fractures out to a distance of 10 to 20 feet from the well bore in a uniform formation. More importantly, as a result of shock reflection off the face of the discontinuity, fractures could propagate as far as 30 to 40 feet to adjacent discontinuities such as nearby steam or hot water passages. Bore shooting would therefore be expected to intersect any nearby natural fracture networks. Bore shooting will create some rubble which must be either cleaned up or allowed to drop to lower levels of the well after the shot.

Massive formation fracturing involves the use of special liquid explosives which are pumped back into a formation prior to detonation. A typical shot could imploy ten to twenty thousand pounds of explosives and is capable of influencing the formation for a hundred feet or more from the well bore. The process requires the use of large pumping equipment and sophisticated controls, and is still in the development stage in the petroleum industry.

An extension of simple bore shooting to achieve a degree of massive formation fracturing is a technique known as repetitive bore shooting in which additional charges are placed in the ever enlarging cavity produced by each previous bore shot. With this method, a series of three or four shots would be expected to influence a radius of up to fifty feet from the well bore.

At present, the explosives employed in a massive fracturing system have thermal stability limitations that prevent their use above 300°F. Therefore, only perforation and bore shooting (perhaps involving repetitive bore shooting) offer immediate potential. Conventional commercial perforating charges can be used in wells with temperatures up to 350°F and beyond if special cooling is employed. In more extreme environments the existing high temperature military explosives are suitable. Several have densities and detonation velocities which are desirable for good shaped charged performance. While cost is not critical, since typical charge weight is on the order of one pound, the effect per unit cost is very low.

For true stimulation, only bore shooting offers economic viability today in high temperature wells. Assuming the use of new low cost geothermal explosives, a typical bore shot treatment involving a few hundred pounds can be done for a cost of a few thousand dollars. When the high cost of drilling geothermal wells is considered, the possibility of achieving economic production or improving output for less than 5% of the well drilling and completion cost is most attractive. Nevertheless, it is a long step from economic and technical feasibility to commercial reality; a major element in

that step is the development of safe hardware and field operational procedures. The entire process, not just the explosive, must be considered and the safety of personnel and equipment are of paramount importance. Therefore, certain conditions must be met in order to qualify an explosive stimulation system for routine commercial use. These conditions include:

1) Two component explosive systems in which only a few pounds of live explosive are handled above ground, the bulk of the charge being armed by mixing two non-detonable components only after the containers have entered the well.

2) Complete thermal stability at maximum well temperature, to insure that self-detonation does not occur in the event that cooling is lost or the charge hangs up in the well.

3) Remote safety interlocks on the initiation mechanism to prevent accidental premature initiation.

4) A reliable, preferably automatic fail-safe method of neutralizing the charge in the well, in case it must be pulled out without detonation.

These conditions will insure that the explosive charges cannot cause massive damage or injury to personnel above ground in case of an accident, and also will minimize the potential for serious damage to a well in the event of a mishap.

Fortunately, these conditions are within the present state of the art, and can be incorporated into the design of charges and supporting hardware today. Given the new developments in low cost geothermal explosives, it appears that geothermal stimulation, using bore hole shooting, can be a commercial reality in less than two years.

SIMULATION OF HEAT TRANSPORT IN FRACTURED, SINGLE-PHASE GEOTHERMAL RESERVOIRS

William G. Gray, Kevin O'Neill and George F. Pinder
Water Resources Program
Department of Civil Engineering
Princeton University
Princeton, N. J. 08540

Although many geothermal reservoirs depend upon fracture permeability to obtain adequate mass flows, relatively little research effort has been directed toward fractured reservoir simulation. This paper outlines the mathematical apparatus necessary to develop a numerical simulator for a fractured, single-phase geothermal reservoir. It is assumed that the fracturing is extensive and well-distributed (though not necessarily uniform) so that it is reasonable to consider a superficial discharge through the fractures as well as the pores. While mass and heat transport are of course coupled in a system of this kind, we have subdivided the ensuing discussion into mass flow and heat flow for clarity of presentation.

Mass Flow Equation

Analytical solutions for the pressure distributions in porous blocks of various shapes and sizes show that the pressure in the interior of a typical block reaches 95% of the value of an initial "step" input imposed on the block surface in a time which is very short relative to the length of time typically required for overall, macroscopic system changes. In addition, recent modeling analyses and examination of pertinent field data by Closmann (1975) support the point of view that for most purposes one may consider both pore and fracture flow fields to be characterized by a single pressure variable. A net flow of mass may exist between one flow regime and the other, but this will be such as to maintain the near equality of pressure. Application of accepted space-averaging techniques (Gray and Lee, 1976) to a point mass balance equation provides the following mass conservation equation:

$$\frac{\partial}{\partial t}(\rho_w \varepsilon_w) = \nabla\cdot[\rho_w \underset{\sim}{v}_w] + S_m = \nabla\cdot[\rho_f \underset{\sim}{v}_f + \rho_p \underset{\sim}{v}_p] + S_m \qquad (1)$$

where ρ_w is the averaged density of all (pore plus fracture) water,

ρ_f is the density of fracture water,

ρ_p is the density of pore water,

ε_w is the void fraction occupied by all water,

v_f is the superficial discharge through the fracture (vector),

$\tilde{v}_p$ is the superficial discharge through the pores (vector), and

S_m is the mass source or sink strength, that is, mass entering or leaving per unit time per unit volume of total medium.

The lefthand side of (1) may be expanded as

$$\frac{\partial}{\partial t}(\rho_w \varepsilon_w) = \rho_w \frac{\partial \varepsilon_w}{\partial t} + \varepsilon_w \frac{\partial \rho_w}{\partial t} \tag{2}$$

$$= \rho_w \alpha_p \frac{\partial p}{\partial t} + \rho_w \alpha_T \frac{\partial T_w}{\partial t} + \varepsilon_w \rho_w \beta_p \frac{\partial p}{\partial t} + \varepsilon_w \rho_w \beta_T \frac{\partial T_w}{\partial t}$$

where ε_f is the void fraction of the fractures,

ε_p is the void fraction of the pores,

p is the incremental fluid pressure,

T_f is the local average fluid temperature in the fractures,

T_{pm} is the local average temperature of the porous medium, and

T_w is the locally averaged temperature of all water defined as

$$T_w = \varepsilon_f T_f + \varepsilon_p T_{pm} \tag{3}$$

The parameters α_p, α_T, β_p and β_T are empirical coefficients defined through the relations:

$$\frac{\partial \varepsilon_w}{\partial t} = \alpha_p \frac{\partial p}{\partial t} + \alpha_T \frac{\partial T_w}{\partial t} \tag{4a}$$

$$\frac{\partial \rho_w}{\partial t} = \rho_w \beta_p \frac{\partial p}{\partial t} + \rho_w \beta_T \frac{\partial T_w}{\partial t} \tag{4b}$$

Superficial fracture and pore discharges may be expressed in terms of incremental pressure gradients, as

$$\underset{\sim}{v}_f = -\left(\frac{\underset{\approx}{k}}{\mu}\right)_f \cdot \underset{\sim}{\nabla} p \tag{5a}$$

$$\underset{\sim}{v}_p = -\left(\frac{\underset{\approx}{k}}{\mu}\right)_p \cdot \underset{\sim}{\nabla} p \tag{5b}$$

where μ is the fluid viscosity,

$\underset{\approx}{k}_f$ is the fracture permeability (tensor), and

$\underset{\approx}{k}_D$ is the pore permeability (tensor)

Under certain conditions $\underset{\approx}{k}_f$ may be considered to be a function of $\underset{\sim}{v}_f$.

Substitution of equations (2) through (5) into (1) yields the following expression for the conservation of all fluid mass:

$$\rho_w(\alpha_p + \varepsilon_w\beta_p)\ \frac{\partial p}{\partial t} + \rho_w(\alpha_T + \varepsilon_w\beta_T)\ \frac{\partial T_w}{\partial t} \tag{6}$$

$$= \underset{\sim}{\nabla} \cdot \left[\left(\frac{\rho \underset{\approx}{k}}{\mu}\right)_f + \left(\frac{\rho \underset{\approx}{k}}{\mu}\right)_p\right] \cdot \nabla p + Sm$$

In addition to the explicit coupling of this equation to the temperature equations through the second term on the lefthand side, temperature dependence also enters implicitly through the changing value of μ .

Heat Flow

The governing equations for heat flow are provided by space averaging of conservation of energy equations written in terms of temperature. For the fracture system, this results in

$$\rho_f c \varepsilon_f\ \frac{\partial T_f}{\partial t} + \rho_f c \underset{\sim}{v}_t \cdot \underset{\sim}{\nabla} T_f - \underset{\sim}{\nabla} \cdot \underset{\approx}{D}_f \cdot \underset{\sim}{\nabla} T_f$$

$$= h(T_{pm} - T_f) + c\, S_{m,f}(T_{s,f} - T_f) \tag{7a}$$

and for the porous medium

$$(\rho c\varepsilon)_{pm} \frac{\partial T_{pm}}{\partial t} + \rho_p c v_{\sim p} \cdot \nabla T_{pm} - \nabla \cdot \underset{\sim}{\underset{\sim}{D}}_{pm} \cdot \nabla T_{pm}$$

$$= h(T_f - T_{pm}) + c\, S_{m,p}(T_{s,pm} - T_{pm}) \qquad (7b)$$

where $(\rho c\varepsilon)_{pm} \equiv \rho_p c \varepsilon_p + \rho_s c_s \varepsilon_s$,

ρ_s is the rock density,

c_s is the specific heat of the rock,

ε_s is the volume fraction of the rock,

c is the specific heat of water,

$\underset{\sim}{\underset{\sim}{D}}_f$ is the tensor coefficient of dispersion for the fractures,

$\underset{\sim}{\underset{\sim}{D}}_{pm}$ is the tensor coefficient of dispersion for the porous medium,

h is a porous medium-fracture heat transfer coefficient relating the time rate of heat transport between those regimes, per volume of the medium, to the temperature difference between the two. $T_{s,f}$ and $T_{s,pm}$ are source or sink temperatures of fracture and pore fluids, respectively. (For withdrawal, the sink temperature is the reservoir fluid temperature and the last terms in 7 vanish).

$S_{m,f}$ is the fracture mass source or sink strength,

$S_{m,p}$ is the pore mass source of sink strength, and

$S_m = S_{m,f} + S_{m,p}$ and the ratio of the two components can be determined using the permeabilities of the two systems.

The superficial velocities in (7) must, of course, be computed using the pressure field through equations (5) and (6). Equations (5), (6), and (7) provide five equations in the five dependent variables T_{pm}, T_f, p, $v_{\sim f}$ and $v_{\sim p}$. These equations have been solved successfully for a variety of hypothetical problems for which analytical solutions exist. The numerical simulator uses isoparametric Hermitean finite elements (Van Genuchten, et al, 1977) to solve in three space dimensions, and a time-centered difference scheme to solve in time.

Figures 1 and 2 show results for an additional fully coupled, one-dimensional, transient test case, subject to the following conditions:

at $x = 0$ $\quad T_{pm} = T_f = 40^{\circ}C$

$t > 0$ $\quad p = 0$

at $x = 100cm$ $\quad T_{pm} = T_f = 0$

$p = -1.0 \times 10^5$ dyne/cm^2

$\frac{1}{\mu} = 5.38 \times 10^2 + (T-150) \times 3.8 - (T-150)^3 \times 2.6 \times 10^{-5}$ cm.sec/g for $0<T<300^{\circ}C$

(Mercer et al, 1975)

$\varepsilon_f = 0.02$, $\varepsilon_p = 0.2$, $\alpha_p = 1.0 \times 10^{-10}$ cm^2/dyne, $\alpha_T = 0$

$\frac{k_f}{\varepsilon_f} = 10^{-7}$ cm^2, $\frac{k_{pm}}{\varepsilon_p} = 3.0 \times 10^{-8}$ cm^2, $\beta_p = 5.0 \times 10^{-11}$ cm^2/dyne

$\beta_T = 5.0 \times 10^{-4}/^{\circ}C$

$\rho_s = 2.5$g/cm^3, $c_s = 0.2$cal/g.$^{\circ}$C, $D_f = 5.0 \times 10^{-4}$ cal/$^{\circ}$C.cm.sec,

$D_{pm} = 3.0 \times 10^{-3}$ cal/$^{\circ}$C cm.sec.

The initial temperature distribution for both fractures and porous medium is displayed on each figure. As expected, a non-zero value of h retards translation of the fracture temperature front, increases translation of the porous medium front, and increases dispersion of both. As the fronts progress, the pressure gradient (not shown) decreases from the initial, essentially isothermal value, due primarily to the decrease in fluid viscosity with rising temperature.

References

Closmann, P. J., "An Aquifer Model for Fissured Reservoirs," Society of Petroleum Engineers Journal, October 1975, 385-398.

Gay, W. G. and P. C. Y. Lee, "On the Theorems for Local Volume Averaging of Multiphase Systems," International Journal of Multiphase Flow, in press 1976.

Mercer, W. M., G. F. Pinder, and I. G. Donaldson, "A Galerkin Finite Element Analysis of the Hydrothermal System at Wairakei, New Zealand," Journal of Geophysical Research, June 1975, 2608-2621.

Van Genuchten, M. T., G. F. Pinder, and E. O. Frind, "Simulation of Two-dimensional Contaminant Transport with Isoparametric Hermitean Finite Elements," Water Resources Research, in press 1976.

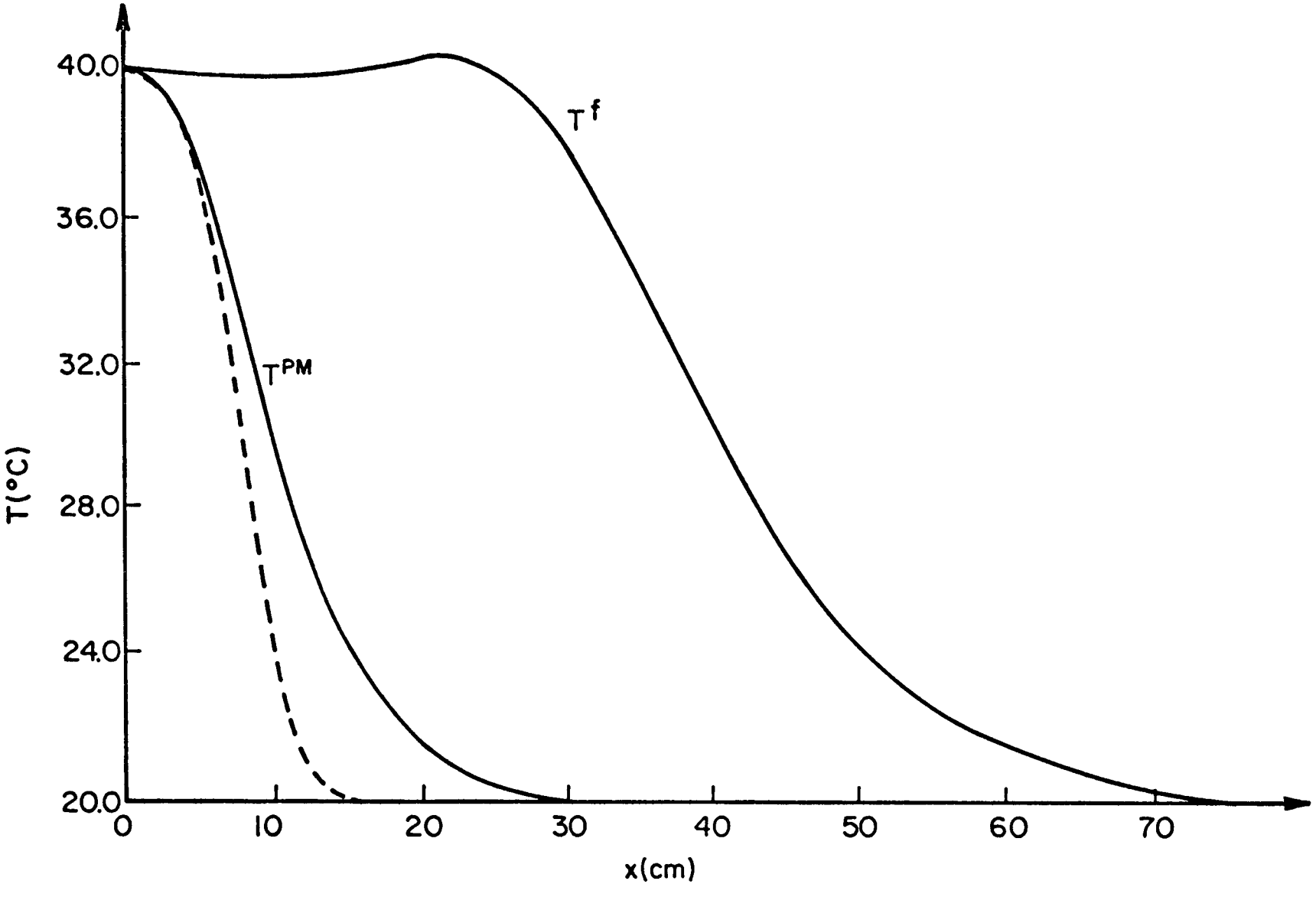

h=0
$t = 3.0 \times 10^3$ sec
DASHED LINE SHOWS INITIAL TEMPERATURE
FIGURE 1

FIGURE 2

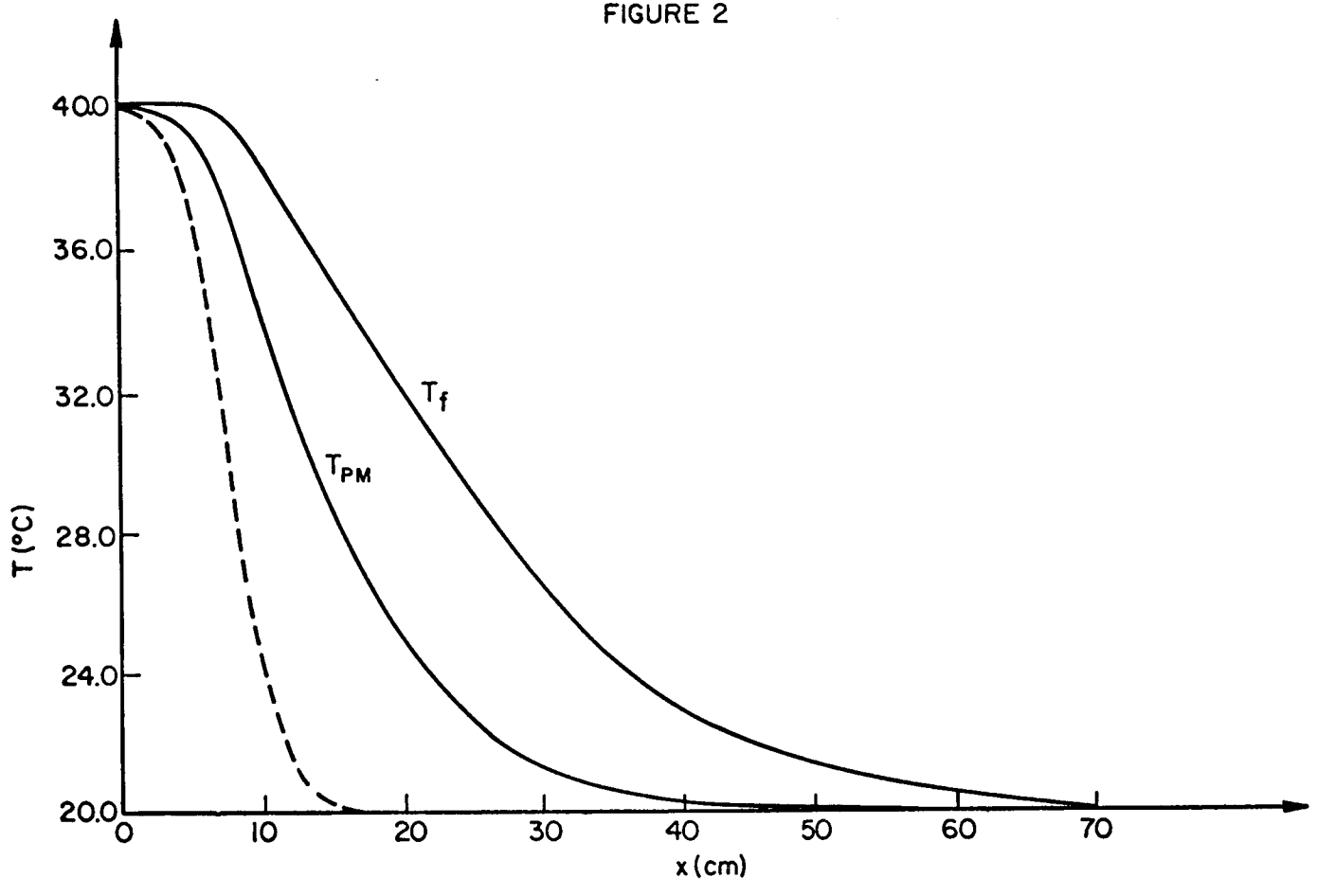

$h = 2.0 \times 10^{-5}$ CAL/cm^2 sec °C
$t = 5.25 \times 10^3$ sec
DASHED LINE SHOWS INITIAL TEMPERATURE

STEAM TRANSPORT IN POROUS MEDIA

A. F. Moench
U. S. Geological Survey
Water Resources Division
345 Middlefield Road
Menlo Park, CA 94025

Numerous investigators have pursued development of large-scale two-phase digital simulation models of vapor-dominated geothermal systems. These represent significant advances in the capability to numerically simulate complex systems. However, the basic physical phenomena which are being modeled are still under investigation. The purpose of this discussion is to present the results of a numerical study in which some of the physical phenomena which may occur in vapor-dominated geothermal reservoirs are examined. These phenomena include: (1) superheating of discharging steam, (2) energy changes due to compressible work, (3) conductive heat transport, and (4) gravitational effects of the steam column. Further details pertaining to this study are available in a report by Moench (1976).

The numerical model used in this study draws upon the concepts of White and others (1971) for a vapor-dominated geothermal system, though of necessity some simplifications have been made. The physical system is idealized as a one-dimensional column of porous or highly fractured rock filled with a mixture of steam and liquid water under high pressure. This reservoir is overlaid by a "cap rock" that has low permeability. At the bottom of the reservoir there is a zone where liquid water saturates the pores. Heat is supplied by a magma chamber at depth and transferred upward through the liquid-saturated zone by conduction and convection. The primary mechanisms for heat transfer through the vapor-dominated zone are vaporization and condensation. Figure 1 illustrates the distributions of temperature and pressure to be expected in this idealized natural system.

The model is designed to determine the time-varying distributions of liquid-water saturation, pressure, and temperature within the vapor-dominated region. These distributions may be due to the withdrawal of steam at either constant pressure or constant discharge. Basic assumptions of the model include the following: (1) liquid water within the vapor zone is stationary, but subject to vaporization, (2) Darcy's law is valid for two fluids, (3) the rock matrix is rigid, (4) local thermal equilibrium occurs between the fluids and rock, (5) negligible viscous dissipation, (6) negligible thermal dispersion, and (7) negligible surface tension effects.

To simulate the vertical flow of steam through variably saturated porous media, two controlling equations are used (see Appendix): a

fluid-flow equation and an energy equation. These equations contain parameters which are dependent upon pressure, temperature, and liquid-water saturation. The energy equation accounts for heat conduction, convection, vaporization, compressible work, and heat storage. These partial differential equations are coupled through the velocity terms, the vaporization terms, the liquid saturation, and the pressure- and temperature-dependent parameters. The equations are solved simultaneously at discrete time intervals by a finite-difference technique.

Results

Figure 2 shows the pressure, temperature, and liquid-water saturation after 10^9 sec (31.6 years) of steam production from the top of a one kilometer column of reservoir rock. This represents the effect of removing about 70% of the mass that was initially available. Steam is produced at a rate which declines with time due to withdrawal at constant pressure. All the liquid water in the top 300 m has been vaporized and steam in this region is superheated.

Temperature distributions "A" and "B" in Figure 2 show the influence of heat conduction and compressible work (as defined by the second term on the righthand side of the energy equation). Distribution "A" shows the temperature profile obtained using the complete energy equation. Distribution "B" shows the temperature profile obtained when the compressible work term is omitted from the calculations. It is clear that compressible work is significant only where superheated steam is present. Both profiles show the temperature increase at the top of the reservoir brought about by conduction from the base of the cap rock at a distance of approximately 50 m. Conduction from the cap rock or other nearby rocks not cooled by the vaporization process may be responsible for the temperature increase of produced steam observed in some wells (Sestini, 1970). The time variation in temperature at the top of the reservoir is shown in Figure 3 for curves "A" and "B". In the early part of the production history, the cooling effect of compressible work counteracts the heating due to conduction from the cap rock.

The effect of eliminating gravity from the calculations upon the pressure and temperature distributions is shown by the dashed lines in Figure 2. Apart from its possible influence upon the vertical distribution of liquid water (not included in this study) the effect of gravity can be safely neglected. The weight of the steam column has little, if any, effect upon reservoir production characteristics.

References

Moench, A.F., 1976, Simulation of steam transport in vapor-dominated geothermal reservoirs, U. S. Geol. Survey open-file report 76-607, 43 p.

Sestini, G., 1970, Superheating of geothermal steam, Geothermics Special Issue, v. 2, pt. 1, p. 622-648.

White, D.E., Muffler, L.J.P., and Truesdell, A.H., 1971, Vapor-dominated hydrothermal systems compared with hot-water systems, Econ. Geology, v. 66, p. 75-97.

APPENDIX

The basic equations used in this study are reproduced here for convenience. Additional details and constitutive relationships are given in the report by Moench (1976).

Flow Equation

$$\frac{\partial}{\partial z}\left[\rho_v \frac{k\, k_r}{\mu_v}\left(\frac{\partial P}{\partial z} - \rho_v g\right)\right] + q + q' = \phi(1-S)\rho_v \kappa \frac{\partial P}{\partial t} - \phi(1-S)\rho_v \beta \frac{\partial T}{\partial t} - \phi \rho_v \frac{\partial S}{\partial t}$$

where

ρ_v	density of the water vapor
μ_v	dynamic viscosity of the water vapor
k	intrinsic permeability
k_r	relative permeability to water vapor
g	acceleration of gravity
ϕ	porosity
S	liquid-water saturation
P	pressure
q	source or sink of steam through wells (positive if source of steam)
q'	source or sink of steam by vaporization or condensation (positive if source of steam)
z	vertical coordinate (positive downward)
t	time
κ	compressibility of water, $\frac{1}{\rho_v}\left(\frac{\partial \rho_v}{\partial P}\right)_T$
β	thermal expansivity of water vapor, $-\frac{1}{\rho_v}\left(\frac{\partial \rho_v}{\partial T}\right)_P$
T	temperature

Energy Equation

$$\frac{\partial}{\partial z}\left(K\frac{\partial T}{\partial z}\right)-c_1 v\frac{\partial T}{\partial z}-Lq'+Q=[c_1+c_2+c_3]\frac{\partial T}{\partial t}-\phi(1-S)\,T\,\beta\frac{DP}{Dt}$$

where

K	effective thermal conductivity
v	average interstitial velocity
c_1	heat capacity of vapor, $\phi(1-S)\rho_v c_{pv}$
c_2	heat capacity of liquid, $\phi S\rho_\ell c_{p\ell}$
c_3	heat capacity of solid, $(1-\phi)\rho_s c_{ps}$
ρ_ℓ	density of liquid water,
ρ_s	density of solid rock particles
c_{pv}	specific heat at constant pressure of vapor
$c_{p\ell}$	specific heat at constant pessure of liquid
c_{ps}	specific heat at constant pressure of solid
L	latent heat of vaporization
Q	energy source or sink by means other than condensation or vaporization (positive if source of heat)
$\frac{D}{Dt}$	substantial derivative, $\frac{\partial}{\partial t}+v\frac{\partial}{\partial z}$

Liquid-Water Saturation Equation

$$\frac{\partial S}{\partial t}=-\frac{q'}{\phi\rho_\ell}$$

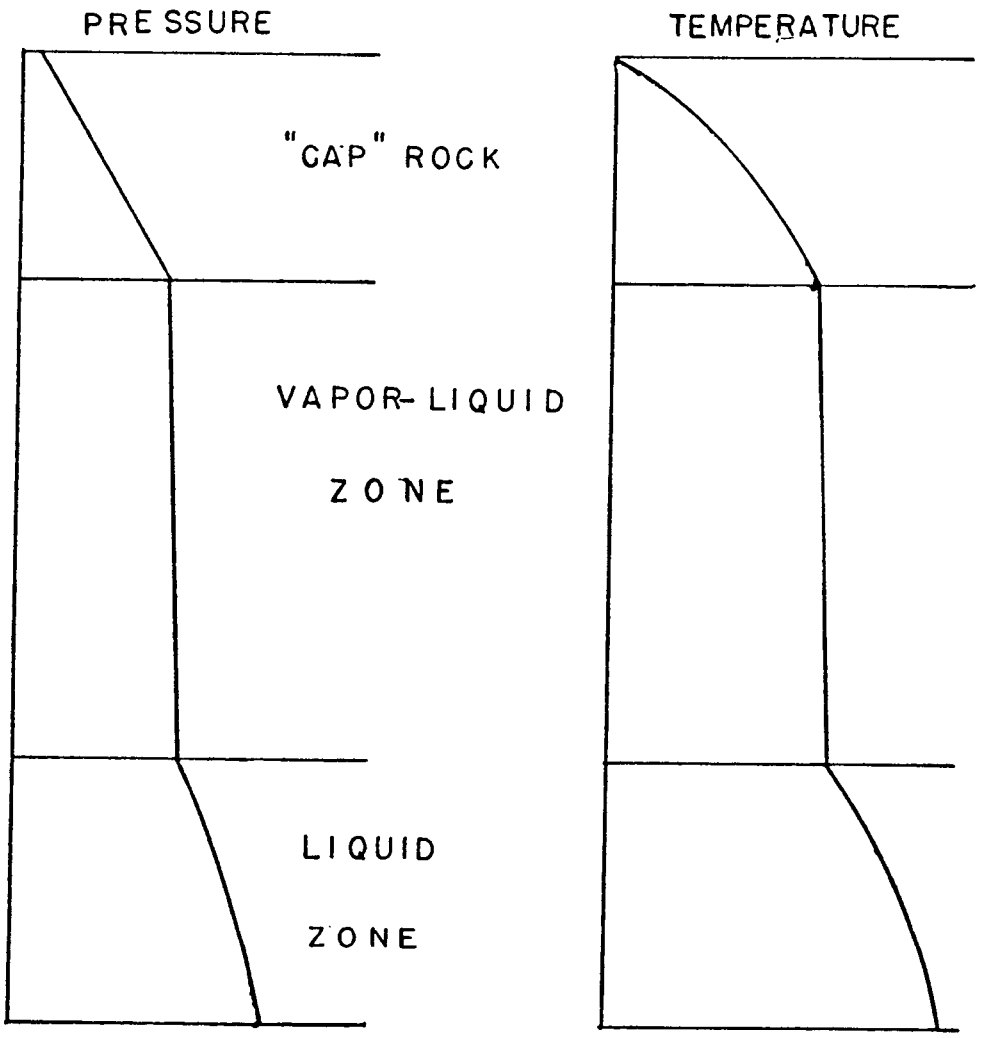

Figure 1. Vertical temperature and pressure distributions in an idealized natural vapor-dominated system.

FIGURE 2. Pressure, temperature and liquid-water saturation distributions in a one-kilometer column of reservoir rock which has been producing steam at a pressure of 10 bars for 10^9 sec. 500 m of cap rock overlie the reservoir. Dashed lines indicate effect of eliminating gravity.

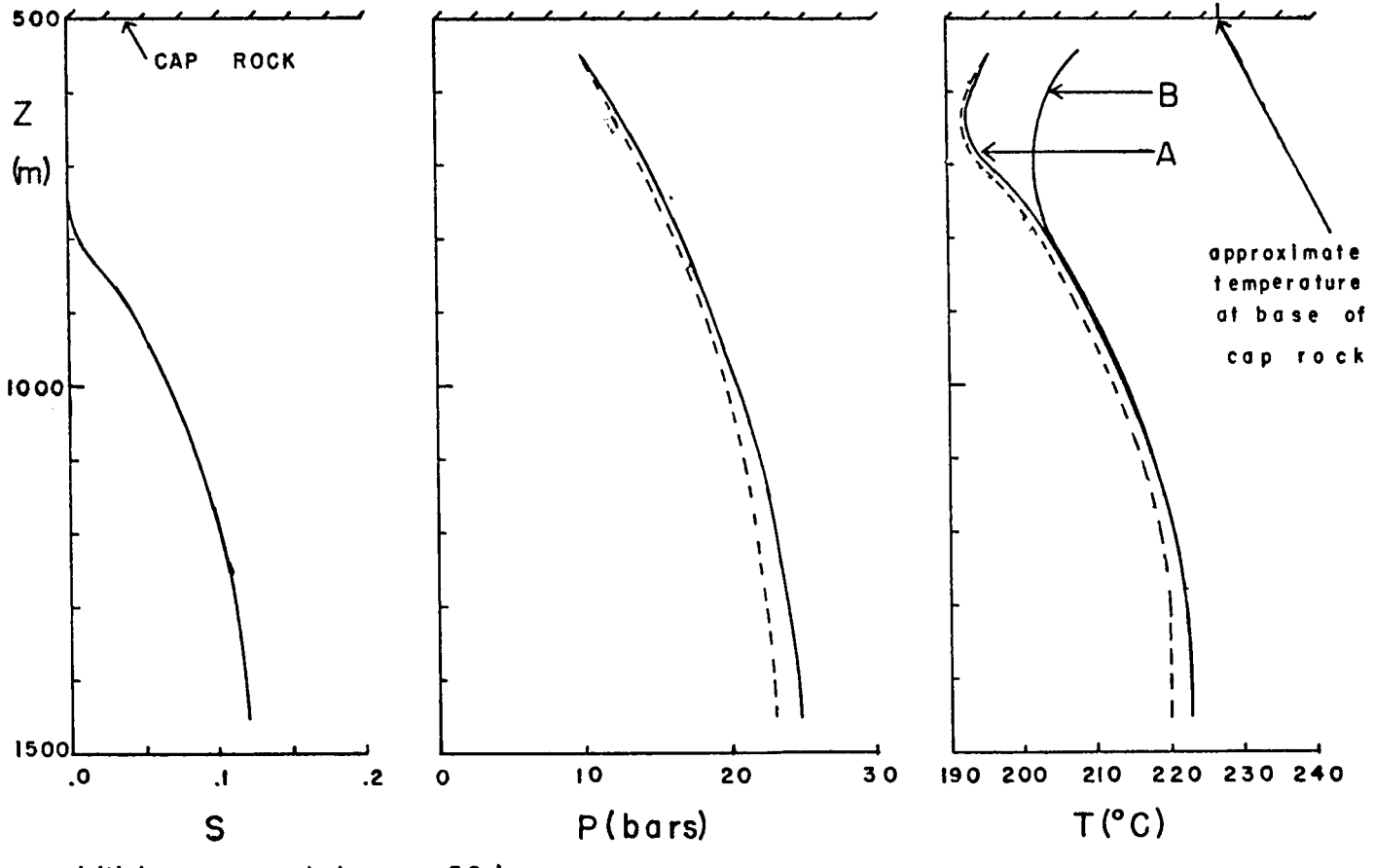

initial pressure at top = 30 bars
initial saturation = 0.2
porosity = 0.2
permeability = 10 md

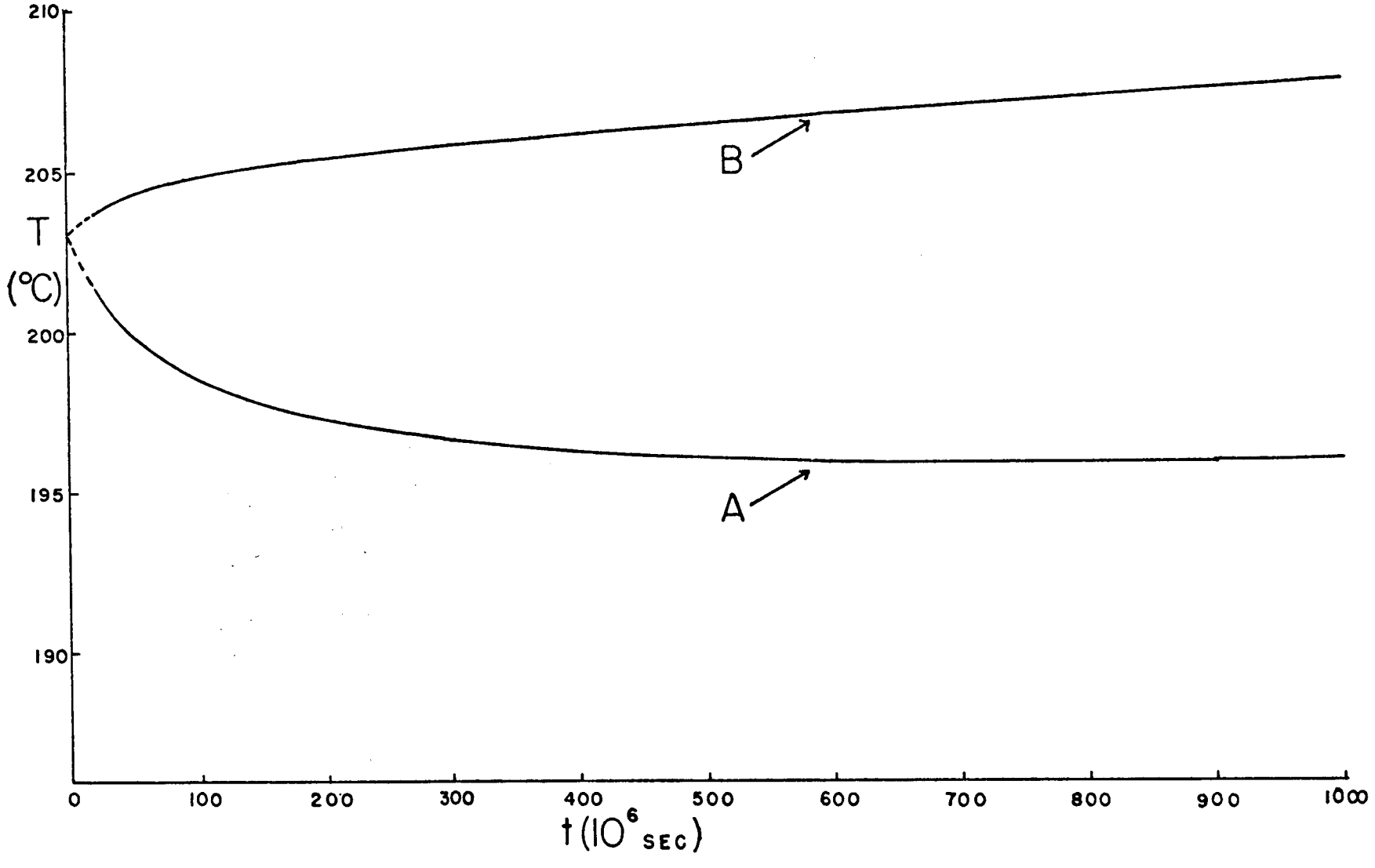

Figure 3. Temperature versus time at top of reservoir for conditions shown in Figure 2.

BUOYANCY INDUCED BOUNDARY LAYER FLOWS IN GEOTHERMAL RESERVOIRS

Ping Cheng*
Department of Petroleum Engineering
Stanford University, Stanford, CA. 94305

Most of the theoretical study on heat and mass transfer in geothermal reservoirs has been based on numerical method. Recently at the 1975 NSF Workshop on Geothermal Reservoir Engineering, Cheng (1) presented a number of analytical solutions based on boundary layer approximations which are valid for porous media at high Rayleigh numbers. According to various estimates the Rayleigh number for the Wairakei geothermal field in New Zealand is in the range of 1000-5000, which is typical for a viable geothermal field consisting of a highly permeable formation and a heat source at sufficiently high temperature.

The basic assumption of the boundary layer theory is that heat convective heat transfer takes place in a thin porous layer adjacent to heated or cooled surfaces. Indeed, numerical solutions suggest that temperature and velocity boundary layers do exist in porous media at high Rayleigh numbers (2). It is worth mentioning that the large velocity gradient existing near the heated or cooled surfaces is not due to viscosity but is induced by the buoyancy effects. The present paper is a summary of the work that we have done on the analytical solutions of heat and mass transfer in a porous medium based on the boundary layer approximations since the 1975 Workshop.

Similarity Solutions to Boundary Layer Equations

Free Convection about a Vertical Impermeable Surface with Uniform Heat Flux

The solution for free convection about a vertical impermeable surface with wall temperature being a power function of distance, i.e., $T_w = T + Ax^{\lambda}$ for $x > 0$ is given by Cheng and Minkowycz (3). The constant heat flux solution can be obtained by a simple transformation of variables and by setting $\lambda = 1/3$ in Ref. 3. The

*Visiting Professor. On sabbatical leave from Department of Mechanical Engineering, University of Hawaii, Honolulu, Hawaii 96822.

expressions for local Nusselt number, the mean Nusselt number, and thermal boundary layer thickness are

$$Nu_x/[Ra_x^*]^{\frac{1}{3}} = 0.7723, \qquad (1)$$

$$\overline{Nu}_L/[Ra_L^*]^{\frac{1}{3}} = 1.029, \qquad (2)$$

$$\frac{\delta_T}{x} = 4.8/[Ra_x^*]^{\frac{1}{3}}, \qquad (3)$$

with $Nu_x \equiv \frac{hx}{k} = \frac{qx}{k(T_W-T_\infty)}$, $\overline{Nu}_L \equiv \frac{qL}{\kappa(\overline{T_W-T_\infty})} = \frac{\bar{h}L}{\kappa}$, $Ra_x^* \equiv \rho_\infty g\beta Kq x^2/\mu\alpha k$, $Ra_L^* \equiv \rho_\infty g\beta KqL^2/\mu\alpha k$, and $\overline{T_W-T_\infty} \equiv \frac{1}{L}\int_0^L (T_W-T_\infty)dx$, where ρ_∞ is the density of the fluid at infinity; g the gravitational acceleration; μ and β the viscosity and the thermal expansion coefficient of the fluid; K the permeability of the porous medium; L the length of the plate; q the surface heat flux; α and κ the equivalent thermal diffusivity and the thermal conductivity of the saturated porous medium. The equivalence of Eqs. (1) through (3) and the corresponding expressions given by Cheng & Minkowycz (3) was shown recently by Cheng (4).

Free Convection about a Horizontal Impermeable Surface with Uniform Heat Flux

The constant heat flux solution for a horizontal impermeable surface can be obtained by a simple transformation of variables and by setting $\lambda = 1/2$ in the solution given by Cheng and Chang (5). The expressions for local Nusselt number, the mean Nusselt number, and thermal boundary layer thickness for the present problem are

$$Nu_x/[Ra_x^*]^{\frac{1}{4}} = 0.8588, \qquad (4)$$

$$\overline{Nu}_L/[Ra_L^*]^{\frac{1}{4}} = 1.288, \qquad (5)$$

$$\frac{\delta_T}{x} = \frac{4.0}{[Ra_x^*]^{\frac{1}{4}}} \qquad (6)$$

Mixed Convection from a Vertical Isothermal Impermeable Surface

The problem of mixed convection from a vertical impermeable surface with a step increase in wall temperature (i.e., $T_w = T_\infty + A$ for $x \geq 0$), embedded in a porous medium is considered by Cheng (6). The expressions for local Nusselt number, average Nusselt number, and thermal boundary layer thickness are

$$\frac{Nu_x}{[Re_x Pr]^{1/2}} = [-\theta'(0)] , \tag{7}$$

$$\frac{\overline{Nu}_L}{[Re_L Pr]^{1/2}} = 2[-\theta'(0)] , \tag{8}$$

$$\frac{\delta_T}{x} = \frac{\eta_T}{[Re_x Pr]^{1/2}} , \tag{9}$$

with $Re_x \equiv \frac{U_\infty x}{\nu}$ and $Pr \equiv \frac{\nu}{\alpha}$ where U_∞ is the velocity outside the boundary layer. The values of $Nu_x/[Re_x Pr]^{\frac{1}{2}}$ and $[Re_x Pr]^{\frac{1}{2}}\delta_T/x$ as a function of Gr_x/Re_x are shown in Figs. 1 and 2, where the corresponding values for free convection about a vertical isothermal plate as given by Cheng and Minkowycz (3) can be rewritten as

$$Nu_x/[Re_x Pr]^{\frac{1}{2}} = 0.444 \left[\frac{Gr_x}{Re_x}\right]^{\frac{1}{2}}, \tag{10}$$

$$[Re_x Pr]^{\frac{1}{2}}\delta_T/x = \frac{6.31}{[Gr_x/Re_x]^{\frac{1}{2}}} , \tag{11}$$

Mixed Convection from a Horizontal Impermeable Surface with Uniform Surface Heat Flux

The expressions for local Nusselt number, average Nusselt number, and thermal boundary layer thickness are given by (4,7)

$$\frac{Nu_x}{[Re_x Pr]^{\frac{1}{2}}} = \frac{1}{[-\phi(0)]} , \tag{12}$$

$$\frac{\overline{Nu_L}}{[Re_L Pr]^{\frac{1}{2}}} = \frac{3}{2[-\phi(0)]}, \tag{13}$$

$$\frac{\delta_T}{x} = \frac{\eta_T}{[Re_x Pr]^{\frac{1}{2}}}. \tag{14}$$

The values of $Nu_x/[Re_x Pr]^{\frac{1}{2}}$ and $[Re_x Pr]^{\frac{1}{2}}\delta_T/x$ as a function of $Ra_x^*/(Re_x Pr)^2$ are given in Ref. 4, where the asymtotes for free convection about a horizontal plate with uniform heat flux are given by Eqs. (4) and (6), which can be rewritten as

$$Nu_x/[Re_x Pr]^{\frac{1}{2}} = 0.8588\ [Ra_x^*/(Re_x Pr)^2]^{\frac{1}{4}}, \tag{15}$$

$$[Re_x Pr]^{\frac{1}{2}}\delta_T/x = 4.0/[Ra_x^*/(Re_x Pr)^2]^{\frac{1}{4}}. \tag{16}$$

The Effect of U_∞ on Heat Transfer Rate and the Size of Hot-Water Zone

To gain some feeling on the order of magnitude of various physical quantities in a geothermal reservoir, consider a vertical impermeable surface at 215°C is embedded in an aquifer at 15°C. If there is a pressure gradient in the aquifer such that groundwater is flowing vertically upward, the values of heat transfer rate and the size of the hot water zone can be determined from Figs. 1 and 2. The results of the computations for U_∞ varying from 0.01 cm/hr to 10 cm/hr are plotted in Figs. 3 and 4 where it is shown that the total heat transfer rate for a vertical surface, 1 km by 1 km, increases from 20 MW to 110 MW, while the boundary layer thickness at x = 1 km decreases from 130 m to 20 m.

Validity of Boundary Layer Approximations

The validity of the boundary layer approximations can be accessed by a comparison of results obtained by similarity solutions to that of numerical solutions of exact partial differential equations, or to experimental data. For free convection in a porous medium between parallel vertical plates separated by a distance H, the correlation equation given by Bories and Combarnous (8) is

$$\overline{Nu}_H = 0.245\ (Ra_H)^{0.625}\ (\frac{H}{L})^{0.397}, \qquad (17)$$

where L is the length of the plate, $\overline{Nu}_H = \frac{\bar{h}H}{k}$ and $Ra_H = \rho g \beta K (T_W - T_L) H/\mu\alpha$. Eq. (17) is valid for Ra_H from 10^2 to 10^3 and for H/L between 0.05 and 0.15[8]. On the other hand, the heat transfer rate as obtained from boundary layer approximations for an isothermal vertical plate (3) is

$$\overline{Nu}_L = 0.888\ (Ra_L)^{0.5}, \qquad (18)$$

which can be rewritten as

$$\overline{Nu}_H = 0.888\ (Ra_H)^{0.5}\ (\frac{H}{L})^{0.5}, \qquad (19)$$

Eqs. (17) and (19) for H/L = 0.05 and 0.15 are plotted in Fig. 5 for comparison. It is shown that they are in good agreement, especially at high Rayleigh numbers where the boundary layer approximations are valid.

Concluding Remarks

As in the classical convective heat transfer theory, boundary layer approximations in porous layer flows can result in analytical solutions. Mathematically, the approximations are the first-order terms of an asymptotic expansion which is valid for high Rayleigh numbers. Comparison with experimental data and numerical solutions show that the approximations are also accurate at moderate values of Rayleigh numbers. For problems with low Rayleigh numbers where boundary layer is thick, higher-order approximations must be used (9).

References

1. Cheng, P., "Numerical & Analytical Study on Heat and Mass Transfer in Volcanic Island Geothermal Reservoirs." Proceedings of 1975 NSF Workshop on Geothermal Reservoir Engineering, pp. 219-224 (1976).

2. Cheng, P., Yeung, K.C., & Lau, K.H., "Numerical Solutions for Steady Free Convection in Island Geothermal Reservoirs." To appear in the Proceedings of 1975 International Seminar on Future Energy Production--Heat & Mass Transfer Problems. Hemisphere Publishing Corporation.

3. Cheng, P. and Minkowycz, W.J., "Free Convection about a Vertical Flat Plate Embedded in a Porous Medium with Application to Heat Transfer from a Dike." Accepted for publication by J. Geophysical Research.

4. Cheng, P., "Constant Surface Heat Flux Solutions for Porous Layer Flows." Submitted for publication to Letters in Heat & Mass Transfer.

5. Cheng, P. and Chang, I-Dee, "Buoyancy Induced Flows in a Saturated Porous Medium Adjacent to Impermeable Horizontal Surfaces." Int. J. Heat Mass Transfer, 19, 1267 (1976).

6. Cheng, P., "Combined Free & Forced Boundary Layer Flows about Inclined Surfaces in a Porous Medium." Accepted for publication by Int. J. Heat Mass Transfer.

7. Cheng, P., "Similarity Solutions for Mixed Convection from Horizontal Impermeable Surfaces in Saturated Porous Media." Accepted for publication by Int. J. Heat Mass Transfer.

8. Bories, S.A. and Combarnous, M.A., "Natural Convection in a Sloping Porous Layer," J.F.M., 57, 63-79 (2973).

9. Cheng, P. and Chang, I-Dee, "Higher-Order Approximations for Convective Heat Transfer in Porous Layers" (in progress).

FIGURE 1. HEAT TRANSFER RESULTS FOR MIXED CONVECTION FROM AN ISOTHERMAL VERTICAL PLATE.

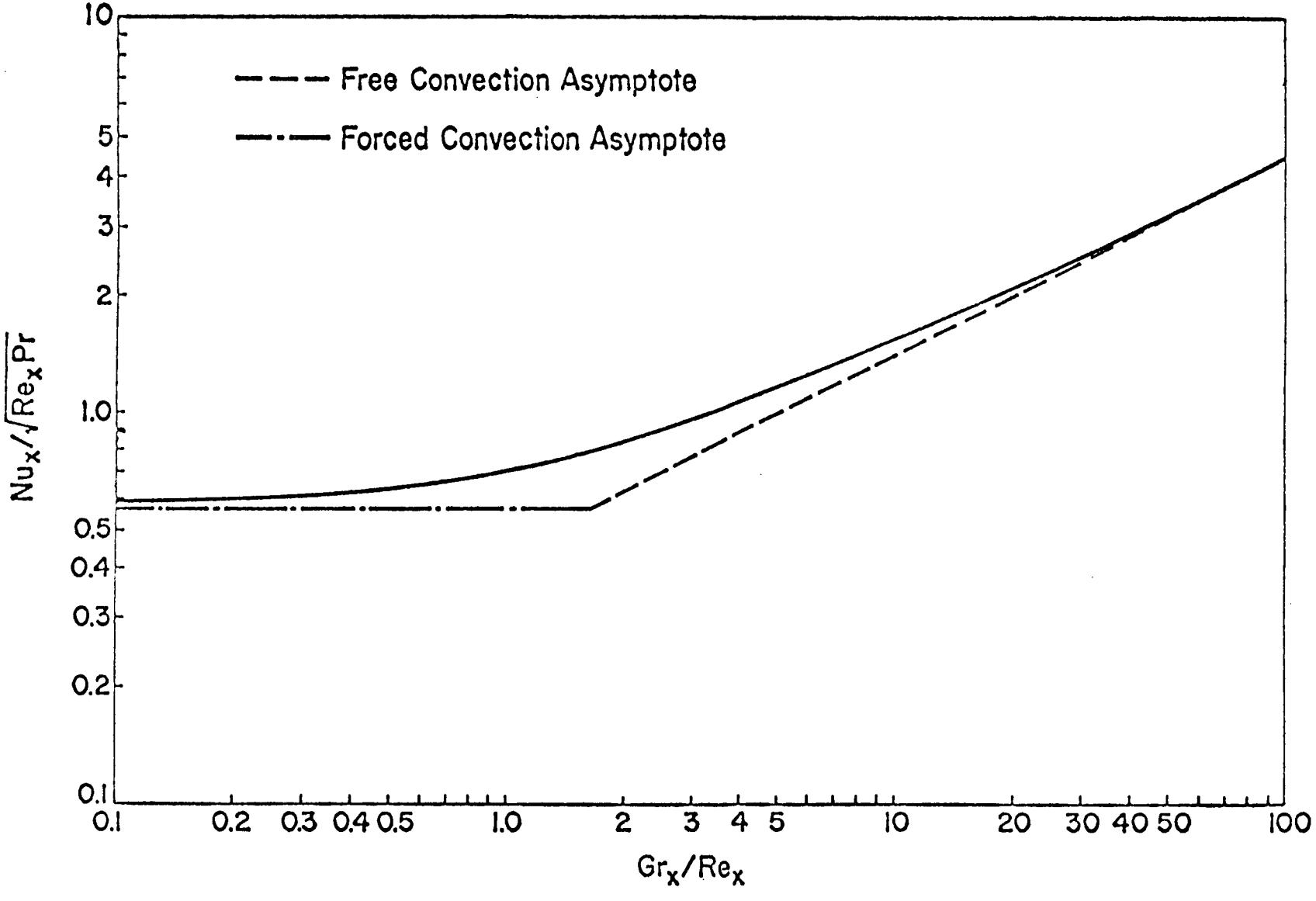

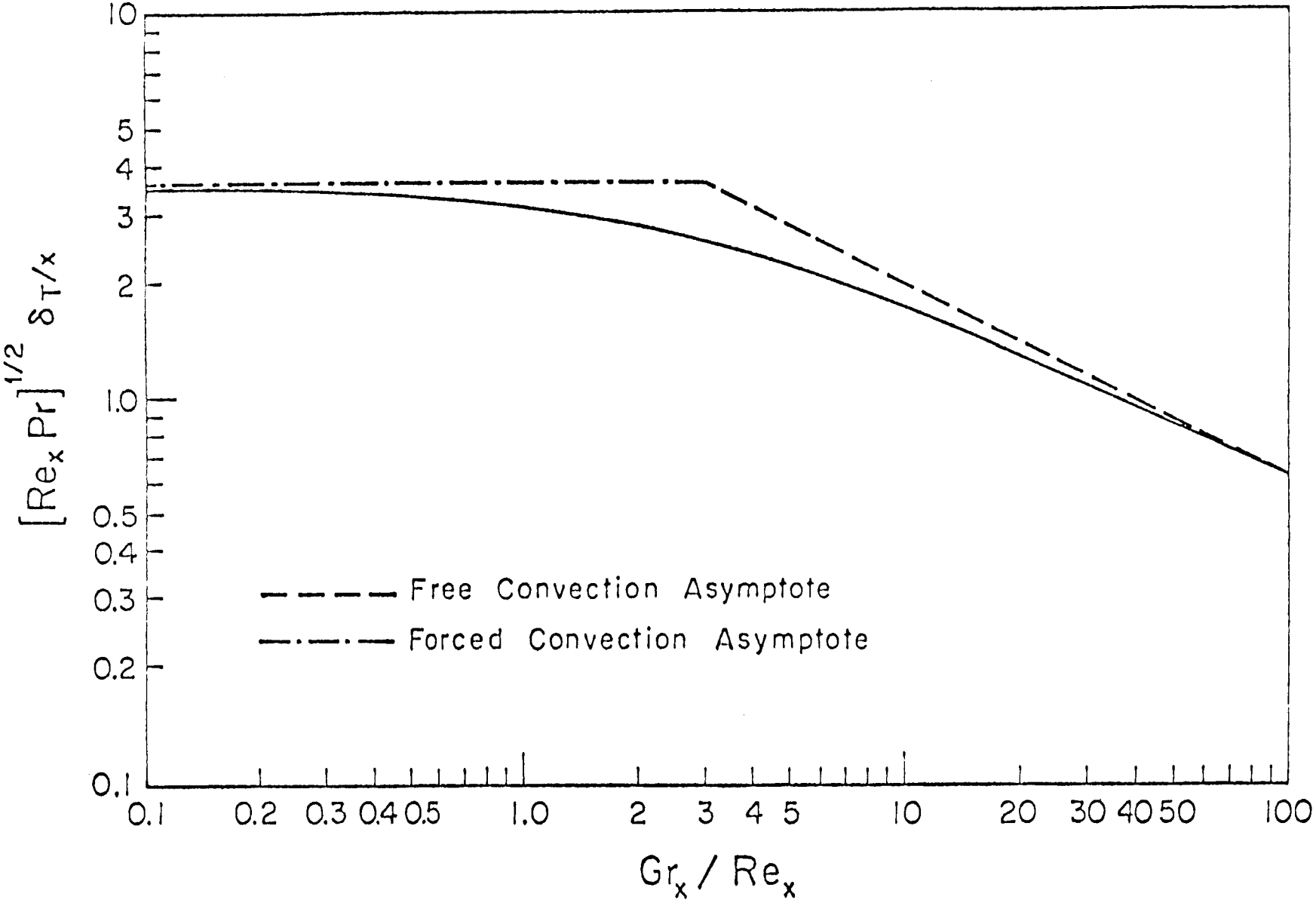

Fig. 2 Boundary Layer Thickness for Mixed Convection From An Isothermal Vertical Plate

FIGURE 3. THE EFFECT OF U_∞ ON TOTAL HEAT TRANSFER RATE FOR MIXED CONVECTION FROM AN ISOTHERMAL VERTICAL HEATED SURFACE IN A GEOTHERMAL RESERVOIR.

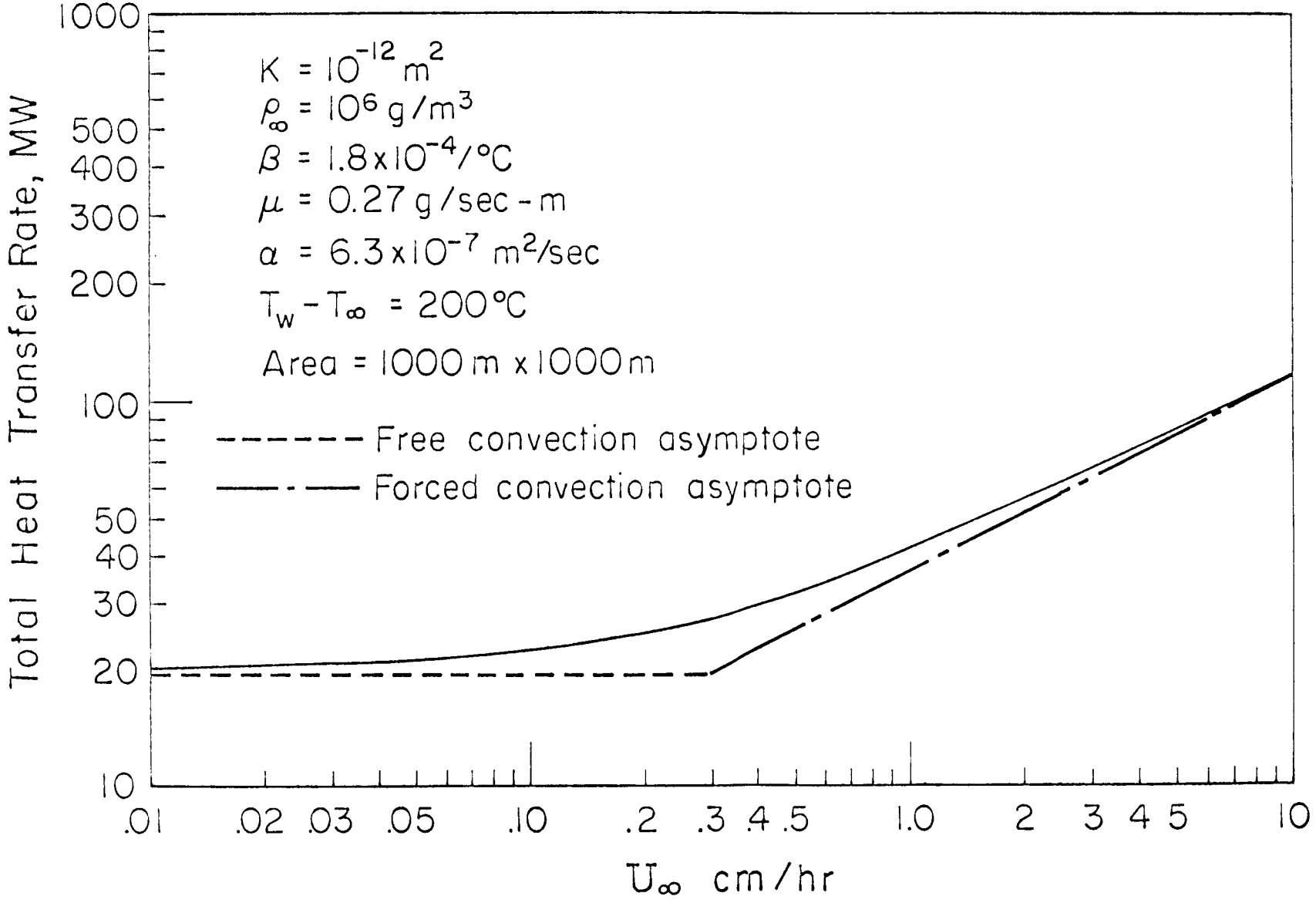

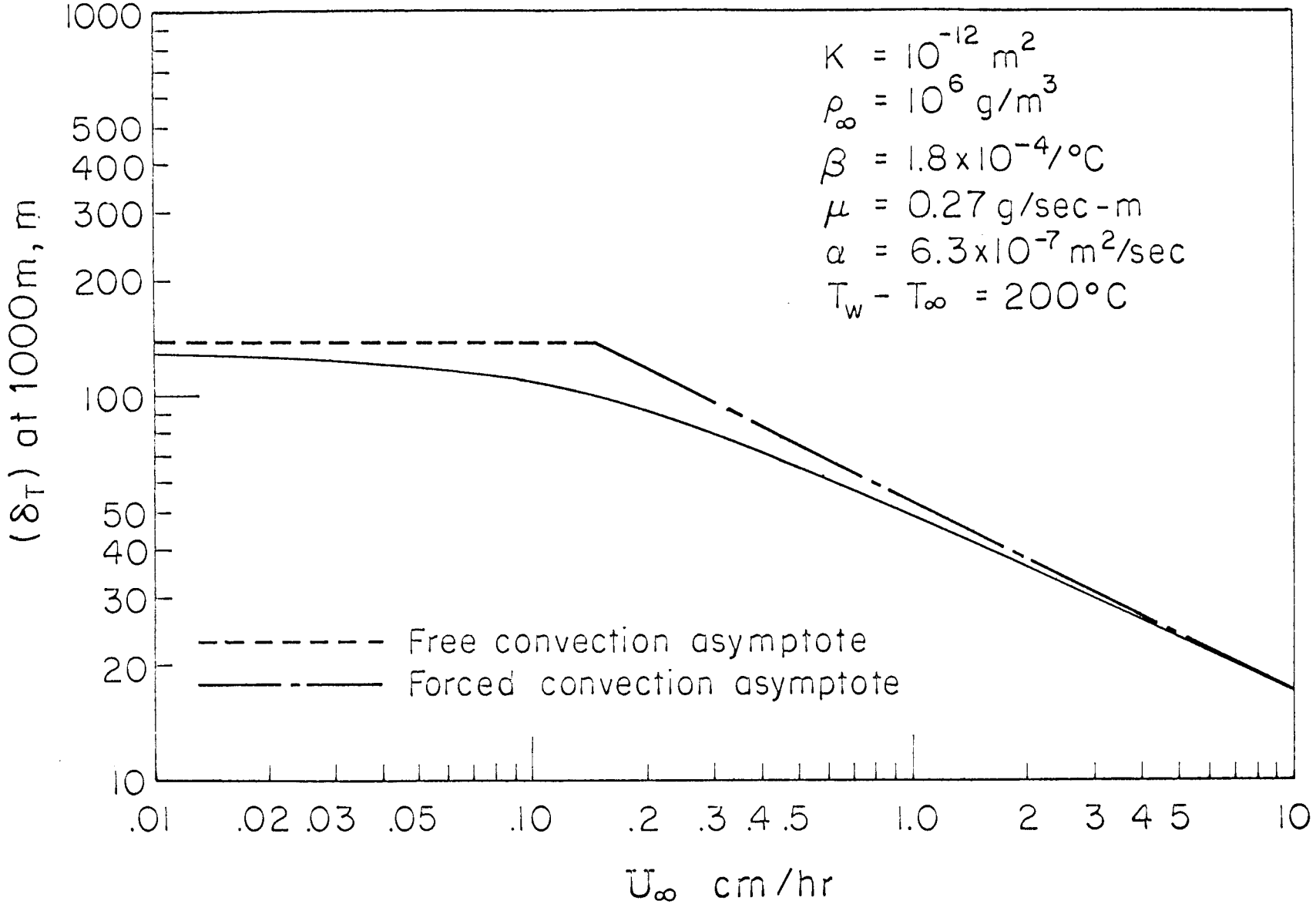

Fig. 4 The Effect of U_∞ on the Boundary Layer Thickness (Size of Hot Water Zone) for Mixed Convection from a Vertical Isothermal Heated Surface in a Geothermal Reservoir

FIGURE 5. COMPARISON OF THEORY AND EXPERIMENT FOR VERTICAL POROUS LAYERS.

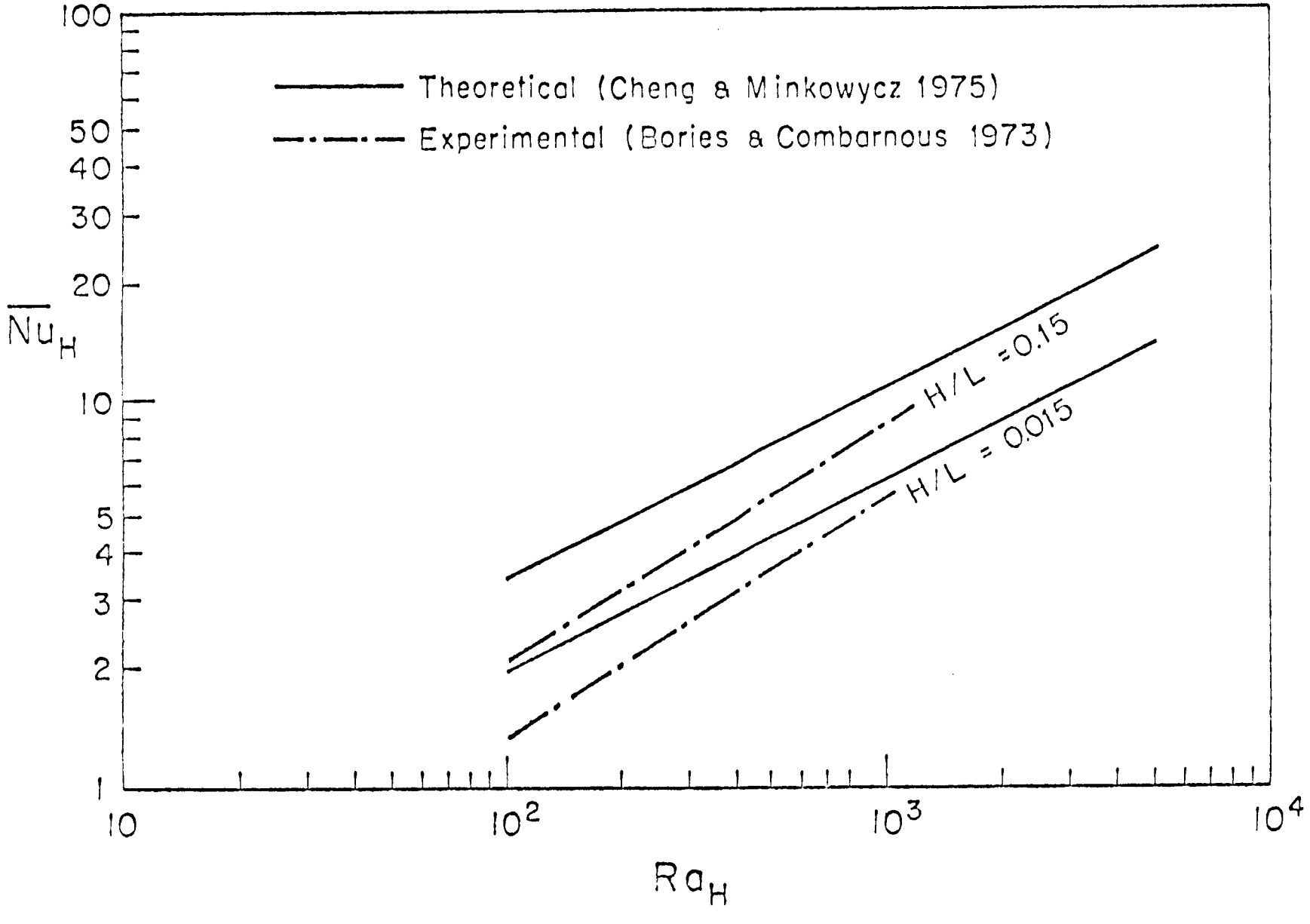

A CALCULATION MODEL FOR THE P-V-T-X PROPERTIES OF GEOTHERMAL BRINES

R. W. Potter, III
U.S. Geological Survey
Menlo Park, CA.
and
J. L. Haas, Jr.
U.S. Geological Survey
Reston, VA.

A set of P-V-T-X data for the highly saline fluids encountered in some geothermal reservoirs is an important prerequisite to the modeling of the chemical and physical behavior of geothermal reservoirs. However, very limited data at the temperatures and pressures encountered in the geothermal systems are available (Potter, 1976). In this paper, we present relatively simple workable models which can be used to predict accurately both the density and vapor pressure of complex brines at elevated temperatures. Together these models yield a parametric equation of state for the vapor-saturated geothermal brine.

There have been attempts to erect theoretical models for calculating the density of complex brines, particularly seawater (Millero, 1973) but generally these models all represent some form of Young's Rule:

$$\phi_{vs} = \Sigma f_i \phi_{vi} \qquad (1)$$

where ϕ_{vs} is the apparent molal volume of the solution, f_i is the mole fraction of component i, and ϕ_{vi} is the apparent molal volume of component i for the total ionic strength of the solution. These models are generally inapplicable to the geothermal case because:

1. The modified Young's Rule defines components as ionic species and sums all the possible combinations of anions and cations. Presently, it is essentially impossible to accurately define the speciation in a highly saline fluid at elevated temperatures.

2. In order to apply the Rule, highly precise ϕ_{vi} data are required for all the species. At the present time densities of the required accuracy are available generally only at temperatures less than 50°C.

3. The modified Young's Rule as used by Millero (1973) assumes the additivity of the infinite-dilution volume properties. Although this holds fairly well for chlorides, it has not been generally documented for carbonates and sulfates. It is also questionable whether predictions based on such assumptions would work for highly saline fluids such as are encountered in the Salton Sea fields.

Since Young's Rule does however define the ϕ_{vs}, it follows by analogy that:

$$d_s = d_o + (d_1-d_o)f_1 + (d_2-d_o)f_2 \ldots (d_n-d_o)f_n \qquad (2)$$

where d_s is the density of the solution; d_o is the density of H_2O; d_1, d_2, d_n are the densities of the binary salt-water systems of the same molality as the solution; and f_1, f_2, f_n are equal to the concentration (molality) of the respective salt divided by the molality of the solution. However, because water is simply one component of each binary solution it follows that:

$$d_s = d_1 + (d_2-d_1)f_2 + (d_3-d_1)f_3 \ldots (d_{n+1}-d_1)f_{n+1} \qquad (3)$$

where $d_1<d_2<d_3 \ldots <d_n$ for computational convenience. To test this relationship the density of NaCl (2.4034 molal)-KCl (1.1311 molal)-H_2O at 25°C was calculated using equations (2) and (3) as well as defining for equation (3) $d_1>d_2>d_3>\ldots d_n$. All three methods yielded the same result, 1.1272 ± 0.0003 g/cm^3, which is in good agreement with the measured value of 1.1274 ± 0.0003 g/cm^3.

The only data of sufficient accuracy for complex solutions at elevated temperatures with which to test the density model are those for seawater (Fabuss et al., 1968). Data for the density of NaCl-H_2O, Kcl-H_2O, and $MgSO_4$-H_2O were taken from Fabuss et al. (1968), for $CaCl_2$ solutions from Potter and Clynne (1976), and for KBr-H_2O and $MgCl_2$-H_2O up to 100°C from the International Critical Tables (National Research Council, 1928). No data above 100°C were available for KBr and $MgCl_2$, hence they were calculated as KCl and $CaCl_2$ respectively. At 100°C the calculated density was 0.9838 + 0.0005 g/cm^3 versus a measured density of 0.9839 ± 0.0005 while at 150°C the calculated density was 0.9443 ± 0.0015 g/cm^3 versus the measured density of 0.9451 ± 0.0010 g/cm^3.

White (1965) lists analyses for a Salton Sea brine sample whose density at 20°C is 1.264 ± 0.005. Based on the chemical analyses the brine can be approximated as a NaCl (2.592 molal)-Kcl (0.953 molal)-$CaCl_2$ (2.216 molal) brine. Using this composition and the data from Potter and Brown (1975, 1976) and Potter and Clynne (1976), the density of the brine was calculated as a function of temperature:

$$d_s = 1.2730 - 3.771 \times 10^{-4}t - 1.407 \times 10^{-6}t^2 \pm 0.002 \qquad (4)$$

Equation (4) yields a density at 20°C of 1.265 ± 0.002 g/cm^3 which is in excellent agreement with the measured density.

Predictive techniques for the vapor pressure of a solution are almost uniformly impractical for brines with a high content of dissolved solids. One technique, however, has proved fairly accurate for extrapolating data, observed at lower temperatures, to as much as 200°C to 300°C above the temperature range of the observations. A modified form of this technique, the reference substance principle (Othmer and Yu, 1968; Othmer and Chen, 1968), was used to derive a function for the vapor pressure of H_2O-NaCl solutions from the freezing temperature to 300°C with a precision of 0.32 percent of the observed vapor pressure (Haas, 1971a and b; 1975a and b).

The reference substance method can be derived from the Clapeyron equation for the vaporization of two liquids. Othmer and Yu (1968) have shown that the temperature T_x of a brine and the temperature T_o of

the H_2O liquid (or reference substance) at the same pressure can be described by an equation of the following from:

$$\ln = T_o = m \ln T_x + c \qquad (5)$$

In the previous work on the H_2O-NaCl system (Haas, 1975a & b), it was found that one can improve the calculation by setting $c = 0$ and $m = (a + bT_x)^{-1}$. Equation 5 can be rewritten:

$$\ln T_o = (a + bT_x)^{-1} \ln T_x \qquad (6)$$

In previous work Haas has shown the model to be applicable to the simple binary system NaCl-H_2O. If one examines equation 6, it becomes obvious that as few as two well-defined observations could be used to predict the remainder of the P-T curve. To test this approach the data of Liu and Lindsay (1971) for a NaCl (1.7065 molal)-Na_2SO_4 (.1190 molal)-$MgCl_2$ (.2690 molal) brine were used at 75° and 100°C to define the constants a and b of equation 6. The calculated vapor pressure at 300°C agreed with the measured value to within 0.5 bars.

In preceding example, data at two temperatures which were 25° centigrade apart were used for the estimation of the vapor pressure. It is obvious that the greater the spread in the known data, the better the estimation, because errors in the known data have considerably less effect. Commonly available data for solutions are: 1) the freezing point depression (for dilute solutions), 2) the normal boiling point elevation where the vapor pressure of the brine is 1 atm or 3) osmotic coefficients near room temperature. From any two of these or from vapor pressures of the brine of interest, the constants a and b of equation 6 may be estimated.

The two models can be used to generate a PVTX grid for a geothermal brine. These data in turn can be used to generate a parametric equation of state from which the energy related thermodynamic properties, e.g. enthalpy, can be extracted.

REFERENCES

Faubuss, B. M., and Korosi, A., 1968, Properties of sea water and solutions containing sodium chloride, potassium chloride, sodium sulfate, and magnesium sulfate: U.S. Off. Saline Water, Res. Develop. Progress Rept. No. 384, 133 p.

Haas, J. L., Jr., 1971a, Thermodynamic correlations for brines: NaCl-H_2O liquid-vapor equilibria (abs): Amer. Geophys. Union. Trans., v. 52, p. 379.

Haas, J. L., Jr., 1971b, The effect of salinity on the maximum thermal gradient of a hydrothermal system at hydrostatic pressure: Econ. Geology, v. 66, p. 940-946.

Haas, J. L., Jr., 1975a, Preliminary "steam tables" for NaCl solutions. Physical properties of the coexisting phases and thermochemical properties of the H_2O component: U.S. Geol. Survey Open file rept. 75-674, 66 p.

Haas, J. L., Jr., 1975b, Preliminary "steam tables" for NaCl solutions. Thermodynamic properties of the coexisting phases and thermochemical properties of the NaCl component: U.S. Geol. Survey Open file rept. 75-675, 68 p.

Liu, C. T., and Linday, W. T., Jr., 1971, Thermodynamic properties of aqueous solutions at high temperatures: U.S. Office of Saline Water, Res. and Development Progress Rept. 722, 124 p.

Millero, F. J., 1973, Seawater - a test of multicomponent electrolyte solution theories. I. Apparent equivalent volume, expansibility, and compressibility of artical seawater: Jour. Soln. Chem., v. 2.

National Research Council, 1928, International critical tables of numerical data, physics, chemistry and technology: New York, McGraw-Hill Book Co.,Inc., v. 3, 444 p.

Othmer, D. R., and Chen, H-T., 1968, Correlating and predicting thermodynamic data: Ind. Eng. Chem., v. 60, no. 4, p. 39-61: Reprinted in Amer. Chem. Soc., 1968, Applied Thermodynamics: Wash, D.C., Amer. Chem. Soc. Publications, p. 155-139.

Othmer, D. R., and Yu, E.S., 1968, Correlating vapor pressures and vapor volumes. Use of reference substance equations: Industrial Engineering Chem., v. 60, no. 1, p. 22-35.

Potter, R. W., II, 1976, An assessment of the status of the available data on the P-V-T properties for the major components in geothermal brines: Proceedings, second U.N. Symposium on the development and use of geothermal resources, San Francisco (in press).

Potter, R. W., II, and Brown, D. L., 1975, The volumetric properties of aqueous sodium chloride solutions from 0° to 500°C at pressures up to 2000 bars based on a regression of the available literature data: U.S. Geol. Survey Open file rept. 75-636, 31 p.

Potter, R. W., II and Brown, D. L., 1976a, The volumetric properties of vapor saturated aqueous potassium chloride solutions from 0° to 400°C based on a regression of the available literature data: U.S. Geol. Survey Open file report 75-243, 6 p.

Potter, R.W., II, and Clynne, M.A., 1976, The volumetric properties of vapor saturated aqueous calcium chloride solutions from 0° to 300°C based on a regression of the available literature data: U.S. Geol. Survey Open file rept. 76-365, 7 p.

White, D. E., 1965, Saline waters of sedimentary rocks, in Fluids in Subsurface Environments - A Symposium: Am. Assoc. Petroleum Geologists Memoir No. 4, p. 342-366.

ONE-DIMENSIONAL CONVECTIVE AND CONDUCTIVE GEOTHERMAL HEAT FLOW

J. C. Martin, R. E. Wegner and F. J. Kelsey
Chevron Oil Field Research Co.
P.O. Box 446, LaHabra, Ca. 90631

A number of research workers have investigated two- and three-dimensional natural convective heat flow in porous media containing a single-phase fluid[1,2]. Results indicate that convective heat flow in geothermal reservoirs can be high with low geothermal gradients within the convection cells.

Single-phase convection can occur only in two or three dimensions; however, it is evident that steam and hot water sometimes exist simultaneously in geothermal areas. The large difference in density between steam and hot water provides a driving force that tends to segregate the two phases, making countercurrent vertical one-dimensional fluid flow theoretically possible.

This paper presents the results of a study of one-dimensional, vertical, two phase, steady-state, geothermal fluid and heat flow. Steam is assumed to be generated at depth by heat conducted from below. The steam flows upward and an equal mass of hot water flows downward within the geothermal reservoir. At the top of the geothermal reservoir the steam condenses into hot water which then flows downward. Above the reservoir the heat flow is again only conductive.

A method of calculating one-dimensional, combined convective and conductive heat flow is presented with calculated examples. The object of the investigation was to understand the one-dimensional convective heat flow that may occur where conditions have been stable long enough for the flow to approach steady-state. Results presented herein apply to unfractured porous media. Similar results should apply to fractured reservoirs and permeable fault zones.

The water is assumed sufficiently fresh that the effects of dissolved solids can be neglected. The surface temperature and heat flow rate are assumed to be known. Capillary pressure and steam and hot water relative permeabilities are used in the analysis; however, the effects of capillary pressure were neglected in the example calculations. The analysis allows the thermal conductivity to vary with temperature and steam or hot water saturation; however, for simplicity a constant value was used in the calculations.

DISCUSSION

Appendix A gives the equations of heat and fluid flow, and the derivation of the two equations below. These can be solved simultaneously to obtain the steam saturation and the temperature-pressure point on the boiling curve as functions of depth.

$$AG_v + BG_d = 1 \tag{1}$$

$$\frac{dp}{dz} = \frac{g\rho_w{}^2\lambda_w + g\rho_s{}^2\lambda_s}{\rho_w\lambda_w + \rho_s\lambda_s} \tag{2}$$

Symbols are defined in Appendix B. If one dimensional, two phase convective flow is possible, equation 1 can be solved for the steam saturation. This result can be used with equation 2 to calculate the pressure gradient.

In equation 1, AG_v is the fractional convective heat flow; BG_d is the fractional conductive heat flow. For a given problem coefficients A and B are constants, and G_v and G_d determine the variations in the convective and conductive heat flow. Both G_v and G_d are functions of the relative permeabilities, the fluid saturations, the temperature-pressure point on the boiling curve, and the fluid properties. In addition, G_v is a function of the steam-hot water enthalpy difference and G_d is a function of the variations in thermal conductivity.

Figure 1 presents the two sets of steam-hot water relative permeability curves used in the calculations. Type II relative permeability curves were included because recent experimental results reported by Brigham[3] indicate high immobile water saturations. Figure 2 presents the variation of G_v with steam saturation for various pressures for Type I relative permeability curves. This curve is "bell" shaped because the mass flow of steam upward must equal the mass flow of water downward. The relative permeability to steam controls the shape of the curve at low values of steam saturations, S_s, and the relative permeability to hot water controls the shape at high values of S_s.

Figure 2 indicates that the temperature-pressure point on the boiling curve also has a strong effect on G_v. At lower temperature-pressure values the relatively high water viscosity depresses the curve, causing the maximum G_v to occur at higher steam saturations. At high temperature-pressure values, the curves are depressed by smaller differences in densities and enthalpies. At critical conditions these differences are zero, hence one-dimensional convection cannot exist.

Figure 3 presents G_d versus S_s for various pressures for Type I relative permeability curves. The sharp decline in G_d at higher S_s results from the low density of steam as compared to that of hot water. The high G_d at low pressures results from the steep slope of the boiling curve, $\psi(p)$.

Figure 4 presents the variation of AG_v, BG_d, and $AG_v + BG_d$ with S_s for Type I relative permeability curves, $T = 435^{\circ}F$, $P = 362$ psia, $k = .010$ darcys, $Kh = 40$ Btu/day-ft-$^{\circ}F$, and $u_h = -6$ Btu/day-ft^2. To satisfy equation 1, $AG_v + BG_d$ must equal 1. Two values of S_s satisfy this condition (Figure 4). The lower steam saturation, S_s1, is associated with conditions approximating a hot water column through which steam is migrating upward and the hot water downward. For a wide range of conditions, the pressure gradient approximates that of hot water, causing a corresponding rapid increase in temperature and pressure with depth. This relatively large temperature gradient can cause significant conductive heat flow.

The higher steam saturation, S_{s2}, is associated with conditions approximating a steam column with a small amount of mobile hot water. In this case there is a wide range of conditions in which the pressure gradient is very low, approximating that of steam. This very low increase in pressure and temperature with depth results in low conductive heat flow.

At a steam-hot water interface or contact, the high steam saturation, S_{s2}, exists above the interface, and the low steam saturation, S_{s1}, exists below it. If capillarity is included, the interface becomes a steam-hot water transition zone, in which capillarity determines the saturation distribution.

Figure 5 presents the results of a series of calculations in which an impermeable zone exists to a depth of 2500 feet, from which a permeable (10 md) geothermal reservoir extends to a depth of 10,000 feet. Below this there is another impermeable zone. The surface temperature is chosen to be $60^{\circ}F$, and the conditions at the top of the reservoir are those used in Figure 4. Both impermeable zones were assigned a thermal conductivity of 40 Btu/day-ft-$^{\circ}F$. Figure 5 presents the variations in temperature, pressure, steam saturation and conductive heat flow with depth for both Type I and Type II relative permeability curves. Only the steam saturation for the S_{s2} solution changes significantly with relative permeability. As mentioned previously, the S_{s1} solution approximates conditions in a hot water column, in which the pressure increases with depth according to a hot water gradient. This requires a corresponding increase in temperature to maintain boiling conditions. The increase in temperature results in significant conductive heat flow. The S_{s2} solution approximates conditions in a steam column, and the low steam density results in low temperature and pressure gradients, and very small conductive heat flow.

Figure 6 presents the results of calculations similar to those of Figure 5, except there is a steam-hot water interface at -10,000 feet. The S_{s2} solution applies from -2500 feet to -10,000 feet and the S_{s1} solution applies below -10,000 feet. Here again only the steam saturation for the S_{s2} solution changes significantly with relative permeabilities. Steam generated at the bottom of the reservoir migrates upward until it reaches the top where it condenses. Throughout the column sufficient phase transfer takes place between the steam and hot water to maintain steady-state heat and fluid flow.

Figure 7 presents an example with and without a steam-hot water interface at 5,000 feet. Both the S_s1 and S_s2 solutions are shown below this depth. The S_s1 solution approaches critical conditions at -15,550 feet. The calculations indicate that convective heat flow does not approach zero to within a few degrees of the critical temperature. This occurs even though the driving force (the difference in density) and the enthalpy difference both approach zero as critical conditions are approached. This seemingly inconsistent result is caused by the very low slopes of the density and enthalpy differences as the critical conditions are approached (Figure 8). Calculations indicate that below the point where critical conditions are reached a single phase exists which is above critical conditions. There is a reduction in the pressure gradient as illustrated in Figure 7 and the heat flow is purely conductive.

Results of calculations not presented herein indicate that it is possible to encounter conditions below the critical beyond which only superheated steam exists. Both S_{s1} and S_{s2} solutions encounter these conditions. They occur at the maximum value of the $AG_v + BG_d$ curve.

Figure 4 indicates that the $AG_v + BG_d$ curve may extend to much lower values in the high S_s range than for the low range. In some cases where A and B are sufficiently large, only S_{s2} solutions exist. Since A and B vary inversely with u_h, these conditions are more likely to occur for low u_h values. Calculations indicate that this type of solution may be valid and have significant convective heat flow over many thousands of feet for low permeabilities even less than 0.1 md. It is conceivable that this type of fluid and heat flow may be taking place at great depths in tectonically active regions where permeability may be being maintained by fracturing. The increased heat flow could be responsible for areas of increased heat flow near faults.

The lower limit of permeability for which physically meaningful solutions can be obtained has not been determined. Numerical solutions have been obtained for extremely small values of permeability and fractional convective heat flow, AG_v. In these solutions the S_s varies in such a manner that both the fluid pressure gradient and the boiling curve conditions are

satisfied. These steady-state solutions assume that all transients have died out. Thus, the lower permeability limit depends on the conditions of the problem and on the time required to reach steady-state.

The results presented in Figures 4-8 are for a total heat flow of -6 Btu/ft^2-day and a reservoir permeability of 10 md. Other calculated results indicate that the overall fluid and heat flow is relatively insensitive to a wide range of conditions.

Conclusions

1. Combined one-dimensional, vertical, convective and conductive heat flow is theoretically possible in geothermal reservoirs. Calculations indicate that this can occur over depths ranging from the surface to below 20,000 feet.

2. In many cases two fluid saturations satisfy the same heat flow rate. One is a high hot water saturation in which hot water is the principal mobile phase. The pressure gradient is approximately that of the hot water. The other fluid saturation is a high steam saturation in which steam is the principal mobile phase, and the pressure gradient is approximately that of steam. Only the steam saturation changed significantly with relative permeability for the two sets of relative permeability curves investigated.

3. For permeabilities greater than 1 md and for high steam saturations, the convective fraction of the heat flow is generally many times the conductive fraction. For high hot water saturations the two fractions are often of comparable magnitudes.

4. Convective heat flows involving high steam saturations can extend to considerably greater depths than those involving high water saturations.

REFERENCES

1. Combarnous, M. A. and Bareis, S. A., "Hydrothermal Convection in Saturated Porous Media", Advances in Hydroscience, Vol. 10, Ven Te Chow Editor, Academic Press, 1975, pp. 231-307.

2. Wooding, R. A., "Methods of Solution of the Equations for Convection in Porous Media, with Geothermal Applications", Workshop on Geothermal Reservoir Engineering, December 15-17, 1975, P. Kruger and H. J. Ramey, Jr., Editors, SGP-TR-12 Stanford Geothermal Program, Stanford University.

3. Brigham, W., "Recent Flow and Equilibria Experiments in the Stanford Geothermal Program", Paper presented at the second Workshop on Geothermal Reservoir Engineering, Stanford University. December 1-3, 1976.

APPENDIX A

The equations used in the numerical solution are derived in this appendix. All equations written in a consistent set of units, and the symbols are defined in Appendix B.

The basic equations are:

Darcy's law for hot water $$u_w = -\lambda_w \left(\frac{\partial p_w}{\partial z} - g\rho_w\right) \qquad (A\text{-}1)$$

Darcy's law for steam $$u_s = -\lambda_s \left(\frac{\partial p_s}{\partial z} - g\rho_s\right) \qquad (A\text{-}2)$$

Continuity equation for mass $$\frac{\partial}{\partial z}(\rho_w u_w + \rho_s u_s) = -\frac{\partial}{\partial t}[\phi(\rho_w S_w + \rho_s S_s)] \qquad (A\text{-}3)$$

Saturations $$S_w + S_s = 1 \qquad (A\text{-}4)$$

Continuity equation for heat $$\frac{\partial u_h}{\partial z} = -\phi \frac{\partial}{\partial t}\left[\rho_w h_w S_w + \rho_s h_s S_s + \left(\frac{1-\phi}{\phi}\right)\rho_r c_r T\right] \qquad (A\text{-}5)$$

Heat flow $$u_h = \rho_w h_w u_w + \rho_s h_s u_s - k_h \frac{\partial T}{\partial z} \qquad (A\text{-}6)$$

Capillary pressure $$p_s - p_w = P_c(S_s, T) \qquad (A\text{-}7)$$

Boiling curve $$T = \psi(p_s, P_c) \qquad (A\text{-}8)$$

The preceding eight equations contain the following eight unknowns u_w, u_s, p_w, p_s, S_s, S_s, T and u_h.

This analysis is restricted to steady-state fluid and heat flow. Thus, all derivations with respect to time are zero, and equation A3 can be integrated to yield

$$\rho_w u_w + \rho_s u_s = c(z) \qquad (A\text{-}9)$$

where c(z) is the constant of integration with respect to time. It represents the mass rate of flow. Because no fluid mass enters or leaves the porous media, the mass of the water flowing downward is equal to the mass of the steam flowing upward, and the net mass flow is zero. Thus c(z) equals zero and

$$\rho_w u_w = -\rho_s u_s \qquad \text{(A-10)}$$

The following equation for $\rho_w u_w$ can be obtained by eliminating u_s, $\frac{\partial p_w}{\partial z}$ and $\frac{\partial p_s}{\partial z}$ from equations A-1, A-2 and A-7.

$$\rho_w u_w = \frac{g(\rho_w - \rho_s)}{\frac{1}{\rho_s \lambda_s} + \frac{1}{\rho_w \lambda_w}} + \frac{(h_s - h_w)\left(\frac{\partial P_c}{\partial S_s}\frac{\partial S_s}{\partial z} + \frac{\partial P_c}{\partial T}\frac{\partial T}{\partial z}\right)}{\frac{1}{\rho_s \lambda_s} + \frac{1}{\rho_w \lambda_w}} \qquad \text{(A-11)}$$

Eliminating $\rho_s u_s$ from equations A-6 and A-10 yields

$$u_h = \rho_w u_w (h_w - h_s) - k_h \frac{\partial T}{\partial z} \qquad \text{(A-12)}$$

Under steady-state conditions, u_h is a constant which is equal to the heat flow rate at the surface.

Combining equations A-11 and A-12 yields

$$u_h = \frac{g(\rho_w - \rho_s)(h_w - h_s)}{\frac{1}{\rho_w \lambda_w} + \frac{1}{\rho_s \lambda_s}} + \frac{(h_s - h_w)\left(\frac{\partial P_c}{\partial S_s}\frac{\partial S_s}{\partial z} + \frac{\partial P_c}{\partial T}\frac{\partial T}{\partial z}\right)}{\frac{1}{\rho_w \lambda_w} + \frac{1}{\rho_s \lambda_s}} - k_h \frac{\partial T}{\partial z} \qquad \text{(A-13)}$$

As is customary in exploratory calculations such as these, the effects of capillarity are neglected, and equations A-11 and A-13 reduce to

$$\rho_w u_w = \frac{g(\rho_w - \rho_s)}{\frac{1}{\rho_w \lambda_w} + \frac{1}{\rho_s \lambda_s}} \qquad \text{(A-14)}$$

and

$$u_h = \frac{g(\rho_w - \rho_s)(h_w - h_s)}{\frac{1}{\rho_w \lambda_w} + \frac{1}{\rho_s \lambda_s}} - k_h \frac{\partial T}{\partial z} \qquad \text{(A-15)}$$

Eliminating u_w and u_s from equations A-1, A-2 and A-10 yields

$$\frac{\partial p}{\partial z} = \frac{g\rho_w^2\lambda_w + g\rho_s^2\lambda_s}{\rho_w\lambda_w + \rho_s\lambda_s} \qquad \text{(A-16)}$$

From equation A-8 (neglecting capillarity),

$$\frac{\partial T}{\partial z} = \frac{d\psi}{dp}\frac{\partial p}{\partial z} \qquad \text{(A-17)}$$

Eliminating $\frac{\partial T}{\partial z}$ and $\frac{\partial p}{\partial z}$ from equations A-13, A-16 and A-17 and converting to nondimensional form yields

$$AG_v + BG_d = 1 \qquad \text{(A-18)}$$

where

$$A = \frac{-k\ h_{wo}\ g\rho_{wo}^2}{u_h\ \mu_{wo}}$$

$$B = -\frac{g\rho_{wo}\ k_h}{u_h}\left(\frac{d\psi}{dp}\right)_o$$

$$G_v = \frac{\frac{\mu_{wo}}{k}\left(\frac{\rho_w - \rho_s}{\rho_{wo}}\right)}{\frac{\rho_{wo}}{\rho_w\lambda_w} + \frac{\rho_{wo}}{\rho_s\lambda_s}}$$

$$G_d = \frac{\left(\frac{d\psi}{dp}\right)\left(\frac{\rho_w^2}{\rho_{wo}}\lambda_w + \frac{\rho_s^2}{\rho_{wo}}\lambda_s\right)}{\left(\frac{d\psi}{dp}\right)_o(\rho_w\lambda_w + \rho_s\lambda_s)}$$

where ρ_{wo}, μ_{wo}, h_{wo} and $\left(\frac{d\psi}{dp}\right)_o$ correspond to boiling conditions at atmospheric pressure.

APPENDIX B

NOMENCLATURE

A, B = nondimensional coefficients (see equation A-18)

$c(z)$ = constant of integration with respect to time (see equations following equation A-9)

G_d, G_v = variable parts of fractional conductive and convective heat flow (see equation A-18)

g = gravitation constant

h = enthalpy

k_h = thermal conductivity

k, k_{rs}, k_{rw} = single phase permeability, relative permeabilities to steam and hot water respectively.

P_c = capillary pressure

p = fluid pressure

S = saturation

S_{s1}, S_{s2} = solutions of equation (1) (see Figure 4)

T = temperature

t = time

u = velocity as given by Darcy's law

u_h = heat flow rate

z = depth

λ = fluid mobility = $\frac{k\ k_r}{\mu}$

μ = viscosity

ϕ = porosity

ρ = density

ψ = boiling curve temperature expressed as a function of fluid pressure (Eq. A-8)

Subscripts

r = rock

s = steam

w = water

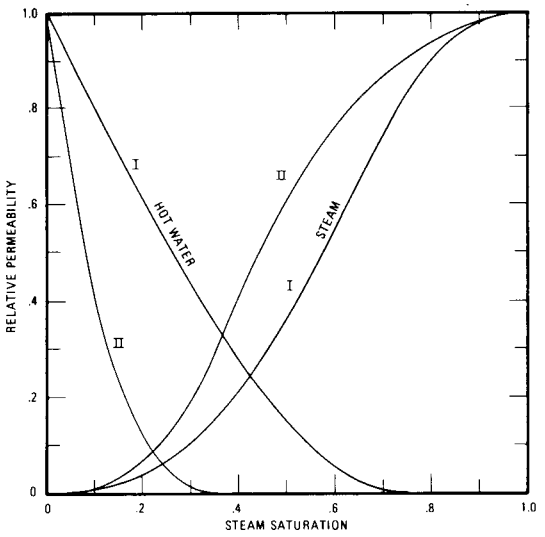

FIGURE 1
STEAM AND HOT WATER RELATIVE PERMEABILITY CURVES USED IN THE CALCULATIONS.

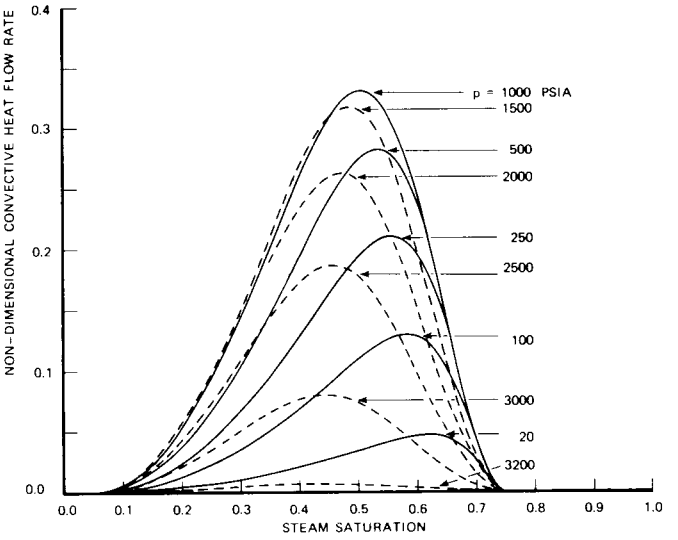

FIGURE 2
THE VARIATION OF THE NON-DIMENSIONAL CONNECTIVE HEAT FLOW RATE, G_v, WITH STEAM SATURATION, S_t, FOR VARIOUS VALUES OF FLUID PRESSURE FOR TYPE I RELATIVE PERMEABILITY CURVES.

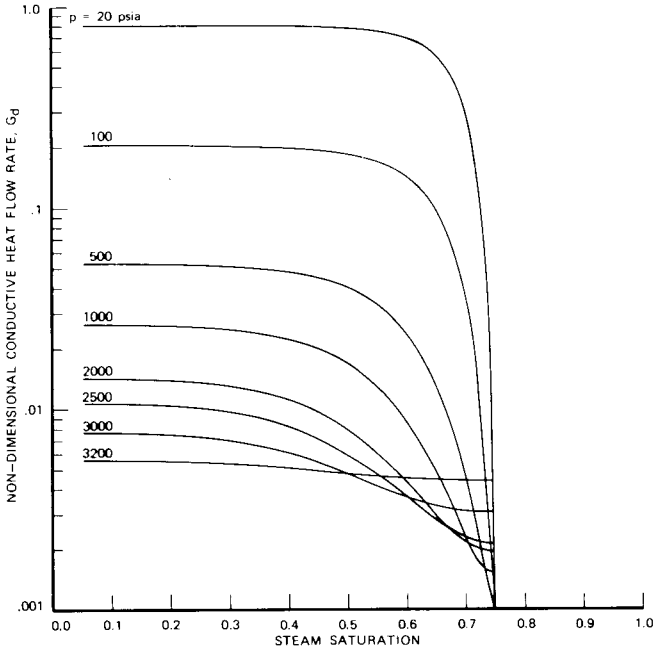

FIGURE 3
THE VARIATION OF THE NON-DIMENSIONAL CONDUCTIVE HEAT FLOW RATE, G_d, WITH STEAM SATURATION FOR VARIOUS VALUES OF FLUID PRESSURE FOR TYPE I RELATIVE PERMEABILITY CURVES.

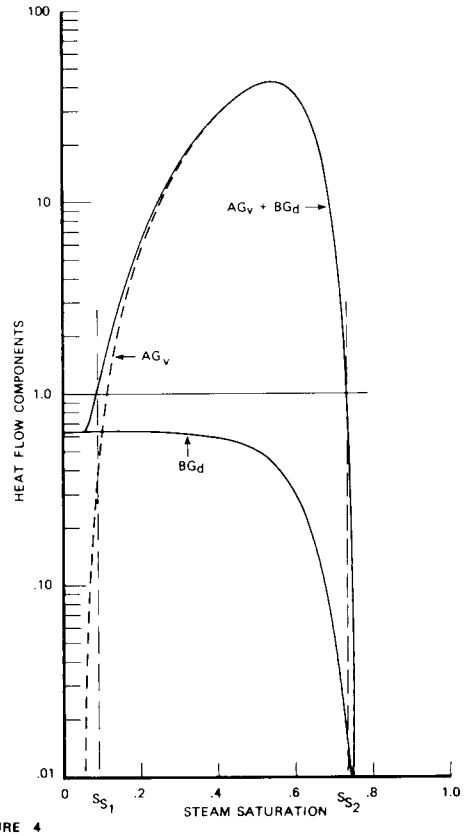

FIGURE 4
THE VARIATIONS OF THE FACTIONAL CONVECTIVE AND CONDUCTIVE HEAT FLOW RATES, AG_v AND BG_d, AND $AG_v + BG_d$ WITH STEAM SATURATION. THE SATURATIONS S_{s1} AND S_{s2} ARE THE TWO SOLUTIONS OF EQUATION (1) FOR TYPE I RELATIVE PERMEABILITY CURVES.

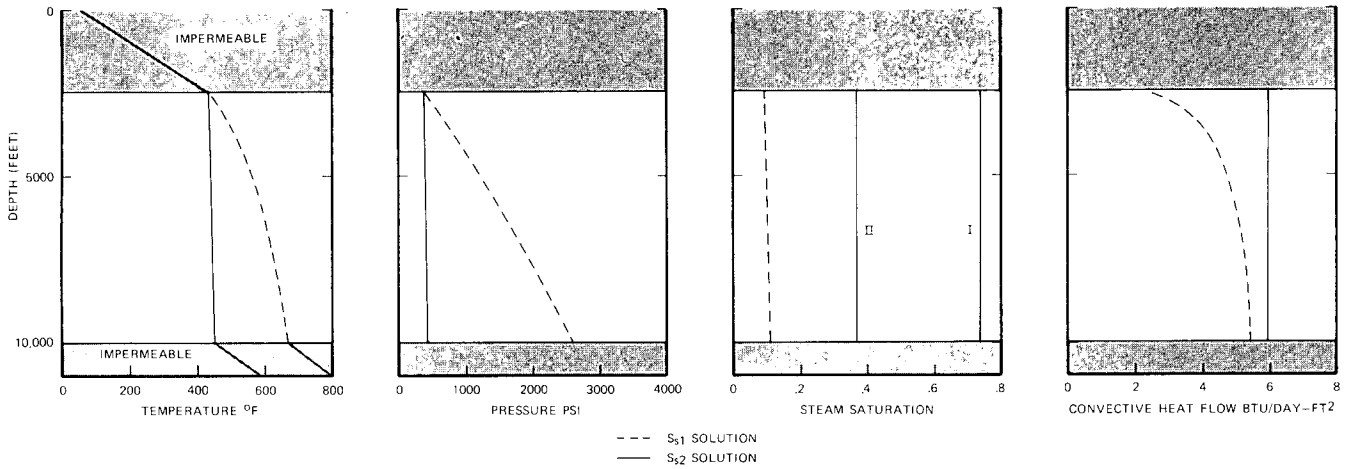

FIGURE 5

CALCULATED RESULTS FOR THE TWO SATURATION SOLUTIONS, S_{s1}, S_{s2}, BEGINNING AT THE TOP OF THE RESERVOIR FOR k = .01 DARCYS, k_h = 40 BTU/DAY–FT–°F, AND u_h = –6 BTU/DAY–FT^2. THE S_{s1} SOLUTION APPROXIMATES HOT WATER COLUMN CONDITIONS AND THE S_{s2} SOLUTION APPROXIMATES STEAM COLUMN CONDITIONS. RELATIVE PERMEABILITY TYPES ARE DENOTED BY I AND II.

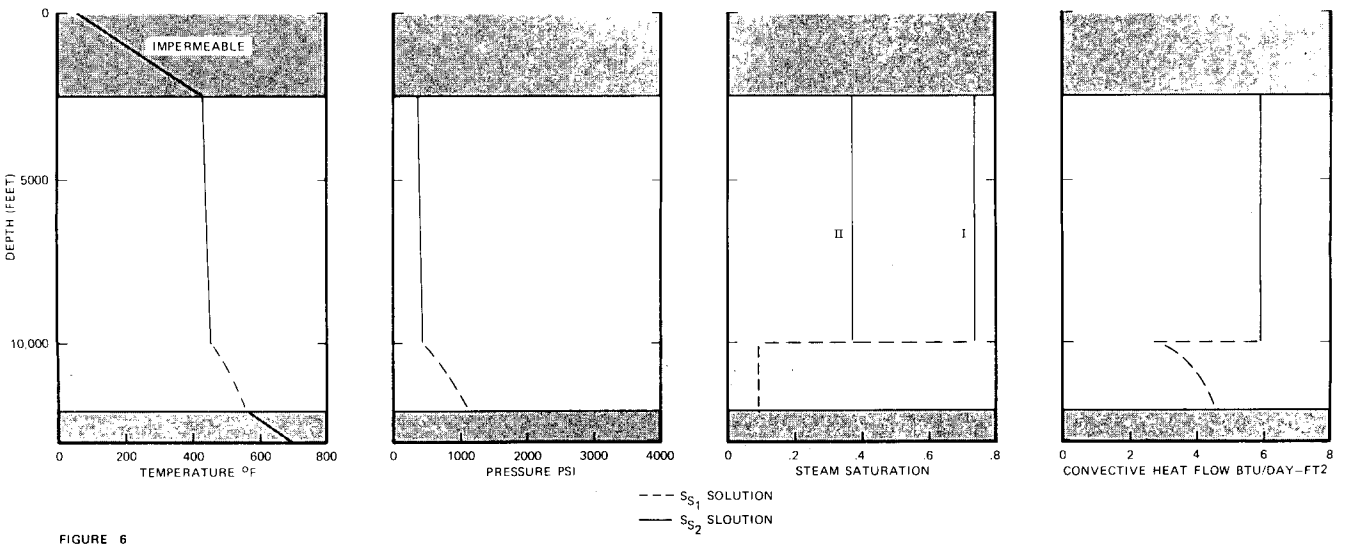

FIGURE 6

CALCULATED RESULTS FOR A HOT WATER–STEAM INTERFACE AT 10,000 FEET FOR SAME PARAMETERS USED IN FIGURE 5. THE S_{s2} SOLUTION APPLIES FROM 2500 TO 10,000 FEET AND THE S_{s1} SOLUTION APPLIES FROM 10,000 TO 12,000 FEET. RELATIVE PERMEABILITY TYPES ARE DENOTED BY I AND II.

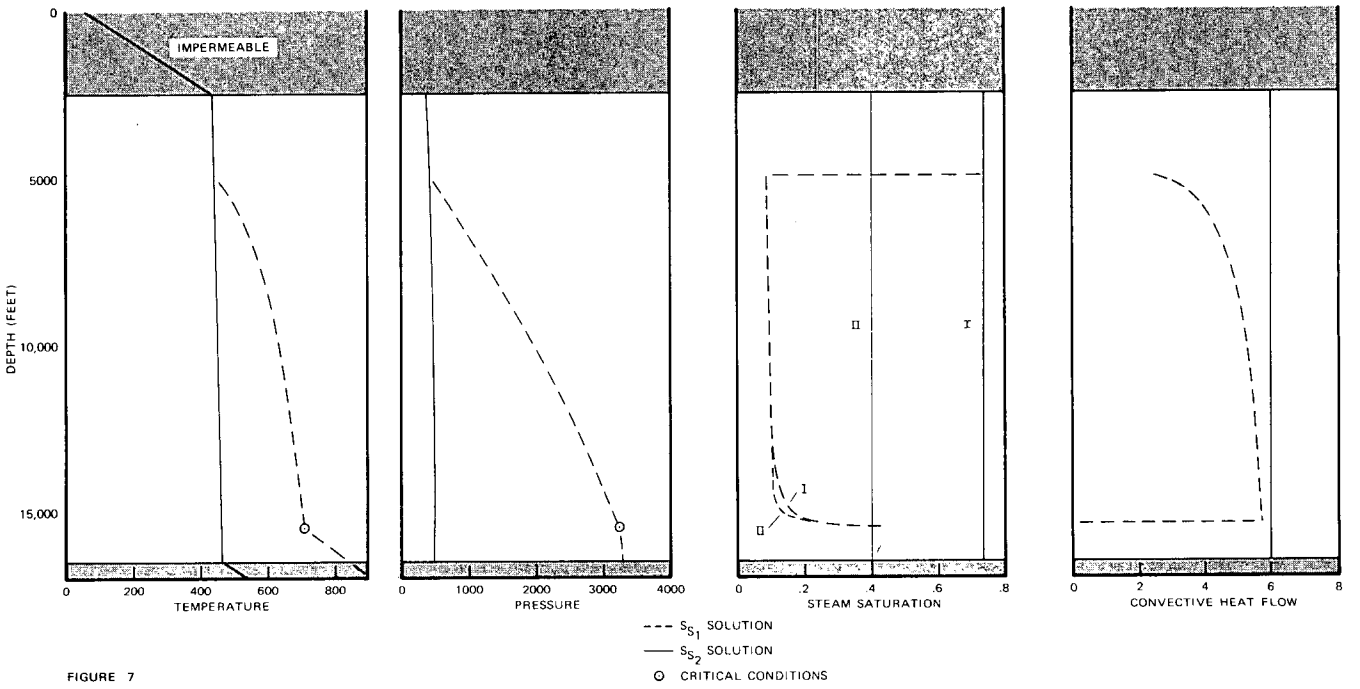

FIGURE 7

CALCULATED RESULTS WITH AND WITHOUT A INTERFACE AT 5000' FOR THE SAME PARAMETERS THOSE USED IN FIGURE 5. RELATIVE PERMEABILITY TYPES ARE DENOTED BY I AND II.

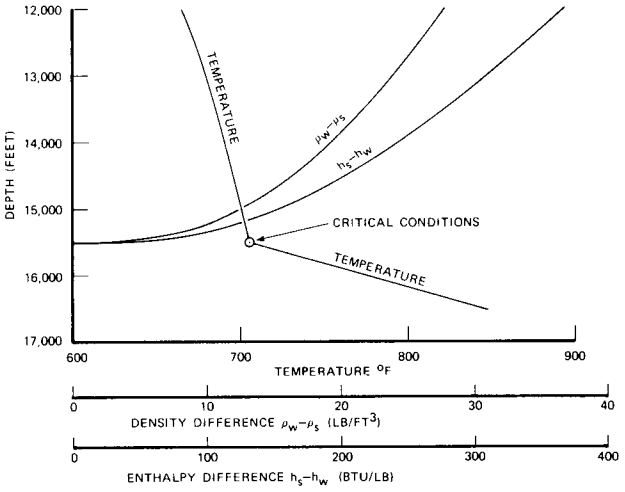

FIGURE 8

THE VARIATIONS OF THE DENSITY AND ENTHALPY DIFFERENCES NEAR CRITICAL CONDITIONS FOR THE S_{s1} SOLUTION PRESENTED IN FIGURE 7.

MODELLING HEAT TRANSFER AND ROCK DEFORMATION PROCESSES IN GEOTHERMAL SYSTEMS

C. Archambeau, D. Holcomb, D. R. Kassoy
J. S. Rinehart, A. Zebib
University of Colorado
Boulder, CO. 80302

The geothermal research program at the University of Colorado encompasses three primary areas of study. These include:

1. Analysis and interpretation of data from the Mesa Anomaly. Development of a physically viable conceptual model of the undeveloped system.

2. Heat and mass transfer in simple models of liquid-dominated geothermal systems. Analysis of flow, temperature and pressure distribution.

3. Rock deformation processes associated with mechanical loading (earth tides, tectonics) and extraction and reinjection of liquids.

During the Second Workshop we will present results of studies on:

(1) Steady Nonlinear Convection on a Saturated Porous Medium with Large Temperature Variation.

(2) The Vertical Convection of Heated Liquid in a Fault Zone in the Geothermal Environment.

(3) The Enhancement of Microfracture Structure in Rocks.

Steady Nonlinear Convection in a Saturated Porous Medium with Large Temperature Variation

Potentially exploitable liquid-dominated geothermal basins must be highly permeable and supplied with heat from below. If the physical situation in these basins is such that significant fluid motion is present, then heat may be convected toward the surface such that high enthalpy liquid is available at relatively shallow depths.

In order to understand the different factors influencing convective motion in a geothermal basin, we consider a simplified model. Our system is a rectangular, homogeneous, isotropic, water-saturated porous medium with rigid boundaries. The vertical sides are insulated, while the upper horizontal boundary is isothermal at a temperature T_o and the lower horizontal boundary is isothermal at a higher temperature T_1. The density and viscosity of the water are functions of the temperature while all other properties are taken as temperature independent. For simplicity, we only consider two-dimensional convection.

The describing equations show that convection will start if the value of the Rayleigh number (R) of the system which is a measure of the ratio of the buoyancy force to the viscous resistance exceeds a critical value (R_c) which is a monotonic decreasing function of the temperature difference $\Delta T = T_1 - T_o$. In this case the amount of heat transfer increases significantly from its conduction value.

Because of the nonlinearity of the describing equations when convection is present, numerical solution of the equations is essential. However, when R is only slightly larger than R_c weakly nonlinear analysis is possible. A result of this analysis shows that the Nusselt number (Nu) which is the ratio of the heat transfer across the system to its conduction value is given approximately by $Nu \approx 1 + \frac{R(R - R_c)}{a+bR+cR^2}$ where a, b and c are functions of ΔT such that for a specific value of R the Nusselt number was found to increase as ΔT increases. These approximate results were used to check the numerical code for values of $R \to R_c^+$

The solution to the full initial boundary value problem which describes natural convection in the system was found by the finite difference method. The parabolic energy equation was solved by the alternating direction implicit method. The elliptic momentum equation was solved by the successive over relaxation method. An initial perturbation is assumed followed by marching in time until a steady state is reached. Estimates of accuracy were found by mesh size reduction.

Our numerical results were checked against published results for constant viscosity computations with good agreement. Excellent agreement with the weakly nonlinear theory was also found for values of $\frac{R}{R_c} \leq 1.2$. It was found that:

1. Although the Nusselt number increases with an increase of ΔT at the specified value of R, a universal curve is found to describe the variation of the Nusselt number with R/R_c for values of $0 < \Delta T \leq 200^oC$.

2. The velocity and temperature distributions are considerably influenced by the viscosity dependence on temperature. The horizontal motion is faster near the lower boundary. The ascending high temperature fluid is moving faster than the colder descending fluid.

3. Thermal boundary layers with strong temperature gradients are found to exist at increasingly smaller values of R/R_c as the temperature difference increases.

4. Temperature distributions with depth cannot always be used to delineate conduction and convection regions.

5. In the upflow section of the convection cell distortion of high temperature isotherms may lead to flashing at relatively shallow depths.

The Vertical Convection of Heated Liquid in a Fault Zone in the Geothermal Environment

There is abundant evidence in Long Valley, the Imperial Valley, the Coso area, Wairakei, Broadlands, and the Rio Grande Rift region among others, which suggests that fault zones are intimately associated with geothermal activity. In many of these areas thermal anomalies and hot springs are aligned with the faults themselves. This juxtaposition implied that the faults provide a path for convecting heated liquid from depth. When the rising hot water intersects a relatively permeable horizontal aquifer a charging process could occur leading to a reservoir of geothermal fluids. In this sense it seems reasonable to suggest that localized geological structure (faults and aquifers) controls the heat and mass transfer in geothermal systems rather than the large scale hydrodynamical convection patterns studied so frequently. With this in mind we have initiated a study of heat and mass transfer in models of a fault zone.

The fault zone is imagined to be a region of heavily fractured rock with a finite transverse dimension (as opposed to a single discrete crack) which extends for some indefinite length along the earth's surface. Microearthquake data suggests that these faults may descend to a depth far in excess of that associated with geothermal reservoirs ($\gtrsim 4$ km). Thus it is assumed that the fault extends through a region of sedimentary material into the basement complex beneath. Due to periodic tectonic activity the fracture system in the fault zone is maintained. Thus the fault region, with a relatively high fracture permeability, can act as a localized conduit for the motion of fluid. In the most general model one imagines that surface water (precipitation, river runoff, etc.) percolates downward over a region of areal extent large compared to that of the fault. Although the general permeability may be insignificant with respect to that of the fault region, the large horizontal area involved permits significant quantities of liquid to reach the hot basement complex. Since the latter is thought to be heavily fractured, liquid from the periphery of the geothermal area can migrate through the hot rocks toward the fault zone. The driving mechanism for this lateral motion at depth is a pressure gradient associated with the difference between the hydrostatic pressure of the cold periphery fluid and that of the hot fluid at the same depth. Hence the fault can be charged with hot water which then rises upward in the channel composed of fractured material. At various horizons in the sedimentary section hot water may leave the fault to charge available aquifers. Should the fault extend to the surface, hot springs may appear.

In our first-order model we imagine a fault zone (extending to the surface) which intersects relatively impermeable sediments (no fluid loss). The zone is modelled as a narrow vertical slab of porous material. In the sedimentary section the walls, assumed to be impermeable, have a temperature that increases linearly with depth. Beneath the contact with the basement complex we assume that mass can pass through the walls which are at a constant high temperature. Two-dimensional solutions are sought for the flow configuration in the vertical slot (the fault as observed in the transverse dimension). Solutions are developed for the fault charging mechanism in the basement complex, for the region of initial cooling of liquid near the contact and the transition to fully-developed flow near the

top of the fault. It is shown that the latter configurations can exist only if the fault zone Rayleigh number is sufficiently small. The analysis also indicates that two-dimensional solutions are possible only if a fault zone is sufficiently narrow, all other physical properties held fixed. For wider faults only three-dimensional flow configurations can exist. Such solutions are given for a limited range of Rayleigh numbers.

The Enhancement of Microfracture Structure in Rocks

A quantitative deterministic model of dilatancy (microfracture development) has been developed that fits the stress-strain relations for confining pressures between 0 and 4 kb. This includes loading, partial unloading and reloading. The description has been tested for rates of 10^{-5} to 10^{-6}/sec.

In connection with geothermal work, modelling is useful in two ways. First, dilatancy represents controllable porosity and this is obviously important to geothermal work. Changing the local stress fields may make it possible to induce a dilatant state with the associated greatly increased permeability. The other side of this is that improper pumping can decrease existing dilatancy. In either case a model is very useful.

Second, in the laboratory, dilatancy has been found to precede and control material failure. Pumping in a geothermal field can lead to dilatancy and failure with possible catastrophic effects on the field and the surroundings. This is not all bad in that a small earthquake may greatly increase fracturing.

The general approach adopted was statistical, based on the sliding grain boundary crack model. Slip on grain boundaries opens cracks that are parallel to the maximum principal stress axis and produces volumetric strain along the minimum compressive stress axis. Distribution functions f_s, f_σ, f_v for the boundary strength, local stress, and crack volume are required. These must depend on the stress invariants. This approach, as opposed to the more common continuum mechanics approach, is closely related to the micro-physics which makes it easier to interpret observations in terms of what is happening at individual cracks. Separating out the various dependencies simplifies the problem of including effects like chemical weakening. If it is known what the chemistry of the fluids does to the crack strength, then by modifying f_s accordingly the effect is included.

The stress invariants $Y = (3/4J_2')^{1/2}$ and $\bar{P} = P - 1/2(\frac{J_3'}{2})^{1/3}$ were chosen as the variables. Y is a measure of the maximum shear traction and $\bar{P}$ represents the average normal traction. As P increases, the frictional force that must be overcome by Y to cause sliding increases. The onset of dilatancy, $Y_D(\bar{P})$, is a measure of the weakest crack and the shape of this curve in $Y - \bar{P}$ space gives the effect of $\bar{P}$ on the failure stress, Y_s. The strength distribution f_s is required to give a cutoff at $Y_D(\bar{P})$. A convenient form, used to describe failure in ceramics, is $f_s(Y_s - Y_D(\bar{P})) = 2a(Y_s - Y_D)\exp(-a(Y - Y_D)2)$. Then the differential number of cracks opening is $dN(Y_s,\bar{P}) = f_s d(Y_s - Y_D)$. The stress distribution f_σ is taken to be a

delta function for a first order theory. The form of the crack volume distribution f_v is unknown but assumed to be invariant, so that its effect can be computed from one value of the dilatancy on the loading curve. Using this approach, biaxial loading curves for confining pressures of 0 to 4 Kb were fit by varying only one constant which reflected the effect of confining pressure on the average crack volume.

Unloading is a very different process from loading in that it is a more linear process, with dilatancy persisting until unloading is complete. Detailed consideration of the local stresses at an open crack suggests that closure is by smooth linear backsliding when the stress falls below the failure stress. The unloading curves are described well by this process. To describe the process we find that three parameters must be obtained from experiment: $Y_D(\bar{P})$, f_v, and a factor related to the number of potential cracks/unit volume.

Implementation of the model in a computer code is straightforward. The finite element method is a natural choice. The effects of cracks can be incorporated in a simple and intuitively appealing way by treating the cracks as dislocations and using the equivalent body force description. This introduces a body force density that can be treated easily by finite elements. It also automatically includes crack interaction effects. Pore pressure effects are handled by using the interacting continua method to calculate the effective stresses. It is not clear how pore pressure will affect the strength of the cracks. Changing, oriented porosity implies that the permeability is anisotropic and variable. It is straightforward to include this effect in a fluid flow finite element code. The overall problem is highly nonlinear and must be solved iteratively.

DERIVATION, BY AVERAGING, OF THE EQUATIONS OF HEAT, MASS AND MOMENTUM TRANSFER IN A GEOTHERMAL RESERVOIR

Guy E. Assens
Lawrence Berkeley Laboratory
One Cyclotron Road
Berkeley, CA 94720

The following paper is an abstract of a report under completion at the Lawrence Berkeley Laboratory (Assens, 1977); the main purpose of this report is to (1) provide a mathematical derivation of the equations describing the transfer of heat, mass and momentum in a geothermal brine reservoir (especially when heat or mass sources are present), and (2) help in the choice of the dependent variables best suited for solving these equations numerically.

The basic tool is an averaging procedure that allows the derivation of the transport equations in a porous medium from the level of the pores, where each of the solid, liquid and fluid constituents is considered as a separate continuum, to a grosser level where the medium in which transport takes place is itself considered as a continuum without reference to its three components.

Two variants of this averaging have been proposed by chemical engineers: Anderson and Jackson (1967) on one hand, Whitaker (1969, 1973) and Slattery (1972) on the other. The former variant has been recently applied to the derivation of the transport of solute (Blake and Garge, 1976) whereas the later was used in relation to the transport of solute (Gray, 1975), a derivation of Darcy's law (Gray and O'Neill, 1976; Neuman, 1976) and the transport of heat in terms of fluid internal energy (Witherspoon et al. 1975) or enthalpy (Faust, 1976).

In the following pages we restrict the scope of our investigation to a one-component fluid and follow the latter of the aforementioned variants, hoping that we may avoid some of the shortcomings noticed in the literature surveyed while obtaining a more complete form of the transport equations.

THE BALANCE EQUATIONS FOR A CONTINUUM

Hypotheses:

(G1) Continuum approximation

(G2) Negligible thermodynamic fluctuations

(G3) Laminar flow regime

(G4) One component fluid

Mass balance:

$$\frac{\partial \rho}{\partial t} + \frac{\partial}{\partial x_j} (\rho v_j) = 0 \qquad (1)$$

Momentum balance (i-direction)

$$\frac{\partial}{\partial t} (\rho v_i) + \frac{\partial}{\partial x_j} (\rho v_i v_j + p\delta_{ij} - \tau_{ij}) - \rho g_i = 0 \qquad (2)$$

Heat balance:

$$\left\{ \begin{array}{l} \frac{\partial}{\partial t} (\rho e) + \frac{\partial}{\partial x_j} (\rho e v_j) \\ \frac{\partial}{\partial t} (\rho h) + \frac{\partial}{\partial x_j} (\rho h v_j) \\ \rho c_v \frac{DT}{Dt} \end{array} \right\} + \frac{\partial}{\partial x_j} \left(-\lambda \frac{\partial T}{\partial x_j}\right) \left\{ \begin{array}{l} + p \frac{\partial v_j}{\partial x_j} \qquad (3e) \\ - \frac{\partial p}{\partial t} - v_j \frac{\partial p}{\partial x_j} \\ - \frac{T\alpha}{\rho\beta} \frac{D\rho}{Dt} \qquad (3t) \end{array} \right\} = \dot{E} + \mu\Phi \qquad (3h)$$

THE AVERAGING PROCEDURE

Definitions:

Consider, within the porous medium, a fixed representative elementary volume (Bear, 1972) R_α (α = S, L, G).

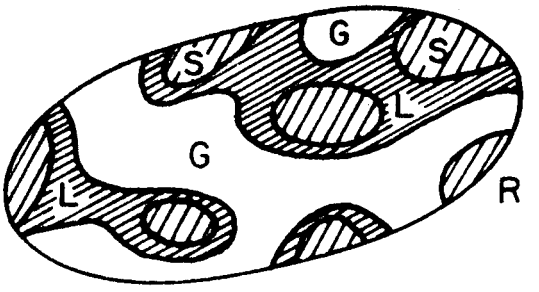

Let ψ_α be any property of the α-phase, defined physically in R_α and mathematically set equal to zero in $R - R_\alpha$.

Phase average: $$\langle\psi_\alpha\rangle \equiv \frac{1}{V}\int_R \psi_\alpha \, dV \tag{4}$$

Intrinsic phase average: $$\langle\psi_\alpha\rangle^\alpha \equiv \frac{1}{V_\alpha}\int_{R_\alpha} \psi_\alpha dV \tag{5}$$

Deviation: $$\tilde{\psi}_\alpha \equiv \begin{cases} \psi_\alpha - \langle\psi_\alpha\rangle^\alpha & \text{in } R_\alpha \\ 0 & \text{in } R - R_\alpha \end{cases} \tag{6}$$

Any quantity, e.g. $\langle\psi_\alpha\rangle$, that has no meaning at a finer level than that of the R.E.V. will be subsequently referred to as "locally" defined, whereas a quantity that exists at the level of the pore, e.g. ψ_α, will be referred to as "pointwise" defined.

Hypotheses:

(G5) characteristic lengths: $d \ll \ell \ll L$

(pore) (R.E.V.) (reservoir)

(G6) good behavior of ψ_α: $$\langle\langle\psi_\alpha\rangle\rangle = \langle\langle\psi_\alpha\rangle\rangle^\alpha = \langle\psi_\alpha\rangle \tag{8a}$$

$$\langle\langle\psi_\alpha\rangle^\alpha\rangle = \langle\langle\psi_\alpha\rangle^\alpha\rangle^\alpha = \langle\psi_\alpha\rangle^\alpha \tag{8b}$$

Theorems:

General transport theorem (Whitaker, 1969):

$$\left\langle \frac{\partial\psi_\alpha}{\partial t} \right\rangle = \frac{\partial}{\partial t}\langle\psi_\alpha\rangle - \frac{1}{V}\int_{S_\alpha} \psi_\alpha w_{\alpha j} n_{\alpha j} \, dA \tag{9}$$

Averaging theorem (Whitaker, 1969; Slattery, 1972):

$$\left\langle \frac{\partial\psi_\alpha}{\partial x_j} \right\rangle = \frac{\partial}{\partial x_j}\langle\psi_\alpha\rangle + \frac{1}{V}\int_{S_\alpha} \psi_\alpha n_{\alpha j} \, dA \tag{10}$$

Modified averaging theorem (Gray, 1975):

$$\left\langle \frac{\partial \psi_\alpha}{\partial x_j} \right\rangle = \varepsilon_\alpha \frac{\partial}{\partial x_j} \langle \psi_\alpha \rangle^\alpha + \frac{1}{V} \int_{S_\alpha} \tilde{\psi}_\alpha \, n_{\alpha j} \, dA \tag{11}$$

Modified transport theorem (Assens, 1977):

$$\left\langle \frac{\partial \psi_\alpha}{\partial t} \right\rangle = \varepsilon_\alpha \frac{\partial}{\partial t} \langle \psi_\alpha \rangle^\alpha - \frac{1}{V} \int_{S_\alpha} \tilde{\psi}_\alpha \, w_{\alpha j} n_{\alpha j} \, dA \tag{12}$$

Nice relations:

$$\frac{1}{V} \int_{S_\alpha} n_{\alpha j} \, dA = - \frac{\partial \varepsilon_\alpha}{\partial x_j} \tag{13a}$$

$$\frac{1}{V} \int_{S_\alpha} w_{\alpha j} \, n_{\alpha j} \, dA = \frac{\partial \varepsilon_\alpha}{\partial t} \tag{13b}$$

THE AVERAGED BALANCE EQUATIONS

Assume that (H1) the average of the product of two or more deviations of variables not strongly dependent on velocity is negligible compared to the product of the averages of these variables.

Mass balances:

Solid - Assume (H2) incompressible, non reacting solid.

$$\frac{\partial \rho_S}{\partial t} = 0 \tag{14}$$

Fluid phase $\alpha (\alpha = L, G)$:

$$\underbrace{\frac{\partial}{\partial t} (\varepsilon_\alpha \langle \rho_\alpha \rangle^\alpha)}_{\text{(storage)}} + \underbrace{\frac{\partial}{\partial x_j} (\langle \rho_\alpha \rangle^\alpha \langle v_{\alpha j} \rangle)}_{\text{(convection)}} + \underbrace{\frac{1}{V} \int_{S_{\alpha\beta}} \rho_\alpha (v_{\alpha j} - w_{\alpha j}) \, n_{\alpha j} \, dA}_{\text{(phase change)}} + \underbrace{\frac{\partial}{\partial x_j} \langle \tilde{\rho}_\alpha \tilde{v}_{\alpha j} \rangle}_{\text{(dispersion)}} = 0 \tag{15}$$

where the dispersion term may be omitted subject to (H3) low correlation between density and velocity.

Momentum balances:

Solid - Assume (H4) indeformable solid matrix

$$v_{Sij} = 0 \tag{16}$$

Fluid - Assume (H5) negligible inertia

$$\langle v_{\alpha i} \rangle^{\alpha} = - \sum_{\beta=L,G} \frac{1}{\varepsilon_\beta \langle \mu_\beta \rangle^\beta} k_{\alpha\beta ij} \left(\frac{\partial}{\partial x_j} \langle p_\beta \rangle^\beta - \langle \rho_\beta \rangle^\beta g_j \right) \tag{17}$$

yields Darcy's formula in the case of a (H6) rigid gas-liquid interface with no slip.

Heat Balances:

Solid - Define the "stagnant" thermal conductivity λ'_S by:

$$- \varepsilon_S \lambda'_S \frac{\partial}{\partial x_j} \langle T_S \rangle^S \equiv - \langle \lambda_S \rangle^S \left(\varepsilon_S \frac{\partial}{\partial x_j} \langle T_S \rangle^S + \frac{1}{V} \int_{S_S} \tilde{T}_S n_{Sj} dA \right) \tag{18}$$

Then, by H1:

$$\left.\begin{array}{l} \dfrac{\partial}{\partial t} \left(\varepsilon_S \langle \rho_S \rangle^S \langle e_S \rangle^S \right) \\ \text{(storage)} \\ \varepsilon_S \langle \rho_S \rangle^S \langle c_{vS} \rangle^S \dfrac{\partial}{\partial t} \langle T_S \rangle^S \end{array}\right\} + \underbrace{\frac{\partial}{\partial x_j} \left(-\varepsilon_S \lambda'_S \frac{\partial}{\partial x_j} \langle T_S \rangle^S \right)}_{\text{(conduction within solid)}} + \underbrace{\frac{1}{V} \int_{S_S} \left(-\lambda_S \frac{\partial T_S}{\partial x_j} \right) n_{Sj} dA}_{\text{(conduction across fluid-solid interface)}} = \langle \dot{E}_S \rangle \tag{19}$$

Fluid - Define the tensor of thermal dispersion $\lambda''_{\alpha ij}$ as follows:

$$\frac{\partial}{\partial x_j} \left(-\varepsilon_\alpha \lambda''_{\alpha ij} \frac{\partial}{\partial x_i} \langle T_\alpha \rangle^\alpha \right) \equiv \frac{\partial}{\partial x_j} \langle \tilde{\rho}_\alpha \tilde{e}_\alpha \tilde{v}_{\alpha j} \rangle + \langle \tilde{p}_\alpha \frac{\partial \tilde{v}_{\alpha j}}{\partial x_j} \rangle \tag{20}$$

Then define the "effective" thermal conductivity tensor:

$$\lambda^*_{\alpha ij} \equiv \lambda'_\alpha + \lambda''_{\alpha ij} \tag{21}$$

Finally assume (H7) negligible viscous dissipation

$$\frac{\partial}{\partial t}\left(\varepsilon_\alpha \langle\rho_\alpha\rangle^\alpha \langle e_\alpha\rangle^\alpha\right) + \frac{\partial}{\partial x_j}\left(\langle\rho_\alpha\rangle^\alpha \langle e_\alpha\rangle^\alpha \langle v_{\alpha j}\rangle\right) + \frac{\partial}{\partial x_j}\left(-\varepsilon_\alpha \lambda^*_{\alpha ij} \frac{\partial}{\partial x_i} \langle T_\alpha\rangle^\alpha\right)$$

(storage) (convection) (conduction within phase α)

$$+ \frac{1}{V}\int_{S_\alpha} \left[(\rho_\alpha e_\alpha + p_\alpha)(v_{\alpha j} - w_{\alpha j}) - \lambda_\alpha \frac{\partial T_\alpha}{\partial x_j}\right] n_{\alpha j}\, dA + \langle p_\alpha\rangle^\alpha \left(\frac{\partial \varepsilon_\alpha}{\partial t} + \frac{\partial}{\partial x_j}\langle v_{\alpha j}\rangle\right)$$

(convection + conduction across interfaces separating phase α from phase β and solid) (pressure work)

$$- \frac{1}{V}\int_{S_{\alpha\beta}} \tilde{p}_\alpha (v_{\alpha j} - w_{\alpha j})\, n_{\alpha j}\, dA = \langle \dot{E}_\alpha\rangle \qquad (22)$$

(residual pressure work) (internal generation)

COMBINING THE AVERAGED EQUATIONS

Fluid momentum balance: Define (locally) the fluid mass flux;

$$\dot{m}_j \equiv \langle\rho_L\rangle^L \langle v_{Lj}\rangle + \langle\rho_G\rangle^G \langle v_{Gj}\rangle \qquad (23)$$

Assume (H8) negligible capillarity, then define (pointwise) the reservoir pressure p:

$$p \equiv \begin{cases} p_S \text{ in } R_S \\ p_L \text{ in } R_L \\ p_G \text{ in } R_G \end{cases} \quad \text{with} \quad \begin{cases} \langle p\rangle = \langle p_S\rangle^S = \langle p_L\rangle^L = \langle p_G\rangle^G \\ p_L = p_G \ (= p) \text{ along } S_{LG} \end{cases} \qquad (24)$$

Then:

$$\dot{m}_j = -\left(\frac{k_L \langle\rho_L\rangle^L}{\varepsilon_L \langle\mu_L\rangle^L} + \frac{k_G \langle\rho_G\rangle^G}{\varepsilon_G \langle\mu_G\rangle^G}\right) k_{ij} \frac{\partial}{\partial x_i}\langle p\rangle + \left(\frac{k_L (\langle\rho_L\rangle^L)^2}{\varepsilon_L \langle\mu_L\rangle^L} + \frac{k_G (\langle\rho_G\rangle^G)^2}{\varepsilon_G \langle\mu_G\rangle^G}\right) g_j \qquad (25)$$

Fluid mass balance: Define (locally) the fluid density $\langle\rho_F\rangle^F$ as follows:

$$\varepsilon_F\langle\rho_F\rangle^F \equiv \varepsilon_L\langle\rho_L\rangle^L + \varepsilon_G\langle\rho_G\rangle^G \tag{26}$$

then:

$$\frac{\partial}{\partial t}\left(\varepsilon_F\langle\rho_F\rangle^F\right) + \frac{\partial \dot{m}_j}{\partial x_j} = 0 \tag{27}$$

Fluid heat balance: Define (locally) the fluid internal energy $\langle e_F\rangle^F$ and internal heat generation rate $\langle\dot{E}_F\rangle$ as follows:

$$\varepsilon_F\langle\rho_F\rangle^F\langle e_F\rangle^F \equiv \varepsilon_L\langle\rho_L\rangle^L\langle e_L\rangle^L + \varepsilon_G\langle\rho_G\rangle^G\langle e_G\rangle^G \tag{28}$$

$$\langle\dot{E}_F\rangle \equiv \langle\dot{E}_L\rangle + \langle\dot{E}_G\rangle \tag{29}$$

Then:

$$\frac{\partial}{\partial t}\left(\varepsilon_F\langle\rho_F\rangle^F\langle e_F\rangle\right) + \frac{\partial}{\partial x_j}\left(\dot{m}_j\langle e_F\rangle^F\right) + \frac{\partial}{\partial x_j}\left(-\varepsilon_L\lambda^*_{Lij}\frac{\partial}{\partial x_i}\langle T_L\rangle^L - \varepsilon_G\lambda^*_{Gij}\frac{\partial}{\partial x_i}\langle T_G\rangle^G\right)$$

$$- \frac{1}{V}\int_{S_s}\left(-\lambda_S\frac{\partial T_S}{\partial x_j}\right) n_{Sj}\, dA + \langle p_L\rangle^L\left(\frac{\partial \varepsilon_L}{\partial t} + \frac{\partial}{\partial x_j}\langle v_{Lj}\rangle\right) + \langle p_G\rangle^G\left(\frac{\partial \varepsilon_G}{\partial t} + \frac{\partial}{\partial x_j}\langle v_{Gj}\rangle\right)$$

$$+ \frac{1}{V}\int_{S_{LG}}\left(\tilde{p}_G v_{Gj} - \tilde{p}_L v_{Lj}\right) n_{Lj}\, dA + \frac{1}{V}\int_{S_{LG}}\left(\tilde{p}_L - \tilde{p}_G\right) w_{Lj} n_{Lj}\, dA = \langle\dot{E}_F\rangle \tag{30}$$

Assume (H9) temperature equilibrium between both fluid phases then define (pointwise) the fluid temperature T_F, (locally) the fluid effective thermal conductivity tensor λ^*_{Fij} and a coefficient of solid-fluid heat transfer h_{SF} (Combarnous and Bories, 1974):

$$T_F \equiv \begin{cases} 0 & \text{in } R_S \\ T_L & \text{in } R_L \\ T_G & \text{in } R_G \end{cases} \qquad \text{with} \qquad \langle T_F \rangle^F = \langle T_L \rangle^L = \langle T_G \rangle^G \tag{31}$$

$$\varepsilon_F \lambda^*_{Fij} \equiv \varepsilon_L \lambda^*_{Lij} + \varepsilon_G \lambda^*_{Gij} \tag{32}$$

$$a h_{SF}(\langle T_S \rangle^S - \langle T_F \rangle^F) \equiv \frac{1}{V} \int_{S_S} (-\lambda_S \frac{\partial T_S}{\partial x_j}) n_{Sj} \, dA \tag{33}$$

with $a \equiv \frac{A_S}{V}$, solid-fluid interfacial area per unit volume of porous medium.

Then

$$\underbrace{\frac{\partial}{\partial t} (\varepsilon_F \langle \rho_F \rangle^F \langle e_F \rangle^F)}_{\text{(storage)}} + \underbrace{\frac{\partial}{\partial x_j} (\dot{m}_j \langle e_F \rangle^F)}_{\text{(convection)}} + \underbrace{\frac{\partial}{\partial x_j} (-\varepsilon_F \lambda^*_{Fij} \frac{\partial}{\partial x_i} \langle T_F \rangle^F)}_{\text{(conduction within fluid)}}$$

$$+ \underbrace{a h_{SF}(\langle T_F \rangle^F - \langle T_S \rangle^S)}_{\text{(conduction across solid-fluid interface)}} + \underbrace{\langle p \rangle \frac{\partial}{\partial x_j} (\langle v_{Lj} \rangle + \langle v_{Gj} \rangle)}_{\text{(pressure work)}} + \underbrace{\frac{1}{V} \int_{S_{LG}} \tilde{p}(v_{Gj} - v_{Lj}) n_{Lj} dA}_{\text{(residual pressure work)}}$$

$$= \langle \dot{E}_F \rangle \quad \text{(internal generation)} \tag{34}$$

Solid heat balance: By H8 and H9,

$$\left.\begin{array}{l} \underbrace{\frac{\partial}{\partial t} (\varepsilon_S \langle \rho_S \rangle^S \langle e_S \rangle^S)}_{\text{(storage)}} \\ \underbrace{\varepsilon_S \langle \rho_S \rangle^S \langle c_{vS} \rangle^S \frac{\partial}{\partial t} \langle T_S \rangle^S}_{} \end{array}\right\} + \underbrace{\frac{\partial}{\partial x_j} (-\varepsilon_S \lambda^*_{Sij} \frac{\partial}{\partial x_i} \langle T_S \rangle^S)}_{\text{(conduction within solid)}} + \underbrace{a h_{SF}(\langle T_S \rangle^S - \langle T_F \rangle^F)}_{\text{(conduction across solid-fluid interface)}}$$

$$= \langle \dot{E}_S \rangle \quad \text{(internal generation)} \tag{35}$$

Solid-fluid heat balance:

Assume (H10) solid-fluid temperature equilibrium then define (pointwise) the reservoir temperature T and (locally) the reservoir effective thermal conductivity tensor λ^*_{ij}:

$$T \equiv \begin{cases} T_F \text{ in } R_L \cup R_G \\ T_S \text{ in } R_S \end{cases} \quad \text{with } \langle T \rangle = \langle T_S \rangle^S = \langle T_F \rangle^F \tag{36}$$

$$\lambda^*_{ij} \equiv \varepsilon_S \lambda^*_{Sij} + \varepsilon_F \lambda^*_{Fij} \quad (\text{with } \varepsilon_S + \varepsilon_F = 1) \tag{37}$$

Then:

$$\underbrace{\frac{\partial}{\partial t}\left(\varepsilon_S \langle \rho_S \rangle^S \langle e_S \rangle^S + \varepsilon_F \langle \rho_F \rangle^F \langle e_F \rangle^F\right)}_{\text{(storage)}} + \underbrace{\frac{\partial}{\partial x_j}\left(\dot{m}_j \langle e_F \rangle^F\right)}_{\text{(convection)}} + \underbrace{\frac{\partial}{\partial x_j}\left(-\lambda^*_{ij} \frac{\partial}{\partial x_i} \langle T \rangle\right)}_{\text{(conduction)}}$$

$$+ \underbrace{\langle p \rangle \frac{\partial}{\partial x_j}\left(\langle v_{Lj} \rangle + \langle v_{Gj} \rangle\right)}_{\text{(pressure work)}} = \underbrace{\langle \dot{E}_S \rangle + \langle \dot{E}_F \rangle}_{\text{(internal generation)}} \tag{38e}$$

Similarly, in terms of (fluid) enthalpy:

$$\frac{\partial}{\partial t}\left(\varepsilon_S \langle \rho_S \rangle^S \langle e_S \rangle^S + \varepsilon_F \langle \rho_F \rangle^F \langle h_F \rangle^F\right) + \frac{\partial}{\partial x_j}\left(\dot{m}_j \langle h_F \rangle^F\right) + \frac{\partial}{\partial x_j}\left(-\lambda^*_{ij} \frac{\partial}{\partial x_i} \langle T \rangle\right)$$

$$- \frac{\partial}{\partial t} \langle p \rangle - \left(\langle v_{Lj} \rangle + \langle v_{Gj} \rangle\right) \frac{\partial}{\partial x_j} \langle p \rangle = \langle \dot{E}_S \rangle + \langle \dot{E}_F \rangle \tag{38h}$$

ELEMENTAL AVERAGING

(Or, how to fit external heat or mass sources, such as wells or leaking boundaries, into the balance equations.)

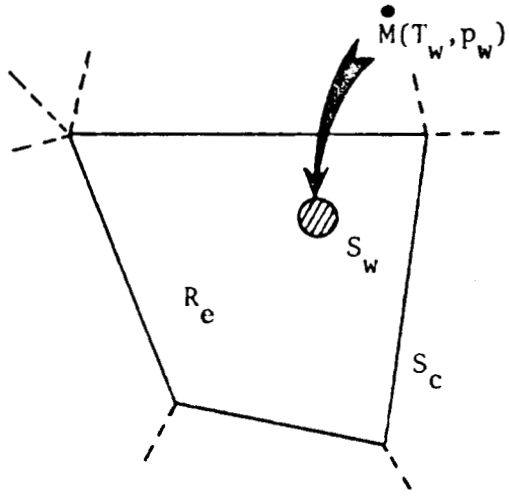

The Procedure

Partition the reservoir into a set of "elements". Any element R_e is bounded by

i) an interface S_c connecting R_e to neighboring elements.

ii) a surface S_w separating R_e from the "outside".

Elemental average:

$$\bar{\psi} \equiv \frac{1}{V_e} \int_{R_e} \langle \psi \rangle \, dV \tag{39}$$

Hypothesis G5 modified:

$$(d<<) \qquad \ell \quad << \quad \ell_e \quad << \quad L \qquad (40)$$

(pore) (R.E.V.) (element) (reservoir)

Divergence theorem:

$$\int_{R_e} \frac{\partial}{\partial x_j} \langle \psi_j \rangle dV = \int_{S_c US_w} \langle \psi_j \rangle n_j dA \qquad (41)$$

Elemental mass balance:

$$\bar{\varepsilon} V_e \frac{\partial \bar{\rho}_F}{\partial t} + \int_{S_c} \dot{m}_j n_j dA = \dot{M} \qquad (42)$$

Elemental momentum balance: Immaterial

Elemental heat balance: By approximation of the pressure term in (38e):

$$V_e \frac{\partial}{\partial t} [(1-\bar{\varepsilon})\bar{\rho}_S \bar{e}_S + \bar{\varepsilon}\bar{\rho}_F \bar{e}_F] + \int_{S_c} \dot{m}_j \langle e_F \rangle^F n_j dA + \int_{S_c} (-\lambda^*_{ij} \frac{\partial}{\partial x_i} \langle T \rangle) n_j dA$$

$$+ \bar{p} \int_{S_c} (\langle v_{Lj} \rangle + \langle v_{Gj} \rangle) n_j dA = V_e (\dot{\bar{E}}_S + \dot{\bar{E}}_F) + \dot{M} (\bar{e}_w + \frac{\bar{p}}{\bar{\rho}_w}) + A_w (\frac{\lambda^*}{\ell_e})_w (\bar{T}_w - \bar{T})$$

(43e)

Alternatively:

$$V_e \frac{\partial}{\partial t} [(1-\bar{\varepsilon})\bar{\rho}_S \bar{e}_S + \bar{\varepsilon}\bar{\rho}_F \bar{h}_F] + \int_{S_c} \dot{m}_j \langle h_F \rangle^F n_j dA + \int_{S_c} (-\lambda^*_{ij} \frac{\partial}{\partial x_i} \langle T \rangle) n_j dA$$

$$- V_e \frac{\partial p}{\partial t} - \int_{R_e} (\langle v_{Lj} \rangle + \langle v_{Gj} \rangle) \frac{\partial \langle p \rangle}{\partial x_j} dV = V_e (\dot{\bar{E}}_S + \dot{\bar{E}}_F) + \dot{M} \bar{h}_w + A_w (\frac{\lambda^*}{\ell_e})_w (\bar{T}_w - \bar{T})$$

(43h)

TOWARD NUMERICAL SOLUTION

The Pressure-Work Term

The main difference between equations (43e) and (43h) lies in the pressure terms in the left side. These terms may be viewed as coupling the heat balance to the mass balance.

An order of magnitude analysis (Appendix B) shows that, under steady state conditions, the contribution of the pressure-work term to the heat balance is systematically lower with equation (43h) than with equation (43e); that term cannot however be neglected, even in equation (43h), since it is of the same order of magnitude as the convection term when the element considered is devoid of any external mass source.

Equation (43h) exhibits an additional pressure term involving the time derivative of the elemental pressure: we expect that term to yield a significant contribution to the heat balance of those elements only that include wells and only for a "short" period of time following every drastic change in the rate of mass generation.

Provided such drastic changes cover a relatively small part of the simulated life span of the geothermal reservoir, we think that, all in all, equation (43h) may be easier to solve than equation (43e).

The Integrated Finite Difference Method

Let us now compare equations (43e) and 43h) from the standpoint of ease in programming by the Integrated Finite Difference Method (Lasseter et al., 1975; Assens, 1976).

The relevant characteristics of that method are that

1) every element may be connected to any number of surrounding elements and

2) the elemental balances are obtained by adding to the storage and generation terms the contribution (fluxes) of every connection.

Using the IFDM, we evaluate the pressure-work term in (43e) as the product of the pressure within R_e by the sum of all the volumetric fluxes across all the connecting surfaces relative to R_e. On the other hand, we found no simple way to evaluate the (integral) pressure-work term in (43h); we however acknowledge that this might be straightforward when using the Finite Element Method.

We are currently looking for a way of approximating the pressure-work term in (43h) so that we may be able to apply IFDM to the solution of that particular equation.

Choosing a Set of Dependent Variables

The selection of (43h) over (43e) implies the choice of the fluid enthalpy as one of the two dependent variables needed to fully describe the behavior of the geothermal system.

The very form of the mass balance equation (42) leads us to the choice of the fluid density as the other variable. A more material reason for that choice is however that the mass balance for the entire reservoir will thus be kept more accurately than if pressure had been taken as the second dependent variable (Pritchett, 1975: in this later case density, then considered as a parameter, would be evaluated indirectly, based on the values of enthalpy and pressure obtained by solving the transport equations. In the former case only density increments are computed, and the values of the density obtained at the end of the previous time step accordingly updated, thus ensuring better "historical" consistency.

Whenever temperature equilibrium is not fully established, as may be the case in the process of storing hot or cold water underground, equation (43h) needs to be replaced by the elemental averages of both equations (34) and (35): the solid temperature is with little doubt best chosen as the third dependent variable then required.

CONCLUSION

Averaging the mass balance equations from the level of the pore to that of a "R.E.V." of porous medium yields an equation the form of which is analogous to that of the basic equations but for the introduction of the porosity and a dispersion term which we expect to be negligible whenever no correlation exists between density and velocity.

The momentum balance equation yields an explicit expression for the velocity, provided inertia is negligible.

The main change from the basic heat balance equation to the averaged equation is the substitution of a tensor of "effective" thermal conductivity of the porous medium for the individual scalar conductivities of each solid, liquid and gaseous constituents.

Since these equations hold only <u>within</u> the porous reservoir <u>stricto sensu</u>, a further step of averaging is required to include the external heat or mass sources such as wells or leaking boundaries: this classical averaging yields equations that express the balance of heat and mass for any element of a partition of the reservoir, in a form suitable for numerical solution.

Comparing the two forms of the heat balance obtained in terms of either fluid internal energy (43e) or enthalpy (43h), we find that, beside a highly transient pressure term in equation (43h), the basic difference lies in a pressure-work term that couples the heat balance to the mass balance: an elementary order of magnitude analysis indicates that coupling is minimum when heat balance is expressed in terms of enthalpy, thus favoring the

selection of the fluid enthalpy as one of the dependent variables that describe the behavior of the reservoir.

This choice however does not allow us to use the Integrated Finite Differences Method in the current state of our art.

Both computational simplicity and mass balance accuracy lead to the selection of the fluid density as second dependent variable, supplemented by the solid temperature whenever solid-fluid temperature equilibrium is not established.

NOMENCLATURE

Whenever relevant, the dimension is listed in the second column in terms of mass (M), length (L), time (t) and temperature (T).

Roman lower case letters

a	(L^{-1})	solid-fluid interfacial area per unit volume of porous medium
c_e, c_h		coupling ratios pressure-work/heat convection
c_v	$(L^2t^{-2}T^{-1})$	specific heat capacity at constant volume
d	(L)	characteristic length of the pore space
e	(L^2t^{-2})	(specific) internal energy
g_i	(Lt^{-2})	i^{th} component of the gravitational acceleration
h	(L^2t^{-2})	(specific) enthalpy
h_{SF}	$(Mt^{-3}T^{-1})$	coefficient of solid-fluid heat transfer
k_{ij}	(L^2)	(second order) tensor of absolute permeability
k_α		relative permeability of the α phase
$k_{\alpha\beta ij}$	(L^2)	second order permeability tensor
ℓ	(L)	characteristic length of the R.E.V.
ℓ_e	(L)	characteristic length of the element R_e
$\dot{m}_j$		j^{th} component of the fluid mass flux
$n_{\alpha j}$		j^{th} component of the unit normal to S_α, directed from R_α outward
p	$(ML^{-1}t^{-2})$	pressure
t	(t)	time
v_j	(Lt^{-1})	j^{th} component of the point velocity
$\bar{v}_j$	(Lt^{-1})	j^{th} component of the elemental velocity
w_j	(Lt^{-1})	j^{th} component of the (point) velocity of S
x_j	(L)	j^{th} coordinate

Roman capital letters

$A_\bullet$	(L^2)	area of $S_\bullet$
$\dot{E}_\alpha$	$(ML^{-1}t^{-3})$	energy generated within the α phase, per unit time, per unit volume
L	(L)	characteristic length of the reservoir
$\dot{M}$	(Mt^{-1})	mass generation rate
$R_\bullet$		any space domain
S_c		boundary between R_e and the surrounding elements
S_w		boundary between R_e and the exterior (with respect to the reservoir).
S_α		boundary between R_α and $R - R_\alpha$
$S_{\alpha\beta}$		boundary between R_α and R_β
T	(T)	temperature
U		mathematical symbol: "union"
$V_\bullet$	(L^3)	volume of $R_\bullet$

Greek lower case letters

α	(T^{-1})	coefficient of (isobaric) thermal expansion
β	$(M^{-1}Lt^2)$	coefficient of isothermal expansion
δ_{ij}		Kronecker symbol
ε		porosity of the porous medium
ε_α		volumetric fraction of the α phase
λ_α	$(MLt^{-3}T^{-1})$	(intrinsic) thermal conductivity of the α phase
λ'_α	$(MLt^{-3}T^{-1})$	stagnant thermal conductivity
$\lambda''_{\alpha ij}$	$(MLt^{-3}T^{-1})$	tensor of thermal dispersion
λ^*_{ij}	$(MLt^{-3}T^{-1})$	tensor of effective thermal conductivity of the porous medium
μ	$(ML^{-1}t^{-1})$	dynamic viscosity
ρ	(ML^{-3})	density
τ_{ij}	$(ML^{-1}t^{-2})$	viscous stress tensor

Greek capital letter

Φ	(t^{-2})	viscous dissipation function

Subscripts

c	connection
e	element
F	fluid
G	gas
i,j,k	spatial coordinates
L	liquid
S	solid
w	exterior
α	phase identifier (α = S, L, G)
β	phase identifier (β = S, L, G)

Mathematical symbols and notations

U	union of two sets
$\bar{\bullet}$	elemental average
$\equiv$	is, by definition, equal to
$\langle\ \rangle$	phase average over R
$\langle\ \rangle^{\alpha}$	intrinsic phase average over R_{α}
$\tilde{\bullet}$	deviation from intrinsic phase average
$\frac{D\bullet}{Dt} = \frac{\partial \bullet}{\partial t} + v_j \frac{\partial \bullet}{\partial x_j}$	substantial derivative
$\nabla_{\bullet}$	gradient

REFERENCES

Anderson, T. B. and R. Jackson, "Fluid Mechanical Description of Fluidized Beds. Equations of Motion", Ind. Eng. Chem. Fundam., 6 (4), 527-639 (1967).

Assens, G. E., Two-phase, Three Dimensional Simulation of Geothermal Reservoirs: Program SHAFT. Lawrence Berkeley Laboratory, to be issued late 1976.

Assens, G. E., Derivation of the Equations Describing Heat, Mass and Momentum Transfer in a Geothermal Brine Reservoir, Lawrence Berkeley Laboratory, report to be issued early 1977.

Bear, J., Dynamics of Fluids in Porous Media, Elsevier, New York (1972).

Blake, T. R. and S. K. Garg, "On the Species Transport Equation for Flow in Porous Media", Water Resources Research, 12 (4), 748-750 (August 1976).

Combarnous, M. and S. Bories, "Modélisation de la convection naturelle au sein d'une couche poreuse horizontale à l'aide d'un coefficient de transfer solide-fluide", Int. J. Heat Mass Transfer, 17, 505-515 (1974).

Faust, C. R., Numerical Simulation of Fluid Flow and Energy Transport in Liquid- and Vapor-Dominated Hydrothermal Systems, Ph.D. Thesis, Pennsylvania State University, Department of Geosciences (1976).

Gray, W. G., "A Derivation of the Equations for Multiphase Transport", Chem. Eng. Sci., 30, 229-233 (1975).

Gray, W. G. and K. O'Neill, "On the General Equations for Flow in Porous Media and their Reduction to Darcy's Law". Water Resources Research, 12 (2), 148-154 (April 1976).

Helgeson, H. C. and D. H. Kirkham, "Theoretical Prediction of the Thermodynamic Behavior of Aqueous Electrolytes at High Pressures and Temperatures: I. Summary of the Thermodyanmic/Electrostatic Properties of the Solvent", Am. J. Sci., 274, pp. 1089-1198 (December 1974).

Lasseter, T. J., P. A. Witherspoon and M. J. Lippmann, "The Numerical Simulation of Heat and Mass Transfer in Multidimensional Two-Phase Geothermal Reservoirs", Proceedings, Second U. N. Symposium on the Development and Use of Geothermal Resources, San Francisco, May 20-29, 1975.

Neuman, S. P., "Theoretical Derivation of Darcy's Law", Acta Mechanica, in press (1976).

Pritchett, J. W., Private communcation (1975).

Slattery, J. D., Momentum, Energy and Mass Transfer, McGraw Hill, New York, 479 pp. (1972).

Whitaker, S., "Advances in Theory of Fluid Motion in Porous Media", J. Ind. Eng. Chem., 61 (12), 14-28, (1969).

Whitaker, S., "The Transport Equations for Multiphase Systems", Chem. Eng. Sci., 28, 139-147, (1973).

Witherspoon, P. A., S. P. Neuman, M. L. Sorey and M. J. Lippmann, "Modeling Geothermal Systems", paper presented at the International Meeting on Geothermal Phenomena and their Applications, Academia Nazionale dei Lincei, Rome, Italy, March 3-5, 1975.

Wukalovitch, M. P., Thermodynamic Properties of Water and Steam, 6th Edition, State Publishing-House of Scientific-Technical Literature, Moscow, 1958; also published by nationally-owned Publishing House "Veb Verlag Technik", Berlin, 1958.

APPENDIX A

The basic assumptions

G1	Continuum approximation
G2	Negliglbe thermodynamic fluctuations
G3	Laminar flow regime
G4	One component fluid
G5	$d << \ell << \ell_e << L$
G6	Good behavior of the variables
H1	The average of the product of two or more deviations of variables not strongly dependent on velocity is negligible compared to the product of the averages of these variables
H2	incompressible, non reacting solid
H3	low correlation between density and velocity
H4	indeformable solid matrix
H5	negligible inertia
H6	rigid gas-liquid interface with no slip
H7	negligible viscous dissipation
H8	negligible capillarity
H9	temperature equilibrium between both fluid phases
H10	solid-fluid temperature equilibrium (optional)

APPENDIX B

Order of magnitude analysis of the pressure-work term

Consider an homogeneous, isotropic, isothermal reservoir with uniform thickness, partitioned into a set of toric elements centered on a fully penetrating well produced at a constant rate $-\dot{M}$.

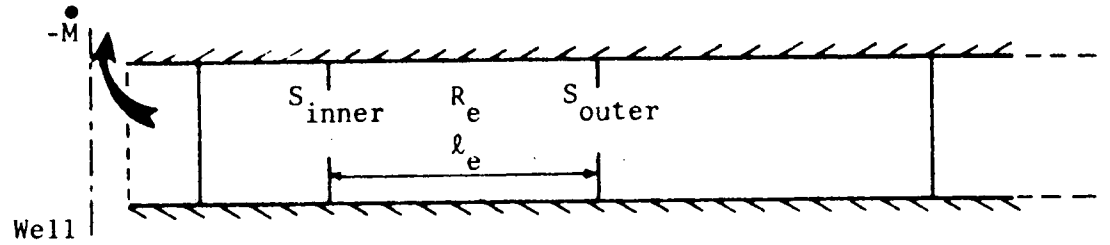

Let the heat convection term (CNV) be the reference with which the magnitude of the pressure-work term (PWK) is to be evaluated.

Case 1

First consider the element immediately surrounding the well and assume that the fluid is one-phase throughout:

$$PWK_e \simeq \bar{p} \int_{S_c} \langle v_j \rangle n_j dA = \bar{p} \frac{\dot{M}}{\langle \rho \rangle_c} \sim \bar{p} \frac{\dot{M}}{\bar{\rho}}$$

$$PWK_h \simeq \bar{v} \nabla \bar{p} V_e \sim \left(\frac{\dot{M}}{\bar{\rho} A_c}\right)\left(\frac{\Delta \bar{p}}{\ell_e}\right)(A_c \ell_e) = \frac{\dot{M} \Delta \bar{p}}{\bar{\rho}}$$

$$CNV_e = \dot{M} \langle e \rangle_c \sim \dot{M} \bar{e} \quad \text{Similarly:} \quad CNV_h \sim \dot{M} \bar{h}$$

Thus:

$$c_e \equiv \frac{PWK_e}{CNV_e} \sim \frac{\bar{p}}{\bar{\rho}\bar{e}} \qquad \text{whereas} \qquad c_h \equiv \frac{PWK_h}{CNV_h} \sim \frac{\Delta \bar{p}}{\bar{\rho}\bar{h}}$$

Let us compare both coupling ratios c_e and c_h:

$$\frac{c_h}{c_e} \sim \left(\frac{\Delta\bar{p}}{\bar{p}}\right)\left(\frac{\bar{e}}{\bar{h}}\right) \sim \frac{\Delta\bar{p}}{\bar{p}}$$

In most cases the element closest to the well is sufficiently narrow for the pressure drop across it to be a small fraction of the average pressure; whence c_h may be expected to be at least one order of magnitude smaller than c_e:

$$\frac{c_h}{c_e} \sim 10^{-1}$$

Let us further particularize our analysis and consider the following "typical" saturated conditions (see e.g. Wukalovitch, 1958):

$T = 293.6\ °C$ $\qquad p = 80\ atm\ (7.9\ 10^6 N/m^2)$

$\rho_L = 725\ kg/m^3$ $\qquad \rho_G = 41.6\ kg/m^3$

$e_L = 1.30\ 10^6\ J/kg$ $\qquad e_G = 2.57\ 10^6\ J/kg$

$h_L = 1.31\ 10^6\ J/kg$ $\qquad h_G = 2.76\ 10^6\ J/kg$

Then:

$$c_e \sim \begin{cases} .8\ 10^{-2} & \text{for steam} \\ 7.\ 10^{-2} & \text{for liquid water} \end{cases}$$

and c_h is at least one order of magnitude smaller.

Case 2:

Then consider any element away from the well and assume that the fluid is one-phase throughout:

$$PWK_e \simeq \bar{p}\left[\int_{S_{inner}} \langle v_j \rangle n_j dA + \int_{S_{outer}} \langle v_j \rangle n_j dA\right] = \bar{p}\left(\frac{\dot{M}}{\langle\bar{\rho}\rangle}_{outer} - \frac{\dot{M}}{\langle\bar{\rho}\rangle}_{inner}\right)$$

$$\sim \frac{\dot{M}\bar{p}\Delta\bar{\rho}}{\bar{\rho}^2} \qquad \text{with } \Delta\bar{\rho} \equiv \langle\rho\rangle_{outer} - \langle\rho\rangle_{inner}$$

$$PWK_e \sim \beta\bar{p}\dot{M}\frac{\Delta\bar{p}}{\bar{\rho}}$$

$$PWK_h \sim \frac{\dot{M}\Delta\bar{p}}{\bar{\rho}}$$

$$CNV_e = \dot{M}(e_{outer} - e_{inner}) \equiv \dot{M}\Delta\bar{e}$$

$$CNV_h = \dot{M}\Delta\bar{h}$$

Thus:

$$c_e \sim \beta\bar{p}\frac{\Delta\bar{p}}{\bar{\rho}\Delta\bar{e}} \quad , \qquad c_h \sim \frac{\Delta\bar{p}}{\bar{\rho}\Delta\bar{h}}$$

$$\frac{c_h}{c_e} \sim \frac{1}{\beta\bar{p}}\frac{\Delta\bar{e}}{\Delta\bar{h}}$$

where $\beta\bar{p} \sim 1$ for steam considered as a perfect gas and (see e.g. Helgeson and Kirkham, 1974):

$$\beta\bar{p} \sim (3.10^{-4} m^2/N)(7.9\ 10^6\ N/m^2) \simeq 2.10^3 \text{ for liquid water}$$

Assuming a piezometric gradient of 10^{-1} and an element width ℓ_e of 100 meters yields the following approximate figures:

$$\Delta\bar{p} \simeq 7.\ 10^4\ N/m^2$$

$$\Delta\bar{e}_L \simeq -\ 180\ J/kg \qquad \Delta e_G \simeq -\ 2800\ J/kg$$

$$\Delta\bar{h}_L \simeq +\ 80\ J/kg \qquad \Delta\bar{h}_G \simeq +\ 3800\ J/kg$$

Then, for liquid water:

$$\frac{c_h}{c_e} \sim 10^{-3} \quad , \quad c_e \sim 10^3 \quad , \quad c_h \sim 1$$

for steam:

$$\frac{c_h}{c_e} \sim 1 \quad , \quad c_e \sim 1 \quad , \quad c_h \sim 1$$

Case 3:

Finally, once again consider any element away from the well but assume that complete flashing (or condensation) occurs within it; given the assumption of isothermal process, the vapor zone lies closest to the well:

$$PWK_e \sim \bar{p}\left(\frac{\dot{M}}{\bar{\rho}_G} - \frac{\dot{M}}{\bar{\rho}_L}\right) = \dot{M}\bar{p}\,\frac{\bar{\rho}_L - \bar{\rho}_G}{\bar{\rho}_L\bar{\rho}_G} \sim \dot{M}\,\frac{\bar{p}}{\bar{\rho}_G}$$

$$PWK_h \sim \bar{v}_G\nabla\bar{p}_G V_{eG} + \bar{v}_L\nabla\bar{p}_L V_{eL} \sim (\bar{v}_G + \bar{v}_L)\,\nabla\bar{p}V_e \sim \left(\frac{\dot{M}}{\bar{\rho}_G A_c} + \frac{\dot{M}}{\bar{\rho}_L A_c}\right)\left(\frac{\Delta\bar{p}}{\ell_e}\right)(A_c\ell_e) \sim \frac{\dot{M}\Delta\bar{p}}{\bar{\rho}_G}$$

$$CNV_e \sim \dot{M}\,(\bar{e}_G - \bar{e}_L) \quad , \quad CNV_h \sim \dot{M}\,(h_G - h_L)$$

Thus:

$$c_e \sim \frac{\bar{p}}{\bar{\rho}_G(\bar{e}_G - \bar{e}_L)} \sim 10^{-1} \quad , \quad c_h \sim \frac{\Delta\bar{p}}{\bar{\rho}_G(\bar{h}_G - \bar{h}_L)} \sim 10^{-3} \quad , \quad \frac{c_h}{c_e} \sim \frac{\Delta\bar{p}}{\bar{p}}\,\frac{\bar{e}_G - \bar{e}_L}{\bar{h}_G - \bar{h}_L} \sim 10^{-2}$$

Summary

Case number		c_e	c_h	c_e/c_h
1	liquid water	10^{-1}	10^{-2}	10^{-1}
	steam	10^{-2}	10^{-3}	10^{-1}
2	liquid water	10^{3}	1	10^{-3}
	steam	1	1	1
3		10^{-1}	10^{-3}	10^{-2}

Table 1

Under steady-state conditions:

i) equation (43h) involves a lesser amount of coupling than does equation (43e).

ii) the pressure-work term cannot be safely neglected.

APPLICATION OF THERMAL DEPLETION MODEL TO GEOTHERMAL RESERVOIRS WITH FRACTURE AND PORE PERMEABILITY

P. W. Kasameyer and R. C. Schroeder*
Earth Sciences Geothermal Group
University of California
Lawrence Livermore Laboratory
Livermore, California 94550

The useful lifetime of a geothermal resource is usually calculated by assuming fluid will be produced from and reinjected into a uniform porous medium. However, most geothermal systems are found in fractured rock. If the reinjection and production wells intersect connected fractures, then reinjected fluid may cool the production wells much sooner than would be predicted from calculations of flow in a porous medium.

We have developed a "quick and dirty" method for calculating how much sooner that cooling will occur (Kasameyer and Schoeder, 1975, 1976). In this paper, we discuss the basic assumptions of the method, and show how it can be applied to the Salton Geothermal Field, the Raft River System, and to reinjection of supersaturated fluids.

Solution for Flow in a Porous Medium

We model a finite hot-water reservoir produced at a constant flow rate with fluid replenished either by reinjection or by cool recharge at the boundaries. We assume that an idealized well distribution can be found which allows a specified flow rate and which produces all of the original fluid from the reservoir before any reinjected fluid has been produced. Further, we assume there is no pressure drawdown or flashing, that the fluid moves with piston displacement through the pores, and that the pore fluid and matrix come to thermal equilibrium instantaneously. All these assumptions lead to an over-estimate of the production temperature.

An analytical solution for this idealized problem of heat transfer has been discussed by Bodvarsson (1974). A steep temperature front moves through the system with no change of shape with time, and with a slower velocity than the fluid front. Ahead of the temperature front, the reservoir retains its initial temperature. Behind the front, enough heat has been taken from the rocks to cool them to the reinjection temperature.

---

* R. C. Schroeder is now with Lawrence Berkeley Laboratory

Solution in the Presence of Fractures

A family of fractures is assumed to exist parallel to the direction of flow. The fractures are characterized by a permeability k_{fr} and a spacing D. (For the results presented here, the fractures are tight enough so that water storage in them is negligible.) The fractures are assumed to have no effect on the pressure field so that the flow stream lines are parallel in the porous rock and in the fractures, but the flow velocities are different.

The solution of a problem with two distinct velocities by a finite difference method (e.g., Kasameyer and Schroeder, 1975) is not efficient if the velocities are quite different. In that case, time steps must be determined by the most rapid velocity and calculations take a long time when fractures are important. An approximate solution requiring a few time steps has been developed. The reservoir is conceptually divided into 10 regions of equal volume. The boundaries of the regions coincide with flow fronts of the reinjected fluid so that the fluid in the pores and the fluid in the fractures both flow through the regions in series (see Figure 1). In each region, we write pairs of approximate equations relating the temperature of the fluid in the fractures averaged throughout the region, T_{fr}, to the average temperature of the saturating fluid, T_s. The 10 pairs of coupled first-order equations are solved analytically by assuming constant coefficients during time intervals which are much longer than those appropriate for the finite-difference method.

The equations for the i^{th} region are presented here in dimensionless form (see Kasameyer and Schroeder, 1976, for the derivations). The times have been multiplied by α = (thermal diffusivity)/$(D/2)^2$.

$$\frac{dT_{fr}}{dt} = \frac{-R_q(1+R_\mu)}{R_\mu(1+R_q)} \frac{M}{\tau^*} (T_{fr}-T_{fro}) + H$$

$$\frac{dT_s}{dt} = \frac{-(1+R_\mu)}{(1+R_q)} \frac{M}{\tau^*} (T_s-T_{so}) - R_\mu H$$

The equations depend only on three dimensionless constants

$$R_q = \frac{\text{Flow in Fractures}}{\text{Flow in pores}}$$

$\tau^* = \alpha\tau$ where τ is the lifetime based on a porous flow calculation.

$$R_\mu = \frac{\text{Heat stored in fractures}}{\text{Heat stored in saturated rock}}$$

The fluid enters the pores and fractures of region i at temperatures T and T_{so}, respectively. These temperatures are determined from the solution for region i-1, or by the reinjection temperature if i=1.

The term H is the heat conducted from the saturated rock into the fractures. That term is approximated by an expression depending only on the time and the instantaneous values and derivatives of the average temperatures.

$$H = \frac{F(t)}{R_\mu}\left[\frac{(1-T_{fr})}{\sqrt{\pi t}} - \frac{2}{R_\mu}\sqrt{\frac{t}{\pi}}\frac{dT_{fr}}{dt}\right] + \frac{2\,[1-F(t)]}{R_\mu}\,(T_s - T_{fr})$$

The function $F(t)$ varies smoothly from one at early times to zero at late times.

The approximation of H is justified by the close agreement of our calculations of the temperature in fractured, impermeable rock with those of Gringarten, et al., (1975), shown in Figure 2. Results presented at the Stanford Workshop in 1975 (Kasameyer and Schroeder, 1975) indicated better agreement between the methods, but those results were for a small range of values of τ^* and were based on the very slow finite-difference calculation with a large number of regions. Our answers differ from those of Gringarten, et al. because 1) we over-estimate the heat transfer to the fracture fluid at early times, and 2) the thermal front is smoothed out at late times because of averaging over large regions.

Correction Factors for Porous Flow Models

A set of calculated production temperature histories are shown in Figure 3. Results from many such calculations can be summarized in one figure by calculating the time, t_f, when the production temperature falls below a specified value. That value would normally be determined from power generating equipment. For the examples presented below, we have chosen a value of 0.8. The ratio of t_f/τ for different fracture systems and production rates is a correction factor for the useful lifetime.

The values of that correction factor for small R_μ are contoured in Figure 4. The contours depend on R_μ and τ^*. For no flow in fractures (Rq < 1) or for slow removal of fluid ($\tau >> 1/\alpha$), the porous medium calculations are correct. If those conditions are not met, the correction factor can be determined from this diagram.

Examples

I. The Salton Sea Field

The τ^* values have been related to fracture spacings (D) by assuming parameters appropriate for the Salton Sea Geothermal Field (Figure 4). Two scales of fracture systems are seen in that field. Fractures are seen in cores with spacings less than a meter. From Figure 4, we see that flow in these fractures will not shorten the useful lifetime of the field. Faults hundreds of meters apart influence the flow in several wells. If these faults carry more than half the fluid, produced and reinjected wells, the useful lifetime may be drastically shorter than predicted from porous flow calculations.

II. A Fracture-Dominated System Like Raft River

If most of the flow is from fractures, then the correction factor depends only on the fracture spacing and the rate at which heat is removed from the system. In Figure 5, we see that the dependence of the correction factor on pumping rate can be strong, and knowledge of the fracture spacing in such a system is crucial for planning exploitation rates.

III. Reinjection of Super-saturated Brines

It may be practical to inhibit silica deposition in a geothermal power plant by brine modification. Acidification of Salton Sea brine inhibits deposition of siliceous scale and decreases rates of precipitation of silica and sulfides long enough to produce power from the brine and reinject it into the ground (Owen, 1975; Owen and Tardiff, 1977). However, the formation around a reinjection well may become badly plugged by silica if the reinjected brine is not reheated rapidly.

The length of time reinjected brine stays cool can be estimated. If the fluid is injected into a porous medium, a steep boundary between warm and cool rock moves at a velocity less than the particle velocity. If R is the fraction of the heat of the reservoir stored in the pore fluid ($R \tilde{} .3$ for 15% porosity), then the temperature moves at velocity RV_p, where V_p is the particle velocity.

Particle paths and temperature boundary locations for radial flow areound a well are shown in Figure 6. A particle injected at time t after the well started flowing remains cool for a period of time, t_c, where

$$t_c = \frac{R}{1-R} t_p \approx .4\ t_p \text{ for } R = .3$$

As shown in Figure 6, brine injected one year after injection begins will remain cool for nearly half a year. Short-term injection tests may not indicate the full potential for injection well damage, because the first brine which is injected will be rapidly reheated. The kinetics of precipitation from super-saturated brines and the temperature dependence of the rates of possible rock-brine interactions must be studied in order to predict the long-term success of reinjection.

References

Bodvarsson, G., On the temperature of water flowing through fractures, J. Geophys. Res., 74, 1967, 1969.

Gringarten, A. C., P. A. Witherspoon, and Y. Onishi, Theory of heat extraction from fractured hot dry rock, J. Geophys. Res., 80, 1120, 1975.

Kasameyer, P. W., R. C. Schroeder, Thermal depletion of liquid-dominated geothermal reservoirs with fracture and pore permeability, in Report of Workshop on Geothermal Reservoir Engineering, Paul Kruger and Henry J. Ramey, Jr. Eds., Stanford Geothermal Program, SGP-TR-12, 1975.

Kasameyer, P. W., and R. C. Schroeder, Thermal depletion of a geothermal reservoir with both fracture and pore permeability. Submitted to J. Geophys. Res., 1976.

Owen, L. B., Precipitation of amorphous silica from high-temperature hypersaline geothermal brines, Lawrence Livermore Laboratory Report, UCRL-51866, 1975.

Owen, L. B. and G. E. Tardiff, Eds., Lawrence Livermore Laboratory Energy Program: brine chemistry and materials status report, UCRL Report (in preparation), 1977.

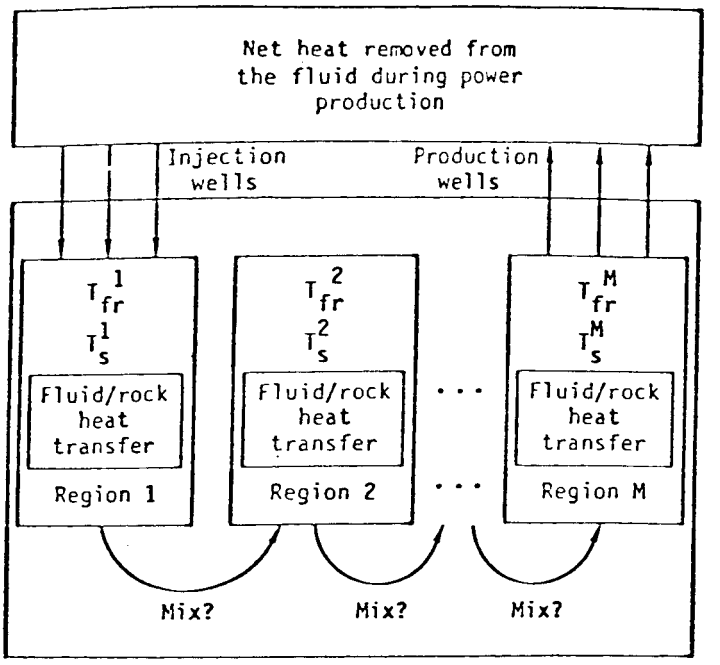

FIGURE 1. Division of reservoir into a small number of regions.

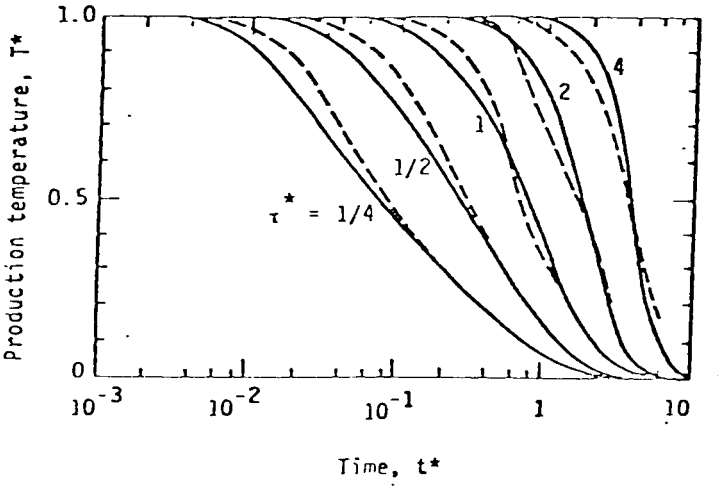

FIGURE 2. Comparison of our calculated curves for the output temperature from fractured impermeable rock (dashed) with those of Gringarten et al., 1975, (solid). Their values have been converted to our dimensionless format, where $t^* = \alpha t$.

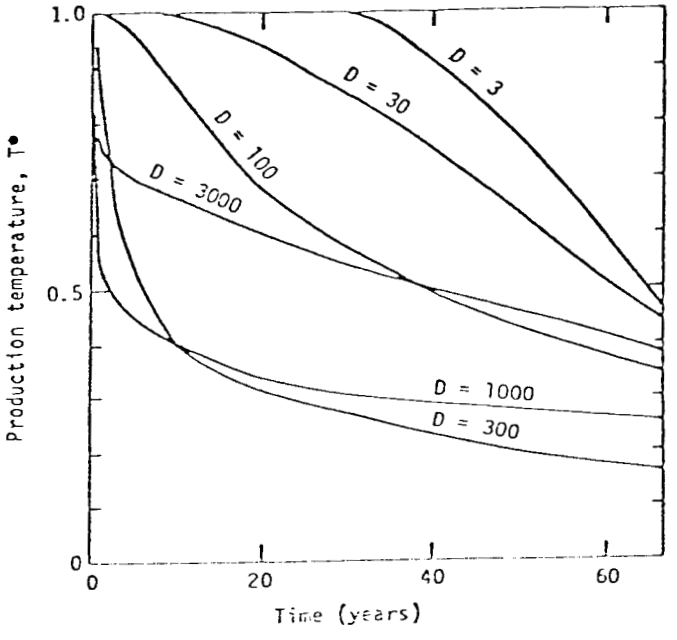

FIGURE 3.

Thermal depletion curves for different fracture spacings D (in meters). The parameters were chosen so that all the original pore fluid would be produced after 20 years, and the useful lifetime (τ) based on the exact porous flow calculation was 66 years.

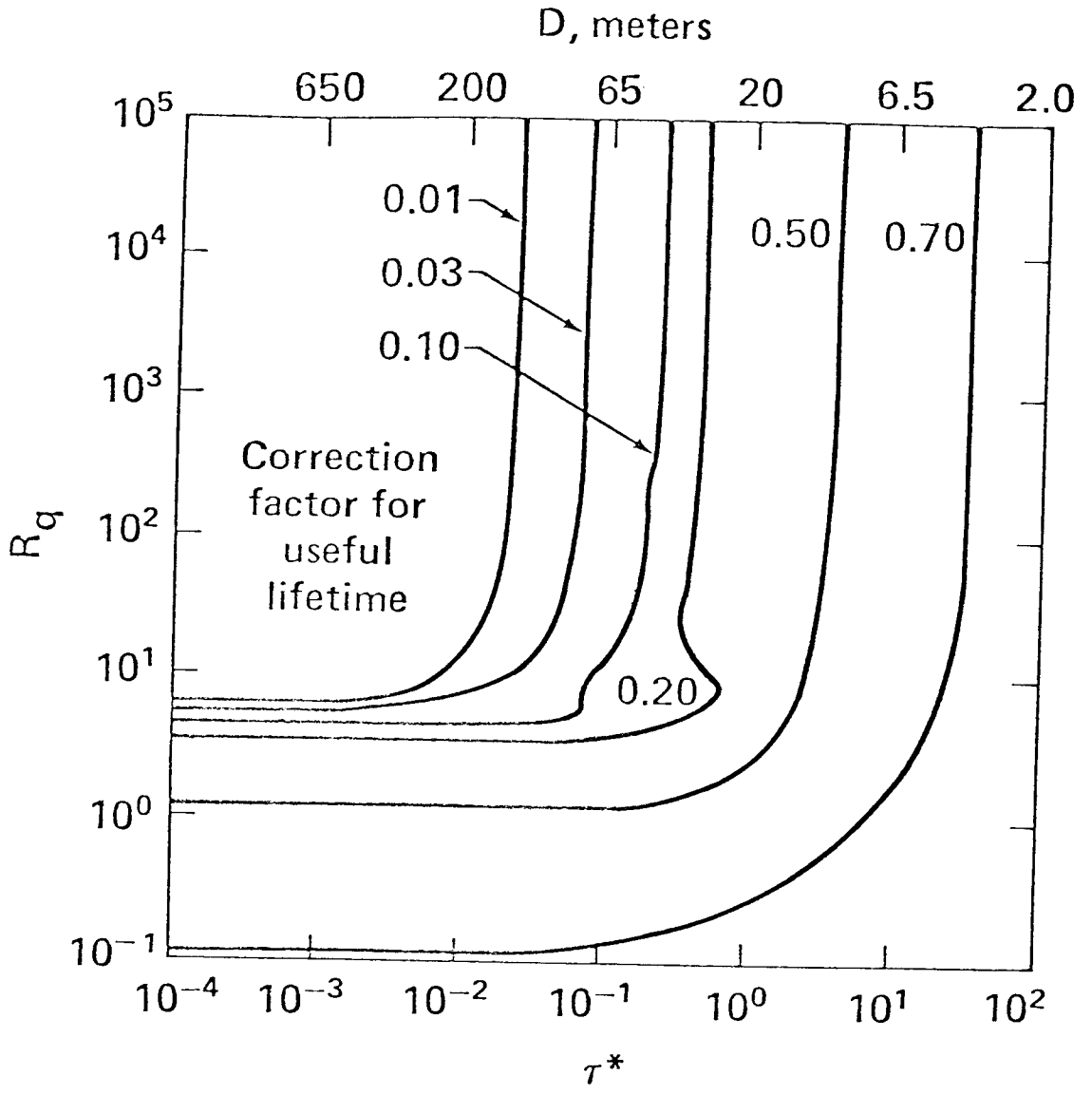

FIGURE 4.

Correction factor for lifetime estimates. The production temperature falls to 0.8 at t'_f. The ratio of t_f/τ is contoured for different flow distribution (Rq) and production rates (τ^*). The contour where the factor equals 0.20 is distorted because of our approximation of term H. The fracture spacings (D) are appropriate for the Salton Sea Field example.

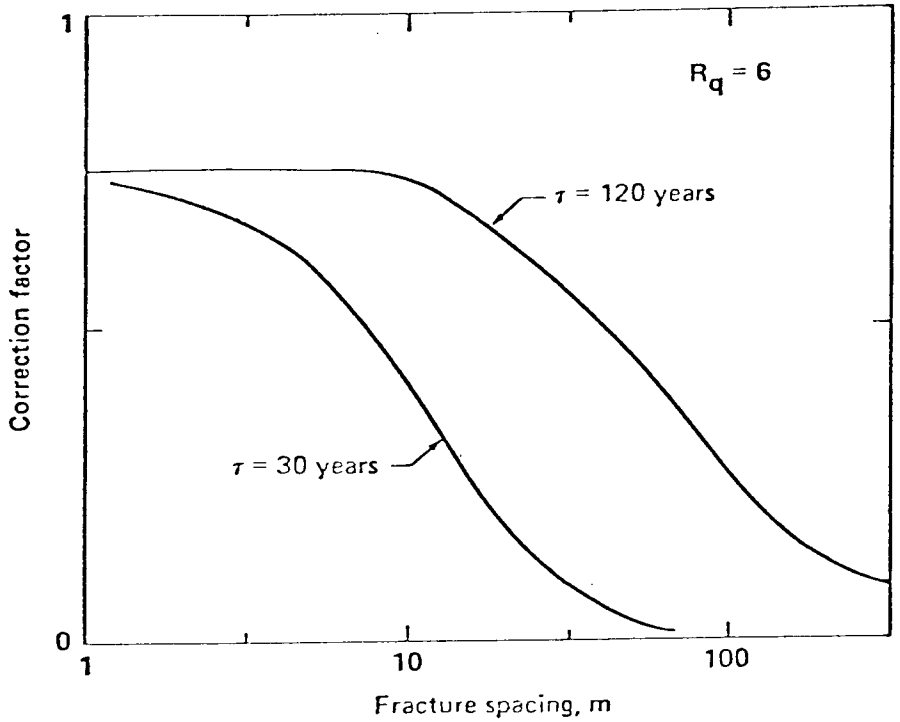

FIGURE 5. The effect of production rate on the correction factor. If the fracture spacing is around 10 meters, more than twice the energy can be removed from the system at the slow production rate (τ = 120 years) as at the fast rate (τ = 30 years).

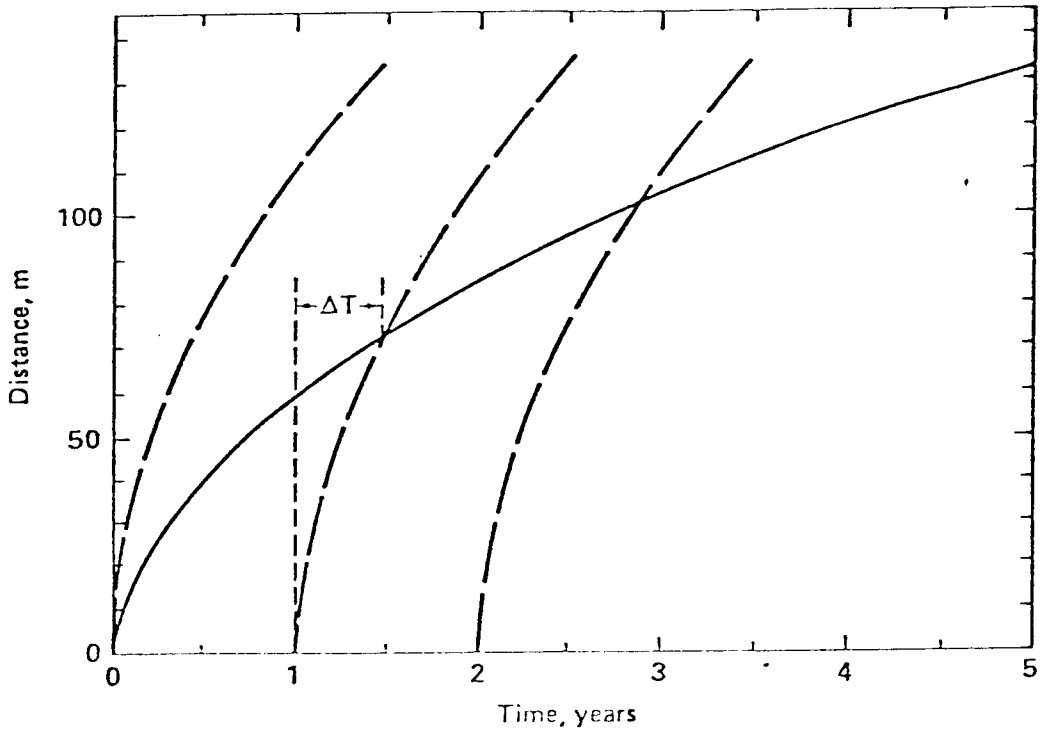

FIGURE 6. Location of temperature front and fluid particles as function of time since reinjection started. The curves in the figure are for (R = 0.3, and radial flow of 0.05 m^3/sec. into a 200m thick aquifer with 20% porosity. The solid line shows the distance to the temperature front. The dashed curves are the trajectories of particles injected at different times. A particle injected one year after injection started remains cool for ΔT years.

MODELING OF TEXAS GULF COAST GEOPRESSURED GEOTHERMAL AQUIFERS

R. M. Knapp, M. H. Dorfman and O. F. Isokrari*
Petroleum Engineering Department
The University of Texas at Austin
Austin, Texas 78712

We would like to report that, at this time, we have coded and tested a model that simulates the behavior of a geopressured geothermal aquifer as it is subjected to production from one or more wells. We have tested this simulator by checking its computed responses against results reported for systems that span the range of the abilities of the simulator.

The general objective of our work was to develop and test a simulator for geopressured geothermal aquifers. The simulator considers the effects of heterogeneous and anisotropic porous media, and the presence of two fluid phases, water and natural gas. The natural gas can exist either in solution or as a separate and distinct flowing phase. The model includes several drive mechanisms which we feel will be significant: these include the water compressibility, the rock matrix compressibility, the changes that occur in pore volume as the aquifer is compacted, the influx of water from adjacent shales either at the edge of the sandstone body or immediately above it or below it, and the expansion of the natural gas either in solution or as a free-phase. We feel that such a model can be used for depletion studies. With the addition of thermal effects it can be used to study the feasibility of reinjection of "cool" used water.

The simulator is the result of combining the momentum transport equation for water and gas with constitutive equations describing the changes of fluid properties with pressure and the changes of formation parameters, such as porosity, permeability and formation thickness with decreasing pore pressure. The resulting equations, shown in the appendix, are solved using finite difference methods to obtain pressure distributions within the aquifer. The energy transport equation can be added to the set of equations and solved to obtain temperature distributions. At the University of Texas, we have done this in a decoupled fashion in order to examine long-term effects. We do not feel that this is adequate for the thermodynamically demanding case of water reinjection.

The goal of the model development was to have a mechanism for performing reservoir engineering studies on potential geopressured geothermal aquifers. The first example of this was performed on a prospect in eastern Kenedy County, Texas, (Knapp and Isokrari, 1976). An isopachous map of the prospect was used to construct a rectangular cube of equal volume and area. This resulted in a reservoir 4.5 miles by 9 miles that was 162 feet thick. At the expected initial pressure of 11,000 psia, the average formation porosity was estimated to be 0.216 and the average permeability was estimated to be

---

*Dr. Isokrari is now with Amoco Production Company, P. O. Box 591, Tulsa, Oklahoma 74102.

18 millidarcies based on well log and core data. The reservoir fluid was assumed to be fresh water at 300°F. Five depletion studies using a single well producing 40,000 BBLS/day were made to investigate the effectiveness of various drive mechanisms. These are shown in Fig. 1. In the first case, the only active producing mechanism was the expansion of the water. It will be noted that the producing well pressure drops to 5,000 psi in about 7 years. We stopped the calculations at that point because 5,000 psi is approximately the hydrostatic pressure at the expected well depth of 13,000 feet. For Case II, a rock matrix compressibility of 7.5×10^{-6} psi^{-1} was added. It can be seen that the well pressure dropped to just below 8,000 psia after 30 years of production. A compaction coefficient of 4.6×10^{-6} psi^{-1} was added for Case III. In this instance, the well pressure remains above 9,000 psia for the full thirty-year producing period. To simulate the effects of shale water influx from off-shore shales, a shale section was added which has a width of 2.5 miles and a length and thickness identical to that of the sandstone formation. The shale porosity at 11,000 psia was assumed to be the same as the sandstone porosity, or 0.216; the initial shale permeability was estimated to be 10^{-4} millidarcies and the shale matrix compressibility was assumed to be 7.5×10^{-4} psi^{-1}. The shale uniaxial compaction coefficient was assumed to be 4.6×10^{-5} psi^{-1}. This run is shown as Case IV. The well block pressure is sustained at a higher level than in the other runs although the amount of support due to shale water influx is not greatly enhanced. Other runs, on a reduced system, show that the effects of underlying sediments are much greater (Knapp and Isokrari, 1976). Finally, the effects of adding 44.1 scf/STB of natural gas to the formation water are shown as Case V in Fig. 1. The small amount of gas along with its very small saturation combine to provide only a small amount of additional pressure support for production.

Since one well would not produce enough water for significant electric power production, the depletion of the aquifer using eleven 40,000 BBLS/day wells was simulated. The average reservoir pressure fell below 7,000 psi in about ten years. The single sand unit could not support a power generation plant for a long enough period of time to depreciate it. There are, however, other sand bodies of a similar size in this prospect that could also be produced, which would extend the useful life of the system.

The model was next used to study the production of natural gas from geopressured geothermal aquifers, (Isokrari and Knapp, 1976). We classified such aquifers into three types based on the natural gas content. In Type 1, the reservoir water is undersaturated with natural gas. However, it could still contain more than 40 standard cubic feet of natural gas per reservoir barrel of water at reservoir conditions. In Type 2 reservoirs, the reservoir water is fully saturated with natural gas and the reservoir may contain a small gas cap. Type 3 is a geopressured gas reservoir. The water is nearly immobile in the reservoir but the adjacent and underlying shales contain water with gas in solution, that may move into the reservoir.

Computer runs were made to generate a variety of data. For Type 1 and Type 2 reservoirs, reservoir pressure variations with natural gas and water production were generated. It was found that substantial amounts of natural gas can be produced over a long period of time.

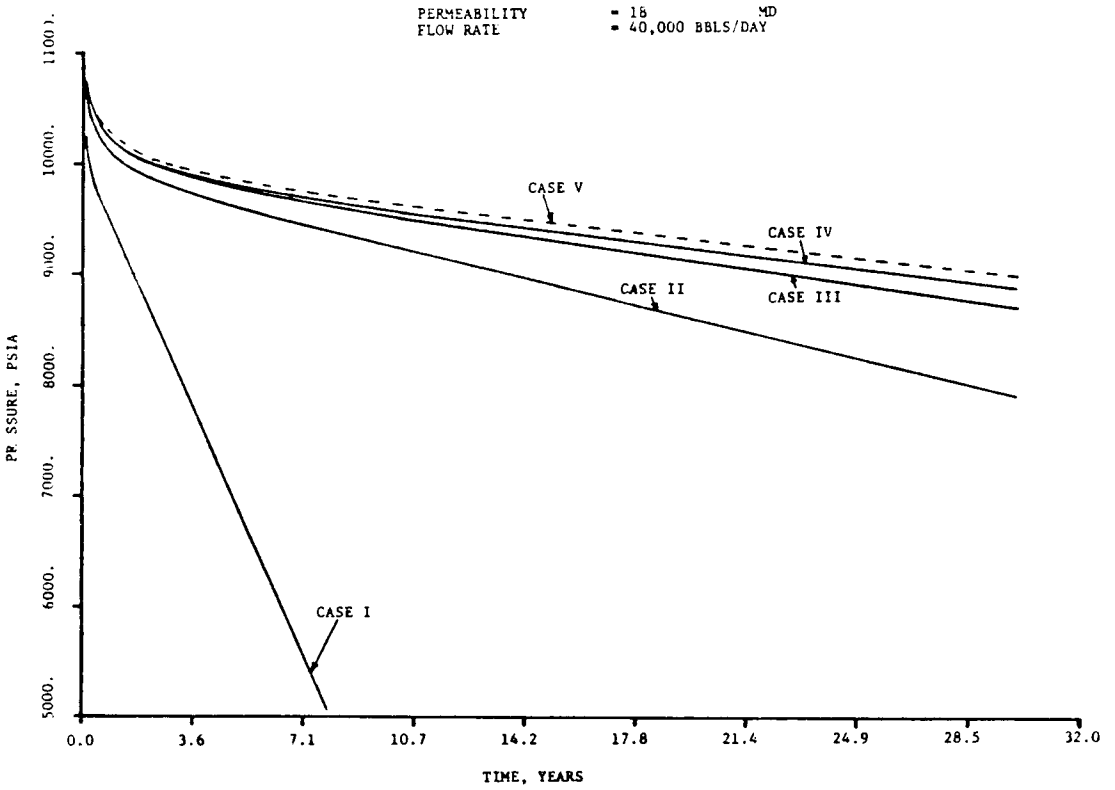

Figure 1

PRESSURE WELL BLOCK PORE PRESSURE OF VARIOUS RESERVOIR DRIVES WITH TIME

The model was used to make areal studies of a bounded hypothetical geopressured gas reservoir, with no shale water influx using different compaction coefficients. It was found the P/Z (average reservoir pressure divided by gas deviation factor) versus cumulative production curve changes significantly with an increase in compaction coefficients.

The model was also used to make cross-sectional studies to assess the effects of shale water influx from adjacent and underlying shales.

Finally, the model was used to simulate the reported production history of the Anderson 'L' zone, a geopressured Frio (Oligocene) gas reservoir in South Texas described by Duggan (1972). Good agreement was obtained between the observed and calculated pressures and water production versus cumulative gas production.

References

Duggan, J. L., 1972, "The Anderson 'L' - An abnormally pressured gas reservoir in South Texas," J. Pet Tech. (Feb. 1972) p. 132-138.

Isokrari, O. F. and R. M. Knapp, 1976, "Natural gas production from geothermal geopressured aquifers," SPE6037, Society of Petroleum Engineers of AIME, 6200 North Central Expressway, Dallas, Texas 75206.

Knapp, R. M. and O. F. Isokrari, 1976, "Aspects of numerical simulation of future performance of geopressured geothermal reservoirs," Proceedings, Second Geopressured Geothermal Energy Conference, Center for Energy Studies, University of Texas at Austin, Austin, Texas (Feb. 23-25, 1976) vol. III.

APPENDIX

The basic equations for a deformable heterogeneous, anisotropic and nonisothermal reservoir as presented by Knapp and Isokrari (1976) are:

Momentum Transport in Water Phase:

$$\bar{\nabla} \cdot \frac{\rho_w K_{rw}}{\mu_w} K(\bar{\nabla}P_w - \frac{\rho_w}{144}\frac{\bar{g}}{g_c}\bar{\nabla}h) + \frac{\rho_{w_{sc}} q_w}{V_P^*} = (\phi S_w(\frac{\partial \rho_w}{\partial P})_T + (\rho_w S_w) \cdot (C_m + C_{rm}(1-\phi)))\frac{\partial P_w}{\partial t}$$

$$+ (\phi\rho_w)\frac{\partial Sw}{\partial t} + (\phi S_w(\frac{\partial Sw}{\partial T})_P)\frac{\partial T}{\partial t} \quad \ldots\ldots\ldots\ldots\ldots\ldots\ldots\ldots\ldots\ldots (1)$$

Momentum Transport in Gas Phase:

$$\bar{\nabla}(\rho_g \frac{K_{rg}}{\mu_g} K(\bar{\nabla}P_g - \frac{\rho_g}{144}\frac{\bar{g}}{\bar{g}_c}\bar{\nabla}h)) + \bar{\nabla}(\rho_w \frac{K_{rw}}{\mu_w} R_{sw} K(\bar{\nabla}Pw - \frac{\rho_w}{144}\frac{\bar{g}}{\bar{g}_c}\bar{\nabla}h)) + \frac{\rho_{w_{sc}} R_{w_{sc}} q_w}{V_P^*}$$

$$+ \frac{\rho_{g_{sc}} q_g}{V_P^*} = (\phi S_g(\frac{\partial \rho_g}{\partial P})_T + \phi S_w R_{sw}(\frac{\partial \rho_w}{\partial P}) + (\rho_w S_w R_{sw} + \rho_g S_g) \cdot (C_m + C_{rm}(1-\phi)))\frac{\partial P}{\partial t}$$

$$+ (\phi\rho_g)\frac{\partial S_g}{\partial t} + (\rho_w R_{sw}\phi)\frac{\partial S_w}{\partial t} + (\phi\rho_w S_w)\frac{\partial R_{sw}}{\partial t} + \phi((S_w R_{sw}(\frac{\partial \rho_w}{\partial T})_P$$

$$+ (1-S_w) \cdot (\frac{\partial \rho_g}{\partial T})_P))\frac{\partial T}{\partial t} \quad \ldots\ldots\ldots\ldots\ldots\ldots\ldots\ldots\ldots\ldots (2)$$

Energy Transport:

$$[(1-\phi)\rho_{rm}C_{vrm} + (S_g\rho_g C_{vg} + (1+R_{sw})\rho_w S_w C_{vw})\phi]\frac{\partial T}{\partial t} + [(\phi\rho_w S_w C_{vw}\bar{V}_w) + \phi(S_g\rho_g C_{vg}\bar{V}_g$$

$$+ S_w\rho_w R_{sw} C_{vw}\bar{V}_w)] \cdot \nabla T = \nabla \cdot [K_m] \cdot \nabla T + \frac{q_w C_{vw} T}{V_P^*}$$

$$+ \frac{q_g C_{vg} T}{V_P^*} + Q \quad \ldots\ldots\ldots\ldots\ldots\ldots\ldots\ldots\ldots\ldots (3)$$

Note that equations (1) to (3) assume that fluid is homogeneous.

$V_p^* = \Delta X_i \, \Delta Z_j \, W_i \, / \, 5.6146$ BBLS

C_m is the uniaxial compaction coefficient, psia $^{-1}$, defined as:

$$C_m = \frac{1 - \frac{\hat{K}}{\hat{K}_{rm}}}{K + \frac{4}{4}\hat{\mu}_P}$$

where:

$\hat{\mu}_P$ is the shear modulus of the porous rock

$\hat{K}(\hat{K}_{rm})$ is the bulk modulus of the porous rock (bulk modulus of the rock matrix)

$$S_w + S_g = 1 \quad \ldots\ldots\ldots\ldots\ldots\ldots\ldots\ldots\ldots\ldots\ldots\ldots\ldots\ldots (5)$$

$$P_g - P_w = P_c(S_w) \quad \ldots\ldots\ldots\ldots\ldots\ldots\ldots\ldots\ldots\ldots\ldots\ldots\ldots\ldots (6)$$

Constitutive Relationships:

1. Porosity - Pressure/temperature relationship for saturated rock:

$$\phi^{n+1} = \phi^n + (1-\phi^n)(C_{rm}+C_m)[\bar{P}^{n+1}-\bar{P}^n]\big|_T + (1-\phi^n)C_{Trm}[T^{n+1}-T^n]\big|_P \quad \ldots\ldots (7)$$

where:

$\bar{P}$ is of the wetting phase

2. Permeability - Pressure/temperature relationship for saturated rock

$$K^{n+1} = K^{n} \left[1.0 + \left(\frac{C_m + C_{rm}}{1 - \phi^{n}}\right)\left(\bar{P}^{n+1} - \bar{P}^{n}\right) + \left(\frac{C_{Trm}}{1-\phi^{n}}\right)\left(T^{n+1} - T^{n}\right)\right] \quad \ldots\ldots\ldots (8)$$

where:

$K^{n+1}(K^{n})$ = new value of permeability (old value of permeability)
Equation (8) can be shown to be equivalent to:

$$K^{n+1} = K^{n} \text{ EXP } \left[\frac{\phi^{n+1} - \phi^{n}}{(1-\phi^{n})(1-\phi^{n+1})}\right] \quad \ldots\ldots\ldots\ldots\ldots\ldots\ldots (9)$$

3. Compaction of a geologic medium due to fluid withdrawal

$$\Delta\bar{Z} = C_m \, \Delta\bar{P} L_Z + C_{TT} \, \Delta T L_Z \quad \ldots\ldots\ldots\ldots\ldots\ldots\ldots\ldots (10)$$

where:

$$C_{TT} = \frac{3 C_{Trm} \hat{K}}{\hat{K} + \frac{4}{3} \mu_P} \quad \ldots\ldots\ldots\ldots\ldots\ldots\ldots\ldots\ldots\ldots (11)$$

NOMENCLATURE

C_{rm}	Rock matrix compressibility, $psia^{-1}$
C_{Trm}	Coefficient of thermal expansion (T^{-1})
C_v	Specific heat of fluid, BTU/lb-^oF
g	Acceleration of gravity
gc	Acceleration constant (32.12 ft/sec/sec)
h	Depth below a reference datum, ft
K	Absolute permeability, tensor (.001127 x md)
K_r	Relative permeability, fraction
K_m	Thermal conductivity of saturated rock, BTU/D-ft-^oF
P	Pressure, psia
$\bar{P}$	Wetting phase pressure, psia
P_c	Capillary pressure, psia
q	Source - sink volumetric flow rate, STB/D
Q	Heat source strength, BTU/Day-ft^3
R_{sw}	Gas solubility in water (lbs/lbs)
S	Saturation, fraction
T	Temperature, ^oF
t	Time, days
$\bar{v}$	Macroscopic velocity, BBLS/D-ft^2
X,Z	X,Z direction, ft
W	Width (for vertical studies), thickness for horizontal studies

Greek

$\Delta X, \Delta Z$	Block dimensions
ρ	Phase density, lbm/ft^3
ϕ	Porosity
μ	Viscosity

Operators

$\nabla\cdot$	Divergence of a vector in fixed coordinate
$\bar{\nabla}\cdot$	Divergence of a vector in deforming coordinates

Subscripts

c	Constant
g	Gas
i	X direction node index
j	Z direction node index
rm	Rock matrix
w	Water

Superscripts

n	Old time level
n+1	New time level

STATUS OF MODELING EFFORTS FOR THE WAIRAKEI GEOTHERMAL FIELD

James W. Mercer and Charles R. Faust
U.S. Geological Survey
Reston, VA.

The theoretical model used in this study is based on an approach that combines the mass, momentum and energy balances for steam and water into two partial differential equations in terms of the dependent variables, pressure and enthalpy. The assumptions used in this formulation and the detailed development of the equations are presented in Faust (1976). The resulting two- and three-dimensional equations are approximated by finite-difference expressions, and are solved using either direct or iterative matrix techniques.

To simulate the production behavior of the Wairakei geothermal field we have chosen a two-dimensional, areal model. Although a three-dimensional model has been developed for applications to field problems, it is preferable to use two-dimensional models whenever possible, in order to avoid excessive data preparation and computing expense. The two-dimensional, areal model is obtained by partially integrating the pressure-enthalpy equations in the Z-dimension. The resulting two-dimensional equations are thus defined in terms of vertically averaged quantities. In averaging these quantities, it is generally assumed that either (1) the fluids have no segregation, or (2) the fluids are completely segregated.

If the fluids are assumed not segregated, then a further simplifying assumption is generally made: that their properties are uniform throughout the thickness of the reservoir. This leads to the easiest evaluation of the vertically averaged terms, since laboratory determined relative permeability curves may be used in the simulation. However, this assumption is very restrictive as it limits the application of the averaged equations to very thin reservoirs or to laboratory experiments.

The assumption that the fluids are completely segregated is less restrictive. It requires that the fluids are in vertical equilibrium. This concept was first introduced in the petroleum literature by Coats, Nielsen, Terhune and Weber (1967) for the reservoirs having a large capillary transition zone. It was later modified by Coats, Dempsey and Henderson (1971) for reservoirs with a small transition zone. The latter case is similar to the conditions in a geothermal reservoir in which a steam cap (or steam-water mixture at the residual water saturation) exists. In applying the concept of vertical equilibrium it is assumed that the fluid potentials are uniform throughout the reservoir thickness. This corresponds to a gravity segregated fluid distribution with the potential of each fluid being uniform in the portion of the column occupied by that fluid, and requires that the reservoir has good vertical communication. Use of the

assumption of vertical equilibrium and of the additional assumption of a relatively uniform temperature distribution throughout the thickness of the reservoir, permits relationships to be derived for vertically averaged fluid properties as functions of average pressure and enthalpy.

To demonstrate the applicability of this approach to solving field problems, we used our areal two-phase model to simulate the geothermal system located at Wairakei, New Zealand. The Wairakei field was the first hot-water hydrothermal system to be utilized for the generation of electricity. Power generation began at Wairakei in 1958, and by 1968 the power stations at Wairakei were providing 192 MW, or approximately 18% of the total electrical requirements of New Zealand's North Island. Although it is believed that the field was originally all hot water, by 1962 lower portions of the reservoir, where most development is occurring, had become two phase and upper portions probably became two phase much earlier.

Our conceptual model of the Wairakei system is basically the same as that outlined in Mercer, Pinder and Donaldson (1975), with the exception that we now allow for mass leakage through the bottom of the reservoir. The Wairakei hydrothermal system is considered to have been at steady state prior to exploitation. The first step in modeling the Wairakei field is therefore the reproduction of the observed virgin or steady state conditions. These results will be used as the initial conditions for the transient model of exploitation. In order to reproduce the steady-state conditions, the following geological and hydrological data are necessary: 1) isopachs of the unconfined aquifer, the Huka Falls confining bed, and Waiora aquifer, where development is occurring; 2) structure map of one of these layers; 3) initial temperature and pressure distributions; 4) parameters such as permeability, porosity, and thermal conductivity for the aquifer and confining bed; and 5) aquifer discharge measurements.

The results of the steady state simulation are used as initial conditions for the transient model. This modeling effort represents an ongoing project, and the results to be presented will describe the current status of our Wairakei simulation.

References

Coats, K.H., Dempsey, J.R., and Henderson, H.: "The use of vertical equilibrium in two-dimensional simulation of three-dimensional reservoir performance," Soc. Pet. Eng. J. (March 1971) 63-71.

Coats, K.H., Nielson, R.L., Terhune, M.H., and Weber, A.G.: "Simulation of three-dimensional, two-phase flow in oil and gas reservoirs," Soc. Pet. Eng. J. (Dec. 1967) 377-388.

Faust, C.R.: "Numerical simulation of fluid flow and energy transport in liquid- and vapor-dominated hydrothermal systems," PhD thesis, Pennsylvania State U., University Park, Pa. (1976).

Mercer, J.W., Pinder G.F., and Donaldson, I.G.: "A Galerkin-finite element analysis of the hydrothermal system at Wairakei, New Zealand," J. Geophys. Res. (1975) 80. No. 17, 2608-2621.

NUMERICAL SIMULATION OF PRODUCTION AND SUBSIDENCE AT WAIRAKEI, NEW ZEALAND

John W. Pritchett, Sabodh K. Garg, D. H. Brownell
Systems, Science and Software
P. O. Box 1620, La Jolla, California 92038

A numerical simulation of the fluid production history at the Wairakei field has been performed in a two-dimensional vertical plane which passes through the principal features of the reservoir. A successful history match, in terms of the pressure decline in the system, was obtained. Details of that simulation have been reported elsewhere (Garg, et al., 1976) but the results are summarized herein for clarity.

As is well known, substantial land surface subsidence has accompanied production at Wairakei. Both the location of the region of maximum subsidence and the character of the deformation are somewhat anomalous, in that the greatest subsidence occurred outside the production area and substantial evidence exists for non-linear rock behavior during production. The reasons for this peculiar behavior are discussed, and speculations are presented concerning the adequacy of existing subsidence-prediction techniques.

Simulation of Wairakei Production History

The Wairakei geothermal system is located north of Lake Taupo and west of the Waikato River (Figure 1); it occupies a surface area of approximately 15 km^2 (Grindley, 1965), and extends westward from the river approximately 5 km. In order to simulate the behavior of the field, we consider a two-dimensional vertical cross-section (line AB in Figure 1) which extends through the main production area and the region of large surface subsidence. The geologic stratification, as determined from wellbore logs (Grindley, 1965; Grange, 1955) is shown in Figure 2. The numerical grid is shown in Figure 3. Most of the fluid production comes from the Waiora formation (see Figure 3). The Waiora formation dips steeply in the east (Figure 2); the exact depth is, however, unknown and, therefore, the indicated depth in Figure 2 may be in substantial error. To the west, the Waiora formation is cut by the much less permeable rhyolites. There are indications that the reservoir extends beyond A in the west (Bolton, 1970); for purposes of the present study this is, however, not very important. The reservoir is assumed to be 3 km thick (in the direction transverse to AB); this yields a surface area of 15 km^2 for the reservoir. The rock properites (permeability, porosity, density, specific heat, thermal conductivity, etc.) are determined from the available field data (c.f., Mercer, et al., 1975) and studies of core samples performed for S^3 by Terra Tek.

The field behavior was simulated from 1953 through 1967 since the subsidence is well documented (for 1967), and the data readily accessible through 1967. Figure 4 shows a comparison of calculated pressure-drop history for the production area with the data. In general the agreement is extremely good. Borehole 36 is of special interest insofar as it lies toward the eastern end of the field; observed pressure drops in borehole 36 are generally lower than those observed elsewhere in the field. This suggests that the Waiora formation in the east has a lower pearmeability than that in the rest of the geothermal field (c.f., Mercer, et al., 1975). The computed pressures for borehole 36 are also in good agreement with the data (see Figure 4).

The behavior of the Wairakei field, under exploitation, is primarily governed by the saturation temperature-pressure relation for water (Bolton, 1970). The upper portions of the reservoir start flashing soon after the production commences (see Figure 5a.); this helps to maintain the reservoir pressures in the early years (Figures 4, 6a). The two-phase boiling region keeps on growing with continued production; in the years 1959-1960, the two-phase flow begins to invade the production horizon (Figure 5b). Field pressures now (1959-1960) begin to drop rapidly (see Figures 4 and 6b) due to the relative permeability effect in two-phase flow. Eventually (around 1964) the entire production region starts to boil (see Figure 5c); this marks the onset of the relative flattening of the pressure drop curve (Figure 4). The above discussion illustrates the dominating influence exercised by boiling on the reservoir pressure response; as a matter of fact, all the important stages (initial flat portion, middle large pressure drop region, and final relatively flat part, Figure 4) in the reservoir pressure history can be traced to boiling in one or another part of the reservoir.

Subsidence at Wairakei

Ground subsidence at Wairakei was first measured in 1956 when benchmark levels were compared with those established in 1950; periodic measurements have indicated that the area affected by subsidence probably exceeds 25 square miles (Hatton, 1970). The area of maximum subsidence (subsidence $\geq$ 0.5 m), however, lies outside the main production region. Cross-section AB (Figures 1-3) passes through the large subsidence region; the intersection of the subsidence region with AB is indicated in Figure 3. The maximum subsidence region, in the shape of an elliptical bowl, overlies the thicker part of Waiora formation (Figure 3). Maximum subsidence at Wairakei (1964-1974) is of the order of 4.5 m; this has been accompanied by horizontal movements of the order of 0.5 m (Stillwell, et al., 1975; see Figure 7).

Pressure profiles (Figures 6a-c) show that the region of largest pressure drop lies directly below the maximum subsidence area; furthermore, the region of large pressure drop to the west of the subsidence region (i.e., in the thinner part of Waiora) is relatively small. This strongly suggests that the subsidence pattern observed at Wairakei is the combined result of the local geology and the fluid production history.

Laboratory measurements have been performed upon core samples from Wairakei by Terra Tek (see Pritchett, et al., 1976). These measurements yielded, among other quantities, the bulk (K) and shear (μ) elastic moduli of the various strata. If the laboratory measurements are taken as correct for the thin surface layers overlying the reservoir (pumice/breccia and Huka Falls formation), we may determine the effective elastic moduli of the Waiora formation through knowledge of (1) the pressure drop history, (2) the measured subsidence history, and (3) the thickness of the Waiora layer. During the interval 1964-1967, reservoir pressures in the Waiora dropped at a rate of 1.77 bars/year, and the mean subsidence rate in that layer was 0.36 m/year. Using a Waiora thickness of 950 meters, we obtain:

$$\left(K + \frac{4}{3}\mu\right)_{\text{Waiora}} = 4.67 \text{ kilobars.}$$

This value is smaller by a factor of nine than that based upon the small-sample laboratory tests discussed above. This large discrepancy implies that either the Waiora formation in the region of maximum subsidence is much thicker than that assumed in the present simulation or that the Waiora formation is intensely fractured. In view of our analysis of the Wairakei production data and also of available geologic data, we lean towards the second of these explanations.

So far it has been assumed that the rock matrix responds to changes in pore pressure as if it were a linear-elastic material (constant elastic moduli K, μ). There exists substantial evidence which suggests that this assumption is rather poor. Figure 7 (from Stillwell, et al., 1975) is a map of the Wairakei field showing both the areas of principal production and of principal subsidence. Within the subsidence area and somewhat to the south of the center of the region is "Benchmark A-97". Stillwell, et al., (1975) presented both detailed subsidence histories for Benchmark A-97 and measured pressure drop histories at the -150 m (M.S.L.) level in the reservoir. Stillwell's data may be cross-plotted as shown in Figure 8, which illustrates the reservoir pressure drop as a function of the downward movement of Benchmark A-97. The "dots" denote time - 1 January of the year indicated in each case. This plot strongly suggests that nonlinear ground movement processes are operating at Wairakei. At early times, the slope of this (psuedo) stress-strain curve is 36 bars/meter of subsidence - at present, the slope is 2.4 bars/meter, lower by a factor of 15.

On the basis of the subsidence data taken over the interval 1 January 1964 - 1 January 1968, and treating the various formations to be homogeneous and linear elastic, we obtained a mean value of $(K + 4\mu/3)_{\text{Waiora}} \approx 4.67$ kb, above. If we make the assumption that the general trend throughout the area of surface subsidence is qualitatively similar to the behavior shown in Figure 8, we can make more definite statements about the behavior of the reservoir rocks. Over the time interval 1964-1967, Figure 8 shows that the average slope of the pressure

drop-subsidence curve at Benchmark A-97 was 12 bars/meter: a factor of three lower than the initial slope but a factor of five greater than the current slope. This suggests that, at early times (1953),

$$(K + 4\mu/3)_{Waiora} \tilde{\sim} \text{ 14 kilobars}$$

and that, at late times (1975),

$$(K + 4\mu/3)_{Waiora} \tilde{\sim} \text{ 0.9 kilobars.}$$

It is comforting to note that the value of 14 kilobars at early times is substantially closer to the laboratory value than the value of 4.67 kb for the period 1964-1967 - it is low by only a factor of three. The difficulty is, of course, to account for the spectacular decrease in apparent elastic moduli with time.

The apparent increase in rock compressibility at Wairakei with time is typical of many reservoirs (for a case study of an oil/gas reservoir see Merle, et al., 1976). A nonlinearity in the mechanical response of the rock may be ascribed to (1) structural failure at late times and/or (2) decrease in bulk modulus with an increase in $\Delta(P_c-P_f)$. Here, P_c is the total (or "confining") pressure and P_f is the pore pressure. Initially, the reservoir rock behaves in a linear-elastic manner with $K + 4\mu/3 \tilde{\sim} 14$ kbars. From the Benchmark A-97 data, we know that this model is probably adequate up to about 1963. At about that time, however, failure must have begun. Hence, it should be possible to estimate, based upon elastically-calculated 1963 shear stresses, the yield strength of the rock. Rock which has yielded should thereafter be assigned an effective incremental shear modulus of zero. The elastically-calculated 1963 response would also enable us to estimate the threshold value of $\Delta(P_c-P_f)$ at which the bulk modulus K starts to decrease with increasing $\Delta(P_c-P_f)$. The functional dependence of K on $\Delta(P_c-P_f)$ would be, of course, determined by history-matching (see also Merle, et al., 1976 in this connection).

The foregoing discussion illustrates the difficulties associated with matching (and predicting for the future) the subsidence history at Wairakei. It is also worthwhile to point out the implications of our analysis of the Wairakei subsidence data for predicting subsidence in a virgin geothermal field. If for example we attempt to predict subsidence in the Salton Sea field due to some specified production/injection strategy, we would necessarily have to use elastic moduli based on measurements of the early-state moduli (derived from seismic measurements, for instance). If, however, in reality the effective moduli were to decline by a factor on the order of 15 during production as they did at Wairakei, we would thereby drastically underestimate the subsidence hazard. Clearly, it would be desirable to determine the appropriate long-term nonlinear stress-strain relations prior to making such theoretical predictions.

At this time it is not clear how these material parameters can be measured. Neither laboratory tests on small core samples nor pre-production seismic measurements are likely to be of much help. It may be possible to obtain some guidance from the analysis of geological, subsidence, and production data for geothermal and oil/gas reservoirs with well documented production and subsidence histories. Such an analysis may help in identifying the mechanisms which cause the nonlinear behavior. Some examples of such mechanisms are:

1. Geological history of the field.
2. Dewatering of interspersed shales.
3. Thermal effects on the mechanical properties of the rock.
4. Chemical dissolution of intergranular cementing minerals by fresh water recharge.
5. Mechanical scouring and weakening of the matrix by fluid motion.

An understanding of these mechanisms, to the extent necessary to assess their relative magnitudes, appears to be required before devising experimental procedures for characterizing rock response and making subsidence predictions at a virgin geothermal field.

REFERENCES

Bolton, R. S., 1970, The behavior of the Wairakei geothermal field during exploitation, Geothermics, Special Issue 2, pp. 1426-1439.

Garg, S. K., J. W. Pritchett, L. F. Rice and D. H. Brownell, Jr., Study of the geothermal production and subsidence history of the Wairakei Field, Proc. 17th U.S. Symposium on Rock Mechanics, Snowbird, Utah, pp. 3B3-1-3B3-5.

Grange, L. I., 1955, Geothermal steam for power in New Zealand, New Zealand DSIR, Bulletin No. 117.

Grindley, G. W., 1965, The geology, structure, and exploitation of the Wairakei geothermal field, Taupo, New Zealand, New Zealand Geological Survey, Bulletin No. 75.

Hatton, J. W., 1970, Ground subsidence of a geothermal field during production, Geothermics, Special Issue 2, pp. 1294-1296.

Mercer, J. W., G. F. Pinder, and I. G. Donaldson, 1975, A Galerkin-finite element analysis of the hydrothermal system at Wairakei, New Zealand, Journal of Geophysical Research, 80, pp. 2608-2621.

Merle, H. A., J. P. Kentie, C. H. C. Van Opstal and G. M. E. Schneider, 1976, The Backaquero study - a composite analysis of the behavior of a compaction drive/solution drive gas reservoir, J. Petroleum Technology, pp. 1107-1115.

Pritchett, J. W., S. K. Garg, D. H. Brownell, Jr., L. F. Rice, M. H. Rice, T. D. Riney and R. R. Hendrickson, 1976, Geohydrological environmental effects of geothermal power production - Phase IIA, Systems, Science and Software Report SSS-R-77-2998, La Jolla, California.

Stillwell, W. B., W. K. Hall and J. Tawhai, 1975, Ground movement in New Zealand geothermal fields, Proc. 2nd U. N. Symp. on the Development and Use of Geothermal Resources, San Francisco, California, pp. 1427-1434.

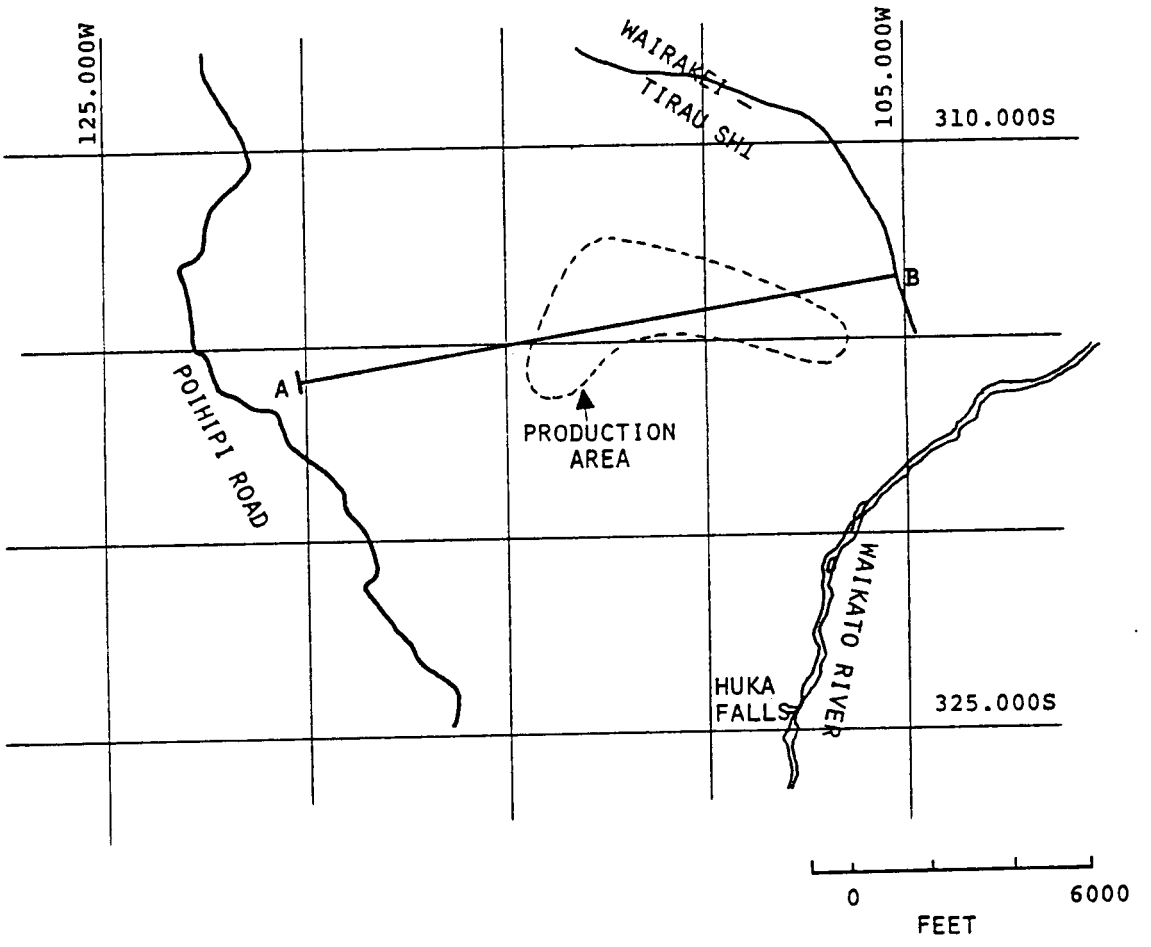

Figure 1. Map showing location of cross-section A-B, of length 5 km, of Wairakei field.

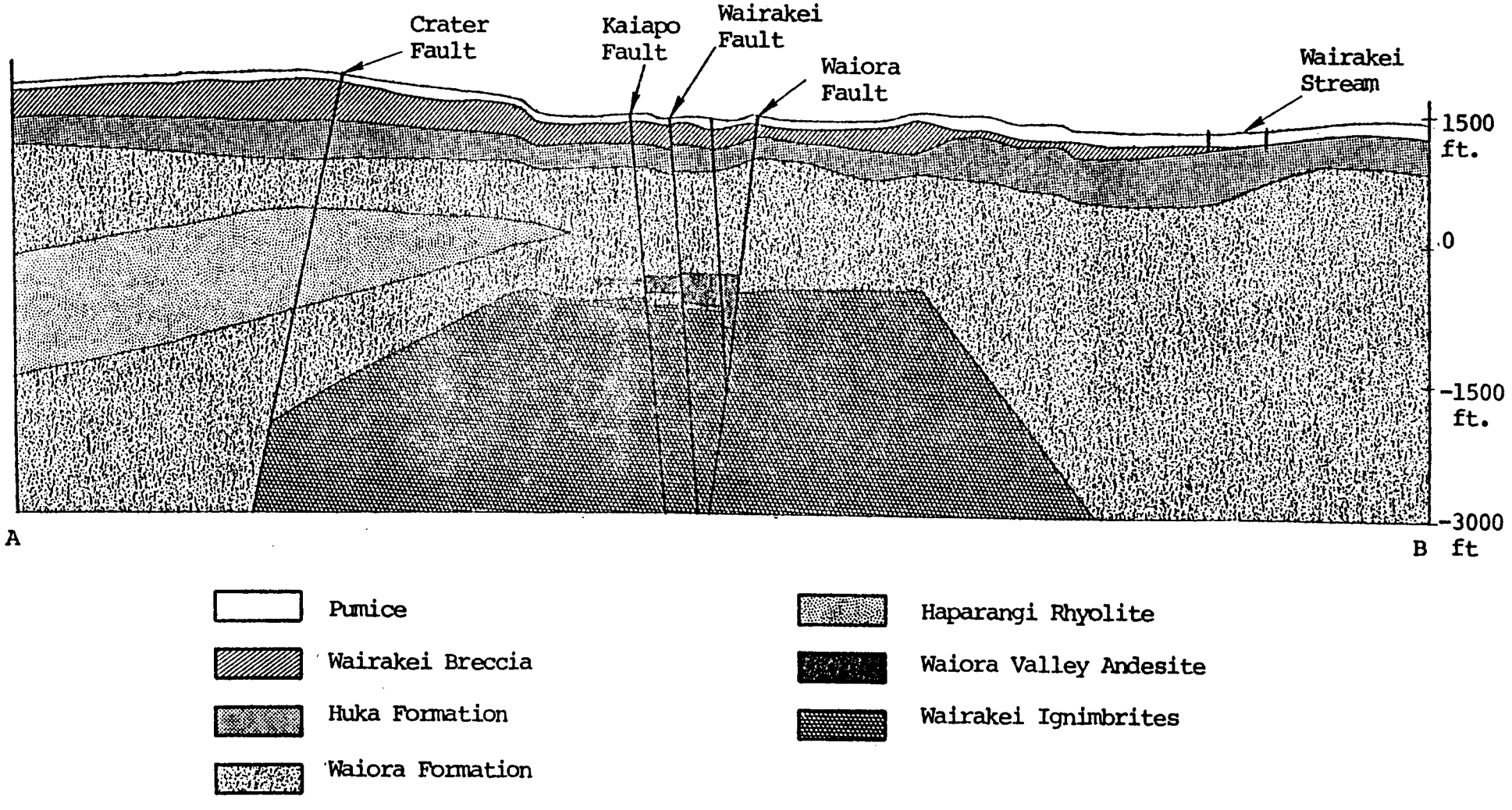

Figure 2. Cross-section of Wairakei field.

Figure 3. Computational grid for two-dimensional vertical cross-section of Wairakei.
X - production region (1967).

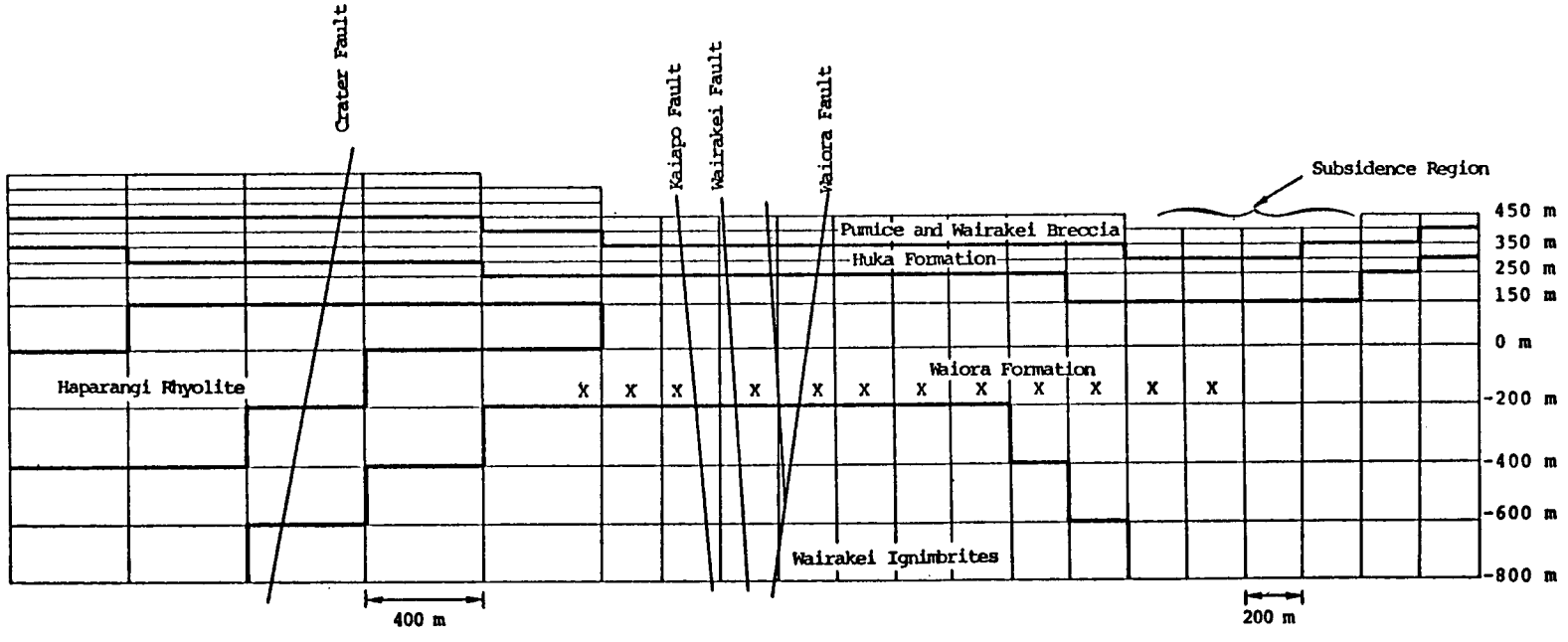

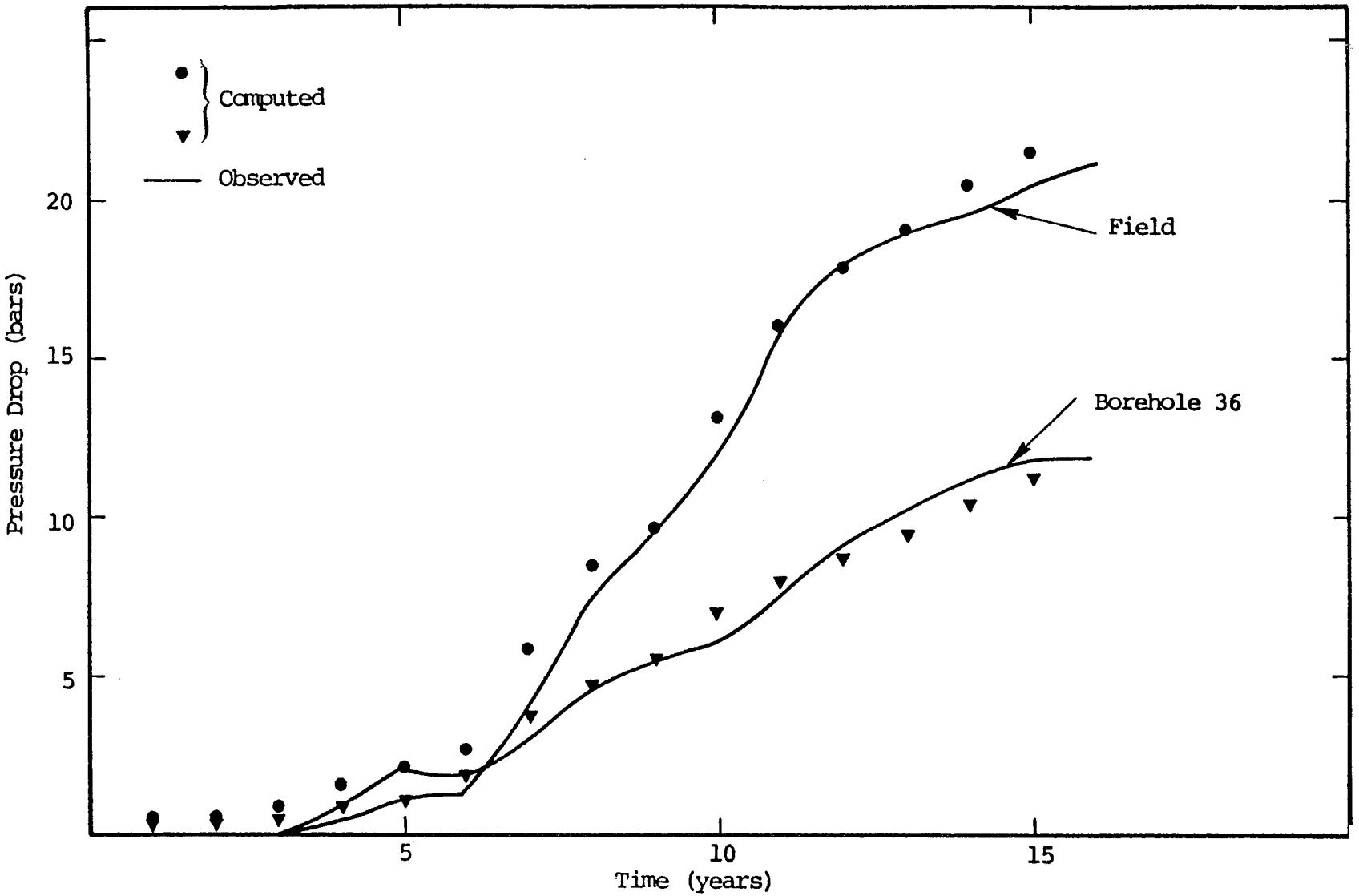

Figure 4. Comparison of calculated pressure drop (field and borehole 36) histories with data.

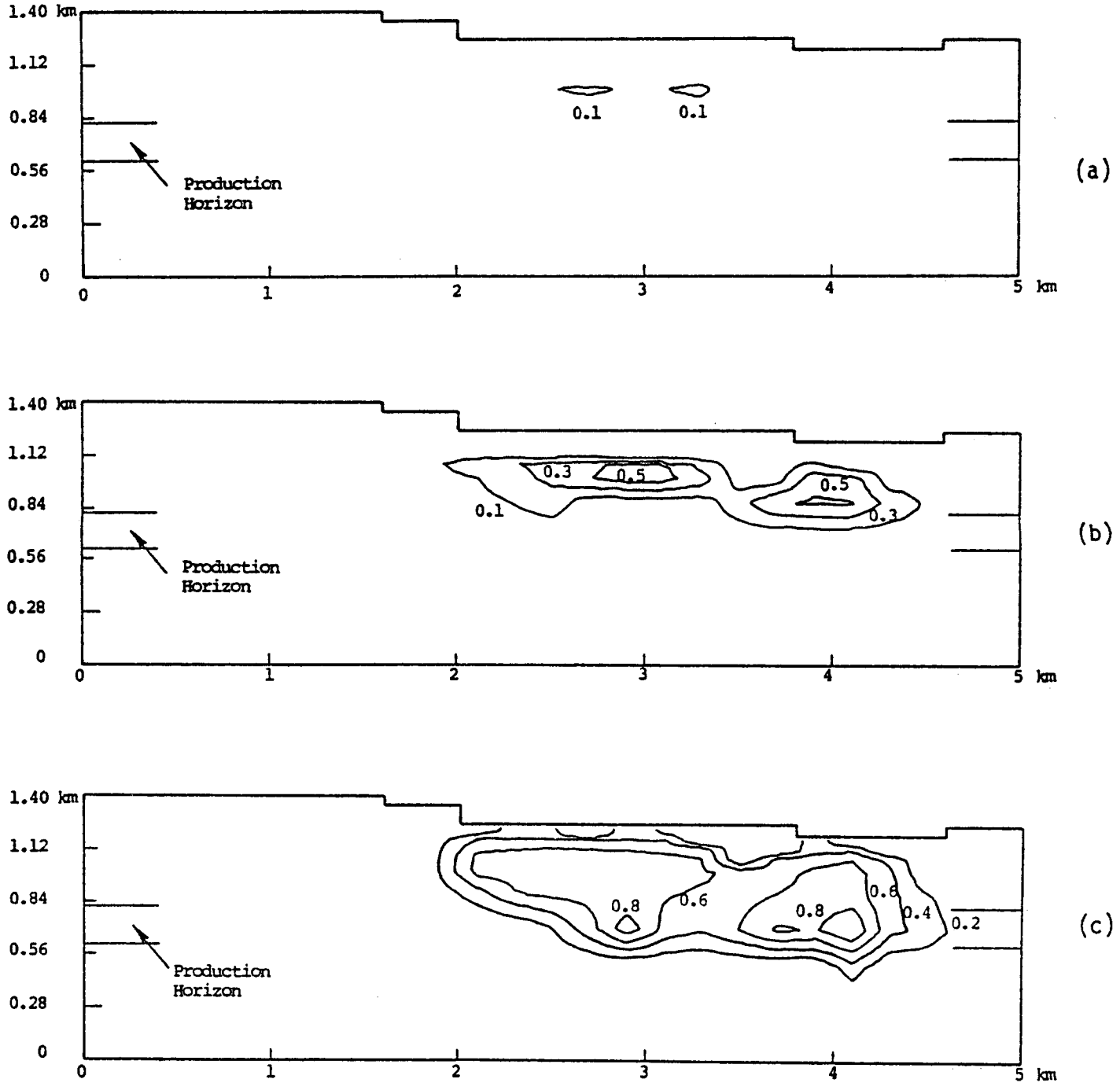

Figure 5. Vapor saturation profiles at the beginning of 1955 (a), 1960 (b), and 1968 (c).

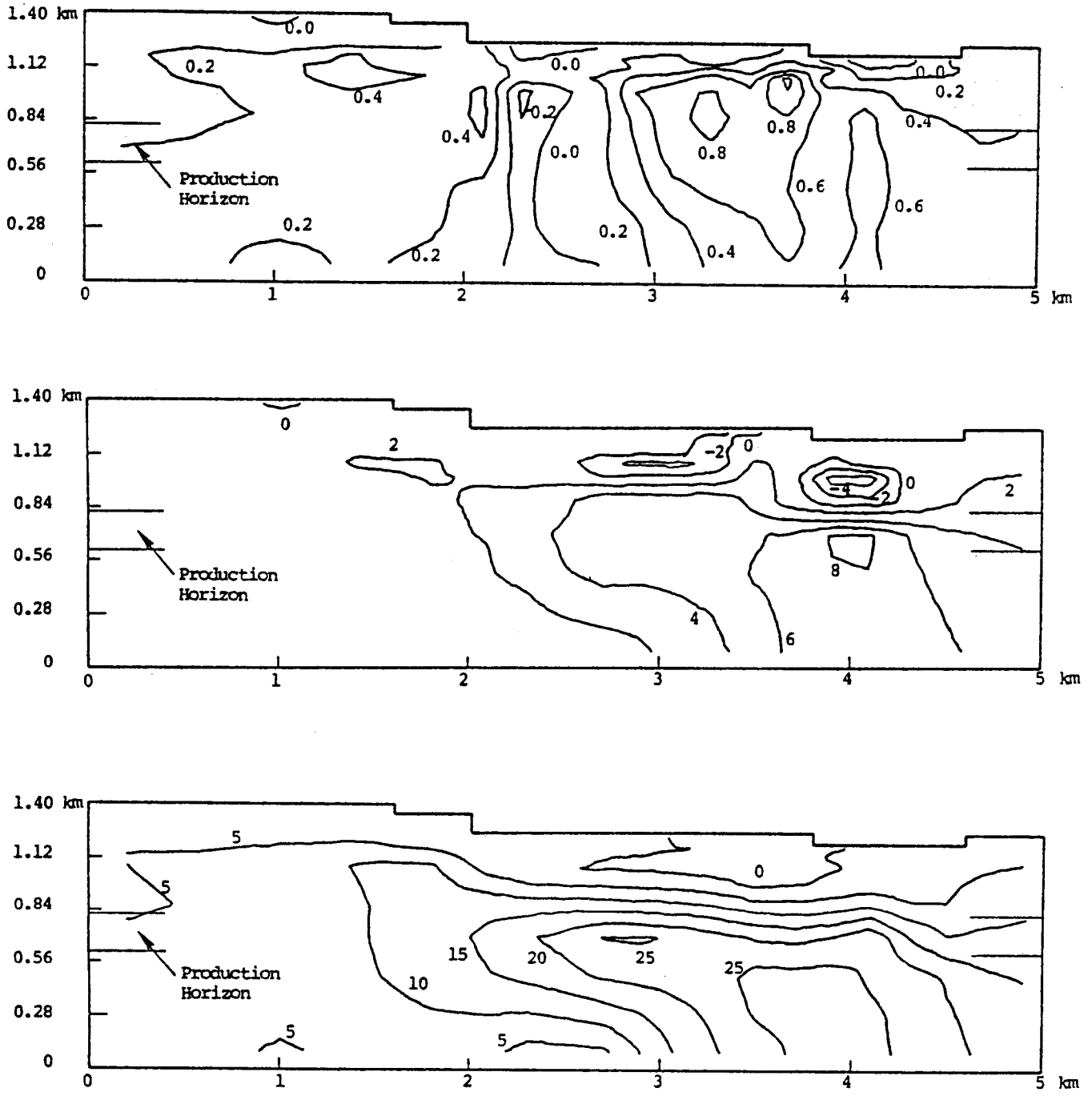

Figure 6. Pressure drop (in bars) profiles at the beginning of 1955 (a), 1960 (b), and 1968 (c).

Figure 7. Total subsidence in meters at Wairakei during period 1964-1974 (Stillwell, et al., 1975).

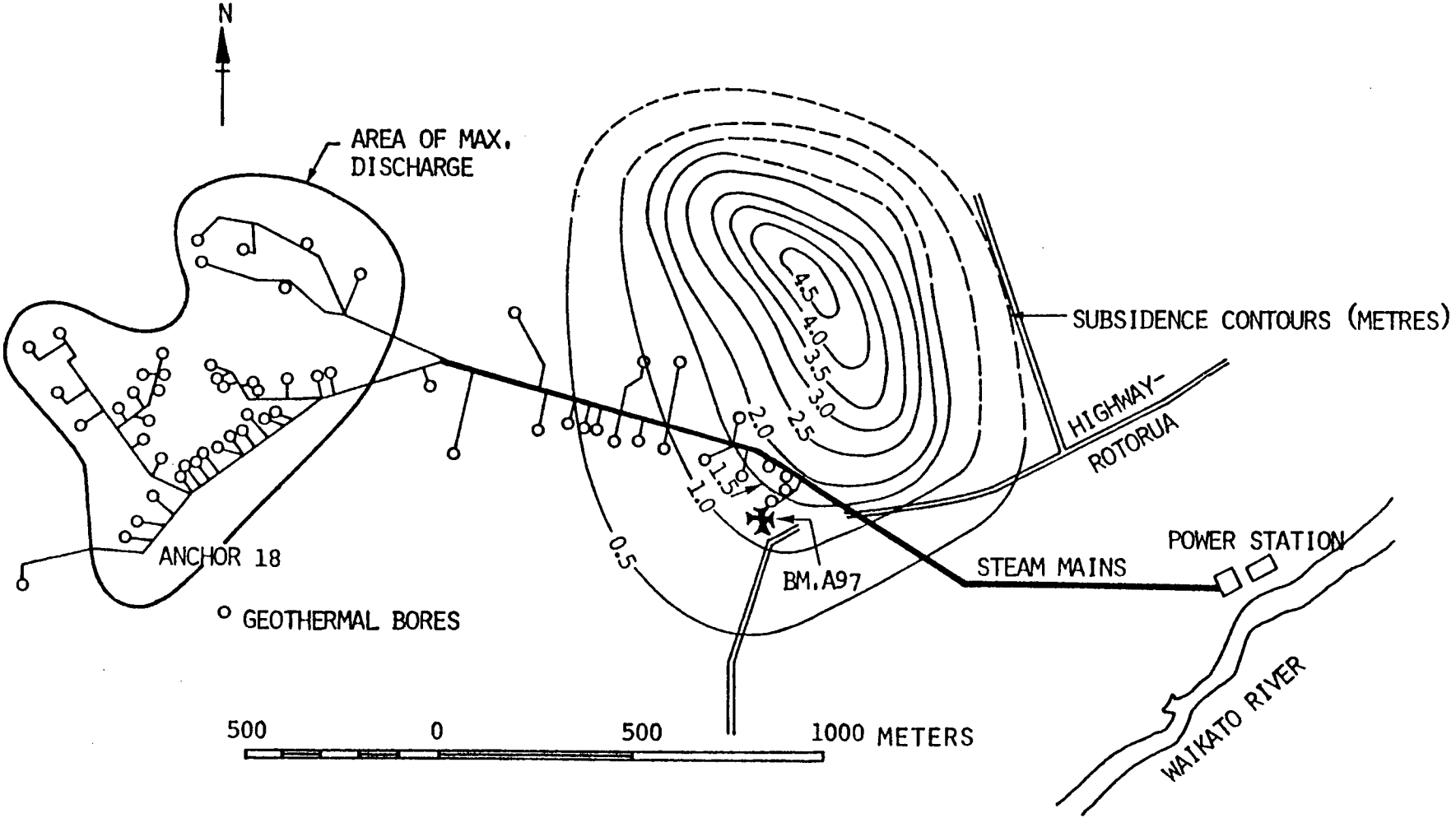

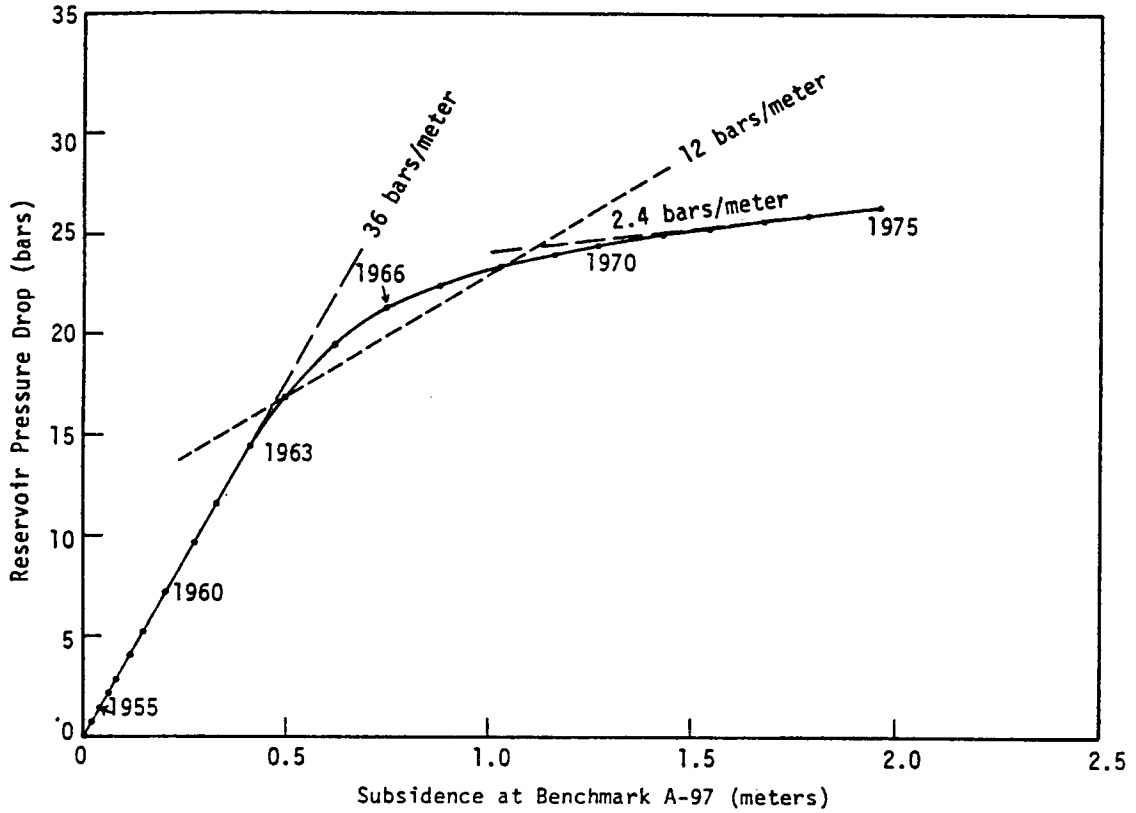

Figure 8. Wairakei subsidence data - reservoir pressure drop versus subsidence at Benchmark A-97.

A MODEL OF THE HYDROTHERMAL SYSTEM OF LONG VALLEY CALDERA, CALIFORNIA

Michael Sorey
U. S. Geological Survey
Water Resources Division
345 Middlefield Road
Menlo Park, CA 94025

Long Valley caldera, an elliptical depression covering 450 km^2 on the eastern front of the Sierra Nevada in east-central California (Fig. 1), contains a hot-water convection system with numerous hot springs and measured and estimated aquifer temperatures at depth of 180°C-280°C. In this study, the results of previous geologic, geophysical, geochemical, and hydrologic investigations of the Long Valley area have been synthesized to develop a generalized conceptual and mathematical model which describes the natural conditions of heat and fluid flow in the hydrothermal system. Because only one deep drill-hole (2 km) has thus far been completed within the caldera, this model must be considered speculative in detail, although its gross features are consistent with known constraints. Details of the work discussed in this summary will be published as a U.S.G.S. open-file report in February, 1977.

Conceptual Model

As illustrated in Figure 2, the conceptual model is three-dimensional, including the area within the topographic boundary of the caldera floor, and extending to a depth of 6 km. For numerical simulation the caldera rocks are divided into five horizontal layers, corresponding in composition and depth to the major rock units identified by the seismic refraction and geologic studies (Hill, 1976; Bailey and others, 1976), and calculations of average depths of fill (F. H. Olmsted, written communication, 1976). Of these, the upper layer, which is 1-km thick, corresponds to the post-caldera sedimentary (glacial, alluvial, and lacustrine) and volcanic (flows and tuffs) rocks and contains the shallow, cold ground-water system. Layer 2, 1-km thick, corresponds to the densely welded Bishop Tuff, a rhyolitic ash flow that erupted 0.7 m.y. ago during caldera formation. Layer 3 includes welded Bishop Tuff, the pre-caldera Glass Mountain Rhyolite, and some granitic and metamorphic basement rocks. Geophysical and geologic studies show that the densely welded tuff forms a continuous layer over the area of the caldera with an average thickness of 1.4 km. It is likely that the welded tuff has retained significant permeability after fracturing. In the conceptual model, a deep, hot ground-water system, i.e. the hydrothermal reservoir, is assumed to occur in layers 2 and 3. Layers 4 and 5 correspond to pre-caldera

basement rocks, which are assumed impermeable but thermally conductive. Two layers were used in this depth interval (3-6 km) to allow more accurate numerical heat flow simulation. The presence of magma below 6 km in the western part of the caldera, which is suggested by seismic, teleseismic, and heat-flow studies, is simulated by a constant (with time) but areally varied temperature distribution at the base of the model.

Hydraulic and thermal properties used in the model are listed in Table 1.

Table 1.--Hydraulic and thermal properties for Long Valley model.

Layer	Thermal conductivities mcal/(s ^{o}C cm)	Heat capacity cal/^{o} C cm^{3})	Intrinsic permeability $m^2 \times 10^{-12}$	Vertical compressibility m^2/N	Porosity
1	2	0.54 - 0.58	0	10^{-9}	0.35
2	5	0.54 - 0.58	0.03 - 0.35	10^{-10}	0.10
3	5	0.54 - 0.58	0.03 - 0.35	10^{-10}	0.05
4	6	0.54 - 0.58	0	10^{-10}	0.05
5	6	0.54 - 0.58	0	10^{-10}	0.05

Layer 1 is considered as an impermeable cap except along parts of the caldera rim, where recharging ground water moves downward along the ring fault, and in the Hot Creek gorge area, where hot water flows upward along faults to discharge in the gorge springs. Ground-water flow is from the higher altitudes along the west and northeast rims to discharge areas at lower altitudes in Hot Creek gorge and at depth through the southeast rim of the caldera. Additional driving force causing flow is provided by density differences between hot and cold parts of the flow system. The effective reservoir transmissivity was evaluated by specifying pressures based on water table altitudes in recharge and discharge areas and adjusting the reservoir permeability distribution to yield the desired mass flux of water.

Numerical Simulation

To permit numerical simulation of heat and fluid flow, each layer of the model is subdivided into 82 grid blocks or nodes along land-net lines (Fig. 3). Finer nodal spacing is used near the dis-

charge areas. Hot water is assumed to discharge only over the surface of the node that includes the springs in Hot Creek gorge, in T3S/R28E-S25, and through the southeast rim as indicated in Figure 3. Only minor differences in computed distributions of pressure and temperature would be expected if a more detailed distribution of hot-water discharge were modeled, because approximately 80 percent of the surface discharge from the thermal reservoir is through the springs in the gorge (Sorey and Lewis, 1976).

The equations and solution procedure used in this study are described in detail by Sorey (1975). The flow equation is

$$\nabla \cdot \left[\rho \frac{k}{\mu} (\nabla P - \rho \bar{g})\right] = C \frac{\partial P}{\partial t} \qquad (1)$$

where

ρ = fluid density
k = intrinsic permeability
μ = dynamic viscosity
P = fluid pressure
$\bar{g}$ = gravitational acceleration vector
C = fluid-rock compressibility
t = time

Equation 1 is based on conservation of mass and Darcy's law for non-isothermal fluid flow in porous media. An assumption inherent in this formulation is that fluid flow in the hydrothermal system, although probably controlled locally by permeable zones along faults, can best be described in large scale as flow in a porous medium in which permeability is distributed effectively throughout.

The energy equation is

$$\nabla \cdot [K_m \nabla T] - \rho c \bar{v} \cdot \nabla T = (\rho c)' \frac{\partial T}{\partial t} \qquad (2)$$

where

K_m = rock-fluid thermal conductivity
T = rock-fluid temperature
$\bar{v}$ = Darcy velocity vector
c = fluid specific heat at constant volume
$(\rho c)'$ = rock-fluid heat capacity

Equation (2) accounts for conductive and convective transfer of heat under steady-state and transient conditions. We assume that thermal equilibrium exists between fluid and solid phases at points of contact and that heat transfer by hydrodynamic dispersion can be neglected in the type of problem considered here (Mercer and others, 1975, p. 2618). Temperature-dependent parameters, μ and c, in Eq. (3) were evaluated from tabulated data (Dorsey, 1968).

The equation of state relating fluid density to temperature is

$$\rho = \rho_o [1-\beta(T-T_o)-\gamma(T-T_o)^2] \qquad (3)$$

where

ρ_o = fluid density at reference temperature T_o

β = thermal expansivity

γ = coefficient for second order fit

Density variations with pressure are neglected.

Simultaneous solutions to the flow and energy equations were obtained by an integrated finite-difference method involving iterative solutions at selected time steps for pressure, temperature, and velocity fields. This numerical procedure offers considerable advantages over standard finite-difference methods in terms of reduced computing times and nodal requirements (Narasimhan and Witherspoon, 1976). The time step used to solve the energy equation is continuously increased by a factor between 1 and 2, with the limitation that the maximum change in nodal temperatures per time step be less than about 10 percent of the maximum total change expected in the system. Because the response times for pressure changes are much smaller than for temperature changes, the flow system essentially equilibrates to a quasi-steady state within each thermal time step. For a simulation period of 35,000 years, approximately 50 thermal time steps were used; for a 350,000 year simulation, approximately 70 time steps were required.

Hydraulic Characteristics

Locations of the principal faults within the caldera, most of which are high angle, normal faults, are also shown in Figure 3. Fractures in the welded tuff associated with these and other faults not delineated at the land surface are considered to provide the major channels for flow in the hydrothermal system. The apparent lack of faulting in the eastern part of the caldera (with the exception of the ring fracture) need not preclude permeable zones in that area which could also occur in brecciated zones between the two major cooling units in the Bishop Tuff (Sheridan, 1968).

Values of intrinsic permeability obtained from the model for a 1-km thick reservoir with a mass flux of 250 kg/s (based on geochemical mixing models and boron discharge into Lake Crowley; Sorey and Lewis, 1976) are listed in Table 2. Interestingly, the Long Valley results of 30-50 millidarcys are within a factor of 3 of the value used by Mercer, Pinder, and Donaldson (1975) for the fractured volcanics of the Wairora aquifer at Wairakei, New Zealand.

Table 2. Intrinsic-permeability data from Long Valley model and other studies.

Data source	Reservoir thickness (km)	Permeability ($\times 10^{-15}$ m^2)
Long Valley model	1	30 - 50[1]
Wairakei model [2]	0.4 - 0.85	100
Long Valley cores [3]	---	0.0005 - 180.
NTS ash flow tuffs [4]	---	0.04 - 10.
NTS welded tuff [5] (fractured)	0.05 - 0.2	5,000 - 30,000

1 Range for two possible cases of reservoir permeability distribution.

2 Wairora aquifer consisting of pumice breccia and vitric tuffs as modeled by Mercer and others (1975).

3 Data for cores of altered rock, flow rocks, and non-welded tuffs.

4 Oak Springs Formation (Keller, 1960).

5 Winograd and others (1971).

Comparisons with measurements on Long Valley cores, and well tests and cores at the Nevada Test Site indicate that the permeability values obtained from the model represent an integration of the effects of fracture permeability over the volume of reservoir rock.

Equivalent of "cold water" hydraulic heads from the model simulations at each node were computed using the relationship

$$H_o = P/(\rho_o g) + Z \qquad (5)$$

where ρ_o = fluid density at reference temperature (10°C) and Z = altitude of node above sea level. An example of the resultant head distribution, in layer 2 at 1.5 km depth as seen in Figure 4, shows the predominant eastward flow toward the Hot Creek gorge area and the effects of recharge from the Glass Mountain area. The existence of deep recharge along the northeastern rim is suggested in part by the results of a 2-km deep test hole recently drilled by private industry 3 km east of Hot Creek gorge, which encountered relatively cool ground-water temperatures within the Bishop Tuff.

Thermal Characteristics

The Long Valley model is constrained by estimates of the natural heat discharge from the caldera. From spring measurements and temperature profiles in wells, the total heat discharge is estimated to be 6.9×10^7 cal/s. Applications of geochemical mixing models indicate that 190-300 kg/s of water at 210°C-282°C discharges upward from the reservoir toward the hot springs, with the highest estimated reservoir temperature corresponding to the lowest mass flux. The model was used to evaluate the depths of fluid circulation for which an underlying magma chamber could supply the required heat flow, equivalent to an average of 15 HFU over the area of the caldera, for various periods of time. The initial thermal condition was the temperature distribution at steady state in the absence of fluid flow.

Studies of saline deposits in Searles Lake, downdrainage from Long Valley (Smith, 1976), indicate that present-day hot spring discharge in the caldera has persisted for only 30,000-40,000 years. Model simulations of heat and fluid flow for a period of 35,000 years show that present-day heat discharge could have been sustained for this period by a magma chamber at 6 km with fluid circulation to 1.5-2.5 km. As shown in Figures 5 and 6, simulated reservoir temperatures at a depth of 1.5 km under the Hot Creek gorge area are near 200°C after 35,000 years with a hot spring discharge of 250 kg/s. Cooler temperatures east of Hot Creek, resulting from recharge along the northeast rim, are consistent with the results reported for the deep test hole.

In contrast, Bailey, Dalrymple, and Lanphere (1976) find evidence of extensive hydrothermal alteration 0.3 m.y. ago which appears to be related to the main magma chamber rather than to the post-caldera eruptive volcanic rocks. Simulation of hot-spring discharge for periods much greater than 35,000 years produces maximum reservoir temperatures significantly cooler than the previous results. Correspondingly, deeper levels of circulation are required to sustain heat flow and reservoir temperatures above 200°C.

In Figure 7, reservoir temperatures under the gorge are plotted as functions of time for two cases of reservoir depth. The initial increase in reservoir temperatures prior to about 10,000 years is due to the arrival of hotter water from the west. Calculation of average ground-water travel times from recharge to discharge areas, based on the time at which reservoir temperature under the gorge begins to decline rapidly (10,000 years), yield values near 2,000 years for a 1-km thick reservoir. Simulation of present-day hot spring discharge for periods greater than about 300,000 years, after which time the system has essentially reached steady state, shows that even for the 2-3-km deep reservoir discharge temperatures fall well below 200°C. The results of these and other simulations with the model indicate that circulation to depths of 4-5 km would be required to sustain present-day thermal conditions over periods of 300,000 years.

Because permeable channels in the basement rocks are unlikely to exist at these depths and in view of the diverse indications of the age of hot spring activity noted above, an alternative hypothesis that discharge from the hydrothermal system has been intermittent in character is preferred. Significant periods of inactivity could have resulted from climatic variations and self-sealing processes which are in evidence today. These possibilities and the adequacy of the simplified hydrothermal model analyzed in this study can only be evaluated by deep drilling in the western part of the caldera.

Under the eastern two-fifths of the caldera, reservoir temperatures measured in the deep test hole and simulated temperatures from the model would seem to preclude the possibility of energy development east of Hot Creek. However, the significance of this area may be its potential contribution of relatively cold ground water to high-enthalpy fluid production from beneath the resurgent dome in the west-central part of the caldera, and (or) its potential for reinjection of hydrothermal fluids. The model analyzed in this study has helped to quantify the relationships between heat and fluid flow and the hydraulic characteristics of the hydrothermal system. Incorporation of additional detail from deep and shallow drilling would enable the model to be used to analyze the potential for, and the effects of, energy development in the Long Valley caldera.

Selected References

Bailey, R.A., Dalrymple, G.B., and Lanphere, M.A., 1976, Volcanism, structure, and geochronology of Long Valley caldera, Mono County, California, Jour. Geophys. Research, v. 81, no. 5, p. 725-744.

Dorsey, N.E., 1968, Properties of ordinary water-substance, Hafner Publishing Co., New York.

Hill, D.P., 1976, Structure of Long Valley caldera, California from a seismic refraction experiment, Jour. Geophys. Research, v. 81, no. 5.

Keller, G.V., 1960, Physical properties of tuffs of the Oak Spring Formation, Nevada, U.S. Geol. Survey Prof. Paper 400-B, p. 396-400.

Lewis, R.E., 1974, Data on wells, springs, and thermal springs in Long Valley, Mono County, California, U.S. Geol. Survey open-file rept. 52 p.

Mercer, J.W., Pinder, G.F., and Donaldson, I.G., 1975, A Galerkin finite-element analysis of the hydrothermal system at Wairakei, New Zealand, Jour. Geophys. Research, v. 80, no. 17, p. 2608-2621.

Narashimhan, T.N., and Witherspoon, P.A., 1976, An integrated finite difference method for analyzing fluid flow in porous media, Water Resources Research, v. 12, no. 1, p. 57-64.

Sheridan, M.F., 1968, Double cooling-unit nature of the Bishop Tuff in Owens Gorge, California (abs), Geol. Soc. America Spec. Paper 115, p. 351.

Smith, G.I., 1976, Origin of lithium and other components in the Searles Lake evaporites, California, in Lithium resources and requirements by the year 2000, U.S. Geol. Survey Prof. Paper 1005, ed. by J. D. Vine, p. 92-103.

Sorey, M.L., 1975, Numerical modeling of liquid geothermal systems, U.S. Geol. Survey open-file rept. 75-613, 66 p.

Sorey, M.L., and Lewis, R.E., 1976, Convective heat flow from hot springs in the Long Valley caldera, Mono County, California, Jour. Geophys. Research, v. 81, no. 5, p. 785-791.

Winograd, I.J., Thordarson, W., and Young, R.A., 1971, Hydrology of the Nevada Test Site and vicinity, U.S. Geol. Survey open-file rept., 429 p.

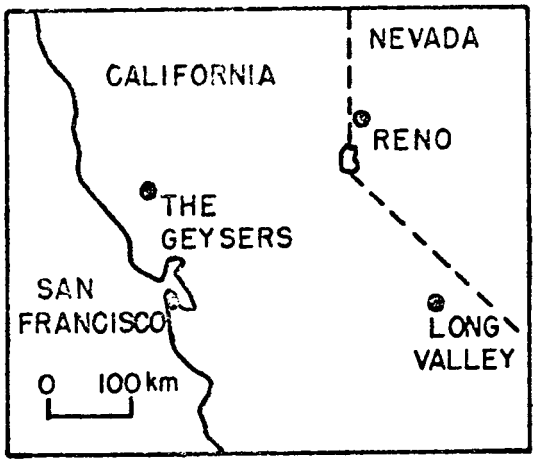

Figure 1. Map showing location of Long Valley and other points of reference.

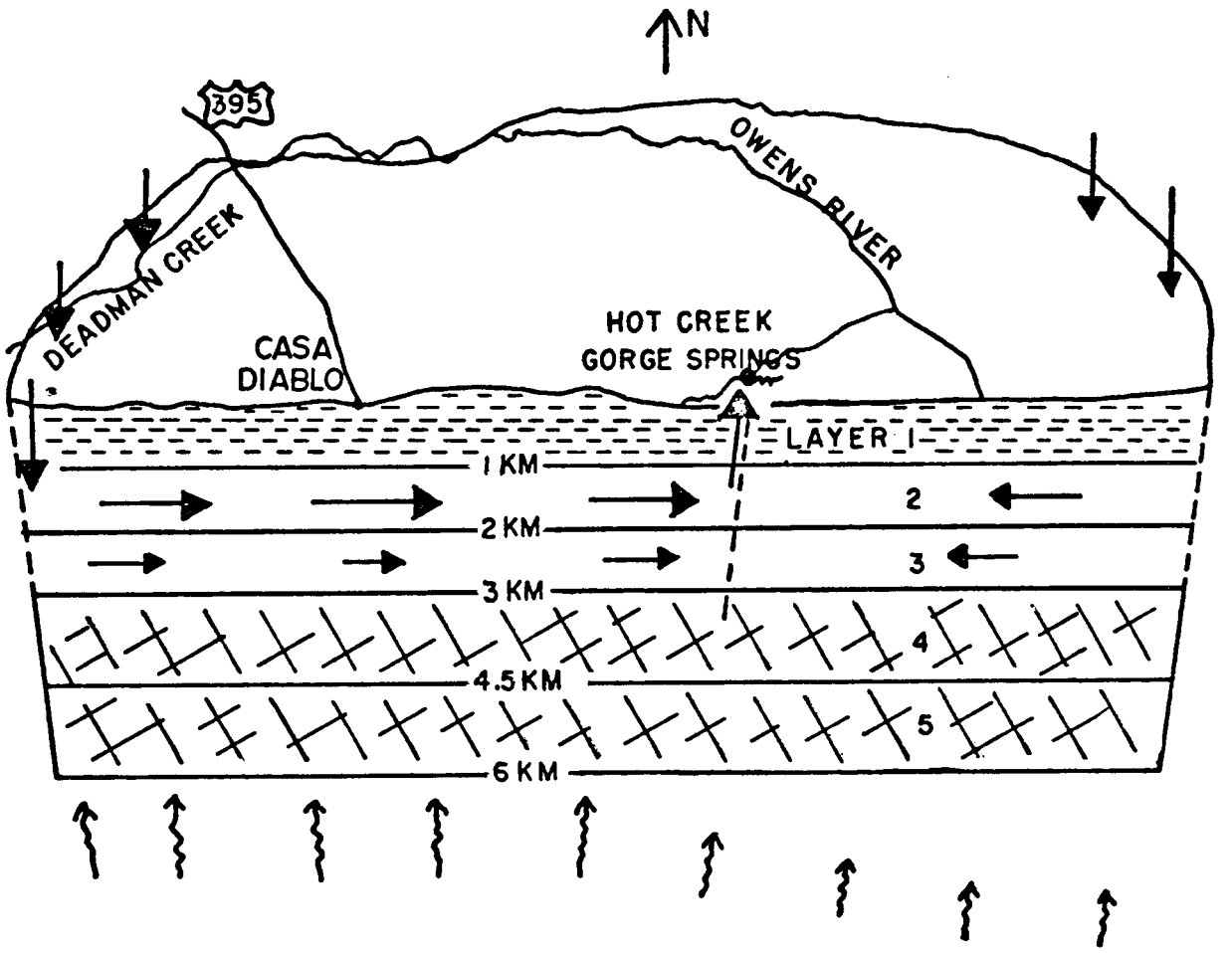

Figure 2. Block diagram showing conceptual model of Long Valley hydrothermal system.

System consists of five horizontal layers having properties listed in text. Patternless layers between depths of 1 and 3 km represent hydrothermal reservoir in fractured, densely welded Bishop Tuff. Recharge to the reservoir is by way of the caldera ring fault in the west and northeast. Discharge is by way of faults and fractures to springs in Hot Creek gorge. Straight arrows indicate ground-water flow; wavy arrows indicate heat flow.

Figure 3. Sketch map of Long Valley caldera showing nodal configuration for numerical simulation of hydrothermal model with uniform reservoir permeability distribution. R denotes recharge node; D denotes discharge node covering Hot Creek gorge. Principal faults are shown as solid heavy lines with ball on downthrown side. Arrow denotes discharge at depth through southeastern caldera rim.

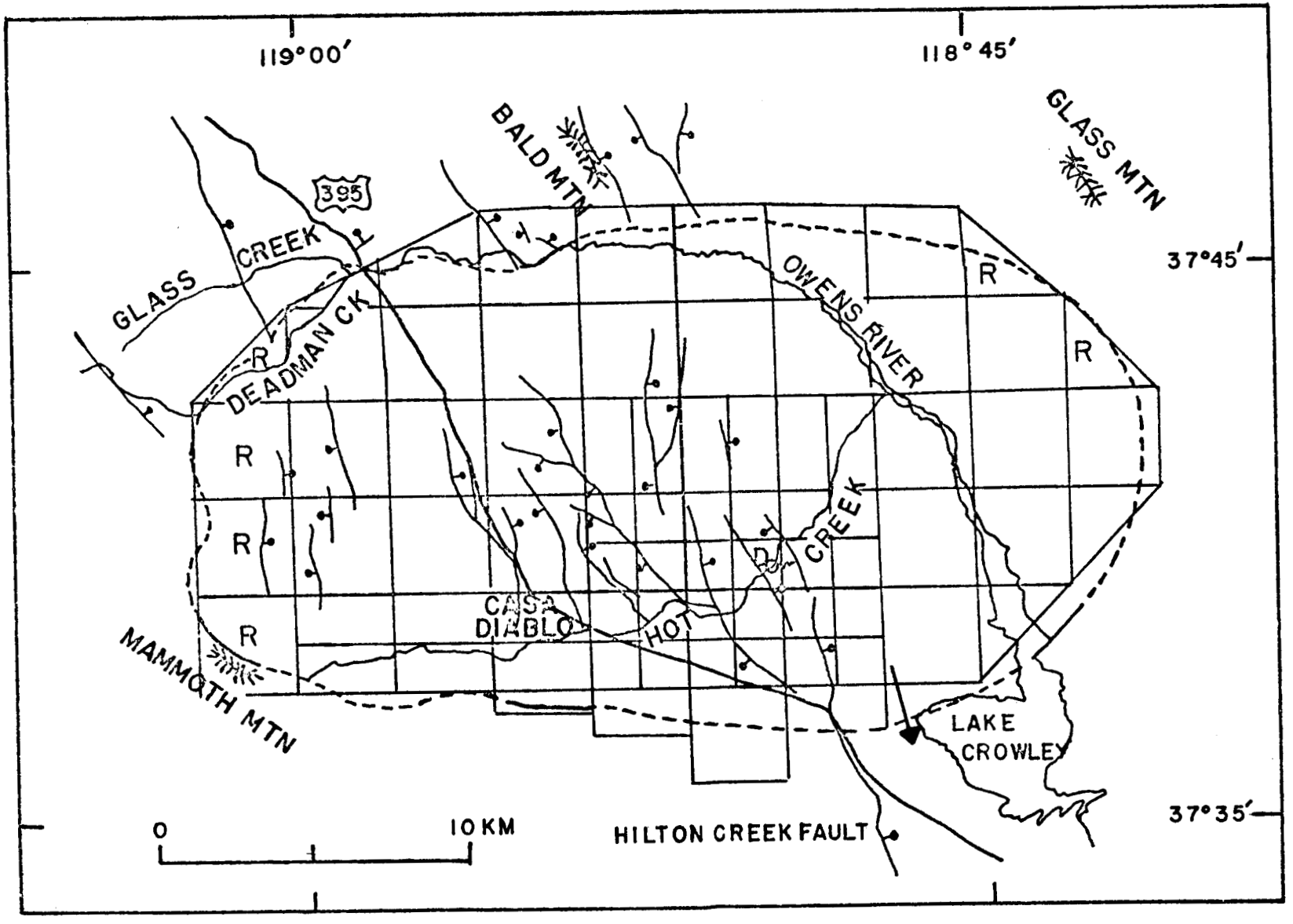

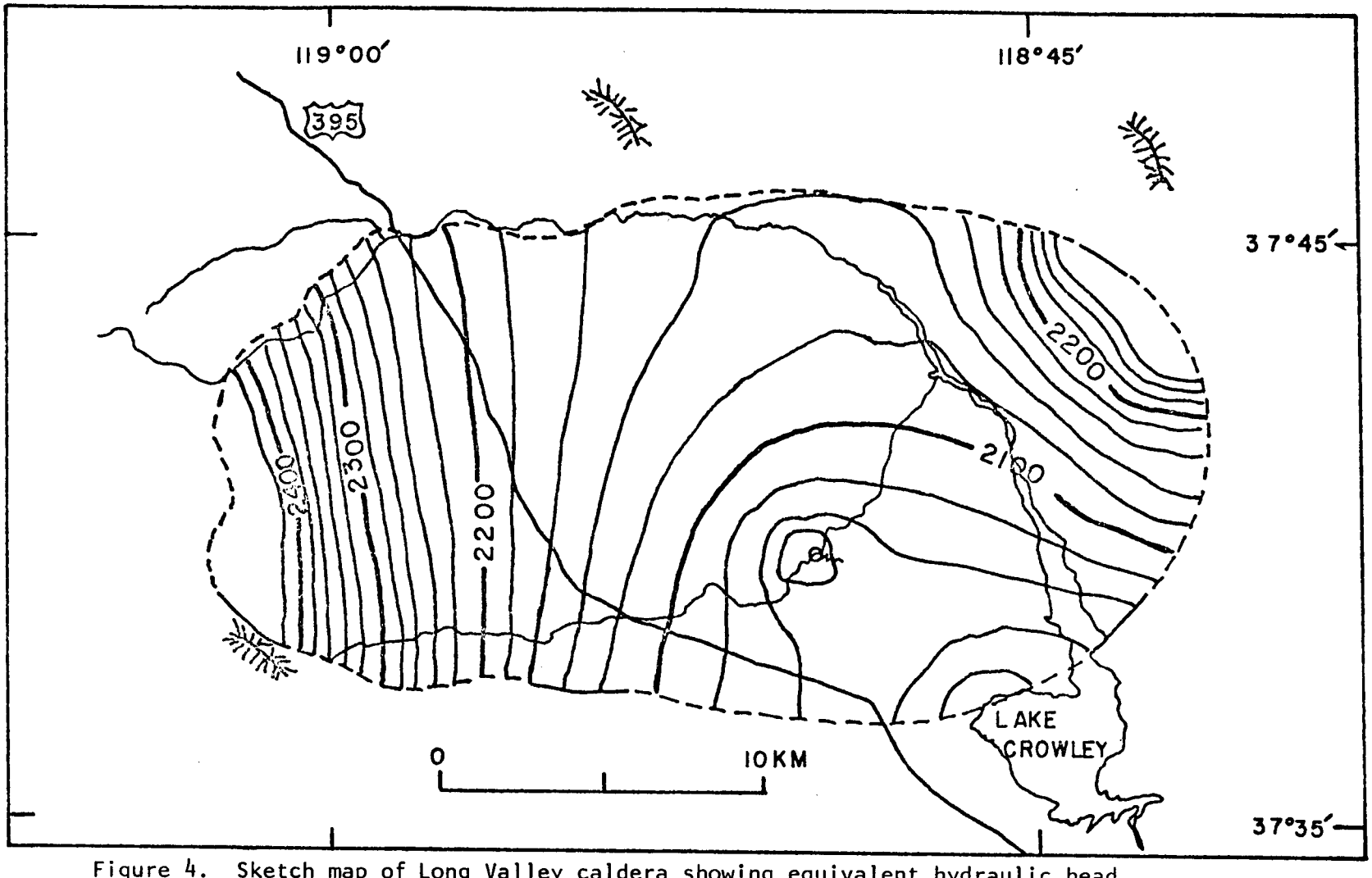

Figure 4. Sketch map of Long Valley caldera showing equivalent hydraulic head at a depth of 1.5 km in reservoir with uniform reservoir permeability of 30 millidarcys, hot-spring discharge of 250 kg/s, and southeast-rim outflow of 110 kg/s. Contours of equivalent hydraulic head in meters above mean sea level. Interval 20 m.

Figure 5. Diagrammatic east-west cross-section of Long Valley caldera showing isotherms in model after 35,000 years with hot-spring discharge of 250 kg/s, southeast-rim outflow of 110 kg/s, and reservoir depth of 1-2 km.

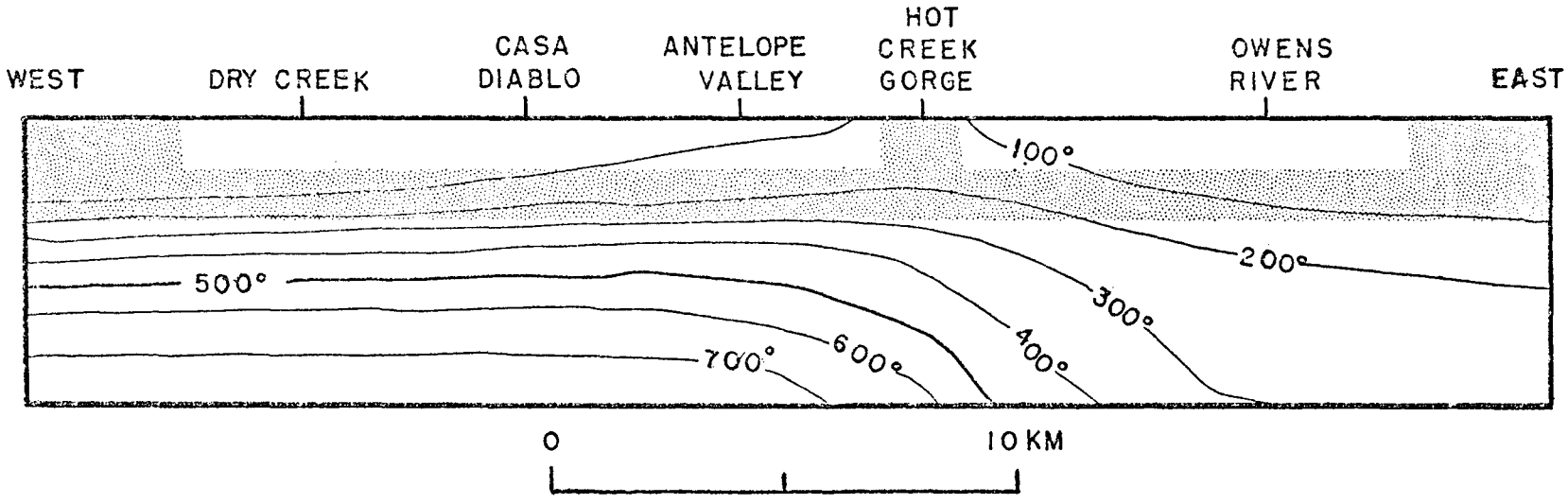

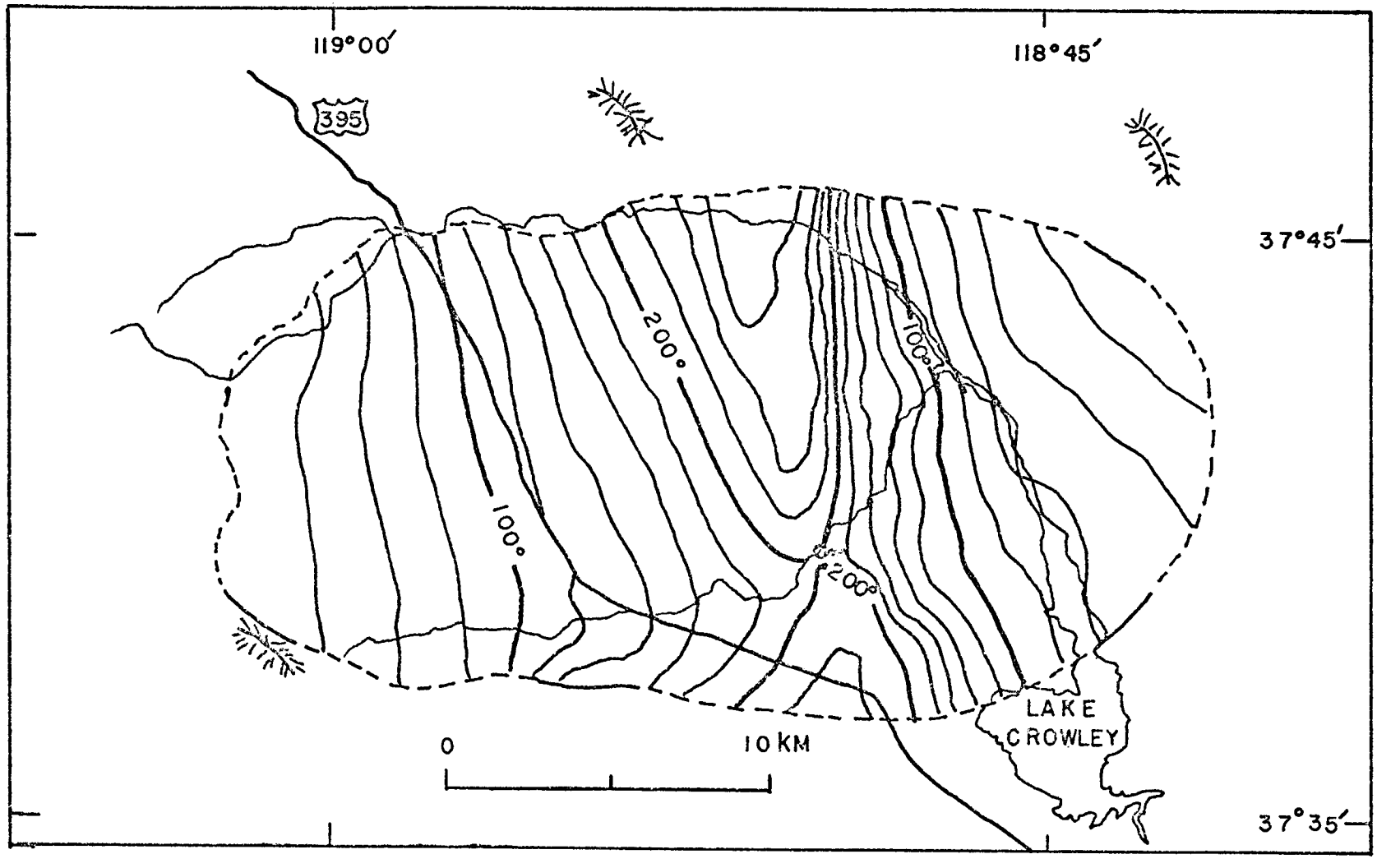

Figure 6. Sketch map of Long Valley caldera showing isotherms at a depth of 1.5 km in reservoir after 35,000 years with hot-spring discharge of 250 kg/s and southeast-rim outflow of 110 kg/s. Lines of equal temperature in degrees Celsius. Interval 20°C.

Figure 7. Transient response since initiation of springflow of average reservoir temperature below Hot Creek gorge for two simulated reservoir depths.

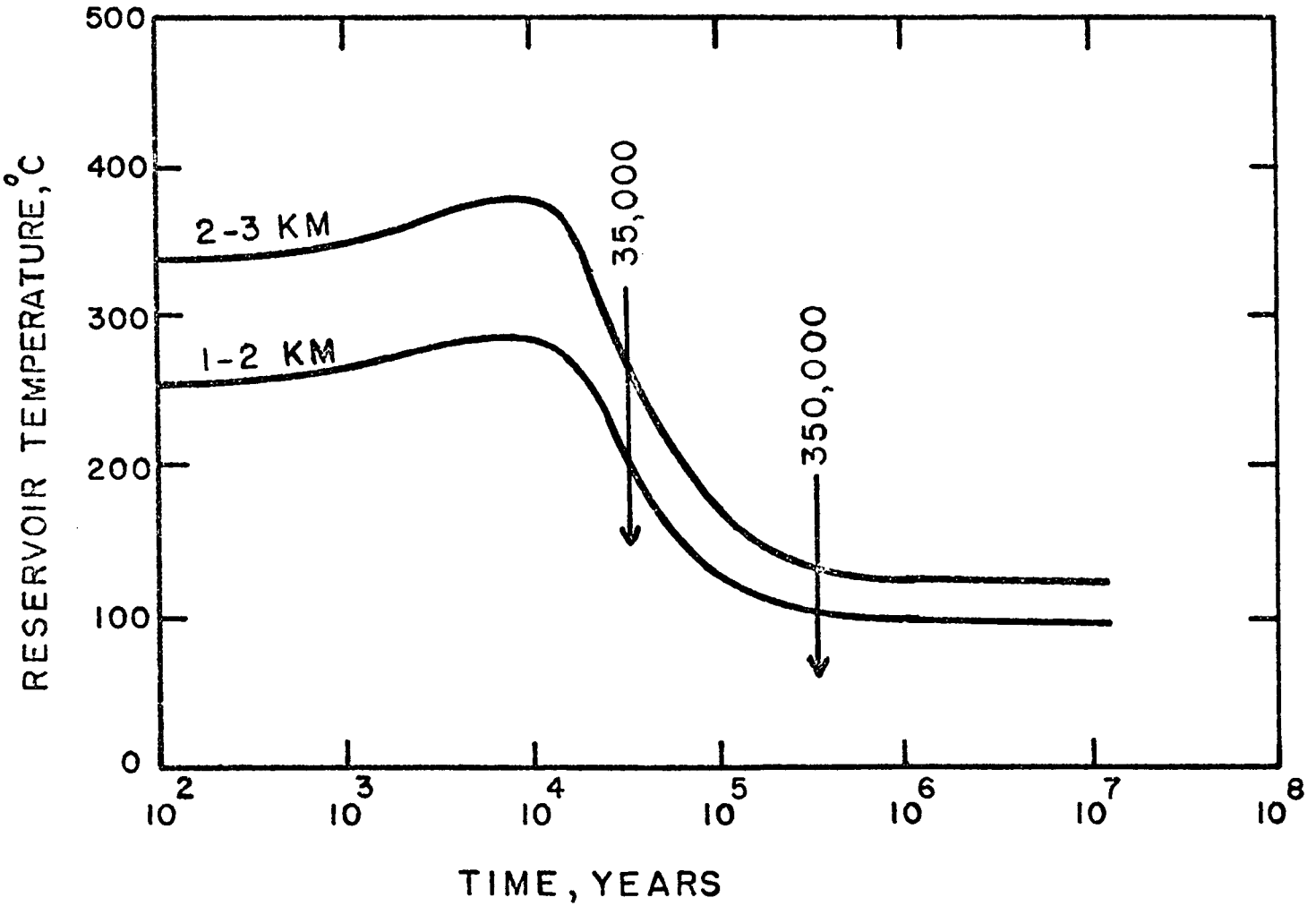

LARGE-SCALE GEOTHERMAL FIELD PARAMETERS AND CONVECTION THEORY

R. A. Wooding
Applied Mathematics Division
D.S.I.R.
Wellington, New Zealand

The question of the depth reached by groundwater in natural recharge to a geothermal field is of interest for geothermal development, since it can affect the nature of the recharge regime during withdrawal, and the volume of water within reach during exploitation. Also, useful inferences may be drawn about the large-scale permeability of the system if the groundwater flow regime is understood.

Evidence for the presence of thermal convection in the groundwater now appears to be well-established, although topographic effects may also be important (Studt and Thompson 1969, Healy and Hochstein 1973). Two regions which serve particularly well as illustrations are (1) the Imperial Valley of Southern California and (2) the Taupo Volcanic Zone of New Zealand. Both exhibit a number of quite well-defined zones of anomalously high heat flow (geothermal fields), separated by distances of 10 to 15 Km, the intervening areas usually having very low heat flow. At Imperial Valley, the fairly permeable sands in which convection is likely to occur are overlain by sediments of low permeability, roughly 0.6 Km in thickness, and thermal conductivity alone without appreciable convection, commonly occurs in these upper layers (Palmer, Howard and Lande 1975). In the case of (2), the heat flow in areas surrounding geothermal fields is depressed practically to zero, and this has been interpreted by Studt and Thompson as being due to downflowing recharge water from precipitation. The water issuing naturally from geothermal fields is predominantly meteoric, but the residence times in the groundwater stage appear to be very long.

It follows that the upper boundary conditions of the two cases must be significantly different. In (1) the upper flow boundary is practically impermeable while, in (2), flow through the upper boundary is almost unimpeded. Idealized conditions which correspond approximately to these cases were introduced by Lapwood (1948); these will be designated as boundary conditions 1 and 2 respectively.

Lapwood calculated critical Rayleigh numbers ($R = R_c$) for neutral stability in a horizontal layer of uniform isotropic porous material, heated from below to maintain a constant temperature difference between the two boundaries. Fluid properties and thermal conductivity of the saturated medium were assumed constant. Although the stability approach does not yield heat-flux Nusselt numbers for convection at supercritical Rayleigh numbers, it provides a useful prediction of the most likely aspect ratio--horizontal wavelength to layer depth--of convection cells under finite amplitude conditions provided that $R - R_c$ is small in comparison with R_c. Also, the approach is convenient for studying the influence of changing fluid or medium properties; many cases can be treated quickly, and likely combinations of parameters may be selected for more detailed study at higher Rayleigh numbers.

Magnitudes of Convection Parameters

Several factors indicate that R/R_c is not very large in the two geothermal zones discussed above. It is likely that heat enters the system by conduction through rock layers from quite shallow, perhaps magmatic, sources. If convection were not present, a thermal anomaly would still exist, with a different spatial distribution, and probably with a heat flow several times normal. The presence of convection will enhance the heat flow, but probably by a factor of order 2, rather than 10. (From a practical point of view, perhaps the most important function of convection is to redistribute and concentrate the heat flow.) A low Nusselt number will be associated with only moderate values of R/R_c.

In round numbers, a 1000°C magma body at a depth of about 5 Km would give rise to a conduction heat flow of 5-10 heat flow units (1 h.f.u. being the world average). If convection were present in the upper part of the 5 Km layer, giving rise to an overall Nusselt number of 2, this would account for the heat flow observed in, for example, the Taupo Volcanic Zone.

A low value of Rayleigh number appears to be consistent with estimated physical parameters, average values from the upper part of the Wairakei field (McNabb, Grant and Robinson 1975). Assuming vertical permeability $K \simeq 7 \times 10^{-11}$ cm^2, cold water viscosity $\mu_o \simeq 10^{-2}$ poise, thermal conductivity $K \simeq 3 \times 10^{-3}$ c.g.s. units, liquid density contrast $\Delta\rho \simeq 0.2$, it is found that

$$R/L = kg\Delta\rho/\kappa\mu_o \qquad (1)$$

$$\simeq 50 \text{ per Km depth.}$$

Here the depth L of the permeable layer is unknown, but it is suggested that it is not more than about 3 Km. It is important to establish whether the convection theory is consistent with this shallow depth of groundwater penetration and the observed 10-15 Km separation of geothermal fields.

Extensions of the Theory

The matrix permeability K and the fluid viscosity μ are involved only through the ratio K/μ--the "mobility"--but in practice this function may be quite complex. This has led to various extensions of Lapwood's work.

Using upper boundary conditions of type 1, Kassoy and Zebib (1976) have considered the case of temperature-dependent viscosity, noting that, for water, μ may change by an order of magnitude over the range of temperatures encountered in geothermal applications. On the other hand, Ribando, Torrance and Turcotte (1976) treated viscosity as constant, and carried out numerical calculations of finite-amplitude convection both for the Lapwood system and for permeability decreasing exponentially with depth.

A peculiar effect observed recently in silica-water systems (H. J. Ramey, Jr., pers. comm.) is that the permeability appears to decrease with rising temperature, perhaps by a factor of 2 or more in a range of a few hundred degrees centigrade. Although an explanation is not forthcoming at this time of writing, it is interesting to note that silica polymerizes in

aqueous solution to form a gel--a property which has been studied in connection with the formation of scale (Marsh, Klein and Vermeulen 1975). Thus the phenomenon may be equivalent to an increase of effective viscosity with temperature, partially counteracting the usual viscosity decrease associated with pure water. For purposes of calculation, this can be incorporated into the assumed temperature-viscosity law.

The Permeability Problem

Permeable media encountered in geothermal areas depart greatly from the simple homogeneous isotropic systems frequently considered in the laboratory and in theory. The Taupo Volcanic Zone exhibits many such complications, in particular the layering produced by a sequence of many thin volcanic deposits, varying in degrees of welding, brecciation, etc., and perhaps interspersed with thin sedimentary lenses, the occasional existence of highly permeable, weathered horizons between successive deposits, and the presence of numerous near-vertical faults trending along the Zone. On the large scale, a fracture-dominated system still appears to be well represented by a Darcy-type flow law, but the permeability is likely to be non-isotropic (H. J. Ramey, Jr., pers. comm.).

Borehole data on which large-scale permeability might be estimated is inadequate, generally because detailed information on fractures and permeable horizons is missed. However, zones of drill circulation loss are recorded, and can give a useful indication of fractures encountered. For the deepest borehole in the Wairakei geothermal field (Bore 121, 2265 metres) circulation losses are encountered frequently down to 1000 m, but only a few cases are noted at greater depths (1680 m and 2250 m, G. Grindley and P. Browne, pers. comm.). This indication of fewer permeable fractures at the greater depths is in accord with the observed hydrothermal alteration (P. Browne, pers. comm.), which implies a lesser through-flow of water. However, there are no other bores of comparable depth at Wairakei to supplement these limited observations.

Attempts to estimate the vertical and horizontal components of large-scale permeability in the area of the Wairakei field (McNabb, Grant and Robinson 1975) indicate that the horizontal permeability could have been anything up to 10 times as great. A contrast as high as this would be consistent with a layered system having very permeable horizons. The vertical faulting could be less important, as there are indications that permeability varies to a lesser extent with horizontal direction.

Stability Analysis from Convection Theory

The basic equations of thermal convection of a variable-viscosity fluid in a saturated medium have been given elsewhere (e.g., Wooding 1975).

A simple, but relevant generalization to anisotropic permeability is realized by assuming horizontal stratification, so that one principal axis of the permeability tensor is vertical and the other two are horizontal. Let γ_1, γ_2 be the ratios of the vertical component of permeability to the two horizontal components. These ratios will be assumed constant although the individual components of permeability may vary with depth.

Suitable scales for the convection problem are the length L (layer depth), the thermal diffusivity κ and the velocity $R\kappa/L$, where R is the Rayleigh number defined in (1). The time scale is $EL^2/R\kappa$, where E is the ratio of the heat capacity of the saturated medium to that of the fluid (Wooding 1957). Also, $\Delta\rho$ is an appropriate density scale.

If z is the dimensionless upward vertical coordinate, the dimensionless density profile corresponding to steady conduction of heat from below is equal to z. Any small perturbation Θ (x, y, z, t) of this profile will give rise to a perturbation velocity field; if w (x, y, z, t) is the vertical component of velocity, let

$$(\theta, w) = (\theta_1(z), w_1(z))\, e^{\lambda\tau} \sin\alpha x \sin\beta y \qquad (2)$$

where τ is dimensionless time and α, β are dimensionless wave numbers. Then the linearized equations give, for the z-dependent functions Θ_1, w_1,

$$D(\sigma D)w_1 - (\alpha^2/\gamma_1 + \beta^2/\gamma_2)(\sigma w_1 + \theta_1) = 0 \qquad (3)$$

$$w_1 = \frac{1}{R}(D^2 - \alpha^2 - \beta^2 - \lambda R)\,\theta_1 \qquad (4)$$

where $D \equiv d/dz$ and $\sigma = (\nu/\kappa)/(\nu/\kappa)_o$, $(\nu = \mu/\rho)$, the suffix o referring to values at the upper boundary. The boundary conditions 1 and 2 give

$$\theta_1 = w_1 = 0 \text{ at } z = 0 \qquad (5)$$

and 1) $\theta_1 = w_1 = 0$ at $z = 1$ (6a)

2) $\theta_1 = Dw_1 = 0$ at $z = 1$ (6b)

where 1) refers to an impermeable upper boundary and 2) to a boundary which is permeable (giving constant pressure).

Results from Stability Analysis

When the ratio ν/κ is constant ($\sigma = 1$), (3) to (6) can be solved analytically, and would include the case where the decrease in kinematic viscosity with depth (due to rising temperature) is balanced by the decrease of permeability with depth--a reasonable approximation to reality.

Figure 1 is a plot of wavenumber α_m and minimum Rayleigh number R_m, for given values of the permeability ratio γ_1, assuming that $\beta = 0$. The curves 1 and 2 correspond to boundary conditions 1 and 2. For any given value of γ_1, the system is more unstable with boundary conditions 2 than with boundary conditions 1. However, the curves 1 and 2 are quite similar in position and shape, and situations involving boundary conditions intermediate between 1 and 2 might be inferred readily. For this reason equal values of γ_1 on the two curves are joined by broken lines. Curves 1 and 2 tend to the same value of R_m as γ_1, and α_m tend to zero; i.e., as

the horizontal-to-vertical permeability ratio increases, the permeability of the upper boundary to fluid flow becomes less significant.

The reduction of α_m with decreasing γ_1 (increasing anisotrophy) is substantial. If, for example, $\gamma_1 \simeq 0.1$--a possible value according to McNabb, Grant and Robinson (1975)--α_m is likely to be in the range 1.4 to 1.8, which corresponds to a horizontal wavelength to layer depth ratio of 4 to 5.2 for hexagonal cells. If this can be extrapolated to finite-amplitude convection in a geothermal zone, a 3 Km depth of groundwater flow would lead to a field spacing of 12 to 15.6 Km, which is plausible when compared with observation.

When σ varies with z, the equations (3) ff. have been solved numerically. Surprisingly, the wavenumber of greatest instability, α_m, is relatively insensitive to variations of viscosity and permeability with depth, even when these approach an order of magnitude. This suggests that if other, unsuspected, factors are not present, the observed field geometry is most strongly influenced by anisotropic permeability.

When the medium also exhibits anisotrophy in the horizontal, it is necessary to consider three-dimensional instability in more detail. Contours of R_c have been plotted as a function of wavenumbers α and β. When the horizontal permeability in the x-direction exceeds that in the y-direction, R_c has a minimum (R_m) at $\beta = 0$ and $\alpha = \alpha_m$. This shows that the most unstable small disturbance consists of two-dimensional rolls with axes at right angles to the direction of maximum permeability. It does not follow, however, that such rolls will be observed at finite amplitudes when $R > R_m$. For example, the effect of variable viscosity may be to impose three-dimensional convection cells upon the system.

A more detailed discussion of these results is given elsewhere (Wooding 1976).

References

Healy, J. and M. P. Hochstein, 1973, Horizontal flow in hydrothermal systems; J. Hydrol. N.Z. 12, 71-82.

Kassoy, D. R. and A. Zebib, 1976, Variable viscosity effects on the onset of convection in porous media; Phys. Fluids 18, 1649-51.

Lapwood, E. R., 1948, Convection of a fluid in a porous medium; Proc. Camb. Phil. Soc. 44, 508-21.

McNabb, A., Grant, M. A. and J. L. Robinson, 1975, Permeability estimates; AMD Tech. Rep no. 34.

Marsh, A. R., III, Klein, G. and T. Vermeulen, 1975, Polymerization kinetics and equilibria of silicic acid in aqueous systems; Lawrence Berkeley Lab. Rep. LBL-4415.

Palmer, T. D., Howard, J. H. and D. P. Lande, 1975, Geothermal development of the Salton Trough, California and Mexico. Lawrence Livermore Lab. Rep. UCRL-51775.

Ribando, R. J., Torrance, K. E. and D. L. Turcotte, 1976, Numerical models for hydrothermal circulation in the oceanic crust; J. Geophys. Res. 81, 3007-12.

Studt, F. E. and G. E. K. Thompson, 1969, Geothermal heat flow in the North Island of New Zealand; N.Z. J. Geol. Geophys. 12, 673-83.

Wooding, R. A., 1957, Steady state free thermal convection of liquid in a saturated permeable medium; J. Fluid Mech. 2, 273-85.

Wooding, R. A., 1975, Methods of solution of the equations for convection in porous media, with geothermal applications. In "Geothermal Reservoir Engineering," P. Kruger and H. J. Ramey, Jr., eds. Stanford Geothermal Program, Rep. SGP-TR-12, 206-12.

Wooding, R. A., 1976, Influence of anisotropy and variable viscosity upon convection in a heated saturated porous layer; AMD Tech. Rep. no. 55.

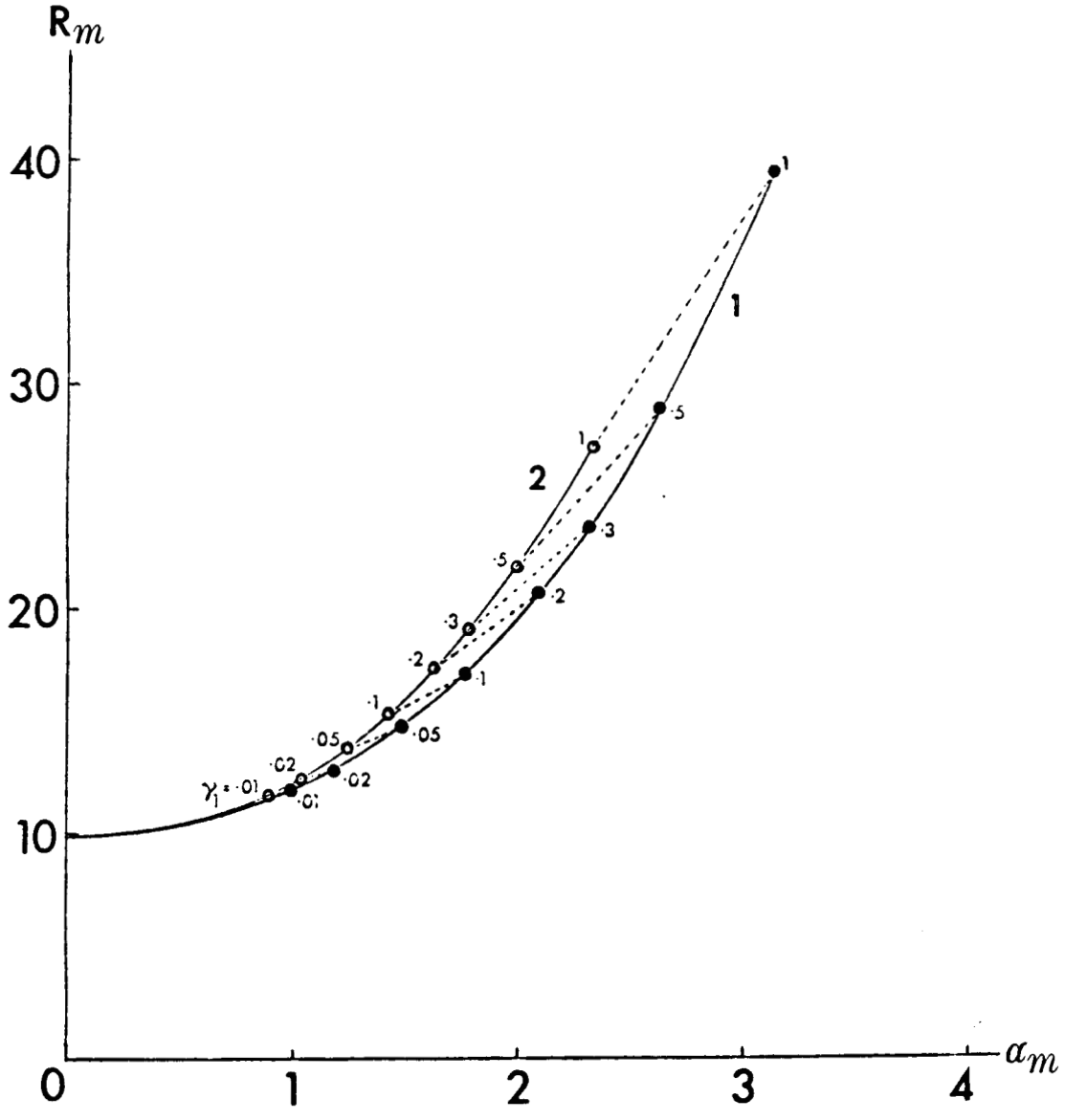

Figure 1. Minimum critical Rayleigh number R_m and the corresponding wavenumber a_m for various vertical-horizontal permeability ratios γ_1.

SUBJECT INDEX

AUTHOR INDEX